

Chiral 'Frustrated Lewis Pair' systems for practical enantioselective hydrogenation and hydrosilylation

by

Dan Mihai Mercea

A dissertation submitted to the

Department of Chemistry, Imperial College London

for the degree of Doctor of Philosophy

August 2019

Abstract

The chemistry of 'Frustrated Lewis Pairs' (FLPs) has been the subject of intense investigation for over a decade now, this activity following the seminal report of Stephan *et al.* concerning the use of a system capable of reversibly binding hydrogen gas in the absence of a transition metal.¹

The explosive development in the field was marked by the discovery of numerous systems which display FLP reactivity and engage in small molecule activation and catalytic reactivity, most notably hydrogenation. To a lesser extent, enantioselective versions of such transformations have also been reported. Perhaps the major limitation which deterred extensive investigation in this area has been the challenging synthesis required to assemble chiral catalysts.

This thesis presents efforts towards the development of practical FLP systems for enantioselective hydrogenation and hydrosilylation as follows:

Chapter 1 surveys the development of the FLP field, with notable developments in terms of structure, reactivity, and mechanistic understanding being covered. Particular attention is given to enantioselective FLP catalysts and to the work carried out for elucidating mechanisms of chirality transfer.

Chapter 2 describes the development of NHC-stabilised borenium ions as catalysts for the FLP hydrogenation and hydrosilylation of *N*-alkyl ketimines, a poorly explored substrate class.

Chapter 3 describes the synthesis of a chiral stannylum ion equivalent and investigations into its catalytic ability in the hydrogenation reaction.

Chapter 4 describes the use of BINOL-derived phosphate salts as Lewis bases in FLP hydrogenation.

Declaration

The results described in this dissertation were obtained by the author (Dan M. Mercea) unless explicitly stated otherwise, and all literature content is referenced as appropriate. The work was carried out by the author in the period October 2015-June 2019 inclusive either in the Department of Chemistry, Imperial College London or at AstraZeneca Macclesfield under the supervision of Prof Matthew J. Fuchter, Dr Andrew E. Ashley, and Dr Alan Steven.

Dan Mihai Mercea

August 2019

Copyright

The copyright of this thesis rests with the author. Unless otherwise indicated, its contents are licensed under a [Creative Commons Attribution-Non Commercial-No Derivatives 4.0 International Licence](https://creativecommons.org/licenses/by-nc-nd/4.0/) (CC BY-NC-ND).

Under this licence, you may copy and redistribute the material in any medium or format on the condition that; you credit the author, do not use it for commercial purposes and do not distribute modified versions of the work.

When reusing or sharing this work, ensure you make the licence terms clear to others by naming the licence and linking to the licence text.

Please seek permission from the copyright holder for uses of this work that are not included in this licence or permitted under UK Copyright Law.

Acknowledgements

I would like to thank my supervisors Matthew Fuchter, Andrew Ashley, and Alan Steven for their guidance and intellectual input, their support throughout my PhD, and their time and effort in helping with the preparation of this manuscript and other pieces of work.

I would like to acknowledge the technical support I received for this work, special mention being due to Peter Haycock for his help with NMR at Imperial College London and to Kevin Leslie and Fiona Bell at AZ Macclesfield for their help with reaction screening. I would like to thank Jochen Brandt for training and past and present members of the Ashley and Fuchter groups for their general help.

I would like to give special thanks to my co-workers in the Fuchter group for their support, understanding, and friendship, in no particular order: James Rushworth, Ollie Bardell-Cox, Raymond Thawani, Jamie Lewis, Nathan Allcock, and Ainoa Zubiaurre.

Last but not least, I would like to thank my parents for all their love and support during my studies.

Abbreviations and common names

1,2-DCB 1,2-dichlorobenzene	Bu butyl
1,2-DFB 1,2-difluorobenzene	C ₇ D ₈ perdeuterated toluene
2,4,6-collidine 2,4,6-trimethylpyridine	C ₇ F ₈ perfluorotoluene
2,6-lutidine 2,6-dimethylpyridine	Cat catechol
9-BBN 9-borabicyclo[3.3.1]nonane	¹³ C ₆ Hex, Cy cyclohexyl
Ac acetyl	Conv. conversion
ACDC asymmetric counterion-directed catalysis	COSY correlated spectroscopy
ACN acetonitrile	Cp cyclopentadienyl
AIBN azobisisobutyronitrile	¹³ C ₃ Pr cyclopropyl
Alk alkyl	d doublet
AN Acceptor Number	d.r. diastereomeric ratio
APCI atmospheric pressure chemical ionisation	DABCO 1,4-diazabicyclo[2.2.2]octane
Ar Aryl	DCM dichloromethane
BAC bis-aminocyclopropenylidene	DIBALH diisobutylaluminium hydride
Benzhydryl diphenylmethyl	DIPP 2,6-diisopropyl phenyl
BINOL 1,1'-Bi-2-Naphthol	DMAP 4-dimethylaminopyridine
Bn benzyl, phenylmethyl	DMSO dimethylsulfoxide
Boc <i>tert</i> -butoxycarbonyl	DOSY diffusion ordered spectroscopy
	e.r. enantiomeric ratio

EI electron ionisation	ⁱ Pr isopropyl
<i>epi</i> - epimeric	IR infrared spectroscopy
Eq. equilibrium	KHMDS potassium hexamethyldisilazane
Equiv. equivalent	m.p. melting point
ESI electrospray ionisation	Me methyl
Et ethyl	Men menthyl
FLP Frustrated Lewis Pair	Mes mesityl, 2,4,6-trimethylphenyl
FWHM Full Width at Half Maximum	Mesitylene trimethylbenzene
GB Gutmann-Beckett (Lewis acidity measurement)	MIC mesoionic carbene
HIBDIO derived from 2,3,10,14,21,22-hexahydroimidazo[4,3- <i>b</i> :5,1- <i>b</i> 0]- bis(3 <i>a</i> S,8 <i>a</i> R)-8,8 <i>a</i> -dihydro-3 <i>a</i> H-indeno[1,3]oxazol-11-ium	MS molecular sieves
HMBC heteronuclear multiple bond correlation	Ms mesyl, methylsulfonyl
HPLC high pressure liquid chromatography	MTBE methyl <i>tert</i> -butyl ether
HRMS high resolution mass spectrometry	NHC <i>N</i> -heterocyclic carbene
HSQC heteronuclear single quantum correlation	NMR Nuclear Magnetic Resonance
IBiox bisoxazoline-derived NHC	Np naphthyl
IPA isopropyl alcohol	Nph neophyl
	Nu nucleophile
	<i>o</i> -tol <i>ortho</i> -tolyl
	pet. Petroleum
	pftb perfluoro <i>tert</i> butanolate

Ph phenyl	^t Bu <i>tert</i> -butyl
Pin pinacol	TEMPO (2,2,6,6-tetramethylpiperidin-1-yl)oxyl
Piv pivalate	Tf trifluoromethylsulfonyl
PMB <i>para</i> -methoxybenzyl	THF tetrahydrofuran
PMHS polymethylhydrosiloxane	THIBO derived from tetrahydroimidazo[4,3- <i>b</i> :5,1- <i>b</i> 0]bis[1,3]oxazol-4-ium
PMP <i>para</i> -methoxyphenyl	TLC thin layer chromatography
Pr propyl	TMP 2,2,6,6-tetramethylpiperidine
PTFE polytetrafluoroethylene	TMS trimethylsilyl
q quartet	TOF turnover frequency
Quinaldine 2-methylquinoline	Toluene methylbenzene
rds rate determining step	Ts tosyl, <i>para</i> -toluenesulfonyl
^s Bu <i>sec</i> -butyl	VT variable temperature
Subst. substrate	WCA weakly coordinating anion
Sulfolane tetramethylene sulfone	Xylene dimethylbenzene
t triplet	
TBAF tetrabutylammonium fluoride	

Units

° degree Celsius

Å Angstroms

atm atmospheres

bar

d days

g grams

h hours

Hz Hertz

J Joules

K Kelvin

L litres

M molar (mol/dm^3)

mol moles

ppm parts per million

s seconds

Table of contents

Abstract.....	2
Declaration.....	3
Copyright.....	3
Acknowledgements.....	4
Abbreviations and common names	5
Units	8
Table of contents	9
List of Figures	15
List of Schemes.....	20
List of Tables	23
1 Chapter 1–Introduction	26
1.1 Lewis acid base theory.....	26
1.2 The frustrated Lewis pair reactivity concept	27
1.2.1 Cooperativity.....	28
1.3 FLP chemistry development.....	30
1.3.1 Small molecule activation	30
1.3.2 Catalytic methodology	34
1.3.3 Mechanistic understanding.....	38
1.3.4 Improving tolerance and substrate scope	40

1.3.5	Other notable reactions.....	43
1.4	Enantioselective FLP chemistry.....	44
1.4.1	Stereochemical probes in FLP-catalysed hydrosilylation.....	45
1.5	Review of catalysts.....	51
1.6	Outlook and project goals.....	60
2	Chapter 2–NHC-stabilised borenium ions.....	63
2.1	Introduction	63
2.1.1	Borenium ions	63
2.1.2	Borenium ions as alternative Lewis acids in FLP chemistry	66
2.1.3	Project goals.....	68
2.2	Catalyst synthesis.....	73
2.2.1	Synthesis of IBiox NHC-boranes	73
2.2.2	Synthesis of borenium cations.....	79
2.3	Catalytic activity.....	84
2.3.1	Hydrogenation	84
2.3.2	Hydrosilylation	103
2.4	Enantioselectivity analysis	127
2.5	Conclusion and future work.....	130
3	Chapter 3–Stannylium ion equivalents.....	133
3.1	Introduction	133
3.1.1	Literature precedent in the field of FLP chemistry	133
3.1.2	Chiral organotin-literature precedent.....	137

3.2	Use of chiral organotin hydrides in enantioselective synthesis.....	140
3.2.1	Under radical conditions.....	140
3.2.2	Under ionic conditions.....	143
3.3	Chiral organotin Lewis acids	144
3.4	Target chiral stannylum ion equivalent and design considerations	144
3.5	Synthesis of a trimethylstannylum cation equivalent (Men_3SnX 167)	147
3.5.1	Proposed synthesis and synthetic options.....	147
3.6	Synthesis	148
3.6.1	Menthyl chloride from menthol	148
3.6.2	Menthylmagnesium chloride 168 formation.....	149
3.6.3	Trimethyltin core formation by alkylation.....	152
3.6.4	Sn-Sn bond cleavage	159
3.6.5	Counterion exchange	163
3.6.6	Trimethyltin hydride preparation	165
3.6.7	Hydride abstraction.....	166
3.7	NMR data interpretation for $\text{Men}_3\text{SnNTf}_2$; Gutmann-Beckett Lewis acidity	168
3.8	Catalytic and stoichiometric studies	170
3.8.1	Hydrogen activation.....	170
3.8.2	Stoichiometric and catalytic reduction studies.....	173
3.9	Conclusions	175
4	Chapter 4—Chiral phosphate Lewis bases	177
4.1	Introduction	177

4.1.1	Literature precedent in the field of FLP chemistry	177
4.1.2	Brønsted acid and Asymmetric Counteranion-directed catalysis.....	180
4.1.3	Envisaged use of chiral phosphate salts as Lewis bases in FLP catalysis	184
4.2	Investigations into catalytic feasibility.....	185
4.2.1	Discussion of relevant NMR methods.....	185
4.2.2	Accessing FLP states.....	191
4.3	Decomposition pathways.....	206
4.4	Attempted catalytic transformations	213
4.5	Conclusions	215
5	Experimental chapter.....	216
5.1	Experimental data concerning Chapter 2	216
5.1.1	Calculation % V_{bur} for 95	216
5.1.2	Catalyst synthesis.....	217
5.1.3	Attempted formation of 108 and coupling of 110	230
5.1.4	Additional characterisation for 95a	230
5.1.5	Additional substrates tested	231
5.2	Experimental data concerning Chapter 3	245
5.2.1	General considerations relevant to Chapter 3.....	245
5.2.2	(-)-MenCl 170	245
5.2.3	'MenMgCl' 168/173 small scale preparation.....	245
5.2.4	'MenMgCl' 168/173 large scale preparation	246
5.2.5	Men ₃ SnCl 151 small scale preparation	246

5.2.6	Men ₃ SnCl 151 large scale preparation.....	247
5.2.7	Men ₆ Sn ₂ 148	247
5.2.8	Men ₃ SnH 152	249
5.2.9	Men ₃ SnNTf ₂ 182	250
5.2.10	Gutmann-Beckett Lewis acidity measurement.....	250
5.2.11	Men ₆ Sn ₂ cleavage using HCl	251
5.2.12	Men ₆ Sn ₂ cleavage using Cp ₂ FeOTf	251
5.2.13	Halide abstraction from Men ₃ SnCl.....	251
5.2.14	Hydrogen activation using Men ₃ SnNTf ₂	251
5.2.15	Stoichiometric reduction of 13g	252
5.2.16	Catalytic reduction of 13g	252
5.3	Experimental Section for chapter 4	252
5.3.1	Purification of racemic [200]H	252
5.3.2	<i>R</i> -[200]Na	253
5.3.3	Racemic [200]Li.....	254
5.3.4	<i>R</i> -[200][Bu ₄ N]	254
5.3.5	<i>R</i> -[201]Na	254
5.3.6	<i>R</i> -[202]Na	255
5.3.7	Hydrogen activation with <i>R</i> -[201]Na in benzene.....	255
5.3.8	Stoichiometric reductions.....	255
5.3.9	Preparation of enamine 205	257
5.3.10	Preparation of racemic amine 206	258

5.3.11	Adduct 207	259
5.3.12	Borane 208	259
5.3.13	Hydrogen activation with 208	259
5.3.14	Attempted catalytic reduction.....	260
6	References	261
7	Appendix	285
7.1	Chapter 2.....	285
7.1.1	Catalyst synthesis.....	285
7.1.2	Proto-deborylation of 95b	291
7.1.3	Stoichiometric reduction	292
7.2	Chapter 3.....	293
7.2.1	Catalyst synthesis and characterisation.....	293
7.2.2	Gutmann-Beckett Lewis acidity measurement.....	302
7.2.3	Men ₆ Sn ₂ cleavage studies	303
7.2.4	Hydrogen activation studies	307
7.2.5	Stoichiometric and catalytic reduction of 13g	309
7.3	Chapter 4.....	311
7.3.1	Preparation and characterisation of phosphate salts and their adducts	311
7.3.2	Hydrogen activation studies	320
7.3.3	Novel borane.....	321
7.3.4	Stoichiometric and catalytic reduction studies.....	324

List of Figures

Figure 1.1 A.Examples of related intramolecular borane/phosphine FLPs reported by Erker	31
Figure 1.2 Variation of acid/base strength in FLPs and inverse FLPs.....	32
Figure 1.3 Reduction transition states for FLP ketimine hydrosilylation.....	48
Figure 1.4 Titanium hydride reduction of ketimines	50
Figure 1.5 Generic description of reduction mechanisms involving pre-activation.....	50
Figure 1.6 Chiral borane reported by Erker.....	59
Figure 1.7 Modular construction of Lewis acids and FLPs	61
Figure 2.1 Borenium ions	63
Figure 2.2 Alternative depictions for borenium ions	64
Figure 2.3 Examples of NHC-stabilised borenium ions.....	66
Figure 2.4 THIBO and HIBDIO NHCs and their use as ligands with variable steric bulk.....	70
Figure 2.5 Target borenium ions.....	70
Figure 2.6 ORTEP diagram showing side-on view of borenium cation 95a	82
Figure 2.7 Gutmann-Becket Lewis acidity measurement	83
Figure 2.8 Choice of model substrates for exploring the prochiral double bond environment.....	92
Figure 2.9 Borane 4f	102
Figure 2.10 Hydrosilylation of substrate 13v	119
Figure 2.11 Hydrosilylation of substrate 13g	120
Figure 2.12 Hydrosilylation of substrate 13g	121
Figure 2.13 Hydrosilylation of substrate 13l	123
Figure 2.14 Hydrosilylation of substrate 13l	124
Figure 2.15 Hydrosilylation of substrate 13l	125
Figure 2.16 Hydrosilylation of substrate 13i	126
Figure 2.17 Graphical representation of enantioselectivity solvent effect	128
Figure 2.18 Graphical representation of enantioselectivity counterion effect	129

Figure 2.19 Examples of chiral MICs	131
Figure 3.1 Hydrogenation and reductive amination catalysed by 132	133
Figure 3.2 Trialkyl stannylum Lewis acids	134
Figure 3.3 Mechanistic proposal for the hydrogenation of imines (A) and ketones (B) using 132	135
Figure 3.4 Mechanistic details for <i>i</i> Pr ₃ SnOTf-catalysed hydrogenation.....	136
Figure 3.5 Examples of compounds featuring chirality at tin	137
Figure 3.6 Configurationally stable penta-coordinate organotin compounds	138
Figure 3.7 Examples of menthyl substituted organotin compounds.....	139
Figure 3.8 Examples of tin (IV) chiral Lewis acids	144
Figure 3.9 Design consideration for target chiral Lewis acid	145
Figure 3.10 Comparison of chirality transfer modes under radical and ionic conditions.....	145
Figure 3.11 Epimeric menthyltin derivatives	155
Figure 3.12 Analysis of Sn-C one bond coupling constants	168
Figure 4.1 Transfer hydrogenation using an axially chiral phosphate salt	181
Figure 4.2 Brønsted acid catalysis and ACDC catalysis	182
Figure 4.3 Catalyst/substrate reactive complex configurations	182
Figure 4.4 Experimental probing of preferred reduction transition states	183
Figure 4.5 Trispentafluorophenyl borane adducts	186
Figure 4.6 ¹¹ B NMR shift correlation with electron density.....	188
Figure 4.7 Franz and Diemoz method for assessing hydrogen-bonding ability.....	190
Figure 4.8 Changes in ³¹ P NMR chemical shifts in BINOL-phosphoric acids	191
Figure 4.9 VT ¹ H NMR for phosphate salt/borane 202 adduct formation.....	195
Figure 4.10 VT ³¹ P NMR (d8-tol) for phosphate salt/borane 202 adduct formation.....	196
Figure 4.11 VT ¹¹ B NMR for phosphate salt/borane 202 adduct formation.....	197
Figure 4.12 VT ¹⁹ F NMR for phosphate salt/borane 202 adduct formation	198
Figure 4.13 ¹¹ B NMR data showing hydrogen activation	200

Figure 4.14 ³¹ P NMR data for stoichiometric reduction using a bulky phosphoric acid	203
Figure 4.15 ³¹ P NMR data for stoichiometric reduction using a non-bulky phosphoric acid	204
Figure 4.16 Stoichiometric reduction of Boc-protected enamine	205
Figure 4.17 Reduction of enamides reported by Antilla	205
Figure 4.18 Comparison of Hantzsch ester and borohydride reducing agents	206
Figure 4.19 NMR data for adduct 207	208
Figure 4.20 NMR data following decomposition of adduct 207	208
Figure 4.21 Possible alternative preparation of borane 208	210
Figure 4.22 Potential hydrogen activation using borane 208	211
Figure 4.23 Attempted hydrogen activation using borane 208	212
Figure 5.1 ¹ H and ¹³ C NMR assignment for catalyst 95a	230
Figure 7.1 ¹ H NMR for 92a	285
Figure 7.2 ¹³ C NMR 92a	285
Figure 7.3 ¹¹ B NMR for 92a	286
Figure 7.4 ¹ H NMR for 92b	286
Figure 7.5 ¹³ C NMR for 92b	287
Figure 7.6 ¹¹ B NMR for 92b	287
Figure 7.7 Isolated product from attempted formation of 108	288
Figure 7.8 ¹¹ B NMR describing attempted coupling of 110	288
Figure 7.9 ¹ H NMR COSY for 95a	289
Figure 7.10 ¹³ C NMR for 95a	289
Figure 7.11 ¹ H NMR HSQC for 95a	290
Figure 7.12 Tetrahedral adducts of 95a	290
Figure 7.13 Hydrolysis of 95b	291
Figure 7.14 Aminolysis of 95b	291
Figure 7.15 Stoichiometric reduction of 13g with 92b	292

Figure 7.16 Stoichiometric reduction of 13k with 92b	292
Figure 7.17 ^1H NMR for MenCl purified by column chromatography	293
Figure 7.18 ^{13}C NMR for MenCl purified by column chromatography	293
Figure 7.19 ^1H NMR for MenMgCl/Men ₂ Mg prepared in an NMR-scale experiment	294
Figure 7.20 ^1H NMR spectra monitoring the conversion of MenCl to MenMgCl/Men ₂ Mg.....	294
Figure 7.21 ^1H NMR spectrum for Men ₃ SnCl crystallised from ethanol	295
Figure 7.22 ^{13}C NMR spectrum for Men ₃ SnCl crystallised from ethanol	295
Figure 7.23 ^{119}Sn NMR spectrum for Men ₃ SnCl crystallised from ethanol	296
Figure 7.24 ^1H NMR for Men ₆ Sn ₂ obtained by slow evaporation of ethanol.....	296
Figure 7.25 ^{13}C NMR for Men ₆ Sn ₂ obtained by slow evaporation of ethanol.....	297
Figure 7.26 ^{119}Sn NMR for Men ₆ Sn ₂ obtained by slow evaporation of ethanol.....	297
Figure 7.27 ^1H NMR for Men ₃ SnH	298
Figure 7.28 ^{13}C NMR for Men ₃ SnH	298
Figure 7.29 ^{119}Sn $\{^1\text{H}\}$ NMR for Men ₃ SnH in CDCl ₃	299
Figure 7.30 ^{119}Sn $\{^1\text{H}\}$ NMR for Men ₃ SnH in C ₆ D ₆	299
Figure 7.31 ^1H NMR for Men ₃ SnNTf ₂	300
Figure 7.32 ^{13}C NMR for Men ₃ SnNTf ₂ in C ₆ D ₆	300
Figure 7.33 ^{13}C NMR for Men ₃ SnNTf ₂ in pentane.....	301
Figure 7.34 ^{119}Sn $\{^1\text{H}\}$ NMR for Men ₃ SnNTf ₂ in C ₆ D ₆	301
Figure 7.35 ^{119}Sn $\{^1\text{H}\}$ NMR for Men ₃ SnNTf ₂ in pentane	302
Figure 7.36 ^{119}Sn $\{^1\text{H}\}$ NMR recorded for Gutmann-Beckett analysis of Men ₃ SnNTf ₂	302
Figure 7.37 ^{31}P $\{^1\text{H}\}$ NMR recorded for Gutmann-Beckett analysis of Men ₃ SnNTf ₂	303
Figure 7.38 ^1H NMR showing progress of Men ₆ Sn ₂ cleavage with HCl.....	303
Figure 7.39 ^{119}Sn $\{^1\text{H}\}$ showing progress of Men ₆ Sn ₂ cleavage with HCl.....	304
Figure 7.40 ^{13}C NMR at the latest analysis time point for the Men ₆ Sn ₂ cleavage with HCl.....	304
Figure 7.41 ^1H NMR showing progress of Men ₆ Sn ₂ cleavage with HOTf	305

Figure 7.42 ^{119}Sn $\{^1\text{H}\}$ showing progress of Men_6Sn_2 cleavage with HOTf	305
Figure 7.43 ^{13}C NMR for isolated product from Men_6Sn_2 cleavage with HOTf.....	306
Figure 7.44 ^1H NMR monitoring Men_6Sn_2 cleavage with Cp_2FeOTf	306
Figure 7.45 ^{119}Sn $\{^1\text{H}\}$ NMR for Men_6Sn_2 cleavage with Cp_2FeOTf	307
Figure 7.46 ^1H NMR for $\text{Men}_3\text{SnNTf}_2$ generated <i>via</i> halide abstraction from Men_3SnCl	307
Figure 7.47 ^{119}Sn $\{^1\text{H}\}$ NMR for $\text{Men}_3\text{SnNTf}_2$ generated <i>via</i> halide abstraction from Men_3SnCl	308
Figure 7.48 ^1H NMR monitoring hydrogen activation with $\text{Men}_3\text{SnNTf}_2$	308
Figure 7.49 ^{119}Sn NMR spectra collected after 21 h in the hydrogen activation with $\text{Men}_3\text{SnNTf}_2$...	309
Figure 7.50 ^1H NMR monitoring stoichiometric reduction of 13g	309
Figure 7.51 ^1H NMR monitoring catalytic reduction of 13g	310
Figure 7.52 $^{119}\text{Sn}\{^1\text{H}\}$ NMR monitoring catalytic reduction of 13g	310
Figure 7.53 Racemic [200]H	311
Figure 7.54 Racemic [200]H	311
Figure 7.55 <i>R</i> -[200]Na	312
Figure 7.56 <i>R</i> -[200]Na	312
Figure 7.57 <i>R</i> -[200]Na	313
Figure 7.58 Racemic [200]Li	313
Figure 7.59 Racemic [200]Li	314
Figure 7.60 Racemic [200]Li	314
Figure 7.61 <i>R</i> -[200][Bu_4N]	315
Figure 7.62 <i>R</i> -[200][Bu_4N]	315
Figure 7.63 <i>R</i> -[200][Bu_4N]	316
Figure 7.64 (<i>R</i>)-[201]Na.....	316
Figure 7.65 (<i>R</i>)-[201]Na.....	317
Figure 7.66 (<i>R</i>)-[201]Na.....	317
Figure 7.67 (<i>R</i>)-[201]Na.....	318

Figure 7.68 (<i>R</i>)-[202]Na.....	318
Figure 7.69 (<i>R</i>)-[202]Na.....	319
Figure 7.70 (<i>R</i>)-[202]Na.....	319
Figure 7.71 (<i>R</i>)-[202]Na.....	320
Figure 7.72 Hydrogen activation with (<i>R</i>)-[201]Na in benzene	320
Figure 7.73 Hydrogen activation with (<i>R</i>)-[201]Na in benzene	321
Figure 7.74 Borane 208	321
Figure 7.75 Borane 208	322
Figure 7.76 Borane 208	322
Figure 7.77 Borane 208	323
Figure 7.78 Borane 208	323
Figure 7.79 Enamine 205	324
Figure 7.80 Enamine 205	324
Figure 7.81 Racemic 206	325
Figure 7.82 Racemic 206	325
Figure 7.83 Hydrogenation of diphenylethene 210	325
Figure 7.84 Hydrogenation of diphenylethene 210	325
Figure 7.85 Hydrogenation of acetophenone 12c	325

List of Schemes

Scheme 1.1 Examples of Lewis acid/base pairs and their reactivity	26
Scheme 1.2 Molecular hydrogen activation using phosphine/borane combinations.....	27
Scheme 1.3 Examples of cooperativity reported by Stahl and Jacobsen.	28
Scheme 1.4 Examples of cooperativity reported by Berkessel and Noyori.....	29
Scheme 1.5 Small molecule activation using FLPs.....	33
Scheme 1.6 Imine hydrogenation catalysed by FLPs.....	35

Scheme 1.7 Examples of Lewis acid catalysed hydrosilylation.	37
Scheme 1.8 Mechanism for Lewis acid catalysed carbonyl hydrosilylation	37
Scheme 1.9 Bond activation transition states	39
Scheme 1.10 General mechanism for catalytic carbonyl FLP hydrogenation.	41
Scheme 1.11 Strategies for FLP catalysed carbonyl hydrogenation.	42
Scheme 1.12 Other notable reactions catalysed using FLPs.....	43
Scheme 1.13 FLP-catalysed C-H activation.	44
Scheme 1.14 Strategies to achieve enantioselective FLP reduction.....	45
Scheme 1.15 FLP reduction of acetophenone 12c with a chiral enantioenriched hydrosilane	46
Scheme 1.16 Complete mechanism for FLP hydrosilylation of ketimines.....	49
Scheme 1.17 Use of chiral boranes in hydrogenation and hydrosilylation	52
Scheme 1.18 Enantioselective hydrogenation reported by Repo.	54
Scheme 1.19 Enantioselective carbonyl hydrosilylation reported by Oestreich.....	55
Scheme 1.20 FLP catalysed ketimine reduction reported by Du.....	56
Scheme 1.21 Enantioselective reduction of carbonyl and silyl enol ethers reported by Du.....	57
Scheme 1.22 Enantioselective FLP reduction reported by Wang.....	58
Scheme 2.1 Preparation strategies for borenium cations.	65
Scheme 2.2 Borenium-catalysed hydrogenation reported in the literature	67
Scheme 2.3 Chirality transfer using chiral borenium ions	68
Scheme 2.4 Synthesis of IBiox NHC-boranes	74
Scheme 2.5 Conversion of bisoxazolines to imidazolium salts	75
Scheme 2.6 NHC-borane adduct synthesis.....	76
Scheme 2.7 Attempted NHC-borane synthesis	77
Scheme 2.8 Synthesis of borenium ions	79
Scheme 2.9 Possible substrate inhibition through C-binding.....	87
Scheme 2.10 Inhibition and decomposition pathways for borenium 95b	87

Scheme 2.11 Stoichiometric reduction of iminium ions.....	89
Scheme 2.12 High-pressure screening for substrate and solvent	96
Scheme 2.13 Brønsted acid catalysed racemisation study.....	98
Scheme 2.14 High-pressure hydrogenation counterion screening	99
Scheme 2.15 Hydrosilylation substrate scope exploration	113
Scheme 2.16 <i>N</i> -alkyl ketimine hydrosilylation substrate scope	115
Scheme 2.17 Catalyst inhibition and bond activation in hydrosilylation.....	117
Scheme 2.18 <i>N</i> -silyliminium ion isomerisation and reduction	118
Scheme 2.19 <i>N</i> -silyliminium ion deprotonation equilibrium.....	119
Scheme 2.20 Fundamental reduction steps	121
Scheme 2.21 Substrate and intermediate protonation equilibria.....	122
Scheme 2.22 Proposed explanation for the reaction profile observed for substrate 131	124
Scheme 2.23 Proposed reduction transition state	130
Scheme 2.24 Opportunities for future development	132
Scheme 3.1 Enantioselective reduction of acetophenone under radical conditions	140
Scheme 3.2 Enantioselective conversion of racemic halides to enantioenriched hydrocarbons	140
Scheme 3.3 Lewis acid-assisted enantioselective reduction	141
Scheme 3.4 Enantioselective reduction with chiral tin Lewis acid/hydride	142
Scheme 3.5 Enantioselective reduction using organotin hydrides under ionic conditions.....	143
Scheme 3.6 Envisaged enantioselective reduction of acetophenone	146
Scheme 3.7 General synthetic plan for the preparation of Men_3SnX	147
Scheme 3.8 Menthol chlorination	149
Scheme 3.9 Preparation of menthyl Grignard reagent from MenCl	150
Scheme 3.10 Menthyl Grignard epimerisation during alkylation reactions.....	153
Scheme 3.11 Proposed pathways leading to formation of 148 and 151 during alkylation.....	156
Scheme 3.12 Cleavage of Sn-Sn bonds	160

Scheme 3.13 Dimer 148 reactivity towards HCl and HOTf	162
Scheme 3.14 Counterion exchange for organotin compounds	163
Scheme 3.15 Sn-H bond cleavage	166
Scheme 3.16 Preparation of $\text{Men}_3\text{SnNTf}_2$	167
Scheme 4.1 General mechanism for enantioselective hydrogenation using chiral Lewis bases	177
Scheme 4.2 Enantioselective hydrogenation using chiral phosphine bases	178
Scheme 4.3 Use of chiral sulfinamides in FLP hydrogenation	179
Scheme 4.4 Transfer hydrogenation of quinolines reported by Shi	180
Scheme 4.5 Chiral phosphoric acid catalysed transfer hydrogenation	180
Scheme 4.6 Envisaged catalytic cycle using BINOL phosphate Lewis bases	184
Scheme 4.7 Water binding to $\text{B}(\text{C}_6\text{F}_5)_3$	187
Scheme 4.8 Competitive binding of $\text{B}(\text{C}_6\text{F}_5)_3$ in 1,4-dioxane	187
Scheme 4.9 Phosphate salt/borane 202 adduct formation	194
Scheme 4.10 Hydrogen activation using phosphate/borane adducts	199
Scheme 4.11 Enantioselectivity changes with metal cations	201
Scheme 4.12 Chiral phosphoric acid/borane stoichiometric reaction	207
Scheme 4.13 Preparation of borane 208	209
Scheme 4.14 Enantioselective ketone reduction reported by Antilla	210
Scheme 5.1 Preparation of enamine 205	257

List of Tables

Table 1.1 Imine hydrogenation results reported by Stephan	35
Table 1.2 Enantioselective ketimine hydrosilylation	47
Table 1.3 Summary of reported selectivity effects	60
Table 2.1 Enantioselective reduction of acetophenone reported by Lindsay and McArthur	69
Table 2.2 $\%V_{\text{bur}}$ values and reported activity	72

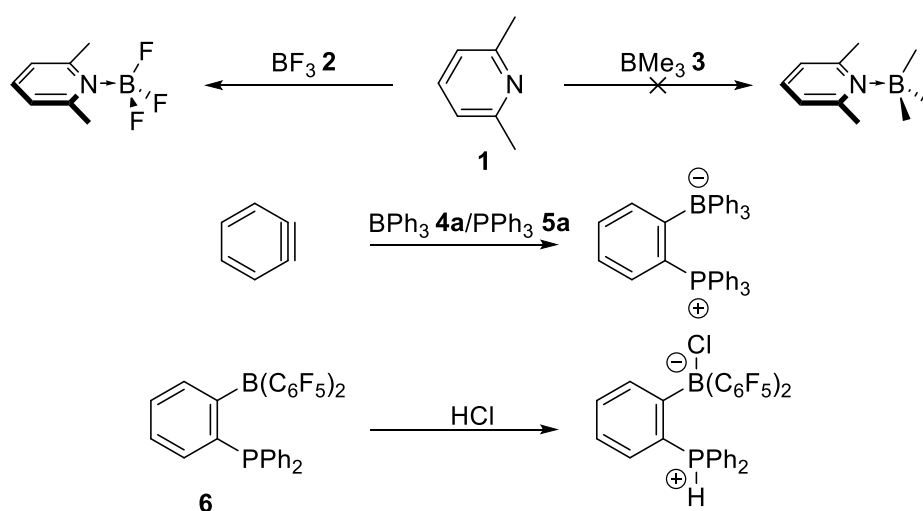
Table 2.3 Summary of yields obtained in the conversion of aminoalcohols to bisoxazolines	74
Table 2.4 NHC-borenum ion comparison.....	81
Table 2.5 NMR scale hydrogenation of <i>N</i> -phenyl and benzyl imines	85
Table 2.6 NMR scale hydrogenation of <i>N</i> - <i>tert</i> butyl imines	86
Table 2.7 Hydrogenation using IBiox-stabilised borenum cations.....	90
Table 2.8 NMR scale hydrogenation reactions	93
Table 2.9 Low-pressure hydrogenation screening.....	95
Table 2.10 High-pressure hydrogenation solvent effect	97
Table 2.11 High-pressure hydrogenation substrate scope screening	100
Table 2.12 High-pressure hydrogenation testing in DCM.....	101
Table 2.13 High-pressure hydrogenation of dialkyl ketimine 13s	101
Table 2.14. <i>N</i> -phenyl ketimine hydrosilylation: catalyst loading.....	103
Table 2.15 <i>N</i> -phenyl ketimine hydrosilylation: setup testing	104
Table 2.16 <i>N</i> -aryl ketimine hydrosilylation: solvent screening.....	106
Table 2.17 <i>N</i> -aryl ketimine hydrosilylation: hydrosilane screening.....	107
Table 2.18 <i>N</i> -aryl ketimine hydrosilylation: additive screening	108
Table 2.19 Catalyst structure variation.....	109
Table 2.20 <i>N</i> -benzyl ketimine hydrosilylation solvent effect.....	110
Table 2.21 <i>N</i> -cyclohexyl ketimine hydrosilylation solvent effect	111
Table 2.22 <i>N</i> -cyclohexyl ketimine counterion effect	112
Table 2.23 Product <i>e.r</i> values/substrate <i>d.r.</i> value comparison for hydrosilylation	126
Table 2.24 Hydrogenation/hydrosilylation <i>e.r</i> values.....	127
Table 3.1 Literature reports for the preparation of trimenthyltin derivatives.....	152
Table 3.2 Preparation of trimenthyltin core	154
Table 3.3 Selected characterisation data for compounds 148 and 151	157
Table 3.4 Metric parameters for dimer 148	158

Table 3.5 Men ₆ Sn ₂ dimer cleavage	161
Table 3.6 Counterion exchange studies	164
Table 3.7 Preparation of Men ₃ SnH	165
Table 3.8 Selected characterisation data for Men ₃ SnH 152	166
Table 3.9 Characterisation data for Men ₃ SnNTf ₂ 182	167
Table 3.10 ¹¹⁹ Sn NMR data for stannylum ion equivalents.....	169
Table 3.11 Hydrogen activation studies.....	171
Table 3.12 Stoichiometric reduction studies	173
Table 3.13 Catalytic reduction studies.....	174
Table 4.1 Effect of ligand binding on ¹⁹ F NMR shifts in C ₆ F ₅ -substituted boranes	185
Table 4.2 ¹¹ B chemical shift values for tetrahedral adducts L-(C ₆ F ₅) ₃	189
Table 4.3 ³¹ P NMR data reported by Ishihara for phosphoric acid/borane adducts	190
Table 4.4 Preparation of chiral phosphate salts	192
Table 4.5 ³¹ P NMR data for phosphate salts	193
Table 4.6 NMR data concerning phosphate salt/borane 4b adduct formation	193
Table 4.7 NMR data comparison for adducts 201 and 202	198
Table 4.8 Stoichiometric reduction studies using borohydrides	202
Table 4.9 Attempted catalytic hydrogenation using phosphate/borane systems	214

1 Chapter 1–Introduction

1.1 Lewis acid base theory

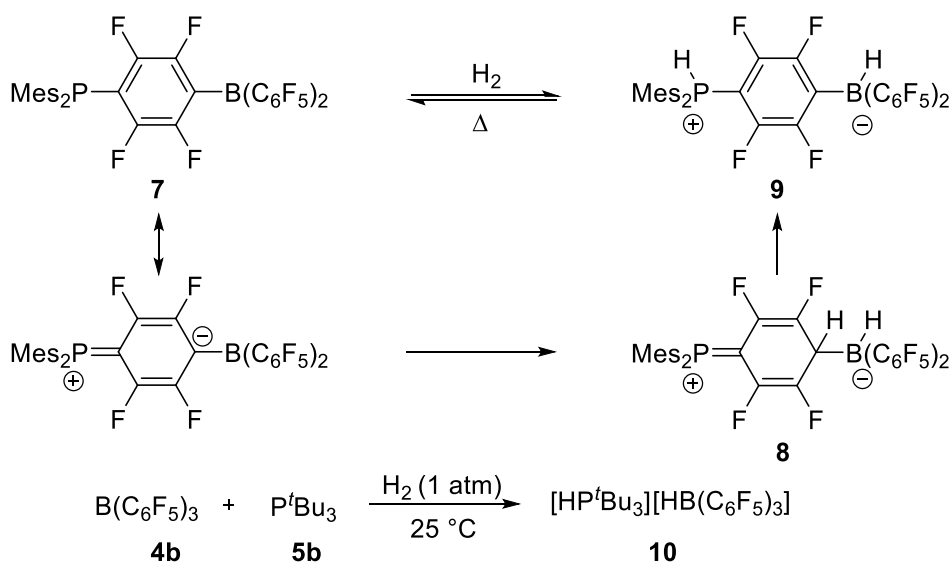
The general description of molecules as acids or bases was presented by G. N. Lewis in 1923 and is currently one of the basic concepts for rationalising and discussing chemical reactivity.^{2,3} A Lewis acid is a molecule which can accept a lone pair of electrons (into an empty orbital); a Lewis base is a molecule which can donate a lone pair of electrons. This process results in the energetically favourable formation of a Lewis acid base adduct containing a new bond (Scheme 1.1). The bond formed by a donor/acceptor interaction rather than by sharing of electrons is called a dative bond. Examples of acid and base combinations, which do not form adducts have been reported.⁴ For example, 2,6-lutidine **1** forms an adduct with boron trifluoride **2**, but not with trimethyl boron **3**. This behaviour is due to increased steric hinderance in the latter combination caused by the methyl substituents within BMe₃. Examples of chemical reactivity arising from combinations of Lewis acids and bases, which cannot form adducts were observed relatively early on,⁵ for example, the pair BPh₃ **4a** and PPh₃ **5a** can add to benzyne. In a more recent example, Piers explored the intramolecular acid/base pair **6** for potential applications in hydrogen storage and showed that **6** can add proton and chloride fragments to the amine and borane components, respectively.⁶



Scheme 1.1 Examples of Lewis acid/base pairs and their reactivity.

1.2 The frustrated Lewis pair reactivity concept

Combinations of sterically hindered Lewis acids and bases, which cannot form the classic Lewis adduct have been named Frustrated Lewis Pairs (FLPs), the term being coined soon after the seminal work of Stephan illustrating the ability of such combinations to cleave dihydrogen (Scheme 1.2).^{1,7,8} The definition of the FLP term has been recently reviewed by Stephan and Fontaine who concluded that FLPs are not defined by their structural features, but by their reactivity.⁹ According to them, FLP chemistry involves the concerted action of a Lewis acid and base pair, separated at the transition state, on a substrate. This definition emphasises the cooperative aspect of FLP reactivity.¹⁰ The conceptual and practical development of FLP chemistry has been covered by numerous reviews.^{10–15}



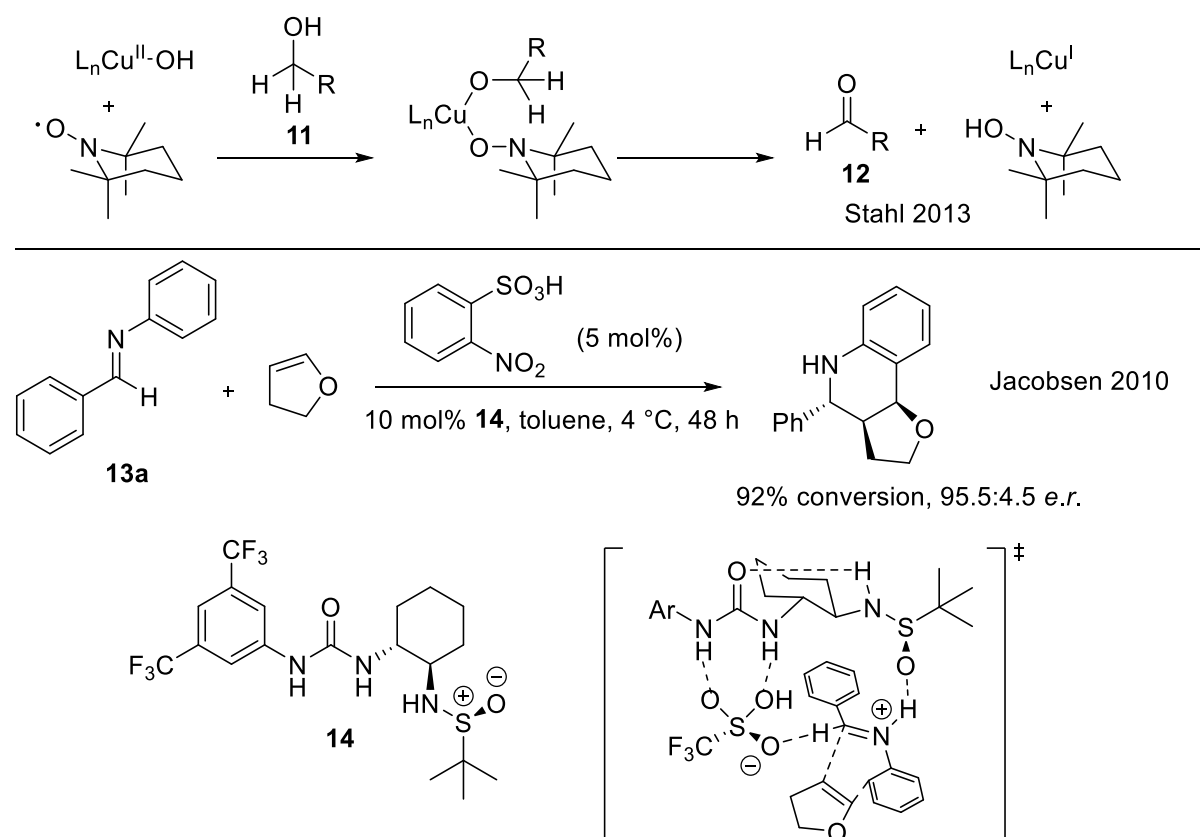
Scheme 1.2 Molecular hydrogen activation using phosphine/borane combinations, reported by Stephan.^{1,7}

The intramolecular phosphine/borane **7** was the first system that illustrated the unprecedented ability for a system lacking transition metals to reversibly bind hydrogen gas (Scheme 1.2).¹ Kinetics studies suggested that hydrogen molecule interaction with the Lewis acidic borane results in hydride and proton binding in vicinal positions in intermediate **8**, followed by intramolecular proton migration to the Lewis basic phosphine fragment, yielding zwitterionic salt **9**. The parent Lewis acid

tris(pentafluorophenyl)borane **4b** displayed similar reactivity in combination with phosphine base **5b**.⁷ The successful nature of the reaction was a result of the combined steric bulk of the two components which prevents classic Lewis adduct formation and of the combined acid/base strength (e.g. **5b** with BMe₃ **4c** affords no reaction). The reaction was in this case not reversible: salt **10** did not liberate hydrogen gas even at 150 °C. Although no evidence existed at the time, it was supposed that cooperative action of the Lewis acid and base is the basis for this reactivity.

1.2.1 Cooperativity

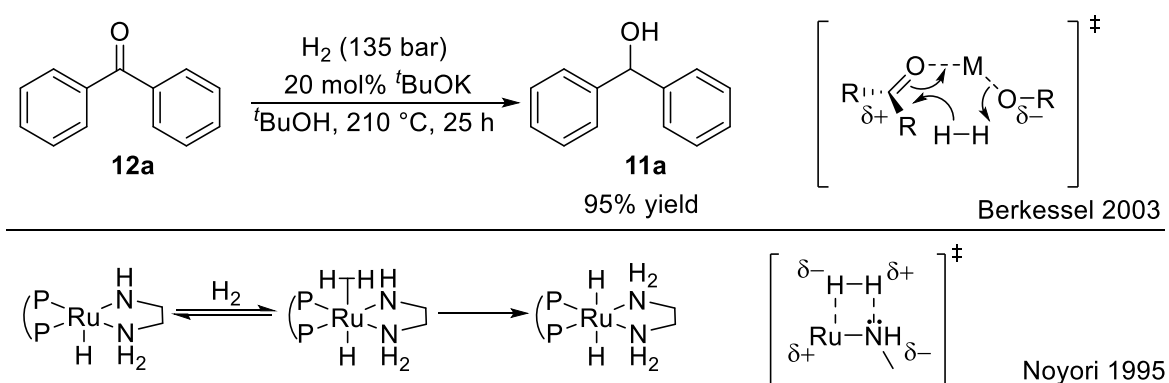
Examples of reactivity resulting from the combined action of two chemical entities, which individually can only deliver such reactivity to a reduced extent or not at all, have been reported in the literature outside the context of frustrated Lewis pair chemistry. Strategies where the two components perform different functions in the catalytic cycle are, although powerful, outside the scope for current discussion.^{16–22}



Scheme 1.3 Examples of cooperativity reported by Stahl and Jacobsen.^{23,24}

A notable example of redox cooperativity (donor/donor, referring to the roles of the species acting on the substrate) has been reported by Stahl and co-workers involving the two-electron oxidation of alcohols **11** to carbonyl compounds (aldehydes) **12** carried out by two one-electron oxidants: a Cu^{II} species and a TEMPO radical (Scheme 1.3).^{23,25} Jacobsen and co-workers reported on the enantioselective Povarov reaction of imine **13a** facilitated by synergistic (donor/acceptor) hydrogen bonding of the activated substrate by bifunctional catalyst **14**.²⁴

A remarkable example of cooperativity is the base-catalysed hydrogenation of carbonyl compounds (e.g benzophenone **12a**) reported by Walling and Bollyky²⁶ and studied by Berkessel and co-workers.²⁷ The latter assigned the reaction to occur *via* a highly ordered transition state (the formation of which is rate limiting) which involves the action of the Lewis acidic substrate and the Brønsted (Lewis) basic alkoxide on the dihydrogen molecule, yielding benzhydrol **11a** directly. This is perhaps the first example of FLP reactivity. The scope of this discovery was probably limited by the forcing conditions required, possibly in part due to the poor ability of the alkali metal cation to organise the transition state, and due to the substrate scope limited to non-enolisable carbonyls. Perhaps the most developed example of synergistic cooperativity outside the FLP field is metal-ligand cooperativity,²⁸ exemplified by the enantioselective ruthenium catalysts reported by Noyori for the hydrogenation of ketones.^{29–33} Activation of hydrogen gas is carried out by the metal centre (effectively acting as a Lewis acid) in combination with an amide ligand acting as a Lewis base.



Scheme 1.4 Examples of cooperativity reported by Berkessel and Noyori.^{27,31}

Following from these examples it could be stated that a cooperative synergistic reaction is defined by donor/acceptor interactions expressed between three or more components and facilitated by their pre-organisation through covalent or non-covalent interactions. These features were shown to be defining for FLP chemistry,^{9,10} and are demonstrated in the following literature discussion. The dramatic development of FLP chemistry was supported by the simplicity and impressive reactivity displayed: two simple components (Lewis acid and base) could carry out a challenging transformation (cleavage of the strong and non-polar H-H bond³⁴) under mild conditions (room temperature and atmospheric pressure).

1.3 FLP chemistry development

Construction of a detailed mechanistic understanding of FLP reactivity was a gradual process outpaced by the explosive development of the practical chemistry. Throughout most of the past decade discussions regarding FLP chemistry were almost entirely focused on the ‘frustrated’ nature of the Lewis pairs employed. This ‘frustration’ was generally seen to result from the significant steric hindrance introduced in the two components. Although tuning the steric profile serves as a useful design principle currently, achieving steric hindrance in the FLP components is not the sole consideration for successful reactivity.³⁵ Among other important factors are the acid and base strengths (more precisely the hydride ion and proton affinities of the acid and base components, respectively, relevant to the hydrogen activation step; see 1.2 for an example) and the chemical stability of the components, chiefly the acid. Examples illustrating the construction of efficient FLP catalysts are presented throughout this chapter.

1.3.1 Small molecule activation

The group of Erker investigated the ability of systems **15,16,17** to activate molecular hydrogen.^{36–38} This series is a useful example showcasing the design of FLP systems beyond simply introducing bulky substituents to prevent adduct formation. All compounds **15–17** exist in the form of an intramolecular phosphine/borane adduct; the FLP state is however readily accessible through an equilibrium with the

open form, proving that FLP reactivity can be accessed from Lewis acid/base adducts. The compounds **15a,b** activate hydrogen gas readily; **17b** reaches a 1:1 equilibrium with the zwitterionic **18**, but **16a,b** do not activate hydrogen.

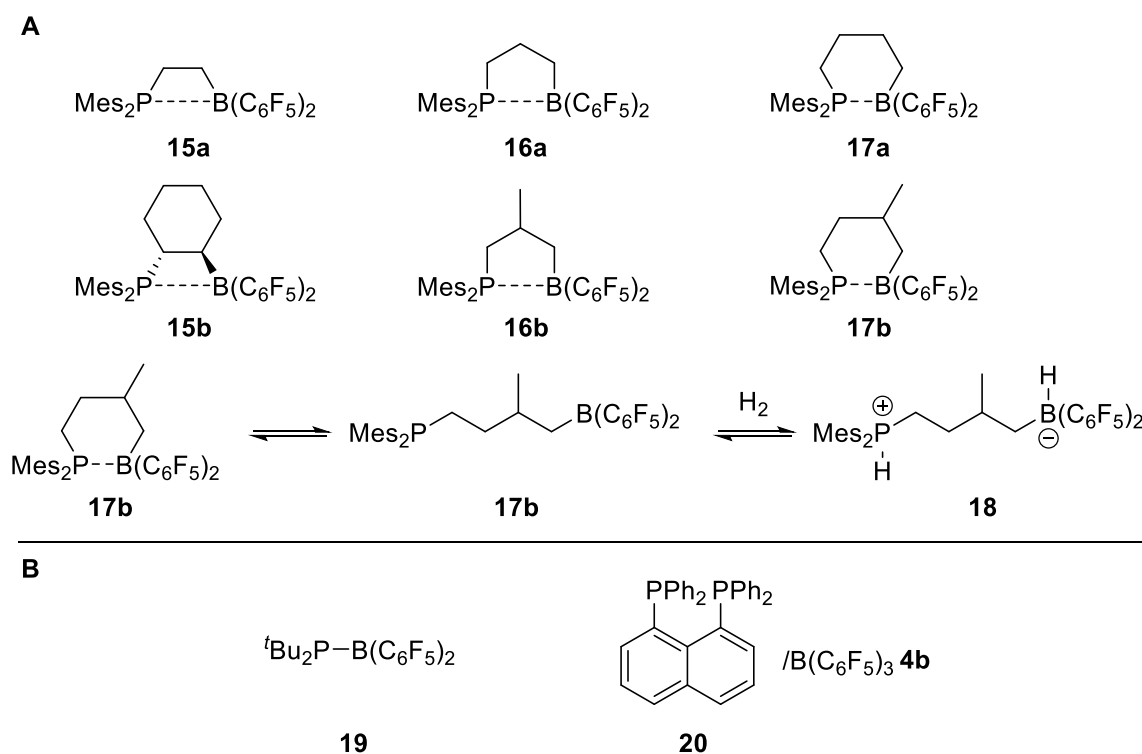


Figure 1.1 A.Examples of related intramolecular borane/phosphine FLPs reported by Erker. B.Other examples of FLPs based on borane/phosphine combinations.^{36–42}

Computational and experimental work indicated that this effect is thermodynamic in nature, with the activation process being exergonic for **15a** and slightly endergonic for **17a**, but strongly endergonic for **16a**. This demonstrates that subtle changes in molecular structure, which cannot be readily rationalised (all the acid and base components can be assumed to have effectively identical strengths) can have an impact on the nature of the bond activation process. Other systems based on combinations of **4b** and phosphines, or intramolecular versions of such combinations, were reported to activate hydrogen gas.^{39–42} The phosphinoborane **19** is a notable example as in this case the availability of free acid and base components is a result of the poor orbital overlap between the phosphorus and boron atoms. The bis-phosphine **20** was notable at the time as it provided readily

reversible hydrogen activation with borane **4b**: hydrogen release taking place at 60 °C. The system **9** reported by Stephan required heating to over 100 °C for hydrogen to be released.

Amine bases can be used as viable alternatives to phosphine bases, as shown by Repo and co-workers with the use of TMP ($pK_aH = 18.6$, ACN;⁴³ Figure 1.2).^{44,45} In a notable extension, Stephan reported the use of 2,6-lutidine **1** in combination with **4b**.⁴⁶ This system represented the first example where the intermolecular Lewis acid/base adduct exists in an equilibrium with the FLP state. It is interesting that due to the lower basicity of 2,6-lutidine ($pK_aH = 14.1$, ACN⁴³), this latter system provides reversible hydrogen activation, in contrast to the TMP system reported by Repo, wherein hydrogen activation is irreversible. The intramolecular *ansa*-aminoborane **21** (which does not present intramolecular binding of the amine fragment) also readily activates hydrogen but does so in a reversible manner, presumably due to the reduction in Lewis acidity of the borane fragment through substitution of a C₆F₅ ring. Such an effect has also been reported by Stephan for the borane **4d**.⁴⁷

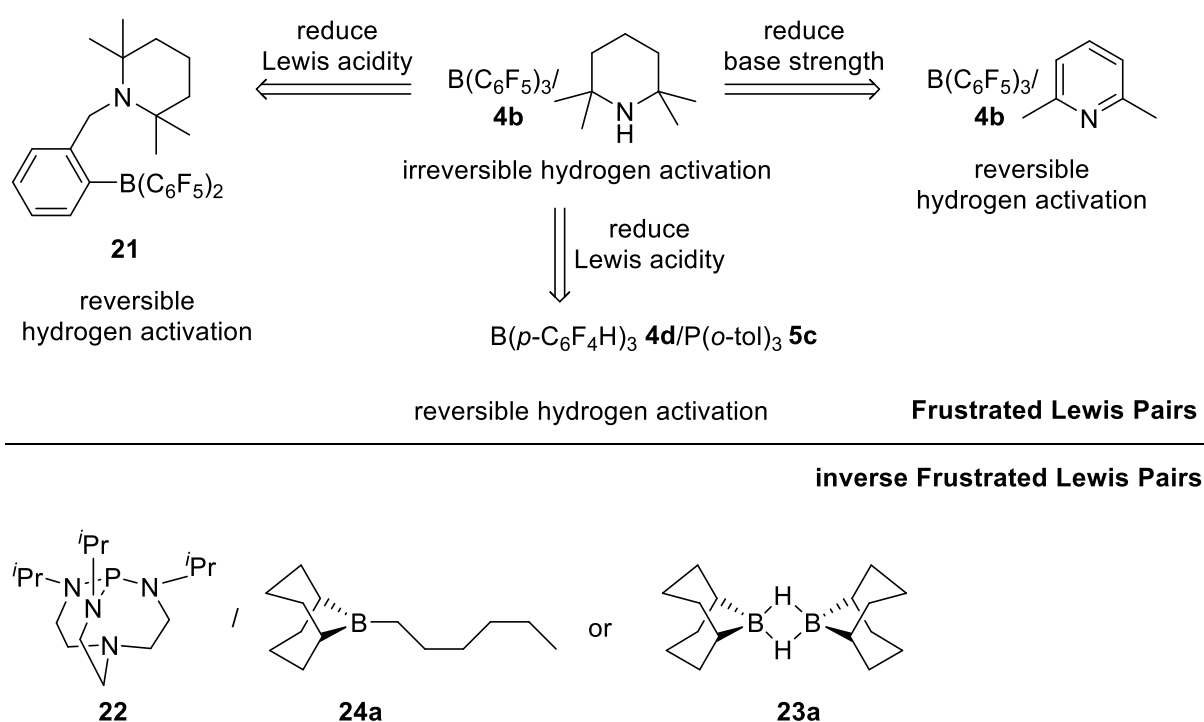
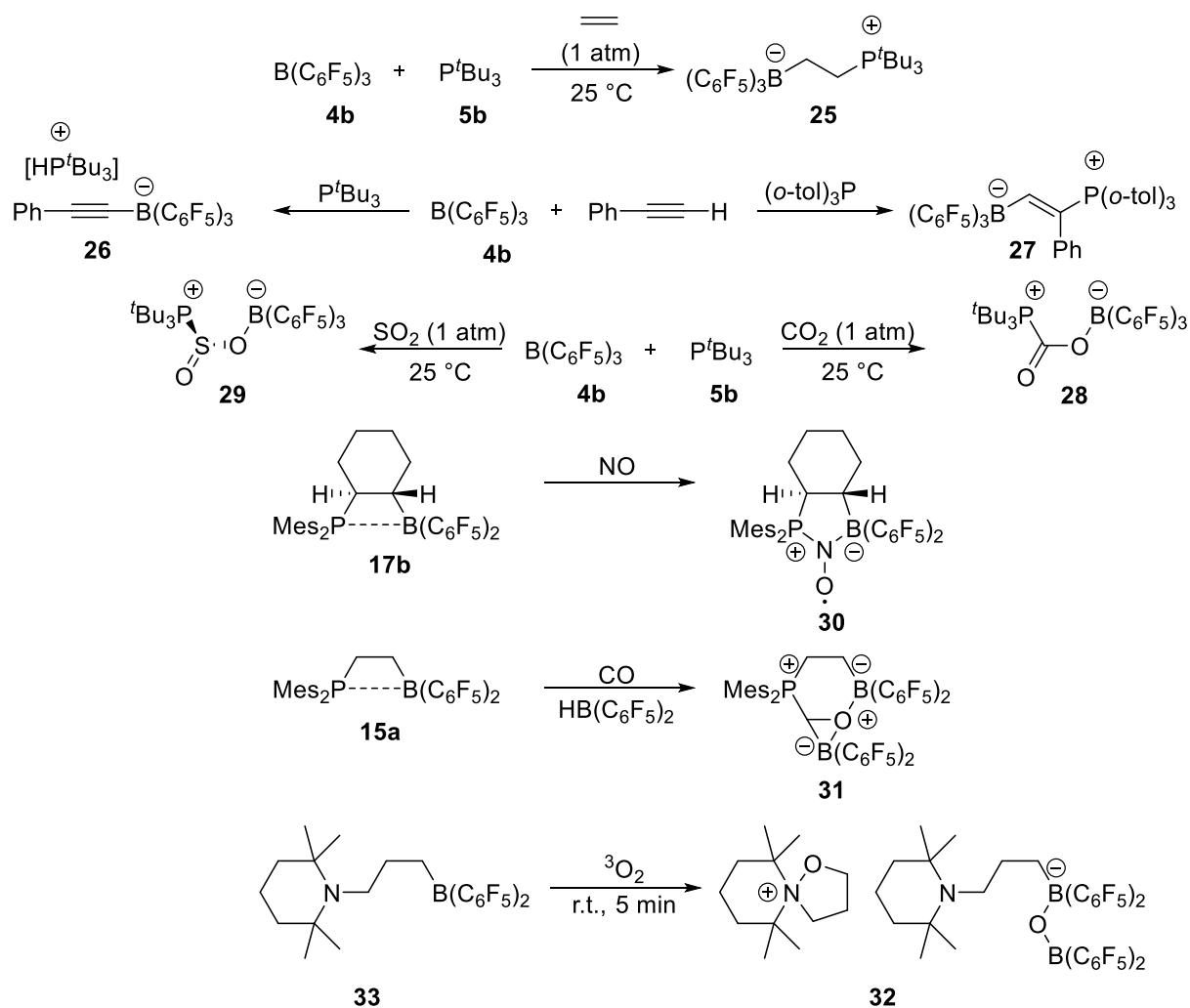


Figure 1.2 Variation of acid/base strength in FLPs and inverse FLPs.

The rapid expansion in the FLP chemistry field has resulted in the development of numerous systems capable of activating hydrogen. In a recent development Krempner and co-workers showed that even weakly Lewis acidic boranes can be used to generate FLPs in combination with superbases.^{48,49} Verkade's superbase **22** ($pK_aH = 29$, ACN^{50}) was shown to activate dihydrogen (2.5 atm) at room temperature in combination with BPh_3 **4a**, 9-BBN dimer **23a** and even 9-hexyl-9-BBN **24a**, examples of what are called 'inverse Frustrated Lewis Pairs'. Further demonstration of the generality of the FLP concept comes with the use of Lewis acids based on other elements. Notable examples are carbon-,⁵¹⁻⁵³ silicon-,^{54,55} tin-,^{56,57} and phosphorus-based Lewis acids.⁵⁸⁻⁶¹

A range of small molecules can be activated using FLPs (Scheme 1.5).



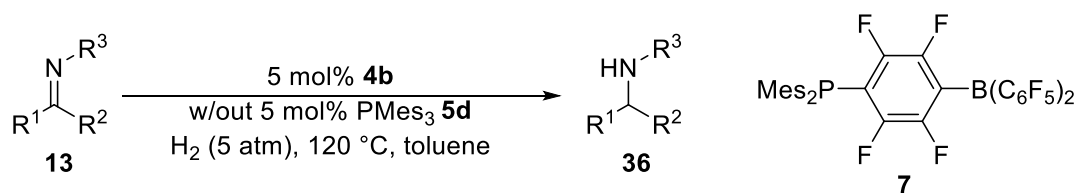
Scheme 1.5 Small molecule activation using FLPs.

Stoichiometric addition of phosphine/borane pairs across alkenes⁸ gives adducts **25**. In the case of terminal alkynes⁶² reaction depends on the nature of the base employed: use of a very basic phosphine **5b** results in deprotonation of the C-H bond giving **26**, whereas the less basic (*o*-tol)₃P **5c** adds to the terminal carbon atom giving **27**. The regioselectivity was explained as resulting from polarisation of the alkyne by the Lewis acid, followed by attack of the nucleophile. Reaction of the pair **4b/5b** with CO₂ gas resulted in immediate formation of adduct **28**.⁶³ SO₂ gas displays similar reactivity to CO₂ forming adduct **29**.⁶⁴ Binding of NO occurs through formation of two new bonds to nitrogen giving adduct **30**, which is a persistent aminoxyl radical.⁶⁵ This example illustrates that FLP reactivity can be exploited to access other reactive species. Carbon monoxide and triplet oxygen also give rise to formation of adducts **31** and **32**, but these reactions are not examples of direct FLP activation. FLP **33** reacts with oxygen *via* a radical pathway,⁶⁶ whereas reductive binding of CO occurs *via* FLP activation of a formylborane.⁶⁷

1.3.2 Catalytic methodology

The great potential of FLPs for small molecule activation was naturally exploited in catalytic applications. Soon after their discovery the intramolecular FLPs **7** and **15a** were used to catalyse the metal-free hydrogenation of imines and enamines.^{42,68} The applicability of the reaction was expanded with the use of **4b** as the Lewis acidic component, and the reduction of nitriles,⁶⁹⁻⁷¹ *N*-heterocycles⁷² and aniline substrates (Table 1.1).^{73,74} The reaction could be carried out in the absence of a phosphine base provided the imine substrate **13** was sufficiently basic. Through this work the general mechanistic cycle depicted in Scheme 1.6 was identified based on a series of key observations. It was shown that the rate of the reaction steps depends strongly on the substrate employed, and that any step can be rate determining. The substrate engages in hydrogen activation directly with the Lewis acidic borane, the process occurring with concurrent activation of the imine substrate by formation of iminium ion pair **34** (formed as a mixture of *E/Z* geometric isomers; the 'double either' nomenclature for double bonds is used throughout this text to represent a mixture of the *E/Z* isomers or undefined double bond

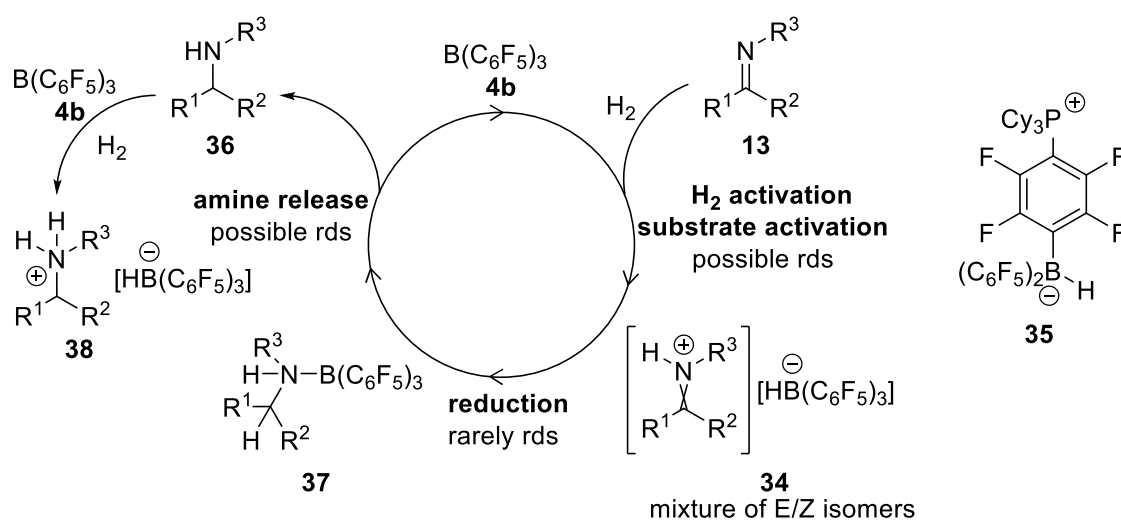
configuration). For poorly basic substrates such as **13b** ($R^1 = \text{Ph}$, $R^2 = \text{H}$, $R^3 = \text{SO}_2\text{Ph}$) the addition of PMes_3 **5d** as cocatalyst or the use of **7** are viable alternatives.



Substrate	R ¹	R ²	R ³	Time	Yield
13c	Ph	H	^t Bu	2 h	89%
13b	Ph	H	SO ₂ Ph	41 h	94%
13b	Ph	H	SO ₂ Ph	8 h (with 5d)	98%
13e	^t Bu	Me	Dipp	48 h	0%

Table 1.1 Imine hydrogenation results reported by Stephan.⁶⁹

Interestingly, **7** achieves faster hydrogen activation (10 min reaction time) than PMes_3 /**4b** pair (24 h).



Scheme 1.6 Imine hydrogenation catalysed by FLPs.

Bulky aldimines **13c** ($R^1 = \text{Ph}$, $R^2 = \text{H}$, $R^3 = \text{^tBu}$), **13d** ($R^1 = \text{Ph}$, $R^2 = \text{H}$, $R^3 = \text{CHPh}_2$) or non-basic **13b** do not cause inhibition of **4b**. More basic substrates favour hydrogen activation and lead to higher reaction rates. Activation of substrates is always required prior to hydride addition, either by protonation or

by binding of Lewis acidic **4b** (only for nitriles). Heating of the substrate **13c** with **35** does not result in reduction even after 24 h at 120 °C.

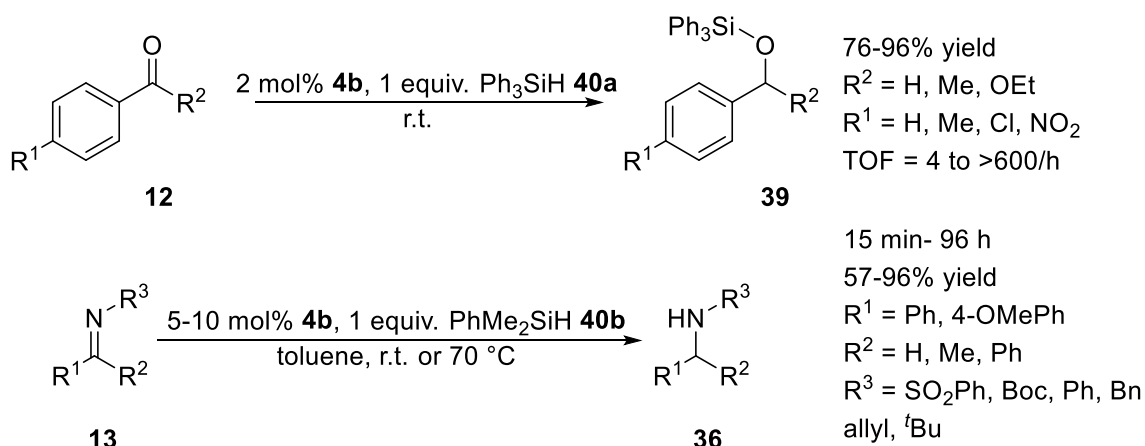
Collapse of iminium ion pair **34** to generate amines **36** is generally a fast process. Isolation of iminium ion/borohydride pairs can be achieved only provided significant steric bulk is present in the parent substrate; **13e** ($R^1 = t\text{Bu}$, $R^2 = \text{Me}$, $R^3 = 2,6\text{-}i\text{Pr}_2\text{C}_6\text{H}_4$) undergoes hydrogen activation with **4b** generating ion pair **34e**, which is stable even at 120 °C.

In contrast to the parent imine substrates, the amine products generally cause inhibition of **4b**. **13c** in combination with **4b** and hydrogen generates the amine adduct **37c** at room temperature; dissociation requires heating to 80 °C, conditions under which further hydrogen activation occurs to generate the ammonium salt **38c**. This latter finding indicates the possibility of auto-catalysis.

The rate of hydrogen activation and of catalyst regeneration is, for most substrates, the main factor determining the success of the process. The catalyst inhibition arising from binding of basic products to borane Lewis acid catalysts is one of the major limitations of the methodology. The reduction of nitriles can only be carried out in the presence of super-stoichiometric amounts of **4b** (with added base) since complete binding of the catalyst occurs. Reduction of aldimine **13f** ($R^1 = \text{Ph}$, $R^2 = \text{H}$, $R^3 = \text{Bn}$) causes irreversible catalyst inhibition through formation of the amine borane adduct **37f**.

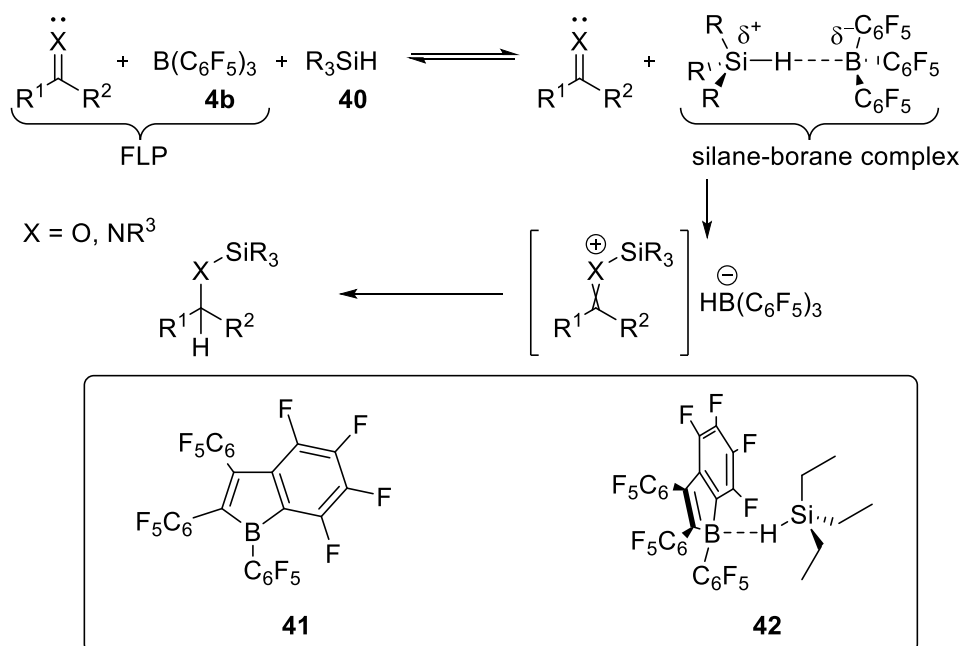
1.3.2.1 Lewis acid catalysed hydrosilylation

The reactivity observed in FLP-catalysed hydrogenation of imines was noted to have parallels in the Lewis acid catalysed (Piers) hydrosilylation (Scheme 1.7).⁶⁹ The reaction was discovered a decade before the seminal work of Stephan,⁷⁵ and through subsequent investigation was shown to be a powerful methodology for the facile reduction of a number of substrate classes: imines (to give free amines **36** following desilylation), aromatic aldehydes and ketones (to give silyl ethers **39**, which can be converted to alcohols through desilylation), esters, and enones using hydrosilanes **40**.^{76,77} Borane **4b** was also able to catalyse dehydrogenative silylation of alcohols⁷⁸ and the reduction of nitro groups,⁷⁹ amides,⁸⁰ and nitriles⁸¹ using hydrosilanes.



Scheme 1.7 Examples of Lewis acid catalysed hydrosilylation.

The catalytic hydrosilylation mechanism of carbonyls and imines was investigated by both Piers and Oestreich. The elegant studies reported by the latter involving the use of stereochemical probes are discussed in detail in section 1.4.1.



Scheme 1.8 Mechanism for Lewis acid catalysed carbonyl hydrosilylation reported by Piers.⁸²

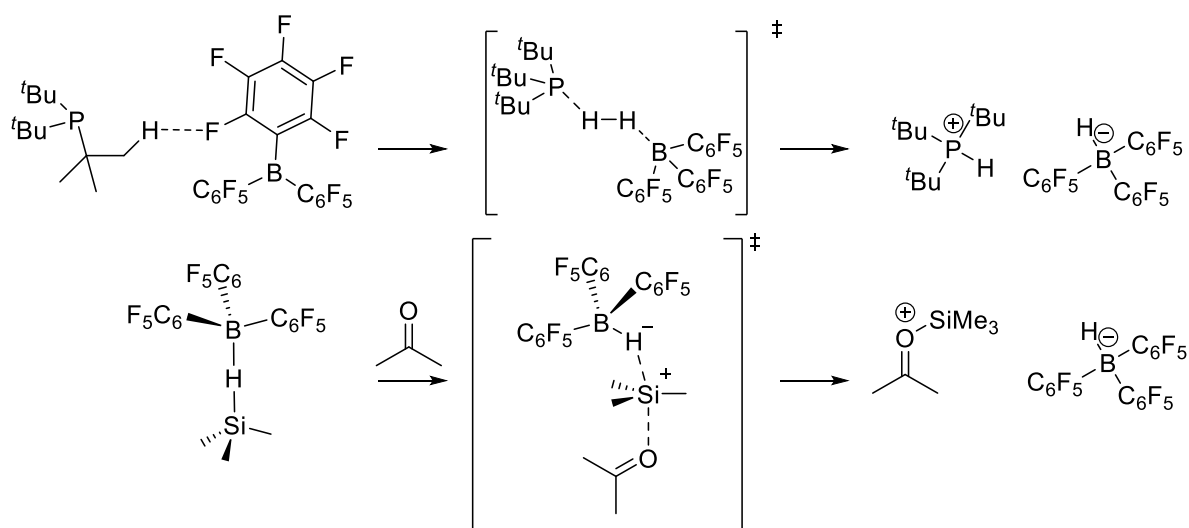
Mechanistic studies performed by Piers indicated reaction to proceed by Lewis acid activation of the Si-H bond followed by substitution at silicon by the substrate with displacement of hydride (Scheme 1.8).⁸² Supportive of this conclusion was the observation that less basic carbonyl derivatives (basicity:

esters < ketones < aldehydes) are reduced more rapidly due to a greater concentration of free borane being present. The relative basicity of different carbonyl derivatives (benzaldehyde, acetophenone, and ethyl benzoate) towards borane **4b** was determined experimentally by Piers.⁸³ The basicity trend is different to that observed towards the proton and indicates that basicity towards the neutral **4b** is controlled by steric effects. In competition experiments the more basic carbonyl substrate is reduced preferentially, indicating that substrates are required to act as nucleophiles. The rate of the process is determined by the concentration of free borane **4b**, which is determined by the position of the adduct formation equilibrium with the substrate, and by the rate at which the free borane and substrate carry out hydrosilane activation. The use of silylium cations as catalysts resulted in ketone deoxygenation being observed, providing indirect evidence that the borane is acting as the hydride shuttle. This was further supported by the selective transfer of H/D from mixtures of silanes with no cross-over products observed. Definitive evidence for this mode of operation was obtained much later with the use of the extremely Lewis acidic **41** which allowed crystallisation of the complex **42** with triethylsilane **40c**.⁸⁴ Crystallographic characterisation indicated significant pyramidalisation at the B atom with a bridging hydrogen atom between the borane and hydrosilane fragments; the bond distances between the boron-hydrogen (1.46(2) Å) and silicon-hydrogen atoms (1.51(2) Å) were similar to those in the individual components and therefore indicative of a Lewis acid/base complex. This study represents one of the most definitive pieces of experimental evidence for the FLP mode of σ -bond activation of hydrosilanes, and by extension, of molecular hydrogen.

1.3.3 Mechanistic understanding

The nature of the σ -bond cleavage process in FLP-mediated dihydrogen activation has attracted considerable attention. Numerous computational studies have probed the nature of this process without reaching a mutual consensus; two schools of thought emerged initially. An early model proposed by Pápai and co-workers rationalised the reaction in terms of a concerted donation/acceptance of electron density.^{85,86} This molecular orbital approach establishes an intuitive mechanism which involves simultaneous $n(\text{base}) \rightarrow \sigma^*(\text{H}_2)$ and $\sigma(\text{H}_2) \rightarrow p(\text{acid})$ donation, mode of

operation which is reminiscent of H₂ activation using transition metal complexes; subsequent work supported this view.^{87–89} The alternative ‘electric field’ model invokes the formation of an electric field between the FLP components: this results in a decrease in energy barrier for dihydrogen activation by polarising the H₂ molecule which, once inside the FLP cavity, is cleaved in an energetically favourable process.^{90–92}



Scheme 1.9 Bond activation transition states reported by Pinter (hydrogen) and Fujimoto (hydrosilane).^{93,94}

More recent efforts have attempted to reconcile the two views.^{93,95,96} Main findings highlight that both the electric field and the orbital interactions play a role in the bond activation process, their relative contributions however depending on the nature of the transition state (early or late), which will in turn depend on the nature of the acid and the base. Regardless of the physical basis for bond cleavage, two salient features of FLP hydrogen activation have been uncovered in all studies: the pre-organisation of Lewis acid and base promoted by intermolecular interactions (formation of the ‘encounter complex’ is favoured by dispersive interactions and C-H...F hydrogen bonding) and the operation of the two components in the bond cleavage step. These findings support the cooperative nature of the FLP activation process. Experimental evidence has been presented for the detection of encounter complexes.^{97–99} The B(C₆F₅)₃ **4b**/PMe₃ **5d** pair associates in solution to a sufficient extent

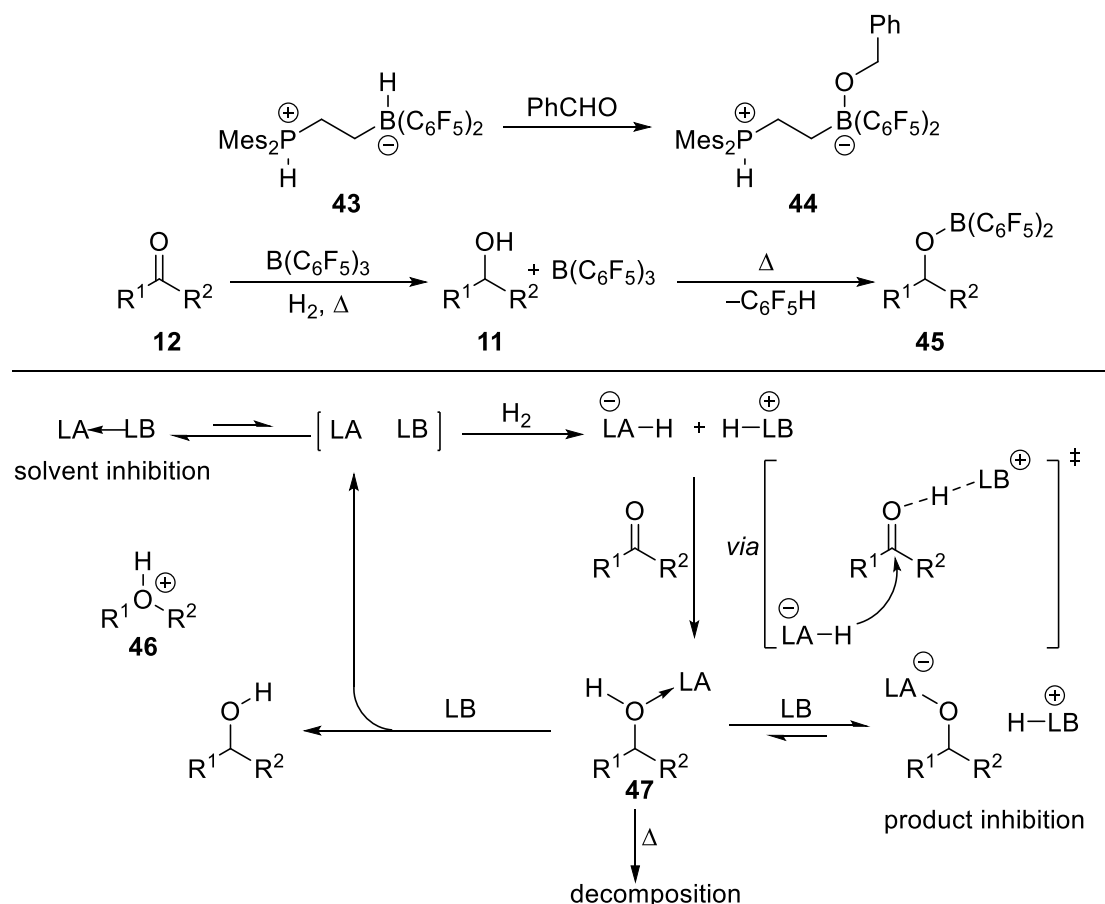
to allow detection of intermolecular CH-F NOE effects. Calorimetric hydrogen activation kinetic studies using the $\text{B}(\text{C}_6\text{F}_5)_3$ **4b**/ PMe_3 **5d** pair revealed the reaction to be best modelled as a termolecular reaction, an observation which indicates the rate of reaction to be limited by the association of the acid and base components; the kinetic isotope effect measured for the reaction (D_2 vs. H_2) was near to unity indicating that bond cleavage is not the rate determining step. Computational work has also been carried out to probe the nature of the hydrosilane activation transition state.⁹⁴

The Scheme 1.9 summarises similarities and differences in the bond activation process; a minor point consists in the different ways that reaction is initiated: for hydrogen activation the key step is formation of the 'encounter complex' whereas for hydrosilane activation formation of the hydrosilane-Lewis acid complex is key. An important point is the difference in transition state geometry: hydrosilane activation takes place with a back-side attack at silicon, whereas hydrogen activation proceeds through a sideways attack. With both experimental and computational work describing a similar reaction mechanism, it results that Lewis acid catalysed hydrosilylation and FLP-catalysed hydrogenation are related transformations.

1.3.4 Improving tolerance and substrate scope

FLP-catalysed hydrogenation displayed a reduced substrate scope compared to hydrosilylation. The latter was first employed for the reduction of carbonyl compounds; early attempts to hydrogenate such substrates under catalytic conditions were unsuccessful (Scheme 1.10). Reduction of benzaldehyde **12b** occurred readily (in the absence of additional activation) with hydride donors such as **7** and **43**^{68,100} to give **44**. Furthermore, it was shown that carbonyl compounds in combination with **4b** can activate hydrogen (at high temperature), resulting in stoichiometric reduction.^{101,102} The product alcohols **11** react with the catalyst leading to formation of borinic esters **45** and preventing turnover. These observations point out to two issues, which prevent catalytic reduction of carbonyls from occurring: irreversible borane inhibition by alkoxide species is observed in the presence of moderately strong bases (the conjugate acids of which are not strong enough to protonate a borane-

alkoxide adduct) and catalyst decomposition occurring by B-C bond cleavage (proto-deborylation) effected by free alcohols at high temperature.

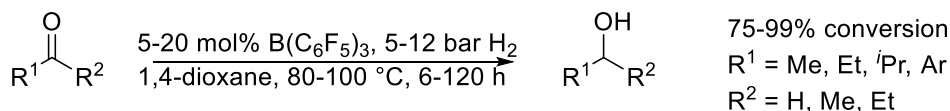


Scheme 1.10 General mechanism for catalytic carbonyl FLP hydrogenation.

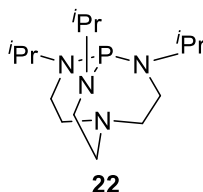
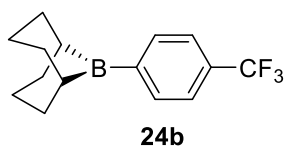
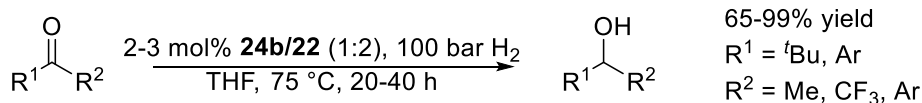
Numerous strategies have been employed to overcome these issues (Scheme 1.11). Using a weak base eliminates catalyst inhibition issues. Our group and the Stephan group reported in parallel the use of ethereal solvents (diethyl ether, 1,4-dioxane, weak bases¹⁰³) as Lewis bases which allowed for successful catalytic hydrogenation of carbonyl substrates.^{104,105} The solvent, present in a significant excess, catalyses hydrogen activation leading to formation of a protonated ether **46**. This species can activate ketones **12** towards reduction, leading to the formation of an alcohol-borane adduct **47**; aldehydes can react with or without assistance from the Lewis acid. Since ethers are not sufficiently strong bases to irreversibly deprotonate adduct **47**, dissociation at high temperature results in liberation of free borane and catalytic turnover. Subsequently, the Stephan group also reported on

the use of solid phase bases (cyclodextrins and molecular sieves).¹⁰⁶ In a natural extension our group has reported on the use of the 1,4-dioxane/**4b** FLP in the hydrogenation of carbonyl substrates under non-anhydrous conditions: the system is tolerant not only of alcohols but also of water.¹⁰⁷

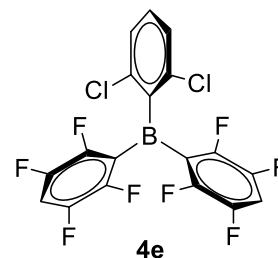
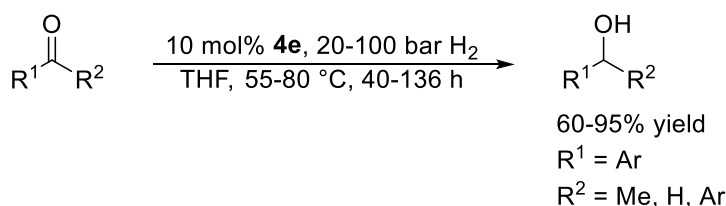
Use of a weakly basic solvent



Use of a weakly Lewis acidic borane



Use of a sterically fine-tuned Lewis acidic borane



Scheme 1.11 Strategies for FLP catalysed carbonyl hydrogenation.

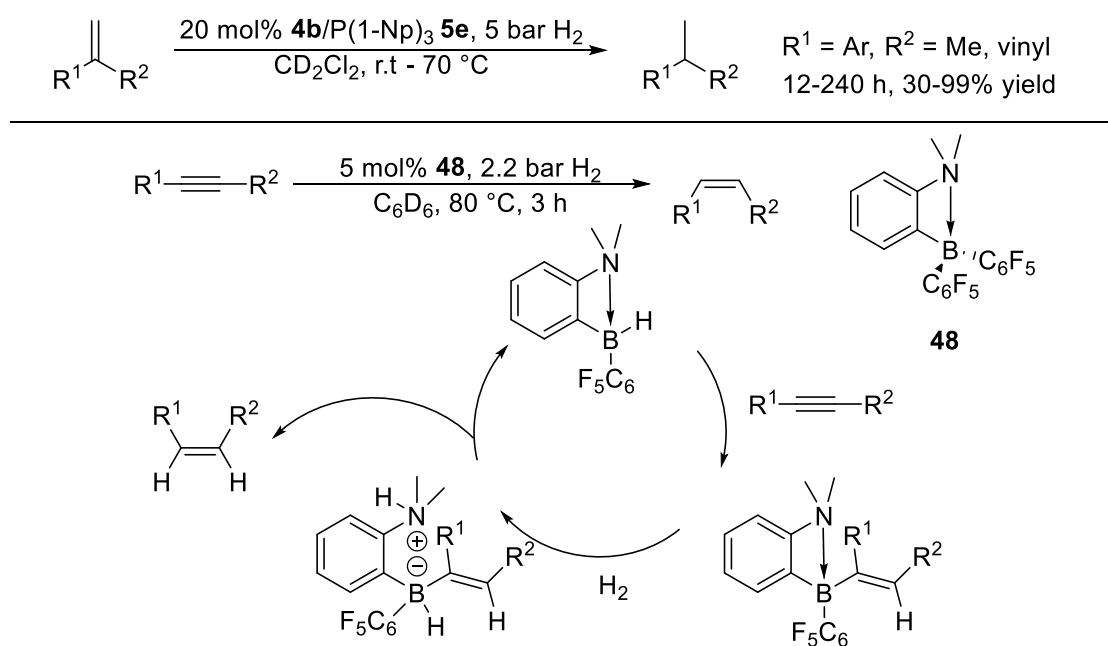
An alternative strategy involves the modification of the Lewis acid. Our group has shown that increasing the steric hindrance in the borane (**4d**, by substituting a C_6F_5 ring for the perchloro analogue) allows for catalytic hydrogenation of a range of substrates to be carried out with the more basic THF ($\text{pK}_a\text{H} = -2.05, \text{H}_2\text{O}$).¹⁰⁸ The increased steric bulk reduces inhibition caused by the solvent. More extensive efforts towards fine tuning of the steric and electronic component in the borane Lewis acid have been reported by the group of Sóos, leading to improved substrate scope and tolerance using borane **4e**.¹⁰⁹⁻¹¹³ The approach taken was termed ‘size exclusion design’ and was aimed at

eliminating undesired reactivity of the borane component allowing it to perform solely in hydrogen gas activation and hydride delivery.

Reducing the Lewis acidity of the borane has also been employed (**24b**, the inverse FLP approach),⁴⁸ leading to a reduction in Brønsted acidity of the product/borane adduct **47**. An interesting approach was reported by our group which investigated reducing the oxophilicity of the Lewis acid rather than its Lewis acidity directly.⁵⁶ Use of a softer Lewis acid (stannylum cation equivalents R_3Sn^+) results in equal hydrogen activation ability, but reduced Brønsted acidity of product/catalyst adducts. Notably, this approach has resulted in significant moisture and thermal tolerance in hydrogenation reactions. These catalysts are the subject of investigation in Chapter 3.

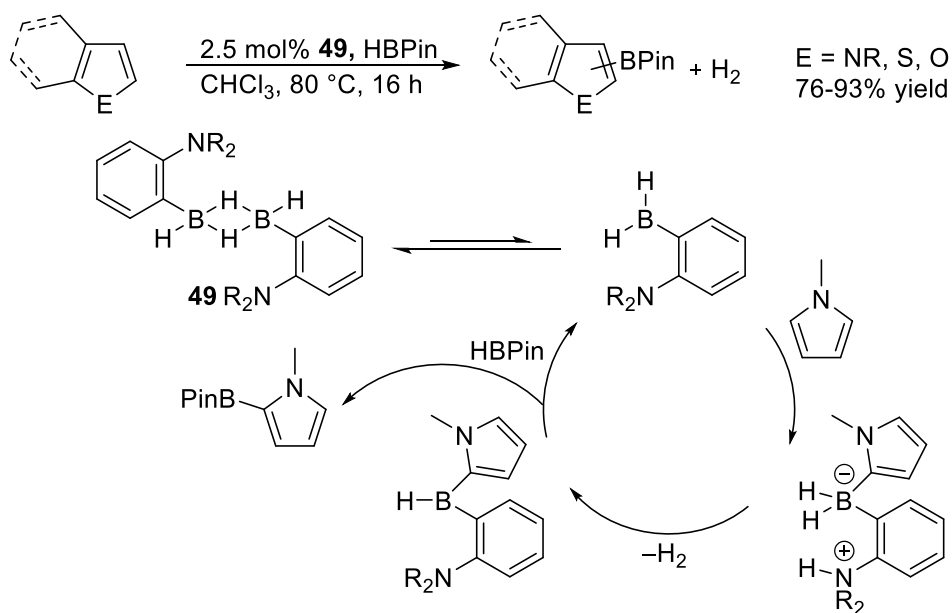
1.3.5 Other notable reactions

The strategies employed previously have been applied for the hydrogenation of alkenes: use of diethyl ether solvent or a very weakly basic phosphine base result in the formation of highly acidic conjugate acids which can protonate alkenes.¹¹⁴⁻¹¹⁷ *Cis*-selective hydrogenation of internal alkynes was achieved using a hydroboration/hydrogen activation/protodeborylation strategy employing pre-catalyst **48**.¹¹⁸



Scheme 1.12 Other notable reactions catalysed using FLPs.

Fontaine and co-workers have notably expanded the scope of FLP procedures with the development of a catalytic C-H borylation procedure using borane **49**.^{119–122}



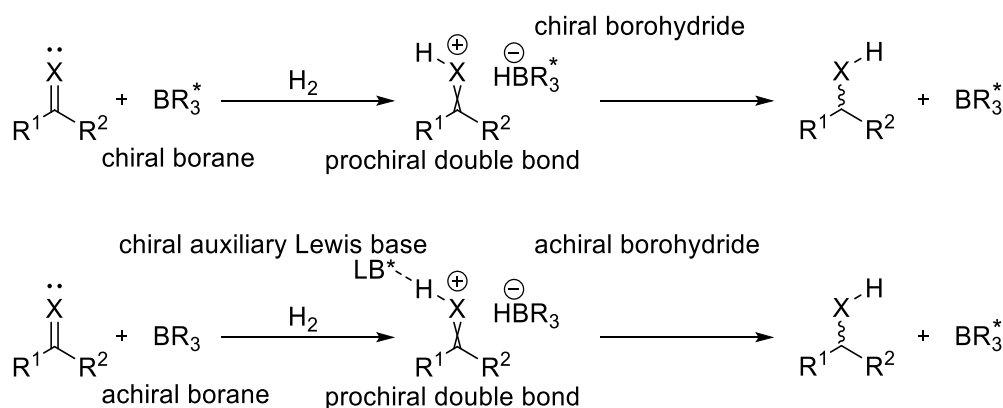
Scheme 1.13 FLP-catalysed C-H activation.

1.4 Enantioselective FLP chemistry

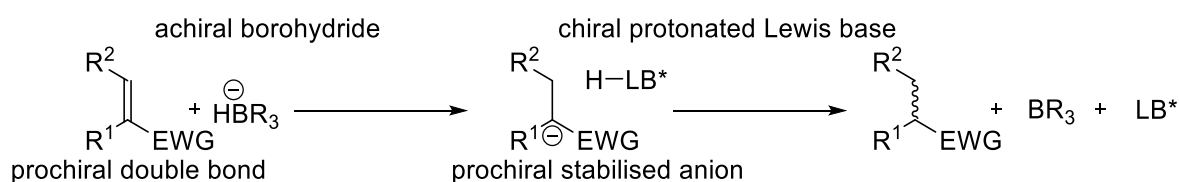
In light of the great synthetic and practical potential of FLP-catalysed hydrogenation and hydrosilylation it is no surprise that enantioselective variants of these reactions became the subject of investigation. Developing such transformations is conceptually simple: use of a chiral Lewis acid will result in formation of an intermediate chiral borohydride. This intermediate will then act to enantioselectively reduce the activated substrate (ketone or imine, activated by protonation or coordination of a silylium cation). Alternatively, use of a chiral Lewis base results in formation of a chiral Brønsted acid which can interact with the activated substrate, rendering its reduction by the achiral borohydride enantioselective. Reduction can for specific substrates (e.g acrylates¹²³) precede the protonation step: chirality can be transferred from a chiral protonated Lewis base to a prochiral anion formed by substrate reduction.

The majority of work reported in the literature is concerned with the use of a chiral Lewis acid, therefore the following discussion provides a review in this area. The use of chiral Lewis bases is an emerging approach and is reviewed in Chapter 4.

Reaction initiated by substrate activation



Reaction initiated by substrate reduction



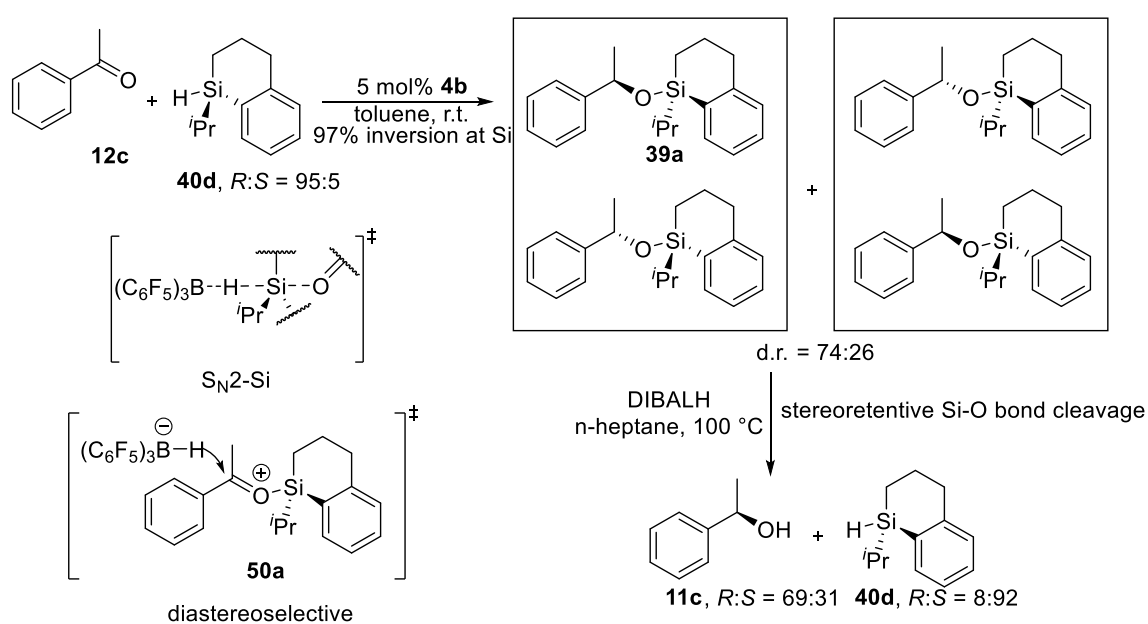
Scheme 1.14 Strategies to achieve enantioselective FLP reduction.

In practice both these transformations raised significant challenges in developing enantioselective versions, with highly enantioselective catalysts being reported only in the past ~6 years. For example, Piers' hydrosilylation of ketones was discovered in 1996¹²⁴ but an enantioselective version (carried out in the absence of an added base) was reported only in 2016.¹²⁵ Alternatively, the use of a chiral Lewis base (different from the substrate) can in theory allow for chirality transfer through interaction between the base and the achiral activated substrate. This strategy has been explored little in the FLP literature. Further discussion is presented in chapter 4.

1.4.1 Stereochemical probes in FLP-catalysed hydrosilylation

Oestreich and co-workers used the enantioenriched chiral hydrosilane **40d** to carry out reduction of acetophenone **12c** mediated by **4b**.^{126,127} The primary product silyl ethers **39a** obtained from the

reduction of acetophenone were isolated with a 74:26 d.r. value. The Si-O bond could be reduced with retention of configuration leading to the recovery of the hydrosilane **40d**. Comparison of the e.r. value for this compound before and after the reaction indicated that reaction had occurred with almost complete (97%) inversion at the silicon atom. This result indicates that hydrosilane activation (with a carbonyl substrate) occurs *via* a S_N2 mechanism at silicon. Reduction of the intermediate silyloxonium cation **50a** proceeds diastereoselectively. A small erosion of enantiopurity was observed in the isolated product alcohol **11c**.

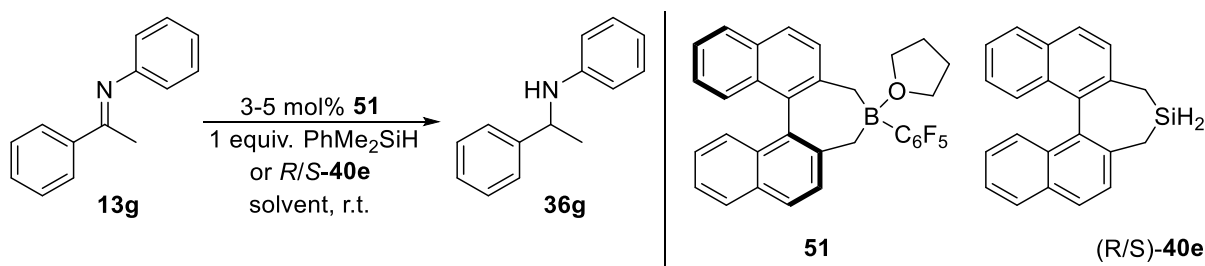


Scheme 1.15 FLP reduction of acetophenone **12c** with a chiral enantioenriched hydrosilane **40d** reported by Oestreich.^{126,127}

Throughout this text enantiomeric ratio (e.r.) is used to discuss enantiopurity of chiral materials. Where literature data was reported using enantiomeric excess (ee), conversion to e.r. was carried out.

To elucidate the mechanism of Lewis acid catalysed ketimine hydrosilylation, subsequent studies were conducted, which notably included the development of a chiral Lewis acid **51** (Table 1.2).^{128,129} Indirect evidence supporting the S_N2 -Si hydrosilane activation mechanism was obtained from observation of reactivity trends similar to those reported by Piers for ketone hydrosilylation: less basic substrates

react faster, except in competition experiments. Questions then remained as to the nature of the enantioselective reduction step: is hydride delivery carried out by the borohydride or by the hydrosilane?



Hydrosilane	Solvent	e.r. <i>R</i> : <i>S</i>
PhMe ₂ SiH 40b	Toluene	49:51
PhMe ₂ SiH 40b	1,2-DFB	33.5:66.5
<i>R</i> - 40e	Toluene	41:59
<i>S</i> - 40e	Toluene	58:42
<i>R</i> - 40e	1,2-DFB	39:61
<i>S</i> - 40e	1,2-DFB	51:49

Table 1.2 Enantioselective ketimine hydrosilylation reported by Oestreich.¹²⁹

Employing both the chiral Lewis acid **51** and chiral hydrosilanes *R/S*-**40e** clear match/mismatch effects on enantioselectivity were observed proving that both fragments are involved in the reduction step (Figure 1.3). Furthermore, a specific solvent effect was observed: use of a high polarity solvent resulted in improved enantioselectivity in reduction carried out using a non-chiral hydrosilane. This observation excludes the possibility of chiral counterion catalysis with the borohydride anion. From here onwards the term solvent effect is used to refer to a significant change in enantioselectivity observed on switching between polar and non-polar solvents: typically DCM/1,2-DFB to toluene.

The low enantioselectivity values in Table 1.2 are perhaps not surprising since chirality transfer is occurring through single point binding, in analogy to the reduction of acetophenone.¹²⁷ Such transition

states will be less organised, situations which can give rise to strong variations in enantioselectivity resulting from changes in reaction parameters. The solvent effect observed with chiral borane **51** and achiral hydrosilane **40b** is one example (Figure 1.3). When two chiral components are used, the interaction between them apparently becomes dominant and reduces the influence of external factors.

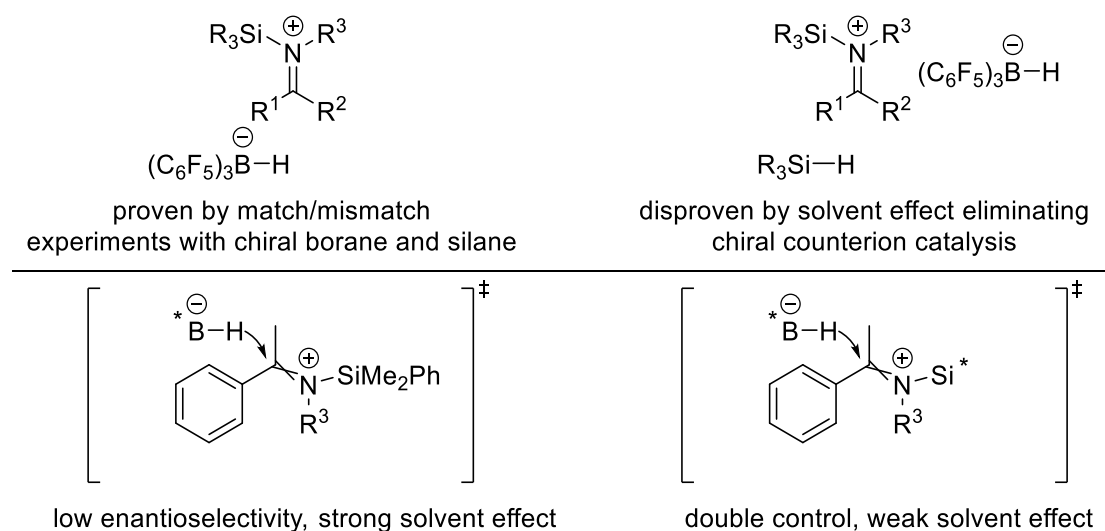
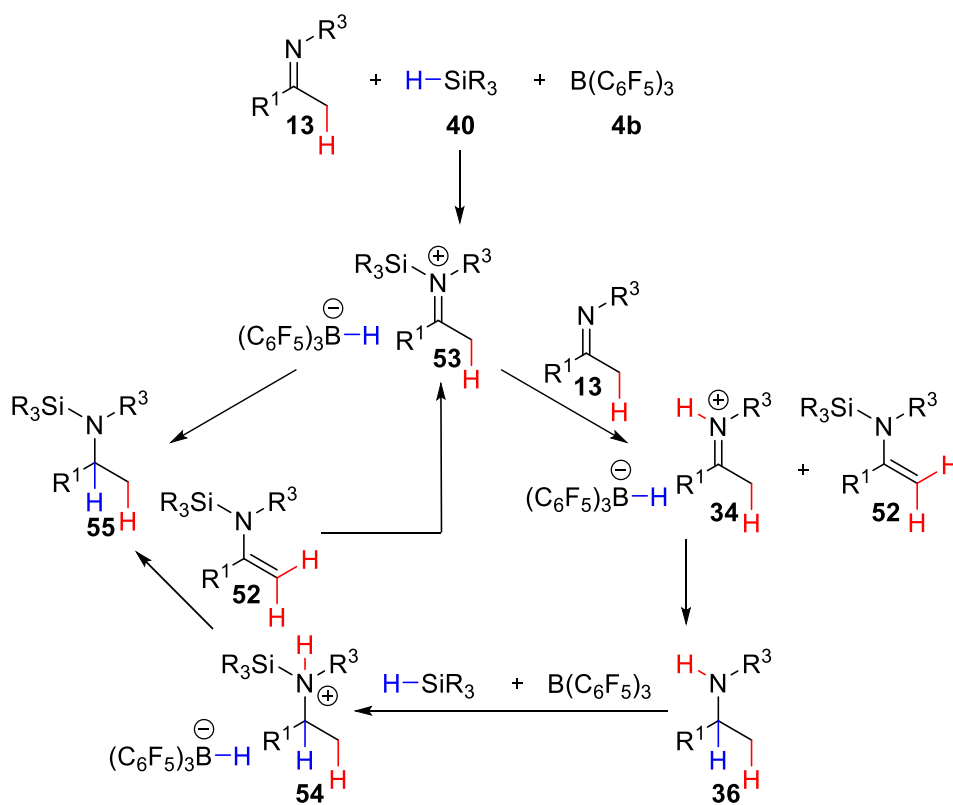


Figure 1.3 Reduction transition states for FLP ketimine hydrosilylation. * is used to describe chiral scaffolds.

The final piece of mechanistic evidence was again provided by the Oestreich group who discovered a new mode of reactivity in the Lewis acid catalysed hydrosilylation of ketimines.¹³⁰ This reactivity was a result of the presence of acidic protons in the α -position of activated ketimines. Careful NMR monitoring revealed the presence of intermediates **52** and **36** in the reaction mixture. Deprotonation of *N*-silyliminium ion **53** by unreacted substrate **13** results in the formation of protoiminium ion **34** and *N*-silylenamine **52**. Rapid reduction of **34** results in formation of free amine **36** as intermediate. Lewis acid catalysed silylation of **36** leads to formation of silylammonium salt **54**, which can act to reprotonate enamine **52** and release final product *N*-silylamine **55**. The authors predict the intermediates **52** and **36** to be present in equal amounts in the reaction mixture. Deuterium labelling experiments confirmed this mechanism: transfer of deuterium from the hydrosilane occurs to the

methine position in the product; formation of deuterated free amine is observed when ketimine labelled at the methyl position is used; deuterium label scrambling is observed in the methine position when mixtures of deuterated and non-deuterated substrates are used (Scheme 1.16).



Scheme 1.16 Complete mechanism for FLP hydrosilylation of ketimines; mechanism reported by Oestreich.¹³⁰

The authors note the great implication for enantioselective FLP methodology development: the selectivity observed depends on the presence of other basic species, reaction conversion, catalyst nature, and loading since reduction of the iminium ions **53** and **34** can proceed with different or opposite selectivity. Surprisingly, no attempts at further qualitative or quantitative correlation of enantioselectivity with reaction profile were made. This is perhaps understandable considering the significant complexity of the reaction mechanism just described.

Before proceeding it is worth discussing the relevance of the *E/Z* geometric isomerism in ketimine substrates. A notable example where the nature of this equilibrium was of direct relevance is the

enantioselective hydrogenation of ketimines or terminal enamines using catalyst **56** reported by Buchwald and co-workers.^{131,132} The active species is postulated to be a chiral titanium hydride which can reduce double bonds in a concerted fashion (Figure 1.4). The *E/Z* geometric isomers of ketimines react at different rates and give rise to opposite enantiomers. This behaviour is reflected in the enantioselectivity outcome being dependent on pressure and substrate *E/Z* ratio and interconversion rate. When terminal enamines or cyclic ketimines are reduced such a behaviour is not observed. Other examples are known.¹³³

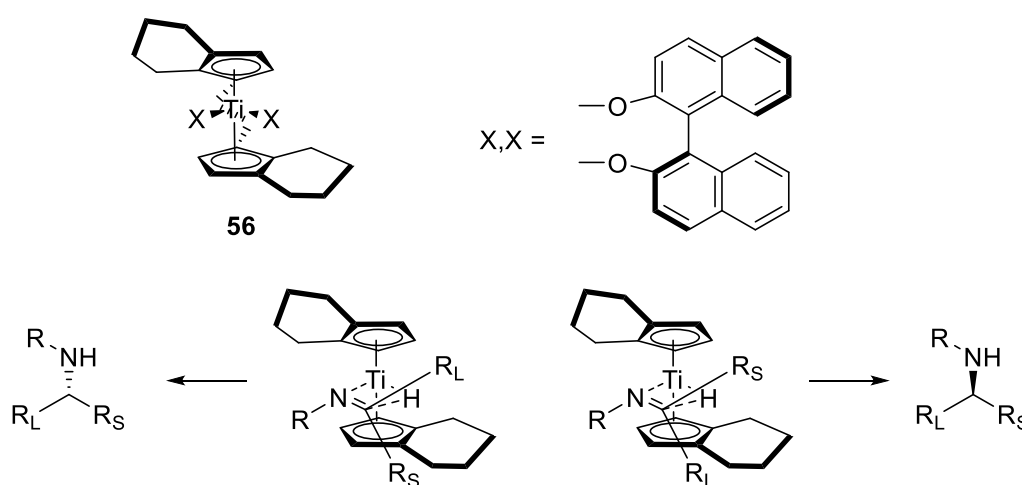


Figure 1.4 Titanium hydride reduction of ketimines reported by Buchwald.^{131,132}

The majority of catalytic systems used for the reduction of double bonds do not react *via* concerted pathways involving the substrate, but by pre-activating the substrate towards reduction (Figure 1.5).

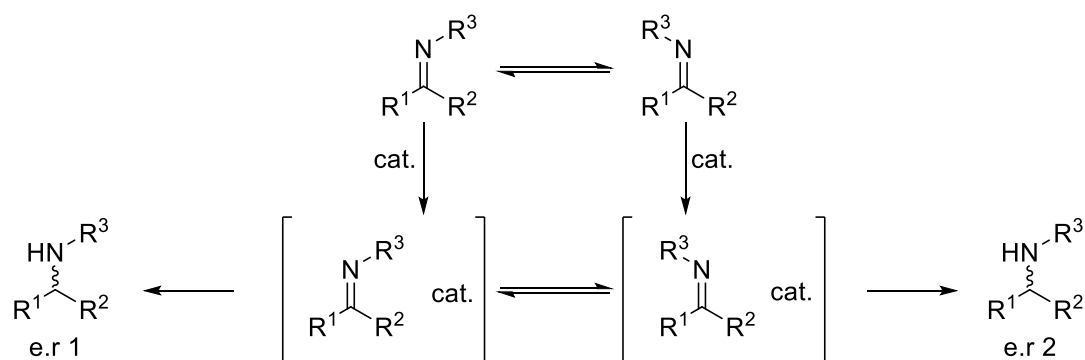


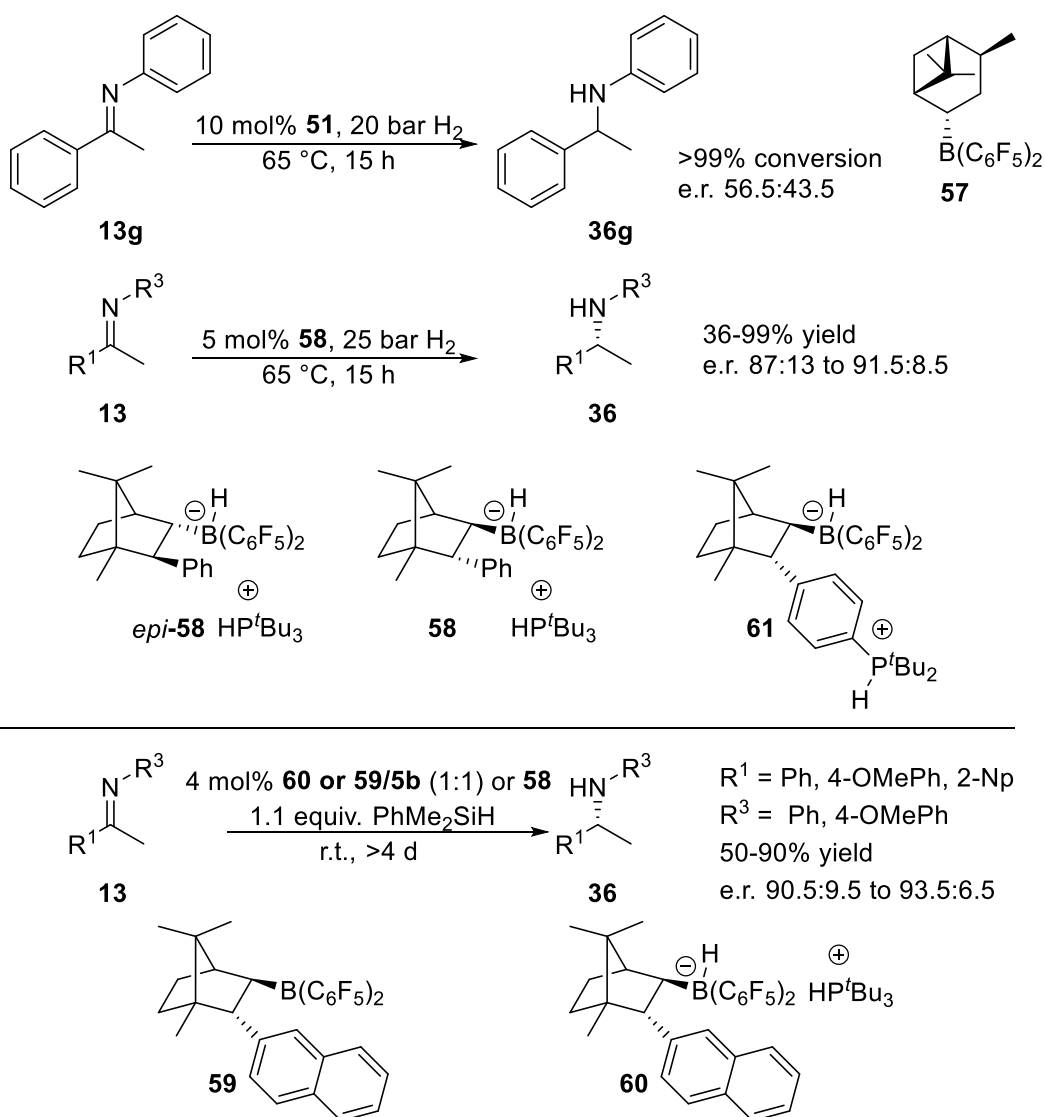
Figure 1.5 Generic description of reduction mechanisms involving pre-activation.

It results that enantioinduction can depend both on the rate of substrate activation and on the rate of activated complex reduction (and relevant isomerisation rates), resulting in no straightforward correlation between substrate *E/Z* ratio and process enantioselectivity being found.^{134–141} A noteworthy study concerning the nature of *E/Z* catalyst interactions and their role in controlling enantioselectivity was reported by Gschwind and co-workers and is briefly discussed in section 4.1.2.1.¹⁴²

1.5 Review of catalysts

Prior to the study from the group of Oestreich and co-workers on the mechanism of enantioselective FLP ketimine reduction (2013), only a few FLP catalytic systems had been reported by the groups of Klankermayer and Repo for the enantioselective hydrogenation or hydrosilylation (*vide infra*). We were surprised to note that in subsequent literature reports no detailed studies were conducted to rationalise the enantioselectivity trends observed with new catalysts used in hydrosilylation reactions. Such efforts may have accelerated development based on improved understanding.

The group of Klankermayer reported the first chiral boranes for FLP hydrogenation reactions (Scheme 1.17). The borane **57** (prepared from α -pinene) was prone to isomerisation by retro-hydroboration;⁷⁰ the isomeric borates **58** and *epi*-**58** (prepared from (+)-camphor) were shown to display different reactivity and selectivity.¹⁴³ The less hindered *epi*-**58** (borane fragment on the endo face) provides faster reduction of *N*-aryl ketimines with a low preference for the *S* enantiomer (74:26 e.r.), unlike **58** which is selective for the *R* enantiomer (89.5:10.5 e.r.). In a related study, Stephan and co-workers demonstrated the importance of the steric bulk of the borohydride reducing agent in the diastereoselective hydrogenation of ketimines using **4b**: common borohydride reducing agents (NaBH₃CN, NaHB(OAc)₃) give rise to significantly lower selectivity.⁷¹ Subsequently, the Klankermayer group used the borane **59** and borate **60** to catalyse the hydrosilylation of *N*-aryl ketimines.¹⁴⁴ The use of borane **59** solely resulted in racemic amine product being formed. The borate **60** or a combination of **59** with phosphine **5b** gave amine product with high enantioselectivity (91.5:8.5 *R:S*).



Scheme 1.17 Use of chiral boranes in hydrogenation and hydrosilylation, reported by Klankermayer.

143

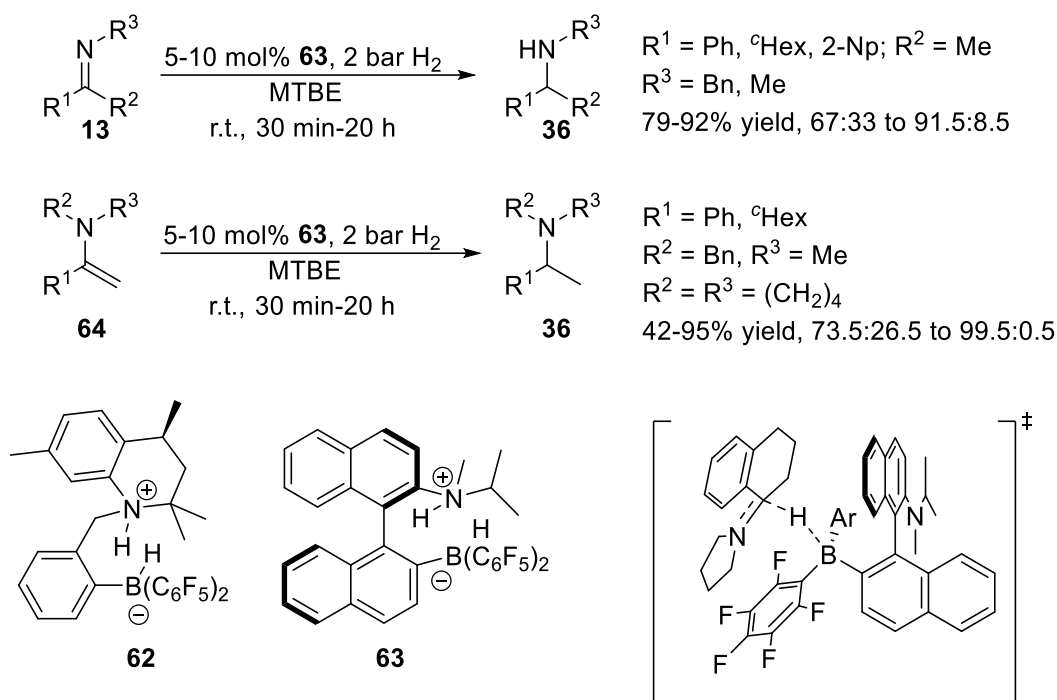
The group recognised this to be a sign of a change in mechanism but interpreted this as resulting from concerted imine reduction by the activated hydrosilane in the absence of phosphine base: hydrogenation carried out by borate **58** was highly selective, conditions under which a similar concerted reaction would have taken place presumably. Addition of phosphine base resulted in formation of a silylphosphonium salt (verified by NMR) and a switch to a stepwise slower and unselective reduction. In a final modification the catalyst **61** was shown to provide similarly high levels of enantioselectivity (86:14 *R:S*) in the hydrogenation reaction, and was air stable and could be

recycled.¹⁴⁵ From here onwards the term phosphine effect is used to refer to large changes in enantioselectivity of a process being observed when run with or without a phosphine additive. The importance of the effect was mentioned by Oestreich and co-workers: '*..the exact role of the phosphane remains to be clarified.*'¹³⁰

Considering the subsequent reports by Oestreich we believe that such a switch in mechanism results from a reduction pathway change from *N*-silyliminium reduction to iminium reduction, a process which converts two molecules of substrate to only one product molecule. The group of Klankermayer reported conversions of ~50% after 4 days in the reduction of ketimine **13g** (defined in Scheme 1.17) in the presence of **5b**. If a switch in mechanism was operating, the increased enantioselectivity suggests that reduction of the protoiminium ion was more selective in this case.

Notable developments in the field were reported by the group of Repo (Scheme 1.18). Rational modification of the intramolecular FLP **21** involving a reduction in basicity of the amine component and a general increase in steric hindrance resulted in the production of *ansa* ammonium borate **62**, which displayed improved activity for an FLP catalyst.¹⁴⁶ The close proximity in space of the base and acid components allowed for hydrogen activation ability to be maintained. The large steric hindrance eliminated issues arising from product inhibition allowing for hydrogenation of unhindered *N*-alkyl ketimines to proceed. Enantioselectivity levels were low, presumably due to the chiral element being installed remotely from the borohydride fragment resulting in little discrimination being effected between diastereomeric hydride transfer transition states. To improve on the situation the axially chiral catalyst **63** was developed.¹⁴⁷ This intramolecular FLP places acid and base components close to the axis of chirality resulting in the creation of a very hindered and well-defined chiral environment. The hydrogenation of non-hindered *N*-methyl ketimines and of *N,N*-substituted enamines **64** (which are *C*-protonated in the α position to generate tetrasubstituted iminium ions, c.f imines are *N*-protonated to give trisubstituted iminium ions) was achieved with high enantioselectivity (up to 99:1 e.r.). Computational studies revealed that selectivity in the rate-determining reduction step is a result

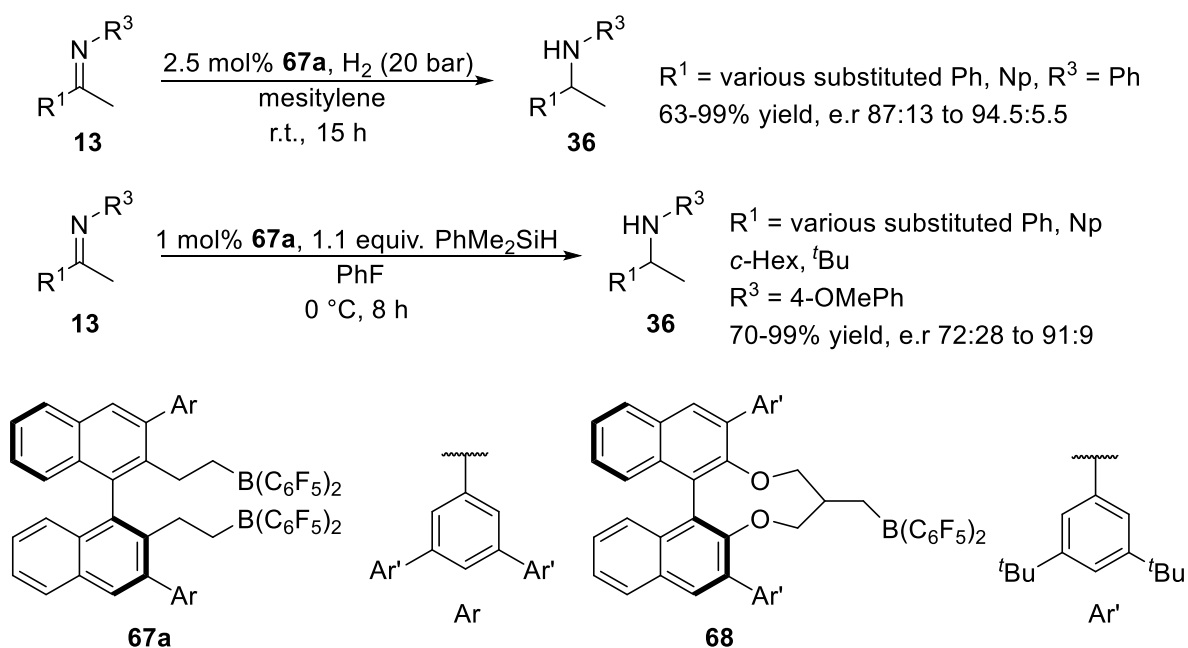
of steric repulsion effects and non-covalent interactions: close contacts were found between the protons in the iminium α position and the amine-substituted naphthyl ring; stacking between one perfluorophenyl ring and the *N*-containing iminium ring (see diagram in Scheme 1.18) was found. It is worth noting the change in enantioinduction: enamines and *N*-methyl substituted **13h** gave the *R*-enantiomers; other substrates (*N*-benzyl ketimines) gave the *S* enantiomer.



Scheme 1.18 Enantioselective hydrogenation reported by Repo.¹⁴⁷

The binaphthyl chiral scaffold has been extensively utilised for catalyst construction and is a ‘privileged’ scaffold in asymmetric catalysis. When the separation between the chiral axis and borane fragment was increased the chiral environment was controlled by substitution in the 3,3’ positions. For example, the unsubstituted borepine **51** catalyses the hydrosilylation of ketimine **13i** ($\text{R}^1 = \text{Ph}$, $\text{R}^2 = \text{Me}$, $\text{R}^3 = \text{Bn}$) with 81:19 e.r, c.f substituted **65**: 91.5:8.5 (**65** defined in Scheme 1.19, reaction not shown).¹²⁹ The borepine scaffold was developed by Oestreich for use in the enantioselective Piers hydrosilylation with catalyst **65**.¹²⁵ The reaction affords alcohols (following desilylation) with high enantiopurity levels (up to 99.5:0.5 e.r.), without the need for an added phosphine base (other basic additives have no effect). Furthermore, it is pointed out that variation in enantioselectivity levels with

upon substituting mesitylene for DCM. The variation in enantioselectivity for various substrates is small, apparently resulting from the structural features of the catalyst exercising tight control in the reduction transition state. It is possible that Lewis acid activation of the substrate is operating with one borane acting as the acid and the other as the hydride donor.

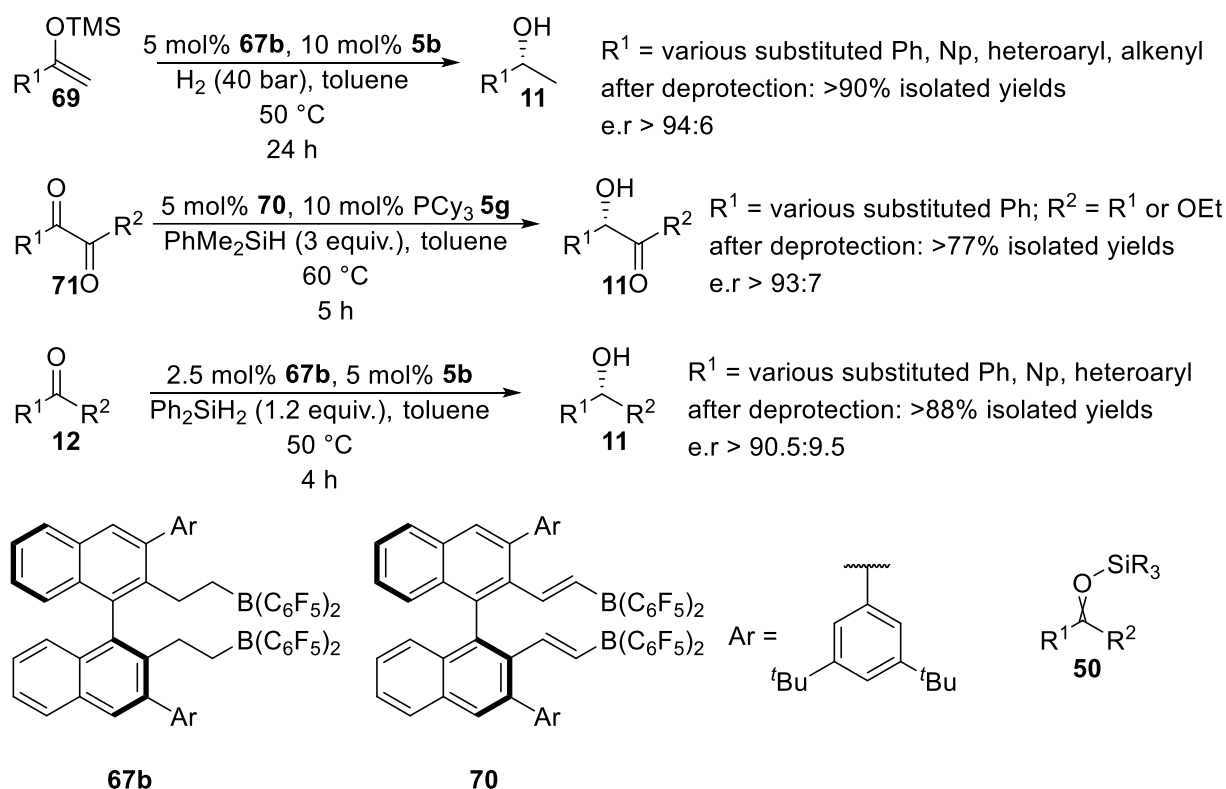


Scheme 1.20 FLP catalysed ketimine reduction reported by Du.¹⁴⁸

In the related hydrosilylation of ketimines,¹⁴⁹ catalyst **67a** afforded appreciable (but slightly lower and more variable) enantioselectivity (72:28 to 91:9) in the absence of phosphine base, and no appreciable solvent effect (DCM/toluene). Replacing the PMP group on the nitrogen atom with a cyclohexyl substituent resulted in lower enantioselectivity levels being observed. In a recent attempt to improve synthetic accessibility, the Du group reported on the catalyst **68** which can be easily prepared from substituted BINOLs.¹⁵⁰

Catalyst **67b** (featuring reduced steric bulk in the 3,3' positions; Scheme 1.21) in combination with 2 equivalents of phosphine **5b** (with respect to catalyst) catalysed the hydrogenation of silyl enol ethers **69** with uniformly excellent enantioselectivity (>94:6 e.r., Scheme 1.21).¹⁵¹ No reaction occurred in the absence of phosphine base and no solvent effect was observed. The related catalyst **70** featuring an

alkenyl linker provided very similar enantioinduction (for the *R* enantiomer) and provided inferior results only with the use of hexane solvent.¹⁵² Interestingly, both catalysts perform best at high concentrations (2 M).

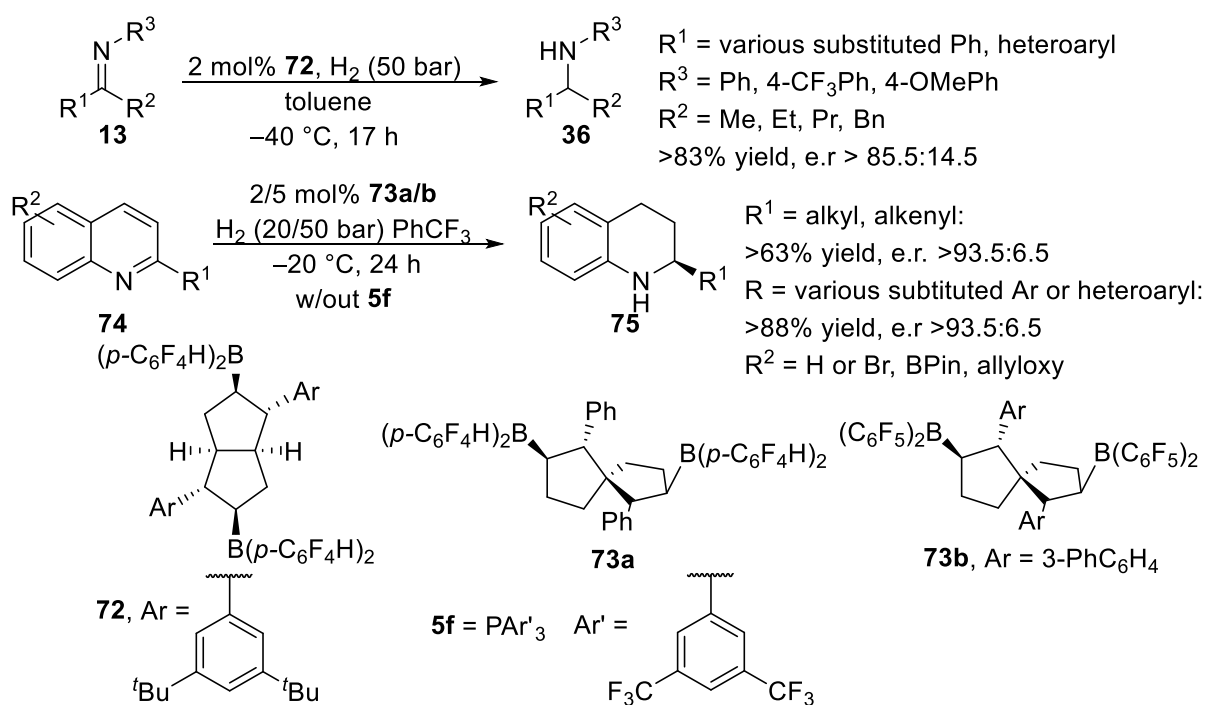


Scheme 1.21 Enantioselective reduction of carbonyl and silyl enol ethers reported by Du.¹⁵²

Having acknowledged the mechanistic connection between hydrogenation of silyl enol ethers **69** and the hydrosilylation of carbonyl compounds (namely reduction of a silyl oxonium cation **50**, defined in Scheme 1.21), Du and co-workers used catalyst **70** in the hydrosilylation of 1,2-dicarbonyls **71** with high selectivity levels (>93:7 e.r.).¹⁵³ A dramatic phosphine effect was observed with PCy₃ **5e** similar to that reported by Klankermayer for catalyst **59**, and interestingly DCM afforded inferior results. Reduction of simple ketones with high enantioselectivity (>90.5:9.5 e.r.) was achieved using catalyst **67b**,¹⁵⁴ this reaction displaying similar behaviour to that observed for 1,2-dicarbonyls: an inversion in enantioinduction was observed on adding phosphine base **5b** and DCM provided inferior results to toluene. Interestingly, the nature of the hydrosilane used also had an effect. Less hindered Ph₂SiH₂

40g gave improved results, but the loading did not have an impact. This stands in contrast with the hydrosilylation protocol reported by Oestreich in which increasing the amount of silane affords better selectivity.¹²⁵ Such effects can arise when a product chiral alkoxy-hydrosilane can compete with the reagent. The Du group have also reported applications of these catalysts for enantioselective reduction of various heterocycle scaffolds.^{155–159}

Following from the work of Du, Wang and co-workers reported bisboranes **72** derived from bicyclic dienes and **73** derived from spirocyclic dienes for use in the hydrogenation of ketimines **13** and quinolines **74** to give tetrahydroquinolines **75** (Scheme 1.22).^{160,161}



Scheme 1.22 Enantioselective FLP reduction reported by Wang.^{160,161}

These catalysts are notable for displaying broad substrate scope and high enantioselectivity (>85.5:14.5 e.r.), but especially for their remarkable activity: catalyst loadings below 2 mol% allow reaction to occur at cryogenic temperatures (<-20 °C).

Other scaffolds have been briefly investigated for the construction of chiral FLP catalysts. Erker and co-workers reported attempts to develop system **76a** for enantioselective hydrogenation of *N*-aryl

ketimines,¹⁶² but the enantioselectivity levels observed were low (up to 84.5:15.5 in the hydrogenation of *N*-aryl substituted ketimines) (Figure 1.6). Control in the reduction step appeared to be effected by the asymmetric carbon centre on which the borane fragment is installed and not the planar chiral ferrocene ring: the related **76b** afforded 63.5:36.5 e.r in the reduction of substrate **13k** ($R^1 = \text{Ph}$, $R^2 = \text{Me}$, $R^3 = \text{'Bu}$).³⁷

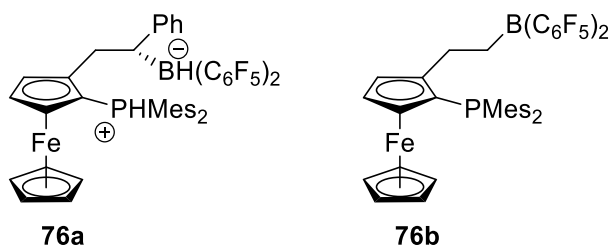
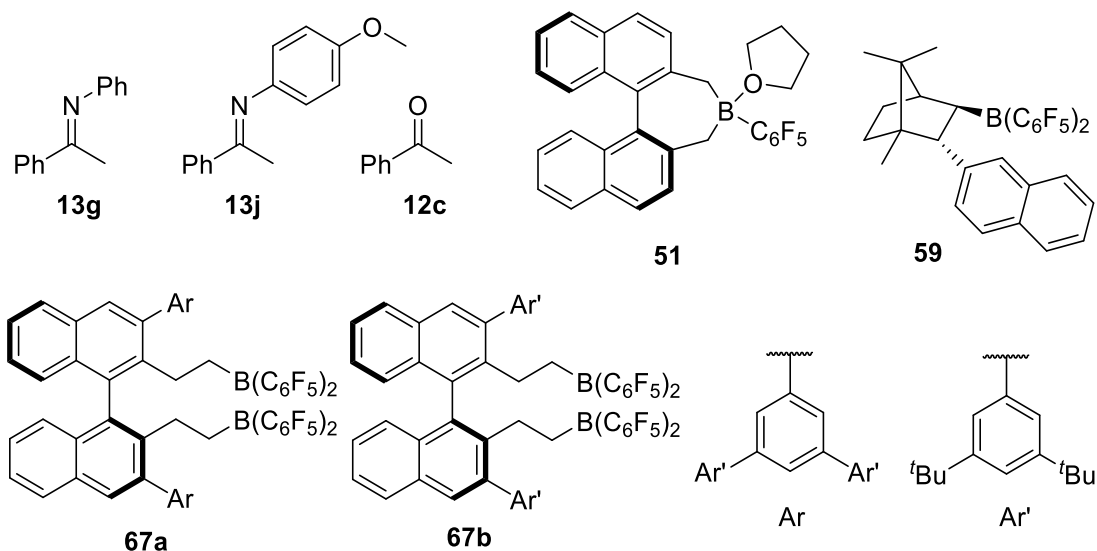


Figure 1.6 Chiral borane reported by Erker.¹⁶²

The Du group have reported enantioselective FLP reduction methodologies relying on the use of chiral Lewis bases. These will be discussed in Chapter 4.

A summary of reported phosphine or solvent effects is presented in Table 1.3.



Catalyst	Phosphine effect	Solvent effect	Reaction
51 ¹²⁹	Mes ₃ P, no effect	Toluene, 41:59 e.r. 1,2-DFB, 33.5:66.5 e.r.	Hydrosilylation, 13g
59 ¹⁴⁴	–, 51:49 e.r. 5b , 89.5:10.5 e.r.	Not investigated	Hydrosilylation, 13g
67a ¹⁴⁹	Not investigated	Toluene, 78:22 C ₆ F ₅ H, 83.5:16.5	Hydrosilylation, 13j
67b ¹⁵⁴	–, 48:52 5b , 94.5:5.5	Toluene, 94.5:5.5 DCM, 65:35	Hydrosilylation, 12c

Table 1.3 Summary of reported selectivity effects; all e.r values reported as *R*:*S*

1.6 Outlook and project goals

One of the main challenges regarding the development of highly Lewis acidic chiral boranes for use in FLP methodology is their challenging synthesis. The most widely employed technique to date is hydroboration of a chiral alkene (diene) precursor with Piers borane (HB(C₆F₅)₂ **23b**),^{163,164} which has been used by Du, Wang, Erker, and Klankermayer. The reaction proceeds cleanly allowing for crude product boranes to be used without isolation or purification. Although this increases catalyst screening speed, considerable effort is required for generating libraries of alkene (diene) precursors (Du, Wang). Alternatively, exchange reactions between chiral organometallics and C₆F₅-substituted haloboranes (Repo, Oestreich) provide access to desired catalysts. This latter approach can be difficult to execute and can pose issues due to by-product contamination. It is perhaps these synthetic challenges, combined with the poor activity of FLP catalysts that have prevented development and adoption of enantioselective FLP methodologies, more than issues regarding moisture- or oxygen-sensitivity. Although the knowledge required to uncover the origins of enantioselectivity exists (cf. the work of Oestreich), no studies aimed at guiding catalyst choice for a target substrate class have been reported, resulting in intensive optimisation efforts being required to achieve high enantioselectivity. Following

from the review of current literature, the question is raised as to what is controlling enantioselectivity: a fine-tuned catalyst structure, the reaction conditions, or a combination thereof? Answering this question could offer opportunities for facile repurposing of known catalysts rather than investing resources for the development of completely new scaffolds. Use of one catalyst for hydrogenation and hydrosilylation, as demonstrated by Du, is of interest due to the complementary benefits of these reactions. This double application of a catalyst also suggests a strategy for investigation. Can the information extracted from comparative studies be used to obtain qualitative information about the fate of reactive prochiral intermediates?

One limitation resulting from construction of Lewis acidic boranes using $B(C_6F_5)_3$ derivatives is the limited opportunity for Lewis acidity tuning: the boranes prepared by Oestreich (one C_6F_5 substituent) are probably not competent hydrogenation catalysts due to insufficient Lewis acidity. Conversely the boranes reported by Du containing two C_6F_5 units can access both reactivity modes.

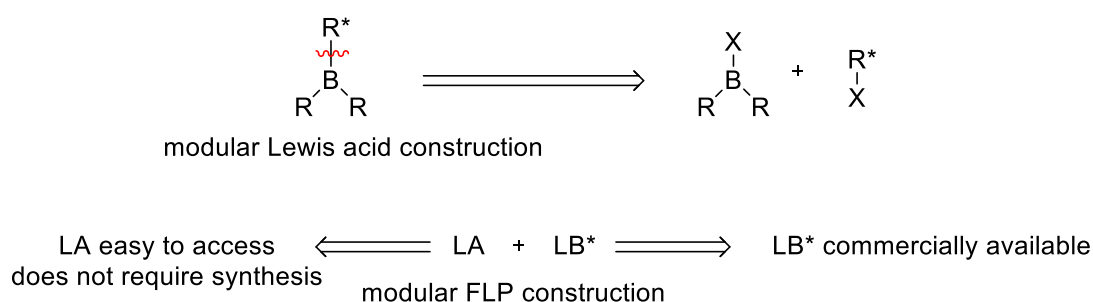


Figure 1.7 Modular construction of Lewis acids and FLPs

We wanted to explore new scaffolds for accessing chiral FLP systems to catalyse hydrogenation and hydrosilylation. To improve practicality we wanted to target systems which are modular in construction and can be accessed using simple transformations starting from commercially available materials. The option to test various borane scaffolds in addition to chiral components would be of use for Lewis acid construction. Screening of combinations of achiral Lewis acids and chiral Lewis bases would offer additional opportunities for expanding the scope of FLP chemistry. Although a detailed

mechanistic investigation was not a priority in the project, we considered the opportunity to make use of the available literature knowledge to support catalyst development.

Three specific aims were set for this project. The following three chapters addresses them as follows:

Chapter 2: Construct a new type of chiral modular Lewis acid and explore its behaviour in hydrogenation and hydrosilylation for various substrates. Use combined reactivity and enantioselectivity data to explore mode of action and improve accessibility and substrate scope of enantioselective FLP protocols.

Chapter 3: Construct a new type of chiral Lewis acid with improved tolerance towards hydroxylic functionality (alcohols and water) to improve the practicality of enantioselective FLP protocols and expand substrate scope to include ketones.

Chapter 4: Develop the use of chiral Lewis bases to provide access to FLP catalysts which can be prepared using commercially available components.

2 Chapter 2–NHC-stabilised borenium ions

The findings from this Chapter have been published as a journal communication.¹⁶⁵ All contributions from other authors are clearly acknowledged in the text.

2.1 Introduction

2.1.1 Borenium ions

Borenium ions are three-coordinate borocation species. These exotic compounds have attracted much attention in both the inorganic and organic chemistry fields.^{166–168} Formation of three covalent σ -bonds can be achieved by the B^+ fragment (2 valence electrons) only if one of the bonding partners can provide a lone pair of electrons (Figure 2.1).

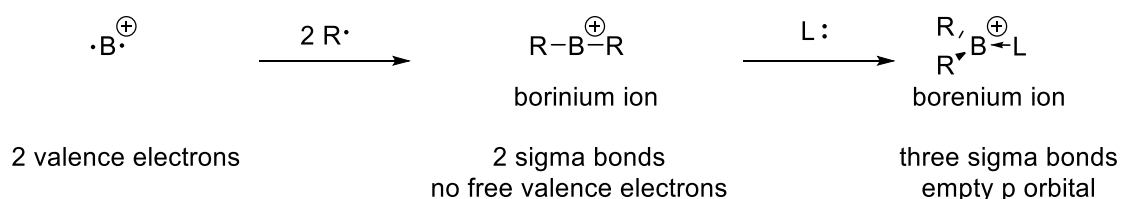


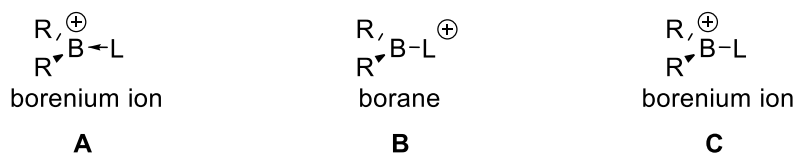
Figure 2.1 Borenium ions

In a borenium species the Lewis acidity exhibited by three-coordinate boranes is enhanced by the presence of the positive charge. The strong tendency for coordination of a second donor makes borenium ions highly reactive. Isolable borenium cations can be generated by including additional stabilising features (steric hindrance, π -bonding) and using weakly coordinating anions.

Different notations have been used to depict borenium ions. The representation **A** (Figure 2.2) placing the positive charge on the boron atom is adopted by Piers, who argues this to be most appropriate considering the lower electronegativity of boron compared to donor atoms (C, N, O) found in the commonly employed ligands (L amines, NHCs), and to be reflective of the chemical behaviour of borenium species.¹⁶⁷ The donors L are generally chosen for their ability to provide extra stabilisation (π -stabilisation through lone pair donation or delocalisation into conjugated systems), this fact

resulting in the positive charge being commonly depicted on the donor atom of the L ligand (representation **B**). For describing species under discussion in this work (donor ligand L used is an NHC) the depiction **C** is used. This is consistent with the argument of Piers but does not emphasise the dative nature of the bond between the B atom and the C atom of the NHC fragment. This notation was adopted in the literature for similar species and is supported by the metric parameters of the B-C bond.¹⁶⁹ Delocalisation of the positive charge is partial due to the system deviating from planarity (Figure 2.2 part B). For review purposes the representation C is used throughout this chapter, unless the original account argues for a different representation.

A. Different depictions of borenium ions



B. Example of a borenium ion and schematic bonding in an NHC-stabilised borenium ion

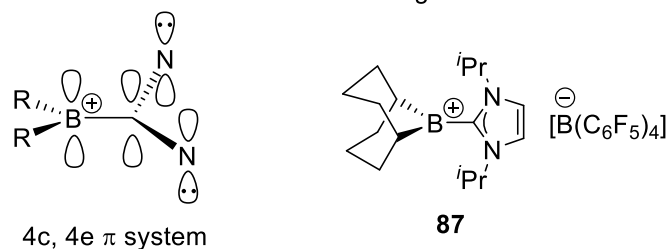
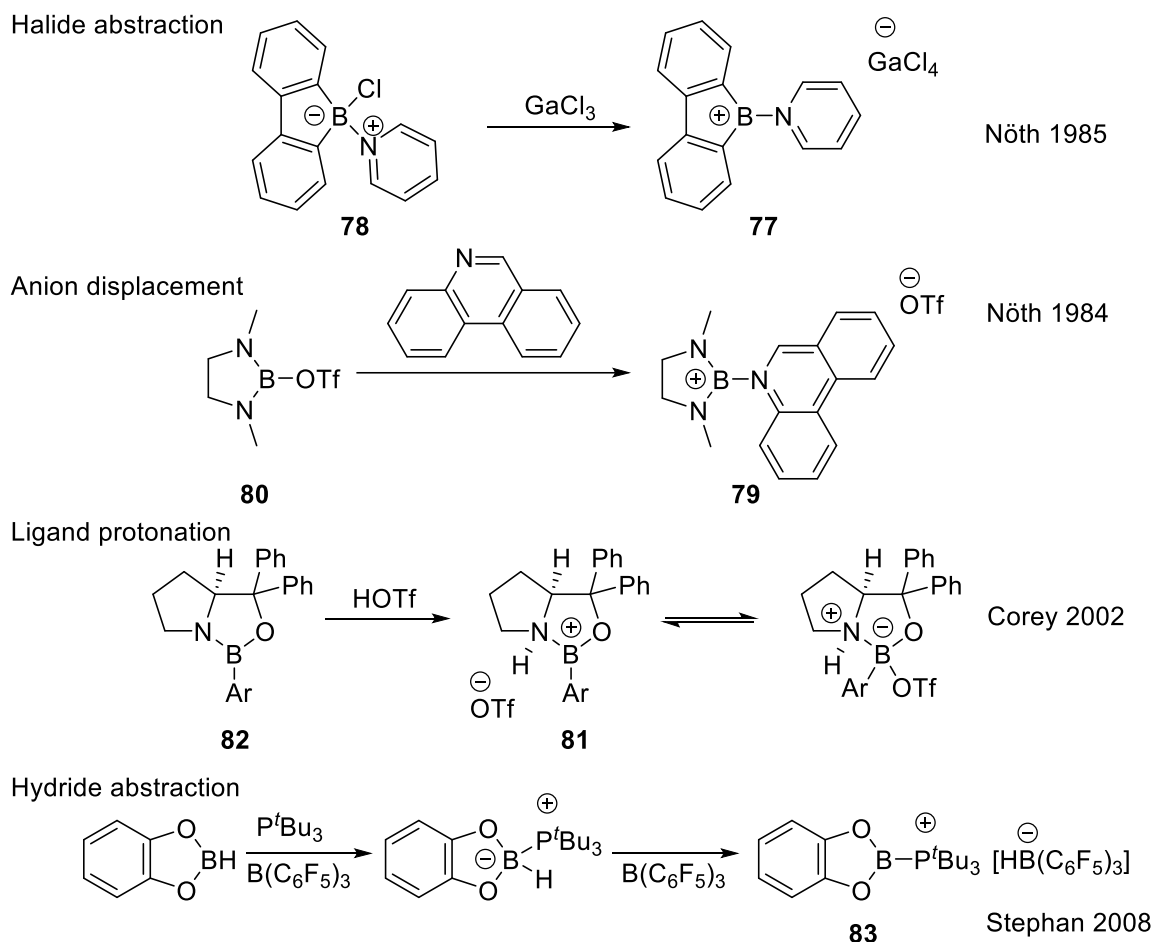


Figure 2.2 Alternative depictions for borenium ions. Example of an NHC-stabilised borenium ion.¹⁶⁹

The borenium cation **77** was prepared and isolated by Nöth using GaCl₃ to abstract chloride from the precursor **78** (Scheme 2.1). Compound **79** could be prepared by counterion displacement (*via* addition followed by elimination) by a nucleophilic amine base on the diazaborolidine **80**.^{170,171} The salt **79** was characterised by crystallography, which confirmed that no triflate anion coordination was occurring. The cationic oxazaborolidine **81** can be prepared by protonating the lone pair of the N atom in the precursor **82**. Such species have found use as Lewis acids in enantioselective catalysis.^{172,173} Hydride abstraction was used to generate borenium salt **83** from neutral starting materials.¹⁷⁴ Computational studies indicated that **83** is best formulated as a borylphosphonium (positive charge mostly resides on the P atom).



Scheme 2.1 Preparation strategies for borenium cations.

These four preparation methods have been used extensively and represent the basis for the synthesis of numerous borenium type systems. The development was in part supported by the availability of weakly coordinating anions (WCAs).¹⁷⁵ This resulted in the preparation of more reactive systems, where stabilising features have been removed from the backbone of the molecule and reside entirely on the ligand L.

2.1.1.1 NHC-stabilised borenium ions

The earliest example of a NHC-stabilised borenium ion **84** was reported by Weber,¹⁷⁶ subsequently, Gabbaï and Lindsay demonstrated that an NHC ligand provides sufficient stabilisation for diaryl¹⁷⁷ **85** and dialkyl borenium cations **86**,¹⁷⁸ respectively, to be prepared (Figure 2.3). The borenium cation **85**

was characterised by crystallography; the ionic nature of **86** was proven by using DOSY NMR to measure cation and anion diffusion coefficients.¹⁷⁹

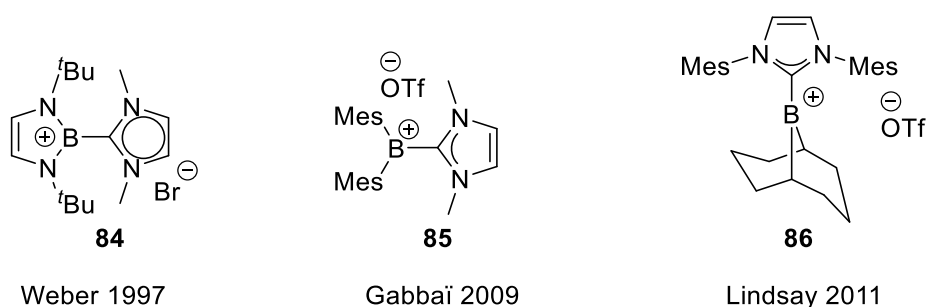
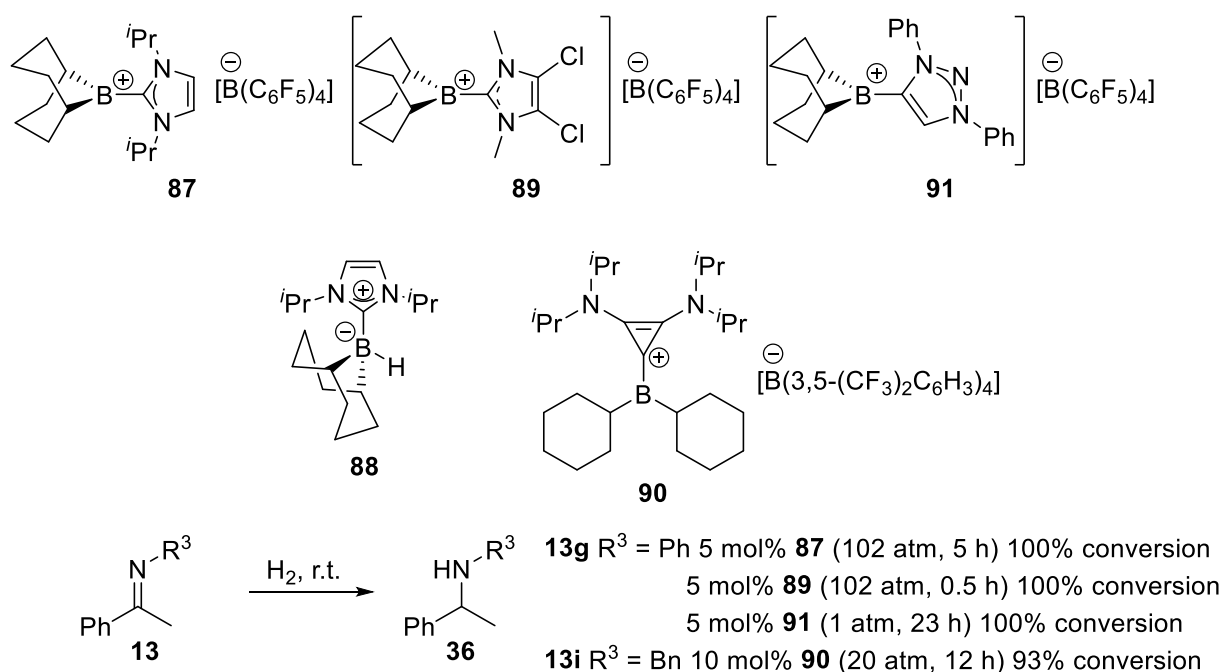


Figure 2.3 Examples of NHC-stabilised borenium ions.

2.1.2 Borenium ions as alternative Lewis acids in FLP chemistry

The reactivity of borenium cations had been explored in both catalytic and stoichiometric manifolds in applications such as C-H bond activation,¹⁸⁰ arene borylation^{181,182} and alkene¹⁸³ and imine¹⁸⁴ hydroboration before the seminal work of Stephan reporting the use of borenium cation **87** to activate hydrogen and catalyse hydrogenation of nitrogen-containing substrates (Scheme 2.2).¹⁶⁹ The success of this catalyst was attributed to the Lewis acidity of borenium cations in combination with the hydricity of NHC-borane **88**.^{185,186} Although **87** was shown to be less hydridophilic than $B(C_6F_5)_3$ **4b** (**88** will transfer hydride to $B(C_6F_5)_3$), it was capable of slowly (48 h) activating hydrogen at room temperature in combination with a phosphine base (P^tBu_3 **5b**) at low pressure (4 bar). The combination of NHC-borane **88** and $[HP^tBu_3][B(C_6F_5)_4]$ was capable of stoichiometrically reducing the hindered imine **13c** ($R^1 = Ph$, $R^2 = H$, $R^3 = ^tBu$). Under catalytic conditions *N*-alkyl **13i** and *N*-aryl imines **13g** and enamines **64** could be readily hydrogenated (<4 h). The high pressure used (102 atm) resulted in rapid reduction, however information regarding catalytic ability at lower pressure was not reported. Presumably, the lower Lewis acidity of borenium **87** compared to $B(C_6F_5)_3$ would have resulted in sluggish reactivity. The steric shielding in **87** appeared sufficient to prevent significant catalyst inhibition by amine products. This was indicated by the fact that heating was not required and bulky additives (e.g. 2-phenylpyridine, 4,4'-dimethyl benzophenone) did not cause inhibition. Therefore, the

major advantage of NHC-stabilised borenium ions over traditional boranes employed in FLP catalysis is the improved functional group tolerance and ability to carry out reactions at room temperature in the absence of significant inhibition effects.



Scheme 2.2 Borenium-catalysed hydrogenation reported in the literature.^{169,187–189}

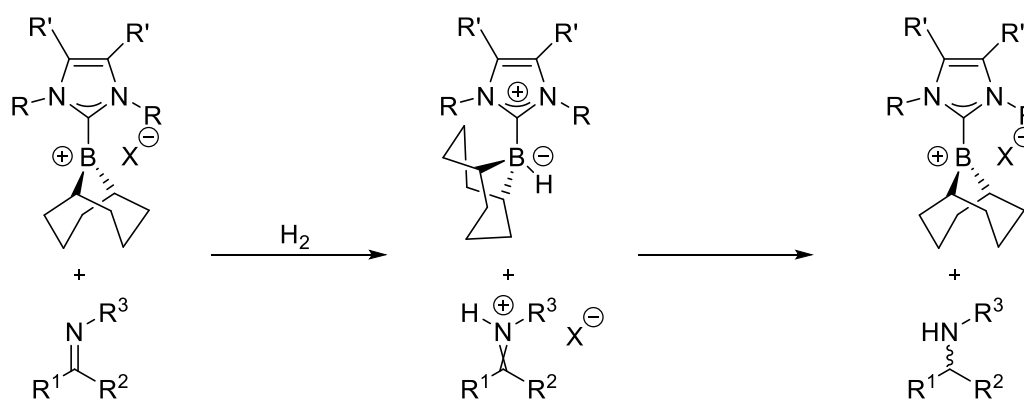
In a follow-up study, optimisation of the catalyst structure resulted in the preparation of, at the time, the most active metal free catalyst for hydrogenation of imines: **89** displayed a TOF number of 940 h⁻¹.¹⁸⁸ The improved catalytic ability resulted from lowering the steric hindrance surrounding the B atom and increasing electrophilicity with the inclusion of electron-withdrawing chlorine substituents in the NHC scaffold, features which resulted in increased rate of hydrogen activation. The lower steric demands made the catalyst prone to inhibition, however: the unhindered, basic imine **13i** could not be hydrogenated. The borenium **90** reported by Speed is the only system to date that can catalyse hydrogenation of unhindered *N*-benzyl ketimines.¹⁸⁹ A subsequent report by the Speed group showed that the success of this system results from the combination of very bulky boron substituents (cyclohexyl rings) with a nonhindered bis-aminocyclopropenylidene (BAC) ligand.¹⁹⁰ This example illustrates that reactivity of borenium cations is not simply a result of overall steric bulk: replacing the

cyclohexyl rings (BCy₂ fragment) with a 9-BBN fragment results in an inactive catalyst for hydrogenation of PMB ketimine **13k**.

Crudden and co-workers reported on the use of mesoionic carbene (MIC) ligands to generate highly active borenium catalyst **91**, which catalysed the room temperature and low pressure (1 atm) hydrogenation of *N*-aryl imines, pyridines and quinolines.¹⁸⁷ Catalyst **91** showed comparable Lewis acidity to B(C₆F₅)₃ (Gutmann Beckett Acceptor Number, see section 2.2.2.3), but was prone to inhibition due to the low steric profile. The improved activity of these catalysts at low pressure is a result of the higher Lewis acidity compared to that of NHC-substituted boranes.

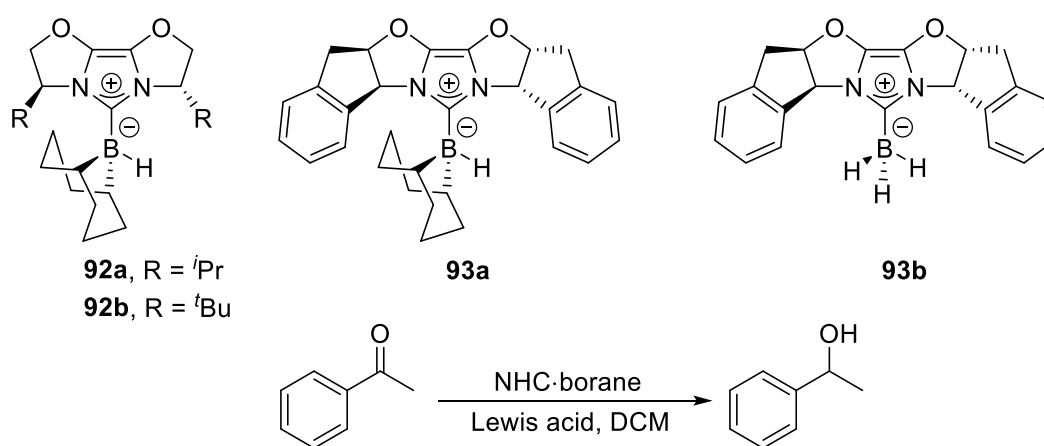
2.1.3 Project goals

Following from the reports of Stephan and Crudden on the use of achiral borenium ions as hydrogenation catalysts, the initial goal of this project was to develop a chiral NHC-stabilised borenium ion and to use it in the enantioselective hydrogenation of nitrogen-containing substrates: imines and *N*-heterocycles. The postulated mechanism of imine hydrogenation using borenium cations involved hydride transfer from an NHC-borane to a protonated iminium substrate. Using a chiral NHC-stabilised borenium would result in the formation of a chiral NHC-borane which could enantioselectively reduce the activated substrate. It appeared that the success of such a procedure would result from good matching of the substrate with NHC-borane.



Scheme 2.3 Chirality transfer using chiral borenium ions.

Only a few examples of diastereoselective transformations using NHC-boranes have been reported,^{191,192} and only one example of an enantioselective transformation using a chiral NHC-borane.¹⁹³ The systems **92** and **93** reported by Lindsay and McArthur were used in the stoichiometric reduction of a number of ketone substrates with high enantioselectivity levels at low temperature (−90 °C) with the aid of a Lewis acid (BF₃). The asymmetric induction was difficult to rationalise and depended on NHC component (THIBO or HIBDIO^{194–196}), boron auxiliary ligands, and Lewis acid (Table 2.1).



NHC-borane	Lewis acid	Temperature	<i>R</i> : <i>S</i>
92a	BF ₃ ·OEt ₂	−90 °C	80:20
92b	BF ₃ ·OEt ₂	−90 °C	8:92
93a	BF ₃ ·OEt ₂	−90 °C	45:55
92a	Sc(OTf) ₃	−78 °C	67:33
93b	Sc(OTf) ₃	−78 °C	12.5:87.5

Table 2.1 Enantioselective reduction of acetophenone reported by Lindsay and McArthur.¹⁹³

The bisoxazolone-derived IBiox NHCs THIBO and HIBDIO were employed by Glorius to prepare catalysts for the Suzuki-Miyaura cross-coupling of *ortho*-disubstituted aryl boronic acids with *ortho*-disubstituted aryl chlorides.^{194–196} The NHCs were shown to be slightly less electron-donating than

standard NHCs such as IMes due to the electron-withdrawing oxygen atoms. The THIBO NHC **94** was shown to have a flexible steric bulk resulting from ring flipping of the cyclohexyl substituents.

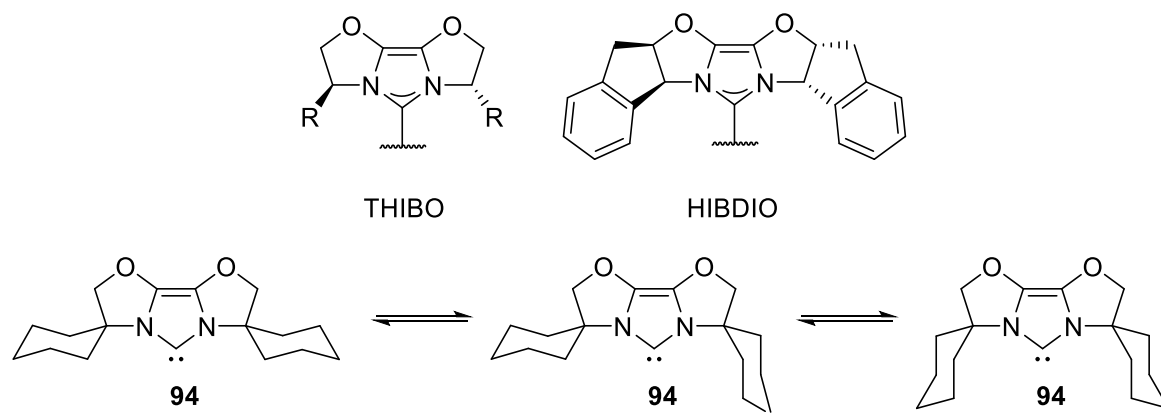
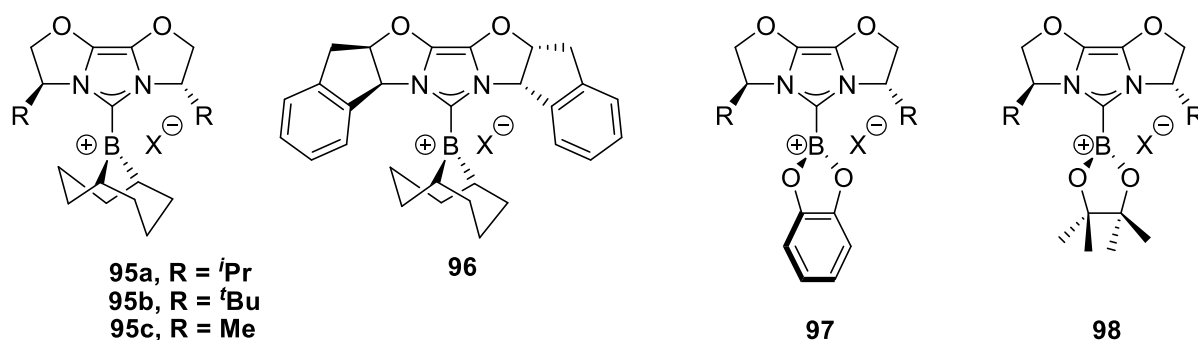


Figure 2.4 THIBO and HIBDIO NHCs and their use as ligands with variable steric bulk.

We planned to use the hydrides **92a,b** and **93a** to generate the corresponding chiral borenium ions **95a,b** and **96**. Additionally, we considered borenium ion **95c** to further explore the role of the R substituents in defining the chiral environment. We reasoned that a similar variable steric profile in the mono-substituted THIBO NHCs to that reported for **94** could be of use in modulating the reactivity of borenium ions.



X = OTf, NTf₂, [B(C₆F₅)₄], {Al[OC(CF₃)₃]₄}, etc.

Figure 2.5 Target borenium ions.

2.1.3.1 Alternative designs under consideration

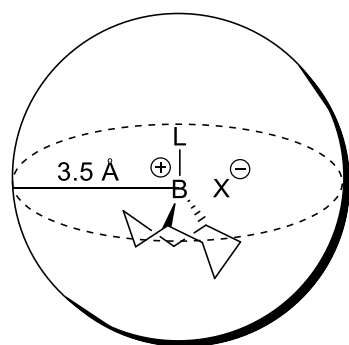
Since the mechanism of chirality transfer from hydrides **92** and **93** appeared to involve interplay between numerous factors, we considered this an opportunity to identify suitable substrates and conditions under which catalysis using borenium ions **95** and **96** would yield high enantioselectivity. Based on the studies of Stephan and Crudden we decided to target imines as initial substrates. We hypothesised that once the required substrate/catalyst complementarity was mapped out, extension to other substrate classes (enamines, heterocycles, etc.) would be possible considering the numerous chiral NHC scaffolds reported.^{197,198}

The 9-BBN core appears to represent a privileged scaffold for the construction of borenium cations intended for hydrogenation catalysis. The rigidity of the borane scaffold is possibly a useful feature to include in alternative designs; other commercially available boranes which fulfil this criterion are catecholborane^{181,199} and pinacolborane (**97** and **98**). We considered the modular structure of NHC-stabilised borenium cations an attractive feature which could allow a library of catalysts to be assembled from the corresponding boranes and selected NHCs.

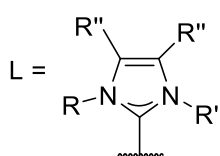
A further point for introducing diversity into a library of borenium catalysts is the counterion. In the accounts by Stephan and Crudden the counterion employed was $[B(C_6F_5)_4]^-$. Since the enantioselective reduction step involves hydride transfer from a neutral NHC-borane to an iminium salt, it is possible that the counterion could play a role in controlling transition state structure.

2.1.3.2 Attempts to quantify steric parameters in NHCs used for borenium preparation

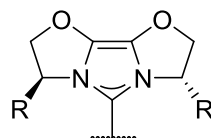
Before commencing synthetic efforts we were interested to quantify the level of steric hindrance found in the NHC systems reported by Stephan^{169,188} and correlate this data with the reported catalytic activity. The resulting trends could then be used to assess the most likely NHC candidates to generate active borenium catalysts. We used the percentage buried volume parameter ($\%V_{bur}$) described by Nolan for NHC ligands.²⁰⁰



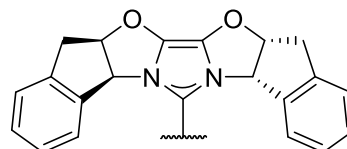
B—L distance = 1.58 Å



NHC



THIBO



HIBDIO

Ligand type	R	R'	R''	%V _{bur}	Conversion (%) ¹⁸⁸
NHC ^a	<i>i</i> Pr	<i>i</i> Pr	H	35.4	35
	Mes	Mes	H	58.9	0
	^t Bu	Me	H	35.4	trace
	Ph	Me	H	36.4	100
	Me	Me	H	29.4	100
NHC ^b	Ph	Me	H	36.4	35
	Me	Me	H	29.4	67
	Me	Me	Me	29.9	21
	Me	Me	Cl	29.8	100
THIBO	Me	-	-	31.5	-
	<i>i</i> Pr	-	-	43.5	-
	^t Bu	-	-	45.3	-
HIBDIO	-	-	-	37.2	-

Table 2.2 %V_{bur} values and reported activity using substrate **13c**, DCM, 102 atm H₂, r.t., 30 min; conversion values reported at 1 mol% (a) and 0.5 mol% (b) catalyst loading.

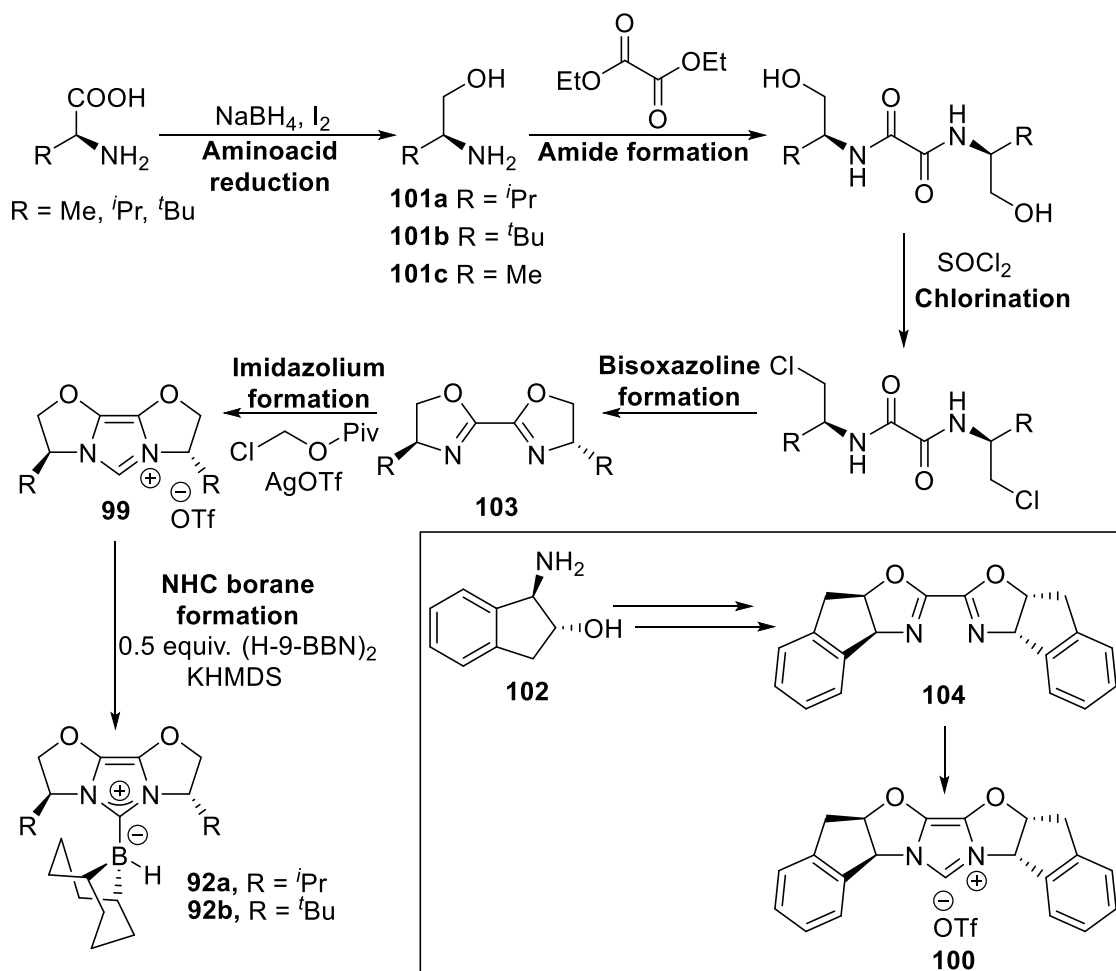
The parameter describes the volume occupied by the ligand within a sphere of arbitrary radius (usually 3.5 Å) centred on the metal atom, with a secondary parameter defined by the ligand-metal distance. Our calculations were performed using generated models (Chemdraw Chem3D) on the online tool Sambvca;²⁰¹ the C_{NHC}-B bond length of 1.58 Å reported experimentally for borenium **87** was used.¹⁸⁸ The standard sphere radius of 3.5 Å was used, a smaller value in comparison to the calculated B-X (X = donor atom in Lewis base component) distance of 4.2 Å required for hydrogen activation.⁸⁵ This choice was justified by the intention to better capture any effects arising from catalyst inhibition. The calculated %V_{bur} values are presented with reported values of the catalytic performance in Table 2.2. %V_{bur} gives an isotropic measure of the steric hindrance resulting in only a qualitative correlation with displayed activity being observed (R = R' = ⁱPr vs R = Me, R' = ^tBu). At the sphere radius employed the effect of substituents present in the distal part of the NHC is minimal, and differences in reactivity are electronic in nature (R'' = H/Me/Cl). For the THIBO ligands (and HIBDIO), the similarly high %V_{bur} values obtained for the series indicated the different placing of steric bulk resulting from tethering of the *N*-substituents. The higher steric hindrance displayed by the ⁱPr and ^tBu substituted THIBO NHC was expected to provide steric shielding in the borenium cations, and possibly eliminate issues resulting from catalyst inhibition. The best reactivity was expected for the methyl substituted **95c**, since its %V_{bur} value was in the range of the active catalysts reported by Stephan.

2.2 Catalyst synthesis

The synthesis of THIBO and HIBDIO NHC pro-ligands, imidazolium salts **99** and **100**, was reported by Glorius^{194–196,202,203} and further developed in our group.²⁰⁴ The synthesis of NHC-borane adducts **92a,b** and **93a** was reported by Lindsay and McArthur.¹⁹³

2.2.1 Synthesis of IBiox NHC-boranes

The general synthetic scheme described in Scheme 2.4 was employed for the synthesis of NHC-borane adducts. Details are presented in the Experimental section.



Scheme 2.4 Synthesis of IBiox NHC-boranes.

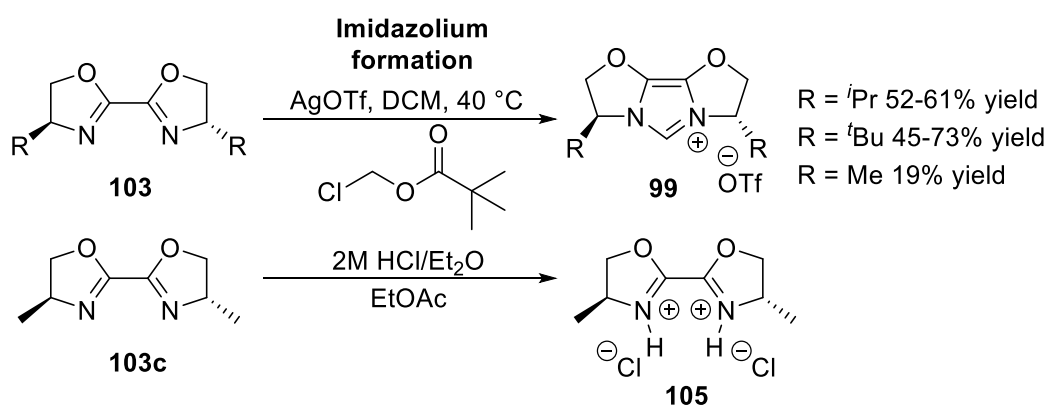
101a-c and **102** were purchased or synthesised following the method of Meyers employing generation of borane *in situ* (**101a** 60% yield, **101b** 62% yield following distillation).²⁰⁵

Substrate	Amide formation	Chlorination	Bisoxazoline formation
101a	83-92%	95%	92%
101b	97%	64%	80%
101c	76%	97%	97%
102	73%	89%	89%

Table 2.3 Summary of yields obtained in the conversion of aminoalcohols to bisoxazolines.

Results for the next three steps which convert amino-alcohols to bisoxazolines (**Amide formation** carried out by reaction with diethyl oxalate; **Chlorination** carried out using thionyl chloride, **Bisoxazoline formation** carried out by cyclisation under basic conditions, Scheme 2.4) are summarised in Table 2.3. Procedures reported by Denmark were also employed.²⁰⁶

Conversion of bisoxazolines **103** and **104** to the imidazolium salts **99** and **100**, respectively, was carried out according to the procedure of Glorius.²⁰³ We observed some variability in our results, particularly on small scale reactions. Since the reaction has to be carried out at fairly high concentration (~0.3 M, e.g. 5 g **104** in 75 mL solvent²⁰³), it is possible that diluting small scale reactions results in poorer reactivity. We have used both the reported methods which involve either separate reagent formation (1.45 equiv. chloromethylpivalate + 1.45 equiv. silver triflate, reagent filtered before use) or a one pot procedure (1.4 equiv. chloromethylpivalate + 1.2 equiv. silver triflate), and carried the reaction with exclusion of moisture, oxygen, and light.

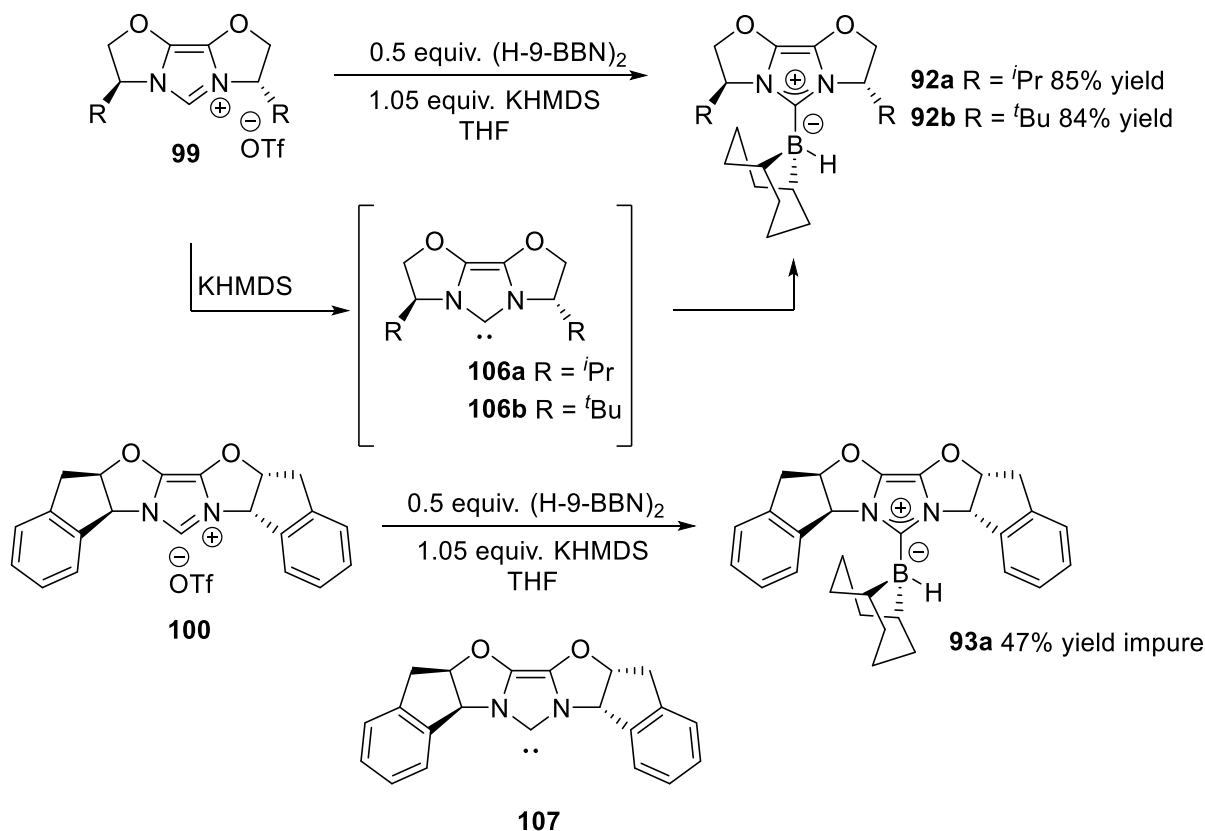


Scheme 2.5 Conversion of bisoxazolines to imidazolium salts.

99c could be isolated on one occasion in 19% yield. Screening of a range of conditions (stoichiometry, concentration) resulted in conversions lower than 30%. We attempted closure of the imidazolium ring using formaldehyde and HCl following the method of Noels.^{207,208} A brief screen of reaction conditions (excess reagent, dehydrating agent) failed to afford any of the desired product. Instead precipitation

of the salt **105** was observed. This compound was prepared separately and characterised by NMR. The conversion of **99c** to borenium **95c** was later performed by Mr Michael Howlett (MSci project).

We also attempted imidazolium ring formation on the bisoxazoline **103a** using formaldehyde and TMSCl following a procedure by Hintermann.²⁰⁹ TMSCl and EtOAc were distilled from calcium hydride and the reaction carried out in a sealed system to prevent TMSCl evaporation. Unfortunately, no product was obtained. Imidazolium salt **99a** could be obtained using the Glorius procedure in 52-61% yield following chromatography and recrystallisation. The reported yield is 80%.¹⁹⁴ Imidazolium salt **99b** was prepared with yields in the range 45-73% following chromatography and recrystallisation. Imidazolium salt **100** was prepared in 44% yield.

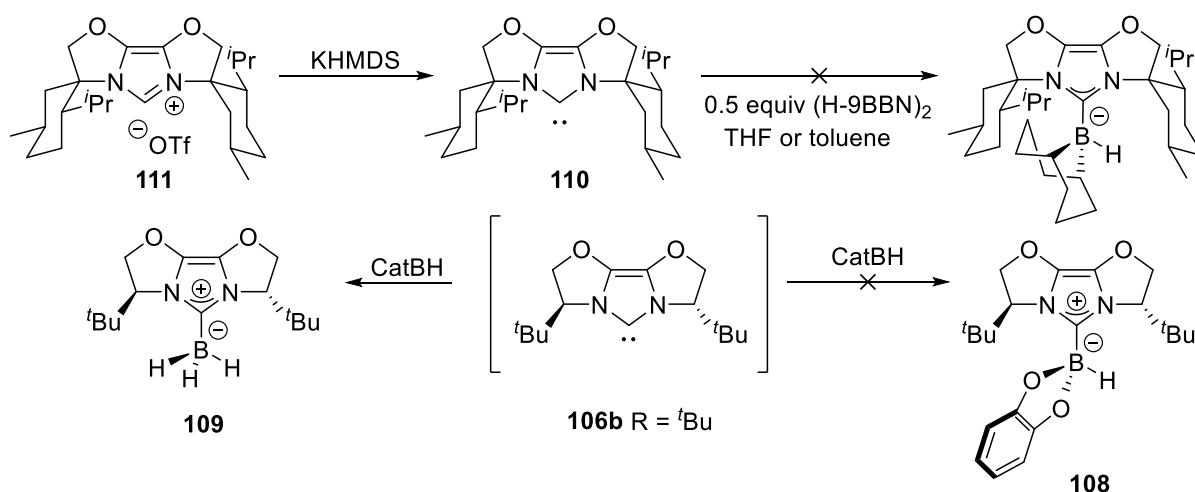


Scheme 2.6 NHC-borane adduct synthesis.

Formation of the borohydrides **92a,b** and **93a** was carried out by imidazolium salt deprotonation using KHMDS (as employed by Stephan and Crudden) and trapping *in situ* of the resulting NHC with 9-BBN

dimer **23a**. NMR scale reactions indicated that under these conditions clean product formation occurred (**92a,b**). Nonetheless, the reactions were found to develop a strong colouration during base addition in the presence of 9-BBN dimer (**92a** and **93a**).

We suspected this to result from instability of the intermediate free NHC. Monitoring solutions of NHC **106a** and **107** by NMR indicated the former to decompose slowly (<7 h) whereas the latter decomposed completely within 15 min. Interestingly, the formation of **92b** proceeded without significant colouration, probably due to the better stability of **106b**. Workup was carried out by solvent removal under high vacuum and extraction of the resulting residue with toluene. Filtration after the solvent switch allowed removal of additional decomposed material together with salt by-product. **92a** was prepared using this method in 85% yield as a pale-yellow powder and was pure by ^1H and ^{11}B NMR. NHC-borane **92b** was prepared in 84% yield; further purification by washing with a toluene/pentane (1:5) mixture resulted in a great reduction in yield (54%). These hydrides were used as prepared, with further purification being possible in the next step. NHC-borane **93a** could not be prepared in pure form using this procedure: it was obtained as a green solid, impure by ^1H NMR (<47% yield, no yield or characterisation reported in the literature¹⁹³).



Scheme 2.7 Attempted NHC-borane synthesis.

Formation of borohydride **108** was attempted following the standard procedure involving NHC generation and trapping *in situ*. Issues resulting from steric bulk were not expected with catecholborane as the reagent. The unexpected formation of **109** (^{11}B NMR -33.9 , q (DCM- d_2), cf. -34.9 , q, (CDCl_3)¹⁹³) was observed. Addition of borane after NHC formation (to exclude reactivity caused by KHMDS) and increasing dilution to prevent unwanted NHC reactivity did not solve this problem. It is possible that redistribution of hydride and catecholate ligands between product/starting material is occurring.

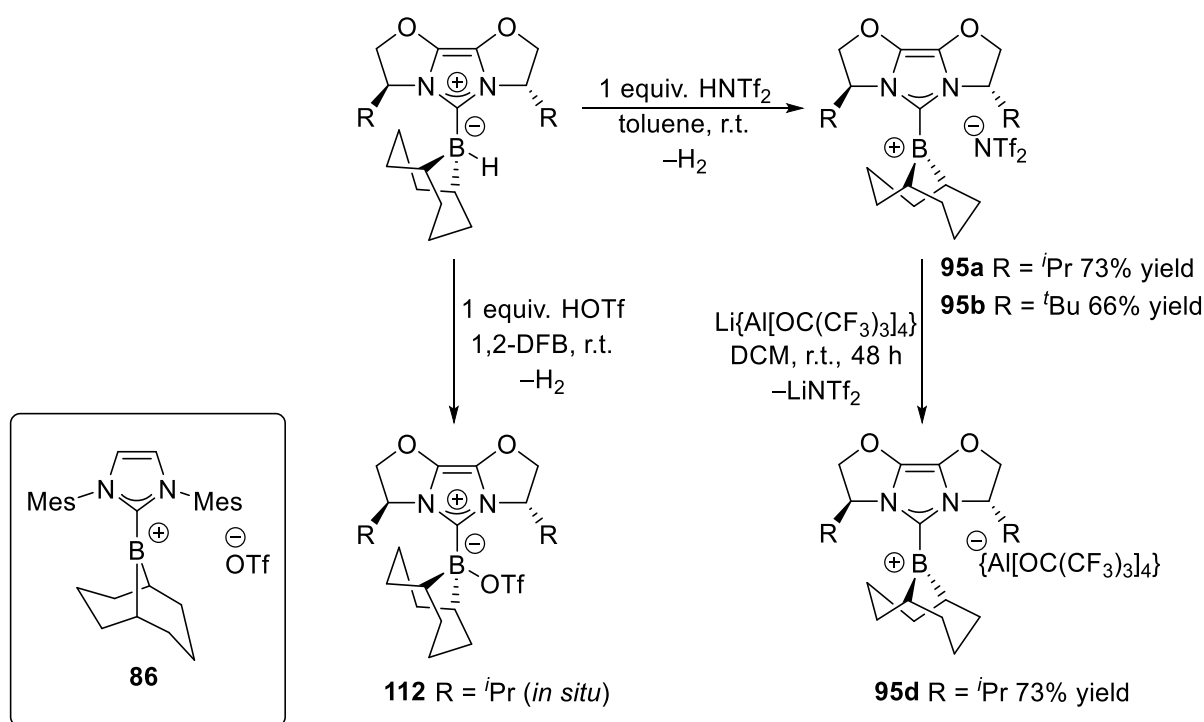
2.2.1.1 Other NHC-borane adducts targeted

As part of our efforts to construct a library of NHC-borane pre-catalysts, we attempted coupling of NHC **110**²¹⁰ with 9-BBN hydride dimer **23a**. NHC **110** could be accessed by *in situ* deprotonation with KHMDS from the commercially available imidazolium salt **111** in the presence of 9-BBN hydride dimer **23a**. Following the standard procedure resulted in formation of two unexpected species: one of type R_2BH_2 (^{11}B NMR -17.6 , t, $J = 75.2$ Hz, singlet observed in the proton decoupled spectrum) and one displaying a ^{11}B NMR shift of ~ 60 ppm. Isolation of the hydride species was not possible by the standard procedure. A similar outcome was observed when the reaction was carried out in toluene; this solvent switch has been used by Speed to prepare unstable NHC-boranes and presumably works by maintaining a low NHC concentration resulting from the slow dissolution of salt precursors in the non-polar solvent.¹⁹⁰ Using salt **111** the R_2BH_2 species slowly formed and decomposed in solution. In both cases (THF and toluene solvent) carbene formation was indicated by the disappearance of the imidazolium proton (^1H NMR) and appearance of a ^{13}C NMR signal (193 ppm) which was assigned to the carbenic carbon.²¹⁰ We believe this unidentified reactivity results from the inability of the exceedingly bulky intermediate NHC to coordinate to boron due to the combined steric bulk of the two components.

2.2.2 Synthesis of borenium cations

2.2.2.1 Hydride abstraction

Hydride abstraction on NHC-borane **92a** was carried out using HNTf₂. This procedure was employed previously by Lindsay¹⁷⁸ and Stephan.¹⁸⁸ The reaction was performed in toluene (≥ 0.05 M); product precipitation was observed during acid addition, together with hydrogen gas evolution. The isolated yield was 90%, with the product exhibiting a clean NMR spectrum, however colouration was noted in the product. Purification performed by crystallisation from a layered DCM/pentane 3:4 mixture at -20 °C resulted in a poor isolated yield of 41%. It was found that increasing the reaction dilution (~ 0.025 M) in combination with slow addition of the acid solution and vigorous stirring allowed precipitation of the product **95a** in a pure microcrystalline state. Following rinsing with toluene the product was obtained as a fine, off-white powder in 73% yield (gram-scale).



Scheme 2.8 Synthesis of borenium ions.

Product **95a** is only sparingly soluble in toluene or 1,2-DCB but soluble in chloroform, DCM and 1,2-difluorobenzene and displays a broad singlet signal in the ¹¹B NMR spectrum at 73 ppm (CD₂Cl₂)

characteristic of tri-coordinate borocations. Further characterisation and comparison with other borenium ions is presented in section 2.2.2.3. Borenium **95b** was prepared in a similar fashion in 66% yield as a crystalline white solid (^{11}B NMR 73 ppm).

The use of HOTf was briefly explored as we were interested to investigate any potential counterion effects on enantioselectivity. In an NMR experiment (1,2-DFB solvent) NHC-borane **92a** was treated with 1 equivalent of HOTf, resulting in the formation of a species **112** displaying a ^{11}B NMR shift of 6 ppm, which was assigned to result from triflate counterion coordination. No signal corresponding to a borenium species was observed at room temperature or at 80 °C. The signal corresponding to adduct **112** was observed to be much sharper at high temperature, suggesting that it exists in an equilibrium with the borenium ion form. It is interesting to note that borenium cation **86** was prepared by Lindsay and McArthur using a triflate counterion. This is probably a result of the much greater steric shielding provided by the IMes NHC ligand.

The NHC-borane **93a** was treated with HNTf_2 in DCM resulting in little gas evolution being observed. ^{11}B NMR indicated that trace hydride was still present after 15 min at r.t., but no borenium ion signal could be detected. It is expected that borenium **96** would be soluble in DCM.

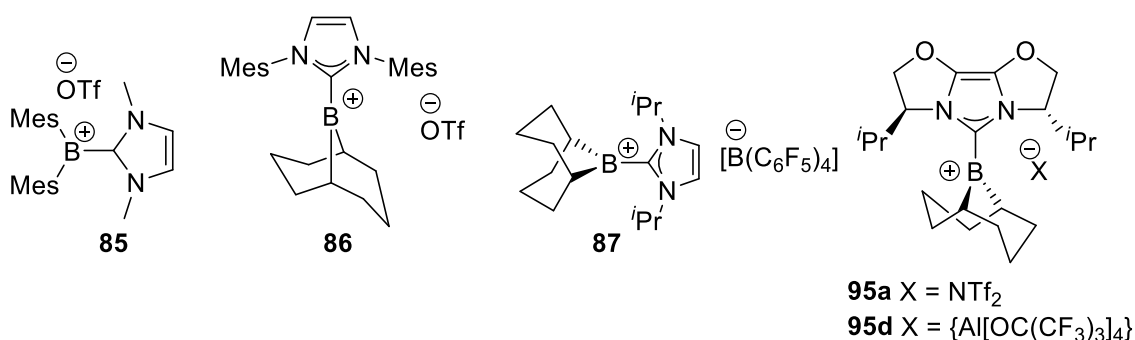
2.2.2.2 Counterion exchange

Having identified the triflimidate counterion as the most coordinating counterion for which a borenium type species is observed for the combination of IBiox NHC and 9-BBN scaffold, we turned to investigating less coordinating counterions. The anion $\{\text{Al}[\text{OC}(\text{CF}_3)_3]_4\}$ is one of the least coordinating anions currently in use.^{175,211} Exchange of triflimidate anion for $\{\text{Al}[\text{OC}(\text{CF}_3)_3]_4\}$ was realised by reaction of **95a** with the potassium (15 min, 63% yield) or lithium (48 h, 73% yield) salts in DCM. An extended reaction time was used for the lithium salt due to it being only sparingly soluble in DCM. The by-product salts were difficult to filter due to being formed as very fine powders. The resulting borenium **95d** was insoluble in benzene or toluene. Initial dissolution was followed by rapid separation of a

denser oil phase. The supernatant did not contain **95d** (assessed by ^{11}B NMR). Product **95d** displayed a ^{11}B NMR shift of 72.5 ppm (1,2-DFB, *vide infra*).

2.2.2.3 Characterisation of borenium triflimide **95a**

Borenium triflimide **95a** was fully characterised by NMR. 2D NMR experiments supported the assigned structure. The broad singlet signal in the ^{11}B NMR spectrum at 73 ppm (CD_2Cl_2) appears in the region of the spectrum characteristic to borenium cations, cf. **85** 66 ppm, **86** 81.4 ppm,¹⁷⁸ **87** 83.8 ppm (Table 2.4).¹⁶⁹ Variation in chemical shift results mostly from changes in the borane scaffold (diaryl **85** vs dialkyl **86**). The borenium ions **95a** and **95d** display essentially identical ^{11}B NMR spectra, providing indirect evidence that anion coordination is not occurring in **95a**, despite the more coordinating counterion.



Borenium cation	^{11}B NMR δ (ppm)	AN	B-C _{NHC} (Å)	D _c /D _a
85 ¹⁷⁷	66	n/a	1.579(7)	n/a
86 ¹⁷⁸	81.4	n/a	n/a	0.85
87 ¹⁶⁹	83.8	n/a	1.580(3)	n/a
95a	73	70.7	1.540(7)	1.06
95d	72.5	n/a	n/a	n/a

Table 2.4 NHC-borenium ion comparison.

Diffusion coefficients for the cation and anion components of **95a** were measured using DOSY NMR studies following the reported method.^{178,179} Values of $1.19 \times 10^{-9} \text{ m}^2/\text{s}$ and $1.12 \times 10^{-9} \text{ m}^2/\text{s}$ were

obtained for the cation and anion component, respectively. The low value of D_c/D_a (1.06) indicates that although no anion binding is occurring, the two components are ion paired, possibly a result of the low solvent polarity (CD_2Cl_2).

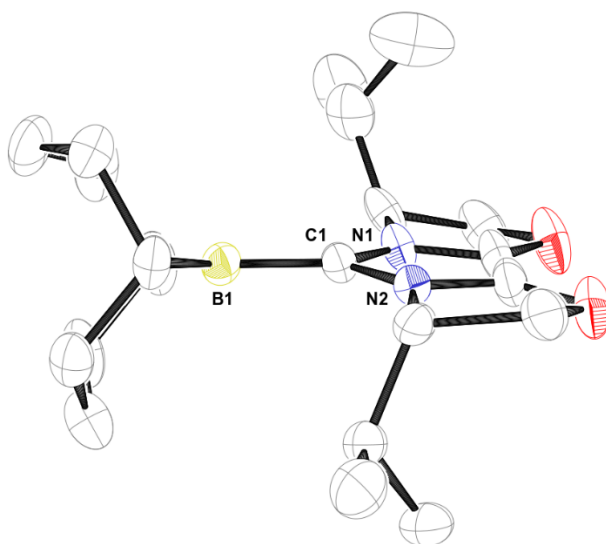


Figure 2.6 ORTEP diagram showing side-on view of borenium cation **95a**. Triflimide counterion and H atoms omitted for clarity. Thermal ellipsoids drawn at 50% probability level. O atoms red, C atoms white, N atoms blue, B atom yellow. Data collection and analysis carried out by Dr Adam Piascik.

Crystallographic characterisation confirmed the ionic nature of **95a** in the solid state (Figure 2.6). Crystals suitable for analysis were grown by vapour diffusion of pentane into a solution of **95a** in 1,2-DFB. The B atom was found in a distorted trigonal planar geometry: \angle (C1-B1-C14) = 123.8(5)°, \angle (C1-B1-C18) = 124.0(5)°, \angle (C14-B1-C18) = 112.2(5)°. No interaction with the anion was found in the solid state, the closest B-O contact being found at 3.656(7) Å. Strong NHC coordination was observed, indicated by the C1-B1 distance of 1.540(7) Å. The torsion angle between the 9-BBN fragment and the imidazolium ring was found to be 13.61° (measured between the mean planes). The conjugated nature of the borenium ion possibly accounts for the slightly shorter B-C_{NHC} distance compared to the precursor **92a** (1.610(3) Å²¹²). The 9-BBN scaffold was found to exist in a boat/chair conformation. This conformation was used in all depictions of IBiox borenium ions, although it does not necessarily reflect

the conformational situation found in solution at room temperature, or effects arising from changing the NHC ligand. Compound **95a** represents the second chiral borenium cation characterised by crystallography.²¹³

It results that in the absence of anion coordination effects, the difference in ¹¹B NMR chemical shift between the compounds **86**, **87** and **95a** is a result of the electronic properties of the IBiox NHC ligand. Since Glorius reported that IBiox NHCs are less electron donating than standard NHCs (IMes),¹⁹⁵ the nature of the effect is not clear and possibly results from the difference in cationic centre being ligated.

NHC-stabilised borenium ions were reported to be weaker Lewis acids than B(C₆F₅)₃. We measured the Lewis acidity of **95a** using the modified Gutmann-Beckett method, attempting to gauge how significant the reduction in Lewis acidity is resulting from the apparent electron-donating properties of the IBiox NHC. Gutmann studied the Lewis acidic properties of solvents by considering the equilibrium shown in Figure 2.7. Any interaction involving the lone pair of the O atom in Et₃P=O (hydrogen bonding, protonation, Lewis acid coordination) will result in a reduction of electron density at the P atom. This process was monitored by ³¹P NMR resulting in the construction of an acceptor number (AN) scale based on reference compounds: hexane (AN = 0) and SbCl₅ (AN = 100).²¹⁴ Beckett applied this method to the study of borane Lewis acids (neat),²¹⁵ and in a final modification Stephan employed a three-fold excess of Lewis acid to ensure complete complexation of B(C₆F₅)₃ derived boranes.²¹⁶ The method has been used extensively for borane Lewis acids.²¹⁷⁻²²⁰

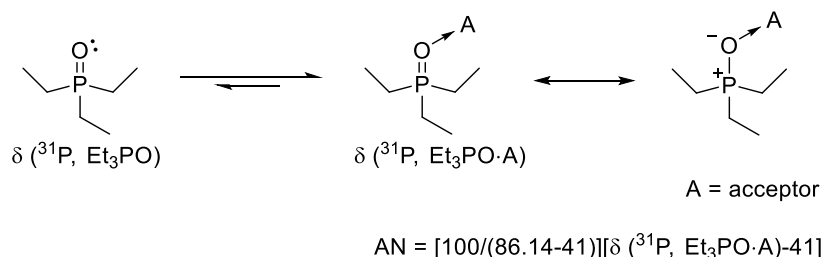


Figure 2.7 Gutmann-Beckett Lewis acidity measurement.

Using this method an acceptor number of 70.7 was measured for **95a**. For reference, the AN value of $B(C_6F_5)_3$ is 78.1.²¹⁹ The equilibrium established was slow on the NMR time scale resulting in broadening of the ^{11}B NMR signal.

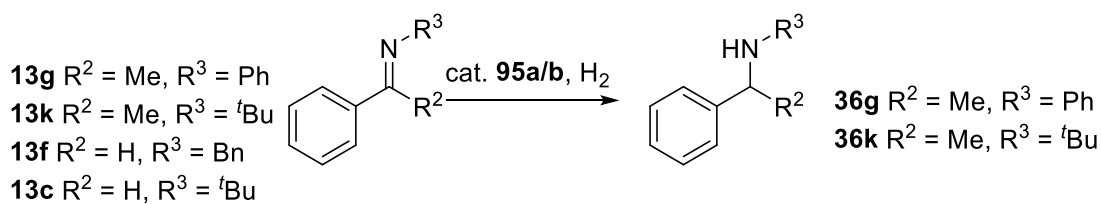
2.3 Catalytic activity

2.3.1 Hydrogenation

2.3.1.1 Low pressure

Model imine substrates investigated were ketimines **13g,k** and aldimines **13f,c**. These substrates are ubiquitous model substrates in FLP methodology development and their study would provide information regarding the essential features of our IBiox-stabilised borenium ions. The ketimines **13g,k** allow for the effect of substrate basicity on reactivity to be explored for sterically hindered substrates and the aldimines **13f,c** allow for further exploration into issues arising from catalyst inhibition. Catalyst generation *in situ* (treating NHC-borane precursors with $HNTf_2$) was generally employed for borenium catalyst **95b**. This approach is useful for screening efforts as it eliminates the need to isolate the moisture-sensitive borenium cations (*vide infra*) and has been used by both Stephan¹⁸⁸ and Crudden.¹⁸⁷ *In situ* catalyst generation was also used in section 2.3.1.2. for further counterion screening. Since most of our investigation concerned the catalyst **95a**, this catalyst was prepared and isolated on scale. This approach, as opposed to *in situ* generation, is faster when the same catalyst is being studied and eliminates potential issues arising from deviations in stoichiometry of the NHC-borane/ $HNTf_2$ mixture.

Screening of low-pressure reaction conditions (<4 bar) is summarised in Table 2.5. Reactions were generally monitored at room temperature before heating. Aldimine **13f** was found to bind borenium cation **95a**, indicated by the presence of a sharp peak in the ^{11}B NMR (-1.8 ppm). A similar adduct has been recently reported by Speed.¹⁹⁰ Evidence of catalytic reduction could not be observed at 80 °C, indicating that substrate binding is strong (entry 1).

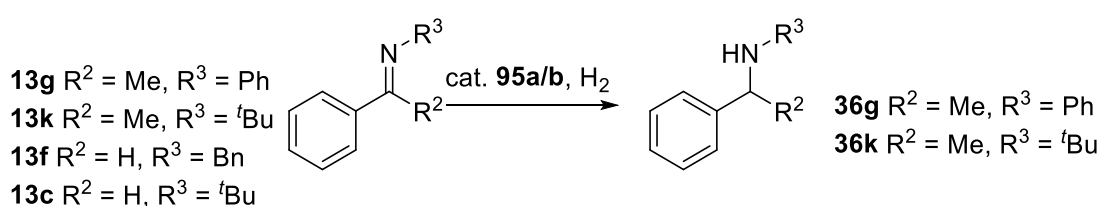


Entry	Subst.	Conditions	95 ^a	Adduct ^{a,b}	Hydride 92 ^c	Conv.
1	13f	10 mol% 95a , DCM-d ₂ , 1 bar, 80 °C, 40 h	–	–1.8	–	0%
2	13g	10 mol% 95a , 10 mol% P ^t Bu ₃ , DCM-d ₂ , 4 bar, 80 °C, 3 h	~74	–	–16.9, d, r.t (29 h)	0%
3	13g	10 mol% 95b , DCM-d ₂ , 1 bar, 50 °C, 3 d	~73	–	–	0%
4	13g	10 mol% 95b , tol-d ₈ , 4 bar, 105 °C, 14 h	insoluble	–	–	0%

Table 2.5 NMR scale hydrogenation of *N*-phenyl and benzyl imines. Reactions carried out in Young's tap NMR tubes. a. analysis carried out before hydrogen addition. b. this peak is heavily obscured by the background signal; its presence is generally difficult to determine definitively. c. analysis during or after the reaction.

The increased steric bulk introduced by the IBiox NHC appears insufficient to prevent coordination of unhindered imines. The ketimine **13g** did not cause significant inhibition of catalyst **95a**, presumably due to its weaker basicity (entry 2). The bulky phosphine **5b** did not cause inhibition either but promoted hydrogen activation at room temperature (accumulation of hydride **92a** after 29 h), this process being accompanied by the formation of several unidentified P containing species (entry 3). Despite this reduction was not observed, presumably due to the poor basicity of substrate **13g** and the weak acidity of the [HP^tBu₃] cation (pK_a>8²²¹). The bulkier **95b** provided similar results in the absence of added phosphine base (entry 3). Increasing the temperature did not result in substrate reduction (entry 4).

Further screening was carried out using the bulky ketimine **13k** (Table 2.6). The bulky aldimine **13c** did not bind boreniums **95a** or **95b** to any discernible extent (entries 1 and 2). However, hydrogen activation or reduction was not observed. This was tentatively assigned to be the result of excessive steric hindrance in the two components preventing hydrogen activation and/or reduction. Any reaction occurring is presumably too slow to overcome the rate of catalyst degradation (*vide infra*). The even bulkier ketimine **13k** again showed no reactivity using either catalyst **95a** or **95b** (entries 3-5).

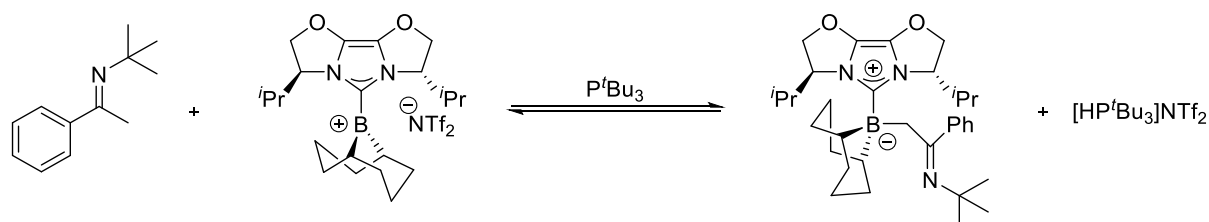


Entry	Subst.	Conditions	95 ^a	Adduct ^{a,b}	92 ^c	Conv.
1	13c	10 mol% 95a , 1 bar, 80 °C, 25 h	~72	–	–	0%
2	13k	10 mol% 95b , 4 bar, 80 °C, 3 d	~72	–	–	0%
3	13k	10 mol% 95a , 10 mol% P ^t Bu ₃ , 4 bar, 80 °C, 65 h	~72	~–6	–	0%
4	13k	10 mol% 95a , 10 bar, r.t. and 50 °C, 24 h	~72	~–6	–	0%
5 ^d	13k	10 mol% 95b , 4 bar, 50 °C, 62 h	~72	–	–	0%

Table 2.6 NMR scale hydrogenation of *N*-*tert*butyl imines. Reactions carried out in Young's tap NMR tubes using DCM-d₂ solvent, unless stated otherwise. a. analysis carried out before hydrogen addition. b. this peak is heavily obscured by the background signal; its presence is generally difficult to determine definitively. c. analysis during or after the reaction. d. reaction carried out in a high-pressure NMR tube

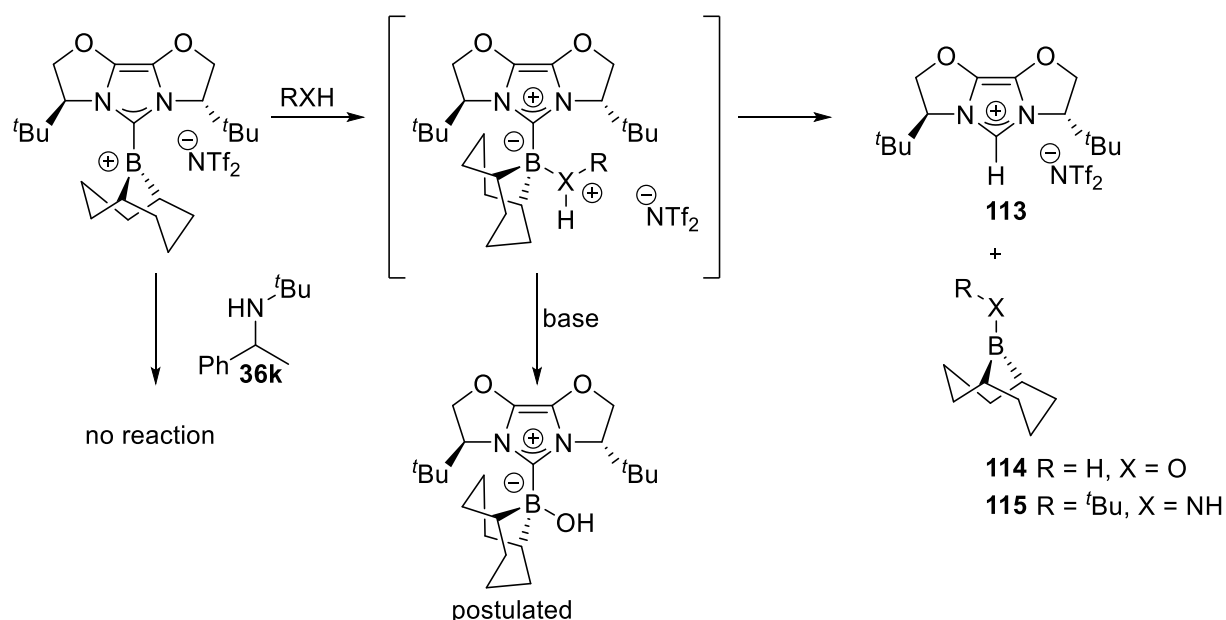
Interestingly, the less bulky **95a** was partially inhibited, possibly resulting from the presence of other nucleophiles in the reaction mixture. It is possible that due to the greater substrate basicity catalyst inhibition by hydroxide anion is occurring (Scheme 2.10). Alternatively, C-binding of the imine

substrate could be occurring. Such behaviour has been reported by Piers for $B(C_6F_5)_3$ **4b** and is presumably favoured by the presence of phosphine base (entry 3; Scheme 2.9).²²² Finally, raising the pressure to 10 bar resulted in no reduction being observed.



Scheme 2.9 Possible substrate inhibition through C-binding.

Catalyst degradation was observed to occur under these reaction conditions. ^{11}B NMR indicated the formation of two sharp signals at 59 and 49 ppm, generally the former being the first observed to form. 1H NMR indicated the formation of imidazolium salt **113** showing a characteristic singlet signal in the 8-9 ppm range. These observations indicate that proto-deborylation is occurring with cleavage of the B-C_{NHC} bond.

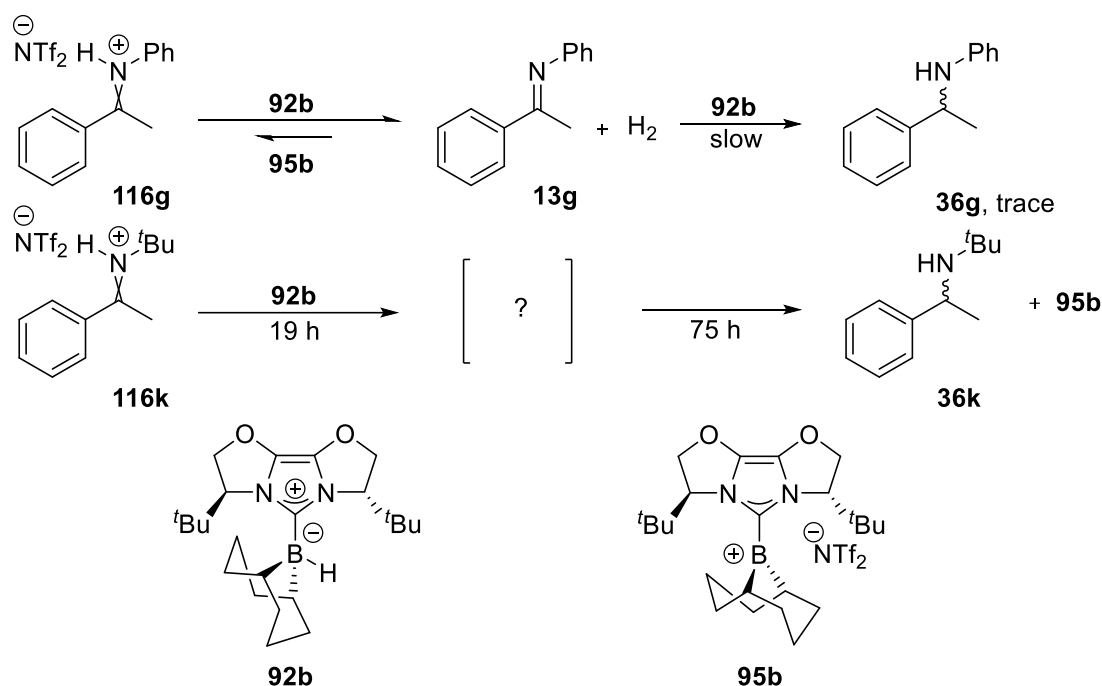


Scheme 2.10 Inhibition and decomposition pathways for borenium **95b**.

To probe mechanisms by which this reaction could occur, the borenium cation **95b** was treated with one equivalent of water or one equivalent $t\text{BuNH}_2$ (Scheme 2.10); decomposition proceeded through proto-deborylation. Remarkably, complete reaction with water required approximately one day, and with $t\text{BuNH}_2$ 9 h. The hydrolysis reaction resulted in the formation of **114** (^{11}B NMR: 58 ppm, cf. reported 58.8, CD_2Cl_2 ²²³); the aminolysis reaction resulted in the formation of **115** (^{11}B NMR: 49 ppm, cf. reported for $\text{Et}_2\text{B-NH}t\text{Bu}$ 46.5 ppm²²⁴). No intermediate tetrahedral adduct was detected, indicating that the rate limiting step is coordination to the extremely hindered boron atom in **95b**. Under basic conditions, it is possible that the transiently present tetrahedral intermediate gets deprotonated, effectively leading to catalyst inhibition by hydroxide. The amine **36k** does not bind or degrade borenium **95b**.

Despite the remarkable water tolerance showed by **95b**, decomposition occurs under reaction conditions due to long reaction times and increased temperatures favouring proto-deborylation. Formation of aminolysis products is a result of imine hydrolysis generating free amine under the reaction conditions, a similar observation having been reported by Klankermayer.⁷⁰ To prevent catalyst decomposition, strict exclusion of moisture was employed through the use of dried glassware (generally $>180\text{ }^\circ\text{C}$); drying of liquid substrates was carried out by storing over activated 4 Å MS and hydrogen gas was dried using a purification column. Trace decomposition was occasionally observed, particularly when hydrogen gas was added at cryogenic temperatures.

Stoichiometric reduction experiments were carried out to assess the ability of **95b** to reduce iminium ions (Scheme 2.11). The ketimine **13g** was treated with one equivalent HNTf_2 (forming iminium ion **116g**), followed by one equivalent **92b**. Immediate hydrogen gas generation was observed (confirmed by ^1H NMR 4.6, s, DCM-d_2) together with formation of ketimine **13g** and borenium **95b**. Only trace reduction to amine **36g** was observed. This result indicates that iminium reduction is disfavoured with respect to hydrogen evolution due to the weak basicity of ketimine **13g**.



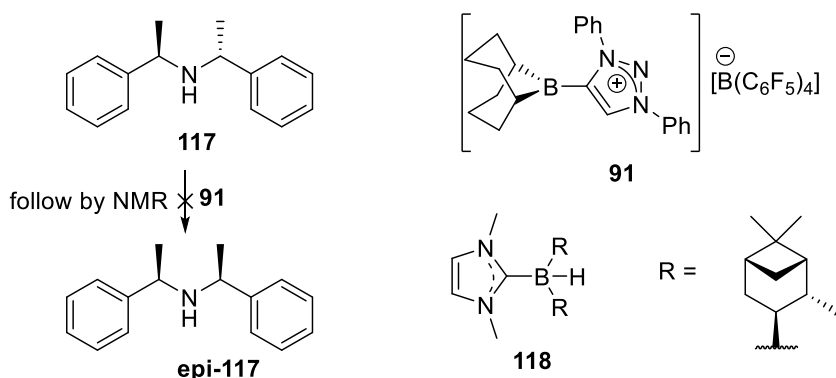
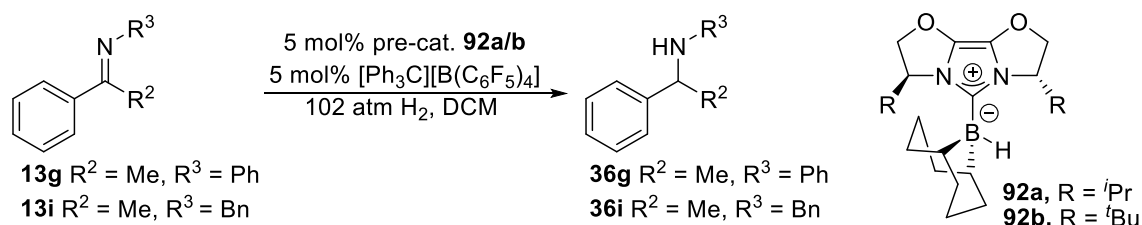
Scheme 2.11 Stoichiometric reduction of iminium ions.

A similar experiment was carried out using ketimine **13k**. Hydrogen evolution was not observed confirming the importance of substrate basicity: more basic substrates will favour hydrogen activation with the weaker Lewis acids **95**. Although the ketiminium ion disappeared after 19 h at room temperature, amine formation proceeded only slowly (up to 75 h) in parallel with borenium **95b** formation. This result indicates that reduction of a hindered substrate (**13k**) is possible using the hindered hydride **92b**, albeit at a very slow rate. The amine product could not be isolated following chromatographic purification.

In summary, our investigation indicates that borenium ions **95a,b** display a similar chemical behaviour to that reported by Stephan for achiral borenium ions: unhindered, basic ketimines cause catalyst inhibition, whereas combinations of bulky substrates and catalyst suffer both from issues in reduction and hydrogen activation.

At this stage of project development, Stephan, Crudden, Mellen and co-workers reported their efforts at developing chiral NHC-stabilised borenium cations for enantioselective hydrogenation applications.²¹² Among the many chiral NHCs that were screened, THIBO IBiox NHCs were tested.

Hydrides **92a,b** were used as pre-catalysts, with catalyst generation achieved by *in situ* hydride abstraction using $[\text{Ph}_3\text{C}][\text{B}(\text{C}_6\text{F}_5)_4]$. Testing was carried out at high pressure (102 atm). The results reported are presented in Table 2.7.



Entry	Substrate	Pre-catalyst	Conditions	Yield	e.r.
1	13g	92b	r.t., 48 h	0%	–
2	13g	92a	0 °C, 12 h	94%	50.5:49.5
3	13g	92a	r.t., 3 h	50%	56:44
4	13g	92a	r.t., 6 h	88%	54.5:45.5
5	13g	92a	r.t., 24 h	100%	53.5:46.5
6	13g	92a	50 °C, 3 h	71%	54:46
7	13i	92a	r.t., 6 h	0%	–

Table 2.7 Hydrogenation using IBiox-stabilised borenium cations, as reported by Stephan, Crudden, Melen and co-workers.²¹²

The ^tBu-substituted borenium cation generated from precursor **92b** showed no activity towards ketimine **13g** (Table 2.7, entry 1). The less hindered borenium cation generated from **92a** displayed good activity at high pressure, but only low enantioselectivity values were reported (results converted to *e.r.*, enantiomer assignment not reported). Interestingly, an increase in selectivity was observed on increasing temperature (entries 2 and 3). Increasing the reaction time at room temperature resulted in better conversion, but reduced selectivity (entries 3-5). Attempts to explain this apparent racemisation were made by following epimerisation of **117** catalysed by **91** (no hydrogen atmosphere included), presumably occurring by reversible hydride abstraction from the benzylic positions of **117**, as with B(C₆F₅)₃. Only trace epimerisation was reported to occur at room temperature (16 h). Further increasing temperature led to a reduction in selectivity (entries 3 and 6). Finally, the unhindered ketimine substrate **13i** was not hydrogenated under the reported conditions. The highest selectivity reported in this account (*e.r.* 60:40; 5% yield, amine **36g**) was obtained at -30 °C using precursor **118**.

Following from this account we decided to focus attention on the borenium ion **95a**, with testing carried out at higher pressures (>10 bar). We were most interested to further explore the factors controlling transfer of chirality: NHC, substrate, reaction conditions, etc.

Following from the stoichiometric reduction studies of Lindsay and McArthur¹⁹³ we concluded that the environment surrounding the prochiral double bond of a carbonyl derivative plays an important role in the transfer of chirality (Figure 2.8). In the case of ketimine reduction, four substituents help define this environment. On the heteroatom side of the double bond, the R³ substituent and the activating group play a key role. Investigations into hydrosilylation would provide an opportunity to explore the latter (hydrogenation uses a proton as electrophile, hydrosilylation uses a silylium group). Variation in steric bulk of the R substituent could be explored by increasing the substitution level in the vicinal position to the nitrogen atom. We noticed that secondary *N*-substituents are seldom used in such chemistry, except for the benzhydryl CHPh₂ substituent which provides excessive steric bulk; most studies favour the use of either primary groups (benzyl), tertiary groups (*tert*butyl) or, predominantly,

aromatic substituents. To address this issue we included substrate **13i** into the choice of test substrates, cf. the work of Du.¹⁴⁹ Initial success obtained using this substrate (*vide infra*) was later followed by studies which revealed that the secondary nature of the cyclohexyl substituent is key to controlling reactivity and selectivity.

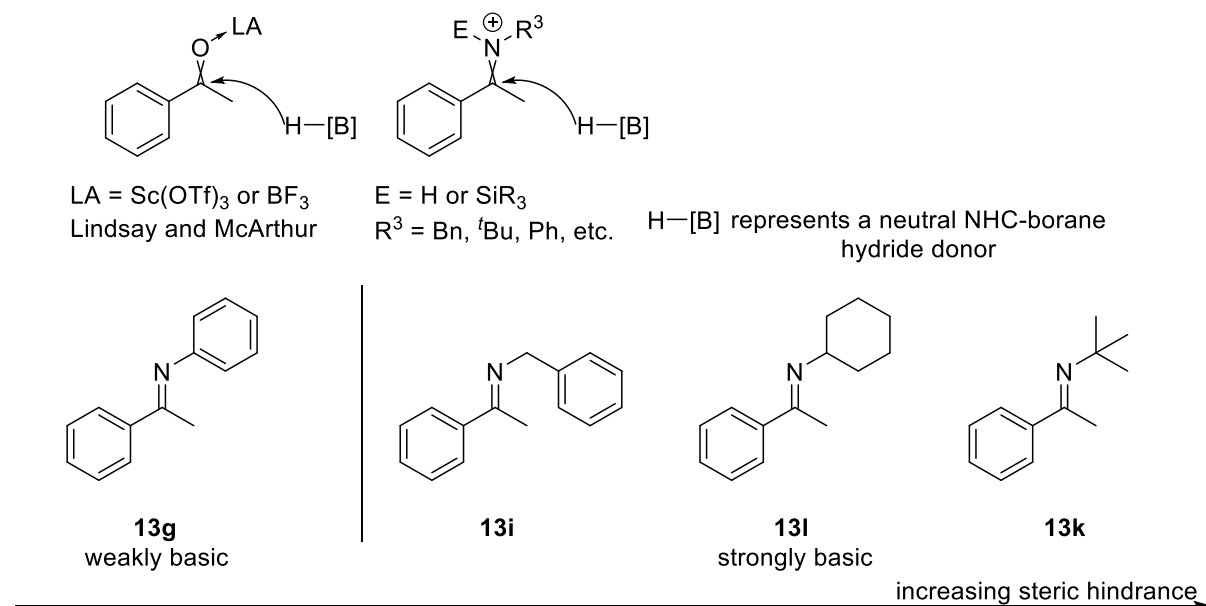
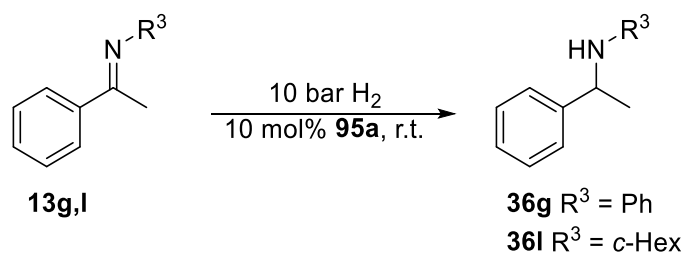


Figure 2.8 Choice of model substrates for exploring the prochiral double bond environment in enantioselective reduction.

2.3.1.2 Testing at higher pressure

We have routinely used high pressure NMR tubes (see experimental details) for carrying out and monitoring hydrogenation reactions. Ketimine hydrogenation reactions carried out using this method are presented in Table 2.8.

Due to the low solubility of **95a** in toluene, very poor reactivity is observed in the hydrogenation of substrate **13g** (entry 1). Good reactivity was observed using DCM as solvent (entry 2). The enantioselectivity observed for this transformation is equal to that reported by Stephan, Cruden, Melen and co-workers (*R:S* 56:44).



Entry	Subst.	Conditions	95^a	92^c	Conv.	e.r. <i>R:S</i>
1	13g	10 mol% 95a , toluene, 10 bar, r.t., 264 h	insoluble	–	3%	58.5:41.5
2	13g	10 mol% 95a , DCM-d ₂ , 10 bar, r.t., 168 h	~72	–	82%	56:44
3	13g	10 mol% 95a , DCM-d ₂ , 10 mol% PMe ₃ 10 bar, r.t., 168 h	~72	–	78%	56:44
4	13g	10 mol% 95a , 1,2-DFB, 10 bar, r.t., 168 h	~72	–	92%	59:41
5 ^d	13I	10 mol% 95a , 1,2-DFB, 10 bar, r.t., 212 h	~72	–6	97%	10:90

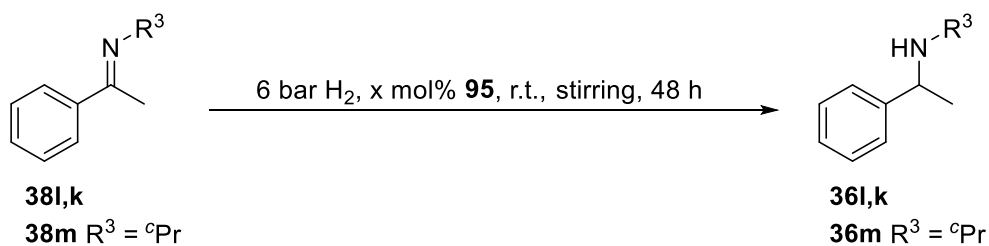
Table 2.8 NMR scale hydrogenation reactions. Reactions carried out in Wilmad high-pressure NMR tubes unless stated otherwise. Tetrahedral adduct formation was not observed (a,b); a. analysis carried out before hydrogen addition. b. this peak is heavily obscured by the background signal; its presence is generally difficult to determine definitively. c. analysis during or after the reaction. d. re-pressurised after 192 h

We attempted to improve the rate of reaction by using a phosphine base additive (entry 3). PMe₃ **5d** was chosen to avoid unwanted reactivity that had been previously observed using P^tBu₃ **5b**. Unfortunately, no improvement in reactivity or enantioselectivity was observed. This is presumably due to the significantly lower basicity of triarylphosphines ($\text{pK}_{\text{aH}} < 3$) compared to that of trialkylphosphines ($\text{pK}_{\text{aH}} > 8$).²²¹ With the phosphine base being of comparable basicity and nucleophilicity to the substrate/product, it is perhaps not surprising that no benefit is attained in hydrogen activation rate or observed enantioselectivity resulting from potential biasing of reaction pathways. Use of the more polar 1,2-DFB resulted in slightly improved reactivity (entry 4). We believe that the reaction is limited by the rate of hydrogen activation (and therefore by the concentration of

hydrogen in solution) and not by the rate of hydrogen diffusion into solution (mass transfer). An experiment carried out using substrate **13g** (10 mol% **95a**, 1,2-DFB) at low pressure (1 bar hydrogen atmosphere) in a large ampule with stirring supported this conclusion: a conversion of 12% was obtained after 4 days at room temperature. Under these conditions it is expected that the solution is saturated in hydrogen gas throughout the reaction and the pressure in the head space does not vary.

Switching the substrate to the more basic, but more hindered **13l** resulted in a slight reduction in reactivity (entry 5). Remarkably, the enantioselectivity of the reaction was much higher, with the opposite enantiomer obtained preferentially (*R*:*S* 10:90). The enantiomer assignment was carried out by comparison of optical rotation values with the literature. *N*-alkyl substituted amines were converted to their *N*-acetyl derivatives **119** by treatment with acetic anhydride/Et₃N. The resulting amides were used to measure enantiomeric ratio by chromatography using chiral stationary phases (HPLC). The *p*-bromobenzoate derivative of **36l** was prepared in an attempt to obtain crystallographic confirmation of the configuration. Crystallisation could be achieved only by water vapour diffusion into methanol, but unfortunately the crystals were not of suitable quality for diffraction studies.

Following this success, we chose to further develop the reduction of secondary *N*-alkyl ketimine substrates. We attempted using a moderate pressure screening reactor (Intek), which allows for running up to 6 reactions in parallel with stirring at pressures up to 6 bar. Results obtained using this setup are presented in Table 2.9. We expected that the combination of moderate pressure and a large head-space (resulting in no significant reduction in pressure throughout reaction) might afford improved reactivity. Unfortunately, very low conversion values were obtained, presumably due to the low pressure employed. Attempts to isolate the reaction product in one case (entry 4) by preparative TLC was unsuccessful, presumably due to the high basicity of the product.

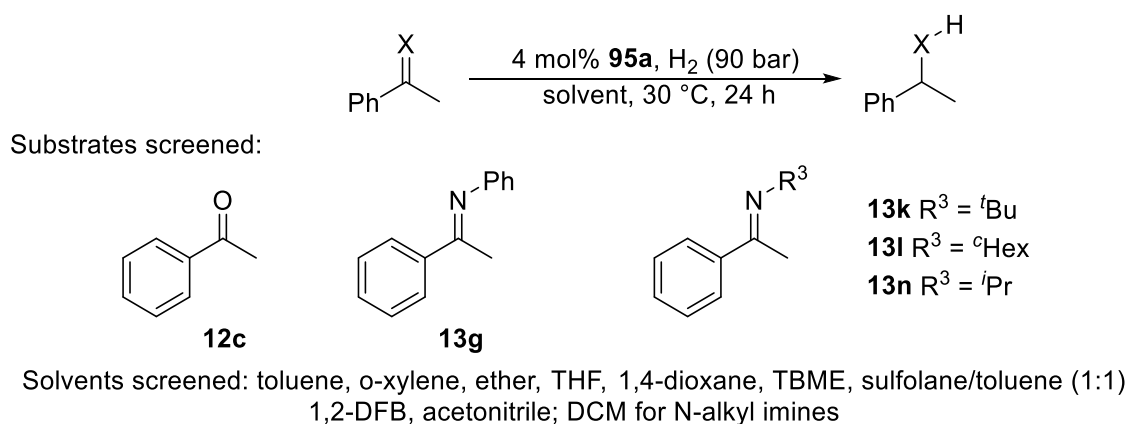


Entry	Subst.	Solvent	Catalyst	Cat loading	Conv.
1	13l	1,2-DFB	95d	10 mol%	0%
2	13l	1,2-DFB	95a	10 mol%	6%
3	13l	1,2-DFB	95a	4 mol%	0%
4	13l	DCM	95a	10 mol%	3%
5	13k	1,2-DFB	95a	10 mol%	0%
6	13m	1,2-DFB	95a	10 mol%	2%

Table 2.9 Low-pressure hydrogenation screening. Reactions were prepared in a glovebox and charged into test tubes. The tubes were placed in the reactor, which was then sealed and removed from the glovebox. The system was connected to the manifold and the atmosphere in the connections replaced with hydrogen (vacuum/backfill cycles). The system was pressurised, sealed and the reactions were magnetically stirred at room temperature.

We next turned to the use of a screening pressure reactor capable of reaching pressures above 100 bar. This equipment was accessible through our collaboration with AstraZeneca. The first screen carried out is presented in Scheme 2.12. A catalyst loading (4 mol%) similar to that employed by Stephan and co-workers was used. Various substrates were screened with focus placed on *N*-alkyl ketimines, given the successful outcome above. Various solvents were tested to establish the effect of solvent on enantioselectivity and reactivity. In the original account by Stephan, DCM was found to

provide superior reactivity to chlorobenzene and toluene.¹⁶⁹ The latter was unsuitable however due to the poor solubility of the ionic boronium catalysts.

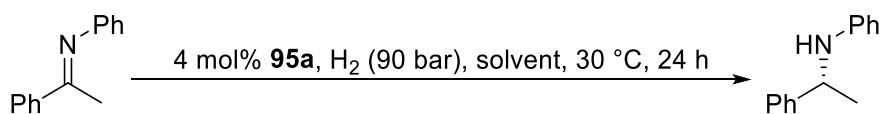


Scheme 2.12 High-pressure screening for substrate and solvent. Adapted from Ref. 165 with permission from The Royal Society of Chemistry.

Unfortunately, at this catalyst loading only substrate **13g** could be hydrogenated. The failure to hydrogenate acetophenone was also reported by Stephan and co-workers and is in part due to the low electrophilicity of acetophenone. We observed no reaction between the NHC-borane **92b** and acetone at room temperature (23 h). Heating to 60 °C (15 h) resulted in partial consumption of acetone with decomposition. The failure to hydrogenate *N*-alkyl ketimines is possibly a result of the presence of trace amounts of moisture, which results in strong catalyst inhibition under the basic reaction conditions. Since all reactions were run in parallel it is reasonable to expect that the levels of water content were similar. It appears that catalyst **95a** displays better moisture tolerance in the presence of the less basic substrate **13g**.

The results of the solvent effect study are reported in Table 2.10. The lack of reactivity observed in THF and ACN is presumably due to the strongly coordinating nature of these solvents (entry 1 and 2). Sulfolane was found to be a compatible solvent (used as a mixture with toluene to depress the freezing point) (entry 8). The great enhancement in reactivity observed with the addition of sulfolane to toluene is most likely due to the former's very high dielectric constant and not due to its catalytic role:

sulfolane is a very weak Brønsted base: $pK_{\text{AH}}(\text{H}_2\text{SO}_4) = -12.9$.²²⁵ The polarity effect is probably offset by its ability to act as a Lewis base causing catalyst inhibition.

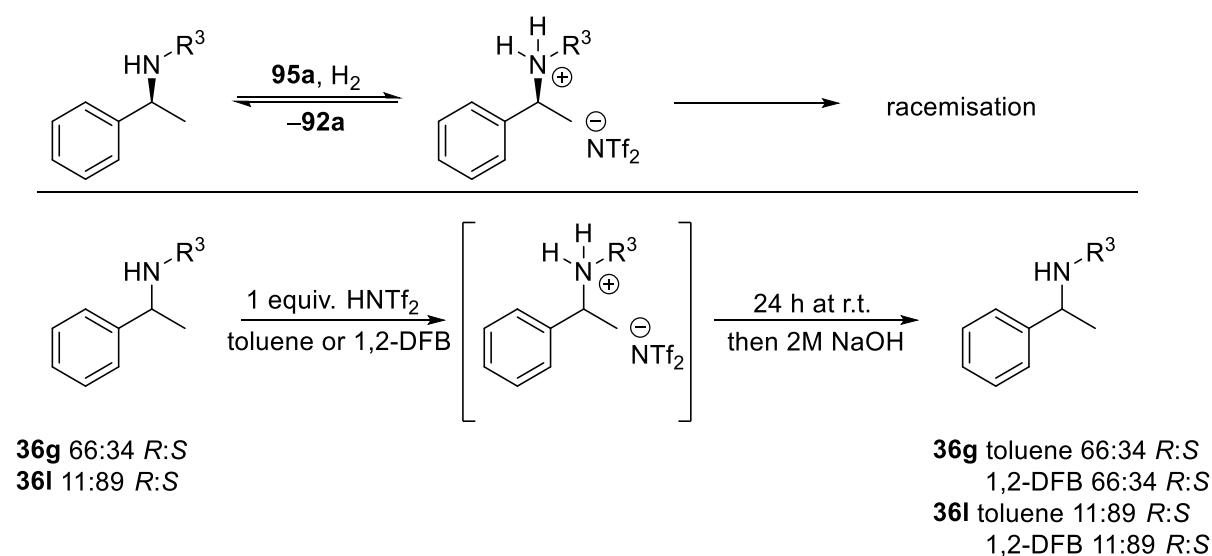


Entry	Solvent (ϵ)	Solvent type	Conv.	<i>R:S</i>
1	ACN (37.5)	Polar, coordinating	0%	–
2	THF (7.6)		3%	55.5:44.5
3	<i>o</i> -xylene (2.57)	Non-polar, non-coordinating	8%	64:36
4	Toluene (2.38)		10%	64:36
5	TBME (4.5)	Non-polar, weakly coordinating	29%	54:46
6	Diethyl ether (4.3)		37%	53:47
7	1,4-Dioxane (2.21)		42%	58:42
8	Sulfolane (44)/toluene ~1:1	Polar, weakly coordinating	53%	58:42
9	1,2-DFB (13.8)	Polar, non-coordinating	100%	59:41

Table 2.10 High-pressure hydrogenation solvent effect. Adapted from Ref. 165 with permission from The Royal Society of Chemistry. Dielectric constants from Handbook of organic solvent properties, Ian M. Smallwood, Wiley, 1996, with the exception of *o*-xylene: CRC Handbook of Chemistry and Physics, 44th ed, 2611-2620; 1,2-DFB²²⁶

The polar, non-coordinating 1,2-DFB was found to give the best reactivity (entry 9). The enantioselectivity observed varied little with the nature of the solvent, with only marginally higher selectivity being observed for hydrocarbon solvents (entry 3,4; toluene *R:S* 64:36). Interestingly, the value obtained was slightly higher than that found for hydrogenation carried out in toluene at 10 bar (Table 2.8 *R:S* 58.5:41.5). Results obtained using 1,2-DFB at the two different pressures are consistent

(10 and 90 bar 59:41 *R:S*). The amine **36g** could be isolated in 91% yield following chromatographic purification (entry 9).

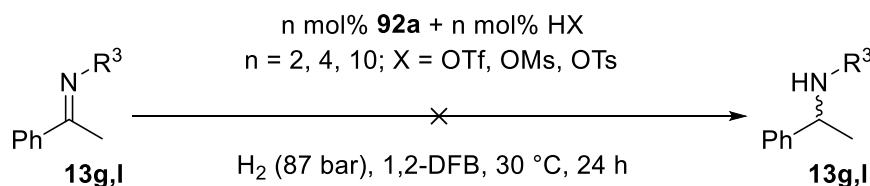


Scheme 2.13 Brønsted acid catalysed racemisation study.

To fully rule out any possibility of a racemisation process, we have investigated Brønsted acid catalysed racemisation, in addition to the investigation carried out by Stephan, Crudden, Melen and co-workers concerning borenium catalysed amine racemisation. Under high pressure conditions, it is possible that hydrogen activation carried out by the amine in combination with the borenium ion results in amine protonation. We fully protonated amines **36g,l** of known enantiopurity using HNTf₂ and measured the enantiopurity after 24 h. No racemisation was observed.

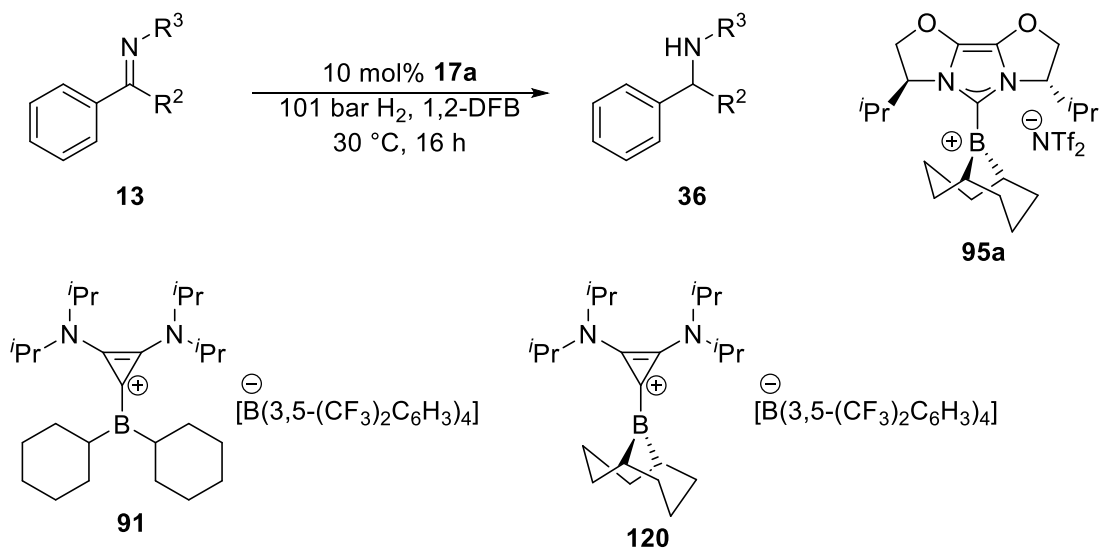
Having identified 1,2-DFB as the most promising solvent we turned to screening various catalyst counterions using **13g,l** as model substrates (Scheme 2.14). NHC-borane **92a** was treated *in situ* with protic acids (HOTf, HOMs, HOTs, all purchased anhydrous or dried). We were interested to investigate the effect the counterion plays on the enantioselectivity. In NMR experiments triflate was found to be coordinating, resulting in no free borenium ion being observed. Nonetheless, we hypothesised that the high reaction pressure might allow for reactivity to be uncovered resulting from presence of small

amounts of free borenium ion. Unfortunately, no reduction could be observed for catalyst loadings up to 10 mol%.



Scheme 2.14 High-pressure hydrogenation counterion screening.

Finally, we decided to explore the substrate scope in the high-pressure hydrogenation of *N*-alkyl ketimines using **95a** and 1,2-DFB or DCM as solvent. Successful reaction required the use of a higher catalyst loading (10 mol%). The reactions described in Table 2.11 were also performed at 4 mol% catalyst loading, but only substrates **13m,r** showed any reactivity under these conditions. The very bulky benzhydryl and ^tBu group (entry 1 and 2, respectively) prevented reaction. The substrates **13i,p** featuring primary non-bulky substituents displayed poor reactivity (entry 3 and 4). Since the substrate **13i** was not found to bind **95a**, it appears that this effect is due to the complex interplay in steric effects between NHC/borane substituents and substrate type, as described recently by Speed.¹⁹⁰ In this work the borenium ion **91** was reported to catalyse hydrogenation of PMB protected ketimine **13j** ($R^1 = \text{Ph}$, $R^2 = \text{Me}$, $R^3 = \text{PMB}$), but the related **120** did not.

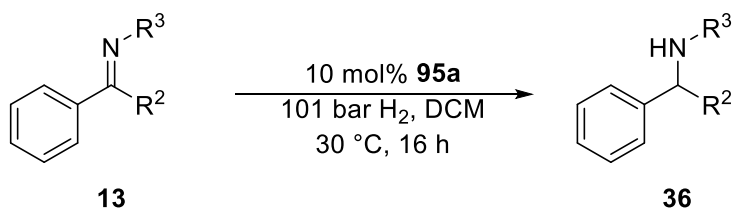


Entry	Substrate	R ²	R ³	Conversion	Isolated yield	e.r. R:S
1	13o	Me	CHPh ₂	0%	n/a	n/a
2	13k	Me	^t Bu	3%	n/a	n/a
3	13i	Me	Bn	8%	n/a	n/a
4	13p	Me	Bu	11%	n/a	n/a
5	13m	Me	^c Pr ^a	14%	n/a	n/a
6	13q	Et	^c Hex	67%	36%	65:35 ^b
7	13l	Me	^c Hex	99%	66%	11:89
8	13r	Me	^c Pent ^c	100%	67%	10:90

Table 2.11 High-pressure hydrogenation substrate scope screening. a. 10% conversion at 4 mol%; b. enantiomers not assigned; c. 6% conversion at 4 mol%.

The secondary, non-bulky substrate **13m** showed similarly poor reactivity (entry 5). It is possible that this effect results either from the small angle in the cyclopropyl ring, or due to a different conformational preference caused by the high *p* orbital character in the ring C-C bonds favouring a perpendicular orientation to the C=N bond.²²⁷ The secondary substrates **13q,l,r** showed good reactivity (entry 6-8). The enantioselectivity found for reduction of **13l** was in agreement with that observed at 10 bar (10:90, *S*:*R*). The similar substrate **13r** also gave positive results (10:90, *S*:*R*). Extension of the alkyl chain in the ketone fragment of the ketimine substrate resulted in a drop in enantioselectivity (**13q**, entry 6, 65:35, enantiomers not assigned).

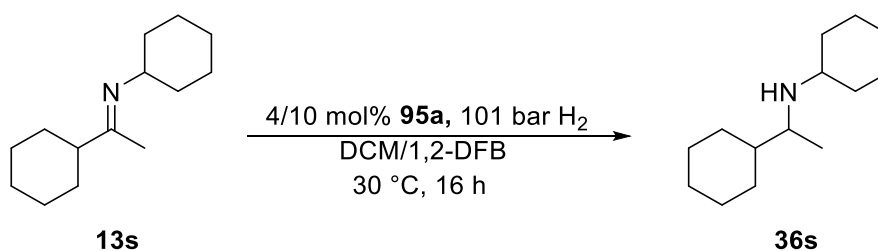
Very similar results were obtained when the reaction was carried out in DCM (Table 2.12).



Entry	Substrate	R ²	R ³	Conversion	Isolated yield	e.r. R:S
1	13l	Me	^c Hex	99%	64%	9:91
2	13i	Me	Bn	7%	n/a	n/a

Table 2.12 High-pressure hydrogenation testing in DCM.

Having explored the effect of substitution on the N-atom and in the alkyl chain of the substrate, we next investigated substrate **13s** to determine the importance of the aromatic ring in the ketone-derived fragment (Table 2.13).



Entry	Catalyst loading	Solvent	Conversion	Isolated yield	e.r.
1	4 mol%	1,2-DFB	100%	66%	50.5:49.5
2	10 mol%	1,2-DFB	100%	65%	50.5:49.5
3	4 mol%	DCM	100%	n/a	n/a
4	10 mol%	DCM	100%	n/a	n/a

Table 2.13 High-pressure hydrogenation of dialkyl ketimine **13s**.

Surprisingly, much better reactivity was observed for this substrate, as full conversion was obtained even at low catalyst loading (4 mol%). It is possible that the higher basicity of substrate **13s** contributes to this effect by favouring hydrogen activation. The product could be isolated either by chromatography or simply by extraction with pentane from the crude reaction mixture. Unfortunately, the product isolated was racemic, indicating that an aromatic substituent in the ketone fragment of the ketimine substrate is essential for enantioselectivity.

From these studies we concluded that a secondary *N*-alkyl substituent such as cyclohexyl or cyclopentyl is sufficiently bulky to prevent catalyst inhibition, but not so bulky as to disfavour hydrogen activation. Smaller substituents (cyclopropyl, benzyl, butyl) are not sufficiently bulky to prevent catalyst inhibition to a sufficient extent. Bulkier substituents (benzhydryl, *tert*butyl) prevent reaction by inhibiting hydrogen activation. Although the steric profile required of a substrate to be effectively hydrogenated was determined, the impact on the enantioselectivity of the process could not be fully determined.

As an alternative strategy to overcome the poor reactivity we investigated the use of **95a** as a catalyst to carry out hydrosilylation. Si-H bonds are weaker than H-H bonds and are polarised, resulting in a lower bond activation energy.^{34,228} Significantly better reactivity is observed in this transformation using weak Lewis acids due to the more facile nature of hydrogen-silicon bond cleavage. For example, borane **4f** has 85% of the Lewis acidity of **4b** B(C₆F₅)₃ but is still competent in the hydrosilylation of carbonyl substrates,²²⁹ borenium **95a** has 91% of the Lewis acidity of **4b**.

The mechanistic similarities between the two reactions (discussed in the introductory chapter) provide a good basis for analysing mechanism of enantioinduction. Furthermore, hydrosilylation is a convenient surrogate for hydrogenation and a useful transformation as specialised equipment is not required.

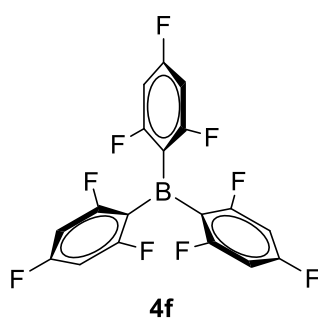
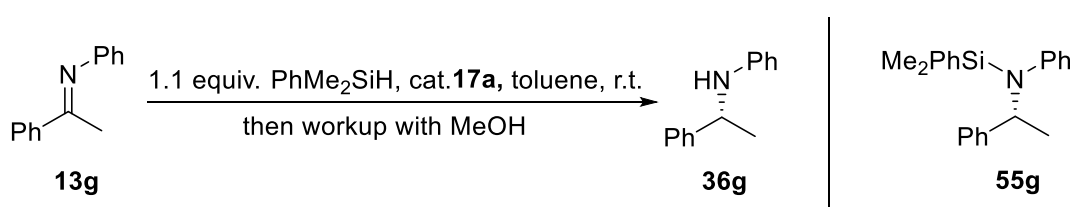


Figure 2.9 Borane **4f**.

2.3.2 Hydrosilylation

2.3.2.1 Optimisation studies for *N*-aryl ketimines

We began our investigation using the model substrate **13g** and reaction conditions reported in the literature (4 mol% catalyst **95a** loading, 1.1 equiv. PhMe₂SiH **40b**, toluene, r.t.).¹⁴⁴ Although **95a** is only sparingly soluble in toluene we were pleased to find good reactivity using PhMe₂SiH as the reducing agent (Table 2.14). Monitoring the reaction by NMR indicated the operation of two reduction pathways, as described previously by Oestreich (see section 1.4.1).¹³⁰ Conversion is reported as the sum of the two amine products found in the reaction mixture: free amine **36g** and *N*-silylamine **55g**.

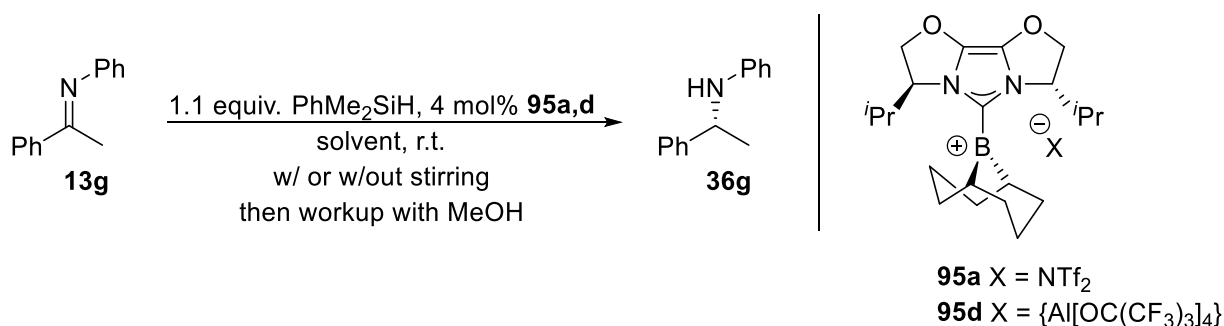


Entry	Catalyst loading	Time	% amine products (NMR)	e.r. (<i>R</i> : <i>S</i>)
1	0 mol%	194 h	0%	—
2	1 mol%	43 h	92%	66:34
3	4 mol%	23 h	93%	66:34
4	10 mol%	19 h	94%	64.5:35.5

Table 2.14. *N*-phenyl ketimine hydrosilylation: catalyst loading. Reactions carried out on a 0.375 mmol scale (0.63 M) in Young's tap NMR tubes.

This approach is used throughout this section, with data concerning the individual amounts of the two reduced products being presented in graphical format (section 2.3.2.4). A control reaction carried out in the absence of catalyst **95a** showed that no background reaction is possible between the two reagents (entry 1). Essentially identical results were obtained at catalyst loadings of 1, 4 and 10 mol%, indicating that the effective catalyst loading in solution was less or equal to 1%. The *R* enantiomer was

obtained consistently with a similar selectivity level to that found in the high-pressure hydrogenation of **13g** in toluene (64:36 *R:S*, Table 2.10).



Entry	Cat.	Setup	Solvent	Time	% amine products (NMR)	<i>e.r R:S</i>
1	95a	NMR tube	toluene	23 h	93%	66:34
2a	95a	Vial, with stirring	toluene	7 h	77%	66.5:33.5
2b	95a	Vial, with stirring	toluene	23 h	90%	66:34
3 ^a	95a	Vial, with stirring	toluene	44 h	98%	65:35
4	95d	NMR tube	toluene	23 h	79%	57:43
5a	95d	Vial, with stirring	toluene	7 h	69%	57:43
5b	95d	Vial, with stirring	toluene	23 h	86%	55:45
6	95d	NMR tube	1,2-DFB	23 h	8%	52:48

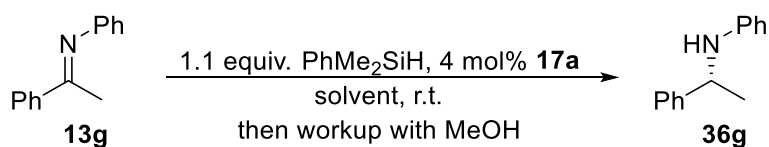
Table 2.15 *N*-phenyl ketimine hydrosilylation: setup testing. a. reaction carried out on double the scale

To further establish that catalysis is taking place in solution and that the heterogeneous nature of the reaction mixture is not having a detrimental impact on the enantioselectivity, we carried out a comparative study using **95a,d** between reactions carried out in NMR tubes without stirring and in vials with stirring (Table 2.15).

Although **95d** was also found to be insoluble in toluene (with separation of an oil phase), we were interested to test whether the less coordinating counterion would offer better reactivity in solution

and possibly better enantioselectivity. Our efforts to use toluene as solvent were motivated by the higher selectivity observed when this solvent was used in the reduction of substrate **13g**. It appeared that the less polar reaction environment results in better selectivity, as found in our hydrogenation solvent screen studies (Table 2.10). Separate vial reactions were carried out for a selection of reaction times. NMR analysis was performed following workup and conversion to free amine product. Very similar results in terms of enantioselectivity and reactivity were observed, confirming that reaction is taking place in solution. To further support this, the catalyst **95d** was tested under homogeneous conditions (entry 6). Surprisingly, no improvement in reactivity and a reduction in enantioselectivity (52:48 *R:S*) was found. Considering the lower selectivity levels obtained using the inert aluminate counterion we decided to focus our efforts at this time on the catalyst **95a**. We attempted carrying out hydrosilylation using the tosylate anion. We assumed that better solubility could be obtained due to the aromatic nature of the anion. Catalyst generation was carried out *in situ* from NHC-borane **92a** and anhydrous tosic acid in toluene to give a crystalline precipitate; no borenium signal could be detected by ¹¹B NMR. After 24 h at room temperature no reduction could be observed, suggesting that the tosylate counterion is too coordinating for any reactivity to be observed.

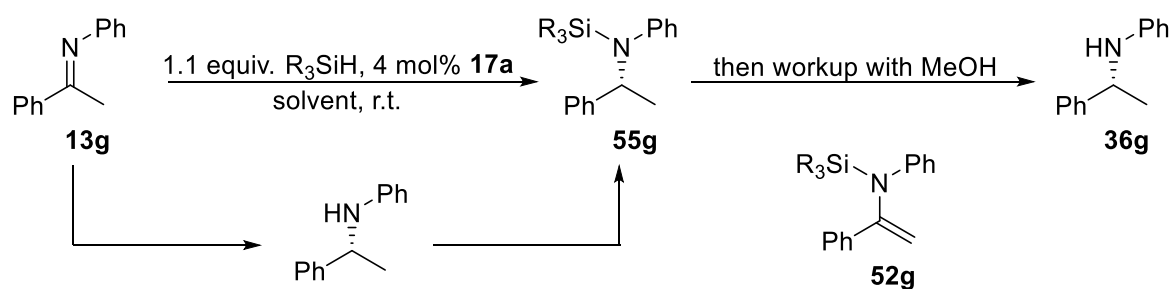
Although the reactivity displayed by **13g** under hydrosilylation conditions was superior to hydrogenation, reaction was sluggish with extended reaction times required for full conversion (entry 3, Table 2.15). We decided to screen various solvents to improve reactivity (Table 2.16). No reaction was observed in pentane, presumably due to the catalyst being completely insoluble (entry 1). Non-polar aromatic solvents afforded comparable selectivity and reactivity (entries 2-4, *R:S* 66:34). Polar halogenated solvents afforded improved reactivity but reduced selectivity (entries 5-9, *R:S* 57:43).



Entry	Solvent	Catalyst loading	Time	% amine products (NMR)	<i>e.r</i> R:S
1	Pentane	0.5 mol%	1 week	0%	–
2	Toluene	4 mol%	23 h	93%	66:34
3	Benzene	4 mol%	24 h	96%	66:34
4	C ₇ F ₈ ^a	4 mol%	45 h	86%	64:36
5	DCM	4 mol%	20 h	98%	53:47
6	1,2-DFB	4 mol%	19 h	100%	57:43
7	1,4-DFB	4 mol%	17 h	96%	59:41
8	1,2-DCB	4 mol%	19 h	100%	59:41
9	C ₆ F ₅ H	4 mol%	6 h	86%	60:40

Table 2.16 *N*-aryl ketimine hydrosilylation: solvent screening. a.perfluorotoluene

We next screened various hydrosilane reducing agents (Table 2.17). Intuitively, varying the nature of the silylium electrophile that activates the imine substrate was expected to result in changes in enantioselectivity. However, we expected the effect to be complicated due to the competitive reduction *via* protonation taking place under hydrosilylation conditions. Indeed, both pathways were found to operate, with intermediates **36g** and **52g** observed by NMR. Variation of the hydrosilane resulted in dramatic effects being observed on the reaction rate, but not on the enantioselectivity. Replacing PhMe₂SiH **40b** for the more hindered Ph₂MeSiH **40g** resulted in a dramatic reduction in reaction rate (entries 1,4 and 3,5). Replacing PhMe₂SiH for Et₃SiH **40c** resulted in a reduction in rate presumably due to both increased steric hindrance and loss of the phenyl ring (entry 6). This group presumably assists in the S_N2-Si process of Si-H bond activation by delocalising positive charge from the Si atom.

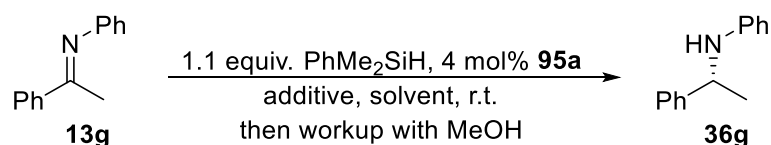


Entry	Solvent	Reducing agent	Time	% amine products (NMR)	<i>e.r</i> <i>R:S</i>
1	Toluene	$PhMe_2SiH$	23 h	93%	66:34
2	Toluene	$PhMe_2SiH$ (5 equiv.)	21 h	100%	64:36
3	1,2-DFB	$PhMe_2SiH$	19 h	100%	57:43
4	Toluene	Ph_2MeSiH	80 days	92%	66:34
5	1,2-DFB	Ph_2MeSiH	286 h	89%	59:41
6	Toluene	Et_3SiH	186 h	88%	67:33
7	Toluene	iPr_3SiH	42 h	0%	–
8	Toluene	$(EtO)_3SiH$	26 h	0%	–

Table 2.17 *N*-aryl ketimine hydrosilylation: hydrosilane screening.

Further increasing the steric bulk by using iPr_3SiH **40h** (entry 7) resulted in no reaction. Increasing the amount of reducing agent improved conversion (entry 1 and 2). It was observed that for different hydrosilanes the selectivity is controlled by the nature of the solvent: in toluene all hydrosilanes give selectivity values in the range 64:36 to 67:33 (*R:S*); in 1,2-DFB values of 57:43 to 59:41 are observed. Surprisingly, the hydrosilane $(EtO)_3SiH$ **40i** affords no reaction (entry 8). This reducing agent has been reported to afford inferior results when weaker Lewis acids are employed as catalysts; this effect possibly results from the electron-withdrawing effect of the O atoms, which destabilise the bond activation transition state.²²⁹ From these results we concluded that the silylium fragment does not appear to be playing an important role in controlling the reduction transition state.

Finally, we investigated the effect of basic or acidic additives (Table 2.18). The addition of phosphine bases has been shown to achieve a dramatic improvement in enantioselectivity, possibly by favouring a more selective reaction pathway. We wanted to test whether this effect was operating, and whether it could be achieved using other basic or acidic additives.



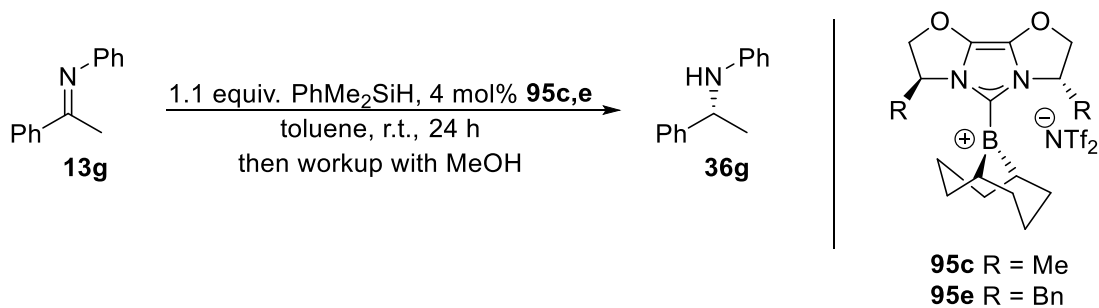
Entry	Catalyst loading	Additive	Time	% amine products (NMR)	<i>e.r R:S</i>
1	1 mol%	–	43 h	92%	66:34
2	1 mol%	1 mol% P ^t Bu ₃	192 h	27%	65:35
3	1 mol%	1 mol% PMe ₃	65 h	90%	66:34
4	4 mol%	4 mol% 2,4,6-collidine	27 h	91%	62:38
5	4 mol%	[CoH]NTf ₂ (saturated)	23 h	96%	63:37
6	4 mol%	HNTf ₂ (50% mol%)	24 h	n/a (biphasic reaction)	64:36

Table 2.18 *N*-aryl ketimine hydrosilylation: additive screening. n/a not available.

Phosphine additives caused no change in enantioselectivity (entries 2 and 3). The strongly basic P^tBu₃ significantly slows down the reaction, presumably by preventing substrate activation. The basic phosphine engages in hydrosilane activation resulting in the formation of a phosphine/silylium cation adduct, as shown by Klankermayer.¹⁴⁴ Transfer of the silylium group to the substrate is presumably rate limiting due to the poor nucleophilicity of the latter compared to the phosphine. The weakly basic PMe₃ caused no change as reported under hydrogenation conditions, again possibly due to its comparable basicity to that of the substrate. We tried using less nucleophilic 2,4,6-collidine to test whether an additive acting mostly as a Brønsted base would afford the desired effect (entry 4), but only a small reduction in selectivity was found. The conjugate acid of 2,4,6-collidine (triflimidate salt)

was employed in entry 5. Acidic additives have not been tested in the literature, to the best of our knowledge. The triflimidate salt of 2,4,6-collidine is insoluble in toluene therefore a saturated solution was used as solvent resulting in good reactivity and slightly lower selectivity being observed compared to the control (entry 5). Addition of half an equivalent of HNTf₂ (with respect to the substrate) results in slow formation of a bi-phasic reaction mixture which prevents analysis in the late stages of the reaction. Product was isolated in 69% yield (~87% purity). No change in selectivity was observed, indicating either that biasing of the reaction pathway is not possible using borenium **95a**, or that neither of the two pathways (*N*-silyliminium and protoiminium) reduction is more selective than the other.

We next investigated the substitution pattern in the NHC component to test whether it would influence reactivity and selectivity. Catalysts **95c,e** were prepared and tested by Mr Michael Howlett, an MSci student in the group. We were surprised to find that variation of the R substituent in the NHC fragment resulted in little variation in enantioselectivity, with only a slight decrease observed for the significantly less hindered **95c**.



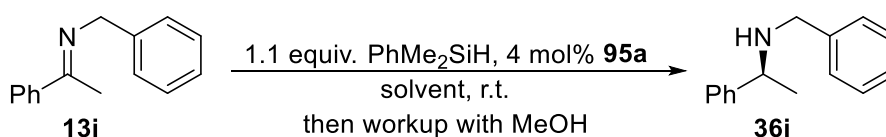
Entry	Catalyst	% amine products (NMR)	e.r. (<i>R</i> : <i>S</i>)
1	95c	71%	57:43
2	95e	100%	64.5:35.5

Table 2.19 Catalyst structure variation. Results obtained by Mr Michael Howlett.

The catalyst **95e** showed higher activity, probably due to it being soluble in toluene at the catalyst loading employed. Having investigated all variables without achieving an improvement in selectivity, we concluded that catalyst **95a** is not suitable for the reduction of *N*-aryl ketimines.

We next carried out reaction development of *N*-alkyl ketimine substrates. Ketimine **13i** was first investigated (Table 2.20). This substrate could not be hydrogenated successfully so no indication of the catalyst's selectivity in the reduction of this typical substrate was available.

2.3.2.2 Optimisation studies for *N*-alkyl ketimines



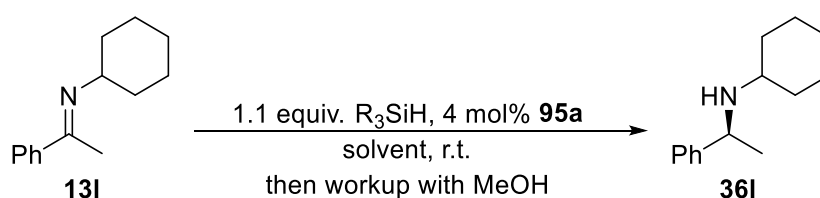
Entry	Solvent	Time	% amine products (NMR)	e.r. <i>R</i> : <i>S</i>
1	Toluene	6 h	100%	38.5:61.5
2 ^a	1,2-DFB	34 h	100%	19:81
3 ^b	DCM	2 h	97%	18:82

Table 2.20 *N*-benzyl ketimine hydrosilylation solvent effect. a. carried out as part of a screen. b. isolated yield was ~100%.

The *S* enantiomer was obtained predominantly (configuration assigned by comparison of optical rotation signs with the literature). Previously, the secondary ketimine **13i** displayed a similar preference for the *S* enantiomer when hydrogenated at low or high pressure (Table 2.11); this is in contrast to substrate **13g** which showed a preference for reduction to the *R* enantiomers under both hydrogenation and hydrosilylation conditions. Surprisingly, substrate **13i** displayed the opposite solvent effect to **13g**: a higher e.r. value was obtained using polar halogenated solvents. Interestingly, ketimine **13i** did not cause discernible catalyst inhibition (by ¹¹B NMR), unlike the aldimine **13f** (Table

2.5). The impressive reactivity observed is therefore a result of facile hydrosilane activation based on both the higher reactivity of the Si-H bond and the high basicity of the substrate.

A similar study was performed using the substrate **13i**. This substrate had previously been hydrogenated with a high selectivity (90:10 *S*:*R*).



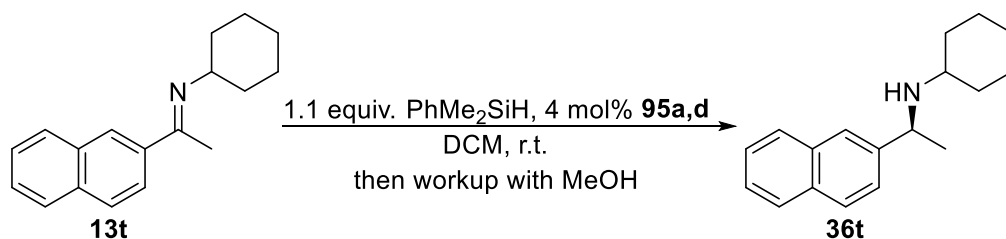
Entry	Solvent	Catalyst	Hydrosilane	Time	% amine products (NMR)	e.r. <i>R</i> : <i>S</i>
1	Toluene	95a	PhMe ₂ SiH	74 h	53%	21:79
2 ^a	Toluene	95c	PhMe ₂ SiH	96 h	65%	23.5:76.5
3 ^b	1,2-DFB	95a	PhMe ₂ SiH	145 h	100%	10:90
4	1,2-DFB	95a	Ph ₂ MeSiH	316 h	68%	10:90

Table 2.21 *N*-cyclohexyl ketimine hydrosilylation solvent effect. a. Result obtained by Mr Michael Howlett b. isolated yield was 91% (~11% (PhMe₂Si)₂O impurity).

A similar preference for the *S* enantiomer and *e.r* value (entry 3, 90:10 *S*:*R*) was observed for substrate **13i** as described previously for its hydrogenation (89:11 *S*:*R* at 90 bar, Table 2.11). The solvent effect was similar to that observed for the primary *N*-alkyl ketimine **13i** (*vide supra*). The reactivity was significantly reduced when a bulkier hydrosilane was used (entry 4). The overall poor reactivity compared to substrate **13i** is probably a result of the greater steric bulk of the cyclohexyl substituent. The less hindered catalyst **95c** provided slightly improved reactivity and comparable selectivity. A mechanistic discussion is presented later (section 2.3.2.4).

The catalysts **95c,e** were not further investigated due to their comparable activity and selectivity to **95a** and due to their more challenging synthesis. In a final attempt to improve the enantioselectivity

level the borenium cation **95d** was investigated using the newly developed reaction conditions (Table Table 2.22). The substrate **13t** featuring a bulkier 2-naphthyl substituent on the C atom of the double bond was included to further test the robustness of our findings and investigate the role this substituent plays in determining enantioselectivity.



Entry	Substrate	Catalyst	Time	% amine products (NMR)	e.r. <i>R</i> : <i>S</i>
1 ^a	13t	95a	31 h	77%	7:93
2 ^b	13t	95d	43 h	78%	4:96
3 ^c	13l	95d	43 h	70%	5:95

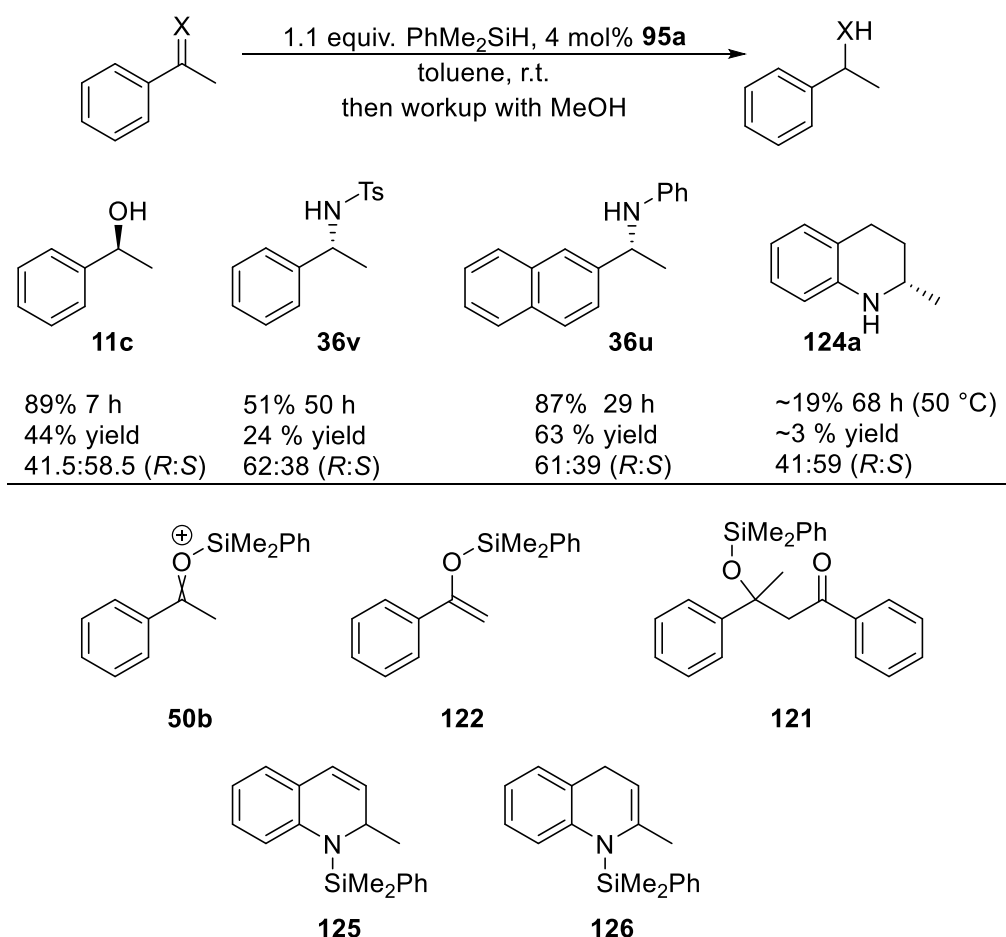
Table 2.22 *N*-cyclohexyl ketimine counterion effect. a. 75% yield, b. 60% yield, c. 60% yield.

Both ketimine substrates **13l,t** were reduced with higher levels of selectivity (*S*:*R* 95:5 and 96:4, respectively) in the presence of the {Al[OC(CF₃)₃]₄} counterion. This trend is opposite to that observed using the *N*-aryl ketimine **13g** (Table 2.15). The reactivity and selectivity found for the two substrates were similar.

In conclusion, two sets of reaction conditions have been developed for hydrosilylation. The reduction of *N*-aryl ketimines is best conducted in a non-polar solvent in the presence of a weakly coordinating anion. The reduction of *N*-alkyl ketimines is best conducted in a polar solvent in the presence of a non-coordinating anion. The nature of these effects is discussed in section 2.4. Using these reaction conditions screening of various substrates was carried out (section 2.3.2.3).

2.3.2.3 Substrate scope

As acetophenone **12c** could not be hydrogenated, we decided to test its hydrosilylation to measure reduction selectivity (Scheme 2.15).



Scheme 2.15 Hydrosilylation substrate scope exploration. Enantiomers assigned based on comparison of optical rotation or HPLC retention times with the literature.²³⁰ Percentage values refer to conversion expressed as percentage of reduced product(s) in the reaction mixture. Yields refer to isolated yields of the depicted product.

The reduction of acetophenone was accompanied by the formation of condensation product **121** (6%, isolated and characterised by ¹H and ¹³C NMR), enoether **122** (5%) and hydrogen gas (confirmed by NMR). Evolution of hydrogen gas rapidly occurs for approximately 5 minutes from reaction mixing. Hydrogen gas is evolved by reaction of borohydride **92a** with silyloxonium **50b**, which is converted to

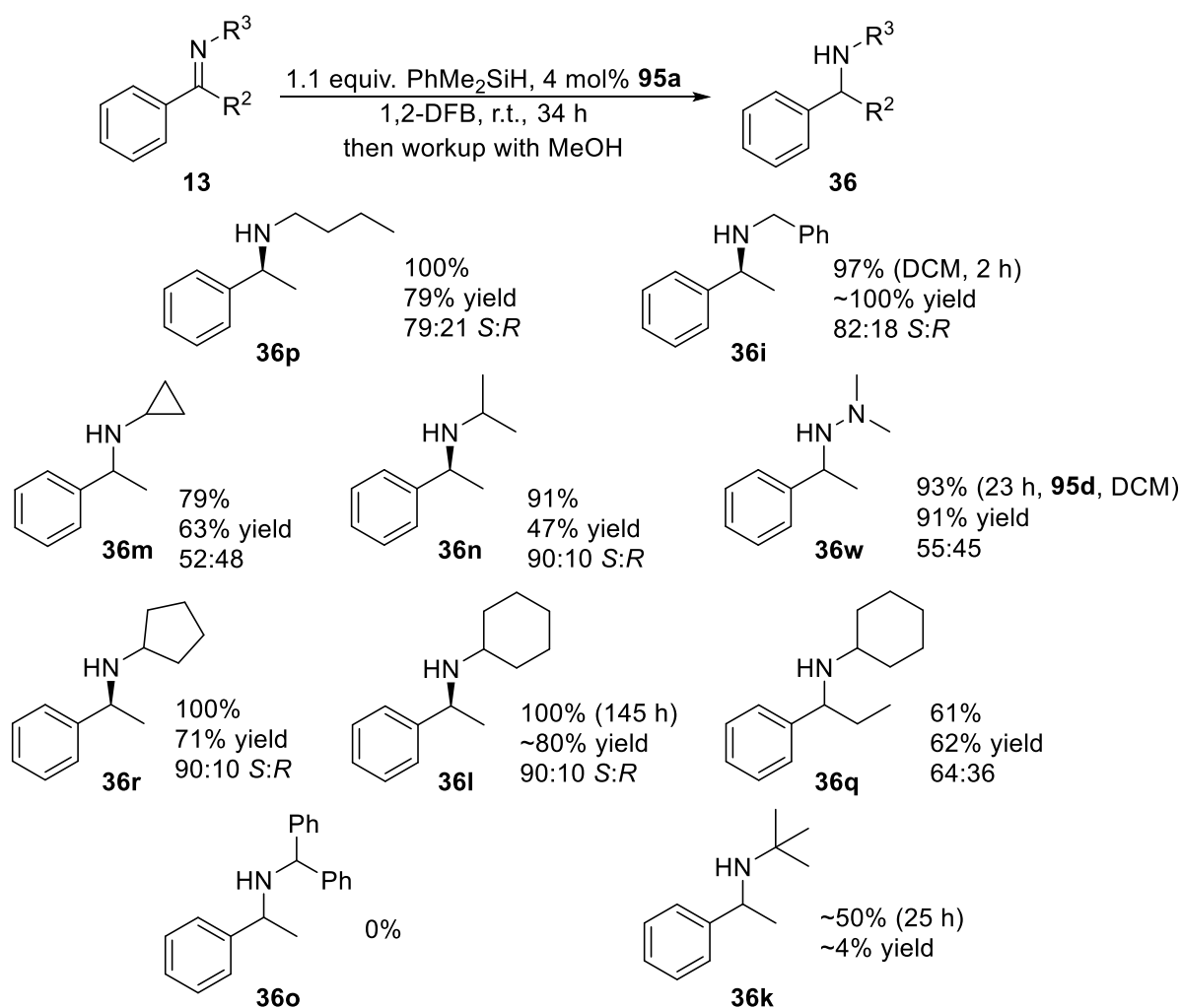
122. Such reactivity has been exploited by Oestreich for the preparation of silyl enol ethers from carbonyl compounds.²³¹ Product **121** is also rapidly formed at the beginning of the reaction, presumably by condensation of **50b** with **122**. Enolether **122** was prepared independently but could not be hydrogenated (4 mol% **95a**, toluene, 4 bar H₂, r.t.) indicating that under hydrosilylation conditions **122** is a by-product and not an off-cycle species. These results are consistent with the need for a strong auxiliary base in the hydrogenation of silyl enol ethers.^{40,151}

The reduction of quinaldine **123a** to **124a** proceeds with significant decomposition, presumably due to the lack of a proton source required for the reduction of intermediates **125** and **126**. The reactivity and selectivity observed for reduction of **13u** to **36u** are comparable to the related substrate **13g**, this trend being consistent with that found for *N*-alkyl derivatives **13l** and **13t**. The poor reactivity of **13v** is presumably due to its poor basicity, this effect having been reported previously (see section 1.3.2 for the reduction of non-basic **13b** reported by Stephan). The presence of the sulfone group appears to influence the selectivity only to a minor extent.

The reduction of *N*-alkyl ketimines afforded more positive results (Scheme 2.16). A similar selection of substrates was used to that employed previously for hydrogenation. Additionally, we employed hydrazone substrate **13w** to further probe the mechanism by which the *N*-substituent is controlling selectivity.

Primary *N*-alkyl ketimines **13i,p** were reduced successfully (~100% conversion). This stands in contrast to the results obtained for hydrogenation where both substrates afforded low conversion values (~10%, Table 2.11). The enantioselectivity levels were similar for the two substrates (79:21-81:18 *S*:*R*), and slightly lower than those observed for secondary *N*-alkyl ketimines (**13r** and **13l** 90:10 *S*:*R*). The similarity between these two substrates indicates that the control on the reduction enantioselectivity is steric in nature: the phenyl ring in the benzyl fragment of **13i** does not appear to be involved in secondary interactions controlling the reduction transition state. The secondary substrates **13m,n** afforded good conversion (79 and 91%, respectively). Previously, **13m** was hydrogenated with low

conversion (14%, Table 2.11). Product **36m** was obtained in almost racemic form after hydrosilylation (52:48). In contrast, product **36n** was obtained with a high enantiomeric purity (90:10 *S*:*R*), equal to that of cyclic secondary *N*-alkyl amines **36l,r**. These results indicate that the geometry at the carbon atom bonded to nitrogen in the alkyl substituent is important in controlling selectivity. The poor selectivity observed for cyclopropyl-substituted **13m** could be due to the small bond angle or due to the different conformational preference of this substrate, as discussed previously (Table 2.11).²²⁷



Scheme 2.16 *N*-alkyl ketimine hydrosilylation substrate scope. Percentage values refer to conversion expressed as percentage of reduced product(s) in the reaction mixture. Yields refer to isolated yields of the depicted product.

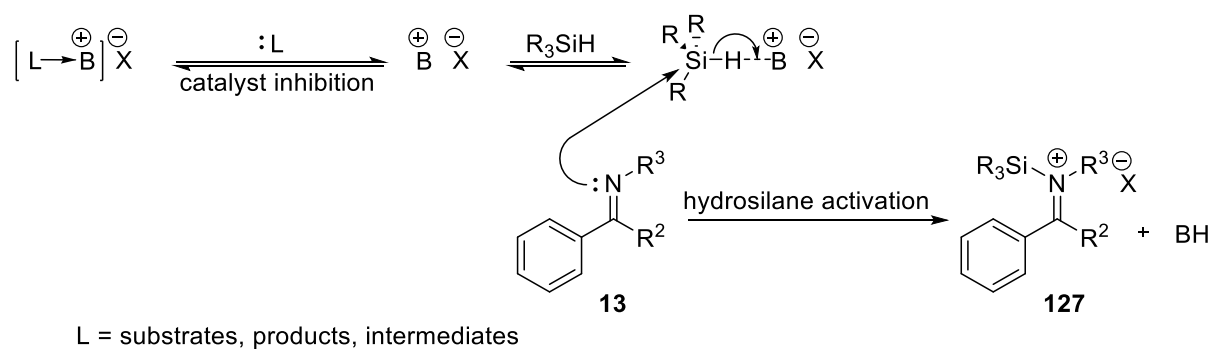
To further test the importance of geometry at the *N*-substituent we employed hydrazone **13w**. Hydrazones and oximes have been reduced successfully using FLP methodology previously.^{232,233} Enantioselective reduction of hydrazones would represent an opportunity to access enantioenriched primary amines through subsequent reduction of the N-N bond. Substrate **13w** displayed good reactivity allowing for the hydrazine **36w** to be isolated in good yield. Analysis of its *N*-acetyl derivative indicated however that essentially racemic material was obtained. It is possible that the poor selectivity results from a different conformational preference, as discussed with substrate **13m**.²²⁷ Substrates **13l,r,q** afforded amine products with enantioselectivity levels similar to those found in hydrogenation (90:10 *S*:*R* **13l,r**, 64:36 **13q**). Substrate **13o** was not reduced, in agreement with hydrogenation results. Substrate **13k** afforded improved reactivity compared to hydrogenation, however reaction proceeded with significant decomposition and only a very small amount of product could be isolated following chromatography.

These results suggest that the rate of reaction is not limited by catalyst inhibition, but by the rate of hydrosilane activation and iminium ion reduction: secondary substrate **13n** is less reactive than primary **13p**; **13l** featuring a larger ring is less reactive than **13r**; **13q** featuring an extended ketone fragment chain is less reactive than **13l**.

The successful enantioselective reduction of *N*-alkyl ketimines represents an advancement in the FLP field. Previously, only non-hindered primary *N*-alkyl ketimines could be hydrogenated enantioselectively using the ansa-ammonium borate **63** reported by Repo.¹⁴⁷ To the best of our knowledge enantioselective hydrosilylation of *N*-alkyl ketimines with FLP methodology has not been reported.

2.3.2.4 Mechanistic analysis

The first factor to consider in rationalising the observed hydrosilylation reaction rates for *N*-aryl and *N*-alkyl ketimines is whether catalyst inhibition is occurring.

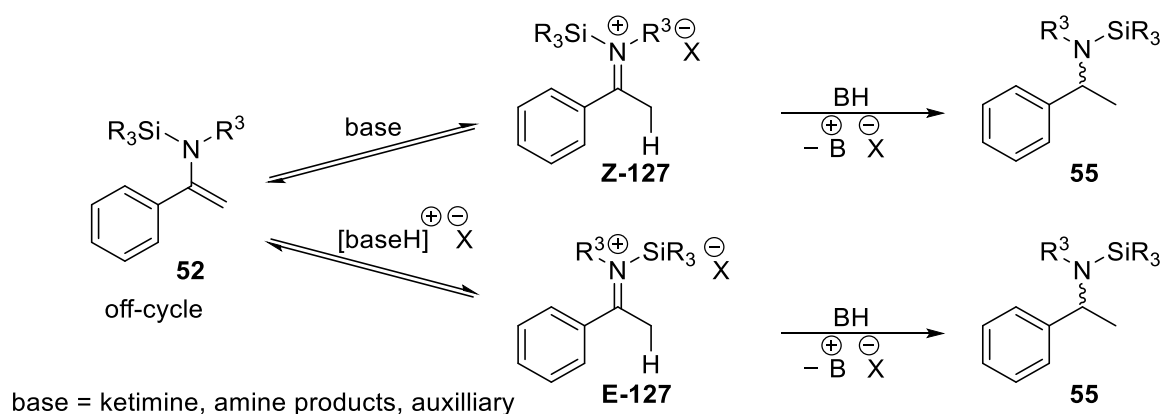


Scheme 2.17 Catalyst inhibition and bond activation in hydrosilylation.

^{11}B NMR analysis of reaction mixtures (at the beginning of reaction) has not indicated formation of a tetrahedral adduct of the catalyst with any of the substrates: acetophenone **12c**, quinaldine **123**, **13g,k,i,l,t,u,v,w**. Since formation of such adducts could not be detected during the progress of the reaction, we assume that none of the reduced products (free amines or *N*-silylamines and silylethers) are causing catalyst inhibition. Since the most non-hindered substrate acetophenone does not cause inhibition, it results that any additional steric hindrance will result in effective protection of the borenium cation from inhibition. The only exception is the inhibition observed with aldimine substrate **13f**, possibly due to its combination of high basicity and low steric hindrance.

Hydrosilane activation is subject to both electronic and steric influence. The presence of groups on the silane component that can stabilise charge build-up on the silicon atom during hydride displacement (an $\text{S}_{\text{N}}2$ type process) will accelerate reaction. This explains the improved reactivity observed with PhMe_2SiH compared to Et_3SiH (Table 2.17). Since three components are involved in the bond-cleavage event (substrate, hydrosilane and borenium cation) the rate of reaction will depend on their combined steric profiles. The borenium ion/hydrosilane interaction can be analysed using the different reactivity found with PhMe_2SiH vs Ph_2MeSiH , and Et_3SiH vs $^i\text{Pr}_3\text{SiH}$. The substrate/hydrosilane

interaction is visible in the improved reactivity detected in the hydrosilylation of primary *N*-alkyl ketimines, as opposed to bulkier secondary *N*-alkyl ketimines and less basic *N*-aryl and *N*-tosyl ketimines.



Scheme 2.18 *N*-silyliminium ion isomerisation and reduction.

The *N*-silyliminium ion **127** (which unlike **53** requires an external reducing agent to react) formed from hydrosilane activation can be reduced using the NHC-borane formed, to give *N*-silylamine **55**. It can alternatively be converted by deprotonation to *N*-silylenamine **52**, an off-cycle intermediate. This mechanism allows for fast geometric isomerisation of **127**. NMR monitoring has allowed detection of intermediates **52** using the distinctive vinylic proton signals in the 4-6 ppm range. Additionally, concentrations of substrates **13**, free amine **36**, and *N*-silylamine products **55** were monitored by ¹H NMR spectroscopy, analysis performed with the aid of a capillary insert containing a reference solution of 1,3,5-trimethoxybenzene solution in C₆D₆ (0.1 M). The insert was calibrated against a solution of 1,4-dinitrobenzene and was added for each reaction to the NMR tube prior to hydrosilane addition. Analysis was carried out at specified time points.

The hydrosilylation of *N*-tosyl ketimine **13v** is a notable example illustrating a limit on a spectrum of reactivity. The substrate, product, and any intermediates are very poorly Brønsted basic due to the strongly electron withdrawing nature of the sulfone functionality. In the absence of basic components in the reaction mixture only very low levels of **52v** are present during the reaction (Figure 2.10). The

reduction of this substrate therefore occurs almost entirely *via* **127v** (and not **116v**, *vide infra*). The hydrosilylation of acetophenone described previously represents an extreme case of this behaviour: the high acidity of **50b** results in hydrogen formation in combination with hydride **92a**.

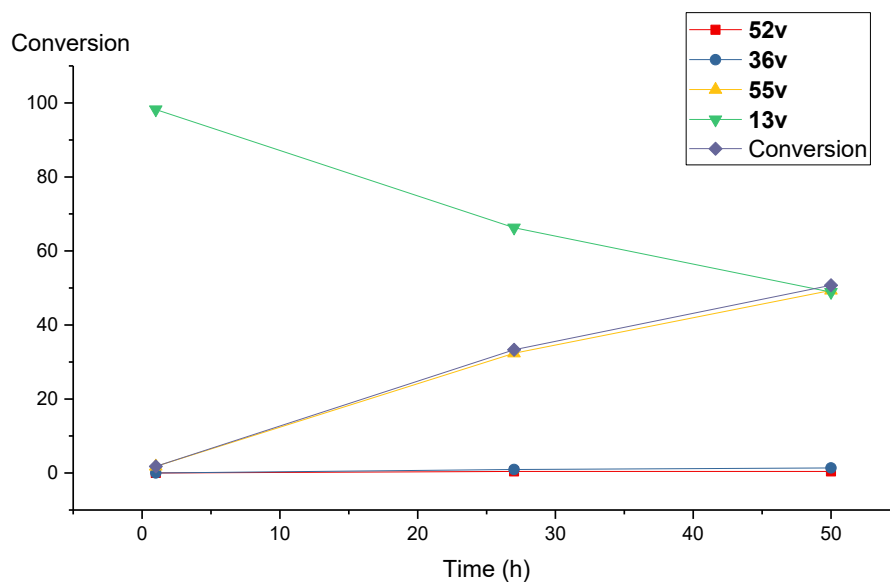
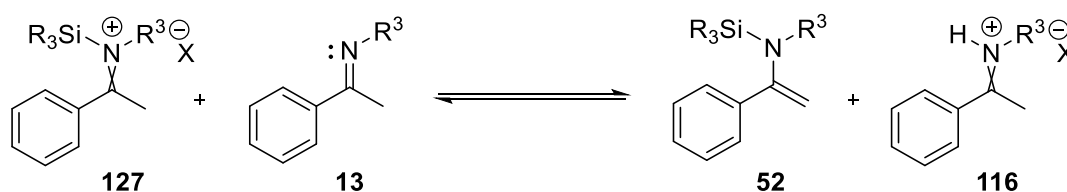


Figure 2.10 Hydrosilylation of substrate **13v**, 4 mol% **95a**, 1.1 equiv. PhMe₂SiH, toluene.

The major component that can act as a Brønsted base is the ketimine substrate, particularly at the beginning of the reaction. Protonation of **13** results in formation of iminium ion **116**, which can also undergo *E/Z* isomerisation and reduction by NHC-borane. The extent to which reduction occurs *via* **127** or **116** depends on the reactivity of **127**: if reduction is slow then deprotonation to form the less hindered and more reactive **116** represents a viable reaction alternative. The pathway for reduction has implications for the observed enantioselectivity, as discussed previously (section 1.4.1).



Scheme 2.19 *N*-silyliminium ion deprotonation equilibrium.

The reaction profile typical of *N*-aryl ketimine reduction is shown in Figure 2.11.

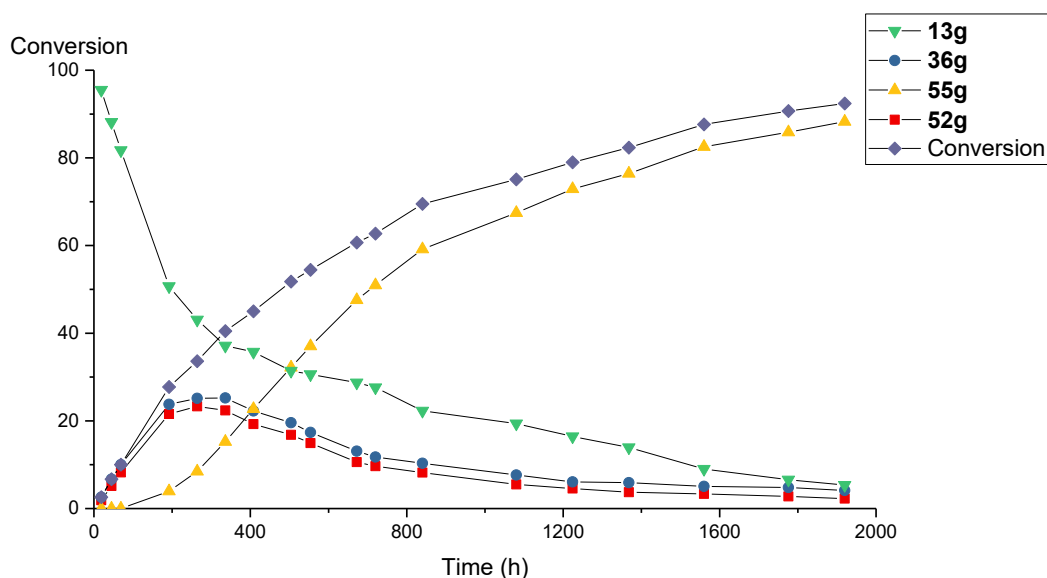
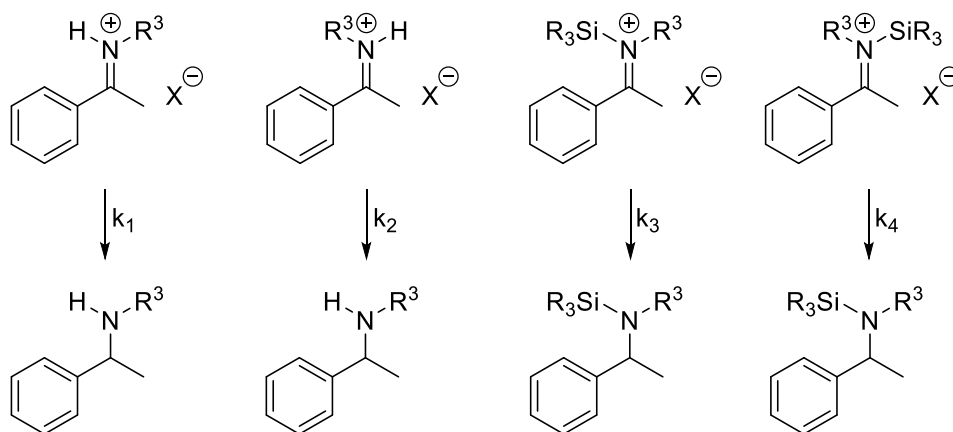


Figure 2.11 Hydrosilylation of substrate **13g**, 4 mol% **95a**, 1.1 equiv. Ph_2MeSiH , toluene. Reproduced from Ref. 165 with permission from The Royal Society of Chemistry.

As reported by Ostreich and co-workers¹³⁰ the free amine **36g** and the intermediate **52g** are present in equal amounts during the reaction, their concentration reaching a maximum of approximately 25%. The substrate is consumed gradually during the reaction. This profile is consistent with the reaction taking place *via* both pathways in parallel. The option of reaction occurring entirely *via* reduction of **116g** can be discounted: such a reaction could not progress past 50% conversion since two molecules of substrate get converted to only molecule of **36g**. It results that by the end of the reaction both pathways will have had to operate at some point. The fundamental rate constants for the reduction of *E/Z* *N*-silyliminium (k_3 , k_4) or *E/Z* protoiminium (k_1 , k_2) ions are determined by the nature of the substrate, the catalyst, and the hydrosilane used for the former (Scheme 2.20). The extent to which these pathways operate is dependent on the concentration of the reactive iminium ions, which in turn is dependent on the concentration of all other species in the reaction mixture. The observed product enantiopurity is therefore expected to change with reaction progress. Monitoring detectable reaction intermediates allows for a qualitative estimate of the pathway operation to be extracted.



Scheme 2.20 Fundamental reduction steps.

Use of a less bulky hydrosilane (PhMe₂SiH, profile not shown) or a more polar reaction solvent (1,2-DFB, Figure 2.12) resulted in a similar profile for the reduction of **13g** to be observed. The characteristic gradual consumption of starting material was observed. Less build-up of intermediates was observed, with their maximum concentrations being estimated to below 15% (cf. Figure 2.11, ~25%).

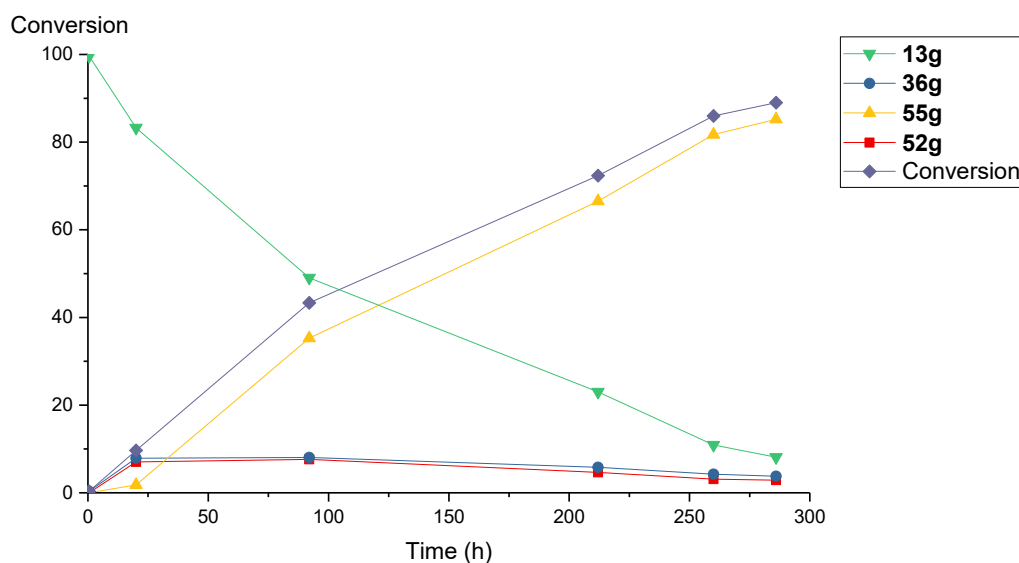
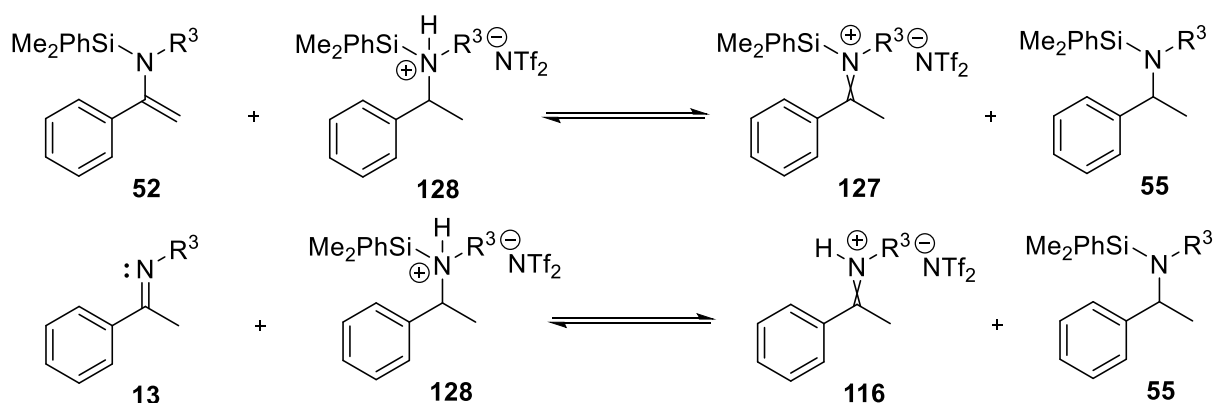


Figure 2.12 Hydrosilylation of substrate **13g**, 4 mol% **95a**, 1.1 equiv. Ph₂MeSiH, 1,2-DFB. Reproduced from Ref. 165 with permission from The Royal Society of Chemistry.

Use of a less hindered hydrosilane will result in the formation of a less sterically hindered silyliminium ion **127g**. This will result in an increased rate of direct reduction, as opposed to deprotonation.

Although the polarity of the solvent is not necessarily expected to increase the rate of iminium reduction, it will favour the rate of free amine **36g** silylation. Since this process is coupled with protonation of the off-cycle enamine **52g**, it is expected that the higher solvent polarity will cause more rapid consumption of intermediates. The overall slow rate of substrate and intermediate consumption observed for **13g** possibly results from the competitive protonation of silylamine product **55g** (Scheme 2.21). As reaction proceeds, accumulation of **55g** will result in the equilibria being shifted towards the left-hand side involving formation of ammonium salts **128**. This effect can be seen as a type of inhibition caused by the Brønsted basicity of the silylamine product. A similar observation was reported by Stephan *et al.* for the metal-free hydrogenation of aniline derivatives to cyclohexylammonium salts, reaction which requires stoichiometric Lewis acid **4b**.⁷³ Although there is no inhibition caused by the products acting as Lewis bases, the low acidity of the cyclohexylammonium salts prevents substrate protonation and leaves the catalyst sequestered as the hydridoborate salt.



Scheme 2.21 Substrate and intermediate protonation equilibria.

Monitoring the hydrosilylation of the basic, sterically hindered **13l** resulted in different reaction profiles being observed. When the reaction was carried out in toluene, no silylamine **55l** formation was observed (Figure 2.13), with starting material being completely converted to intermediates **52l** and **36l**. This effect is presumably caused by the increased steric hindrance and basicity of substrate **13l**. The silyliminium **127l** is very sterically hindered, therefore complete deprotonation by the basic **13l** occurs preferentially to reduction. The less hindered **116l** is then reduced to free amine **36l**. The

reaction stalls at ~50% conversion. Extending the reaction time to 74 h achieves only 53% conversion. (Table 2.21).

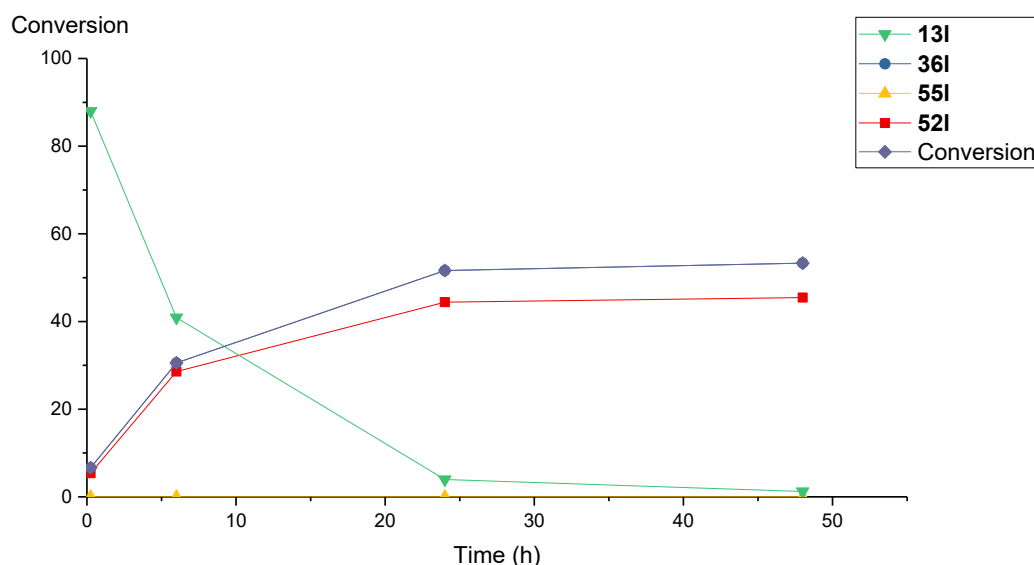
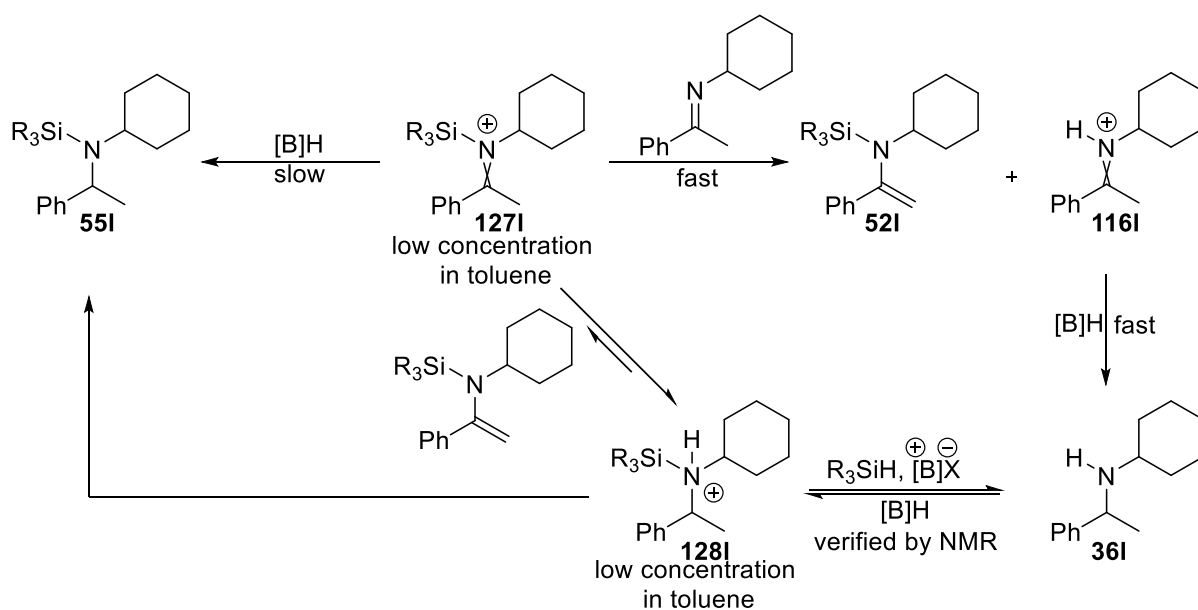


Figure 2.13 Hydrosilylation of substrate **13I**, 4 mol% **95a**, 1.1 equiv. PhMe₂SiH, toluene. Reproduced from Ref. 165 with permission from The Royal Society of Chemistry.

This effect appears to be steric in nature, as indicated by two observations: with the less hindered **95c** reaction proceeds slowly after the halfway point (Table 2.21); when the very bulky substrate **13k** is reduced reaction takes a similar course with only **36k** and **52k** being detected. We postulated the inability to convert intermediates to final products could be due to the silylation of amine **36I** not occurring. A control experiment carried out using a mixture of **95a**, PhMe₂SiH, and amine **36I** (1:1:2) indicated that this process is an equilibrium: trace formation of **55I** was observed by ¹H NMR, together with **92a** detected by ¹¹B NMR. This result suggests that reaction should be possible in toluene since formation of the silylammonium salt **128I** is required for the *N*-silylenamine **52I** to be re-introduced in the catalytic cycle. Nonetheless, the equilibria described previously (Scheme 2.21) are expected to cause inhibition: the greater basicity of the amine products **36I** and **55I** could result in a low concentration of the poorly reactive **127I** preventing reaction.



Scheme 2.22 Proposed explanation for the reaction profile observed for substrate **13I**.

Much improved reactivity was observed in 1,2-DFB (Figure 2.14), with reaction proceeding to completion. The product **55I** could be isolated by extraction from the reaction mixture and was characterised by 1D and 2D NMR.

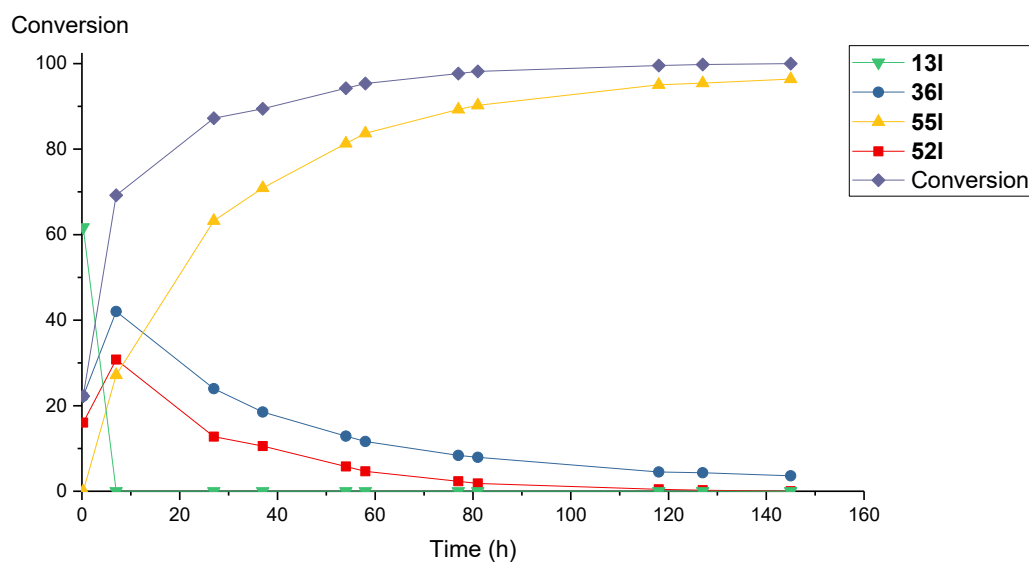


Figure 2.14 Hydro-silylation of substrate **13I**, 4 mol% **95a**, 1.1 equiv. PhMe₂SiH, 1,2-DFB. Reproduced from Ref. 165 with permission from The Royal Society of Chemistry.

The reaction was found to take place in essentially two stages. The first stage (up to 7 h) is described by reactivity similar to that observed in toluene: predominant conversion of starting material to intermediates **52i** and **36i**. Partial conversion of intermediates to final product **55i** begins to take place during this time which explains the concentration of intermediates less than 50%. Such a process also takes place at a much lower rate when the reaction is carried out using the bulkier Ph₂MeSiH (Figure 2.15). Notable is also the rather significant difference in concentration between **52i** and **36i**. This is possibly a result of the greater basicity of reaction components derived from **13i** (compared to the *N*-aryl substituted **13g**, see Figure 2.11), but the source of this effect is not apparent.

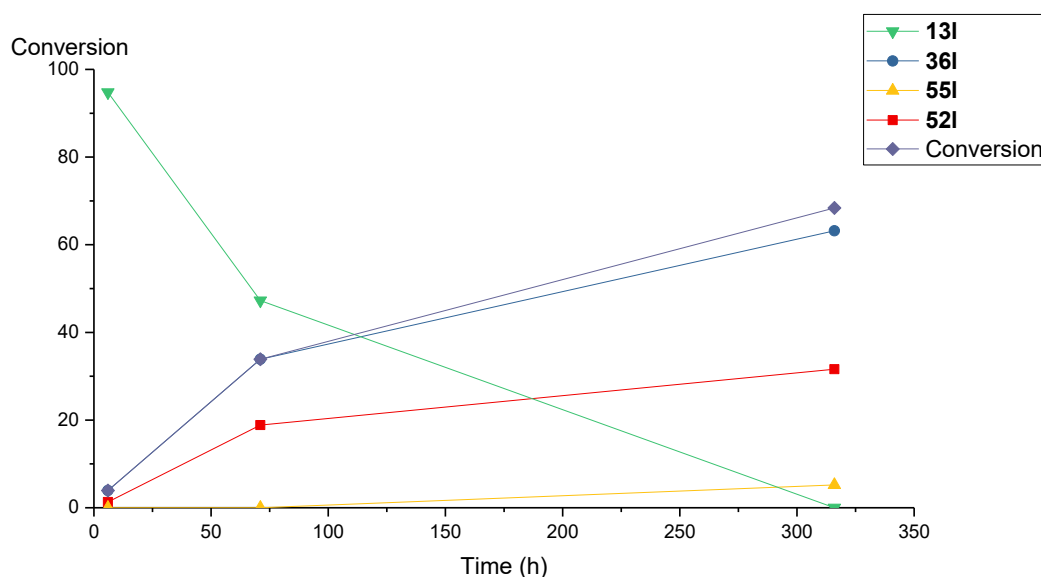


Figure 2.15 Hydrosilylation of substrate **13i**, 4 mol% **95a**, 1.1 equiv. Ph₂MeSiH, 1,2-DFB. Reproduced from Ref. 165 with permission from The Royal Society of Chemistry.

Conversion of intermediates to final product is slow and is most likely limited by the rate of reduction of **127i**. This unique behaviour (almost complete separation of pathways) observed for **13i** results from the poor reactivity of **127i** and the high basicity of **13i**. Further evidence that the effect is steric in nature comes from analysing the reactivity of unhindered, basic *N*-benzyl ketimine **13i** (Figure 2.16). The overall higher reactivity is a result of rapid hydrosilane activation and rapid reduction of **127i**. Deprotonation of **127i** is competitive due to the high basicity of **13i**.

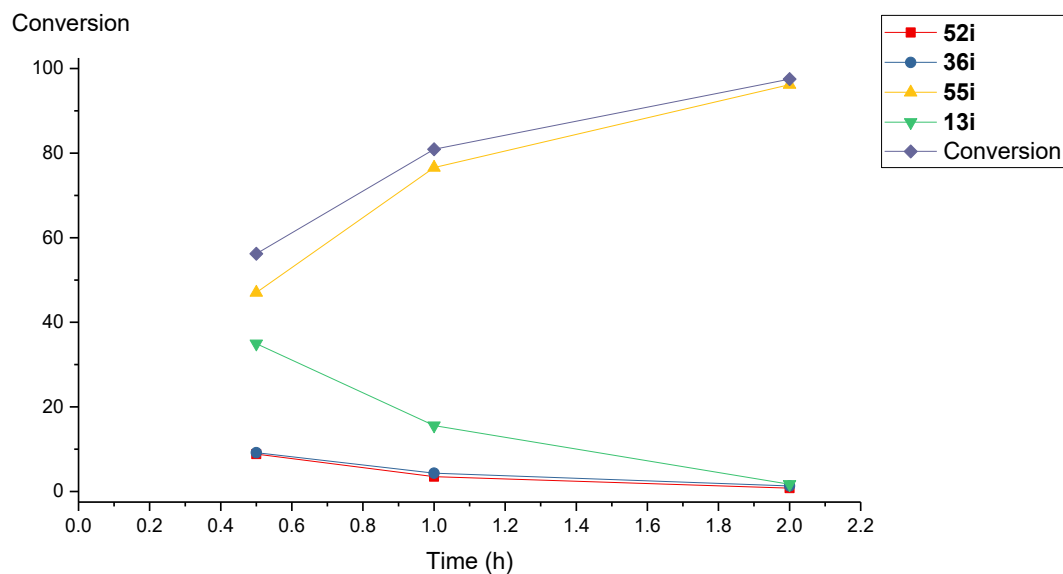


Figure 2.16 Hydrosilylation of substrate **13i**, 4 mol% **95a**, 1.1 equiv. PhMe₂SiH, DCM.

The observed enantioselectivity values (e.r.) are generally lower than the *E/Z* ratios of ketimine substrates (Table 2.23).

Substrate 13	Ketimine d.r.	Amine product e.r.
13i	14.3:1	4.2:1
13l	20:1	8.9:1
13m	16.7:1	1:1
13n	7.7:1	9:1
13p	18.2:1	3.8:1
13q	2:1	1.8:1
13r	16.7:1	9:1
13w	14.6:1	1:1
13t	12.5:1	13.3:1

Table 2.23 Product e.r values/substrate d.r. value comparison for hydrosilylation of *N*-alkyl ketimines.

Substrate **13q** is an exception (e.r 64:36; *E/Z* ratio 2:1). Since both silyliminium **127q** formation and its reduction are slow compared to the rate of *E/Z* isomerisation in **13q**, it is expected the selectivity to be determined by reduction of the most reactive isomer of **127q**. The hydride **92a** could be observed by ¹¹B NMR in the hydrosilylation of *N*-alkyl ketimines, supporting that iminium ion reduction is slow.

2.4 Enantioselectivity analysis

The enantioselectivity levels observed for various substrates were found to be similar in the two related processes, hydrogenation and hydrosilylation, when the same solvent was used (Table 2.24).

Substrate	Reaction			
	Hydrogenation		Hydrosilylation	
	Toluene	1,2-DFB	Toluene	1,2-DFB
13g	64:36	59:41	65:35	57:43
13l	n/a	11:89	21:79	10:90
13q^a	n/a	65:35	n/a	64:36
13r	n/a	10:90	n/a	10:90

Table 2.24 Hydrogenation/hydrosilylation *e.r* values reported as (*R:S*). a. enantiomers not assigned.

Since it is recognised that reduction of a protoiminium ion **116** can take place under hydrosilylation conditions, and that it is this sole reaction pathway that can operate under hydrogenation conditions, two hypotheses can be raised to explain the observed enantioselectivity effect. The first would be that hydrosilylation is taking place entirely *via* reduction of the protoiminium ion **116**. This can be discounted based on the reaction analysis presented previously. The second hypothesis states that both reduction of protoiminium ion **116** and silyliminium ion **127** is taking place with similar enantioselectivity levels. We believe this to be the case. The similar enantioselectivity levels obtained in the reduction of **13g** with various hydrosilanes (Table 2.17) further supports this hypothesis: the variation in structure of ion **127** resulting from changing the silyl fragment will presumably have a similar (apparently negligible) effect to that brought about by replacing the silyl fragment with a

proton. We also believe that the lack of a phosphine effect (see section 1.5) observed in the hydrosilylation of **13g** (Table 2.18) is possibly caused by this similarity in selectivity. In their report of a phosphine effect in hydrosilylation, Klankermayer and co-workers suggested that the additional base is shifting the mechanism towards the more selective reduction of protoiminium species.¹⁴⁴

The solvent effect observed in the hydrosilylation catalysed by **95a** is graphically represented in Figure 2.17.

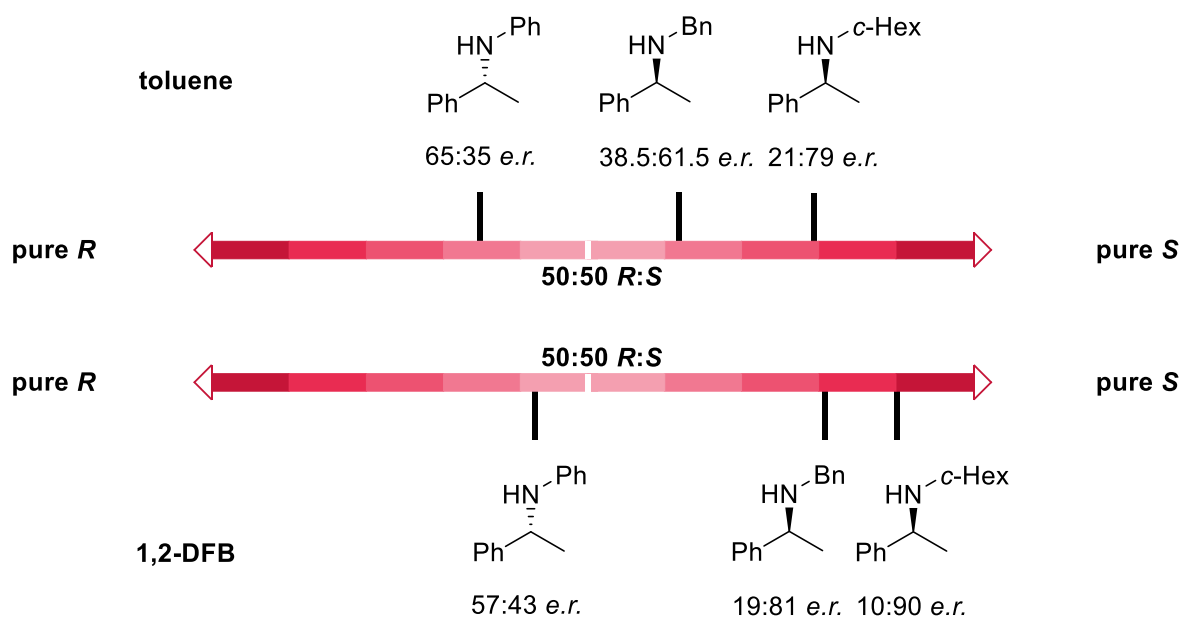


Figure 2.17 Graphical representation of enantioselectivity solvent effect.

The cause for the different behaviour observed between *N*-aryl and *N*-alkyl ketimines stems from the different intrinsic selectivity of the two substrates classes: the former preferentially produces the *R* enantiomer with low selectivity whereas the latter produces the *S* enantiomer with greater enantioinduction. The solvent effect is consistent as switching from toluene to 1,2-DFB results in all cases in an increased preference for formation of the *S* enantiomer. For **13g** this translates to an apparent reduction in enantioselectivity.

The enantioselectivity levels observed in the hydrosilylation of *N*-aryl and *N*-alkyl ketimines with different counterions is presented in Figure 2.18. As shown in Scheme 2.20 the counterion is involved

in the enantiodetermining reduction steps: an iminium ion is consumed and the borenium ion catalyst is regenerated. The effect found on switching from NTf_2 to $\{\text{Al}[\text{OC}(\text{CF}_3)_3]_4\}$ is consistent with a slightly increased preference for the *S* enantiomer observed with the weakly coordinating aluminate counterion.

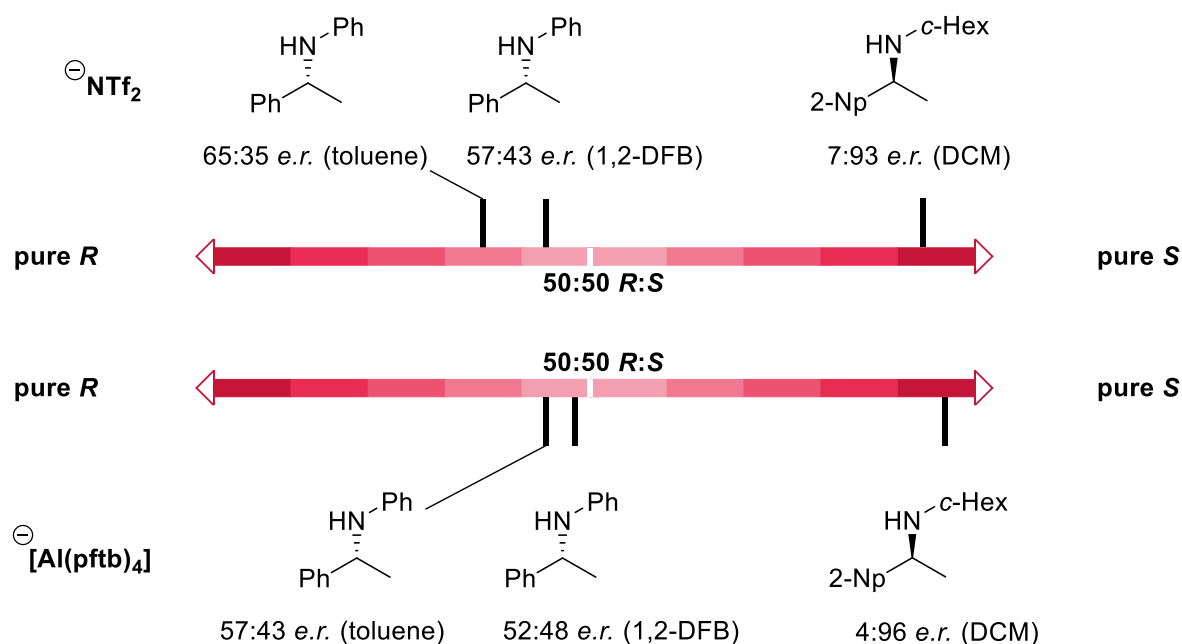
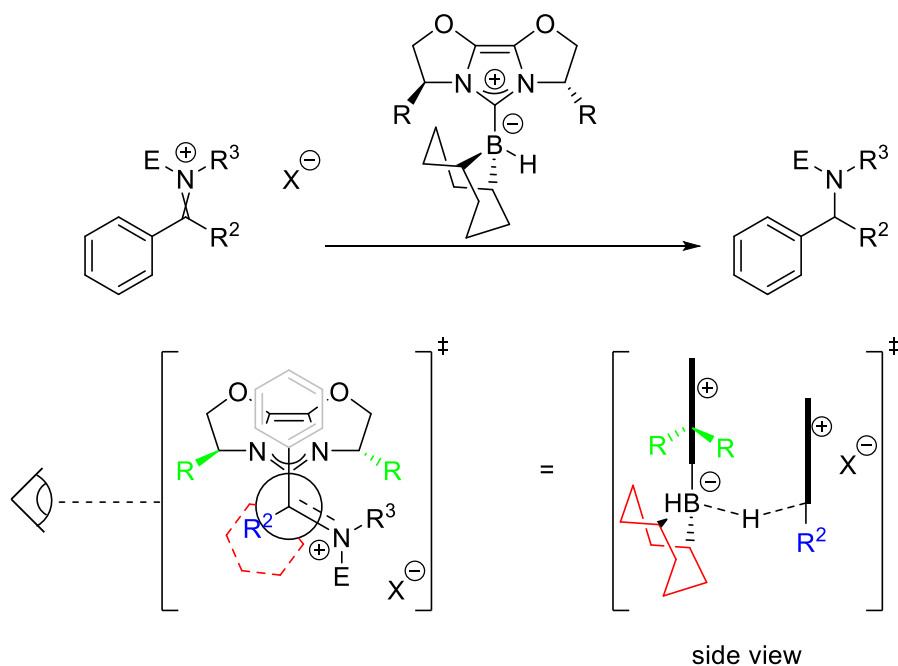


Figure 2.18 Graphical representation of enantioselectivity counterion effect.

All these results indicate that the enantioselectivity of reduction catalysed by **95** is a result of interaction between iminium ion **127/116** and reducing agent **92**, the solvent modulating this interaction.

One suggested transition state is depicted in Scheme 2.23. The aryl ring in the ketone fragment possibly stacks with the imidazolium fragment. The large secondary *N*-alkyl substituent (R^3) controls the transition state by facing away from the *R* substituent of the imidazolium fragment. The substitution pattern in the *R* group has a lesser impact since these fragments can point away from R^3 . The electrophile and alkyl chain of the ketone-derived fragment (R^2) are pointing towards a fairly open region of space where the rigid 9-BBN framework is tilted away. Increasing the length of this alkyl chain results in a detrimental effect.



Scheme 2.23 Proposed reduction transition state.

2.5 Conclusion and future work

Chiral IBiox-stabilised borenium ions have been prepared, isolated, and characterised. Their reactivity in hydrogenation and hydrosilylation was explored and shown to be consistent with that expected of neutral Lewis acids employed in such transformations (solvent effect, phosphine effect). Differences arising from the ionic nature of borenium ion catalysts are minor and manifest themselves in the reduction step where the counterion accompanies the iminium ion which is being reduced by a neutral NHC-borane. The particular suitability of these borenium ions as catalysts for the reduction of secondary *N*-alkyl ketimines apparently results from their molecular complementarity with such substrates, and not due to variations in reaction mechanism. The study presented herein will hopefully be of value for future catalyst development efforts by highlighting the importance of both catalyst design and of mechanistic analysis.

Use of computational modelling for the iminium reduction steps could help identify the relevant catalyst/substrate interactions. With this knowledge, judicious variation of catalyst structure could be

carried out to improve reactivity and selectivity. The reactivity would be most likely improved by an increase in Lewis acidity. Preparation of more catalytically competent, more Lewis acidic, chiral MIC (mesoionic carbene)-stabilised borenium ions represents one option. To the best of our knowledge only three examples of chiral MICs have been reported (Figure 2.19).^{234–236} Although these scaffolds are not suitable for the construction of borenium cations due to the presence of donor atoms in **129** and **130** and the need to resolve axially chiral **131** (by equilibration to the more stable diastereomer of the bis-silver complex), it is possible that functional group modification will allow for their use in the future.

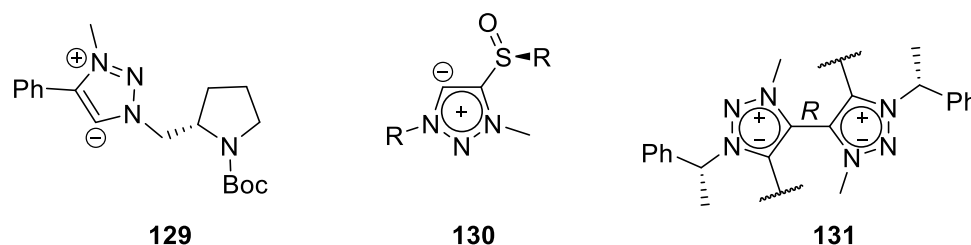
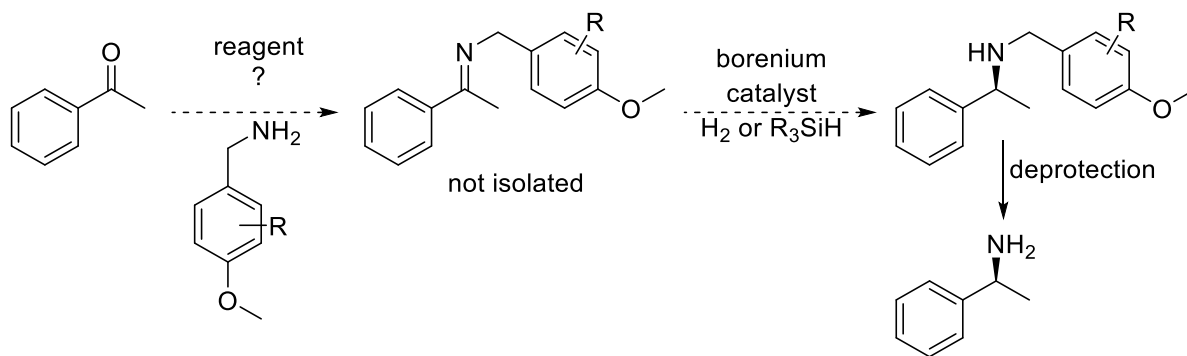


Figure 2.19 Examples of chiral MICs.

Further exploration of compatible *N*-protecting groups is required for substrate scope expansion. Use of protecting groups which can be removed using standard methodology is desirable (e.g. PMB) as this would allow access to enantioenriched primary amines. Increasing the steric bulk of such protecting groups by substitution is one possible way of assuring high enantioselectivity. Improving the practicality of enantioselective FLP procedures could support their adoption. Our current protocol requires the preparation and isolation of substrate ketimines prior to their reduction. Although the moisture sensitivity of borenium cations makes them presumably incompatible with direct reductive amination procedures, modification of the current protocol to a ‘one-pot’ procedure is an attractive idea. One possible way of achieving this is by using a solid-state reagent which would effect ketimine formation prior to the addition of borenium catalyst and reducing agent.



Scheme 2.24 Opportunities for future development of borenium-catalysed preparation of enantioenriched amines.

3 Chapter 3–Stannylum ion equivalents

3.1 Introduction

3.1.1 Literature precedent in the field of FLP chemistry

Recently, our group reported on the use of $i\text{Pr}_3\text{SnOTf}$ **132** as a chemical equivalent for a stannylum cation in FLP hydrogenation chemistry, in conjunction with amine bases (Figure 3.1).⁵⁶

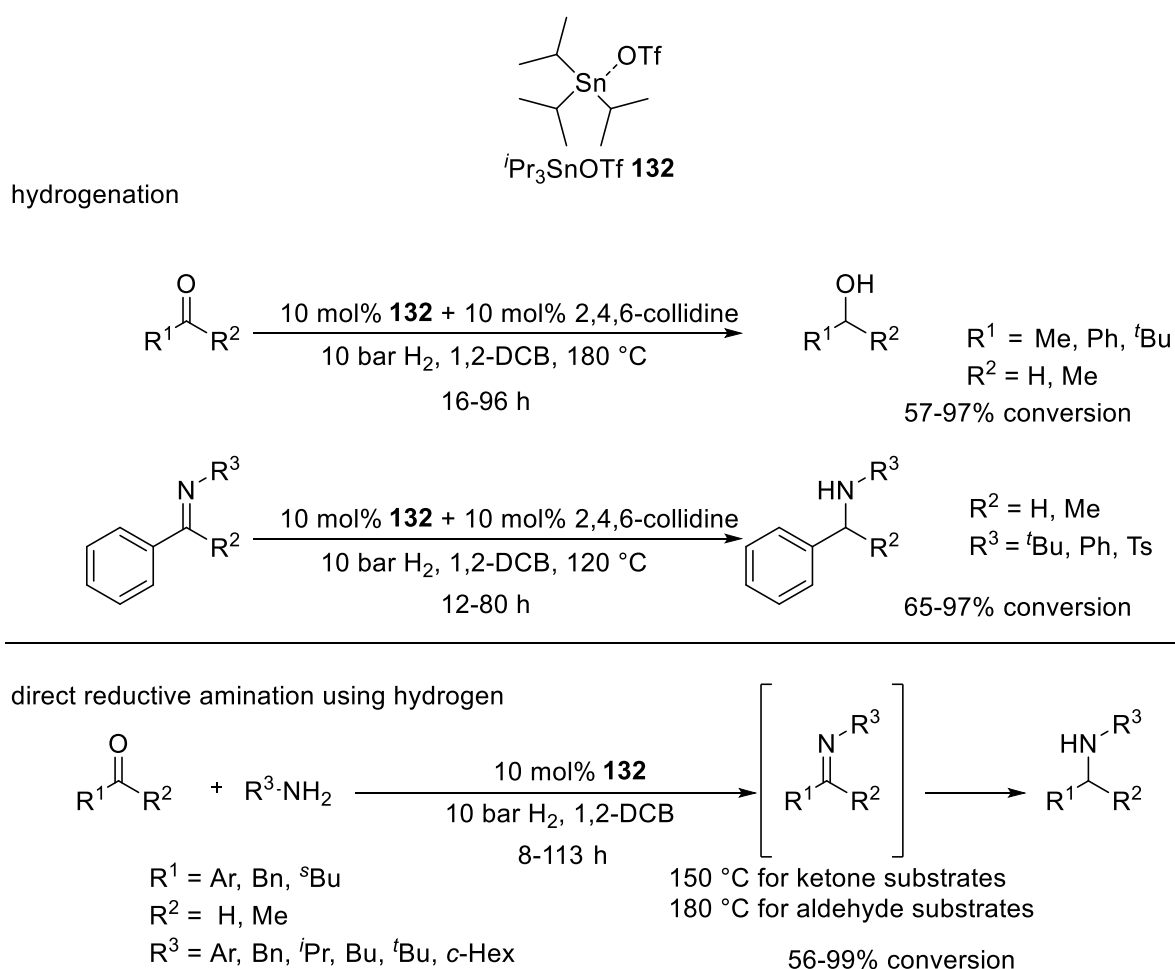


Figure 3.1 Hydrogenation and reductive amination catalysed by **132**.

A broad range of substrates could be reduced including imines, carbonyls, enamines and electron deficient alkenes. The system displayed water tolerance, with similar reactivity observed under anhydrous conditions and in the presence of more than two equivalents of water with respect to the catalyst (formation of the dihydrate $i\text{Pr}_3\text{SnOTf} \cdot 2\text{H}_2\text{O}$ was found to occur when **132** was stored under

air). The class of trialkylstannylium ion equivalents was chosen for development of an enantioselective catalyst tolerant of hydroxyl functionality based on the known tolerance displayed by **132**. The success of this system was attributed to the weak acidity of the stannylium cation water adducts (e.g. $n\text{Bu}_3\text{Sn}\cdot x\text{H}_2\text{O}$, $\text{pK}_a(\text{H}_2\text{O}) = 6.25^{237}$), which renders them compatible with basic functionality (see section 1.3.2). The steric hindrance imposed by the presence of the three secondary alkyl groups weakened coordination of the triflate counteranion sufficiently for the system to be able to activate molecular hydrogen in combination with amine bases, i.e. ‘internal frustration’ imparts cationic character on the Sn centre. This comes in contrast to previous reports, which indicated that $n\text{Bu}_3\text{SnOTf}$ **133** was not sufficiently Lewis acidic to participate in molecular hydrogen activation.²³⁸

In a subsequent report, $i\text{Pr}_3\text{SnOTf}$ **132** was used to carry out catalytic reductive amination using hydrogen gas as the reducing agent to generate both *N*-aryl and *N*-alkyl amines.²³⁹ This application illustrates the great water tolerance displayed by **132** and its stability under forcing conditions. The system is limited in that high temperatures are nonetheless required to allow dissociation of the adducts formed between amine or alcohol products and the active catalyst **132**, indicating that further design optimisation is required to increase reactivity.

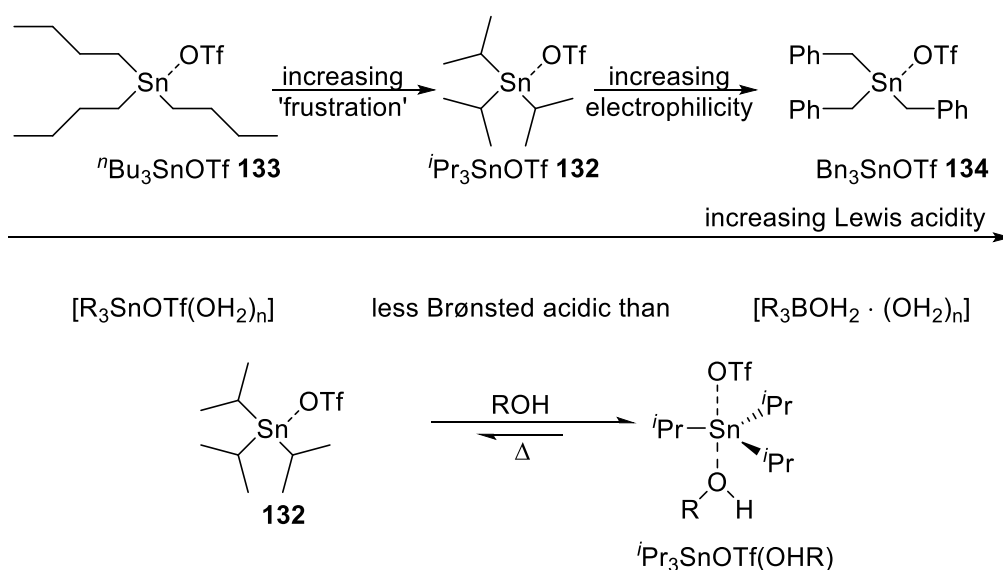


Figure 3.2 Trialkyl stannylium Lewis acids.

The Lewis acidity of $^i\text{Pr}_3\text{SnOTf}$ **132** (Gutmann-Beckett AN = 68) is comparable to that of borenium **95a** (AN = 70.7), but lower than that of borane $\text{B}(\text{C}_6\text{F}_5)_3$ **4b** (AN = 78.1²¹⁹). Variation of the trialkyl stannylum core to improve Lewis acidity was investigated with the use of Bn_3SnOTf **134**.²⁴⁰ This compound showed greater Lewis acidity (AN = 74) than **132** due to the stronger electron withdrawing nature of the benzyl groups, feature which translated into improved hydrogen activation ability. Catalytic ability was limited due to catalyst decomposition initiated by Bn_3SnOTf **134**/ Bn_3SnH **135** exchange leading to formation of Bn_4Sn .

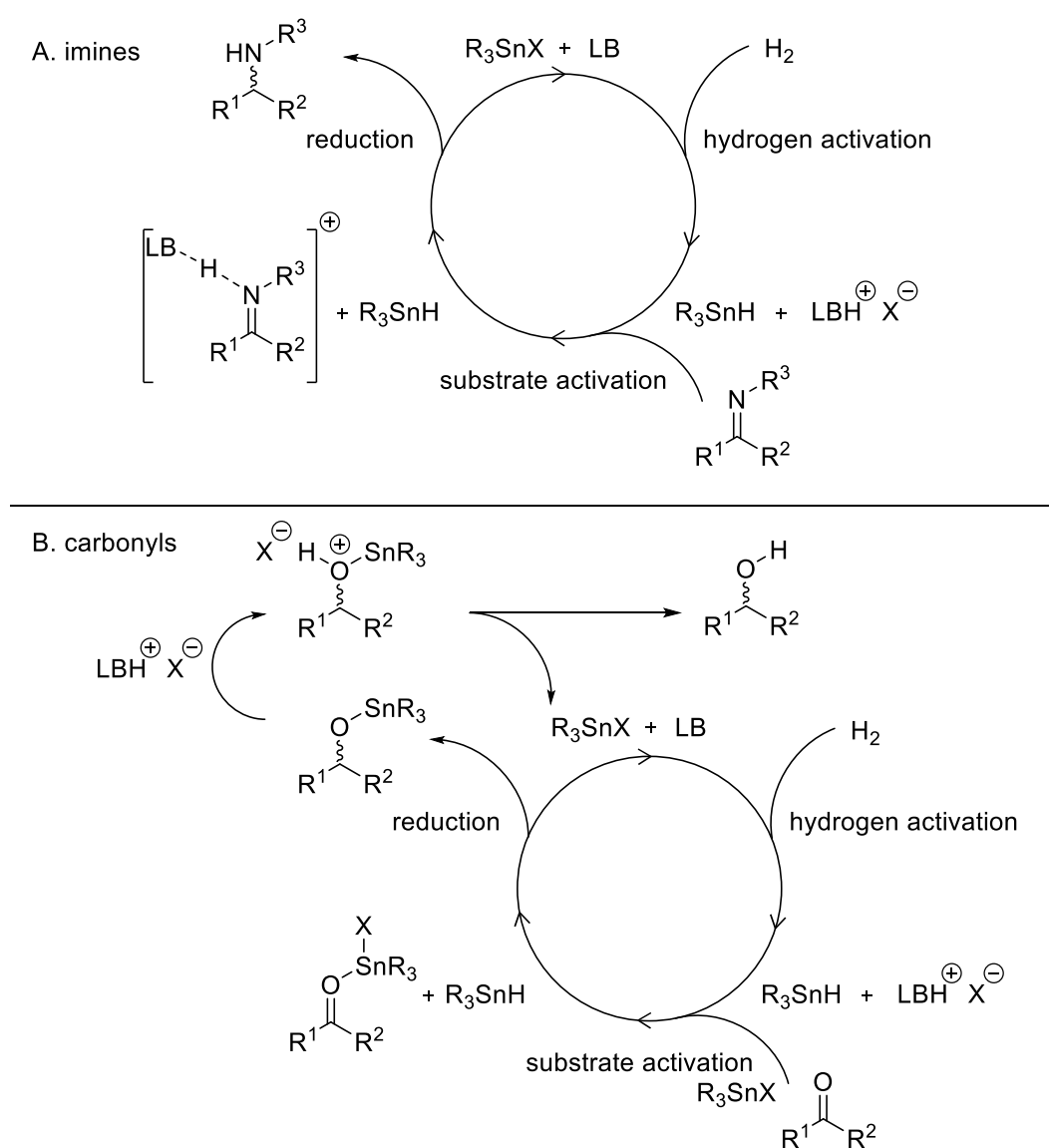


Figure 3.3 Mechanistic proposal for the hydrogenation of imines (A) and ketones (B) using **132**.

Further development of the trialkyl stannylum catalytic system appeared to require further increase in steric bulk, whilst maintaining use of the secondary alkyl group to provide stability. Replacement of the triflate counteranion with weakly coordinating anions was expected to improve reactivity.

The reaction mechanisms described in Figure 3.3 were proposed to operate in the hydrogenation catalysed by $i\text{Pr}_3\text{SnOTf}$ **132**.⁵⁶ The mechanism proposed for imine substrates is similar to borane-catalysed hydrogenation involving substrate activation through hydrogen bonding/protonation. For the reduction of carbonyl compounds, Lewis acid ($i\text{Pr}_3\text{SnOTf}$) activation of substrates was postulated to operate due to the lower Brønsted basicity of these substrates.

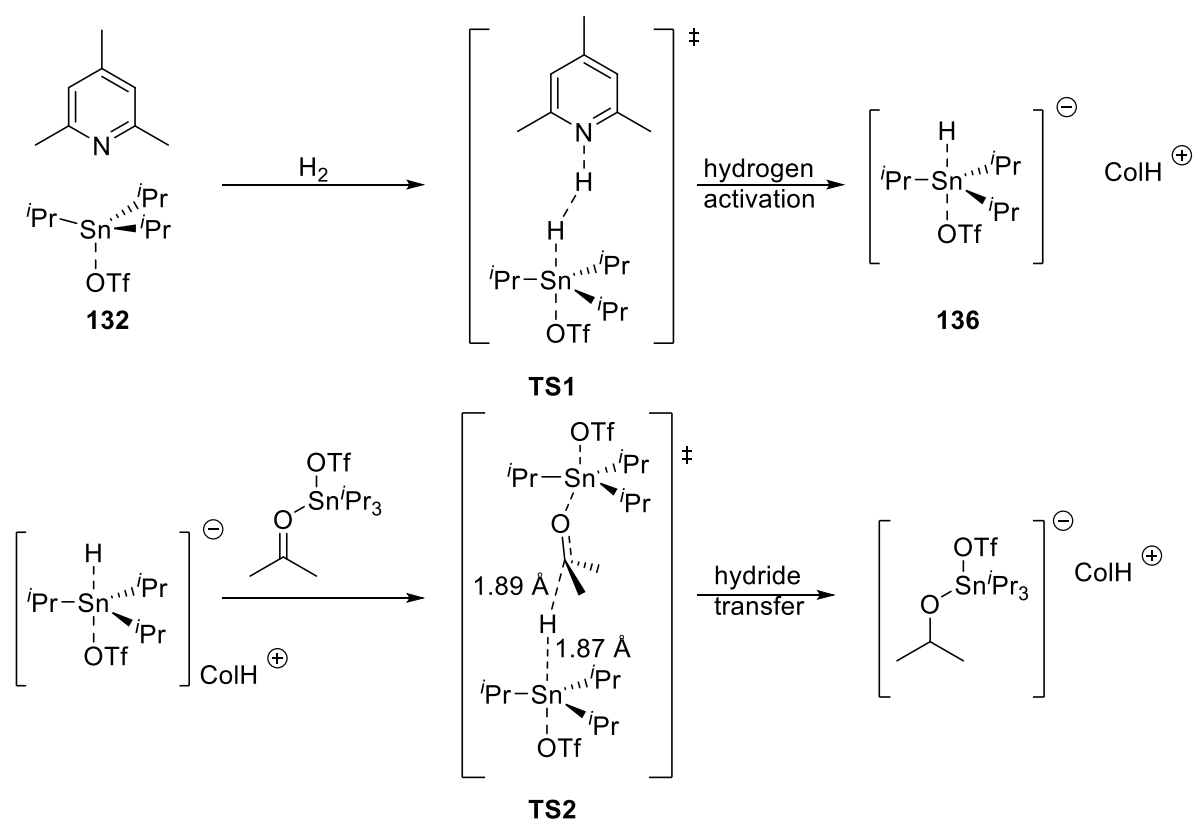


Figure 3.4 Mechanistic details for $i\text{Pr}_3\text{SnOTf}$ -catalysed hydrogenation, reported by Swapan.²⁴¹

These mechanistic proposals are supported by computational studies (Figure 3.4).^{241,242} Additional important features which emerge from these studies are the nature of the hydrogen activation process and the nature of the hydride reducing agent. Hydrogen activation occurs with the triflate counterion coordinated to the tin centre, in a trigonal bipyramidal structure **TS1**. This leads to the

formation of $^i\text{Pr}_3\text{SnH}(\text{OTf})$ **136** which is postulated to be the active reducing agent. Although triflate anion dissociation is slightly thermodynamically favoured, the greater hydricity of **136** vs $^i\text{Pr}_3\text{SnH}$ **137** makes the former the dominant reducing agent. This effect has potential implications in enantioselective transformations as it changes the nature of the enantiodetermining **TS2**.

3.1.2 Chiral organotins-literature precedent

Tetravalent tin adopts a tetrahedral coordination geometry similarly to its congener carbon. It results that there are two relevant types of chirality found in organotin compounds: chirality at tin and chirality at carbon.

3.1.2.1 Chirality at tin

Chirality at tin has been reviewed by Gielen (Figure 3.5).²⁴³ The optically pure alcohol **138** (stereochemistry not assigned) was prepared from the optically pure menthyl ester **139**, which was obtained following a classical resolution strategy.

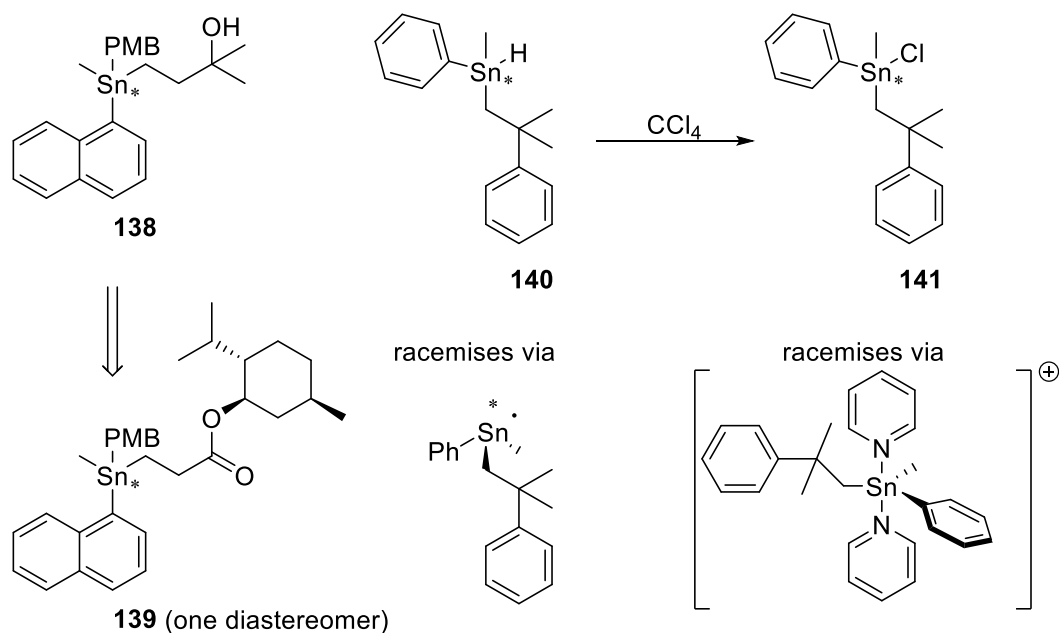


Figure 3.5 Examples of compounds featuring chirality at tin.

Optically-enriched tin hydrides **140** have been prepared by enantioselective reduction,²⁴⁴ but have been shown to be prone to racemisation by a radical mechanism.²⁴⁵ Hydride **140** can be converted by exchange with CCl_4 with retention to the corresponding chloride **141**. This latter compound undergoes racemisation catalysed by weak nucleophiles (pyridine).²⁴⁶ The proposed mechanism involves an achiral pentacoordinate complex resulting from substitution followed by addition of a second molecule of pyridine.

Configurationally stable penta-coordinate Sn complexes can be prepared by the inclusion of an internal nucleophile in the molecule (**142** and **143**, Figure 3.6).²⁴⁷ NMR studies show that for **142** inversion of configuration is slow on the NMR timescale even at 120 °C due to a high energy barrier for Berry pseudorotation.²⁴⁸ The compound **143** exists as two diastereomers in almost equal proportion in solution, however preferential crystallisation of the less soluble (S)_C(S)_{Sn} isomer allows it to be characterised in the solid phase and in solution at low temperature (-55 °C). At higher temperatures (-13 °C) epimerisation does occur, the mechanism responsible being again postulated to involve the action of a nucleophile (traces) to generate the neutral hexa-coordinate complex **144**.

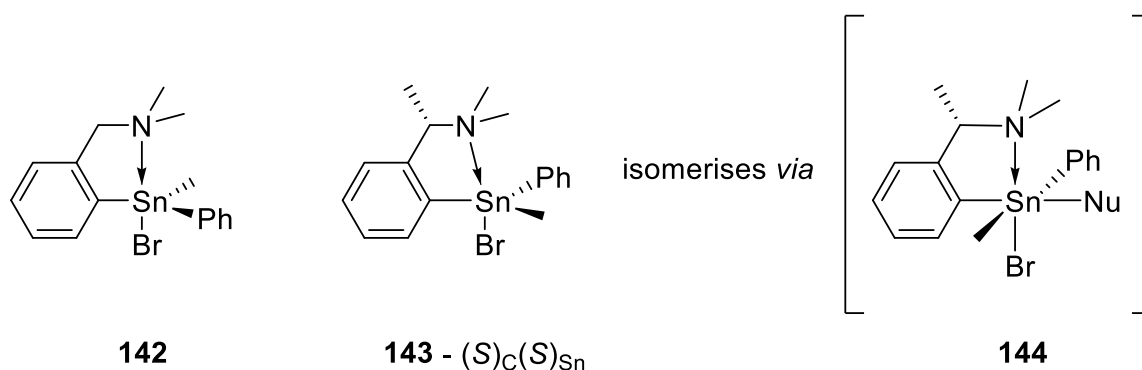


Figure 3.6 Configurational stable penta-coordinate organotin compounds.

3.1.2.2 Chirality at carbon

Further development of chiral organotin reagents focused on appending chiral substituents to the tin atom. These substituents were generally rendered chiral by the presence of one or more carbon

stereocentres or, more rarely, by an axis of chirality. An extensively employed chiral ligand was the (-)-menthyl ligand ((-)-Men = Men) due to its facile sourcing from the chiral pool (Figure 3.7). Schumann and Wassermann reported the preparation of menthyl-substituted hydrides **145**²⁴⁹ and subsequently of the dimethylamino stabilised derivative **146**.²⁵⁰ Numerous menthyl-tin derivatives were synthesised by Podestá: trimethyltin derivatives **147** and dimer **148**²⁵¹ and neophyl substituted derivatives **149a,b**.²⁵² Jousseau and Santini reported the preparation of dimethyltin derivatives **150** and trimethyltin derivatives **151** and **152**.²⁵³

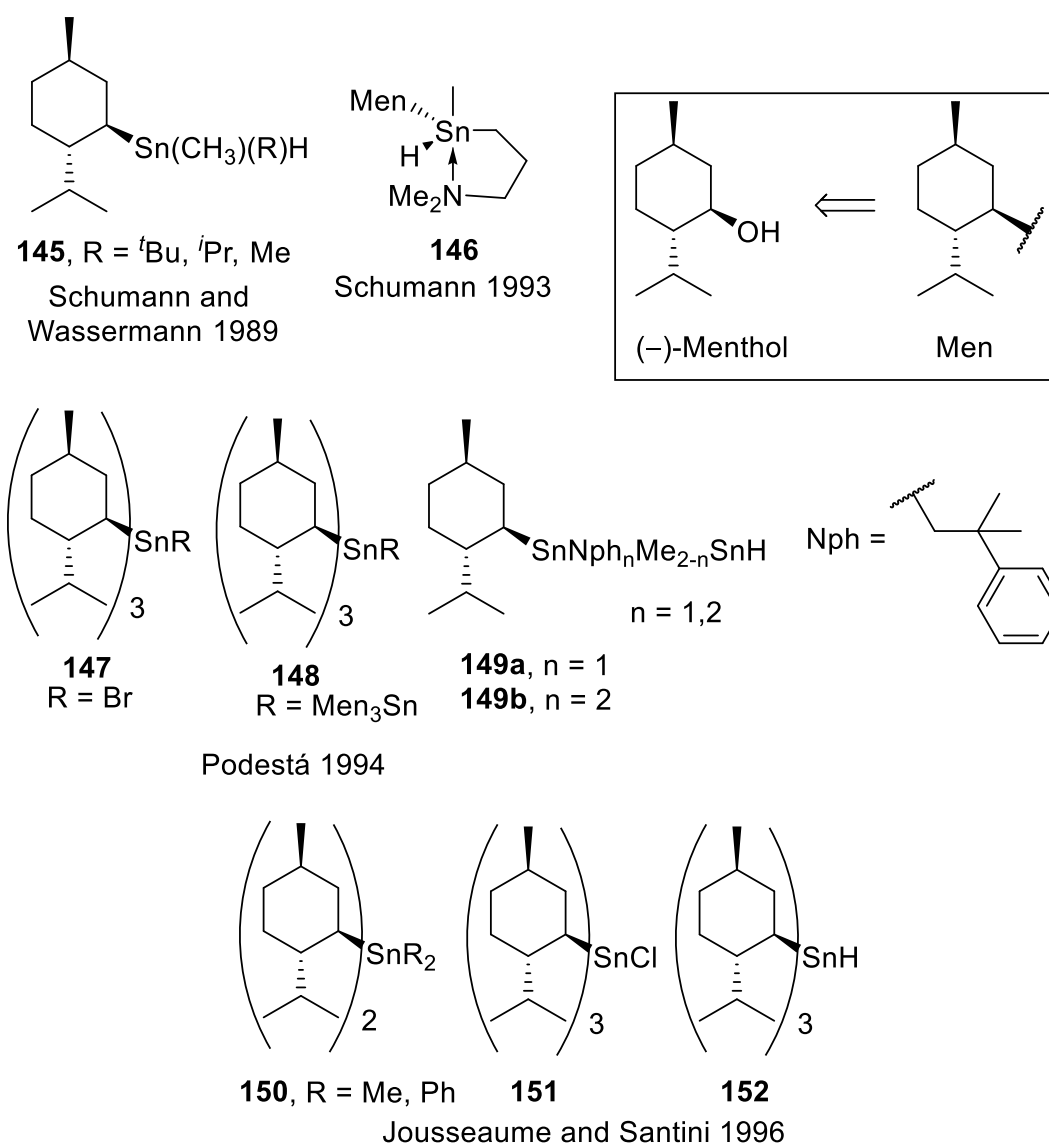
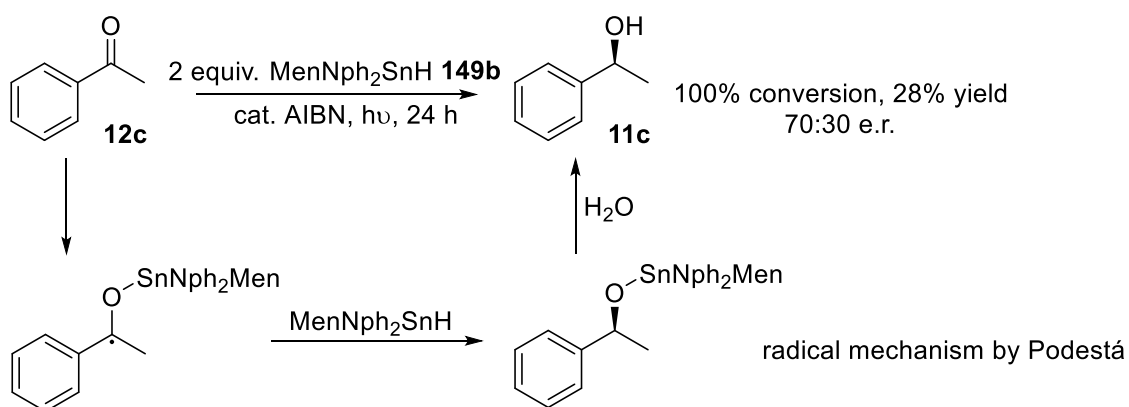


Figure 3.7 Examples of menthyl substituted organotin compounds.

3.2 Use of chiral organotin hydrides in enantioselective synthesis

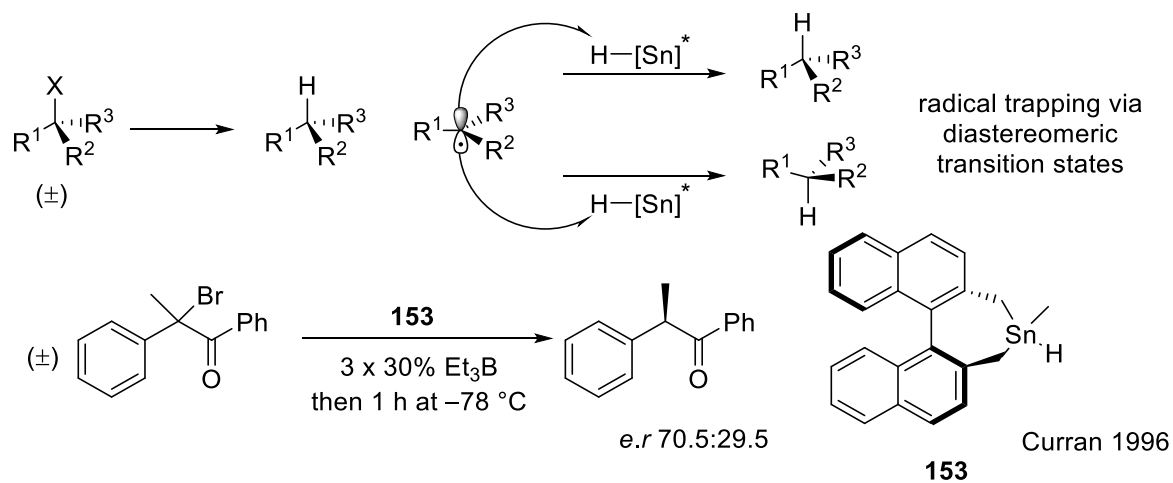
3.2.1 Under radical conditions

Dineophyl-substituted hydride **149b** carried out the reduction of acetophenone under radical conditions (AIBN) with a 70:30 e.r. selectivity.²⁵²



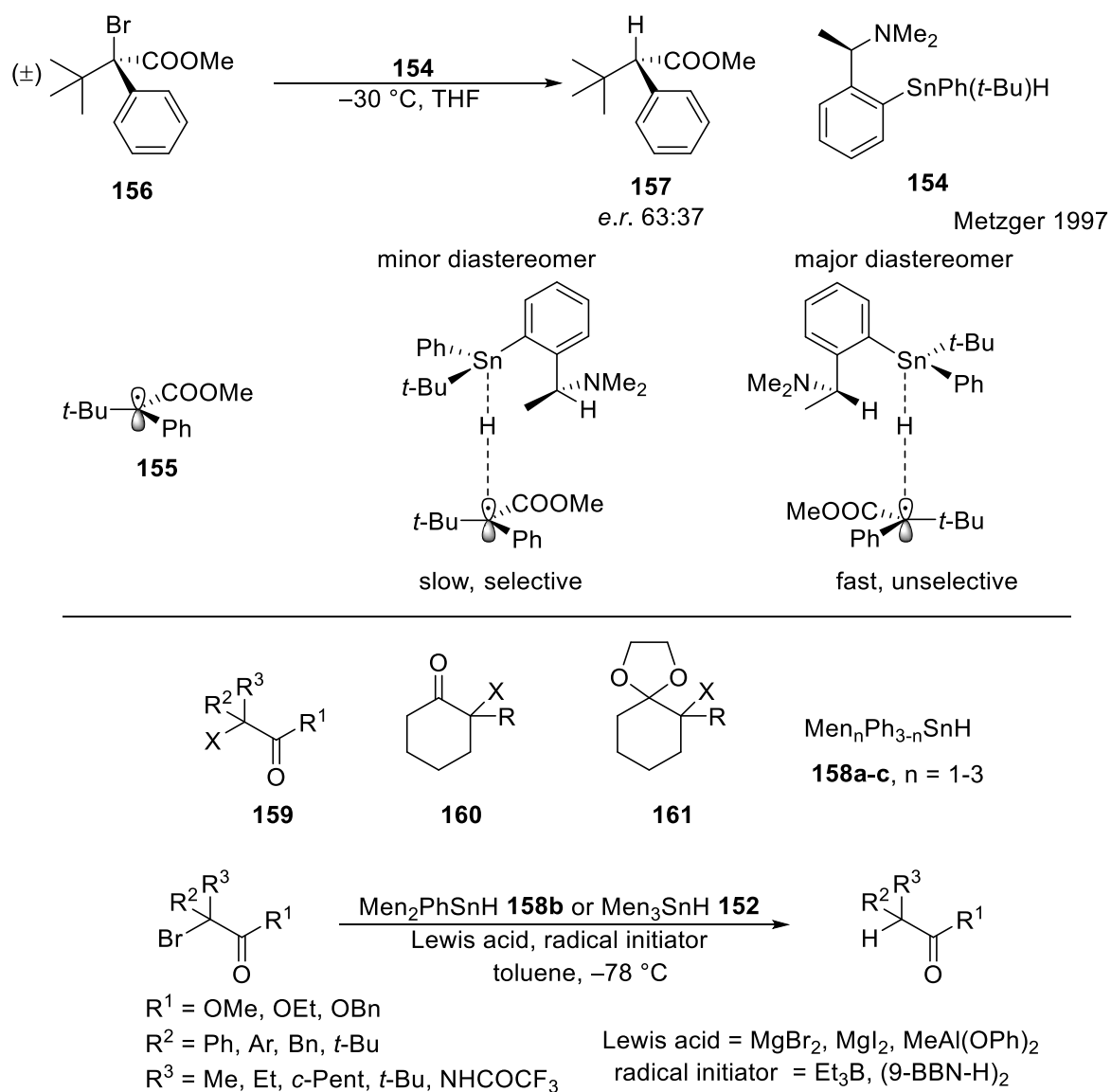
Scheme 3.1 Enantioselective reduction of acetophenone under radical conditions.

Although this reported reduction of a prochiral double bond was a promising result, at the time extensive efforts were devoted for the use of new chiral organotin hydrides for enantioselective reduction of organohalides. This process would achieve the conversion of a racemic organohalide containing a sp^3 C-X bond to an enantioenriched hydrocarbon derivative (Scheme 3.2).



Scheme 3.2 Enantioselective conversion of racemic halides to enantioenriched hydrocarbons.

Transfer of chirality is achieved by trapping a prochiral radical with a chiral radical trap. In an early account, Nanni and Curran described the preparation of axially chiral **153**, this compound being one of the few examples of organotin reagents which contain an axis of chirality.²⁵⁴

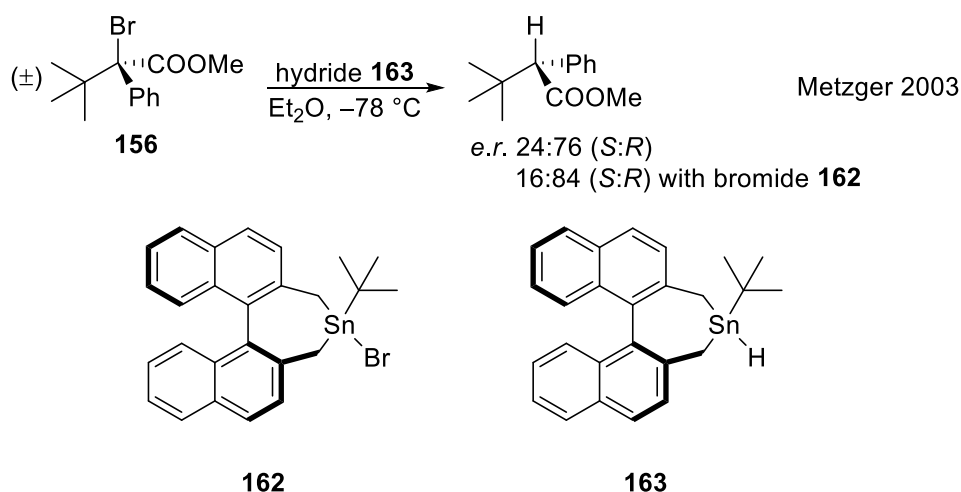


Scheme 3.3 Lewis acid-assisted enantioselective reduction.

In a comprehensive study concerning the transfer of chirality from enantioenriched organotin hydrides **154** to prochiral radicals **155**, Metzger *et al.* reported enantioselectivity levels up to 63:37 in the reduction of α -bromo esters **156** to esters **157** (Scheme 3.3).²⁵⁵ They postulated that the poor selectivity arises in the rapid reduction carried out by the major diastereomer of the reagent. Schiesser

et al. continued the development of chiral organotin hydride reagents featuring the menthyl substituent (Scheme 3.3).^{256–258}

The series of menthyl-substituted stannanes **158** afford scalemic mixtures of very low enrichment levels (e.r. <58:42) in the reduction of the various esters **159**, **160**, **161**. This was proposed to be a result of the large Sn-C distance (3.5 Å calculated) in the hydrogen atom transfer step.²⁵⁹ This large distance results in inefficient chirality transfer from the chiral organostannane to the prochiral C-centred radical. When the same reductions are carried out in the presence of stoichiometric amounts of Lewis acids (with respect to the substrate) selectivity levels as high as 99:1 can be obtained for a range of substrates, including amino acid precursors.²⁵⁸ This effect was attributed to the larger effective steric profile of the prochiral radicals resulting from Lewis acid coordination to the vicinal carbonyl functionality. This mode of operation is supported by the observation that the sense of enantioinduction is controlled by the stannane **158** and not by the Lewis acid, when a chiral version of the latter is used. The steric bulk of the magnesium-based Lewis acids is postulated to arise due to their promoting dimer formation, i.e. one ester unit is providing the steric bulk for another radical fragment during the reduction step.

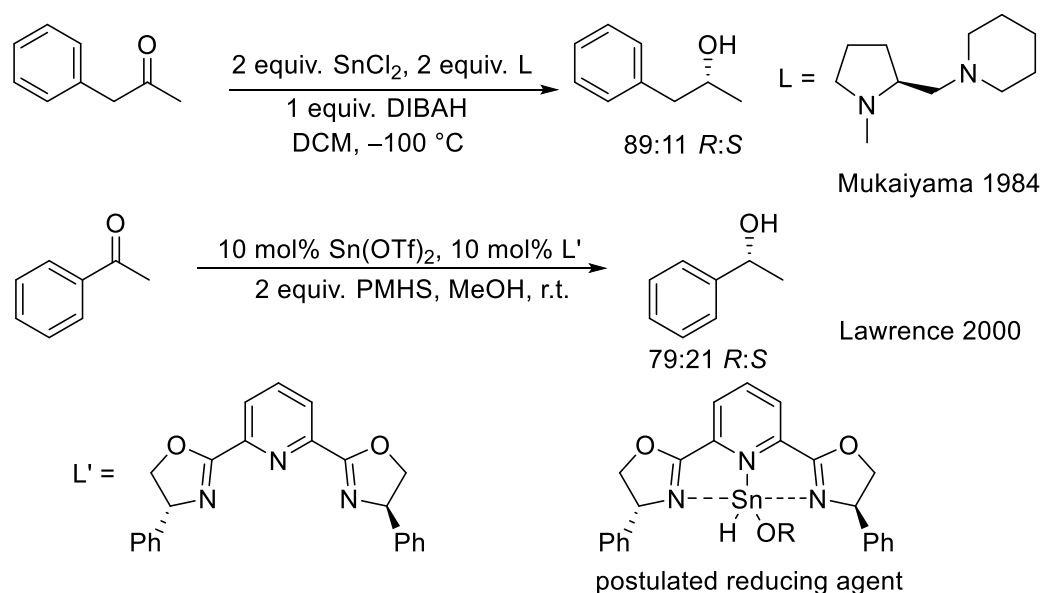


Scheme 3.4 Enantioselective reduction with chiral tin Lewis acid/hydride.

Building on the early work of Curran and exploiting the use of Lewis acids as additives, Metzger employed a combination of bromide **162** and hydride **163** to obtain improved selectivity levels in the reduction of bromoester **156** (Scheme 3.4).²⁶⁰ Menthyl-substituted organotin reagents have been explored as chiral modifiers for heterogeneous Pt-based catalyst for the hydrogenation of 3,4-hexanedione.^{261,262}

3.2.2 Under ionic conditions

Rare examples of enantioselective reductions carried out using tin reagents under ionic conditions have been reported in the literature to proceed with enantioselectivity levels, which although modest were higher than those reported under radical conditions. These reagents used tin in the oxidation state II and chiral amine ligands (Scheme 3.5).^{263,264} The reduction procedure reported by Mukaiyama presumably involves a chiral tin (II) hydride, the reaction requiring the use of a non-donor solvent. A similar intermediate was postulated in the catalytic reduction by Lawrence.²⁶⁴ Selectivity is potentially a result of intramolecular hydride transfer resulting from substrate coordination.



Scheme 3.5 Enantioselective reduction using organotin hydrides under ionic conditions.

3.3 Chiral organotin Lewis acids

Organotin halides display weak Lewis acidity, however their reactivity has been studied little in comparison to that of the hydrides. Kuivila reported the synthesis of numerous haloorganotins using common terpene compounds as sources of chirality. No applications of these compounds were reported.²⁶⁵ Chiral organotin halides or triflates based on the binaphthyl framework **164**, **165** have been investigated as catalysts for the resolution of racemic diols and, briefly, for the Diels-Alder reaction.^{266–269} The use of oxazolines as intramolecular donors has been reported.^{270,271} A recent report described the chiral haloorganotin **166** which is stabilised by an agostic interaction.²⁷²

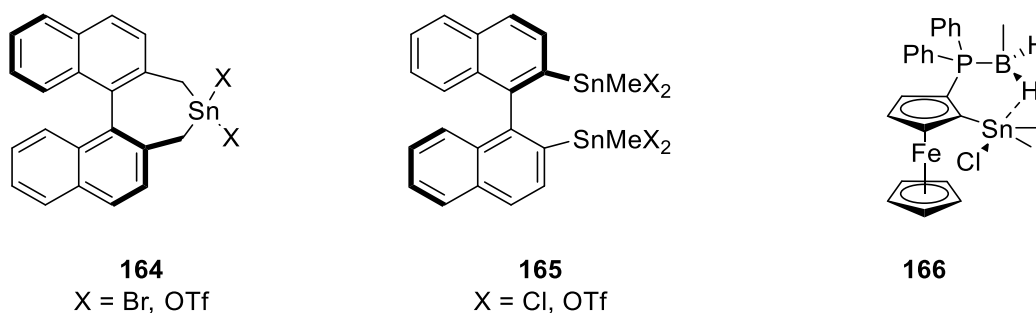


Figure 3.8 Examples of tin (IV) chiral Lewis acids.

3.4 Target chiral stannylum ion equivalent and design considerations

We planned to synthesise the chiral organotin Lewis acid **167** that would be sufficiently strong (have sufficient stannylum ion character resulting from the use of weakly coordinating anions and bulky substituents) to take part in hydrogen activation to generate the hydride form **152**, which could then act as a reducing agent towards an activated carbonyl substrate or derivative (Figure 3.3 and Figure 3.9).

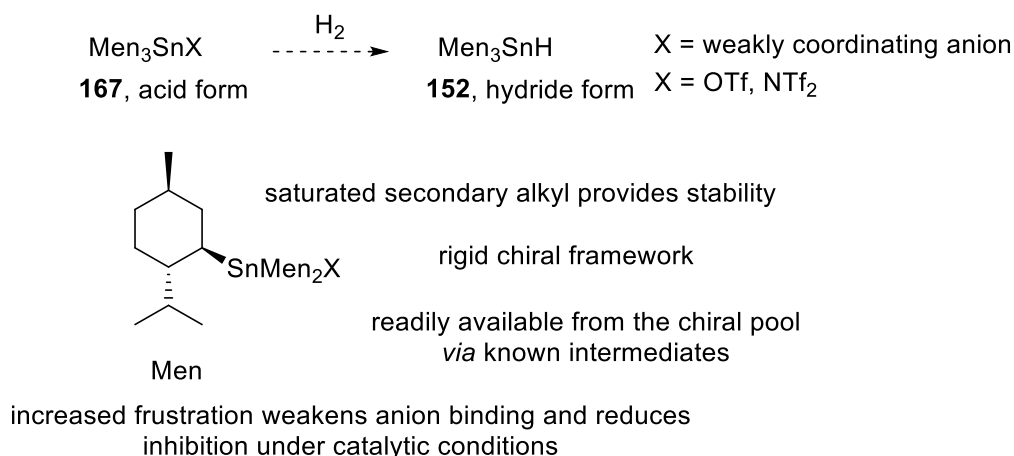


Figure 3.9 Design consideration for target chiral Lewis acid.

We postulated this system to hold potential as a catalyst for the enantioselective hydrogenation of carbonyls, substrates for which so far FLP-type catalytic systems have not been reported. Attractive features considered are the demonstrated tolerance of tin-based Lewis acids towards alcohols and precedent for their use in enantioselective transformations.

Hydride transfer has been postulated to occur *via* an ionic mechanism under FLP conditions,^{56,241,242} unlike with the majority of methodology using chiral tin hydrides (section 3.2.1).²⁵⁴ An analysis of the analogous envisaged modes of chirality transfer in the enantiodetermining step is presented in Figure 3.10. The reduction of carbonyl derivatives (ketones) is expected to be particularly susceptible to effects arising from the steric bulk of the trialkyltin core due to the involvement of two such fragments in the reduction step.

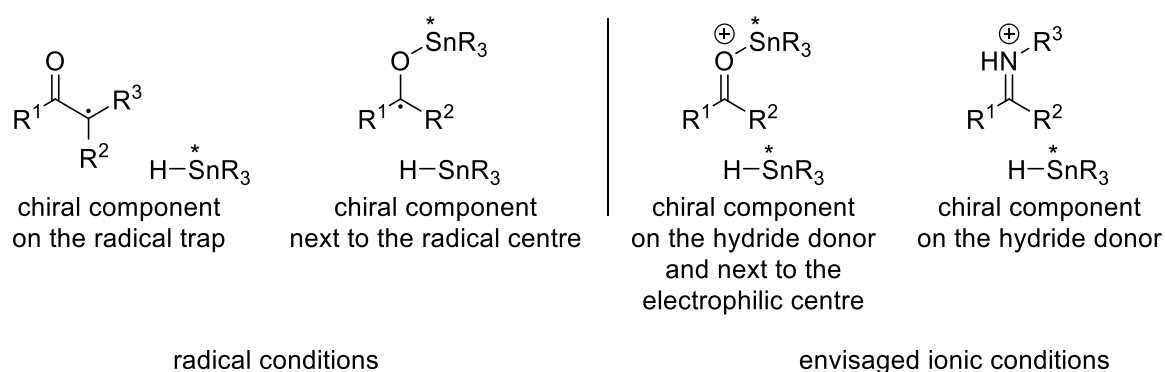
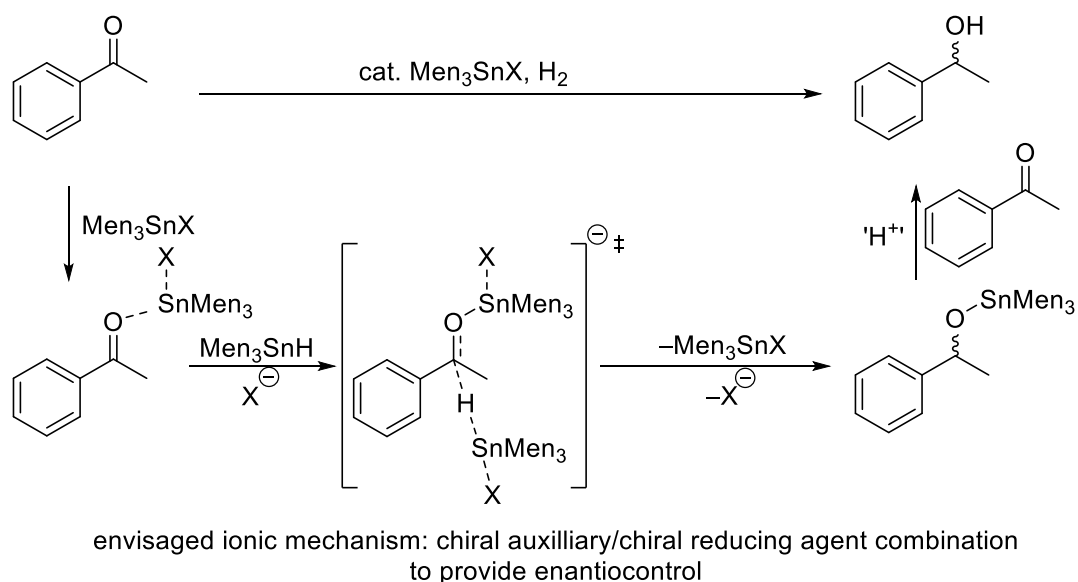


Figure 3.10 Comparison of chirality transfer modes under radical and ionic conditions.

The saturated alkyl fragments (bonded through secondary carbons) should provide a stability level comparable to that observed for the tri-*isopropyl*stannylum core. The increased steric hindrance provided by the bulky menthyl fragments should increase the level of ‘frustration’ thereby increasing activity by weakening counteranion and nucleophile (amines, alcohols) binding. Furthermore, the presence of two bulky chiral fragments during the enantiodetermining reduction (for carbonyl substrates) could potentially lead to an improved level of enantioselectivity. The potential downside to having such bulky substituents would be a reduction in rate for hydride delivery from the hydride form **152** to activated substrates (Scheme 3.6 and Figure 3.10). The preliminary results reported by Podestá for the reduction of acetophenone under radical conditions indicated to us the potential of the menthyl moiety for controlling transfer of chirality under ionic conditions. We were interested to investigate whether the ionic nature of the transition state would translate to better enantiocontrol resulting from a more organised transition state. The expected distance over which chirality transfer would occur (3.76 Å) is comparable to that reported previously under radical conditions (3.5 Å).^{241,259}

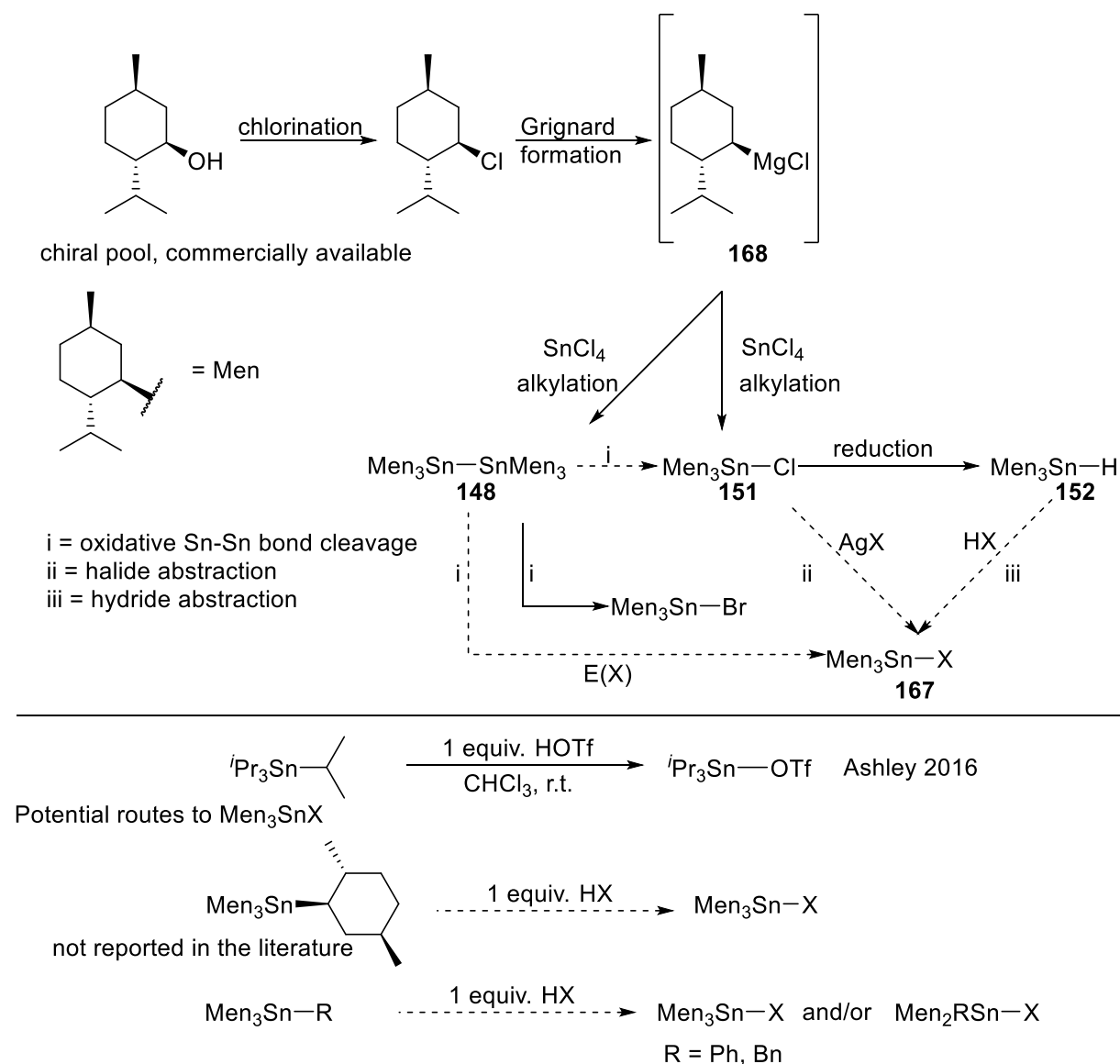


Scheme 3.6 Envisaged enantioselective reduction of acetophenone.

3.5 Synthesis of a trimethylstannylum cation equivalent (Men_3SnX **167**)

3.5.1 Proposed synthesis and synthetic options

A general synthetic plan is presented in Scheme 3.7.



Scheme 3.7 General synthetic plan for the preparation of Men_3SnX .

Formation of the trimethyltin core represents a key step in the synthetic plan. Its preparation has been described using menthyl Grignard **168** to alkylate SnCl_4 generating either hexamethylstannane **148** or trimethyltin chloride **151**. $i\text{Pr}_3\text{SnOTf}$ **132** has been synthesised by treating $i\text{Pr}_4\text{Sn}$ with HOTf ,⁵⁶ process which involves cleavage of a Sn-C bond. Protodealkylation of stannanes was reported early on

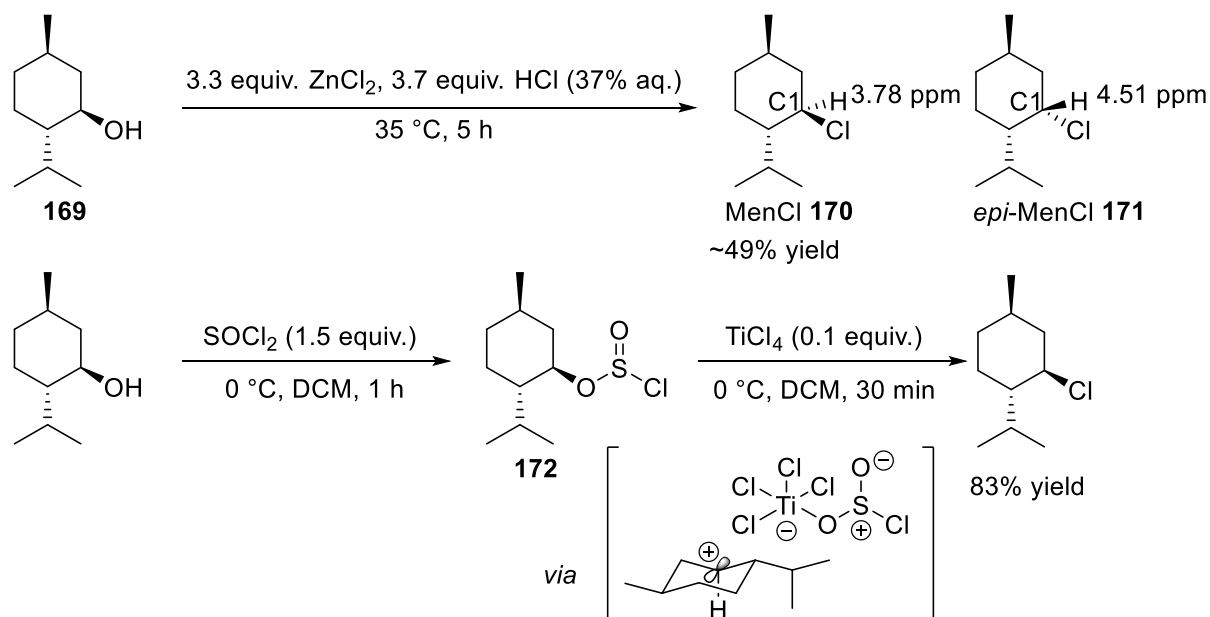
by Sasin.²⁷³ By analogy **167** could be prepared from the precursor Me_4Sn . This compound has not been reported in the literature, failures in its preparation being attributed to the excessive amount of steric bulk which would have to be accommodated around the tin atom.²⁶¹ The use of a 'dummy' ligand attached to the trimethyltin core represents an option, however issues related to chemoselectivity can arise. The alternative strategies depicted in Scheme 3.7 were considered.

3.6 Synthesis

3.6.1 Menthyl chloride from menthol

Conversion of natural levo-menthol **169** to levo-menthyl chloride **170** was first reported by Smith and Wright using the Lucas reagent (Scheme 3.8).²⁷⁴ Following this procedure (50 g scale) yielded a product of high diastereomeric purity (>100:1, C1(Cl)H 3.78 ppm, CDCl_3 ; in the epimeric **171** this proton is found at 4.51 ppm²⁷⁵) but otherwise impure. Distillation at 15 mbar allowed collection of a fraction boiling at 101-104 °C (29 mL, ~27 g, ~49% yield) which showed partial improvement in purity as assessed by NMR (high field region) as well as removal of most of the colouration. It was found that elution through silica (pentane) assisted in further removal of colouration. Attempted distillation at atmospheric pressure was unsuccessful with fractions of lower purity collected between 200 and 250 °C.

Belluci, Lepore *et al.* recently published a modern method for alcohol chlorination involving formation of the ester **172** with thionyl chloride, followed by TiCl_4 catalysed rearrangement.²⁷⁶ The conversion proceeds with retention of configuration at C1. The authors propose reaction to occur by TiCl_4 coordination to the sulfoxyl oxygen atom of **172**, which initiates dissociation to a non-planar carbocation stabilised by hyperconjugation, found as an ion pair with the chlorosulfite- TiCl_4 counteranion. This anion then delivers chloride to the accessible side of the carbocation to generate **170** with retention.

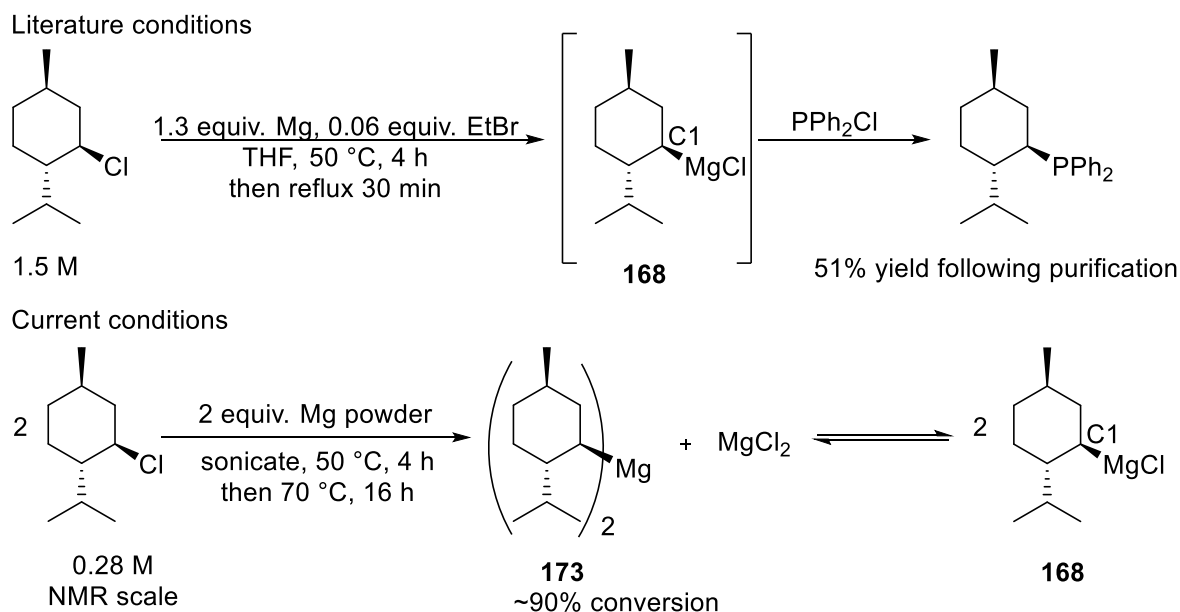


Scheme 3.8 Menthol chlorination.

Using these conditions similar results were obtained compared to the Smith procedure. Purification by column chromatography (1 g scale reaction) yielded **170** of high purity. This procedure was difficult to scale up due to the low polarity of the product (**170** travels at the solvent front with pentane). When distillation (58 °C, 1 mbar) was employed a yield of 83% was obtained. Generally, further purification was carried out and it was found that very slow distillation (<1 mbar, 30-40 °C heating block temperature) afforded almost pure product. The menthyl chloride obtained from these procedures was diastereomerically pure (confirmed by ^1H and ^{13}C NMR).

3.6.2 Menthylmagnesium chloride **168** formation

The preparation of menthyl Grignard reagent **168** was reported by Tanaka and Ogata.²⁷⁷ This procedure is cited in all preparations of menthyltin reagents, however experimental details regarding this step are generally not included. In the original report Tanaka and Ogata use EtBr as an initiator and carry out this reaction at 50 °C,²⁷⁸ followed by reflux. Formation of Grignard reagents generally occurs with loss of stereochemical information due to the radical nature of the process.²⁷⁹



Scheme 3.9 Preparation of menthyl Grignard reagent from MenCl.

In a study involving trapping of MenMgCl **168** with PPh₂Cl (Grignard formation carried out at room temperature),²⁸⁰ Dakternieks reports that no (*epi*-Men)PPh₂ could be detected in the crude mixture, indicating that Grignard formation is occurring with retention of configuration.

Borsdorf *et al.* reported on the use of ¹¹⁹Sn NMR spectroscopy as a probe for the determination of diastereomeric composition of organotin compounds.²⁸¹ The use of an inverse-gated decoupling technique makes integration of signals possible by reducing intensity loss caused by the negative nuclear Overhauser factor. The large NMR shift scale allows differentiation of diastereomeric species, however generally separations of less than 1 ppm are reported (for a 400 MHz spectrometer).²⁸¹ Therefore, the presence of more than one stereocentre in the menthyl fragment provides a convenient handle for NMR monitoring of epimerisation at the C1 centre by the use of ¹¹⁹Sn NMR in addition to ¹H NMR, as employed by Tanaka and Ogata. For menthyl/*epi*-menthyl substituted stannanes higher chemical shift differences have been reported; e.g. MenSnPh₃ and *epi*-MenSnPh₃ $\Delta\delta$ (¹¹⁹Sn) = 3.1 ppm.²⁸⁰

We have carried out an NMR study concerning the formation of **168**. All THF used for these reactions was purified by distilling under a nitrogen atmosphere from sodium/benzophenone ketyl (purple

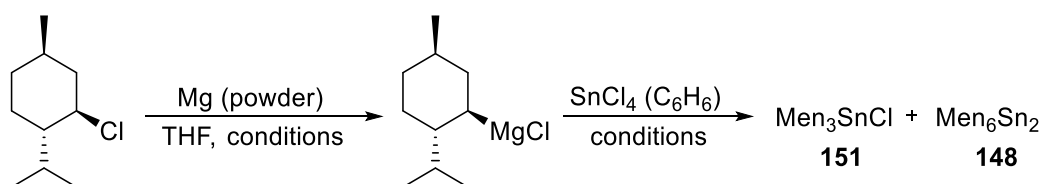
colour) and storing in ampules sealed with Teflon stopcocks. Further degassing was carried out by the freeze-pump-thaw technique. Mg (powder) was treated with dibromoethane (0.06 equiv.) in THF-d₈, in an inert atmosphere glovebox. Following heating to 75 °C for 30 min (sealed Young's tap NMR tube), the formation of ethene could be detected by ¹H NMR (5.36 ppm, s), indicating the activity of this Mg source. Afterwards, 1 equiv. MenCl **170** was added and the sealed NMR tube was heated to 75 °C, with analysis carried out at specified time points. Reaction was seen to progress as indicated by disappearance of starting material and appearance of a new multiplet (believed to correspond to C1(Mg)H, -0.14 ppm) and consumption of Mg and formation of a white solid, possibly MgCl₂ resulting from the known Schlenk equilibrium.²⁸² This suggests that the reagent being formed is in fact of the form Men₂Mg **173**. Under alkylation conditions, re-equilibration to MenMgCl **168** is expected due to the presence of MgCl₂. Reaction was slow with only an estimated 65% conversion observed after reflux for 38 h. This could be due to low magnesium metal activity, the poorly reactive substrate, or due to the lack of stirring. Formation of Grignard reagents under NMR conditions has been reported previously for reactive substrates, however variability in rate is expected.^{283–287} Smith reported preparation of MenMgCl **168** in 55% yield using sublimed magnesium.²⁷⁴

We attempted to improve the reactivity of our Mg source by subjecting commercially available Mg powder to a series of washes: 1M HCl (aq.) followed by rinsing with distilled water, methanol, and finally diethyl ether before drying under high vacuum at 150 °C. The resulting powder was stored in an inert atmosphere glovebox (N₂). The Grignard formation reaction was repeated, no initiator was used, and the reaction was subjected to ultrasonication at a temperature of 50 °C for 4 h (no Grignard formation could be detected at 50 °C) and then to heating to 70 °C for 16 h. Consumption of Mg was observed and analysis by NMR indicated ~90% conversion from MenCl **170** to Men₂Mg **173**. This Mg source was deemed suitable and used for future experiments. This methodology could not be easily scaled-up due to limitations in carrying out large scale reactions in sealed systems and limitations related to ultrasonication equipment (bath size). Therefore, conventional three-necked round bottom flasks were used, with heating carried out under reflux conditions. Lack of substantial Mg conversion

(as assessed visually) was generally observed, therefore an excess was used. The characteristic black colouration associated with Grignard solutions was observed, and qualitative evidence for Grignard formation was obtained in a large-scale experiment by treating an aliquot of the solution with D₂O. Analysis of the resulting crude product indicated deuterium incorporation (²H NMR, CHCl₃, 1.29 ppm).

3.6.3 Trimenthyltin core formation by alkylation

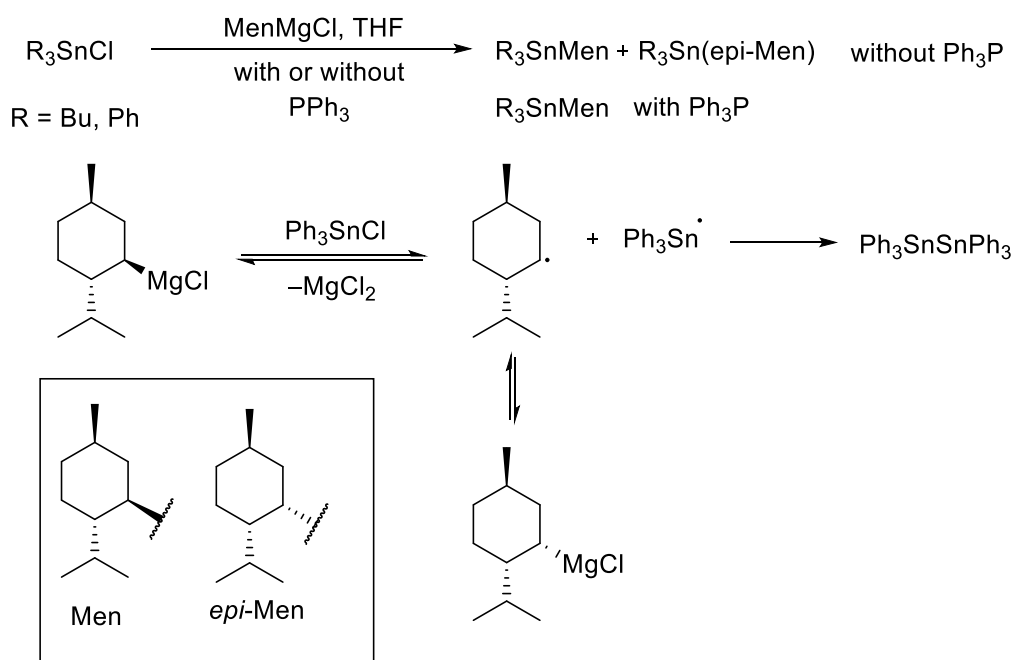
A summary of the literature conditions for trimethyltin formation is presented in Table 3.1.



Procedure	MenMgCl/SnCl ₄	Rxn. conditions	Workup	Yield
Podestá 1994 ²⁵¹	5	Reflux 4 h; r.t. 12 h	10% HCl _(aq.)	40.5% 148
	8	idem	idem	46.6% 148
Jousseaume 1996 ²⁵³	8.5	n/a	30% HCl _(aq.)	52% 151
Podestá 2012 ²⁶²	6	60 h reflux	10% HCl _(aq.)	59.8% 148

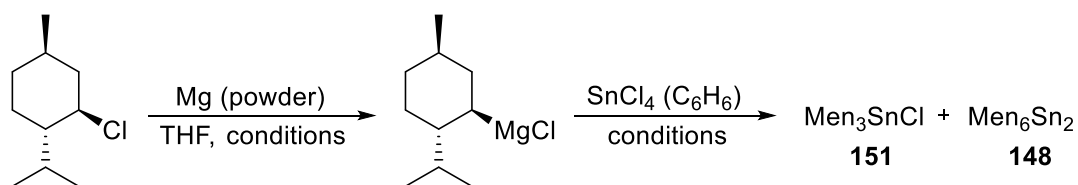
Table 3.1 Literature reports for the preparation of trimethyltin derivatives.

Experimental investigation into the nature of this alkylation process has not been reported in these accounts, however Dakternieks²⁸⁰ and later Podesta²⁶¹ discuss issues concerning epimerisation of the menthyl ligand during organotin alkylation for other substrates (Scheme 3.10). In the account of Dakternieks²⁸⁰ the point is also raised as to how the formation of Men₃SnCl **151** (Jousseaume) is possible using essentially the same procedure as that for the generation of Men₆Sn₂ **148**. In a subsequent account Podesta comments that both products are formed, together with Men₂SnCl₂, however experimental details as to how to control this reaction are not given.²⁶²



Scheme 3.10 Menthyl Grignard epimerisation during alkylation reactions, reported by Dakternieks.²⁸⁰

A summary of our efforts towards the synthesis of Men_3SnCl or Men_6Sn_2 is presented in Table 3.2. Monitoring was carried out with the use of ^{119}Sn NMR, either on crude mixtures obtained following workup, or on aliquots collected from the reaction and worked up similarly. 1H NMR provided little information since menthyl-derived organotin species showed similar spectral characteristics, and mixtures could not be analysed. Interestingly, only very small amounts of unreacted $MenCl$ **170** could be detected. Due to the low sensitivity of ^{119}Sn NMR, it is possible that minor species were not always detected. Generally, complex mixtures were observed with numerous signals in the range 120 to -250 ppm. The species relevant to the following discussion are the Men_3SnCl **151** which appears as a sharp signal at 106 ppm ($CDCl_3$) and the dimer Men_6Sn_2 **148** which gives a weak, broad signal at ~ 18 ppm ($CDCl_3$).



Entry	Mg/MenCl/SnCl ₄ (scale)	Conditions (Time)		Product (yield)
		Grignard formation	Alkylation	
1	3/3/1 (0.06 mmol)	70 °C (16 h) ^{a,b,c}	70 °C (17 h)	—
2	10.3/8.5/1 (0.2 mmol)	50 °C (3 h) ^d	75 °C (17 h)	151+148
3	10.3/8.5/1 (0.2 mmol)	70 °C (20 h) ^e	70 °C (4 h)	151 (46%)
4	7.2/6/1 (0.28 mmol)	70 °C (15 h) ^f	70 °C (4 h)	151 (25%)
5	3/3/1 (0.28 mmol)	70 °C (5 h) ^{f,g}	70 °C (3 h) + r.t. (11 h)	151
6	7/7/1 (2.8 mmol)	70 °C (5 h) ^f	70 °C (4 h) + r.t. (12 h)	151 (36%)
7	7/7/1 (2.8 mmol)	60 °C (14 h) ^a	65 °C (20 h)	151 (37%)
8	7/7/1 (28 mmol)	70 °C (14 h) ^h	85 °C (17 h)	Unidentified (6 g)
9	8/8/1 (16.9 mmol)	70 °C (16 h) ⁱ	80 °C (3.5 h)	151 (4%)
10	7/5.2/1 (30 mmol)	70 °C (3 h) ^{e,h,i}	70 °C (4 h) + r.t. (12 h)	148 (6%)
11	8/8/1 (7.1 mmol)	Barbier ^B	80 °C, (7 h) + r.t. (17 h)	—

Table 3.2 Preparation of trimethyltin core. Grignard reagent preparation was carried out using concentrations of MenCl of approx. 1-1.5M, unless stated otherwise; SnCl₄ was added as a solution dissolved in a small volume of benzene. Filtration of the Grignard reagent solution was carried out through Celite, unless stated otherwise; Workup using 30% HCl(aq.) was carried out in all cases; Yields are reported for isolated products following crystallisation from EtOH; a. magnesium consumption was observed. b. sonication was used for initiation; c. ~0.3 M; d. EtBr initiator was used; e. (CH₂Br)₂ initiator was used; f. heating carried out with ultrasonication; g. ~0.5M; h. Grignard reagent solution was not filtered; i. ~0.8M.

Another species which was consistently observed displayed a sharp signal at 95 ppm (CDCl_3). This species occasionally co-crystallised with the desired product Men_3SnCl . The ratio of these two species was observed to vary during the reaction: after 1.5 h **151**/unknown = 1:3.2; after 3.5 h reflux 1:1.9. Other species observed showed sharp signals at 112 and 109 ppm (CDCl_3). In the large-scale reaction described in entry 8 one of these products was part of the isolated product. These species can be possibly assigned to the epimeric forms **174**, **175**, **176**.

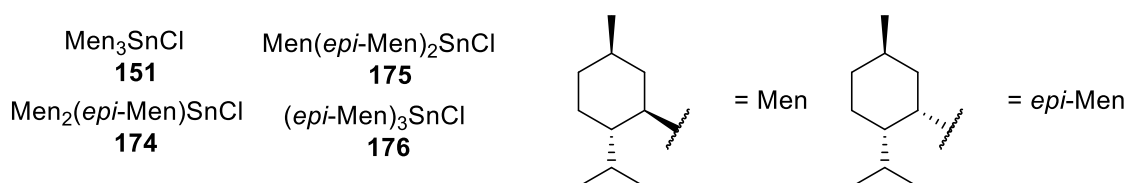
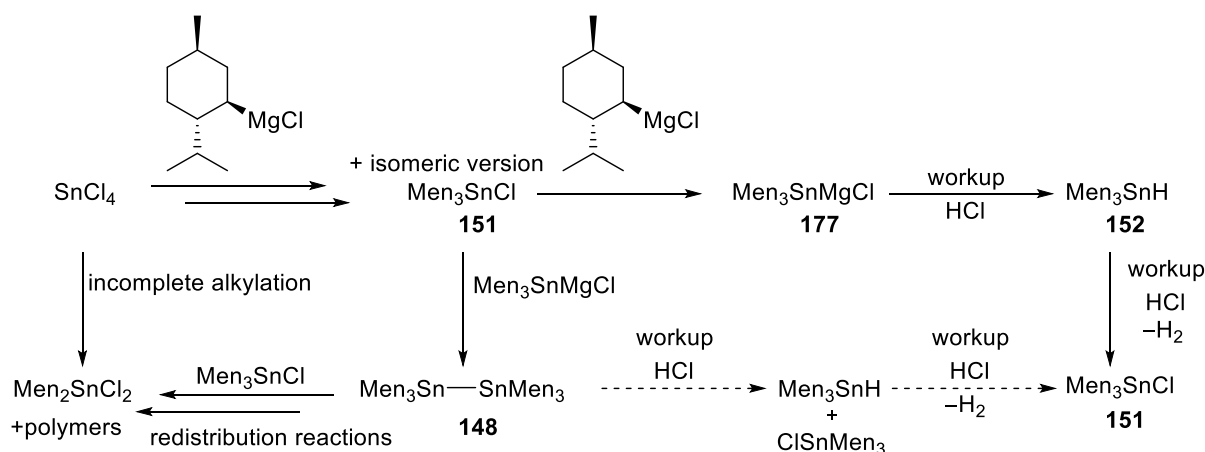


Figure 3.11 Epimeric menthyltin derivatives.

We have found that using a larger amount of the alkylating agent and extending its formation time have a beneficial effect on the reaction yield (entries 1-5, Table 3.2). This is understandable considering that successive alkylation presumably becomes more difficult due to electronic and steric factors, meaning that higher reagent concentration is required in the reaction environment. Reactions carried out at lower concentration provided inferior results (entries 1, 5, 11). For reactions containing sufficient Grignard reagent a reaction time of 4 h at reflux is sufficient (entry 3), however extending this time does not appear to be detrimental (entries 6 and 7). Increasing the scale of the reaction was found to be detrimental (entry 7 and 8), however this could be due to the higher reaction temperature employed in the larger scale reaction. Shorter reaction times at higher temperature (entry 8 and 9) allowed isolation of a small amount of **151**. On one occasion we obtained preferential crystallisation of the dimer **148**, even though this did not appear to be the dominant product in the crude reaction mixture (entry 10). Use of Barbier type conditions (addition of MenCl to a mixture of Mg and SnCl_4 in THF) gave rise to no identifiable product formation (entry 11).²⁸⁸ Purification of both Men_3SnCl **151** and Men_6Sn_2 **148** is reported *via* crystallisation from ethanol of the crude reaction product, however no experimental details are included.^{251,280} We have dissolved the crude products in a minimum

amount of ethanol required to form a solution. Product **151**, when present in sufficient amount, crystallised rapidly, the process being initiated by sonication or stirring. Product **148** crystallised by slow evaporation over the course of weeks. From our efforts we can conclude that both **148** and **151** are formed as reaction products to various extents. A plausible mechanistic scheme is described in Scheme 3.11.



Scheme 3.11 Proposed pathways leading to formation of **148** and **151** during alkylation.

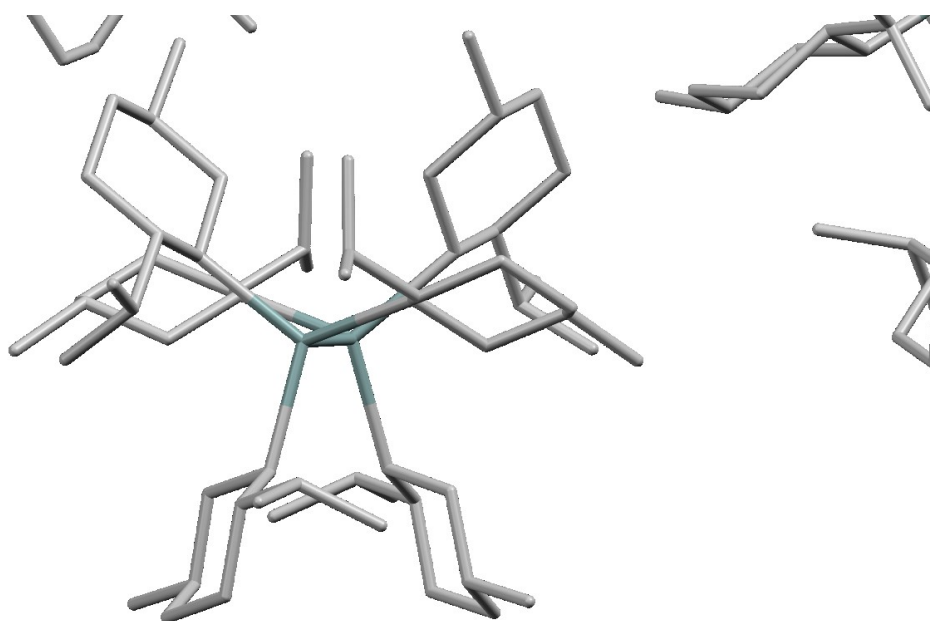
The primary product expected from the reaction is **151**. This can be transmetallated to form a stannyl anion equivalent **177**,^{289,290} which can act to alkylate **151** thereby forming the dimer **148**. This product can also form by a radical pathway as described by Dakternieks, which supported by the observation of epimerisation products, or *via* reaction between **177** and unreacted MenCl .^{280,290} Redistribution reactions between these two products are possible, as described by Wells.²⁹¹ If the trimethylstannyl anion **177** is present in the reaction mixture, it will get converted to **151** during workup, *via* the hydride **152** with hydrogen gas generation. Gas generation was noticed in the workup phase, particularly for large scale reactions (e.g entry 9). Magnesium metal had been filtered from the Grignard solution before use in the alkylation step, therefore hydrogen generation by reaction between Mg and HCl can be discounted. The possible evolution of *p*-menthane from Grignard quenching can also be discounted since this hydrocarbon is not a gas at room temperature. We have not investigated the nature of the gas being released, however we believe it is plausible for H_2 to be formed by one of the processes

described in Scheme 3.11. The cleavage of the dimer **148** is further explored in section 3.6.4.

	Men ₃ SnCl 151		Men ₆ Sn ₂ 148	
	Found	Literature ²⁵³	Found	Literature
¹ H NMR	See Experimental Chapter	—	CDCl ₃ : 0.91 (d, <i>J</i> = 6.7 Hz), 0.86 (d, <i>J</i> = 6.2 Hz), 0.8 (d, <i>J</i> = 6.7 Hz)	CDCl ₃ : 0.91 (d, <i>J</i> = 6.8 Hz), 0.86 (d, <i>J</i> = 5.9 Hz), 0.8 (d, <i>J</i> = 6.7 Hz) ²⁵¹
¹³ C NMR (<i>J</i> ¹³ C- ¹¹⁷ / ¹¹⁹ Sn, Hz)	CDCl ₃ : 46.4 (10.4), 43.9, 40.5 (19.3), 35.5, 35.5, 35.4, 27.2, 22.7, 22.3, 16.9	CDCl ₃ : 46.7 (11), 43.7 (329), 40.9 (17.6), 35.6 (65), 35.3, 35.3, 27.4 (67), 22.8, 22.3, 17	C ₆ H ₆ : 47 (15.7), 46.3, 40.2 (179.8, 34.8), 37.2 (59.4), 36.2, 34.9, 28.2 (45.7), 23, 22.6, 17.8	CDCl ₃ : 46.3 (19, 14), 45.5, 39.6 (196.4, 34), 36.5 (63.7), 35.7, 34.4 (11.8), 27.6 (48.2), 22.4, 22.1, 17.3 ²⁵¹
¹¹⁹ Sn NMR	CDCl ₃ : 106.2 C ₆ H ₆ : 92.3	C ₆ D ₆ : 93.6	C ₆ H ₆ : 19.2 (br)	CDCl ₃ : 21.2 ²⁸⁰ 18.8 ²⁵¹
Mass spectrometry	(ESI) 578.3768 [M(¹²⁰ Sn)- Cl+CH ₃ CN] ⁺	(EI) 571, 539, 434, 276, 260	(ESI) 1114.7490 [M(^{116,120} Sn)+CH ₃ CN+3 H] ⁺	Loss of menthyl group by ESI ²⁸⁰
[α] _D (c, C ₆ H ₆)	-123.8 (0.29, 25°C)	-80.9 (1.25, 20 °C)	-205.2 (2.56, 25°C)	-214 (c = 0.99, 20 °C) ²⁵¹
m.p.	128.6-129.7 °C	131.2-131.6 °C	dec. 250 °C	>280 °C ²⁸⁰

Table 3.3 Selected characterisation data for compounds **148** and **151**. For full data see Experimental chapter.

Characterisation data collected on the two products **148** and **151** are presented in Table 3.3 together with data reported in the literature. Comparison confirms the identity of the products prepared. In addition to this data, we have been able to confirm the structure of product **148** by crystallographic characterisation. Since all pathways leading to the formation of **148** involve **151** as an intermediate, this constitutes indirect evidence for the structure of **151**. X-ray quality crystals of **148** were grown by slow cooling of a hot (100 °C) 1,4-dioxane solution (21 mg/mL).



Molecule	Sn-Sn bond distance (Å)	Dihedral angle
A	2.8930(6)	21.96
B	2.9162(7)	25.46
C	2.9073(6)	24.85

Table 3.4 Metric parameters for dimer **148**. Molecule C depicted in POV-Ray image. Hydrogen atoms omitted for clarity. Grey = carbon, Cyan = tin; Data collection and analysis performed by Dr Andrew White.

Compound **148** crystallised with three crystallographically independent molecules in the asymmetric unit. All molecules contained 6 menthyl fragments, the absolute stereochemistry being confirmed by

measurement of the absolute structure parameter (Flack parameter = $-0.024(6)$). Interestingly, the molecules exhibit an almost eclipsed conformation (Table 3.4).

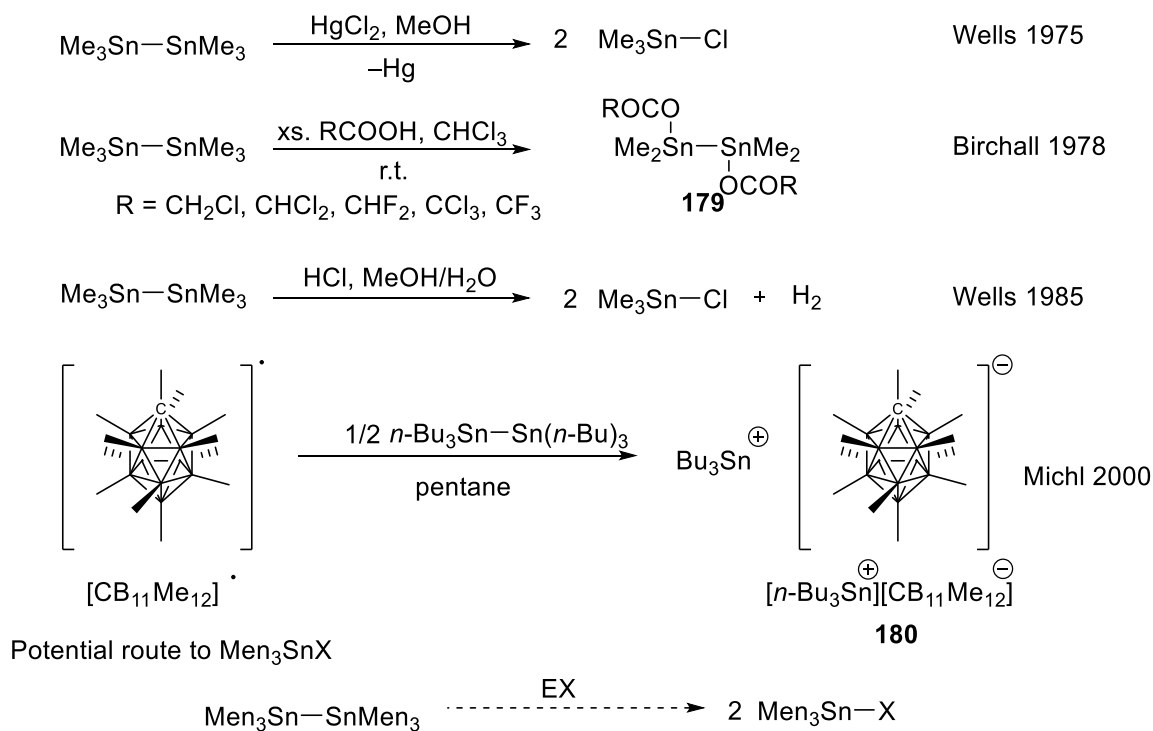
Dihedral angles were measured using three-atom ($\text{Sn}_1\text{-Sn}_2\text{-C}_{\text{menthyl}}$) mean planes. All Sn-C bonds were very similar in length (2.21-2.24 Å). The Sn-Sn bonds displayed consistent lengths as well (~ 2.9 Å). For comparison, the related compound hexacyclohexylditin²⁹² displays a staggered conformation (60°), a Sn-Sn bond length of 2.805(1) Å, and a Sn-C bond length of 2.154(5) Å. The elongated Sn-Sn and Sn-C bonds and the reduced dihedral angle in **148** are presumably a result of the additional steric demands of the menthyl substituent.

In conclusion, we have been able to prepare products containing the trimenthyltin core **148** and **151**, however challenges associated with scale up of these processes have hindered progress. The highest quantities of **151** produced in single reactions were in the ~ 0.5 g range and on one occasion 1 g of the dimer Men_6Sn_2 **148** could be isolated. Next, we explored options for converting these products to the desired trimenthylstannylum species **167**. It appears that successful formation of trimenthyltin products relies, in part, on the development of procedures for the large-scale preparation of the MenMgCl reagent **168**. We have briefly explored the preparation of MenLi as an alkylating reagent.²⁹³ Following reflux at 50°C for 17 h (using lithium pellets), no organolithium reagent formation could be observed by ^1H NMR.

3.6.4 Sn-Sn bond cleavage

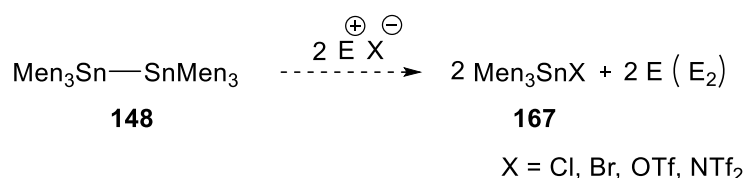
Having prepared a significant amount of Men_6Sn_2 (1 g), we considered synthetic routes to achieve conversion to the desired Men_3SnX **167** compounds. The cleavage of Sn-Sn^{251} and $\text{Sn-C(H}_3)^{249}$ bonds using Br_2 provides access to menthyltin bromides. Oxidative cleavage of the simple Me_6Sn_2 dimer **178** by different reagents has been investigated in the literature. Successful cleavage using HgCl_2 ,²⁹⁴ Me_2SnCl_2 ,²⁹⁵ and SnI_2 or $\text{GeCl}_2\cdot\text{PPh}_3$ was reported,²⁹⁶ however subsequent reactivity negates the synthetic utility.^{291,297} The potential use of protic acids has been described, however the reactivity observed is dependent on the nature of the acid. Birchall and Johnson used haloacetic acids to prepare

derivatives **179**, the reaction proceeding with Sn-C bond cleavage.²⁹⁸ Wells *et al.* reported that Sn-Sn and Sn-C bond cleavage are competitive processes when HCl is used as the acid source.²⁹⁹ The use of an oxidising agent featuring a poorly coordinating counterion to cleave a Sn-Sn bond would provide direct access to the desired **167** species. Such a procedure has been notably used by Michl *et al.* to generate a tributylstannylum cation equivalent **180**.³⁰⁰



Scheme 3.12 Cleavage of Sn-Sn bonds.

Cleavage of the Sn-Sn bond using Br₂ is a good starting point for synthesis (*via* reduction to Men₃SnH **152** followed by hydride abstraction, Scheme 3.7). We carried out this bromination procedure on a small scale,²⁵¹ however in our hands we observed the formation of 4 species by ¹¹⁹Sn NMR (91.2 major CCl₄, reported 105 CDCl₃; entry 1, Table 3.5). Prompted by the work of Wells, Jousseume, and Michl concerning the cleavage of Sn-Sn bonds (Scheme 3.12), we wondered whether direct conversion of Men₆Sn₂ to the desired Men₃SnX compounds **167** is possible. Such a transformation would then allow for a short, two step synthesis of Men₃SnX compounds **167** starting from MenCl **170**.



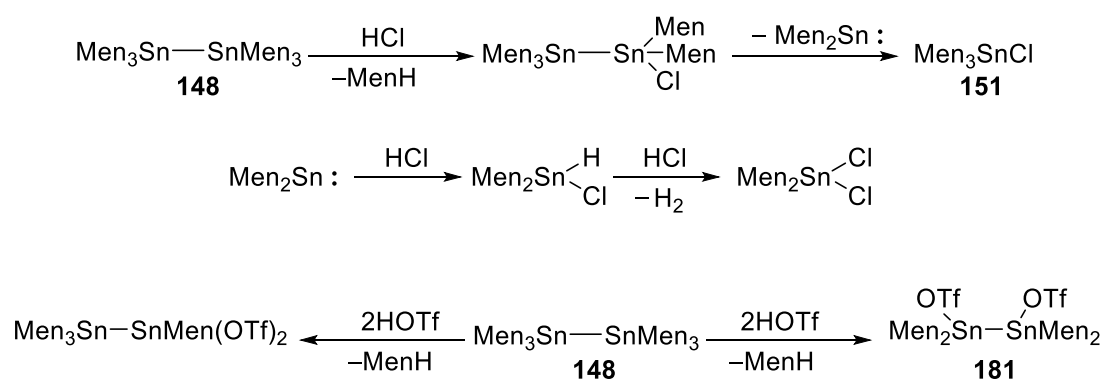
Entry	Oxidant	Conditions	Results
1	Br ₂	CCl ₄ , r.t., 17 h	Four Sn species formed
2	30% HCl _{aq}	THF, r.t., 1 h	No reaction
3	4M HCl (10 equiv.)	1,4-Dioxane, 80 °C, 49 h	Men ₃ SnCl formation (+H ₂)
4	HOTf (1 equiv.)	1,4-Dioxane, 80 °C, 24 h	No reaction
5	HNTf ₂ (1 equiv.)	1,4-Dioxane, 80 °C, 22 h	No reaction
6	HOTf (1 or 2 equiv.)	C ₆ H ₆ , 60 °C, 3 days	Sn-C bond cleavage
7	AgNTf ₂ (2 equiv.)	1,2-DFB, r.t.	Men ₃ SnNTf ₂ (δ _{Sn} = 362, 1,2-DFB)
8	Cp ₂ FeOTf (2 equiv.)	1,2-DFB, r.t., ~4 h	Men ₃ SnOTf (δ _{Sn} = 236, 1,2-DFB)

Table 3.5 Men₆Sn₂ dimer cleavage.

We carried out a small screen of oxidising agents, with reaction monitoring carried out by NMR. We aimed to develop a procedure which would allow for clean conversion to Men₃SnX **167** (preferably one species containing Sn formed only). We deemed this necessary as the products **167** are expected to be reactive, and therefore extensive purification techniques would be cumbersome to execute. We targeted X = OTf and NTf₂, option which dictated our choice of oxidising agents. Nonetheless, we started our investigation by considering the use of HCl as an oxidant to establish whether cleavage of the Sn-Sn bond in Men₆Sn₂ **148** is possible under alkylation workup conditions or otherwise (entry 2, Table 3.5). The reaction was carried out for 1 h with vigorous stirring (biphasic mixture). The starting material was recovered unchanged (¹H and ¹¹⁹Sn NMR analysis). We conclude that conversion of **148** to Men₃SnCl **151** during workup for the alkylation step (section 3.6.3) is most likely not occurring.

More interesting results were obtained when a 4M HCl/1,4-dioxane solution was used (entry 3). The starting material is poorly soluble at room temperature in this solution, however slow reaction was

found to occur when heating to 80 °C, leading to the formation of a major species tentatively assigned as **151** (^{119}Sn NMR: 86 ppm, cf. 88.4 ppm in THF-d8) *via* an intermediate (97.6 ppm), together with the formation of H_2 gas (^1H NMR, sealed NMR tube, 4.52 ppm, 1,4-dioxane¹⁰⁵). ^1H and ^{13}C NMR analysis suggested that a complex mixture was forming. Next, we investigated the use of HOTf and HNTf₂ in 1,4-dioxane, however under these conditions we were not able to observe any reaction (entries 4 and 5). We tried using benzene as solvent since cleavage of the Sn-Sn bond was postulated to occur *via* the undissociated form of the electrophile.²⁹⁹ Addition of 2 equiv. HOTf to a solution of **148** in benzene led to precipitate formation. Only very slow reaction could be observed at room temperature by ^1H NMR (23 h). Heating to 60 °C for 3 days led to the formation of a new species with similar ^1H NMR profile to the starting material. Hydrogen formation was not observed. This new species could be isolated from the reaction mixture following solvent removal and extraction with pentane and displays a ^{119}Sn NMR shift of 226 ppm (C_6H_6) and a symmetrical structure, as indicated by ^{13}C NMR (10 C environments). We have assigned this species **181** to result from Sn-C bond protolysis (Scheme 3.13). The crystalline material deposited from the reaction was found to be insoluble in DCM, which suggests it might be of inorganic or polymeric nature,²⁹⁹ or a ditriflate.³⁰¹ The reaction carried out with 1 equiv. HOTf was found to proceed in a similar fashion. We believe these results are possibly indicative of the reaction pathways shown in Scheme 3.13.²⁹⁹

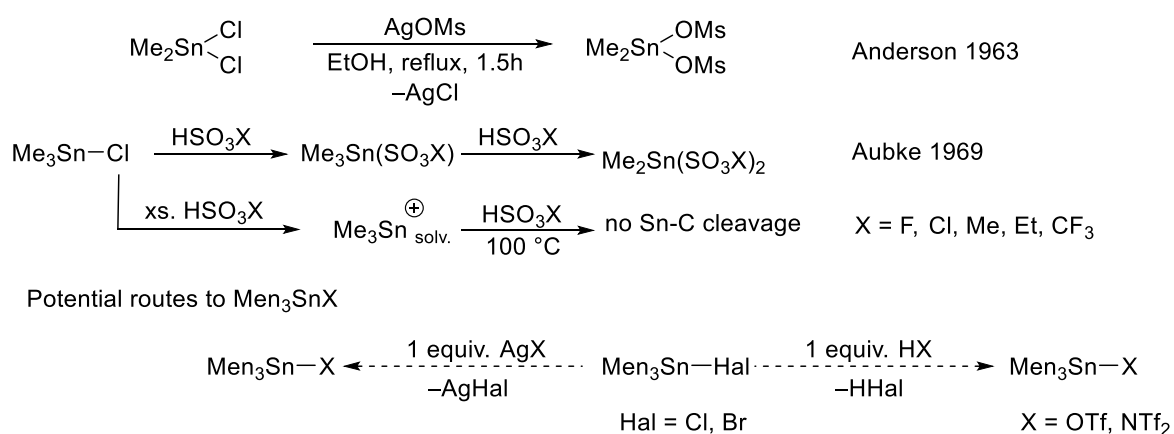


Scheme 3.13 Dimer **148** reactivity towards HCl and HOTf.

We turned to the use of established oxidising agents.³⁰² Commercially available AgNTf₂ was successful at rapidly converting the dimer **148** to the desired Men₃SnNTf₂ **182** (entry 7; 362 ppm, 1,2-DFB). The product was independently generated from **151** and AgNTf₂ and from Men₃SnH **152** and HNTf₂ (see section 3.6.5). We also investigated the mild oxidising agent Cp₂FeOTf (entry 8). Formation of a new species was observed to occur rapidly (30 min, 236 ppm, 1,2-DFB) and a gradual change in colour from deep blue to orange occurred over ~4 h indicating reduction of the ferrocenyl cation to ferrocene. After 29 h potential stannylation of ferrocene was observed. Optimisation of the reaction time to prevent secondary reactivity should allow preparative use of this reaction.

3.6.5 Counterion exchange

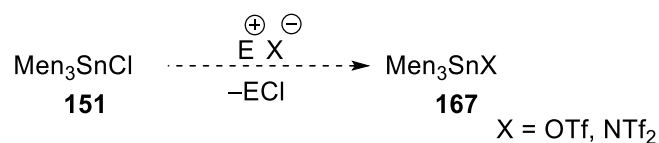
Substitution of a coordinating counterion such as halide for a less coordinating anion in a metathesis reaction could be applied for the synthesis of **167**. Such a process has been exploited early on for the synthesis of tin(IV) compounds through exchange with silver salts³⁰³ or displacement of a weaker acid by a stronger acid.^{304,305}



Scheme 3.14 Counterion exchange for organotin compounds.

In parallel with our efforts towards the oxidative cleavage of the dimer **148**, we investigated replacement of the chloride anion in **151** for a more weakly coordinating OTf or NTf₂ anion (Table 3.6). Silver salts were successfully used to achieve generation of the desired Men₃SnX (X = OTf **183**, NTf₂ **182**) species for NMR scale experiments (entries 1-3). Mixing of the reagents led to immediate

formation of a black precipitate. We believe this to be a result of the extreme light sensitivity of the nanoparticulate AgCl generated, which decomposes to metallic silver.



Entry	Reagent, solvent	¹¹⁹ Sn NMR
1	AgNTf ₂ , C ₆ H ₆	342 (C ₆ H ₆)
2	AgOTf, C ₆ H ₆	218 (C ₆ H ₆)
3	AgNTf ₂ , 1,2-DFB	361 (1,2-DFB)
4	HOTf, DCM-d ₂ , 120 °C	273 (DCM-d ₂)+ 94

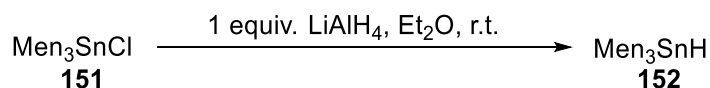
Table 3.6 Counterion exchange studies.

Alternatively, low levels of Men₆Sn₂ **148** could have been present in **151** although this would not justify the extent to which the phenomenon occurred. We suspected that the silver residues and other decomposition products could interfere with catalytic activity, therefore we attempted to remove them by allowing sufficient time for precipitation to occur before filtering through Celite®. We obtained successful results using such solutions (see hydrogen activation section 3.8.1). Nonetheless, we sought alternative methods for the preparation of **167** for isolation. We attempted to displace HCl with HOTf by the method of Aubke (entry 4).³⁰⁵ Formation of a new species by ¹¹⁹Sn NMR was suggestive of successful reaction (273 ppm, DCM-d₂), however even strong heating could not drive the reaction to completion. This led to formation of the previously reported impurity (94 ppm) possibly by action of HCl or rearrangement. Kuivila reported a similar displacement reaction to be an equilibrium.³⁰¹

3.6.6 Trimethyltin hydride preparation

Having investigated a range of options for generation of **167**, we decided that most appropriate would be preparation of the known Men_3SnH **152**, followed by hydride abstraction with HOTf or HNTf_2 , a preparation analogous to that used in chapter 2 for borenium cation **95**.

Men_3SnH **152** has been prepared in the literature from the corresponding chloride **151** by Jousseume, however full experimental details were not included.²⁵³ The original procedure using LiAlH_4 was reported by Schumann and Wassermann and employed a reaction time of 5 h.²⁴⁹ Purification is generally reported to be carried out by high vacuum distillation or chromatography.²⁵² Our efforts at preparing Men_3SnH **152** are described in Table 3.7



Entry	Conditions	Results
1	21 h	~90% purity crude; decomposes on silicagel
2	6 h	No hydride formation detected
3	21 h	~ 10% conversion; decomposes during distillation
4	0.4 M, 24 h, purified LiAlH_4	52% yield

Table 3.7 Preparation of Men_3SnH . Reactions carried out at r.t. with stirring at a concentration of ~0.1M unless otherwise stated.

In entry 1, the reaction was successful however the product obtained was contaminated with another hydride type species (~10%, assumed Sn-H type, -174 ppm, CDCl_3). Attempted purification by column chromatography led to complete decomposition of the material. We assumed that the long reaction time could be causing decomposition, therefore we ran the reaction for 6 h (entry 2). We couldn't detect any hydride formation by ^{119}Sn NMR in the crude product. In a different trial (entry 3) we obtained only very low conversion (~ 10% based on ^{119}Sn NMR) using the same conditions as in entry 1. Attempted distillation using a vacuum bridge led to almost complete decomposition, a small

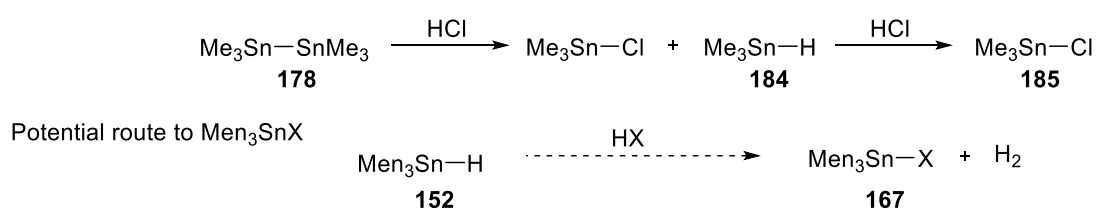
amount of the Men_6Sn_2 **148** dimer forming in this process. Finally, carrying out the reaction using purified LiAlH_4 resulted in successful reaction: the crude product was isolated in 52% yield with no detectable tin-containing impurities being present. Sampling of the reaction supported our previous findings: after 4.5 h no hydride formation could be detected, however after 21 h complete conversion of Men_3SnCl **151** to Men_3SnH **152** was found. We believe these results could be explained by the heterogeneous nature of the reaction mixture: LiAlH_4 is only sparingly soluble in Et_2O . The product was characterised by ^1H , ^{13}C and ^{119}Sn NMR. Data are presented in Table 3.8.

Men ₃ SnH 152		
	Found	Literature ²⁵³
^1H	C_6D_6 : 5.48 (^1H , $^1J(^1\text{H}-^{117/119}\text{Sn}) = 1374/1438$ Hz), CDCl_3 : 4.92 (^1H , $^1J(^1\text{H}-^{117/119}\text{Sn}) = 1358/1420$ Hz)	CDCl_3 : 5.23
^{13}C ($J^{13}\text{C}-^{117/119}\text{Sn}$, Hz)	C_6D_6 : 47.8, 43.3, 36, 35.8, 34.5, 33.9, 27.3, 23, 22.4, 16.4	CDCl_3 : 47.7 (16), 43.8 (16.8), 37.8 (60.5), 36, 34.4 (339), 33.8 (18), 27.2 (53), 23, 22, 16.3
^{119}Sn	C_6D_6 : -103.8 CDCl_3 : -103.5 $^{1/3/2}J(^{119}\text{Sn}-^{13}\text{C}) = 339.8/59/17.4$ Hz	C_6D_6 : -102.9

Table 3.8 Selected characterisation data for Men_3SnH **152**. For full data see Experimental chapter.

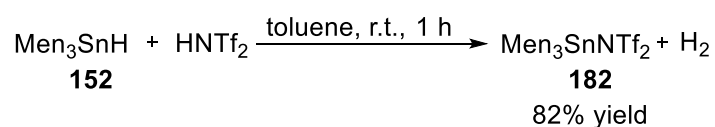
3.6.7 Hydride abstraction

Wells *et al.* proposed HCl cleavage of dimer **178** to occur *via* the tin hydride Me_3SnH **184**, which is then converted by acid to the corresponding chloride Me_3SnCl **185**.



Scheme 3.15 Sn-H bond cleavage.

Having obtained the desired Men_3SnH we investigated its reaction with HNTf_2 in C_6H_6 . Acid addition led to immediate gas evolution, the reaction solution remaining clear. NMR analysis indicated formation of the desired $\text{Men}_3\text{SnNTf}_2$ (341 ppm, C_6H_6). We performed this reaction on a preparative scale (0.19 mmol) in toluene. The reagents were combined with stirring and gas evolution took place over the course of ~10 min. After 1 h the solvent was removed to give $\text{Men}_3\text{SnNTf}_2$ **182** as a white solid (82% yield).



Scheme 3.16 Preparation of $\text{Men}_3\text{SnNTf}_2$.

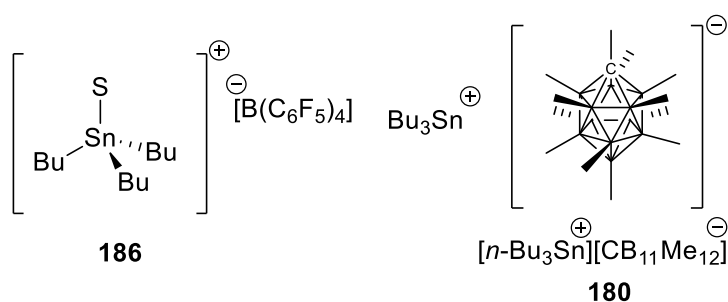
$\text{Men}_3\text{SnNTf}_2$ **182** was found to be soluble in hydrocarbon solvents (benzene, toluene) unlike the parent compound ${}^i\text{Pr}_3\text{SnOTf}$ **132**. Remarkably, **182** was found to be soluble in pentane. Characterisation was carried out by ${}^1\text{H}$, ${}^{13}\text{C}$, ${}^{119}\text{Sn}$ and ${}^{19}\text{F}$ NMR (Table 3.9).

	$\text{Men}_3\text{SnNTf}_2$ 182	
	C_6D_6	Pentane
${}^1\text{H}$	2.68-2.35 (2m, 2H), 1.47 (m, 5H), 1.14-0.58 (13H): 0.98 (d, $J = 6\text{Hz}$)	2.64 (m), 2.33 (m), 1.82 (m)
${}^{13}\text{C}$ (J ${}^{13}\text{C}$ - ${}^{117}/{}^{119}\text{Sn}$, Hz)	49, 46.5, 39.8 (22.5), 38.9 (31.8), 35.4, 35.1, 27.4, 22.5, 22.1, 17.1	118.6 (CF_3), 47.9, 45.7, 38.8 (20.6), 37.3 (30.8), 34.5, 34.2, 26.5 (69.4), 20.9 (x2), 15.8; additional peaks: 30.8, 29, 24.9
${}^{119}\text{Sn}$ (J ${}^{119}\text{Sn}$ - ${}^{13}\text{C}$, Hz)	342.8; FWHM = 8.7 Hz	308.5 (238, 66); FWHM = 8.5 Hz
${}^{19}\text{F}$	-77.9	-79.8

Table 3.9 Characterisation data for $\text{Men}_3\text{SnNTf}_2$ **182**.

of a weak tetrahedral adduct with the solvent.³¹¹ Since our value was measured in pentane, solvent which has no donor ability, we propose that $\text{Men}_3\text{SnNTf}_2$ **182** retains its tetrahedral structure in solution; additional lowering of the 1J (^{119}Sn - ^{13}C) value occurs possibly due to the lengthening of the Sn-N bond and due to the electron-donating ability of the Men ligands.

The ^{119}Sn NMR characteristics of $\text{Men}_3\text{SnNTf}_2$ **182** are worth comparing, in conjunction with measured values of Gutmann-Beckett AN, with those of the compounds $^i\text{Pr}_3\text{SnOTf}$ **132**, Bu_3SnOTf **133**, Bn_3SnOTf **134**, **180** and **186**.³⁰⁰



	133 ³⁰¹	186 ³¹¹	180 ³⁰⁰	132 ⁵⁶	134 ²⁴⁰	$\text{Men}_3\text{SnNTf}_2$ 182		
Solvent	CDCl_3	CD_2Cl_2	C_6D_{12}	CDCl_3	CDCl_3	C_5H_{12}	C_6D_6	<i>o</i> - $\text{C}_6\text{H}_4\text{F}_2$
^{119}Sn δ	168.4	349	454.3	156	87.4	308.5	342.8	361.2
FWHM (Hz)	n/a	n/a	~800	130	48.4	8.5	8.7	17
1J (^{119}Sn - ^{13}C) (Hz)	382.8	278	n/a	316	271.2	238	n/a	n/a
GB AN	64.2	n/a	n/a	68	74	79.1		

Table 3.10 ^{119}Sn NMR data for stannylum ion equivalents.

The high chemical shift value for $\text{Men}_3\text{SnNTf}_2$ **182** is indicative of significant stannylum ion character. The ^{119}Sn NMR chemical shift depends on the nature of the R groups and solvent and cannot be used solely to assess stannylum ion character and Lewis acidity. When compounds featuring the same R groups are compared, it does provide a useful indication of stannylum character (Bu_3SnOTf **133**, **180**, **186**, Table 3.10; Men_3SnOTf **182** and $\text{Men}_3\text{SnNTf}_2$ **183**, Table 3.6). The solvent affects observed stannylum ion character as well: $\text{Men}_3\text{SnNTf}_2$ **182** shows progressively higher chemical shift in the

series: pentane < benzene < 1,2-difluorobenzene; complex formation with the solvent is likely involved in causing this effect.³¹¹

The value of $^1J(^{119}\text{Sn}-^{13}\text{C})$ is a useful measure to assess the extent of trigonalisation of the Sn atom, but is, as discussed, affected by the nature of the R groups. The observed trend for $^1J(^{119}\text{Sn}-^{13}\text{C})$ in the series R_3SnOTf ($\text{Bu} > ^i\text{Pr} > \text{Bn}$) is the opposite to the trend observed for the measured Lewis acidity.

The peak width for the ^{119}Sn NMR signal is a further measure which can be used to assess stannylum ion character.³⁰⁰ In the absence of sufficient steric shielding, aggregation effects lead to broadening by exchange processes, e.g. boranyl complex **180**. Increasing steric hindrance (in the series $^i\text{Pr} < \text{Bn} < \text{Men}$) leads to a reduction in aggregation effects and sharpening of the NMR ^{119}Sn signal. The values observed for **182** are particularly remarkable and we believe are a result of steric shielding and sufficiently strong intramolecular interaction with the weakly coordinating NTf_2 anion.

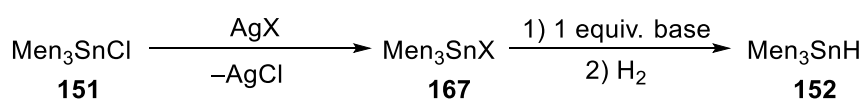
The Lewis acidity of **182** was measured using the standard procedure employed for borenium **95** (chapter 2). A complex between Et_3PO and $\text{Men}_3\text{SnNTf}_2$ was formed, supported by the observation of Sn-P coupling in both ^{119}Sn (189.1 ppm, d, $^2J = 198$ Hz) and ^{31}P NMR (76.7 ppm, $^2J(^{31}\text{P}-^{117}/^{119}\text{Sn}) = 189/198$ Hz, $^1J(^{31}\text{P}-^{13}\text{C}) = 66$ Hz); and by the downfield shift for Et_3PO . In contrast to the situation observed with borenium **95**, the excess $\text{Men}_3\text{SnNTf}_2$ **182** was almost undetectable by ^{119}Sn NMR, possibly due to interaction with resulting NTf_2 anion. The measured AN = 79.1 indicates that **182** is a stronger Lewis acid than $^i\text{Pr}_3\text{SnOTf}$ **132**, Bn_3SnOTf **134** and $\text{B}(\text{C}_6\text{F}_5)_3$ **4b**. The Lewis acidity varies inversely with the ^{119}Sn signal linewidth, suggesting that improved Lewis acidity is a result of the increased steric 'frustration' provided by the bulky menthyl ligand.

3.8 Catalytic and stoichiometric studies

3.8.1 Hydrogen activation

In entry 1 (Table 3.11), **182** was generated by treating **151** with AgNTf_2 . Even after 3 d a small amount of what appeared to be **151** could be detected (92.6 ppm, C_6H_6). Following filtration (Celite®), two

equivalents of 2,6-lutidine were added. This did not cause disappearance of the $\text{Men}_3\text{SnNTf}_2$ **182** signal (342 ppm), indicating that adduct formation with the base does not appear to be proceeding.



Entry	Halide abstraction	Hydrogen activation	Results
1 ^{a,b}	AgNTf ₂ , C ₆ H ₆ , 3 d	2,6-lutidine, 120 °C, 2 h	No H ₂ activation
2 ^b	AgOTf, C ₆ H ₆ , 6 h	2,6-lutidine, 120 °C, 24 h	No H ₂ activation
3 ^c	AgNTf ₂ , 1,2-DFB (0.043 M), 24 h	DABCO, r.t., 17 h	H ₂ activation
4 ^c	Men ₃ SnNTf ₂ 1,2-DFB (0.017 M)	DABCO, r.t., 72 h	H ₂ activation

Table 3.11 Hydrogen activation studies. Halide abstraction was carried out at room temperature with 1 equiv. Ag salt unless otherwise stated; reactions were filtered before using for hydrogen activation studies. a. 2 equiv. AgNTf₂ and 2 equiv. 2,6-lutidine used; b. 4 bar H₂; c. 10 bar H₂

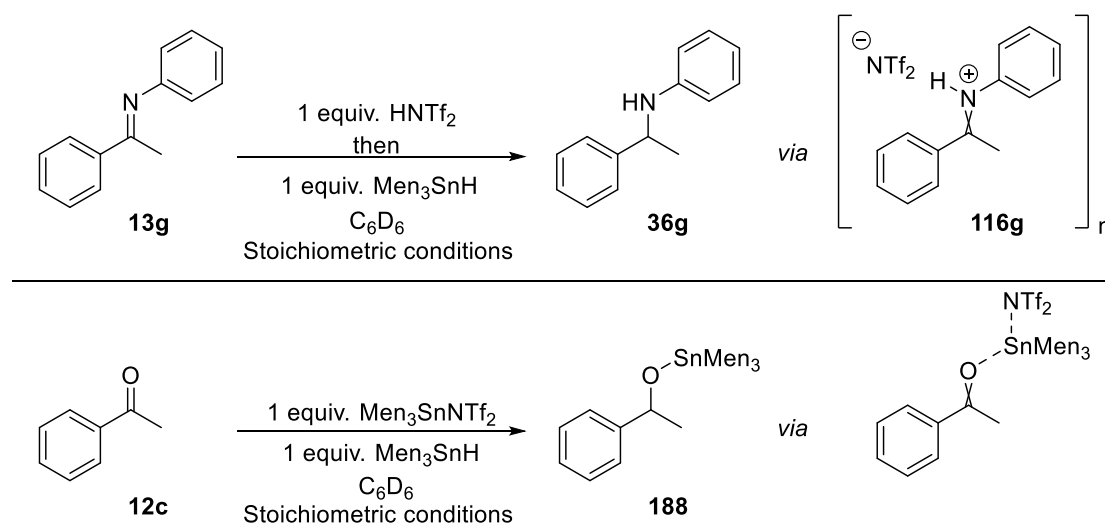
However, peaks corresponding to lutidine (~2.2, 6.4 ppm) were broadened suggesting reversible interaction to be occurring. Following addition of hydrogen gas (to 4 bar), no hydride formation could be detected by ¹H or ¹¹⁹Sn NMR at room temperature (17 h) or after heating to 120 °C (2 h). Slow conversion of the signal at 342 ppm to the one at 92.6 ppm could be observed. We believe this to result from the presence of trace water in commercially available AgNTf₂ and the introduction of moisture during pressurising, which is leading to the conversion of Men₃SnNTf₂ to (Men₃Sn)₂O **187**. This is supported by the resolution of peaks corresponding to the formation of 2,6-lutidinium cation (¹H 12.79, 6.39, 2.31 ppm). It would appear then that Men₃SnCl and (Men₃Sn)₂O have very similar chemical shifts. For subsequent experiments AgNTf₂ was further dried under vacuum and the experiment in entry 1 was repeated using anhydrous AgOTf. In this case complete conversion to Men₃SnOTf **183** was observed (218 ppm, C₆H₆). Addition of lutidine did not cause any change in the ¹¹⁹Sn NMR spectrum. Following addition of hydrogen (4 bar) no evidence of hydrogen activation could be observed at r.t. (51 h), 60 °C (19 h) or 120 °C (24 h). Remarkably, ¹¹⁹Sn NMR indicated Men₃SnOTf

183 to be stable even after prolonged heating to 120 °C. Again, resolution of peaks corresponding to lutidine/lutidinium species was observed. At this point we considered whether the presence of residual Ag⁺/Ag could be the cause for this behaviour, by catalysing decomposition of any **152** being formed. This was prompted by the observation that addition of lutidine to a clear solution of **183** caused formation of a crystalline precipitate, which with time turned dark in colour. Nonetheless, it appeared that although a stronger Lewis acid than *i*-Pr₃SnOTf **132**, Men₃SnNTf₂ **182** is not strong enough to give stoichiometric activation of hydrogen using a weak base (lutidine) in a nonpolar solvent (benzene) at low pressure. We then decided to carry out hydrogen activation using **182** and the strong base DABCO (pK_aH = 8.82, H₂O) in 1,2-DFB at a higher hydrogen pressure (entry 3). We attempted to shield the reaction from light, however formation of dark, metallic precipitate following halide abstraction was observed nonetheless. Following filtration and DABCO addition we observed the disappearance of the ¹¹⁹Sn signal characteristic to **182** and the appearance of broad signals in the ¹H NMR spectrum corresponding to a slow exchange equilibrium between free acid/base and the adduct. This is in contrast to the behaviour observed for DABCO/**132**, system which is found in rapid exchange.⁵⁶ Following addition of hydrogen (10 bar) successful hydrogen activation was observed at room temperature (17 h): peaks corresponding to Men₃SnH **152** were observed by ¹H NMR (5.32 ppm) and ¹¹⁹Sn NMR (-105 ppm), and to [DABCOH]⁺ by ¹H NMR (10.94, 2.99). Recording of the ¹¹⁹Sn NMR spectrum without decoupling proved the nature of the Men₃SnH formed: the sharp singlet split to a weak broad doublet (*J* = ~1430 Hz).

The successful synthesis of Men₃SnNTf₂ **182** allowed us to repeat this experiment (entry 4). Similar results were obtained. At this lower concentration (0.017 as opposed to 0.043 M) we observed the reaction to proceed slowly over 72 h, which suggests that hydrogen activation could be rate determining under catalytic conditions.

3.8.2 Stoichiometric and catalytic reduction studies

We began by testing the ability of Men_3SnH **152** to reduce an imine substrate under ionic conditions. Substrate **13g** was protonated using HNTf_2 (entry 1, Table 3.12). This led to the formation of the iminium ion **116g**. The spectrum of this species in C_6D_6 is complex, with two environments observed for the NH proton (11.71, 11.61, 1H), and 7 environments for the Me group (2.58-1.89, 3H).

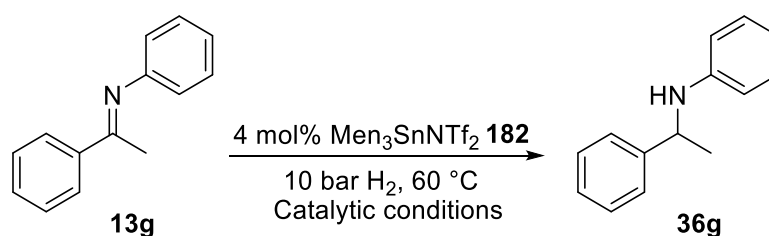


Entry	Substrate	Conditions	Conversion	e.r. (<i>R:S</i>) ^a
1	13g	r.t., 21 h	86 %	56:44
2	12c	100 °C, 40 h	22 %	–

Table 3.12 Stoichiometric reduction studies. Conversion determined by NMR on the reaction mixture by integration against a capillary insert or by relative integration. a. determined by chiral HPLC on products purified by column chromatography; enantiomers assigned by referencing of HPLC traces.

Addition of **152** initiated reduction: NMR analysis carried out soon thereafter indicated formation of amine **36g**. ^{119}Sn NMR indicated at this point only the presence of **152**. After 21 h at room temperature almost complete Men_3SnH **152** consumption is observed together with formation of $\text{Men}_3\text{SnNTf}_2$ **182**. This is remarkable indicating that no interaction between **182** and the amine **36g** is occurring. The selectivity of this reduction was disappointing with an e.r. of 56:44 measured following product

isolation. A stoichiometric reduction of acetophenone **12c** using stoichiometric Lewis acid **182** and reducing agent **152** was next attempted (entry 2). This reaction requires in principle only catalytic amounts of Lewis acid, however a stoichiometric amount was used to avoid issues resulting from inhibition. No interaction between **12c** and **182** was observed, however upon addition of hydride **152** a strong decrease in the intensity of the stannylum signal was detected by ^{119}Sn NMR. No reduction was observed at room temperature. Temperature was increased in 20 °C increments, with the reaction allowed to proceed for sufficient time (17-28 h) before re-analysing. Very slow build-up of a new product was observed (^1H NMR 5.04 ppm, septet). A final conversion to what is assigned as $\text{PhCH}(\text{Me})\text{OSnMen}_3$ **188** of 22% was achieved after 40 h at 100 °C. The reaction was worked up with a 15% KF solution. The crude material contained a significant amount of organotin material; following chromatographic purification we were not able to isolate any 1-phenylethanol **11c**. We believe that both these results (slow reduction of an iminium and failed reduction of acetophenone) are the result of the very high steric hindrance present in Men_3SnH **152**. Interestingly, we were not able to observe $\text{Men}_3\text{SnNTf}_2$ **182** by ^{119}Sn NMR in the presence of excess (25 equiv.) **13g**.



Entry	Conditions	Conversion	e.r. (<i>R:S</i>) ^a
1	C ₆ H ₆ , 19 h	0 %	-
2	1,2-DFB, 19 h	4 %	48:52
3	4 mol % 2,4,6-collidine, 1,2-DFB, 84 h	14 %	48:52

Table 3.13 Catalytic reduction studies. Conversion determined by NMR on the reaction mixture by integration against a capillary insert or by relative integration. a. determined by chiral HPLC on products purified by column chromatography. enantiomers assigned by referencing of HPLC traces.

Under catalytic conditions (entry 1, Table 3.13) we were not able to see any reduction occurring at temperatures up to 60 °C in benzene. Switching to a more polar solvent (entry 2, Table 3.13) and the addition of auxiliary base (entry 3) allowed reaction to proceed, however no great improvement in rate was observed resulting from base addition.

The Men_3SnH **152** formed under these reaction conditions was persistent and could be observed by ^1H and ^{119}Sn NMR after cooling the reaction to room temperature. We believe this behaviour, in contrast to that of $^i\text{Pr}_3\text{SnOTf}$ **132**, indicates that catalysis is limited by the rate of substrate reduction and by the rate of hydrogen activation (due to steric hindrance and not due to weak Lewis acidity), and not due to catalyst inhibition. Lewis acid **132** displays a great improvement in catalysis rate upon the addition of 2,4,6-collidine (to aid hydrogen activation) and a reduction in rate when DABCO is employed. This latter observation was interpreted to result from an inability to protonate ROSn^iPr_3 complexes in the presence of DABCO.⁵⁶ All the observations are consistent with the idea that the dramatically higher steric shielding in **182** resolves issues requiring ‘frustration’ but leads to hindrance in reduction steps.

The enantioselectivity levels observed in the reduction of **13g** are disappointing under both stoichiometric (r.t.) and catalytic conditions. We believe this could be due to the nature of the hydride reducing agent **152**. The shape of the reagent is essentially ‘spherical’ with very little differentiation in environments realised by the three Men fragments. The ionic nature of the hydride delivery step does not appear to result in sufficient organisation of the transition state to overcome the detrimental effect of the large C-Sn separation.

3.9 Conclusions

The novel strong Lewis acid $\text{Men}_3\text{SnNTf}_2$ **182** has been prepared and isolated. NMR characterisation indicates that **182** exists as a monomeric species exhibiting stannylum ion character, even in non-polar, non-coordinating solvents such as pentane. This remarkable property results from the steric shielding provided by the bulky menthyl groups, in combination with the weak donor ability of the

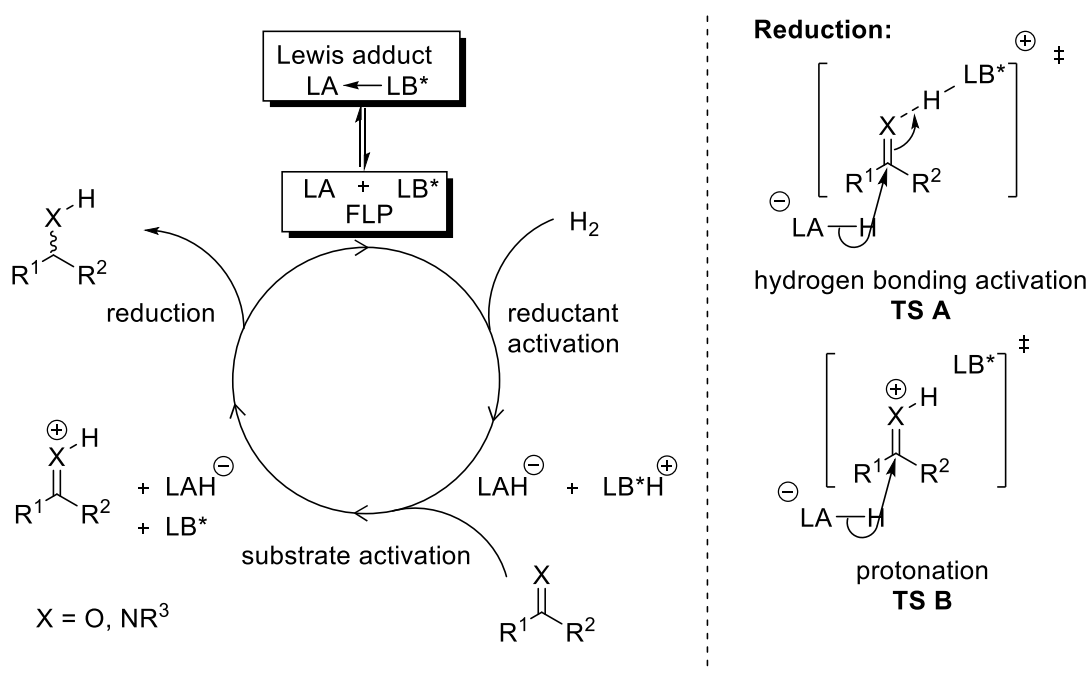
NTf₂ anion. In agreement with its structure, **182** displays high Lewis acidity in the Gutmann-Beckett test (AN = 79.1). Compound **182** is capable of activating hydrogen at room temperature in combination with a strong amine base (DABCO) and of catalysing the hydrogenation of ketimine **13g** at 60 °C. Although the rate of reaction is very slow at this temperature, it indicates the value of ‘increasing frustration’ as a strategy for developing more active catalysts than **132**, which catalyses the same transformation at 120 °C. Unfortunately, enantioselectivity in the reduction of **13g** was negligible.

In the future, exploration of derivatives of the type Men₂RSnX, where R = ethyl, isopropyl, etc., could provide improved reactivity and enantioselectivity, resulting from a reduction in steric bulk and better differentiation of chiral environments.

4 Chapter 4–Chiral phosphate Lewis bases

4.1 Introduction

Scheme 4.1 describes that chirality in the enantiodetermining reduction step can be transferred from the Lewis base component if interaction with the activated substrate occurs before hydride delivery from the achiral LAH. The schematic **TS A** and **TS B** detail potential mechanisms by which transfer of chirality from the Lewis base could occur when carrying out reduction. In their extensive review of organocatalysis performed using chiral phosphoric acids, Rueping *et al.* propose structures similar to **TS A** and **TS B** (Scheme 4.1) as idealised modes of activation carried out by a chiral phosphoric acid on a Brønsted basic imine substrate.³¹² Experimental evidence is discussed in section 4.1.2.1.

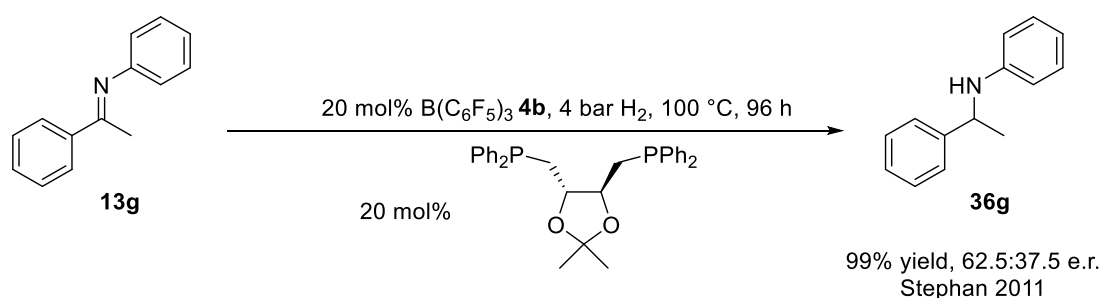


Scheme 4.1 General mechanism for enantioselective hydrogenation using chiral Lewis bases.

4.1.1 Literature precedent in the field of FLP chemistry

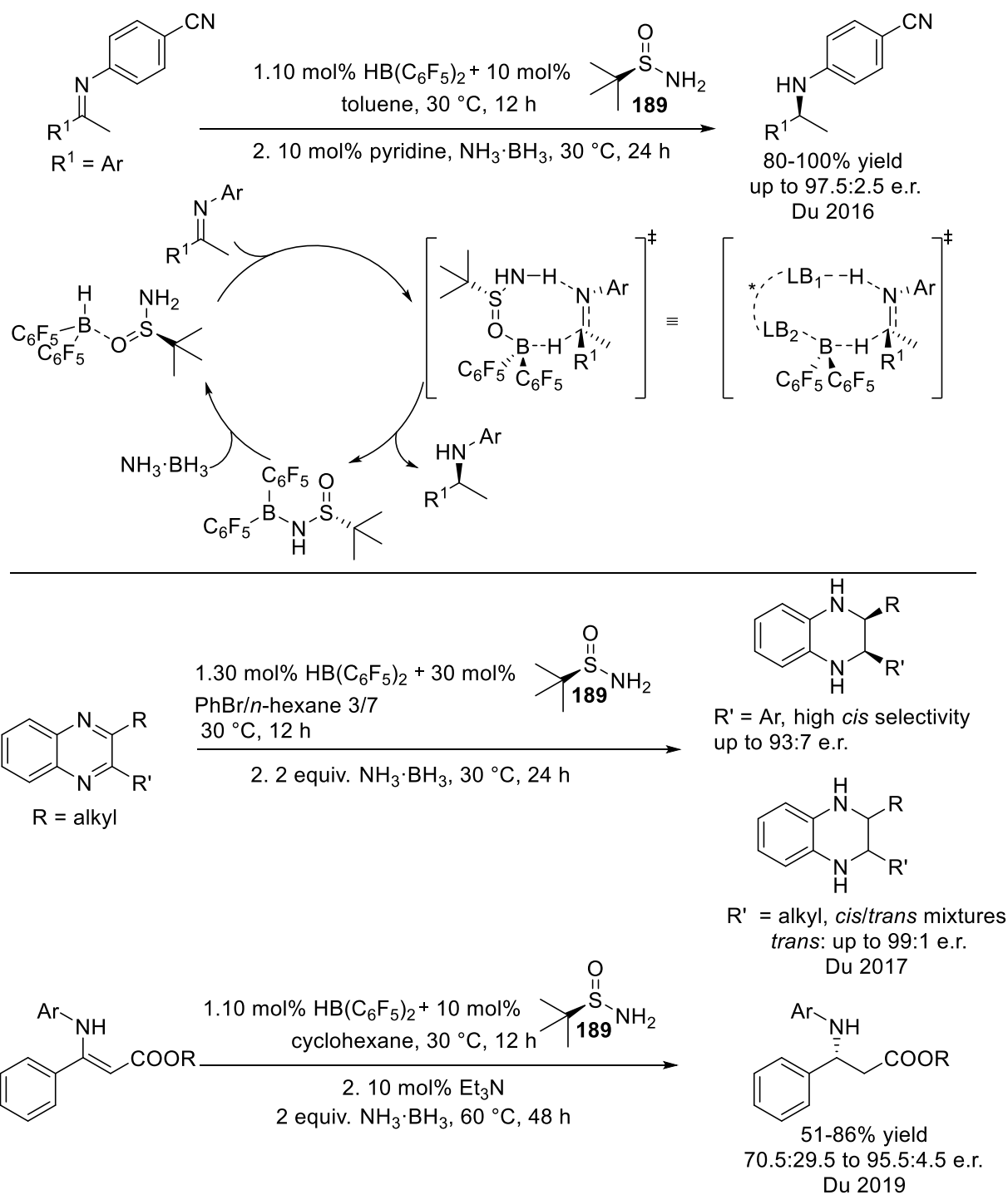
Early on, Stephan *et al.* considered the use of a chiral Lewis base and investigated chiral phosphine bases for the hydrogenation of the model substrate **13g**,³¹³ but the results were disappointing (62.5:37.5 e.r., Scheme 4.2). Although it is probable that the high temperature required for catalysis

to occur is in part the cause for the low selectivity observed, the authors themselves remark that ‘Employing a chiral phosphine is only going to impact the induced chirality if it remains in close proximity to the iminium as the hydride is transferred to the imine carbon center. The above data suggest that NH/P hydrogen bonding is weak at best and thus has a minimal effect.’ From this analysis we can see that, *a priori*, the mechanism of activation was assigned as depicted in **TS B** (Scheme 4.1) based on the knowledge available at the time of imine activation in FLP hydrogenation catalysis.



Scheme 4.2 Enantioselective hydrogenation using chiral phosphine bases reported by Stephan.³¹³

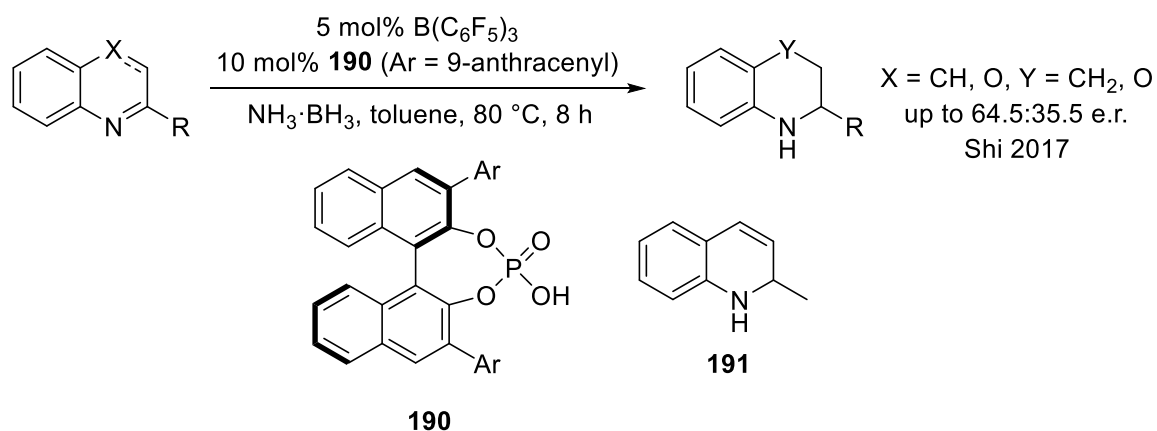
More recently, Du has explored the use of the chiral sulfinamide **189** in combination with Piers’ borane **23b** and showed this system to be competent in the transfer hydrogenation of *N*-aryl imine substrates (Scheme 4.3)³¹⁴ The proposed mechanism involves a concerted transfer of both hydride and proton fragments to the substrate, this being supported by experimental and computational investigation. Conceptually, this is made possible by the presence of two Lewis basic sites in the chiral base component (O and N lone pair in the sulfinamide). It is therefore possible to visualise this system as an ‘intramolecular’ FLP carrying out reduction of the imine substrate *via* a transition state of the type **TS A** (Scheme 4.1). This catalytic system was subsequently adapted for the transfer hydrogenation of 2,3-quinoxalines³¹⁵ and β -*N*-substituted enamino esters.³¹⁶ In an interesting extension of this methodology, the Du group used chiral phosphoric acids to catalyse the enantioselective reduction of *N*-aryl ketimines and β -*N*-substituted enamino esters with ammonia borane. The postulated reducing agent was a chiral phosphoric acid-derived ammonia borane: the reaction does not require a Lewis acid for generation of the reducing agent.³¹⁷



Scheme 4.3 Use of chiral sulfinamides in FLP hydrogenation, reported by Du.³¹⁴

Shi *et al.* have reported preliminary work attempting to carry out the enantioselective transfer hydrogenation of quinolines and 1,4-benzoxazines using borane **4b** and BINOL-derived phosphoric acid **190** as a source of chirality.³¹⁸ The mechanism of FLP-catalysed hydrogenation of quinaldine **123a**

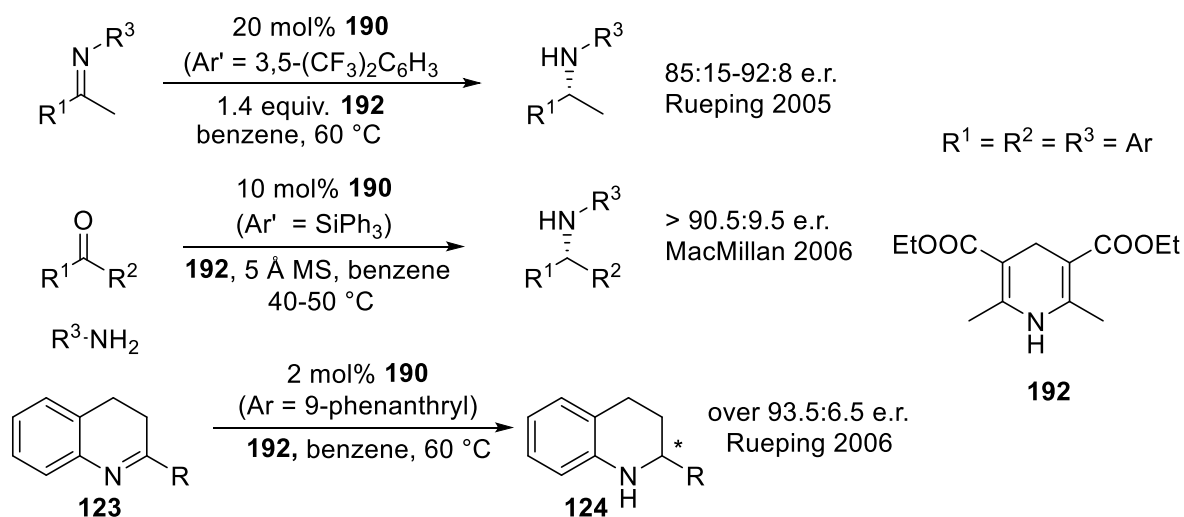
was investigated by Soós using computational and deuterium labelling studies,¹¹⁰ and indicated that the dihydroquinoline **191** is involved as a reducing agent.



Scheme 4.4 Transfer hydrogenation of quinolines reported by Shi.³¹⁸

4.1.2 Brønsted acid and Asymmetric Counteranion-directed catalysis

In the early 2000s numerous reports described the use of Brønsted acids (namely chiral phosphoric acids) to catalyse enantioselective addition reactions to imines. Among the nucleophiles employed were enol ethers,^{319,320} phosphonates,³²¹ enols,³²² furans,³²³ and amines.³²⁴



Scheme 4.5 Chiral phosphoric acid catalysed transfer hydrogenation.

Notably, the use of dihydropyridines (Hantzsch esters **192**) as reducing agents with this methodology has allowed for the development of enantioselective transfer hydrogenation^{325,326} and reductive amination protocols (Scheme 4.5).³²⁷ Rueping reported the enantioselective transfer hydrogenation of 2-quinolines **123**.³²⁸

Following from this work, List and Mayer reported the use of the salt **193** to catalyse enantioselective transfer hydrogenation of α,β -unsaturated aldehydes.³²⁹ They postulated that chirality transfer occurs in a cationic transition state mediated by potential CH-O hydrogen bonding between the iminium ion and the chiral phosphate counteranion, and coined the term asymmetric counteranion-directed catalysis for this mode of operation.

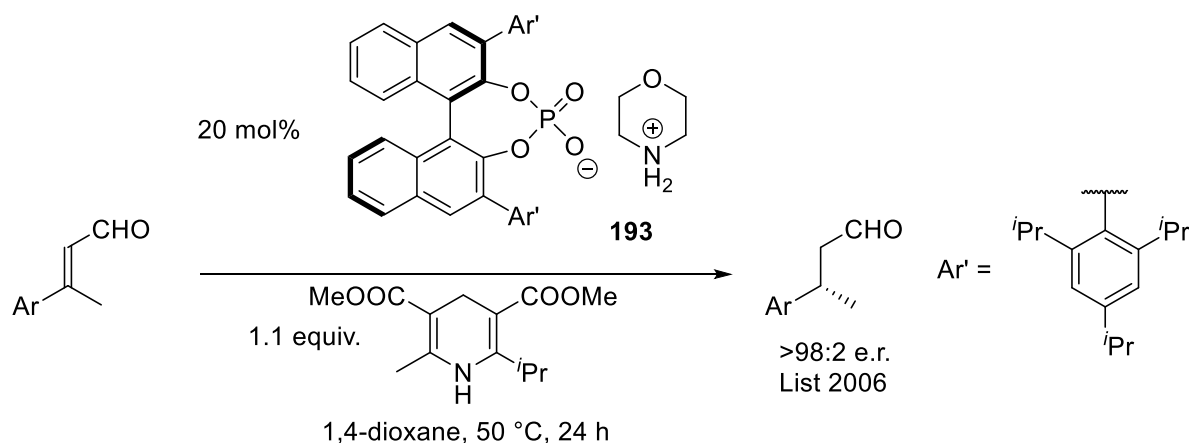


Figure 4.1 Transfer hydrogenation using an axially chiral phosphate salt reported by List.³²⁹

The development of this field has been reviewed by Toste *et al.*,³³⁰ and List and Mahlau.³³¹ The latter define asymmetric counteranion-directed catalysis (ACDC) in the following manner: ‘*Asymmetric counteranion-directed catalysis refers to the induction of enantioselectivity in a reaction proceeding through a cationic intermediate by means of ion pairing with a chiral, enantiomerically pure anion provided by the catalyst.*’.

Attempts to use weakly coordinating chiral anions led to negligible enantioselectivity levels being observed.^{332–334}

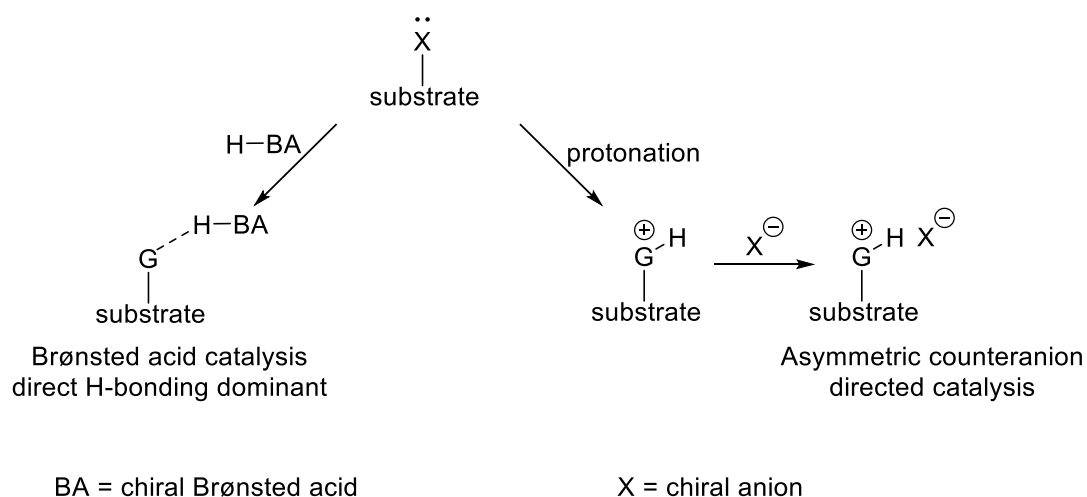


Figure 4.2 Brønsted acid catalysis and ACDC catalysis.

4.1.2.1 Mechanistic background in enantioselective transfer hydrogenation using chiral phosphoric acids

Detailed experimental studies characterising the interactions occurring between various imines and chiral phosphoric acids (Figure 4.3), carried out by Rueping, Gschwind *et al.*, provide experimental support for the postulated mechanism for reduction of imines by Hantzsch esters **192**.^{335–337}

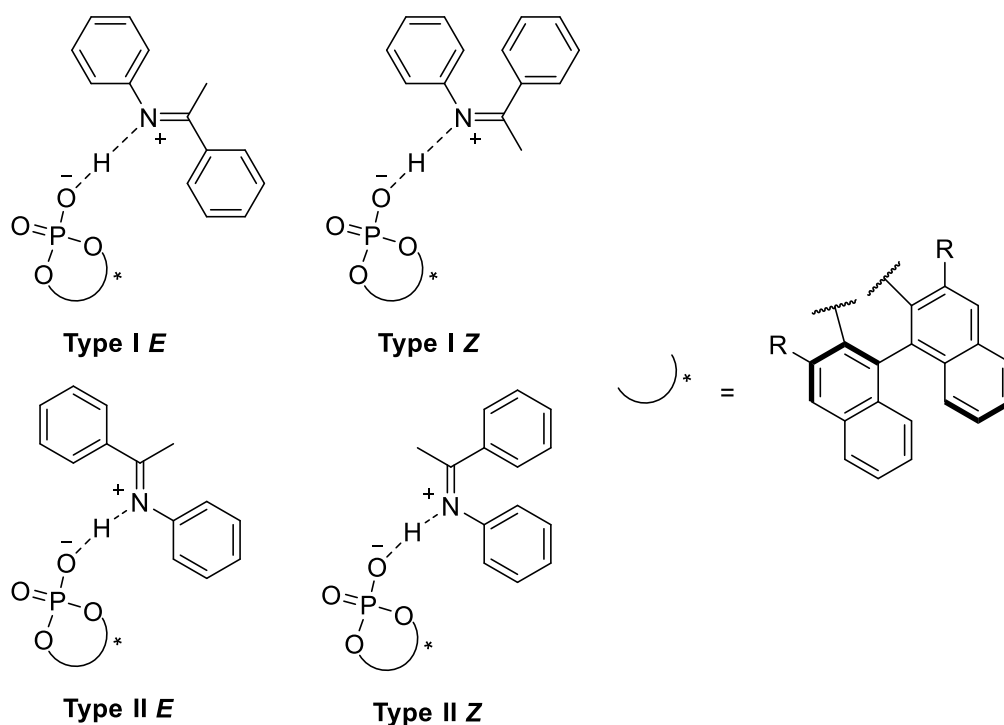


Figure 4.3 Catalyst/substrate reactive complex configurations reported by Gschwind.^{335,336}

The reactivity of each of these complexes with a nucleophile (Hantzsch ester or malonate) was probed experimentally by photochemically biasing the imine *E/Z* equilibrium (Figure 4.4).³³⁸ It was found that the reaction pathway is dependent on the nature of the nucleophile used: for reactions carried out with Hantzsch ester transition states accessed from the *Z* complex are lower in energy, for a malonate the *E* transition states were lower in energy. This result indicates that the nature of the nucleophile reacting with a chiral phosphoric acid activated substrate can have a significant impact on the enantioselectivity. These results indicate that the discrepant results obtained by Shi and Rueping (Scheme 4.4 and Scheme 4.5) in the reduction of quinolines is potentially caused by the different reducing agents used (borohydrides vs Hantzsch esters).

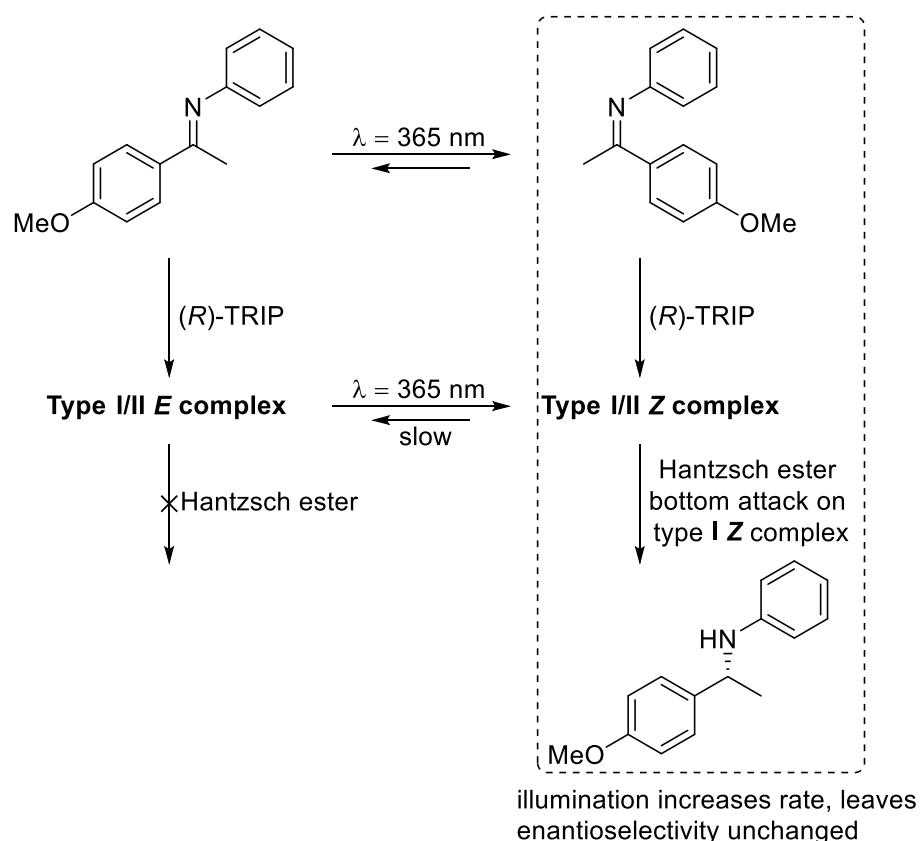


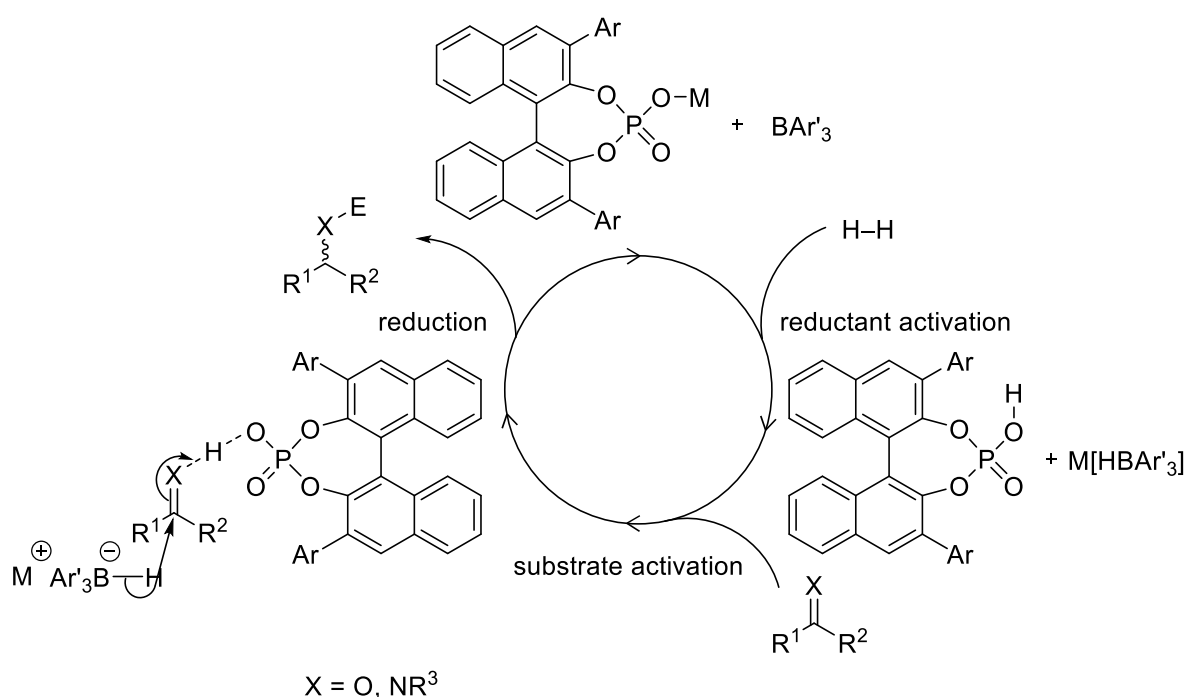
Figure 4.4 Experimental probing of preferred reduction transition states reported by Gschwind.¹⁴²

Following from the work of Rueping and Gschwind we conclude that, in contrast to the interpretation of Stephan and co-workers, both **TS A** and **TS B** and any other intermediate state, or combinations thereof, are *a priori* compatible with chirality transfer, the successful nature of the process being

dependent on the individual components involved. It does indeed appear less likely that **TS B** will support efficient transfer of chirality in the absence of a directed bonding interaction, however this is possible on account of other interactions (electrostatic, dispersion forces, π -stacking) operating that help organise the transition state (cf. ACDC).

4.1.3 Envisaged use of chiral phosphate salts as Lewis bases in FLP catalysis

Drawing from the substantial background work concerning imine activation by chiral phosphoric acids, we decided to investigate the use of chiral phosphoric acids/chiral phosphate salts in FLP catalysis. The potential to easily screen a variety of FLP systems comprised of an achiral borane Lewis acid and a phosphate salt, derived from commercially available BINOL-phosphoric acids, was considered particularly attractive.



Scheme 4.6 Envisaged catalytic cycle using BINOL phosphate Lewis bases.

Scheme 4.6 describes the envisioned design and function of these types of FLP systems. The success of the enantioselective reduction step would depend on the following factors:

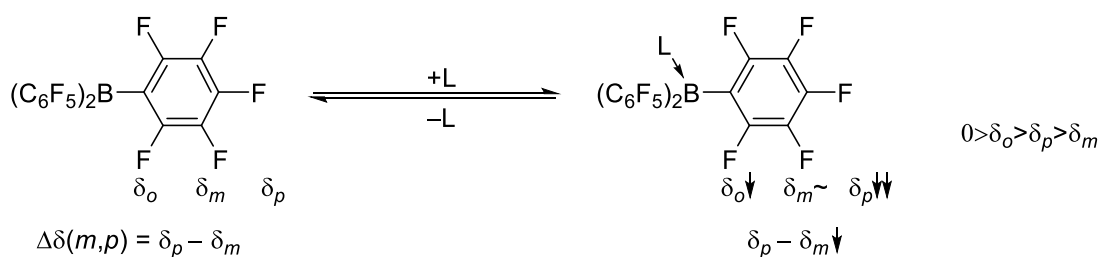
- Determining the appropriate chiral phosphoric acid/substrate combination. This aspect has been widely explored in the field of organocatalysis using chiral phosphoric acids.
- Successful use of the borohydride salt reducing agent. Variation of the metal counterion is a potential avenue for investigation, since coordination to the P=O functionality is expected to provide additional control in the transition state

4.2 Investigations into catalytic feasibility

4.2.1 Discussion of relevant NMR methods

4.2.1.1 ¹⁹F-NMR

Numerous detailed investigations have been performed on the coordination chemistry of B(C₆F₅)₃ **4b**.³³⁹ A detailed discussion is beyond the scope of this work, therefore essential features will be discussed by way of examples chosen for their chemical relevance to this work. The value of $\Delta\delta(m,p-F)$, the difference in chemical shift between the *meta* and *para* fluorine atoms in the pentafluorophenyl rings of a borane moiety, is a useful measure for assessing the coordination state of the boron atom in fluoroaryl substituted boranes.^{76,340–343} It was developed by Horton and de With and measures the changes in electron density in the para position of the C₆F₅ rings on coordination/de-coordination of a ligand from the boron atom (Table 4.1).



$\Delta\delta(m,p-F) L \cdot B(C_6F_5)$	Type of complex
<3 ppm	$[HB(C_6F_5)]^-$
~8 ppm	$L \cdot B(C_6F_5)_3$
>15 ppm	$B(C_6F_5)_3$

Table 4.1 Effect of ligand binding on ¹⁹F NMR shifts in C₆F₅-substituted boranes.

The bulky nature of boranes of the type $B(C_6F_5)_x(C_6Cl_5)_y$ **4** ($y=3-x$, and derivatives) can result in chemical inequivalence being observed by ^{19}F NMR for adducts formed on nucleophile coordination, resulting from slow rotation about B-(C_6F_5) and L-B bonds on the NMR timescale.

Piers investigated the adducts **194a-d**, **195**, **196** formed between $B(C_6F_5)_3$ **4b** and carbonyl derivatives PhCOX (X = H, Me, OEt, $N(iPr)_2$),⁸³ or imines.²²² VT ^{19}F NMR was used to analyse the nature of the rotational processes occurring in the borane moiety: rotation about B-(C_6F_5) bonds in carbonyl derivatives becomes slow with decreasing temperature, eventually leading to detection of individual environments. With the bulkier imines such behaviour can be observed at room temperature.

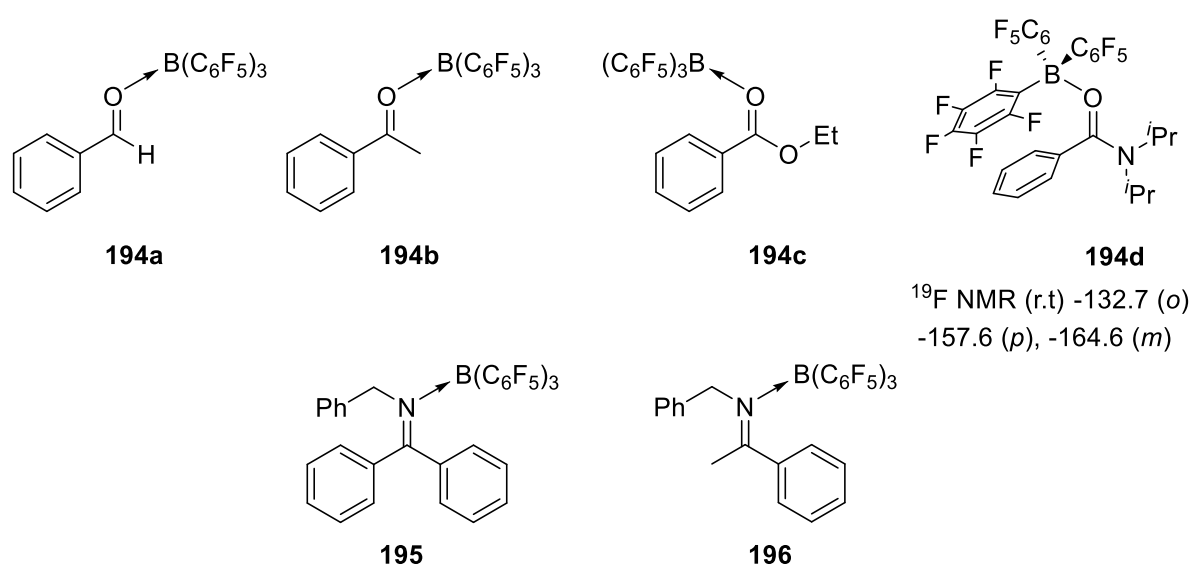
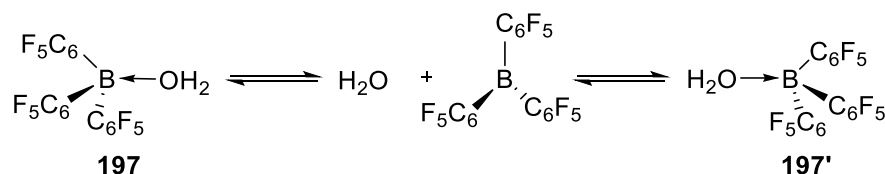


Figure 4.5 Tris(pentafluorophenyl) borane adducts.

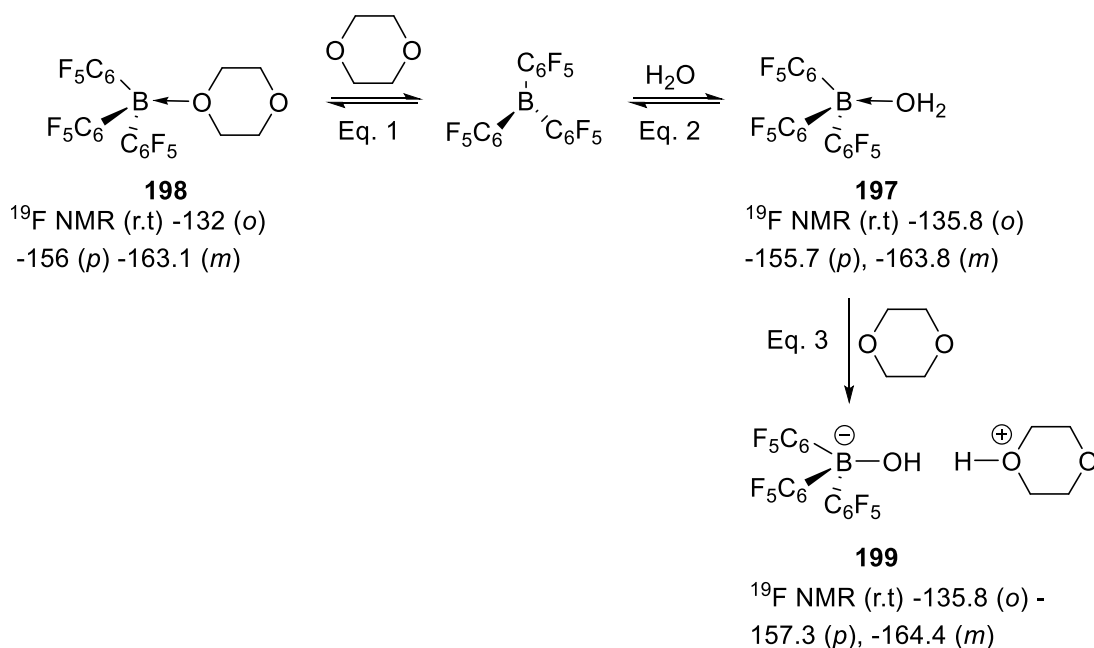
The complex NMR behaviour was a result of conformational effects and occurred in the absence of chemical exchange processes. Such processes can be relevant and are perhaps most clearly illustrated for the very small nucleophile water. The behaviour of $B(C_6F_5)_3 \cdot nH_2O$ **197** systems was studied in detail by Norton, Friesner, Parkin *et al.*³⁴⁴ and Beringhelli.³⁴⁵ For $n < 1$ (conditions under which only mono-adduct formation is occurring), a fast chemical equilibrium is established at room temperature (in toluene) leading to observation of broad, chemical shift averaged signals by ^{19}F NMR. Lowering the

temperature reduces the rate of exchange allowing for the free borane and the adduct **197** to be observed individually (Scheme 4.7).



Scheme 4.7 Water binding to $\text{B}(\text{C}_6\text{F}_5)_3$ as described by Beringhelli.³⁴⁵

A more complicated behaviour arises when two different donors are competing for binding the borane. When the equilibrium **1** (Scheme 4.8) was studied in C_7D_8 , VT ^{19}F NMR indicated the presence of free borane at high temperature (380 K). As the temperature is decreased to 300 K the equilibrium is shifted towards adduct **198** formation (one set of broad signals), indicated by a significant change in chemical shift in the *p*-F signal. Further lowering the temperature down to 190 K results in observation of conformers, indicated by the observation of two sets of signals. In the presence of excess 1,4-dioxane (solvent), free borane cannot be observed at temperatures as high as 370 K. The improved rate of chemical exchange at high temperature leads to observation of sharper signals.¹⁰⁵



Scheme 4.8 Competitive binding of $\text{B}(\text{C}_6\text{F}_5)_3$ in 1,4-dioxane.¹⁰⁷

Treating a solution of borane in 1,4-dioxane with water (up to 1 equivalent) leads to formation of hydroxyl adduct **199**, indicated by the appearance of a new sharp set of signals. Due to the significantly stronger donor ability of the hydroxyl anion, adduct **199** is not involved in exchange equilibria. Treating a solution of water adduct **197** with 1,4-dioxane (1 equivalent) results in formation of the characteristic set of sharp signals of hydroxy adduct **199**. This process is accompanied by an upfield shift of the *p*-F resonance.¹⁰⁷

4.2.1.2 ¹¹B NMR

This technique has been used in conjunction with ¹⁹F NMR to study the coordination chemistry of B(C₆F₅)₃ and derivatives. It is useful for assessing the coordination state of the boron atom, with transition from tri-coordinate to tetra-coordinate state being accompanied by large changes in chemical shift. Smaller structural changes give rise to small changes in chemical shift, such changes being best interpreted only within series of structurally related compounds.

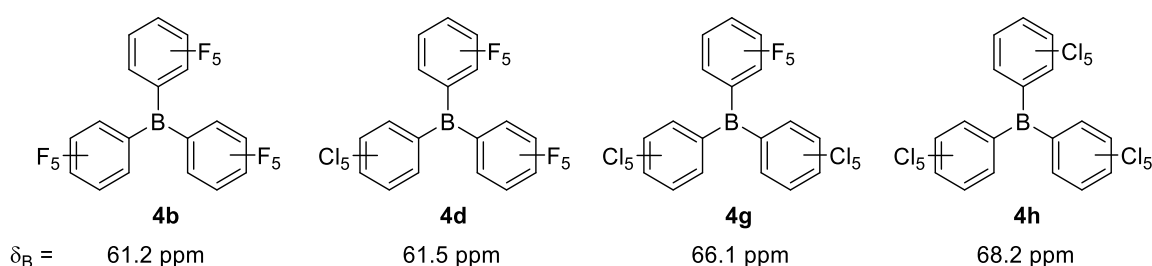


Figure 4.6 ¹¹B NMR shift correlation with electron density.

In the series B(C₆F₅)_x(C₆Cl₅)_y (y=3-x) changes in the ¹¹B NMR shift were assigned to a decrease in electron density at the boron atom, this assignment being possible with support from computational work (Figure 4.6).²¹⁹

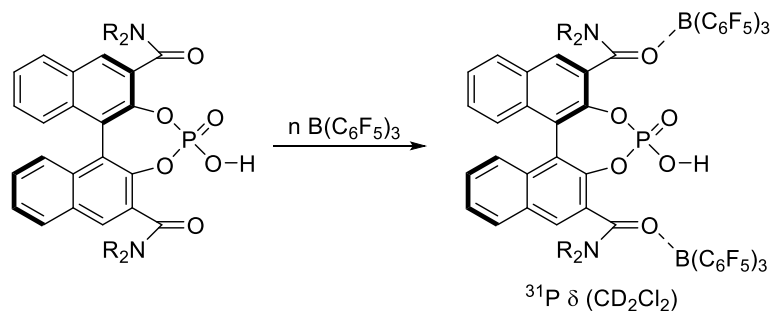
The Table 4.2 presents reported ¹¹B NMR shifts for various adducts L·(C₆F₅)₃.

Entry	Ligand L	¹¹ B NMR shift
1	B(C ₆ F ₅) ₃ ²¹⁹	61.2
2	PhCOOEt ⁸³	19.2
3	PhCHO	5
4	PhCON(<i>i</i> Pr) ₂	-0.05
5	PhCMeNBn ²²²	-4.7
6	1,4-dioxane ¹⁰⁷	5.6
7	H ₂ O	4.6
8	OH	-2.1
9	H ⁷⁷	-25.5 (d, J = 58 Hz)
10	Me ³⁴²	-14.1
11	C ₆ F ₅ ³⁴⁶	-16.7

Table 4.2 ¹¹B chemical shift values for tetrahedral adducts L·(C₆F₅)₃. Values were reported in non-donor solvents: CD₂Cl₂, C₇D₈, C₆D₆, C₆D₅Br or 1,2-DFB with the exception of entry 6 (1,4-dioxane) and entry 11 (CD₃CN).

4.2.1.3 ³¹P NMR

Table 4.3 contains ³¹P NMR data reported by Ishihara on chiral phosphoric acid/B(C₆F₅)₃ complexes.³⁴⁷ The small variation in ³¹P NMR chemical shift on complexation of the carbonyl functionality at room temperature indicates that ³¹P NMR could be used as a sensitive probe for changes in molecular structure. In practice this is not always feasible due to the much greater response seen when the coordination environment changes at the O(P) atom, ie. phosphate group acting as a Lewis base. This sensitivity has been extensively exploited both in solid-state and solution phase investigations of Lewis/Brønsted acidity.³⁴⁸



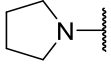
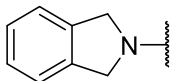
NR ₂	n	³¹ P NMR δ (CD ₂ Cl ₂ , 195 K)	³¹ P NMR δ (CD ₂ Cl ₂ , 298 K)
	1	-20.1, -14, -11.3	n/a
	2	4.1	n/a
	0	n/a	4
	1	Multiple peaks -12 to -7 and 4 to 6	n/a
	2	-0.7	4.6

Table 4.3 ³¹P NMR data reported by Ishihara for phosphoric acid/borane adducts.³⁴⁷

A notable example for solution phase studies is the Gutmann-Beckett method for measuring Lewis acidity (see section 2.2.2.3). In a natural extension, Franz and Diemoz have recently reported on the use of triethylphosphine oxide as a probe for measuring the H-bonding strength of numerous Brønsted acids (Figure 4.7).³⁴⁹ The observed variations in chemical shift ($\Delta\delta = \delta(\text{Et}_3\text{PO}\cdot\text{HD}) - \delta(\text{Et}_3\text{PO})$) were as high as 24 ppm, cf. the chemical shift of un-complexed Et₃PO is 50.3 ppm).

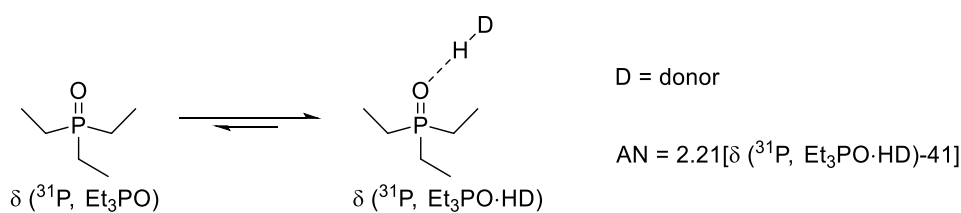


Figure 4.7 Franz and Diemoz method for assessing hydrogen-bonding ability.³⁴⁹

Aggregation effects can impact observed spectral characteristics. An example of this has been reported by Ishihara *et al.* (Figure 4.8).³⁵⁰ To conclude, ³¹P NMR can be used to assess changes in both

covalent and non-covalent bonding in phosphate derivatives. Specialised techniques can be used to construct a detailed picture on the chemical behaviour of chiral phosphoric acids in solution.³⁵¹

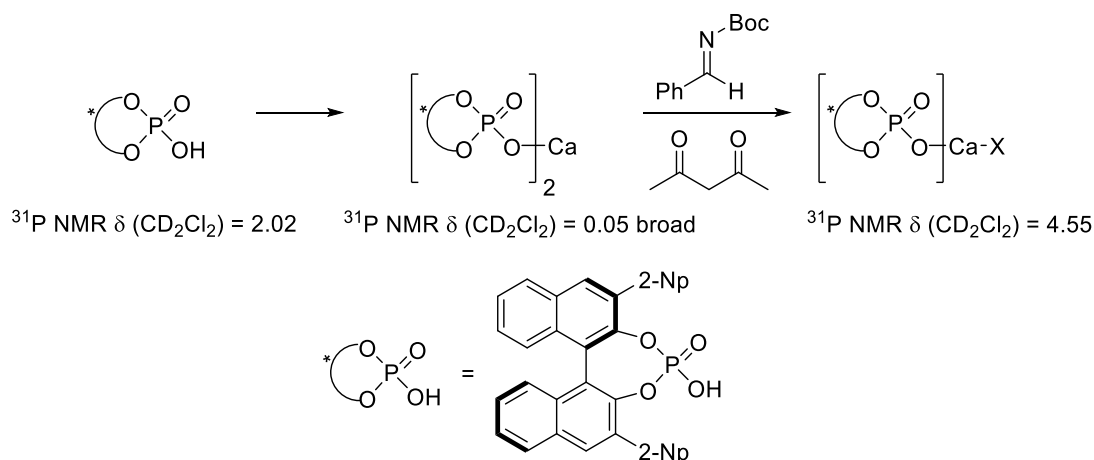


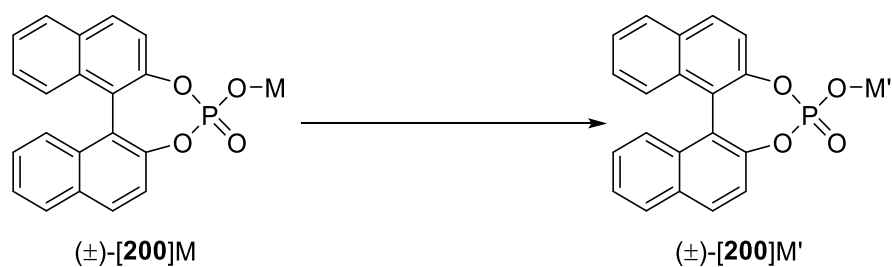
Figure 4.8 Changes in ^{31}P NMR chemical shifts in BINOL-phosphoric acids, reported by Ishihara.³⁵⁰

4.2.2 Accessing FLP states

We began our studies by investigating the feasibility of molecular hydrogen activation using phosphate salts. We hypothesised that the following factors would be relevant:

1. Coordination of the phosphate salts (*via* the (P=)O atom) to the borane Lewis acid and the lability of the resulting adducts
2. Lewis (Brønsted) basicity of the phosphate salts.

Phosphate salts **200** have been investigated by the group of Ishihara and others.^{350,352–355} The preparation of these salts was carried out by treating the chiral phosphoric acid with the corresponding methoxide salts in DCM/methanol (Table 4.4).³⁵⁰ We observed that under these reaction conditions slow product degradation occurred. We postulated that this could be due to the nucleophilic nature of the methoxide anion (residual or formed from equilibrium deprotonation of methanol by the salt **200**). We attempted to modify this procedure by using the bulkier *tert*butoxide anion as a base and using DCM as the only solvent.



Substrate	Product	Conditions	Yield
$(\pm)\text{-[200]H}$	$(\pm)\text{-[200]Li}$	LiOtBu (1 equiv.), DCM, r.t., 1.5 h	<93% (97% ^{31}P NMR) ^a
$(R)\text{-[200]H}$	$(R)\text{-[200]Na}$	NaOMe (1 equiv.), DCM:MeOH 1:1, r.t. 23 h	81% (94% ^{31}P NMR)
$(R)\text{-[200]Na}$	$(R)\text{-[200][Bu}_4\text{N]}$	$[\text{Bu}_4\text{N}]\text{Cl}$ (1 + 0.5 equiv.), CDCl_3	<i>(in situ)</i>

Table 4.4 Preparation of chiral phosphate salts. a. the amount of $t\text{BuOH}$ in the isolated product could not be estimated due to its poor solubility.

Under these conditions degradation occurred even after a reaction time of 1.5 h. Furthermore, the *tert*butanol by-product could not be removed after drying under high vacuum (4 days) or by azeotropic removal with DCM under high vacuum. Further screening of bases will be required to reliably prepare phosphate salts.

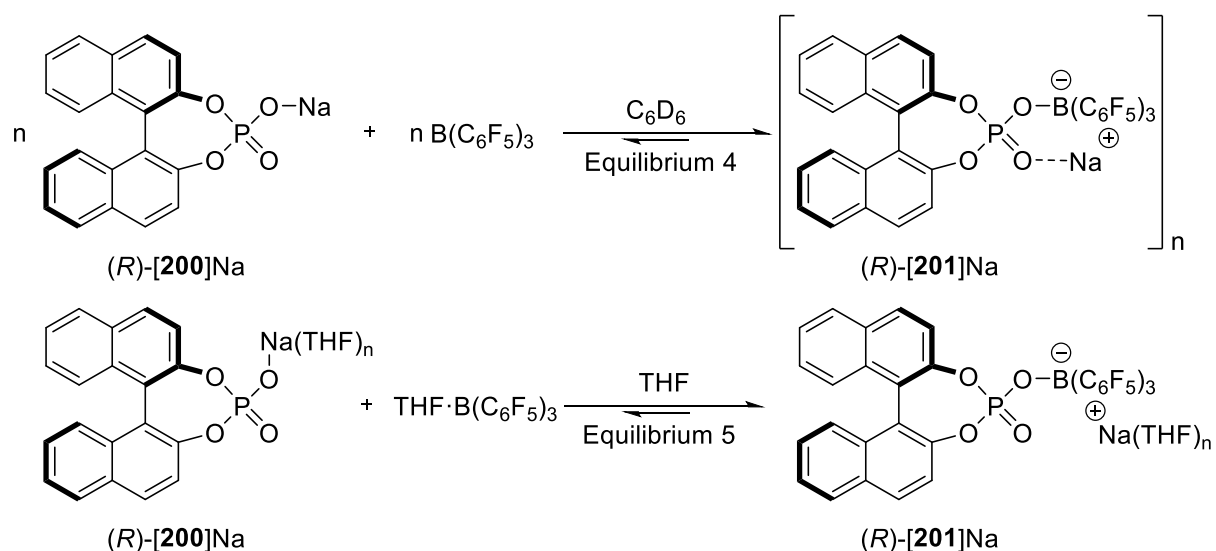
The solubility properties and NMR data for the compounds **200** are presented in Table 4.5. The sodium salt shows improved solubility compared to the lithium salt. Both salts give rise to broad, unresolved ^{31}P NMR spectra in non-polar solvents due to strong aggregation effects. Use of donor solvents (THF, DMSO) results in measurement of resolved ^{31}P NMR spectra. Replacement of the Na sodium cation for the inert Bu_4N cation was carried out in chloroform. Partial resolution of the ^1H and ^{31}P NMR spectra could be observed after the addition of one equivalent of reagent, and then an additional 0.5 equivalents. Although no direct interaction between the anionic phosphate group and the cation is possible in this case, ion pairing and aggregation are still occurring due to the low solvent polarity (CDCl_3).

M	$\delta(^{31}\text{P})$ ($\text{C}_6\text{D}_6/\text{tol-d8}$)	Solubility	$\delta(^{31}\text{P})$ (CDCl_3)	Solubility	$\delta(^{31}\text{P})$ (d6-DMSO)	Solubility
H	–	insoluble	6.6 ^a	sparingly	3.8	soluble
Li	n/a	n/a	6.6 (br)	insoluble	6	poorly
Na ^b	~7 (v. weak)	insoluble	8.2 (br)	Soluble	6.5	soluble
ⁿ Bu ₄ N	n/a	n/a	7	soluble	n/a	n/a

Table 4.5 ³¹P NMR data for phosphate salts. NMR shifts externally referenced (capillary insert) against

85% H₃PO₄ (aq.). a. ¹H NMR indicated presence of analyte in solution.

The coordinating ability of salt (*R*)-[**200**]Na towards **4b** was investigated in benzene, the solvent being chosen for its lack of Lewis basic functionality. The boranes **4b** and **4d** were prepared by Dr Daniel Scott.

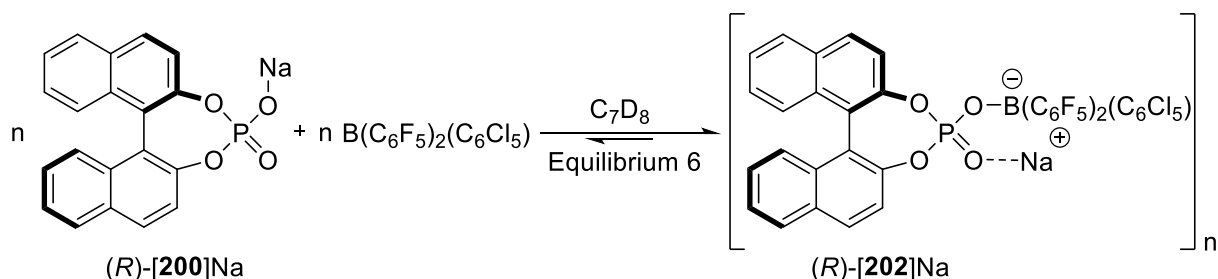


Entry	Compound	Solvent	$\delta(^{11}\text{B})$	$\delta(^{31}\text{P})$	$\delta(^{19}\text{F})$	$\Delta\delta(m,p-F)^{340}$
1	(<i>R</i>)-[201]Na	C ₆ D ₆	-1.8 (br)	-2.6 (br)	-137 (br), -157.8 (br), -163.9 (br)	6.1
2	(<i>R</i>)-[201]Na	THF	-4.4	-6.6	-134.8, -163.9, -168.8	4.9
3	4b	THF	-0.8	n/a	-136.9, -161.5, -168.3	6.8
4	(<i>R</i>)-[200]Na	THF	n/a	7.5	n/a	n/a

Table 4.6 NMR data concerning phosphate salt/borane **4b** adduct formation.

The salt (*R*)-[**200**]Na displayed poor solubility in benzene (very weak signals can be observed by ^{31}P NMR at $\delta = \sim 10$ and ~ 8 ppm); addition of the borane **4b** results in dissolution (10-15 min with strong shaking) leading to the formation of a homogeneous solution. NMR analysis revealed the formation of a new major species **201**, assigned as the Lewis acid/base adduct formed between the two components (Table 4.6). This adduct displays broad ^1H , ^{31}P , ^{11}B NMR, and ^{19}F NMR signals, probably due to a slow exchange process occurring on the NMR time scale and/or aggregation effects. Phosphate salt **200** has no appreciable steric hindrance at the two distal O atoms, which makes coordination to **4b** favourable. The reversible nature of the process is probably a result of the weak Lewis basicity of the phosphate group. The equilibrium 5 was studied in THF (Table 4.6, Entry 2). Under these conditions a set of sharp peaks was observed in the ^1H , ^{31}P , ^{19}F and ^{11}B NMR spectra. The higher solvent polarity and the Lewis basicity of the solvent eliminates aggregation effects by binding sodium cations. The observed ^{31}P NMR shift suggests that coordination to $\text{B}(\text{C}_6\text{F}_5)_3$ is occurring, in analogy to the situation observed in benzene. The chemical shift values (^{11}B NMR and the ^{19}F NMR) observed for adduct **201** (entry 2) are significantly different to those of THF-**4b** adduct (entry 3), providing support for its structure assignment.

The bulkier borane $\text{B}(\text{C}_6\text{F}_5)_2(\text{C}_6\text{Cl}_5)$ **4d** was next investigated. The increased steric hindrance was expected to reduce the strength of phosphate base binding. The equilibrium 6 established between the phosphate salt (*R*)-[**200**]Na and $\text{B}(\text{C}_6\text{F}_5)_2(\text{C}_6\text{Cl}_5)$ **4d** was studied in toluene- d_8 (Scheme 4.9).



Scheme 4.9 Phosphate salt/borane **202** adduct formation.

Following partial dissolution of the sodium salt (sonication for 1 h) a cloudy solution was obtained. NMR analysis did not provide conclusive evidence for the nature of the equilibrium established: ^{11}B NMR indicated the presence of free borane and formation of a new species (-2.8 ppm), presumably the phosphate/borane adduct **202**. After 15 h at rt a clear solution was obtained; no change was observed by NMR. ^{19}F NMR indicated only free borane to be present. A variable temperature NMR study was carried out to elucidate the nature of this system (Figure 4.9 to Figure 4.12).

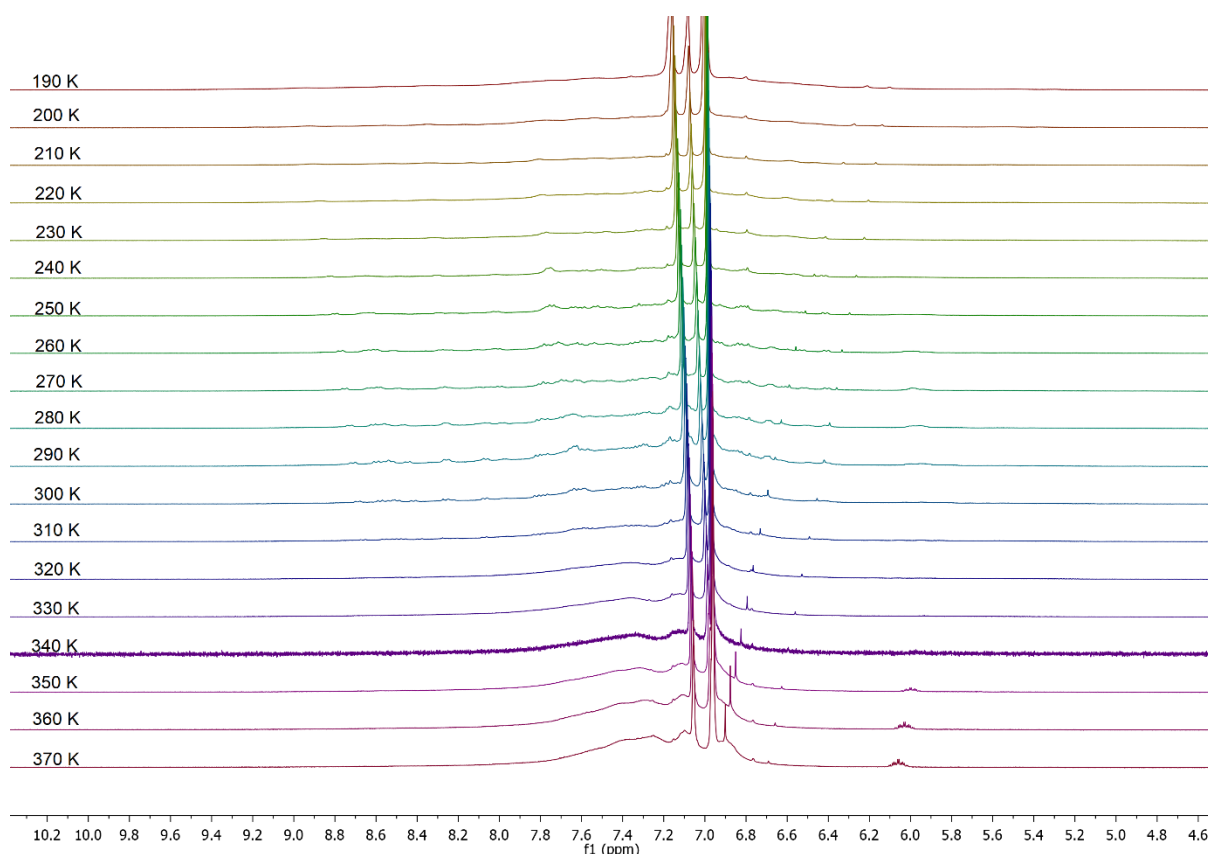


Figure 4.9 VT ^1H NMR for phosphate salt/borane **202** adduct formation.

The system was first cooled from room temperature down to 190 K. It was then heated from room temperature up to 370 K. Analysis performed after cooling back down to room temperature indicated that the system returned to its room temperature state. ^1H NMR indicated a broad profile in the aromatic region of the spectrum over the entire temperature range with few resolved peaks (Figure 4.9). Formation of a new species was detected starting at ~ 60 °C: multiplet at 6.06 ppm (370 K) which is indicative of the formation of pentafluorobenzene (compared with an authentic sample) resulting

from protodeborylation. This observation is corroborated by the detection of the corresponding signals by ^{19}F NMR. More useful information regarding equilibrium **6** could be extracted from the ^{31}P , ^{11}B and ^{19}F NMR spectra.

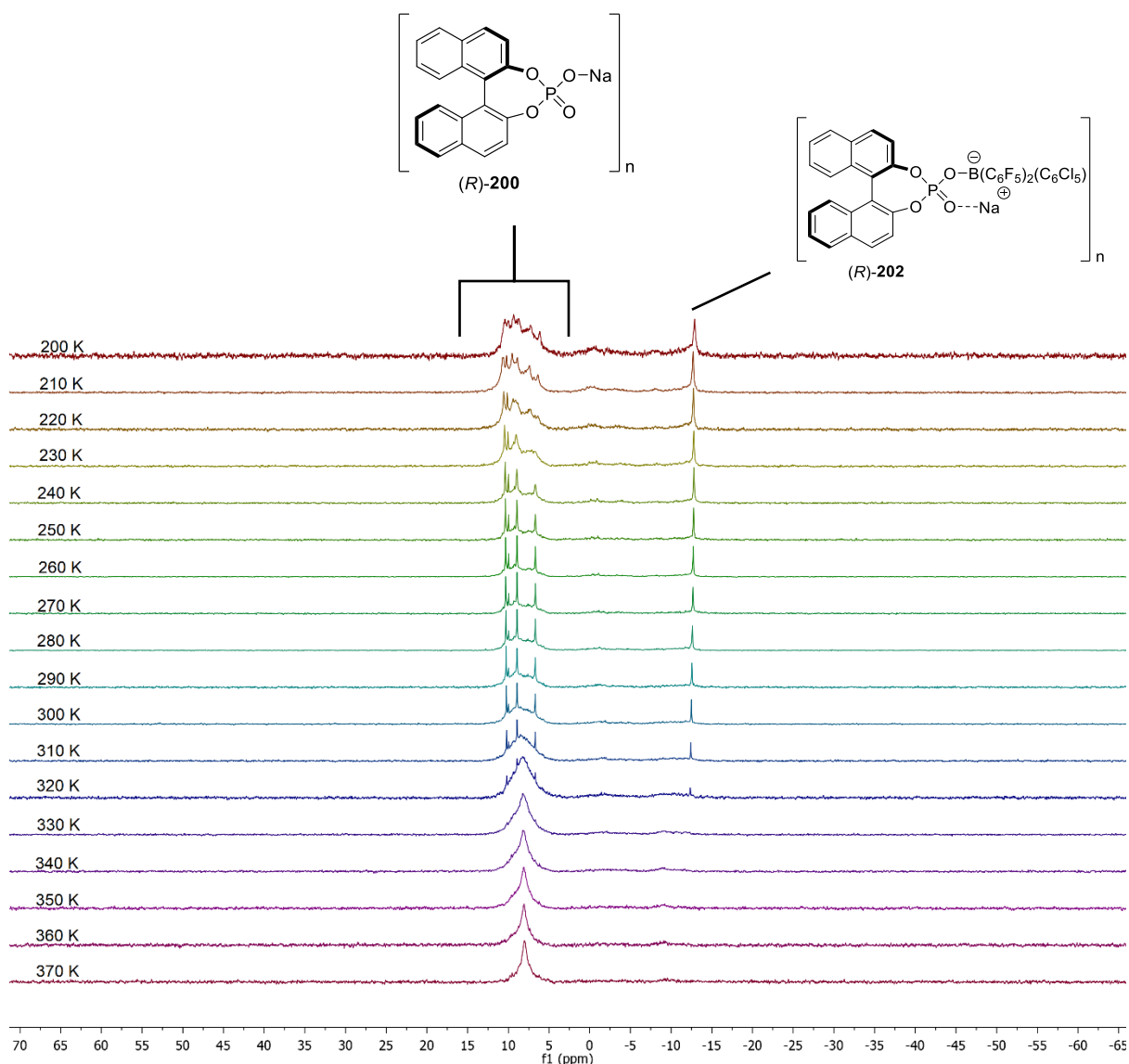


Figure 4.10 VT ^{31}P NMR (d8-tol) for phosphate salt/borane **202** adduct formation.

^{31}P NMR presented two regions of interest: 5-10 ppm and -10 to -15 ppm (Figure 4.10). The former is specific to un-coordinated phosphate salts and the latter to the adduct **202**. In the free salt region a transition is observed between a complex mixture of 6 species at 200 K to 3 species at 280 K and finally to one species at 370 K. This behaviour is consistent with the existence of slow exchange equilibria between different aggregates. With increasing temperature dissociation occurs, together with shifting

into a rapid exchange regime between species present. In the phosphate/borane adduct region a single species can be detected in the range 200-320 K. These data support the existence of an equilibrium between free borane and borane/phosphate adduct, which becomes shifted towards adduct formation below 320 K.

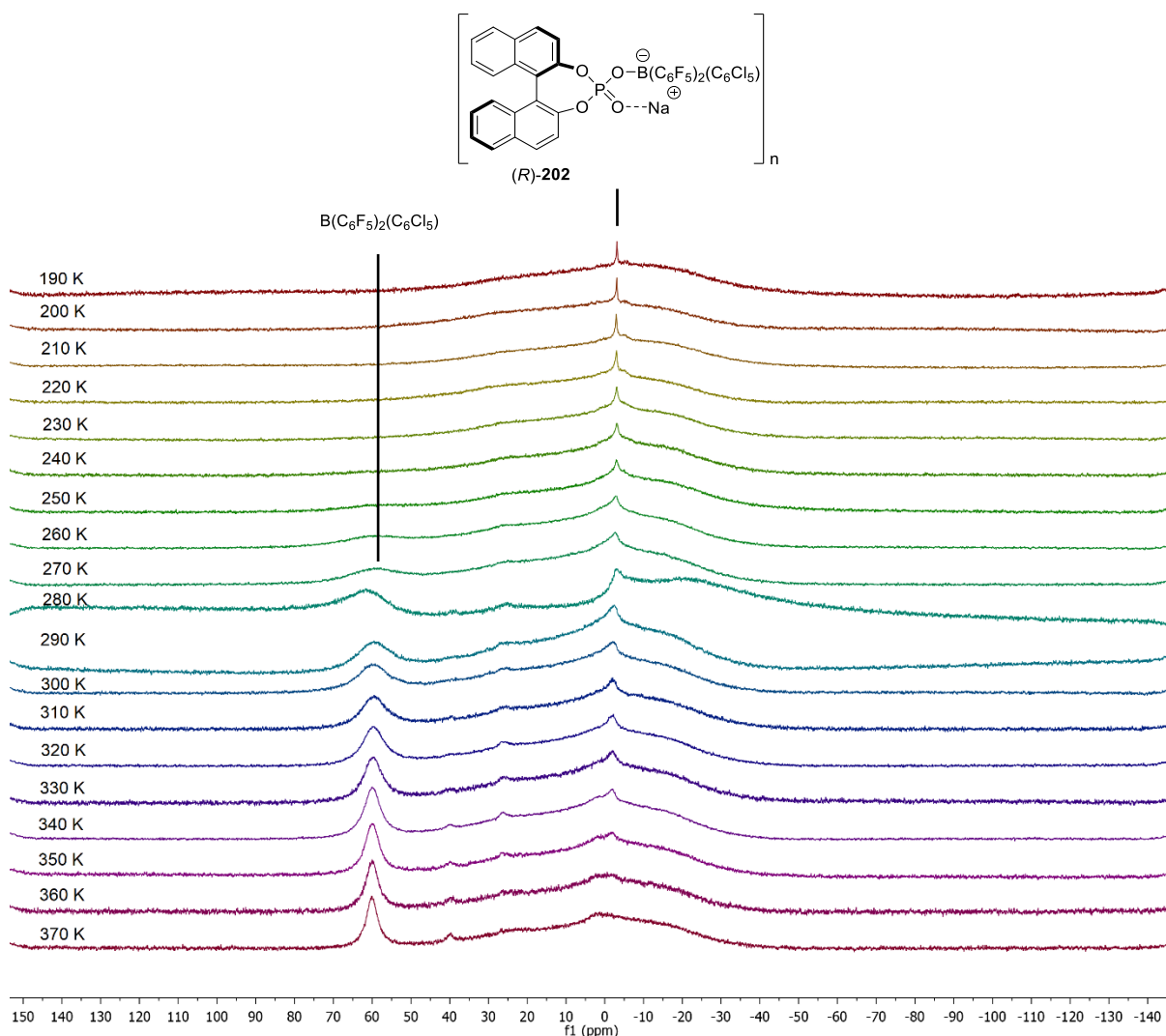


Figure 4.11 VT ^{11}B NMR for phosphate salt/borane **202** adduct formation.

This conclusion is supported by the ^{11}B NMR spectra (Figure 4.11). An adduct is detected at -3.2 ppm (190 K). Up to 250 K no appreciable amount of free borane (60 ppm) can be detected. With increasing temperature the extent of dissociation increases such that at ~ 360 K the adduct becomes almost undetectable. The detection of oxyborane species (25, 40 ppm) supports the occurrence of protodeborylation. ^{19}F NMR (Figure 4.12, see overleaf) indicated only the presence of free borane

across the whole temperature range ($\Delta\delta(m,p\text{-F}) = 20.3$ ppm, 190 K; 18.2 ppm, 370 K). The adduct **202** is presumably undetectable by ^{19}F NMR.

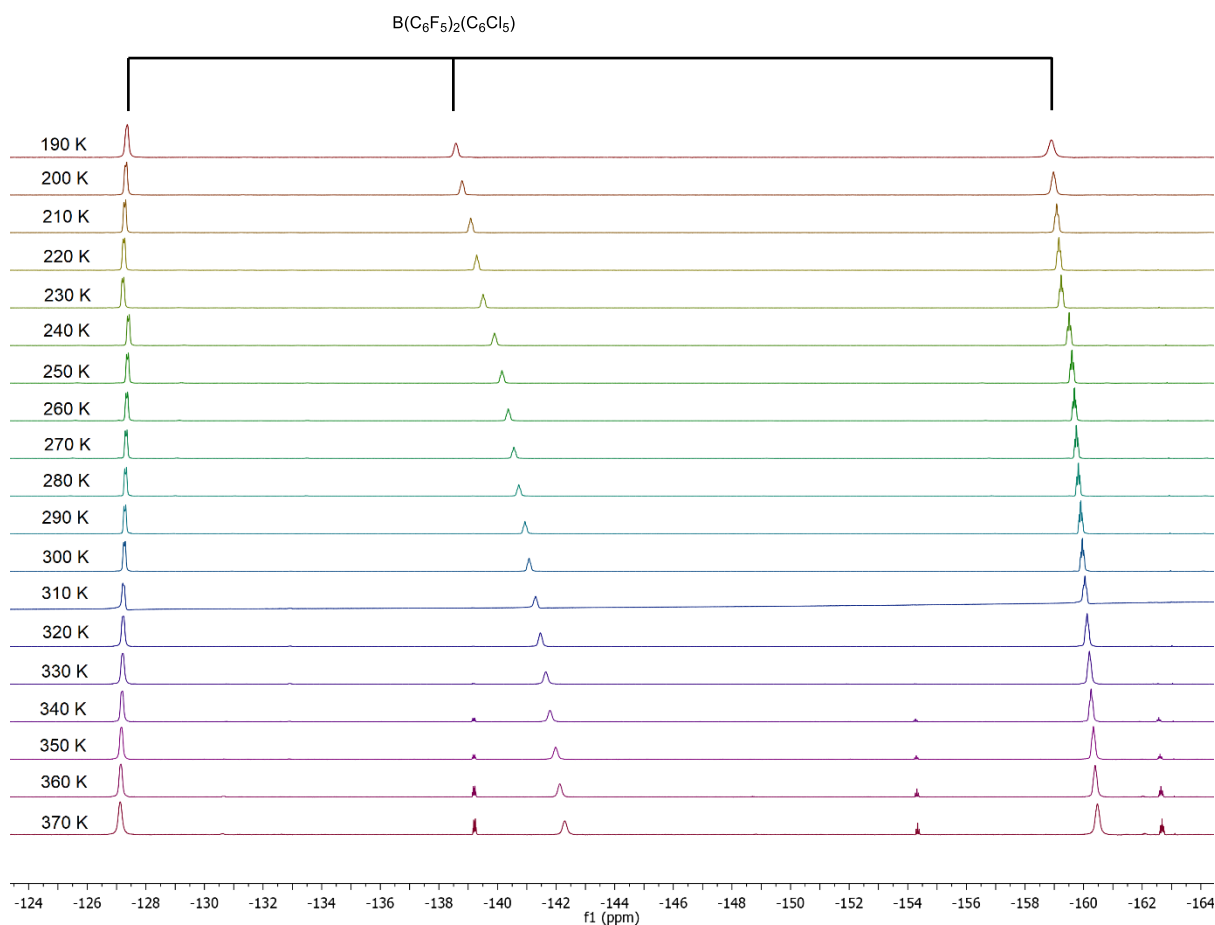


Figure 4.12 VT ^{19}F NMR for phosphate salt/borane **202** adduct formation.

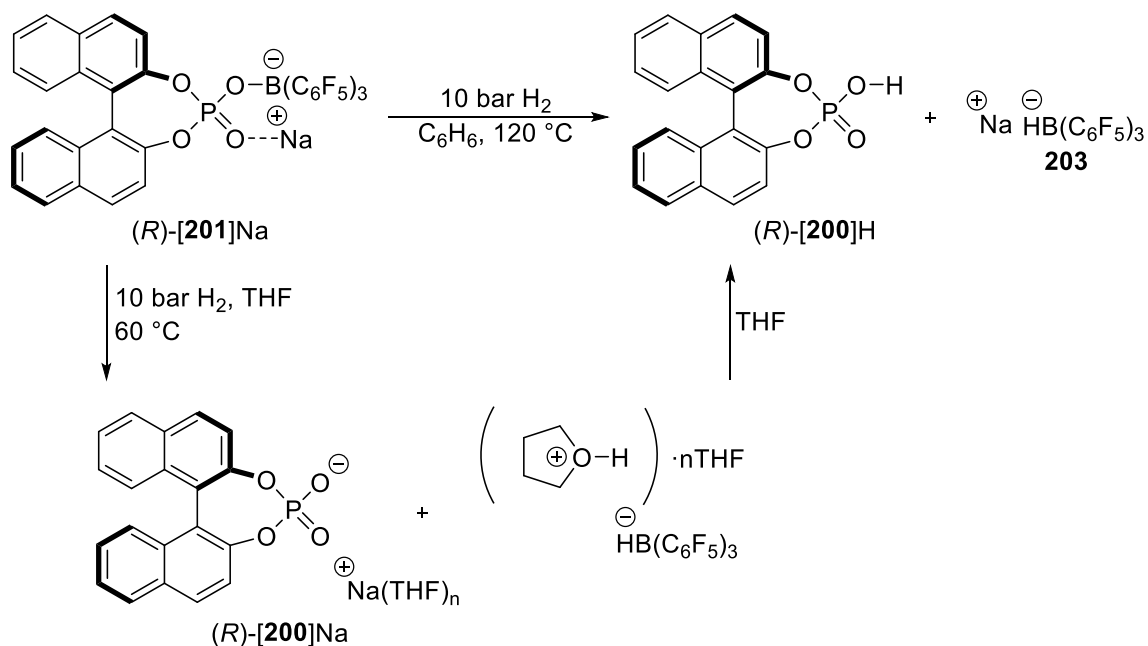
A comparison of the NMR spectra of adducts (*R*)-**[201]**Na and (*R*)-**[202]**Na (at room temperature) is presented in Table 4.7. The upfield shift in the ^{31}P NMR signal suggests a monomeric structure for **202** resulting from the increased steric bulk of the borane component.

Adduct	Solvent	$\delta(^{11}\text{B})$	$\delta(^{31}\text{P})$	$\delta(^{19}\text{F})$	$\Delta\delta(m,p\text{-F})^{340}$
(<i>R</i>)- [201] Na	C_6D_6	-1.8 (br)	-2.6 (br)	-137 (br), -157.8 (br), -163.9 (br)	6.1
(<i>R</i>)- [202] Na	Tol-d8	-2.2 (br)	-12.5	(-127.3, -141.1, -160)	(18.9)

Table 4.7 NMR data comparison for adducts **201** and **202**.

4.2.2.1 Dihydrogen activation

The ability of adduct (*R*)-[**201**]Na to activate hydrogen was investigated in benzene and THF.



Scheme 4.10 Hydrogen activation using phosphate/borane adducts.

The reactions were carried out at a pressure of 10 bar hydrogen gas and assessed using ^{11}B NMR (monitoring for the distinctive borohydride signal). No reaction was observed at room temperature; the temperature was increased in $20\text{ }^\circ\text{C}$ increments with sufficient time provided for reaction to occur before repeating the analysis. In benzene formation of the borohydride **203** was first observed at a temperature of $100\text{ }^\circ\text{C}$, with better reactivity observed at $120\text{ }^\circ\text{C}$ (separate reaction). At the latter temperature reaction was also seen to occur at a hydrogen pressure of 4 bar. Nonetheless, the reaction was very slow in both cases with progress observed by heating over the course of a week. At this point the characteristic signals of borohydride **203** could be seen both by ^{11}B NMR ($-26.3\text{ d}, J = 75.6\text{ Hz}^{77}$) and by ^1H NMR (2.5, br d, $^1J = 114\text{ Hz}$). Additionally, the formation of the $[\text{B(C}_6\text{F}_5)_4]^-$ anion was observed ($^{11}\text{B } \delta = -17.3^{346}$), indicating that decomposition is occurring. Accumulation of borohydride in quantities allowing for NMR detection is not required for catalytic application, meaning that such a system could find potential use.

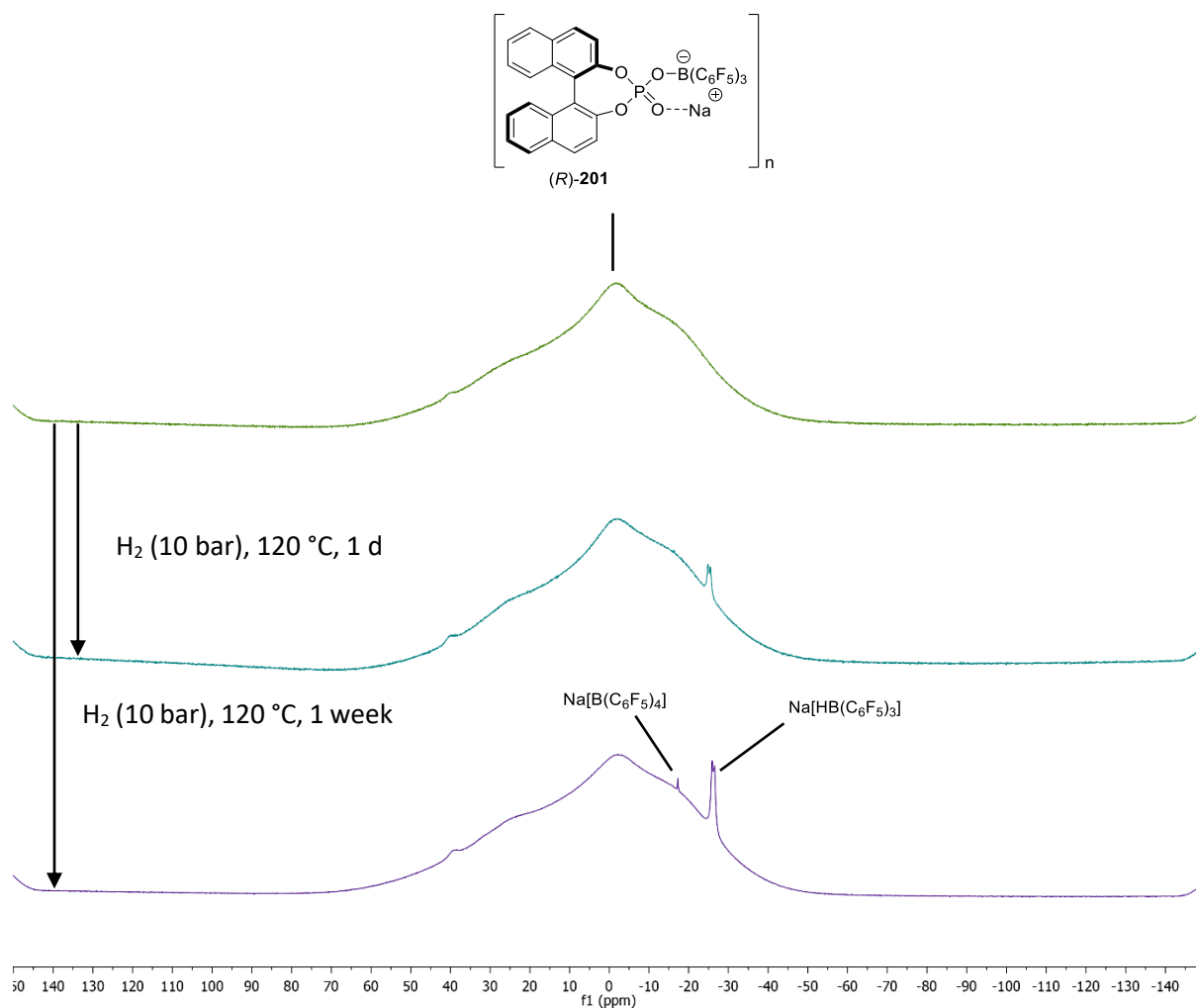


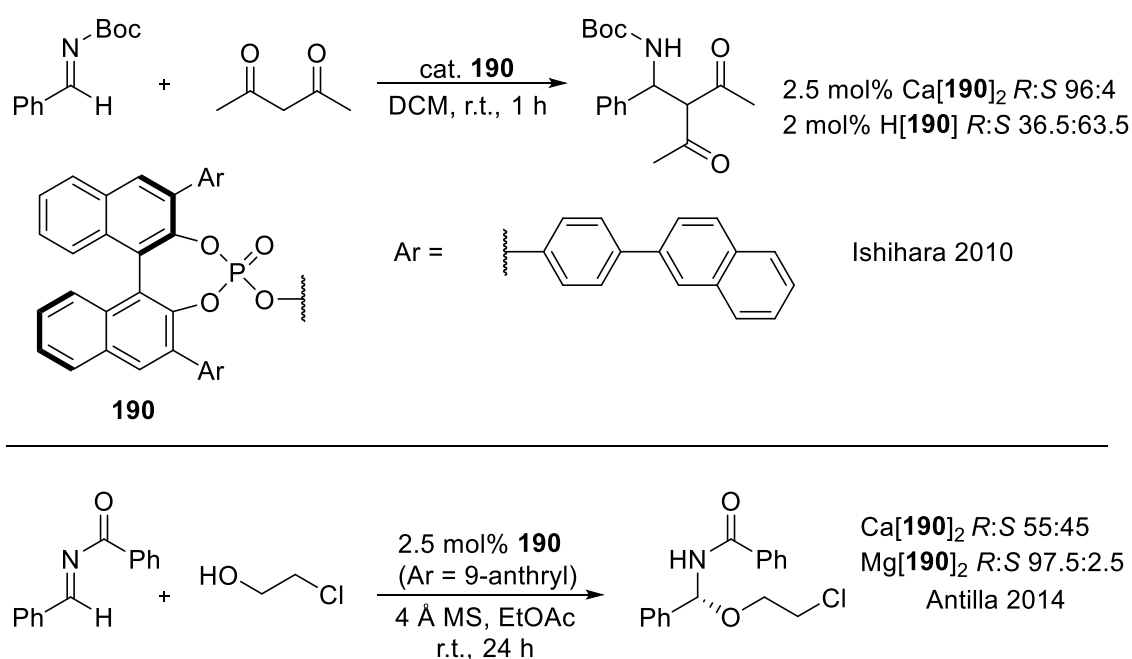
Figure 4.13 ^{11}B NMR data showing hydrogen activation using phosphate/borane adduct **201**.

We attempted to reduce the temperature required for hydrogen activation by using THF as solvent. THF was chosen for its higher polarity and known ability to function as a catalytic Lewis base. The formation of trace borohydride **203** was first observed (-26.6 , d, $J = 94.6$ Hz) at 60 °C (43 h). The nature of the product was confirmed by collecting the ^{11}B $\{^1\text{H}\}$ spectrum (doublet signal collapses to singlet). It is not possible to confirm whether the phosphate salt is acting as a stoichiometric base in this process as no changes were observed in the recorded ^{19}F and ^{31}P NMR spectra.

4.2.2.2 Stoichiometric reduction studies

Having proven that hydrogen activation is possible, we turned to assessing the ability of a chiral phosphoric acid/[HB(C₆F₅)₃] borohydride couple to reduce imine substrates with transfer of chirality.

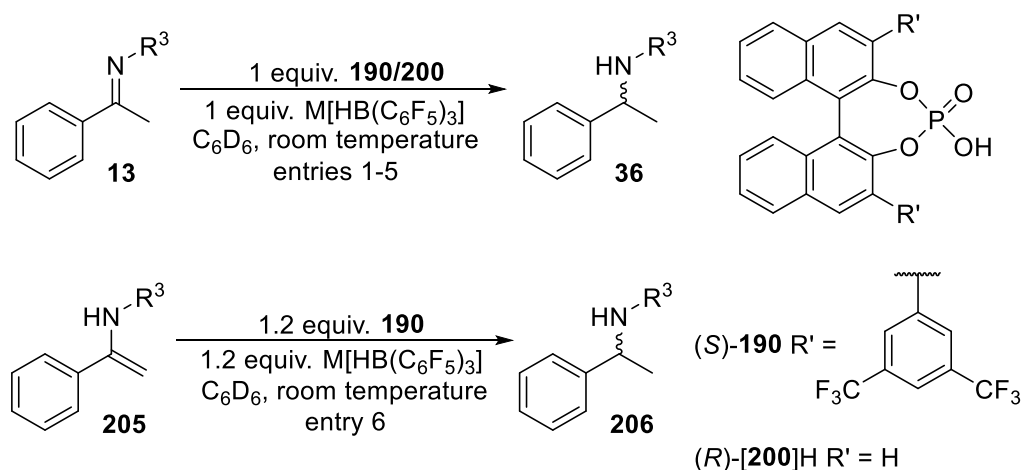
Procedures involving nucleophile addition to unsaturated carbonyl derivatives under chiral phosphate **190** catalysis have been reported to be strongly dependent on the metal counterion present (Scheme 4.11).^{350,356–359} It appears that the presence of coordinating protecting groups on the N atom of the imine substrate has a beneficial role, likely due to providing opportunity for coordination of the metal cation.



Scheme 4.11 Enantioselectivity changes with metal cations.

We hypothesised that the use of BINOL-derived chiral phosphate salts could provide a means of achieving reduction of other substrate types in addition to classical imines. As a natural extension we wanted to investigate the reduction of Boc-protected imines and potentially carbonyls. The coordinating nature of the Boc protecting group would allow for additional control in the hydride transfer step, *via* coordination of metal cations. Under FLP hydrogenation catalysis, a borohydride of the type M[H(BAr)₃] would act to deliver nucleophilic hydride, the success of the procedure therefore

depending on the compatibility of this reagent with the other reaction components. The borohydrides $\text{Na}[\text{HB}(\text{C}_6\text{F}_5)_4]^{360}$ **203** and $[\text{nBu}_4\text{N}][\text{HB}(\text{C}_6\text{F}_5)_4]^{77}$ **204** were prepared according to literature procedures and their reactivity towards imine model substrates **13g** and **13k** in the presence of chiral phosphoric acids was assessed (Table 4.8).



Entry	R^3	(R)-[200]H or (S)-190	M	Time	Conversion	e.r. (<i>R</i> : <i>S</i>)
1	^t Bu	<i>R</i> , $\text{R}' = \text{H}$	Bu_4N	63 h	0%	-
2	Ph	<i>R</i> , $\text{R}' = \text{H}$	Bu_4N	63 h	66% ^a	50:50
3	Ph	<i>R</i> , $\text{R}' = \text{H}$	Na	30 min	90%	50:50
4	Ph	<i>S</i> , $\text{R}' = 3,5\text{-(CF}_3)_2\text{C}_6\text{H}_3$	Bu_4N	43 h	88%	52:48
5	Ph	<i>S</i> , $\text{R}' = 3,5\text{-(CF}_3)_2\text{C}_6\text{H}_3$	Na	30 min	87%	54:46
6	COO^tBu	<i>S</i> , $\text{R}' = 3,5\text{-(CF}_3)_2\text{C}_6\text{H}_3$	Na	15 min	81%	52:48

Table 4.8 Stoichiometric reduction studies using borohydrides. a. possibly due to insufficient amount of phosphoric acid; product formation observed after 30 min.

The ketimines **13g** and **13k** were chosen due to having significantly different basicity. We wanted to investigate the effect this would have on the strength of the substrate/chiral phosphoric acid interaction and whether this would result in an improvement in selectivity. The enamine **205** was investigated to test whether the coordinating nature of the carbamate functionality would result in improved enantioselectivity in reduction to **206** through improved transition state organisation.

Additionally, the Boc protecting group is an attractive option to use as it can be easily removed following enantioselective reduction resulting in the formation of an enantioenriched primary amine.

The sterically hindered, basic imine **13k** was not reduced by this combination of reagents (Entry 1, Table 4.8). Superior reactivity was observed in the reduction of imine **13g** when sodium counterion was employed (entries 3 and 5). The reduction of substrate **13g** with the sterically hindered phosphoric acid (*S*)-**190** (Ar = 3,5-(CF₃)₂C₆H₃) in the presence of the innocent cation ⁿBu₄N was significantly slower (analysed after 30 min, 19 h and 43 h) than the corresponding reduction in the presence of sodium cation (entries 4 and 5, Table 4.8). Monitoring by ³¹P NMR for these reactions is presented in Figure 4.14. The data is consistent with formation of the phosphate/borane adducts as by-products.

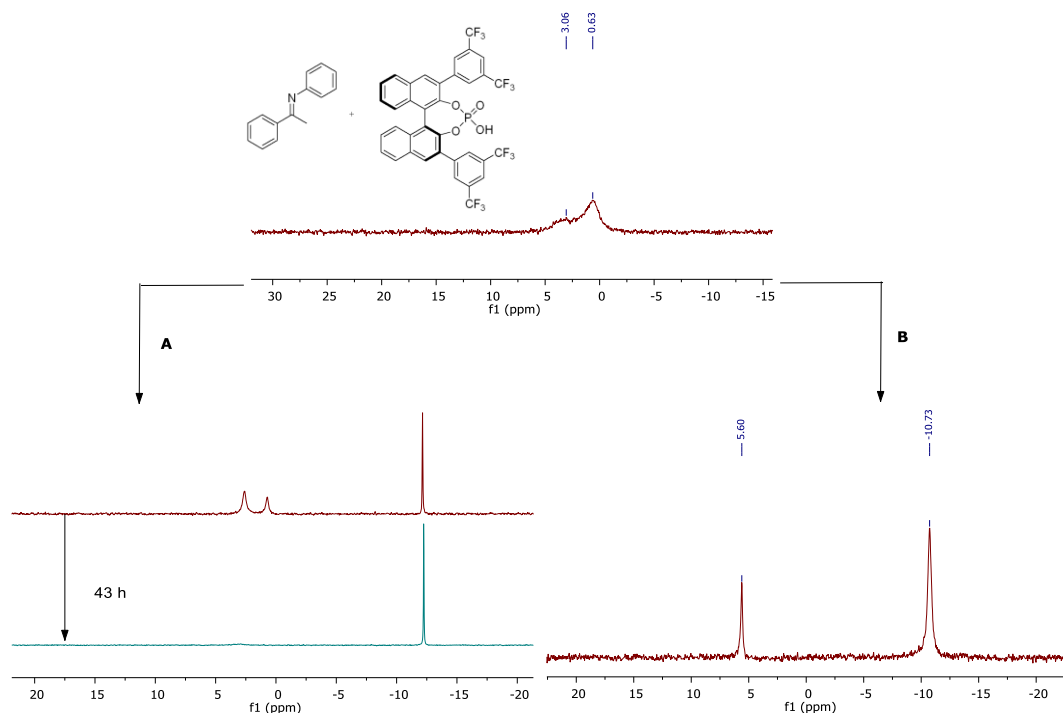


Figure 4.14 ³¹P NMR data for stoichiometric reduction using a bulky phosphoric acid; reactions carried out in C₆D₆; **A.** reagent [ⁿBu₄N][HB(C₆F₅)₄] **204**; **B.** reagent Na[HB(C₆F₅)₄] **203**

A similar process is found to occur when the un-substituted acid (*R*)-[**200**]H was used, although aggregation effects appear to be more significant (Figure 4.15).

The selectivity of these processes was negligible, with essentially racemic material obtained under all conditions. The organocatalytic reduction of imines reported by Rueping provides a good comparison with this work (cf. Scheme 4.5). Under catalytic conditions (20 mol% (*R*)-**190** (Ar = 3,5-(CF₃)₂C₆H₃)) in benzene at 60 °C a e.r. value of 86:14 (*R*:*S*) was reported for amine **36g**.³²⁵ We believe this higher selectivity is mostly a result of the different reducing agent being used (borohydride **203** vs. Hantzsch ester **192**).

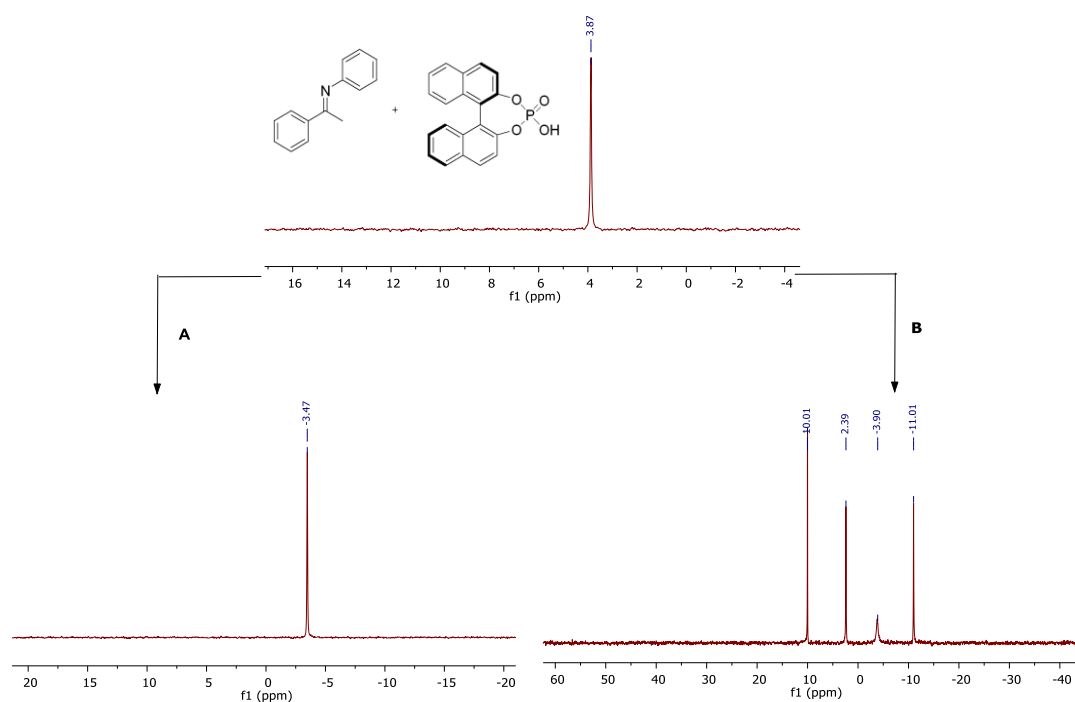


Figure 4.15 ³¹P NMR data for stoichiometric reduction using a non-bulky phosphoric acid; reactions carried out in C₆D₆; **A**. reagent [¹⁸Bu₄N][HB(C₆F₅)₄] **204**; **B**. reagent Na[HB(C₆F₅)₄]³⁶⁰ **203**

Reduction of enamine **205** (entry 6) was again very fast (15 min, no further change observed up to 4 h), but proceeded without any selectivity. Interaction between the chiral phosphoric acid and the enamine was observed, but the exact nature of the reactive species was not established. (Figure 4.16). Addition of hydride led to consumption of these reactive species and formation of the desired amine **206** (determined by comparison with a reference NMR recorded in C₆D₆). ³¹P NMR indicated a simple transformation from (*S*)-**190** (Ar = 3,5-(CF₃)₂C₆H₃) (6.2 ppm) to the corresponding phosphate/borane adduct (-10.4 ppm), confirmed by ¹⁹F NMR (-136.1, -158.2, -164.2; cf. Table 4.7).

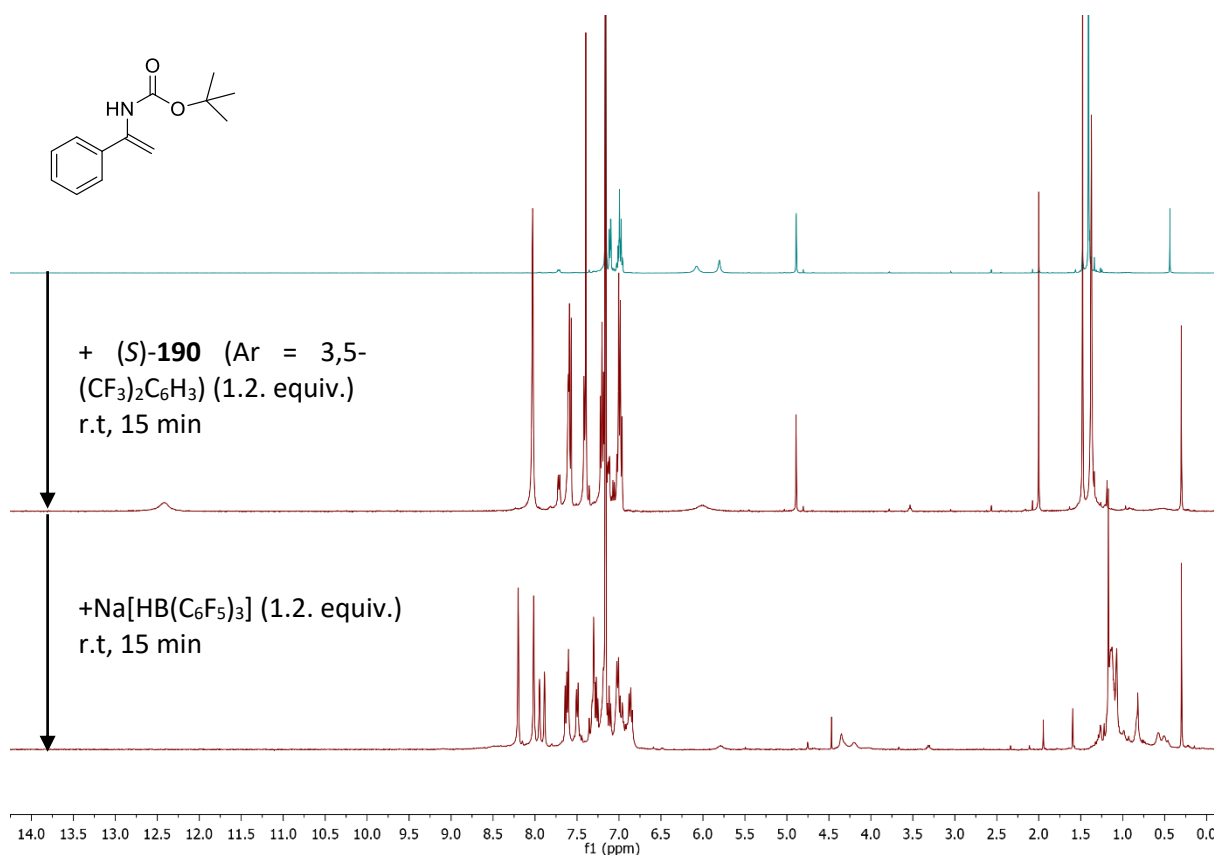


Figure 4.16 Stoichiometric reduction of Boc-protected enamine.

No enantioselectivity was observed under these conditions. An organocatalytic reduction of enamides was reported by Antilla (Figure 4.17).³⁶¹ The reaction was postulated to occur *via* isomerisation of the substrate to the imine form, which is then protonated. Acetic acid cocatalyst assists with the iminium formation, but reduction occurs only in the presence of phosphate counterion.

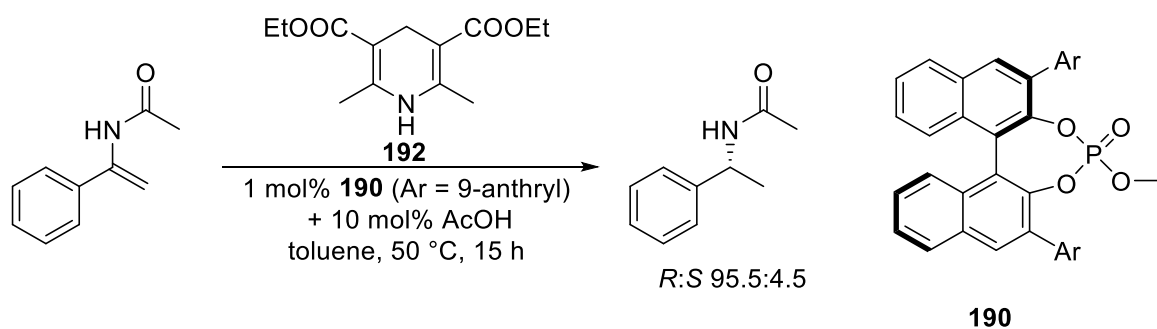


Figure 4.17 Reduction of enamides reported by Antilla.³⁶¹

The success of the reaction appears to be a result of using Hatzsch ester **192** as a hydride source. This could be due to two causes: the much bulkier nature of the borohydride disrupts hydrogen bonding

in the reduction transition state between the substrate and chiral phosphoric acid and/or the lack of functionality allowing for interaction between the phosphoric acid and the reducing agent (dihydropyridines are activated by hydrogen bonding between the NH donor and the acceptor PO fragment of the phosphoric acid³¹²) (Figure 4.18).

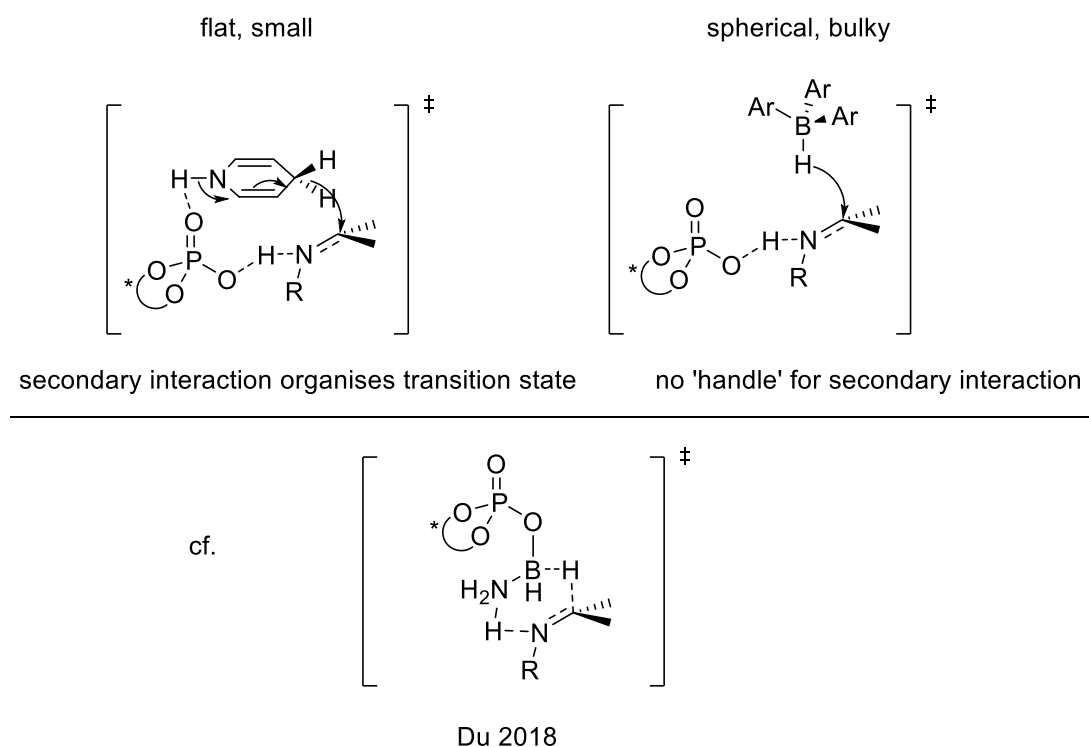


Figure 4.18 Comparison of Hantzsch ester and borohydride reducing agents.

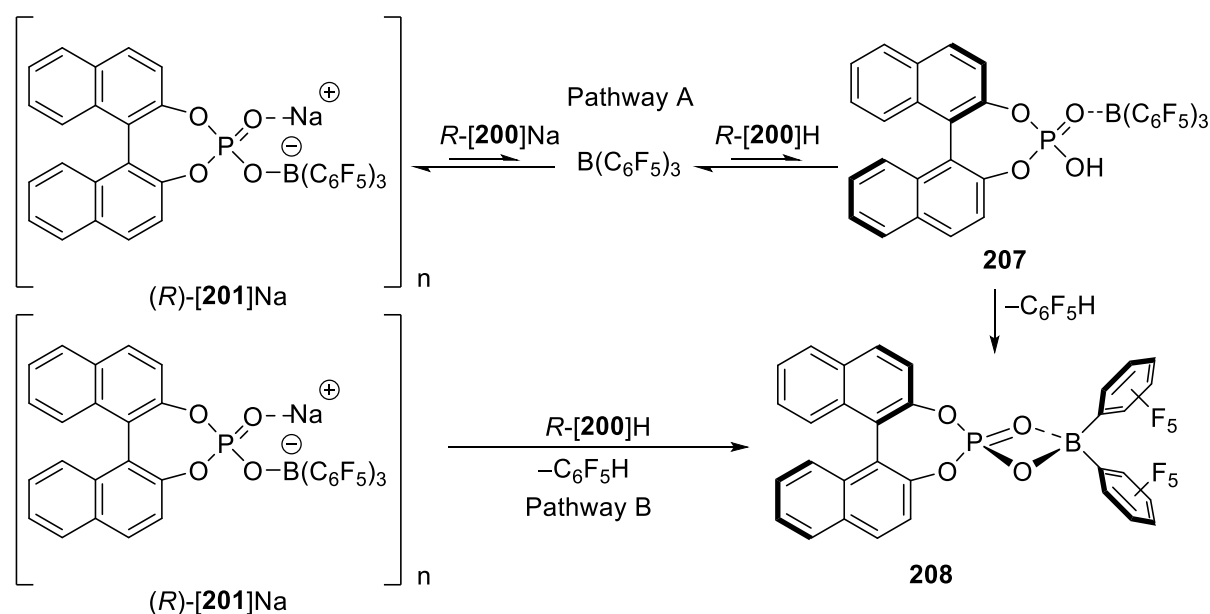
This conclusion also appears to be consistent with the related work of Du and co-workers who demonstrated successful use of chiral phosphoric acids to generate chiral ammonia borane-derived reagents for the reduction of ketimines.³¹⁷ In this case the chiral fragment is in proximity of the prochiral carbon atom of the substrate and the secondary hydrogen bonding interactions help organise the transition state.

4.3 Decomposition pathways

During the hydrogen activation experiment described in section 4.2.2.1 we noticed (by ¹⁹F NMR, -140.7, -155.6, -163.9, sharp multiplets, ratio 2:1:2) the formation of a by-product which was assigned as pentafluorobenzene. This was corroborated by the observation of a signal in the proton

NMR spectrum at 5.8 ppm (C_6D_6). Both the 1H and ^{19}F NMR spectra were compared to those recorded for an authentic sample of C_6F_5H in C_6D_6 .

Proto-deborylation is a common decomposition pathway for $B(C_6F_5)_3$,¹⁰² and could occur by the two pathways depicted in Scheme 4.12.



Scheme 4.12 Chiral phosphoric acid/borane stoichiometric reaction.

The borane/phosphoric acid adduct **207** was accessed from a mixture of the two components. When the two components were mixed in C_6D_6 , almost complete dissolution of the phosphoric acid occurred and NMR analysis of the resulting mixture revealed the formation of a new species assigned as the adduct **207** (Figure 4.19). This adduct was found to be unstable in solution at room temperature, decomposing slowly (20 h) to two new species which were assigned based on the stoichiometry suggested by the 1H and ^{19}F NMR spectra (Figure 4.20). Small variations in rate were observed between NMR and preparative scale (<0.6 mmol), with progress assessed by monitoring disappearance of adduct **207** by ^{31}P NMR (up to 44 h).

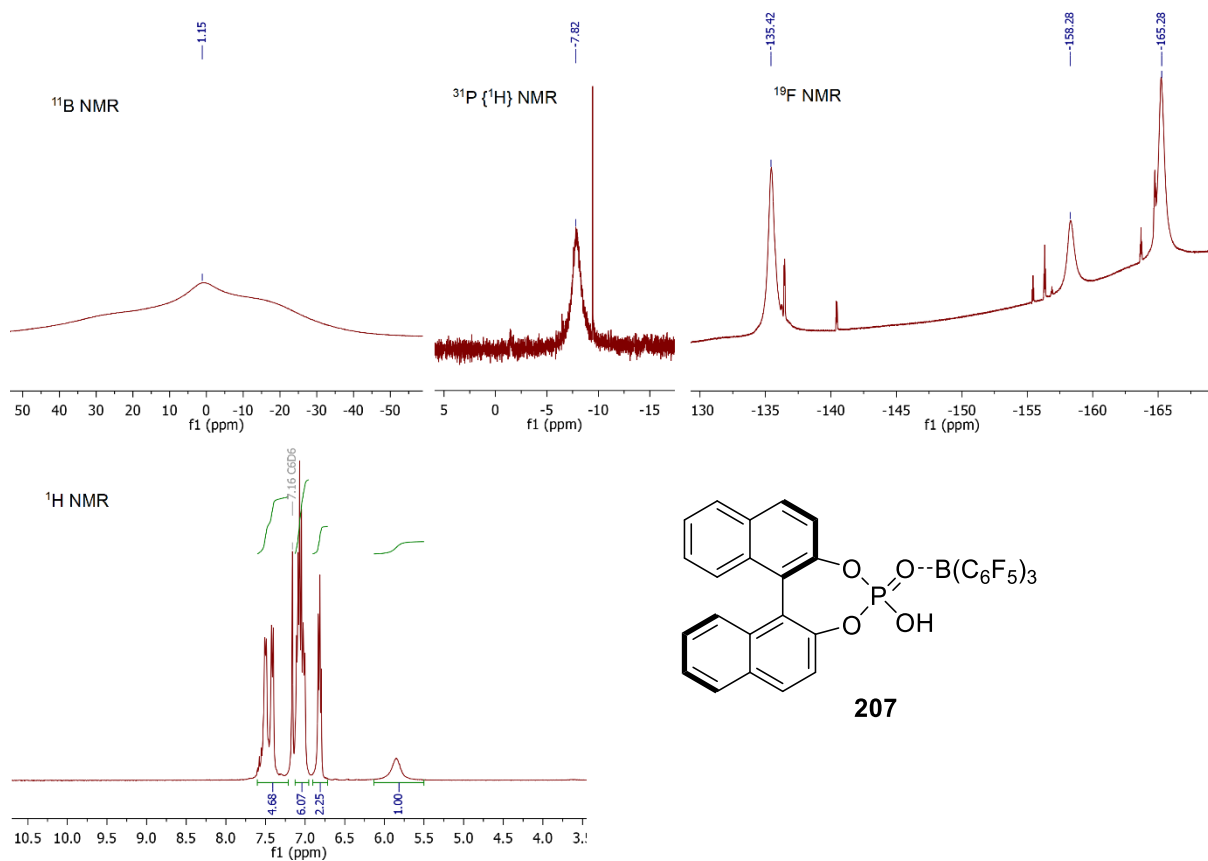


Figure 4.19 NMR data for adduct **207**.

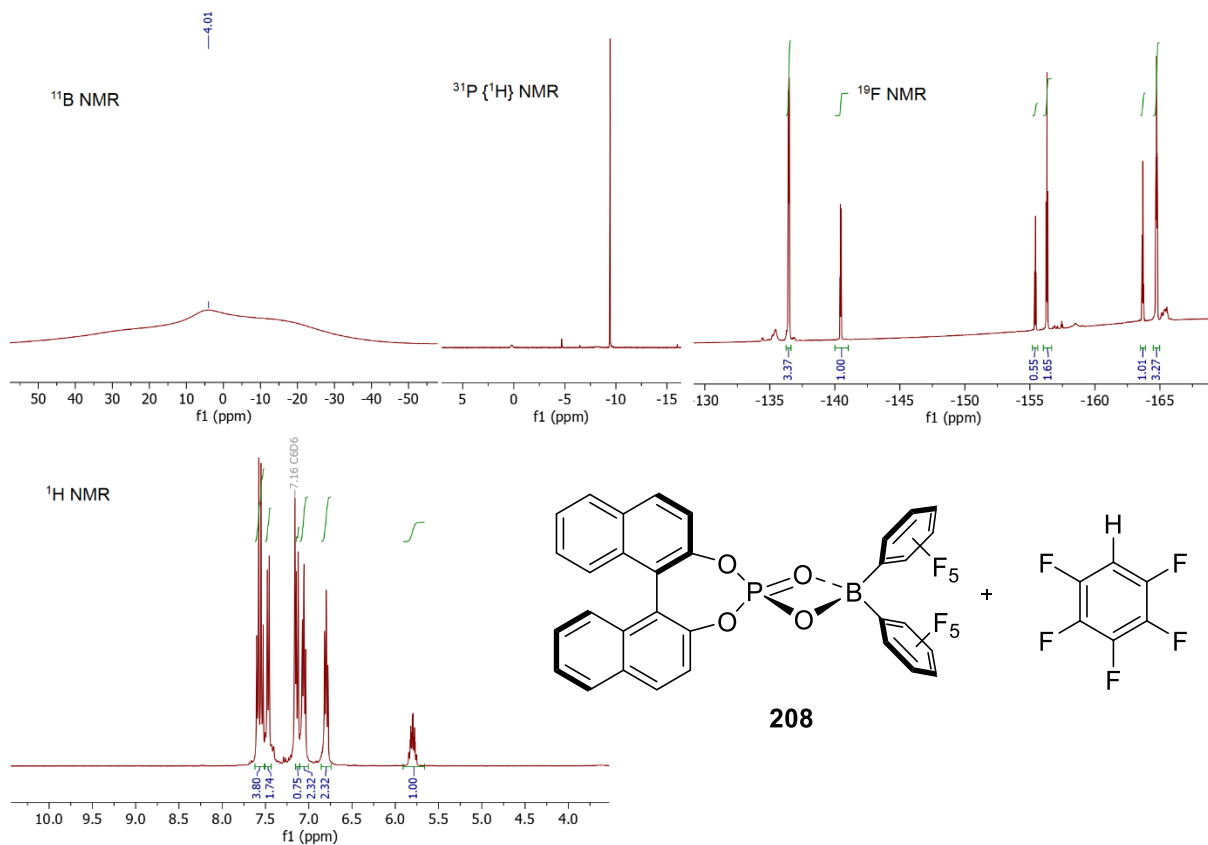
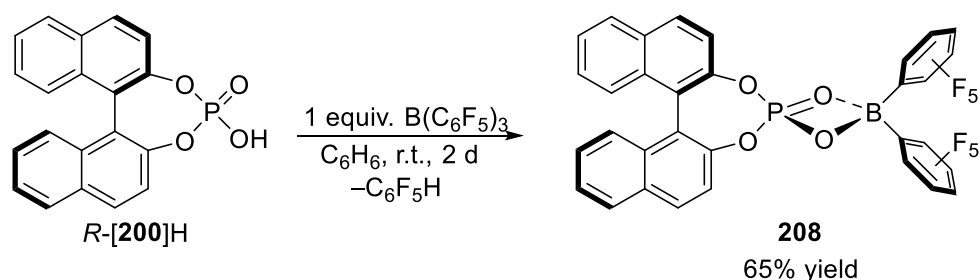


Figure 4.20 NMR data following decomposition of adduct **207**.

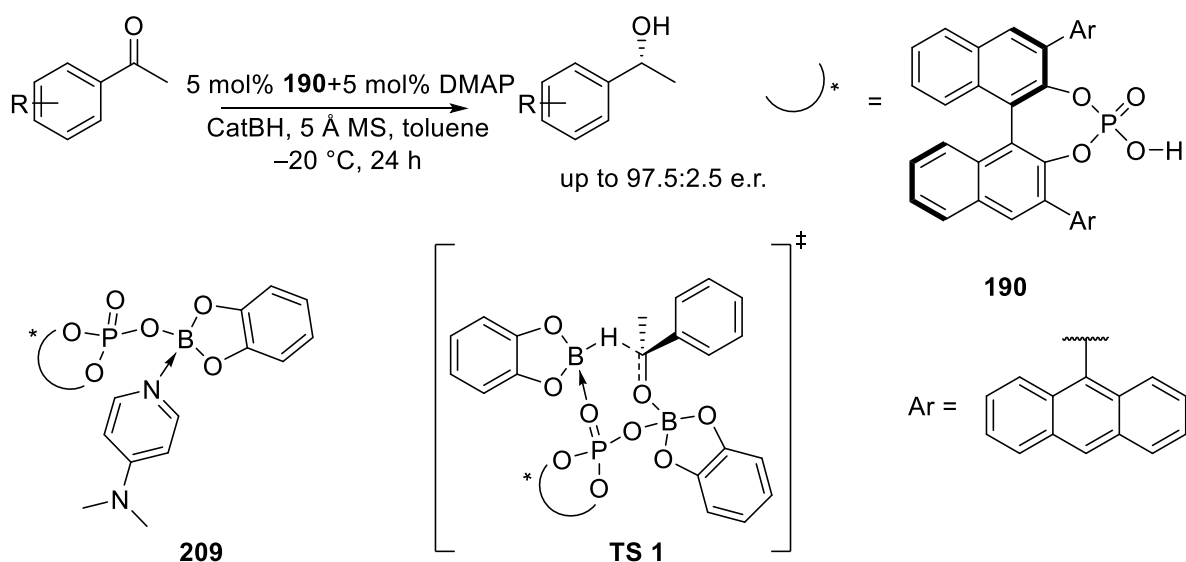
Isolation of the postulated product **208** was achieved in 65% yield following removal of volatiles and crystallisation from a DCM/pentane mixture (Scheme 4.13).



Scheme 4.13 Preparation of borane **208**.

NMR characterisation in C_6D_6 of the purified material supported the postulated structure. ^{31}P NMR showed the presence of a sharp peak at -9.4 ppm which indicates that the species is monomeric and that borane coordination is occurring to the $\text{P}=\text{O}$ fragment. ^{11}B NMR showed a broad peak at 3 ppm, indicative of a tetra-coordinated boron atom. The broad nature of this peak suggests that the structure is dynamic (Figure 4.22, see later). A similar DMAP adduct **209** reported by Antilla displayed a ^{11}B NMR of 6.1 ppm (Scheme 4.14).³⁶² ^{19}F NMR confirms the tetra-coordinate nature of the boron atom: sharp multiplets are observed in the ratio of 2:1:2 at the following chemical shifts -137.1 (*o*), -158.1 (*p*), -166.1 (*m*); $\Delta\delta(m,p-F) = 8$ ppm (cf. Table 4.1). Numerous conditions were tested for the recrystallisation of borane **208**, but crystals of suitable quality for crystallographic study could not be obtained.

Antilla reported on the use of chiral phosphate catalyst **209** to achieve reduction of ketones with catecholborane (Scheme 4.14).³⁶² A cooperative mechanism was proposed to be operating (**TS 1**) involving concerted activation of borane and substrate by the phosphate: the reducing agent has 'borohydride' character.



Scheme 4.14 Enantioselective ketone reduction reported by Antilla.³⁶²

Compound **208** could possibly be prepared from the reaction of Piers borane with the phosphoric acid (*R*)-[**200**]H, this preparation bearing resemblance with the work of Du (Figure 4.21).³¹⁴

Compound **208** could not be directly observed in the previously described hydrogen activation (section 4.2.2.1; see relevant experimental section) and stoichiometric reduction studies, presumably due to its interaction with free phosphate salt/phosphoric acid present under the reaction conditions.

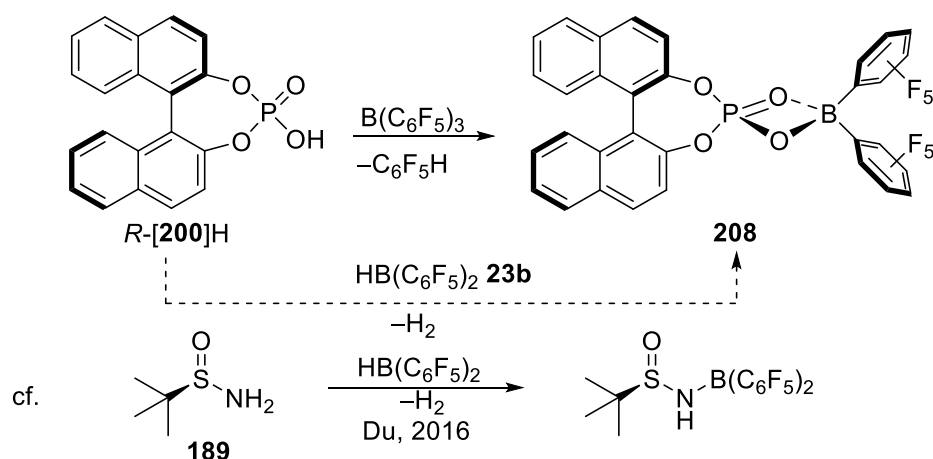


Figure 4.21 Possible alternative preparation of borane **208**.

Under hydrogen activation conditions protodeborylation is slow, probably due to the equilibrium shown for pathway A being shifted towards phosphate salt adduct (*R*)-[**201**]Na (Scheme 4.12).

Considering the potential catalytic activity of borane **208**, hydrogen activation experiments were performed at 10 bar in donor solvents (THF or 1,4-dioxane). Although the open form of borane **208** can be considered as an intramolecular FLP (PO group acting as a weak base), hydrogen activation by this mechanism was considered unlikely due to the low basicity of the PO functionality, reason for which an external base (solvent) was employed.

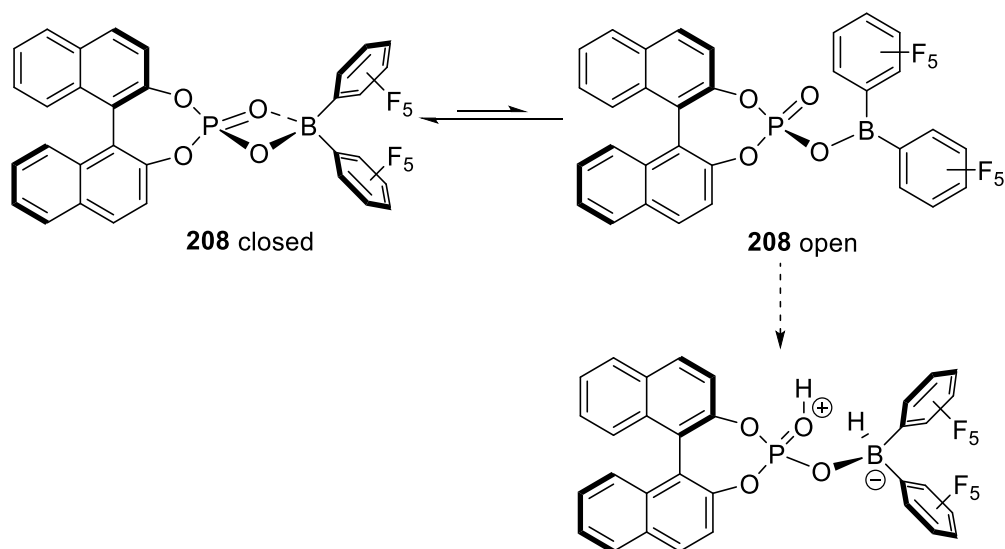


Figure 4.22 Potential hydrogen activation using borane **208**.

The ^{31}P , ^{19}F and ^{11}B spectra of borane **208** recorded in donor solvents (THF, 1,4-dioxane) were very similar to those observed in non-donor solvents, suggesting that the intramolecular P=O to B donation is strong enough to prevent coordination of external donors. In THF solvent, a slow reaction was observed at room temperature (18 h) following pressurising with hydrogen gas (10 bar). Heating to 50 °C (25 h) increased the rate, leading to observation of new peaks by ^{31}P NMR, ^{19}F NMR and ^{11}B NMR (Figure 4.23).

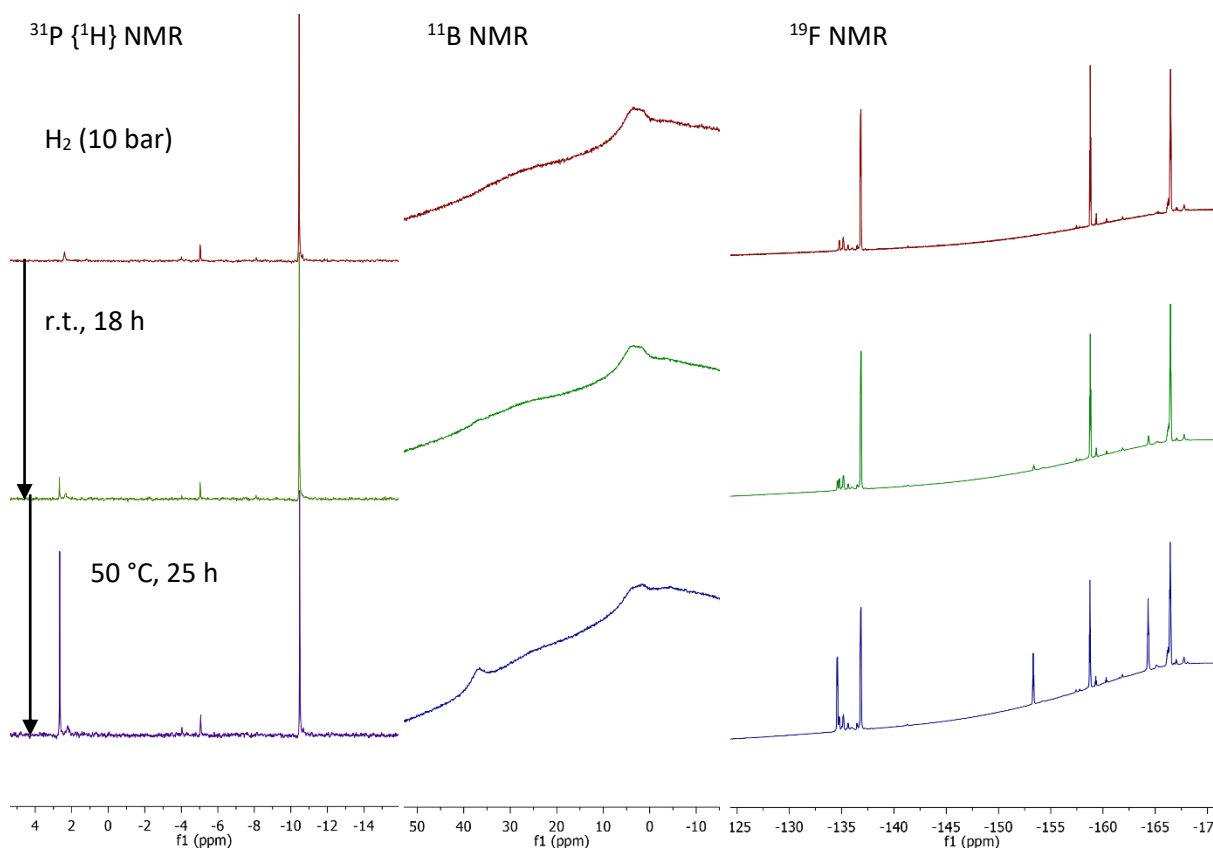


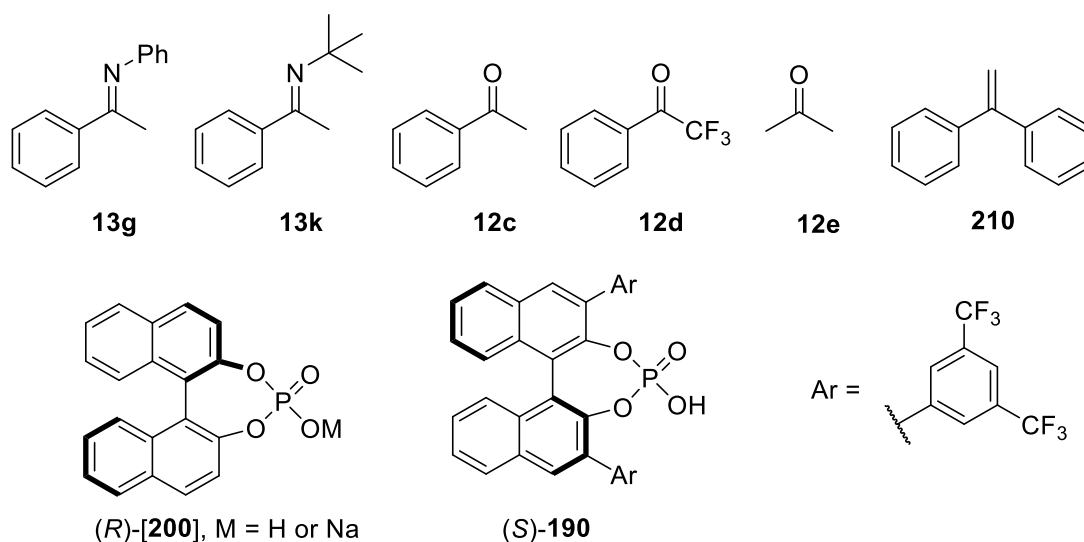
Figure 4.23 Attempted hydrogen activation using borane **208**.

These data suggested that further degradation was occurring, with formation of free phosphoric acid and C_6F_5H . 1H NMR indicated the formation of a significant amount ($>70:1$ with respect to borane **208**) of what appeared to be polymerised THF (3.33, 1.55, $\sim 1:1$). Additionally, small peaks were observed at 4.2 ppm, which together with the other spectral data suggests that ring opening of THF has partially occurred. It is not possible from these results to determine whether polymerisation was Brønsted or Lewis acid catalysed (ie. whether hydrogen activation preceded polymerisation). A similar process was not found to occur in 1,4-dioxane. When the latter reaction was repeated in the presence of a catalytic amount of $B(C_6F_5)_3$ **4b** (10 mol%) a similar negative result was obtained. These results suggest that borane **208** is potentially a strong Lewis acid, reason for which it was investigated in catalytic applications together with the phosphate/**4b** system.

4.4 Attempted catalytic transformations

A range of attempted hydrogenation reactions are summarised in Table 4.9. Except for entries 4-6, all other reactions did not result in discernible product formation by ^1H NMR. In the entries 1-3 performed with imine substrates the reaction mixture before hydrogenation contained a monomeric version of a phosphate/borane adduct (imine acting as a base), as indicated by ^{11}B (~ -3 ppm) and ^{31}P NMR (~ -7 ppm). Following heating under a hydrogen atmosphere partial or complete decomposition was observed as indicated by the formation of pentafluorobenzene (^{19}F NMR), oxyboranes (^{11}B NMR) and free phosphoric acid (^{31}P NMR). The reactions 4-7 indicated before hydrogenation the presence of adduct (*R*)-[**201**]Na, in either aggregate form (entry 6, presumably due to the lack of donor properties of alkene **210**) or monomeric form (entries 4, 5, 7). Following heating under a hydrogen pressure a similar course was observed to that described for the attempted reduction of imines: hydrogen activation is followed by protodeborylation (see experimental section), with minimal reduction of substrates occurring. In the case of acetophenone (entry 5) approximately stoichiometric reduction was observed; the resulting alcohol was dehydrated under these reaction conditions to styrene. Remarkably the alkene **210** (entry 6) was also reduced in approximately stoichiometric amount, presumably on account of the high Brønsted acidity of phosphoric acid/**4b** adduct **207**. Trace reduction of acetone was observed (formation of two isopropyl septets, 4.12, 4.3 ppm) however no estimate of conversion could be made due to decomposition of the remainder of the starting material. Similarly, ^{19}F NMR indicated trace reduction of ketone **12d** (entry 4, series of doublets at -79.3).

Borane **208** decomposed under the reaction conditions leading to no reduced product formation. The extensive deborylation observed is a result of the high temperature required to achieve hydrogen activation. In future work, use of lower reaction temperatures could improve conversion, however the rate of reaction is expected to remain very slow. To address these issues, the use of donor solvents (THF, etc.), more polar solvents (1,2-DFB) and higher hydrogen pressures are expected to improve reactivity.



Entry	Subst.	Borane	Chiral component	Reaction conditions	Conv.
1	13k	4b (10 mol%)	(<i>R</i>)-[200]H (10 mol%)	4 bar H ₂ , C ₇ D ₈ , 120 °C, 90 h	0%
2	13g	4b (10 mol%)	(<i>R</i>)-[200]H (10 mol%)	4 bar H ₂ , C ₇ D ₈ , 120 °C, 19 h	0%
3	13g	4b (10 mol%)	(<i>S</i>)- 190 (10 mol%)	10 bar H ₂ , C ₆ D ₆ , up to 80 °C, 20 h	0%
4	12d	4b (5 mol%)	(<i>R</i>)-[200]Na (5 mol%)	10 bar H ₂ , C ₆ H ₆ , 120 °C, 48 h	trace
5	12c	4b (5 mol%)	(<i>R</i>)-[200]Na (5 mol%)	10 bar H ₂ , C ₆ H ₆ , 120 °C, 92 h	~7%
6	210	4b (5 mol%)	(<i>R</i>)-[200]Na (5 mol%)	10 bar H ₂ , C ₆ H ₆ , 120 °C, 7 d	~9%
7	12e	4b (5 mol%)	(<i>R</i>)-[200]Na (5 mol%)	10 bar H ₂ , C ₆ H ₆ , 120 °C, 24 h	trace
8	13g	208 (10 mol%)	-	10 bar H ₂ , THF, 50 °C, 14 h	0%
9	12c	208 (10 mol%)	-	10 bar H ₂ , THF, 50 °C, 14 h	0%

Table 4.9 Attempted catalytic hydrogenation using phosphate/borane systems. Conversions estimated by relative integration and represent maximum values; see Experimental section; ¹⁹F NMR used for entry 4.

4.5 Conclusions

The chemistry of BINOL-derived phosphate salt/borane FLPs was explored. Such systems were capable of activating hydrogen gas; the rate of reaction was slow, most likely due to the poor basicity of the phosphate salts. Screening under catalytic or stoichiometric conditions has revealed that weakly basic substrates are potentially suitable, in agreement with the weakly basic nature of the phosphate component. The system suffers from the known drawbacks associated with $B(C_6F_5)_3$ resulting from tendency towards protodeborylation. Stoichiometric reductions afforded negligible levels of enantioselectivity, apparently due to the nature of the bulky borohydride reducing agent $[HB(C_6F_5)_3]$. In future work it is expected that standard optimisation (see section 4.4) will solve issues regarding reactivity. Improving enantioselectivity levels appears to be a more challenging task and will require further screening of directing groups and additives or the preparation of custom boranes or other Lewis acids capable of engaging in hydrogen activation.

5 Experimental chapter

Copies of relevant NMR spectra can be found in the Appendix.

5.1 Experimental data concerning Chapter 2

General experimental procedures, catalyst characterisation, substrate preparation and characterisation, product purification procedures and characterisation data relevant to this chapter can be accessed at: <http://www.rsc.org/suppdata/c9/cc/c9cc02900a/c9cc02900a1.pdf>.

Details regarding catalyst synthesis and characterisation of intermediates and characterisation data for other substrates and products is included here.

5.1.1 Calculation %V_{bur} for **95**

SambVca@MoLNnaC https://www.molnac.unisa.it/OMtools/sambvca_result.php

Results : Volumes in Angs³

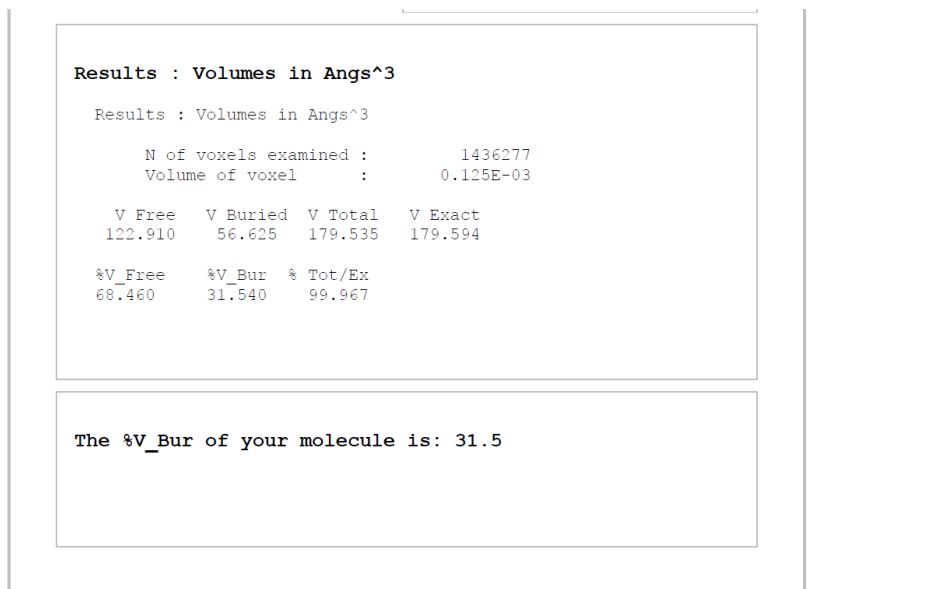
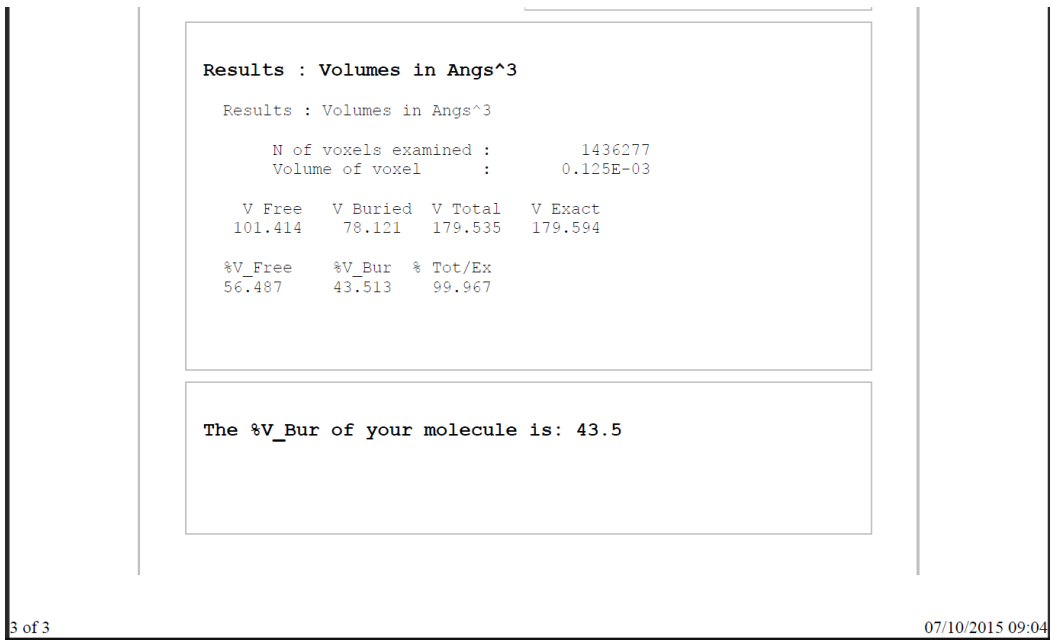
Results : Volumes in Angs³

N of voxels examined :	1436277
Volume of voxel :	0.125E-03

V Free	V Buried	V Total	V Exact
98.243	81.291	179.535	179.594

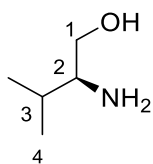
%V_Free	%V_Bur	% Tot/Ex
54.721	45.279	99.967

The %V_Bur of your molecule is: 45.3



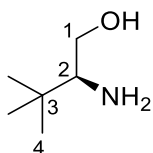
5.1.2 Catalyst synthesis

(S)-valinol 101a



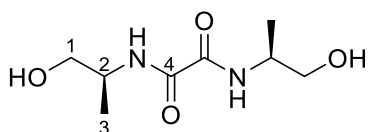
A 3-neck flask was charged with sodium borohydride (3.9 g, 102.5 mmol, 2.4 equiv.), THF (110 mL), and (*S*)-valine (5 g, 42.7 mmol, 1 equiv.). The reaction was cooled in an ice bath before a solution of iodine (10.9 g, 42.7 mmol, 1 equiv.) in THF (30 mL) was added slowly *via* an addition funnel. After the gas evolution ceased the solution was heated to reflux for 22 h. After cooling to r.t., methanol was added slowly until the solution became clear. After stirring for 2 h the solvents were removed on a rotary evaporator; to the resulting residue KOH aqueous solution (84 mL, 20% w/v) was added. Following stirring for 4 h, the solution was extracted with DCM (3×84 mL). The organic phase was dried overnight on sodium sulfate and the solvent removed. The resulting residue was distilled on a Kugelrohr apparatus (75 °C at 0.035 mbar) to yield the product as a clear oil (2.73 g, 26.5 mmol, 62 % yield). ¹H NMR (400 MHz, CDCl₃): 3.61 (dd, *J* = 10.7, 3.9 Hz, 1H, H1), 3.27 (dd, *J* = 10.6, 8.6 Hz, 1H, H1), 2.53 (m, 1H, H2), 2.17 (br s, 3H), 1.55 (m, 1H, H3), 0.9 (d, *J* = 4.8 Hz, 3H, H4), 0.88 (d, *J* = 4.9 Hz, 3H, H4). ¹³C NMR (125 MHz, CDCl₃) 64.8 (C1), 58.6 (C2), 31.5 (C3), 19.4 (C4), 18.5 (C4). Data in agreement with the literature.³⁶³

(*S*)-*tert*-leucinol 101b



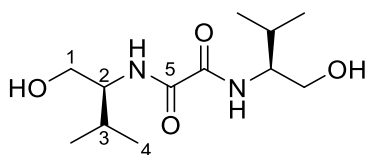
Prepared analogously to (*S*)-valinol using (*S*)-*tert*-leucine (5 g, 38.2 mmol, 1 equiv.). Product obtained as a clear oil (2.76 g, 23.6 mmol, 62 % yield). ¹H NMR (400 MHz, CDCl₃): 3.7 (dd, *J* = 10.3, 3.9 Hz, 1H, H1), 3.19 (t, *J* = 10.1 Hz, 1H, H1), 2.49 (dd, *J* = 10.2, 3.9 Hz, 1H, H2), 0.89 (s, 9H, H4). In agreement with the literature.³⁶⁴

N,N'-bis[(2*S*)-1-hydroxy-2-methylpropan-2-yl]ethanediamide



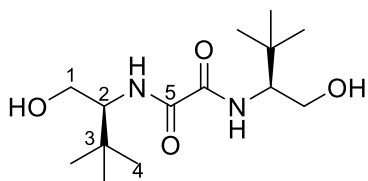
Diethyl oxalate (4.52 mL, 33.3 mmol, 1 equiv.) and (*S*)-alaninol (5.2 mL, 66.7 mmol, 2 equiv.) were added sequentially to THF (200 mL). The resulting solution was heated to 65 °C and acetic acid (0.2 mL, 3.3 mmol, 0.1 equiv.) was added. Stirring at this temperature was maintained for 16 h, during which time the product precipitated. Filtration and drying *in vacuo* yielded the product (5.2 g, 25.3 mmol, 76% yield) as a white powder. Product can be recrystallised from methanol. m.p. (MeOH) 168-172 °C; Elemental analysis %C calculated: 47.05, found: 47.16; %H calculated: 7.9, found: 7.88; %N calculated: 13.72, found: 13.56; R_f 0.39 (DCM/MeOH 9:1); ^1H NMR (400 MHz, DMSO- d_6) 8.32 (d, J = 8.6 Hz, 2H, NH), 4.77 (t, J = 5.7 Hz, 2H, OH), 3.81 (m, 2H), 3.36 (m, 4H), 1.07 (d, J = 6.8 Hz, 6H, H₃); ^{13}C NMR (100 MHz, DMSO- d_6) 159.5 (C₄), 63.8, 47.1, 16.6 (C₁); HRMS (ESI⁺) calculated for C₈H₁₇N₂O₄ ([M+H]⁺): 205.1188; found : 205.1182; IR ν_{max} /cm⁻¹ 3380 (OH), 3288 (NH), 1655 (CO).

***N,N'*-bis[(2*S*)-1-hydroxy-3-methylbutan-2-yl]ethanediamide**



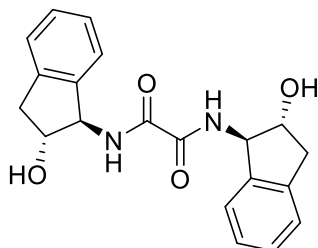
Diethyl oxalate (1.7 mL, 12.5 mmol, 1 equiv.) was added to a solution of (*S*)-valinol (2.7 g, 26.2 mmol, 2.1 equiv.) in toluene (68 mL). The solution was stirred under heating at 90 °C for 16 h. The solution was cooled slowly and allowed to stand for 2 h before being filtered. The product was washed with an approximately equal volume of pentane and dried to yield the product (2.68 g, 10.4 mmol, 83% yield) as a white powder. R_f 0.28 (DCM/MeOH 19:1); ^1H NMR (400 MHz, DMSO- d_6) 8.14 (d, J = 9.6 Hz, 2H, NH), 4.67 (t, J = 5.3 Hz, 2H, OH), 3.55 (m, 2H), 3.48 (m, 4H), 1.85 (m, 2H, H₃), 0.87 (d, J = 6.6 Hz, 6H), 0.81 (d, J = 6.6 Hz, 6H); ^{13}C NMR (100 MHz, DMSO- d_6) 159.9 (C₅), 61, 56.8, 28.5 (C₃), 19.6 (C₄), 18.7 (C₄); Spectral data in agreement with the literature;²⁰⁶ HRMS (ESI⁺) calculated for C₁₂H₂₅N₂O₄ ([M+H]⁺): 261.1814; found: 261.1816; IR ν_{max} /cm⁻¹ 3405 (OH), 3286 (NH), 1647 (CO).

***N,N'*-bis[(2*S*)-1-hydroxy-3,3-dimethylbutan-2-yl]ethanediamide**



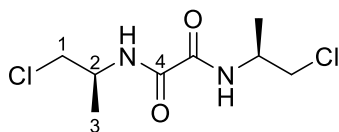
Prepared analogously to *N,N'*-bis[(2*S*)-1-hydroxy-3-methylbutan-2-yl]ethanediamide using diethyl oxalate (1.52 mL, 11.2 mmol, 1 equiv.) and *L-tert* leucinol (2.76 g, 23.6 mmol, 2.1 equiv.). The toluene was removed on a rotary evaporator to give the product as a white powder. (3.13 g, 10.9 mmol, 97 % yield). ¹H NMR (400 MHz, CDCl₃) 7.5 (d, *J* = 11.5 Hz, 2H, NH), 3.89 (dd, *J* = 11.6, 3.3 Hz, 2H), 3.77 (m, 2H), 3.59 (dd, *J* = 11.6, 8.9 Hz, 2H), 3.35 (br s, 2H, OH), 0.94 (s, 18H, H₃); ¹³C NMR (100 MHz, CDCl₃) 161.3 (C5), 61.6, 61, 33.5 (C3), 26.9 (C4); In agreement with the literature.³⁶⁵ HRMS (ESI+) calculated for C₁₄H₂₉N₂O₄ ([M+H]⁺): 289.2127; found: 289.2130; IR ν_{max}/cm⁻¹ 3391 (OH), 3303 (NH), 1653 (CO).

***N*¹,*N*²-bis[(1*R*,2*R*)-2-hydroxy-2,3-dihydro-1*H*-inden-1-yl]oxalamide**



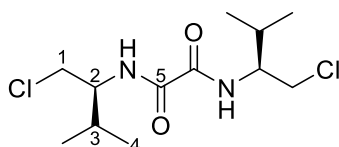
Prepared analogously to *N,N'*-bis[(2*S*)-1-hydroxy-2-methylpropan-2-yl]ethanediamide using (1*R*,2*R*)-*trans*-1-amino-2-indanol (1 g, 6.7 mmol, 2.1 equiv.) and diethyl oxalate (0.44 mL, 3.24 mmol, 1 equiv.). The crude product obtained following filtration was washed with THF and CHCl₃ to give a white solid (836 mg, 2.4 mmol, 73% yield). ¹H NMR (400 MHz, DMSO-*d*₆): 9.1 (d, *J* = 9 Hz, 2H), 7.2 (m, 6H), 7.08 (m, 2H), 5.37 (d, *J* = 6 Hz, 2H), 5.09 (t, *J* = 7.9 Hz, 2H), 5.41 (m, 2H), 3.15 (dd, *J* = 7.3, 15.5 Hz, 2H), 2.72 (dd, *J* = 7.9, 15.3 Hz, 2H). ¹³C NMR (100 MHz, DMSO-*d*₆): 160.6, 141.1, 139.8, 127.6, 126.6, 124.6, 123.6, 76.9, 61.5, 38.7. In agreement with the literature.²⁰⁴

***N,N'*-bis[(2*S*)-1-chloropropan-2-yl]ethanediamide**



N,N'-bis[(2*S*)-1-hydroxy-2-methylpropan-2-yl]ethanediamide (4.9 g, 24 mmol, 1 equiv.) was suspended in toluene (196 mL), the resulting suspension heated to 60 °C, and then thionyl chloride (5.1 mL, 69.7 mmol, 2.9 equiv.) was added. The reaction mixture was stirred at 60 °C for 1 h, then at 90 °C for 14 h. After cooling to r.t. the reaction was added to a 20% KOH aqueous solution (350 mL) together with DCM (700 mL) and stirred. The aqueous layer was separated and stirred again with 700 mL DCM for 30 min. The combined organic phases were dried over sodium sulfate and evaporated to yield the product as a white powder (5.58 g, 23.3 mmol, 97 % yield). R_f 0.08 (DCM/pet. ether 1:1); ^1H NMR (400 MHz, DMSO- d_6) 8.78 (d, J = 9 Hz, 2H, NH), 4.06 (m, 2H), 3.67 (m, 4H), 1.17 (d, J = 6.9 Hz, 6H, H3); ^{13}C NMR (100 MHz, DMSO- d_6) 159.4 (C4), 47.3, 46.8, 17.8 (C3); HRMS (ESI+) calculated for $\text{C}_8\text{H}_{16}\text{N}_2\text{O}_3\text{Cl}$ [M-Cl+H $_2\text{O}$]: 223.0849, found: 223.0851; IR ν_{max} /cm $^{-1}$ 3278 (NH), 1656 (CO), 732 (C-Cl).

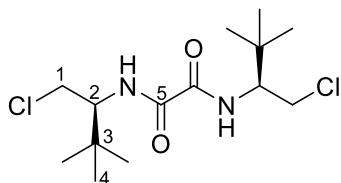
***N,N'*-bis[(2*S*)-1-chloro-3-methylbutan-2-yl]ethanediamide**



Prepared analogously to *N,N'*-bis[(2*S*)-1-chloropropan-2-yl]ethanediamide using *N,N'*-bis[(2*S*)-1-hydroxy-3-methylbutan-2-yl]ethanediamide (2.68 g, 10.3 mmol, 1 equiv.) and thionyl chloride (1.67 mL, 22.7 mmol, 2.2 equiv.), 90 °C for 1.5 h. White powder (2.9 g, 9.8 mmol, 95% yield). R_f 0.33 (DCM/pet. ether 1:1); ^1H NMR (400 MHz, CDCl_3) 7.56 (d, J = 9.8 Hz, 2H, NH), 3.91 (m, 2H), 3.68 (m, 4H), 2.04 (m, 2H), 1.00 (d, J = 6.7 Hz, 6H, H4), 0.96 (d, J = 6.7 Hz, 6H, H4); ^{13}C NMR (100 MHz, CDCl_3) 159.5 (C5), 56.1, 45.8, 29.4 (C3), 19.4 (C4), 18.7 (C4); In agreement with the literature;²⁰⁶ HRMS (APCI)

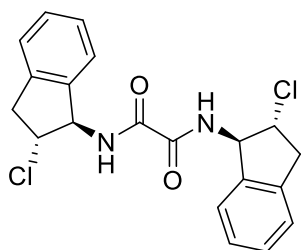
calculated for $C_{12}H_{23}N_2O_2Cl_2$ ($[M-H]^+$): 297.1131, found: 297.1121; IR ν_{max}/cm^{-1} 3276 (NH), 1657 (CO), 734 (C-Cl).

***N,N'*-bis[(2*S*)-1-chloro-3,3-dimethylbutan-2-yl]ethanediamide**



Prepared analogously to *N,N'*-bis[(2*S*)-1-chloropropan-2-yl]ethanediamide using *N,N'*-bis[(2*S*)-1-hydroxy-3,3-dimethylbutan-2-yl]ethanediamide (3.13 g, 10.9 mmol, 1 equiv.) and thionyl chloride (1.75 mL, 23.9 mmol, 2.2 equiv.), 90 °C for 2 h. The organic phase was washed with water (60 mL), brine (100 mL) and dried on sodium sulfate. The resulting cloudy solution was filtered and then evaporated to yield the product as an off-white powder (2.26 g, 7 mmol, 64% yield). Elemental analysis %C calculated: 51.7, found: 51.84; %H calculated: 8.06, found: 8.07; %N calculated: 8.61, found: 8.79; 1H NMR (400 MHz, $CDCl_3$) 7.48 (d, $J = 11.3$ Hz, 2H, NH), 4.02 (m, 2H), 3.82 (dd, $J = 11.9, 3.7$ Hz, 2H), 3.49 (dd, $J = 11.6, 9.3$ Hz, 2H), 1.0 (s, 18H, H₄); ^{13}C NMR (100 MHz, $CDCl_3$) 160.1 (C₅), 59.8, 44.5, 35.2 (C₃), 26.8 (C₄); HRMS (ESI⁺) calculated for $C_{14}H_{27}N_2O_2Cl_2$ ($[M+H]^+$): 325.1450, found: 325.1439; IR ν_{max}/cm^{-1} 3365 (NH), 1685 (CO), 726 (C-Cl).

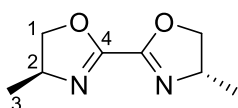
***N*¹,*N*²-bis((1*R*,2*R*)-2-chloro-2,3-dihydro-1*H*-inden-1-yl)oxalamide**



Prepared analogously to *N,N'*-bis[(2*S*)-1-chloropropan-2-yl]ethanediamide using *N*¹,*N*²-bis((1*R*,2*R*)-2-hydroxy-2,3-dihydro-1*H*-inden-1-yl)oxalamide (800 mg, 2.27 mmol, 1 equiv.) and thionyl chloride (0.82 mL, 11.4 mmol, 5 equiv.), 110 °C (16 h); cool to -20 °C then isolate product by filtration; crude

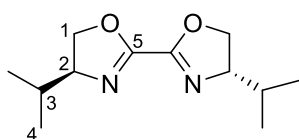
product was washed with toluene and pentane to give a white solid (782 mg, 2 mmol, 89% yield). ¹H NMR (400 MHz, DMSO-d₆, poorly soluble) 9.48 (d, *J* = 8.9 Hz, 2H), 7.28 (m, 6H), 7.18 (m, 2H), 5.44 (t, *J* = 8.6 Hz, 2H), 4.78 (q, *J* = 7.9 Hz, 2H), 3.55 (dd, *J* = 7.7, 15.8 Hz, 2H), 3.12 (dd, *J* = 8.4, 15.6 Hz, 2H); ¹³C NMR (100 MHz, DMSO-d₆) 160.3, 140.1, 139.2, 128.3, 127.3, 124.5, 123.4, 62.2, 61.3. In agreement with the literature.²⁰⁴

(4*S*,4'*S*)-4,4'-dimethyl-4,4',5,5'-tetrahydro-2,2'-bi-1,3-oxazole 103c



N,N'-bis[(2*S*)-1-chloropropan-2-yl]ethanediamide (5.6 g, 23.2 mmol, 1 equiv.) and KOH (3 g, 53.3 mmol, 2.3 equiv.) were suspended in methanol (345 mL). The resulting suspension was heated to 65 °C and refluxed for 1.5 h during which time it became clear and a precipitate was generated. The reaction mixture was dried on a rotary evaporator and to the resulting residue water (450 mL) was added. The resulting suspension was extracted with DCM (2×250 mL) and the combined organic phases were dried on sodium sulfate for 1 h before being evaporated to yield the product as a white powder (3.77 g, 22.5 mmol, 97% yield). Elemental analysis %C calculated: 57.13, found: 57.04; %H calculated: 7.19, found: 7.08; %N calculated: 16.66, found: 16.47; *R*_f 0.43 (DCM/MeOH 30:1); ¹H NMR (400 MHz, CDCl₃) 4.51 (dd, *J* = 9.6, 8.3 Hz, 2H), 4.38 (m, 2H), 3.97 (t, *J* = 8.1 Hz, 2H), 1.33 (d, *J* = 6.5 Hz, 6H, H₃); ¹³C NMR (100 MHz, CDCl₃) 154.8 (C₄), 74.9, 62.6, 21 (C₃); HRMS (ESI+) calculated for C₈H₁₃N₂O₂ ([M+H]⁺): 169.0977, found: 169.0979; IR *v*_{max}/cm⁻¹ 1618 (C=N).

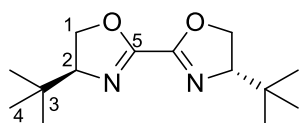
(4*S*,4'*S*)-4,4'-di-*iso*-propyl-4,4',5,5'-tetrahydro-2,2'-bi-1,3-oxazole 103a



Prepared analogously to: (4*S*,4'*S*)-4,4'-dimethyl-4,4',5,5'-tetrahydro-2,2'-bi-1,3-oxazole using *N,N'*-bis[(2*S*)-1-chloro-3-methylbutan-2-yl]ethanediamide (1.09 g, 3.66 mmol, 1 equiv.) and methanolic

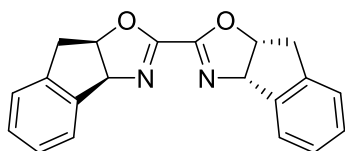
KOH solution (1.16 M, 7.2 mL, 8.4 mmol KOH, 2.3 equiv.), 65 °C (2.5 h). White powder (754 mg, 3.4 mmol, 92 % yield); R_f 0.47 (DCM/MeOH 50:1); ^1H NMR (400 MHz, CDCl_3) 4.44 (m, 2H), 4.16-4.07 (m, 4H), 1.86 (m, 2H, H3), 1.03 (d, $J = 6.6$ Hz, 6H, H4), 0.92 (d, $J = 6.6$ Hz, 6H, H4); ^{13}C NMR (100 MHz, CDCl_3) 154.7 (C5), 73.3, 71.2, 32.6 (C3), 19.1 (C4), 18.4 (C4); In agreement with the literature;²⁰⁶ IR $\nu_{\text{max}}/\text{cm}^{-1}$ 1617 (C=N).

(4*S*,4'*S*)-4,4'-di-*tert*-butyl-4,4',5,5'-tetrahydro-2,2'-bi-1,3-oxazole 103b



N,N'-bis[(2*S*)-1-chloro-3-methylbutan-2-yl]ethanediamide (1.96 g, 6 mmol, 1 equiv.) was dissolved in THF (94 mL) and to the resulting solution an ethanolic sodium hydroxide solution (0.41 M, 31 mL, 12.7 mmol, 2.1 equiv.) was added. Stirring for 20 min resulted in a cloudy solution forming, which was thereafter heated to 80 °C for 2.5 h. Analogous workup: water (50 mL), DCM (3×100 mL). White solid (1.22 g, 4.8 mmol, 80 % yield). R_f 0.37 (DCM/MeOH 100:1); ^1H NMR (400 MHz, CDCl_3) 4.36 (dd, $J = 10.1$, 8.5 Hz, 2H), 4.22 (t, $J = 8.9$ Hz, 2H), 4.06 (dd, $J = 10.5$, 9.3 Hz, 2H), 0.93 (s, 18H, H4); ^{13}C NMR (100 MHz, CDCl_3) 154.6 (C5), 76.8, 69.6, 33.8 (C3), 26.0 (C4); In agreement with the literature.³⁶⁶ HRMS (ESI+) calculated for $\text{C}_{14}\text{H}_{25}\text{N}_2\text{O}_2$ ($[\text{M}+\text{H}]^+$): 253.1916, found: 253.1914; IR $\nu_{\text{max}}/\text{cm}^{-1}$ 1620 (CN).

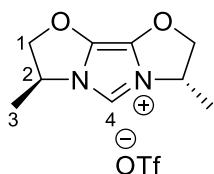
(3*aS*,3'*aS*,8*aR*,8'*aR*)-3*a*,3'*a*,8*a*,8'*a*-tetrahydro-8*H*,8'*H*-2,2'-biindeno[1,2-*d*]oxazole 104



Prepared analogously to: (4*S*,4'*S*)-4,4'-di-*tert*-butyl-4,4',5,5'-tetrahydro-2,2'-bi-1,3-oxazole using N^1, N^2 -bis((1*R*,2*R*)-2-chloro-2,3-dihydro-1*H*-inden-1-yl)oxalamide (700 mg, 1.8 mmol, 1 equiv.) and NaOH ethanolic solution (0.4 M, 16.9 mL, 6.75 mmol, 3.75 equiv.), 70 °C (40 min). The volatiles were removed on a rotary evaporator. The crude reaction mixture was purified by flash column

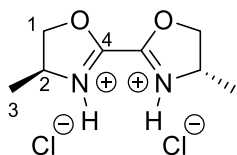
chromatography (~30 g silicagel, DCM:MeOH 50:1 to 10:1). Product was obtained as a light brown solid (506 mg, 1.6 mmol, 89% yield). m.p. (DCM) = 208 °C; $[\alpha]_D^{25} = 324.1$ (c = 1.54, DCM); $^1\text{H NMR}$ (400 MHz, CDCl_3) 7.52 (m, 2H), 7.25 (m, 6H), 5.75 (d, $J = 8.1$ Hz, 2H), 5.49 (m, 2H), 3.42 (m, 4H). $^{13}\text{C NMR}$ (100 MHz, CDCl_3) 155.3, 140.5, 139.6, 129, 127.6, 125.8, 125.4, 84.6, 77.2, 39.5; In agreement with the literature.²⁰⁴

(3*S*,7*S*)-3,7-dimethyl-2,3,7,8-tetrahydroimidazo[4,3-*b*:5,1-*b'*]bis[1,3]oxazol-4-ium triflate 99c



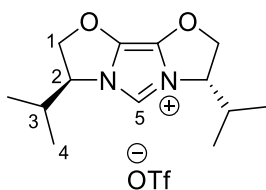
In a round-bottomed flask was weighed AgOTf (89 mg, 0.35 mmol, 1.45 equiv.). Under light free conditions DCM (0.86 mL) was added followed by chloromethylpivalate (0.05 mL, 0.35 mmol, 1.45 equiv.). This mixture was stirred at r.t. for 45 min after which the supernatant solution was taken with a syringe and transferred to a microwave vial containing (4*S*,4'*S*)-4,4'-dimethyl-4,4',5,5'-tetrahydro-2,2'-bi-1,3-oxazole (40mg, 0.24 mmol, 1 equiv.). After being sealed the reaction was stirred under light-free conditions at 40 °C for 20 h and then concentrated. The resulting residue was purified by flash column chromatography (DCM/MeOH 20:1) to yield the product as a hygroscopic brown oil (15 mg, 0.05 mmol, 19% yield). $^1\text{H NMR}$ (400 MHz, CD_3OD) 8.48 (s, 1H, H4), 5.22 (d, $J = 8.8, 7.2$ Hz, 2H), 4.99 (m, 2H), 4.7 (dd, $J = 8.8, 7.4$ Hz, 2H), 1.66 (d, $J = 6.9$ Hz, 6H, H3); $^{19}\text{F NMR}$ (376 MHz, CDCl_3) -78.5.

Protonated bisoxazoline 105



$^1\text{H NMR}$ (400 MHz, DMSO- d_6) 8.77 (d, $J = 9$ Hz, NH), 4.06 (m, 2H, H2), 3.67 (m, 4H, H1), 1.17 (d, $J = 6.7$ Hz, 6H, H3); $^{13}\text{C NMR}$ (100 MHz, DMSO- d_6) 159.4 (C4), 47.3 (C1), 46.8 (C2), 17.8 (C3).

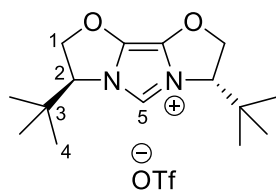
(3*S*,7*S*)-3,7-di(propan-2-yl)-2,3,7,8-tetrahydroimidazo[4,3-*b*:5,1-*b'*]bis[1,3]oxazol-4-ium triflate 99a



Silver triflate (1.22g, 4.75 mmol, 1.2 equiv.) was dried under high vacuum at 90 °C for 9 h in a reaction vial wrapped with aluminium foil. The vial was then rapidly sealed with a septum and placed under a nitrogen atmosphere. A solution of (4*S*,4'*S*)-4,4'-di-*iso*-propyl-4,4',5,5'-tetrahydro-2,2'-bi-1,3-oxazole (885 mg, 3.95 mmol, 1 equiv.) in DCM (13.4 mL) was added followed by chloromethylpivalate (0.8 mL, 5.6 mmol, 1.4 equiv.) and the reaction vial sealed. The reaction was stirred at 40 °C for 19 h with the exclusion of light before being concentrated on a rotary evaporator. The resulting residue was purified by flash column chromatography (125 mL silicagel, 30 mL fractions, DCM/acetone 3 : 1). The resulting compound after being dissolved almost completely in THF (5 mL) was crystallised by the successive addition of toluene (25 mL) and pentane (8 mL) to this solution. Removing the supernatant and drying yielded the compound as white, small crystals (860 mg, 2.2 mmol, 56% yield). $[\alpha]_D^{24} = 46.3$ ($c = 2.46$, DCM); reported value: $[\alpha]_D^{20} = 55$ ($c = 1$, DCM);¹⁹⁴ m.p. (THF/toluene/pentane) 112-116 °C; ¹H NMR (400 MHz, CDCl₃) 8.81 (s, 1H, H5), 5.07 (m, 2H), 4.93 (m, 2H), 4.84 (m, 2H), 2.36 (m, 2H, H3), 1.05 (d, $J = 7$ Hz, 6H, H4), 1.00 (d, $J = 7$ Hz, 6H, H4); ¹³C NMR (100 MHz, CD₃CN) 127, 115.3, 81, 64.9, 31.8 (C3), 17.5 (C4), 17.2 (C4); ¹⁹F NMR (300 MHz, CD₃CN) -79.3; In agreement with the literature;¹⁹⁴ HRMS (ESI+) calculated for C₁₃H₂₁N₂O₂ (M⁺ imidazolium cation): 237.1603, found: 237.1600; IR $\nu_{\max}/\text{cm}^{-1}$ 3112, 2969, 1731, 1532, 1480.

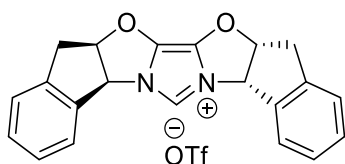
Note: These reactions are more conveniently carried out using ampoules equipped with Young's taps; this method was used for further scale up.

(3*S*,7*S*)-3,7-di-*tert*-butyl-2,3,7,8-tetrahydroimidazo[4,3-*b*:5,1-*b'*]bis[1,3]oxazol-4-ium triflate 99b



Prepared analogously to (3*S*,7*S*)-3,7-di(*propan*-2-yl)-2,3,7,8-tetrahydroimidazo[4,3-*b*:5,1-*b'*]bis[1,3]oxazol-4-ium triflate using silver triflate (1.22 g, 4.75 mmol, 1.2 equiv.), (4*S*,4'*S*)-4,4'-di-*tert*-butyl-4,4',5,5'-tetrahydro-2,2'-bi-1,3-oxazole (1 g, 3.95 mmol, 1 equiv.), DCM (13.4 mL), chloromethylpivalate (0.8 mL, 5.6 mmol, 1.4 equiv.) at 40 °C (19 h); flash column chromatography (200 mL silicagel, 50 mL fractions, DCM/acetone 6 : 1 and then polarity increased to 2 : 1 to collect remaining product). The resulting compound (approx. 1 g) was dissolved almost completely in THF (3 mL) and recrystallised by the successive addition of toluene (15 mL) and pentane (5 mL) to this solution; off-white small crystals (945 mg, 2.3 mmol, 58 % yield). m.p. (THF/toluene/pentane) 121-125 °C; Elemental analysis %C calculated: 46.37, found: 46.46; %H calculated: 6.08, found: 6.08; %N calculated: 6.76, found: 6.83; ¹H NMR (400 MHz, CDCl₃) 8.55 (s, 1H, H5), 5.06 (m, 2H), 4.91 (m, 2H), 4.84 (m, 2H), 1.06 (s, 18H, H4); ¹³C NMR (100 MHz, CDCl₃) 126, 120.8 (q), 117.2, 78.9, 68.3, 34.2 (C3), 25.5 (C4); ¹⁹F NMR (300 MHz, CDCl₃) -78.4; In agreement with literature;²⁰³ HRMS (ESI+) calculated for C₁₅H₂₅N₂O₂ (M⁺ imidazolium cation): 265.1916, found: 265.1909; IR ν_{max}/cm⁻¹ 3108, 2969, 1732, 1519, 1482.

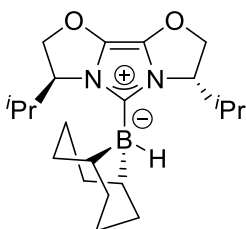
Imidazolium salt 100



Prepared analogously to: (3*S*,7*S*)-3,7-dimethyl-2,3,7,8-tetrahydroimidazo[4,3-*b*:5,1-*b'*]bis[1,3]oxazol-4-ium triflate using AgOTf (529 mg, 2.06 mmol, 1.45 equiv.), (3*aS*,3'*aS*,8*aR*,8'*aR*)-3*a*,3'*a*,8*a*,8'*a*-

tetrahydro-8H,8'H-2,2'-biindeno[1,2-d]oxazole (450mg, 1.42 mmol, 1 equiv.), DCM (~7 mL), chloromethylpivalate (0.3 mL, 2.06 mmol, 1.45 equiv.) at 40 °C (15 h). flash column chromatography (~29 g silicagel, DCM/MeOH 50:1) to give the product as a yellow solid (378 mg). Recrystallised from THF (1.5 mL) with toluene (6 mL) and pentane (6 mL) to give a crystalline off-white solid (301 mg, 0.63 mmol, 44% yield; after extensive drying it contains ~6% toluene). $[\alpha]_D^{25} = -145.1^\circ$ ($c = 2.9$, DCM); m.p. = 210-214 °C; $^1\text{H NMR}$ (400 MHz, CDCl_3) 9.45 (s, 1H), 7.83 (m, 2H), 7.33 (m, 6H), 6.34 (d, $J = 6.4$ Hz, 2H), 6.1 (m, 2H), 3.51 (m, 4H). $^{13}\text{C NMR}$ (100 MHz, CDCl_3) 139.8, 135, 130.9, 129, 126.1, 125.4, 120.8 (q, $J = 321.7$ Hz, CF_3), 114.4, 95.3, 67, 38.4. $^{19}\text{F NMR}$ (376 MHz, CDCl_3) -78.3 ; In agreement with the literature.²⁰³

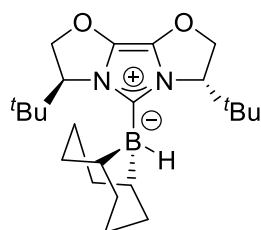
Borohydride **92a**



(3*S*,7*S*)-3,7-di(propan-2-yl)-2,3,7,8-tetrahydroimidazo[4,3-*b*:5,1-*b'*]bis[1,3]oxazol-4-ium triflate (1.15 g, 2.98 mmol, 1 equiv., pre-dried by heating to 90 °C under high vacuum) and 9-BBN dimer **23a** (364 mg, 1.49 mmol, 0.5 equiv.) were dissolved in THF (~40 mL) in an ampule. To the resulting solution was slowly added with vigorous stirring a solution of KHMDS (626 mg, 3.13 mmol, 1.05 equiv.) in THF (~20 mL) *via* double-ended needle. The solution turns orange and a crystalline precipitate is formed. The reaction was stirred at room temperature for 2 h. Solvent was removed under high vacuum to give a brown oil which partially crystallises. The residue was dissolved in toluene (~20 mL) and the resulting solution was decanted using a canula equipped with a glass microfibre filter. The resulting clear solution was concentrated to give a yellow solid (906 mg, 2.53 mmol, 85% yield). $^1\text{H NMR}$ (400 MHz, CD_2Cl_2) 4.72 (m, 4H), 4.49 (m, 2H), 2.55 (m, 2H), 1.84 (m, 5H), 1.67 (m, 5H), 1.52 (m, 3H), 1.38 (m, 1H), 0.97 (d, $J = 7.2$ Hz, 6H), 0.93 (br s, 1H, BH), 0.78 (d, $J = 7.2$ Hz, 6H); $^{13}\text{C NMR}$ (100 MHz, CD_2Cl_2) 124.1,

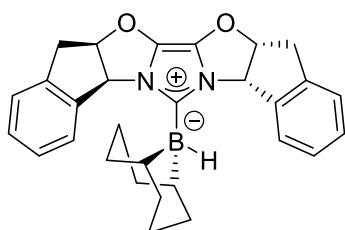
76.6, 62.7, 36.9, 36.2, 33.1, 32.8, 30.5, 26.1, 25.5, 19.3, 14.9; ^{11}B NMR (128 MHz, CD_2Cl_2) -17 (d, $J = 78$ Hz). NMR data is in agreement with reported values.¹⁹³

Borohydride **92b**



Prepared analogously using (3*S*,7*S*)-3,7-di-*tert*-butyl-2,3,7,8-tetrahydroimidazo[4,3-*b*:5,1-*b'*]bis[1,3]oxazol-4-ium triflate (200 mg, 0.48 mmol, 1 equiv.), 9-BBN dimer (59.6 mg, 0.24 mmol, 0.5 equiv.) solution in THF (3 mL), freshly prepared solution of KHMDS (102 mg, 0.5 mmol, 1.05 equiv.) in THF (3.6 mL); room temperature for 16 h. Filtration through a small Celite® plug using toluene (1.5 mL) afforded an almost colourless clear solution which was concentrated to give an off-white solid (157 mg, 0.41 mmol, 84% yield). This compound was washed twice with a mixture of toluene and pentane (1.2 mL, 1:5) to afford 100 mg of a white solid. ^1H NMR (400 MHz, CD_2Cl_2) 4.85 (d, $J = 9.3$ Hz, 2H), 4.64 (m, 2H), 4.52 (d, $J = 5.5$ Hz, 2H), 1.4-2.07 (m, 14H), 1.07 (s, 18H), 0.60 (br s, 1H, BH); ^{13}C NMR (100 MHz, CD_2Cl_2) 124.5, 79.5, 68.8, 39.2, 35.5, 34.9, 32.6, 32, 27.9, 26.1, 25.4; ^{11}B NMR (128 MHz, CD_2Cl_2) -16.8 (d, $J = 84$ Hz); In agreement with the literature.²¹²

Borohydride **93a**



Prepared analogously using **100** (106 mg, 0.208 mmol, 1 equiv.), 9-BBN dimer (25.4 mg, 0.104 mmol, 0.5 equiv.), KHMDS (43.8 mg, 0.219 mmol, 1.05 equiv.), THF (4 mL); room temperature (3 h); Crude was extracted with benzene (5 mL) and filtered through Celite®. The brown solution was concentrated

to give a green solid (44 mg, ~0.01 mmol, ~47% yield, impure); ^1H NMR (400 MHz, C_6D_6) 8.23 (m, 2H), (7.12, 7, 6.8, m, 21H), 5.51 (m, ~1H), 4.49 (m, ~2H), 3.1-0.97 (48H); ^{13}C NMR (100 MHz, C_6D_6) 140.6, 137.9, 129.7, 128.6, 125.2, 124.1, 94.7, 66.8, 37.3, 36.3, 36.3, 34.4, 33.5, 26.6, 26.6; ^{11}B NMR (128 MHz, C_6D_6) -16.2 (br d).

5.1.3 Attempted formation of **108** and coupling of **110**

99b (50 mg, 0.12 mmol, 1 equiv., pre-dried) and KHMDS (26 mg, 0.13 mmol, 1.08 equiv.) were reacted in THF (0.9 mL) for 10 min. Next a solution of CatBH (0.16 M, prepared by dilution of a commercial solution, 0.75 mL, 0.12 mmol, 1 equiv.) was added leading to the solution becoming cloudy. After 16 h the solvent was removed under high vacuum. The residue was extracted with toluene (2×1 mL) and filtered through Celite® to give a clear yellow solution.

Imidazolium salt **111** (20.7 mg, 0.038 mmol, 1 equiv.) and 9-BBN dimer (4.6 mg, 0.019 mmol, 0.5 equiv.) were weighed into a Young's tap NMR tube and dissolved in THF (0.3 mL). A KHMDS (7.5 mg, 0.038 mmol, 1 equiv.) solution in THF (0.7 mL) was added leading to formation of a pale brown solution and a crystalline precipitate. The solvent was removed under high vacuum after NMR analysis was carried out; the residue was extracted with toluene (~1 mL) and filtered through Celite® to give a clear solution.

5.1.4 Additional characterisation for **95a**

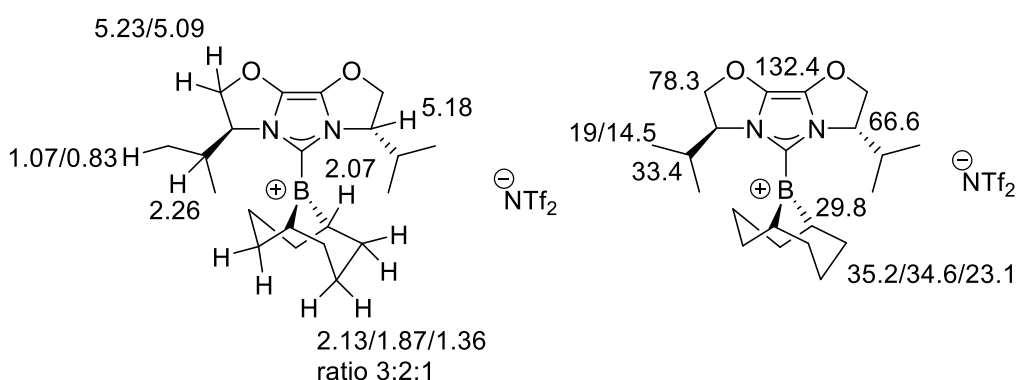


Figure 5.1 ^1H and ^{13}C NMR assignment for catalyst **95a**.

5.1.5 Additional substrates tested

The following general procedures have been adapted from reference 165 with permission from the Royal Society of Chemistry.

General procedure for hydrosilylation:

A solution containing the substrate (0.375 mmol, 1 equiv.) and catalyst (0.015 mmol, 0.04 equiv) was prepared using the indicated solvent (0.6 mL). The reaction was initiated by hydrosilane addition using a microsyringe (0.41 mmol, 1.1 equiv.). The reaction was sealed (either in a Young's tap NMR tube or glass vial), mixed, and allowed to proceed at room temperature. The reaction was quenched with methanol and purified by flash column chromatography (10-15 g silicagel) or preparative TLC (20x20 cm, 0.2 cm).

General procedure for hydrogenation:

A solution containing the substrate (0.375 mmol, 1 equiv.) and catalyst (0.038 mmol, 0.1 equiv) was prepared using the indicated solvent (0.6 mL) in a HPLC vial. Hydrogenation was carried out in a Symyx SPR system using a 48-well plate at 101 bar H₂, 30 °C, and with agitation provided by circular motion (500 rpm). Alternatively, the reaction was carried out in a Wilmad high pressure NMR tube (10 bar H₂, room temperature). Purification was carried out by flash column chromatography (I.D ~2.5 cm, ~10.15 g silicagel) or by preparative TLC (20x20 cm, 0.2 cm).

General procedure for the synthesis of *N*-alkyl ketimines:

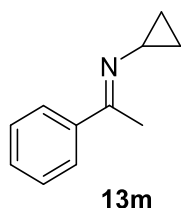
To a stirred solution of acetophenone (3.5 mL, 30 mmol, 1 equiv.) in pentane (500 mL) was added the amine (150 mmol, 5 equiv.) resulting in formation of a cloudy solution. Next was added TiCl₄ (1.65 mL, 15 mmol, 0.5 equiv.) which lead to the formation of a voluminous, coloured precipitate. The reaction was stirred at room temperature and monitored by collection of aliquots for NMR analysis. The reaction was filtered and the volatiles removed under low or high vacuum. The resulting oils were stored over activated 3 or 4 Å molecular sieves.

General procedure for the synthesis of racemic amines:

Ketimine (100 mg, x mmol) and sodium borohydride (y mg, 2x mmol) were combined and next methanol (generally 1 mL) was added. The reaction was stirred at room temperature for the specified amount of time. The solvent was removed and the resulting residue was extracted, generally with DCM. The organics were concentrated and the resulting crude product was purified by flash column chromatography (10-15 g silicagel).

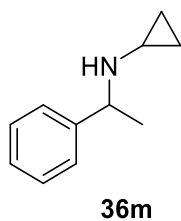
General procedure for the synthesis of *N*-acetyl derivatives

To a solution of amine (< 30 mg) in DCM (<1 mL) was added Et₃N (2 equiv., approximate volume) and then acetic anhydride (4 equiv., approximate volume). The reaction was allowed to take place at room temperature for the indicated period of time. The volatiles were removed and the resulting residue was purified by flash column chromatography (~1-2 g silicagel).



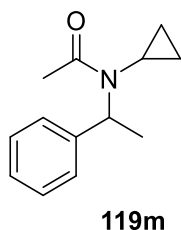
Prepared according to the standard procedure for *N*-alkyl ketimine synthesis (22 h reaction time, 96% yield, pale yellow clear oil).

d.r. = 18.6: 1; ¹H NMR (400 MHz, CDCl₃) 7.74 (m, 2H), 7.37 (m, 3H), 3.13 (m, 1H), 2.38 (s, 3H), 0.96 (m, 4H); ¹³C NMR (100 MHz, CDCl₃) major isomer: 163.7, 141.5, 129.1, 128.3, 126.4, 34.2, 16, 9.1; In agreement with the literature,³⁶⁷ HRMS (ESI+) calculated for C₁₁H₁₄N ([M+H]⁺) 160.1126, found 160.1126; IR (neat, cm⁻¹) 3084, 3055, 3004, 1626, 1445, 1359, 1280, 1025, 1016, 919, 758, 742, 691, 571.



A racemic sample was prepared according to the standard procedure. Purification using pentane/EtOAc (10:1 to 4:1, +1% Et₃N) to give a colourless oil (69% yield).

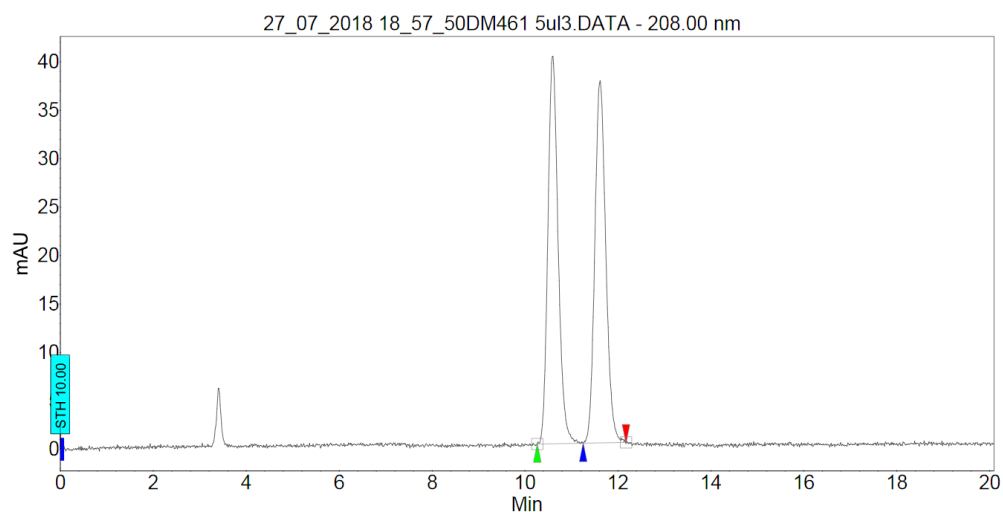
From the standard hydrosilylation procedure (carried out in a vial) the product was obtained following preparative TLC purification as a clear yellow oil (37.9 mg, 0.235 mmol, 63% yield). $[\alpha]_D^{25} = 0^\circ$ (c 1.74, CH₂Cl₂, 52:48 e.r.); ¹H NMR (400 MHz, CDCl₃) 7.33 (m, 4H), 7.24 (m, 1H), 3.86 (q, *J* = 6.8 Hz, 1H), 1.97 (m, 1H), 1.75 (br s, 1H), 1.37 (d, *J* = 6.8 Hz, 3H), 0.35 (m, 4H); ¹³C NMR (100 MHz, CDCl₃) 146.2, 128.5, 126.9, 126.8, 58.6, 29.1, 23.8, 6.6; In agreement with the literature;³⁶⁸ HRMS (ESI+) calculated for C₁₁H₁₆N ([M+H]⁺) 162.1283, found 162.1289; IR (neat, cm⁻¹) 3023, 3004, 2960, 2925, 1492, 1451, 1367, 1014, 759, 697.



A racemic sample was obtained following the standard acetylation procedure. Purification by flash column chromatography (pentane/EtOAc 1:1) to give a pale-yellow oil (96% yield).

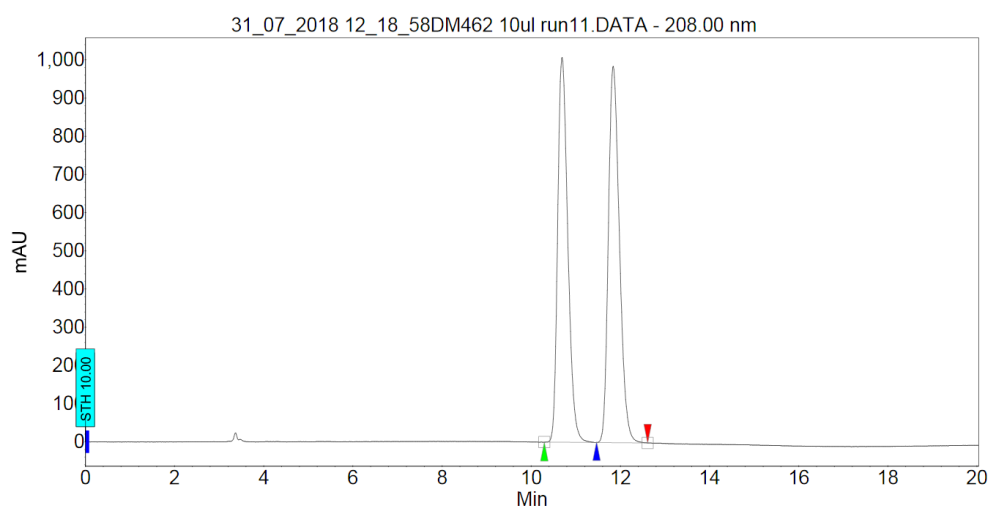
$[\alpha]_D^{25} = 0^\circ$ (c 0.47, CH₂Cl₂, 52:48 e.r.); ¹H NMR (400 MHz, CDCl₃) 7.26 (m, 5H), 5.79 (m, br, 1H), 2.48 (m, 1H), 2.3 (s, 3H), 1.67 (d, *J* = 7.2 Hz, 3H), 0.72 (m, 1H), 0.62 (m, 2H), 0.46 (m, 1H); ¹³C NMR (100 MHz, CDCl₃) 174.1, 143, 128.3, 126.8, 52.7, 29.8, 28.6, 23.4, 17.2, 9.4, 7.4; HRMS (ESI+) calculated for C₁₃H₁₈NO ([M+H]⁺) 204.1388, found 204.1381; IR (neat, cm⁻¹) 2978, 2936, 1647, 1448, 1388, 1314, 1030, 753, 701.

HPLC: Chiralcel OD-H, IPA/hexane 5:95, 1 ml/min, 208 nm detection, *t* = 10.6 min, *t* = 11.6 min.



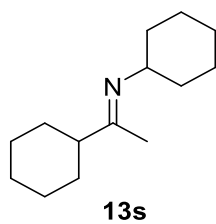
Peak results :

Index	Name	Time [Min]	Quantity [% Area]	Height [mAU]	Area [mAU.Min]	Area % [%]
1	UNKNOWN	10.586	50.03	40.0	10.2	50.034
2	UNKNOWN	11.612	49.97	37.4	10.2	49.966
Total			100.00	77.4	20.4	100.000

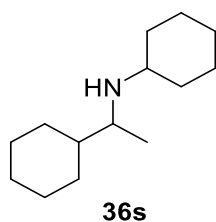


Peak results :

Index	Name	Time [Min]	Quantity [% Area]	Height [mAU]	Area [mAU.Min]	Area % [%]
1	UNKNOWN	10.693	48.37	1007.6	265.3	48.365
2	UNKNOWN	11.839	51.63	985.2	283.2	51.635
Total			100.00	1992.7	548.5	100.000

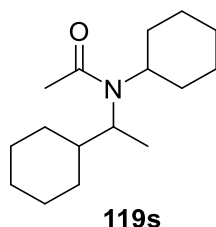


Prepared according to the standard procedure for *N*-alkyl ketimine synthesis. (7 h reaction time, 73% yield, pale-yellow clear oil). dr = 16.7: 1; ^1H NMR (400 MHz, CDCl_3) 3.2 (m, 1H), 2.14 (m, 1H), 1.73 (s), 1.8-1.12 (m, 24H); ^{13}C NMR (100 MHz, CDCl_3) 170.9, 58.9, 51.2, 33.8, 30.4, 26.3, 25.9, 25.2, 14; In agreement with the literature.³⁶⁹ HRMS (ESI+) calculated for $\text{C}_{14}\text{H}_{26}\text{N}$ ($[\text{M}+\text{H}]^+$) 208.2065, found 208.2065; IR (neat, cm^{-1}) 2921, 2850, 1653, 1447, 1370, 1359, 1347, 889, 842.



A racemic sample was prepared according to the standard procedure. Purification by flash column chromatography using pentane/EtOAc (4:1, +1% Et_3N) to give a colourless oil (91% yield).

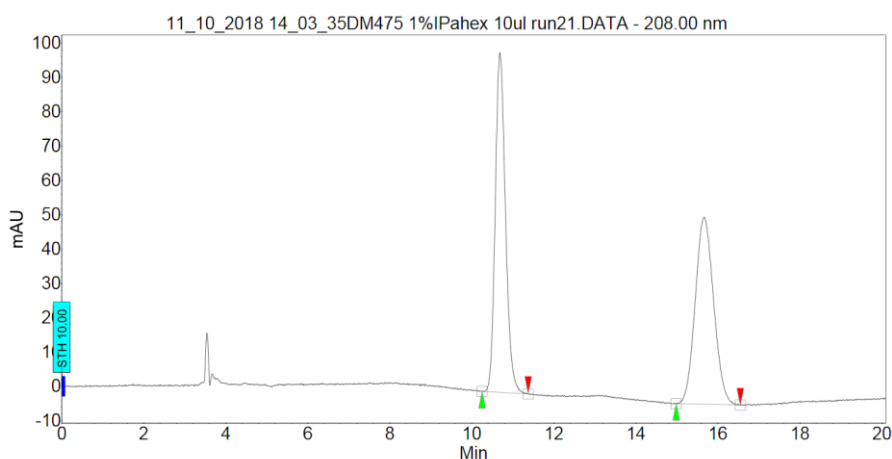
The compound was obtained from the standard hydrogenation procedure (screening method). The crude reaction mixture was concentrated and then extracted with pentane twice. The extract was filtered and concentrated to give a clear colourless oil (51 mg, 0.24 mmol, 65% yield). ^1H NMR (400 MHz, CDCl_3) 2.54 (m, 1H), 2.44 (m, 1H), 1.83 (m, 2H), 1.67 (m, 8H), 1.32-0.9 (m, 14H), 0.95 (d, $J = 6.4$ Hz); ^{13}C NMR (100 MHz, CDCl_3) 54.2, 54.1, 43.3, 34.8, 34, 30.3, 28.1, 27, 26.9, 26.7, 26.4, 25.5, 25.4, 17.8; In agreement with the literature;³⁶⁹ HRMS (ESI+) calculated $\text{C}_{14}\text{H}_{28}\text{N}$ ($[\text{M}+\text{H}]^+$) 210.2222, found 210.2226; IR (neat, cm^{-1}) 2919, 2849, 1447, 1372, 1259, 1098, 888, 800, 711.



A racemic sample was obtained following the standard acetylation procedure. Purification by flash column chromatography (pentane/EtOAc 9:1) to give a colourless oil (74% yield).

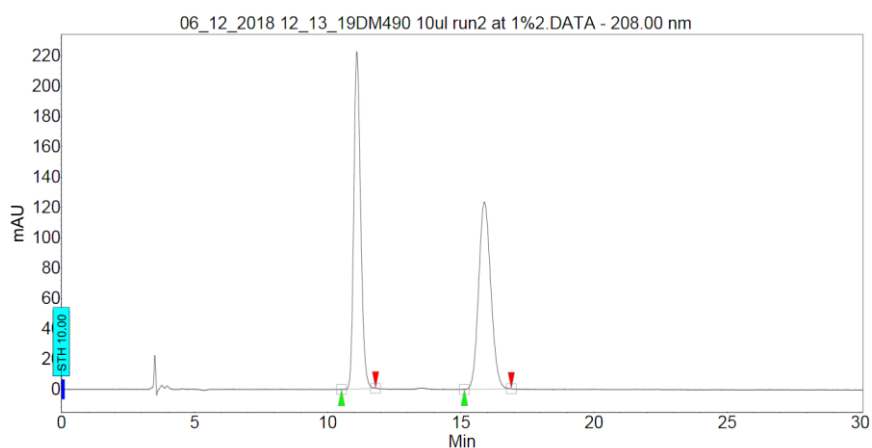
¹H NMR (400 MHz, CDCl₃) unresolved 3.41 (m, 1H), 2.86-2.46 (m, 2H), 2.09 (m, 3H), 1.92-0.66 (m, 25H), 1.18 (d, J = 7.3 Hz); ¹³C NMR (100 MHz, CDCl₃) unresolved 170.5, 169.9, 60.4, 56.1, 41, 40.2, 32.2, 31.5, 31.3, 30.2, 29.6, 26.9, 26.7, 26.6, 26.4, 26.3 (x2), 26.2, 26, 25.5, 25.3, 24.3, 23.8, 20.9, 17.8, 16.7; HRMS (ESI+) calculated for C₁₆H₃₀NO ([M+H]⁺) 252.2327, found 252.2334; IR (neat, cm⁻¹) 2920, 2849, 1635, 1429, 1367, 1308, 1302, 1192, 1137, 997, 892.

HPLC: Chiralcel OD-H, IPA/hexane 1:99, 1 ml/min, 208 nm detection, t = 11.1 min, t = 15.9 min.



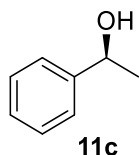
Peak results :

Index	Name	Time [Min]	Quantity [% Area]	Height [mAU]	Area [mAU.Min]	Area % [%]
1	UNKNOWN	10.679	50.25	98.9	28.6	50.250
2	UNKNOWN	15.666	49.75	54.6	28.3	49.750
Total			100.00	153.5	56.9	100.000



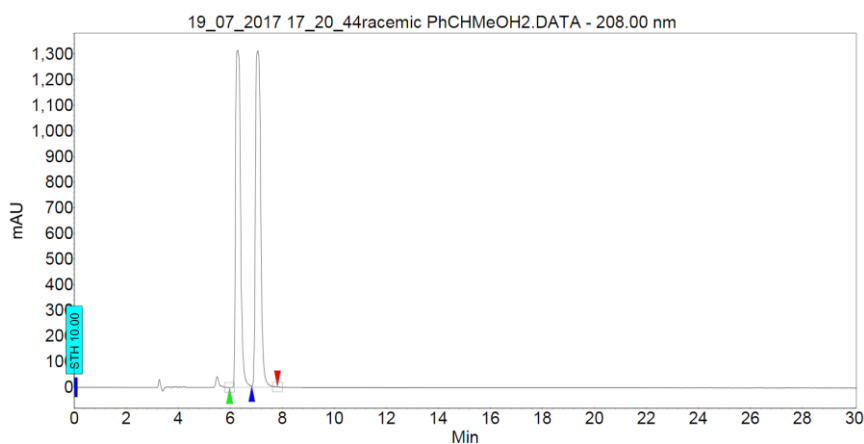
Peak results :

Index	Name	Time [Min]	Quantity [% Area]	Height [mAU]	Area [mAU.Min]	Area % [%]
1	UNKNOWN	11.093	50.46	222.4	66.5	50.456
2	UNKNOWN	15.879	49.54	123.3	65.3	49.544
Total			100.00	345.7	131.8	100.000



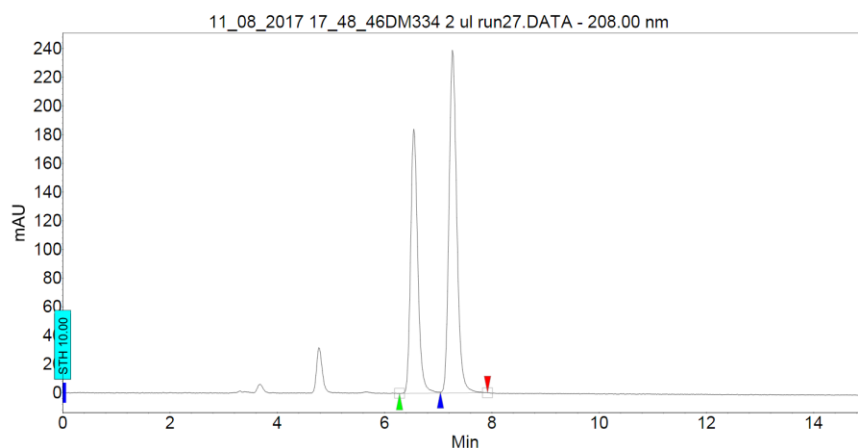
Workup of a typical hydrosilylation reaction (0.375 mmol acetophenone) was carried out using a methanolic TBAF solution. The crude product was purified by flash column chromatography (pentane/DCM 1:4) to give the product as a pale-yellow oil (20 mg, 0.16 mmol, 44% yield). $[\alpha]_D^{24} = -20.9^\circ$ ($c = 0.19$, CHCl_3 , 58.5:41.5 e.r.), reported: $[\alpha]_D^{20} = -48^\circ$ ($c = 0.17$, CHCl_3 , 96.5:3.5 e.r.); ^{125}H NMR (400 MHz, CDCl_3) 7.37 (m, 4H), 7.28 (m, 1H), 4.9 (q, $J = 6.3$ Hz, 1H), 1.92 (br s, 1H), 1.5 (d, $J = 6.4$ Hz, 3H); ^{13}C NMR (100 MHz, CDCl_3) 145.9, 128.6, 127.6, 125.5, 70.6, 25.3.

HPLC: Chiralcel OD-H, IPA/hexane 10:90, 1 ml/min, 208 nm detection, $t_R = 6.5$ min, $t_S = 7.3$ min.



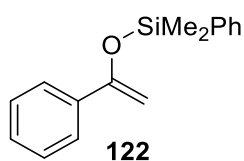
Peak results :

Index	Name	Time [Min]	Quantity [% Area]	Height [mAU]	Area [mAU Min]	Area % [%]
1	UNKNOWN	6.293	48.81	1315.4	292.3	48.812
2	UNKNOWN	7.066	51.19	1311.7	306.5	51.188
Total			100.00	2627.1	598.9	100.000

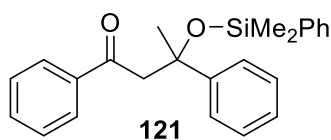


Peak results :

Index	Name	Time [Min]	Quantity [% Area]	Height [mAU]	Area [mAU.Min]	Area % [%]
1	UNKNOWN	6.547	41.48	184.2	28.6	41.483
2	UNKNOWN	7.267	58.52	239.0	40.4	58.517
Total			100.00	423.2	69.0	100.000

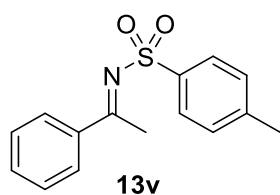


Prepared according to a literature procedure from acetophenone (2.9 mL, 25 mmol, 1 equiv.).³⁷⁰ Purification by distillation (115 °C at 0.1 mbar) afforded the product as a clear colourless oil (1.3g, 5.19 mmol, 21% yield, ~90% purity with (PhMe₂Si)₂O). ¹H NMR (400 MHz, CDCl₃) 7.72 (m, 4H), 7.42 (m, 6H), 4.97 (d, *J* = 1.3 Hz, 1H), 4.45 (d, *J* = 1.3 Hz, 1H), 0.61 (s, 6H); ²⁹Si {¹H} NMR 8.1 (s); ¹³C NMR (100 MHz, CDCl₃) 155.6, 137.5, 137.4, 133.6, 130, 128.4, 128.2, 128.1, 125.4, 91.6, -1.1. In agreement with reported.

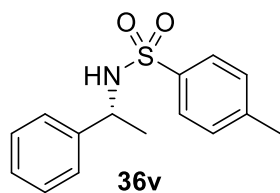


Workup of a typical hydrosilylation reaction (0.375 mmol acetophenone) was carried out using an aqueous TBAF solution followed by extraction with DCM. The crude product was purified by flash column chromatography (pentane/EtOAc 10:1) to give the product as an oil (~4% yield). ¹H NMR (400 MHz, CDCl₃) 7.9 (d, *J* = 8.2 Hz, 2H), 7.49 (m, 3H), 7.3 (m, 11H), 3.59 (d, *J* = 13.4 Hz, 1H), 3.1 (d, *J* = 13.6

Hz, 1H), 1.8 (s, 3H), 0.16 (2 s, 6H); ^{13}C NMR (100 MHz, CDCl_3) 198.8, 148, 139.5, 138.4, 133.4, 132.8, 129.3, 129.1, 128.3, 128.2, 127.8, 127.1, 125.4, 54.2, 27.8, 0.8.

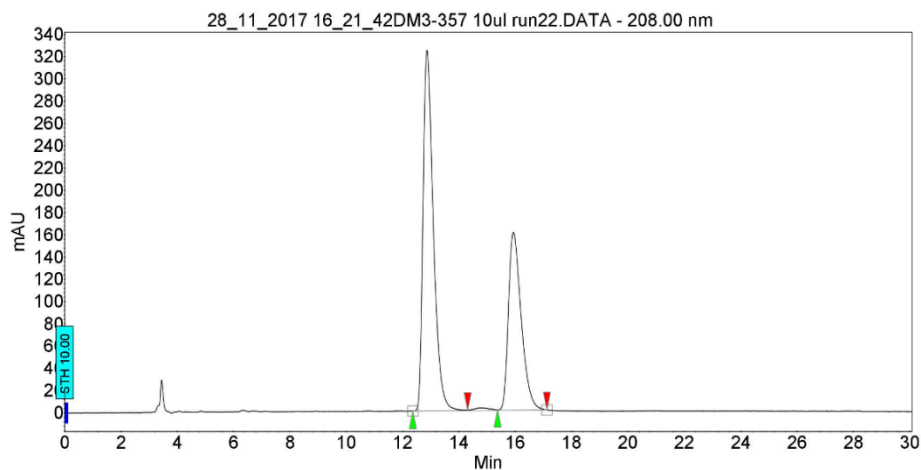


Prepared according to a literature procedure from acetophenone (3.5 mL, 30 mmol, 1 equiv.).³⁷¹ Purification was carried out by flash column chromatography (~400 mL silicagel, pentane/EtOAc 10:1 to 5:1, to give an oily solid) followed by trituration with pentane (4×7 mL) to give the product as a white crystalline solid (532 mg, 1.95 mmol, 6.5% yield). ^1H NMR (400 MHz, CDCl_3) 7.91 (m, 4H), 7.53 (m, 1H), 7.37 (m, 4H), 2.99 (s, 3H), 2.44 (s, 3H); ^{13}C NMR (100 MHz, CDCl_3) 179.9, 143.6, 138.8, 137.6, 133.3, 129.6, 128.7, 128.4, 127.2, 21.7, 21.3. Data in agreement with the literature.³⁷²



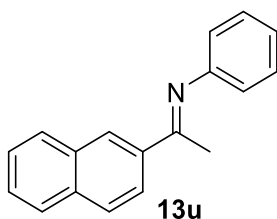
Prepared using the typical hydrosilylation procedure carried out in a Young's tap NMR tube. Purification was carried out by flash column chromatography (9×3 cm, pentane/EtOAc 13:1 to 5:1) to give the product as a clear colourless oil (24.7 mg, 0.09 mmol, 24% yield). Evaporation from chloroform gives a white solid. ^1H NMR (400 MHz, CDCl_3) 7.61 (m, 2H), 7.2 (m, 5H), 7.09 (m, 2H), 4.66 (d, J = 6.4 Hz, 1H), 4.46 (quintet, J = 6.8 Hz, 1H), 2.39 (s, 3H), 1.43 (d, J = 7 Hz, 3H); ^{13}C NMR (100 MHz, CDCl_3) 143.6, 142.4, 138, 129.9, 129, 128, 127.6, 126.6, 54.1, 24, 22.

HPLC: Chiralcel OD-H, IPA/hexane 10:90, 1 ml/min, 208 nm detection, t_R = 12.9 min, t_S = 15.9 min. Enantiomer assignment was carried out by comparison of HPLC traces with the literature (identical column).³⁷³



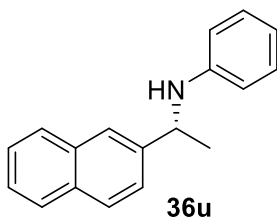
Peak results :

Index	Name	Time [Min]	Quantity [% Area]	Height [mAU]	Area [mAU.Min]	Area % [%]
1	UNKNOWN	12.866	62.07	323.8	137.0	62.073
2	UNKNOWN	15.932	37.93	159.7	83.7	37.927
Total			100.00	483.5	220.7	100.000



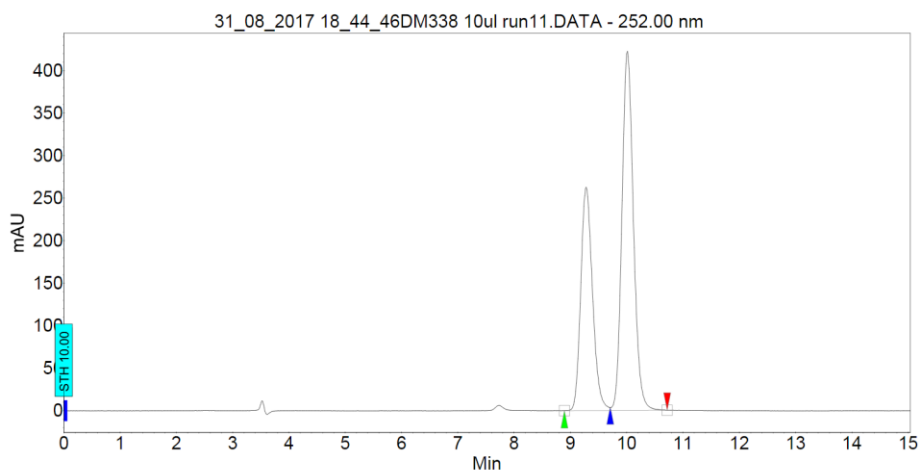
Prepared according to a literature procedure from 2-acetonaphthone (5.17 g, 30.4 mmol, 1 equiv.).

³⁷⁴ Purification was carried out by trituration with pentane (2×~10 mL) to give the product as a yellow powder (1.49 g, 6.08 mmol, 20% yield). ¹H NMR (400 MHz, CDCl₃) 8.36 (s, 1H), 8.24 (d, *J* = 8.5 Hz, 2H), 7.92 (m, 3H), 7.54 (m, 2H), 7.38 (t, *J* = 7.7 Hz, 2H), 7.12 (t, *J* = 7.5 Hz, 1H), 6.86 (d, *J* = 7.7 Hz, 2H), 2.37 (s, 3H). ¹³C NMR (100 MHz, CDCl₃) 165.4, 151.9, 137, 134.6, 133.1, 129.1, 129.1, 128.1, 127.8, 127.8, 127.3, 126.5, 124.4, 123.4, 119.6, 17.5. In agreement with reported.



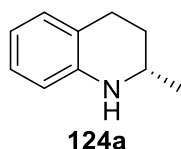
Prepared using the standard hydrosilylation procedure carried out in a Young's tap NMR tube. Purification carried out by flash column chromatography (pentane/EtOAc 100:1) to give the product as an almost colourless oil (58 mg, 0.23 mmol, 63% yield). ^1H NMR (400 MHz, CDCl_3) 7.81 (m, 4H), 7.51 (d, $J = 8.8$ Hz, 1H), 7.45 (m, 2H), 7.08 (t, $J = 7.9$ Hz, 2H), 6.64 (t, $J = 7.3$ Hz, 1H), 6.56 (d, $J = 8.2$ Hz, 2H), 4.65 (q, $J = 6.8$ Hz, 1H), 4.13 (br s, 1H), 1.6 (d, $J = 6.7$ Hz, 3H). ^{13}C NMR (100 MHz, CDCl_3) 147.4, 142.9, 133.7, 132.9, 129.3, 128.6, 128, 127.8, 126.1, 125.6, 124.5, 124.4, 117.4, 113.5, 53.9, 25.2.

HPLC: Chiralcel OD-H, IPA/hexane 10:90, 1 ml/min, 252 nm detection, $t_s = 9.3$ min, $t_R = 10$ min. Enantiomer assignment was carried out by comparison of HPLC traces with the literature (identical column).³⁷⁵



Peak results :

Index	Name	Time [Min]	Quantity [% Area]	Height [mAU]	Area [mAU.Min]	Area % [%]
1	UNKNOWN	9.280	38.76	262.6	63.3	38.760
2	UNKNOWN	10.013	61.24	422.4	100.0	61.240
Total			100.00	685.0	163.4	100.000

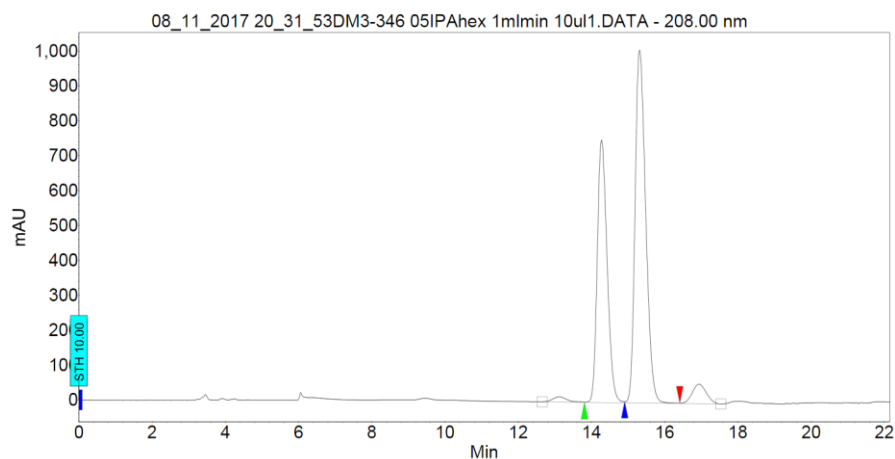


Carried out using the standard hydrosilylation procedure, carried out in a Young's tap NMR tube, reaction temperature was 50 °C. Purified by flash column chromatography (~ 50 mL silicagel, pentane/EtOAc 20:1) to give the product as an oil (1.8 mg, 0.012 mmol, 3% yield). ^1H NMR (400 MHz,

CDCl₃) 6.96 (m, 2H), 6.6 (td, *J* = 7.4, 1 Hz, 1H), 6.47 (dd, *J* = 8.4, 1.1 Hz), 3.69 (br s, 1H), 3.4 (m, 1H), 2.9-2.68 (m, 2H), 1.93 (m, 1H), 1.59 (m, 1H), 1.21 (d, *J* = 5.9 Hz).

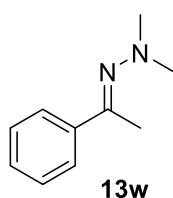
HPLC: Chiralcel OD-H, IPA/hexane 0.5:99.5, 1 ml/min, 208 nm detection, *t_R* = 14.3 min, *t_S* = 15.3 min.

Enantiomer assignment was carried out by comparison of HPLC traces with the literature (identical column).²⁹²



Peak results :

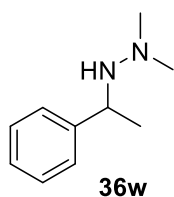
Index	Name	Time [Min]	Quantity [% Area]	Height [mAU]	Area [mAU.Min]	Area % [%]
1	UNKNOWN	14.279	40.76	752.1	234.0	40.758
2	UNKNOWN	15.306	59.24	1010.6	340.1	59.242
Total			100.00	1762.6	574.1	100.000



Prepared according to the standard procedure for *N*-alkyl ketimine synthesis using Et₃N as auxiliary base (4 equiv.); scale: 6 mmol acetophenone; 53 h. Purification was carried out by distillation: acetophenone was removed slowly at 30 °C (5 mbar); then the product was distilled rapidly at 100 °C with the receiving flask cooled in dry ice. Clear yellow oil (575 mg, 3.55 mmol, 59% yield).

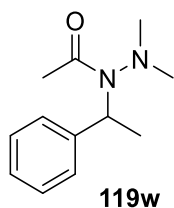
d.r. = 14.6:1; ¹H NMR (400 MHz, CDCl₃) 7.74 (m, 2H), 7.36 (m, 3H), 2.61 (s, 6H), 2.36 (s, 3H); ¹³C NMR (100 MHz, CDCl₃) 162.2, 139.2, 129.3, 128.4, 126.5, 47.4, 15.7; In agreement with the literature;³⁷⁶ HRMS (ESI+) calculated for C₁₀H₁₅N₂ ([M+H]⁺) 163.1235, found 163.1227; IR (neat, cm⁻¹) 2985, 2951,

2892, 2852, 2816, 2771, 1685, 1607, 1571, 1465, 1444, 1359, 1299, 1264, 1202, 1021, 1003, 947, 758, 691, 635, 562.



A racemic sample was obtained following the standard procedure; purification using pentane/EtOAc with 1% Et₃N to give a yellow oil (33 mg, 0.2 mmol, 33% yield). Although exposure to air caused degradation of this material satisfactory characterisation could be obtained.

Sample obtained following the standard hydrosilylation procedure. Purification by preparative TLC to give the product as a yellow oil (56 mg, 0.34 mmol, 91% yield). $[\alpha]_D^{25} = +4.3^\circ$ (c = 5.1, CDCl₃). ¹H NMR (400 MHz, CDCl₃) 7.28 (m, 8H), 4.03 (q, J = 6.5 Hz, 1H), 3.79 (br s, 2H), 2.45 (s, 6H), 1.31 (d, J = 6.8 Hz, 3H); ¹³C NMR (100 MHz, CDCl₃) 145.2, 128.5, 127.1, 126.8, 57.1, 48.1, 22.7. HRMS (ESI+) calculated for C₁₀H₁₅N₂ ([M+H]⁺) 163.1235, found 163.1235. IR (neat, cm⁻¹) 2926, 2852, 2806, 1670, 1492 1472, 1451, 1361, 1018, 890, 775, 758, 690.

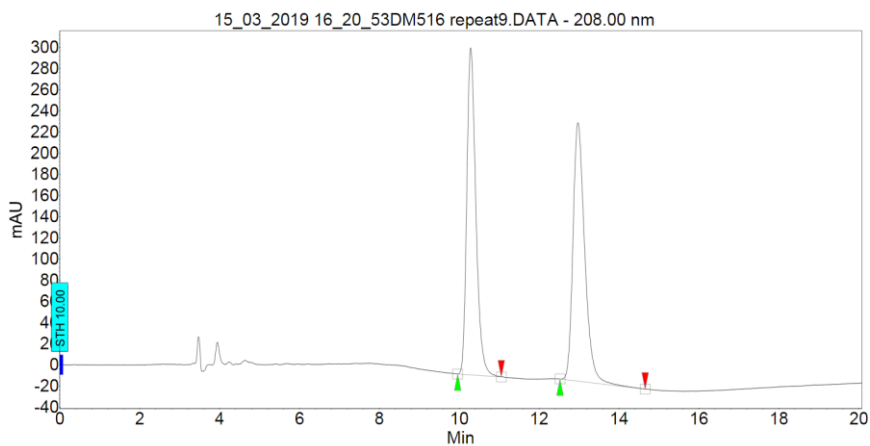


A racemic sample was obtained following the standard acetylation procedure. Purification: pentane/EtOAc 10:1 to 4:1 to give a clear colourless oil (4.5 mg, 0.02 mmol, 18% yield).

$[\alpha]_D^{24} = +7.3^\circ$ (c = 0.27, CDCl₃); ¹H NMR (400 MHz, CDCl₃) unresolved 7.4 (m, 1H), 7.31 (m, 3H), 7.21 (m, 1H), 4.86 (q, J = 7 Hz, 1H), 2.9-2.49 (3 singlets, 5H), 2.35-2.11 (4 singlets, 4H), 1.77 (d, J = 7.3 Hz, 2H), 1.62 (d, J = 7.1 Hz, 1H); ¹³C NMR (100 MHz, CDCl₃) 173.4, 142.2, 128.4, 128.2, 127.9, 127.6, 126.9, 58.9, 51.9, 44.8, 44.3, 24.1, 23.1, 19.2, 17.8; HRMS (ESI+) calculated for C₁₂H₁₉N₂O ([M+H]⁺) 207.1497,

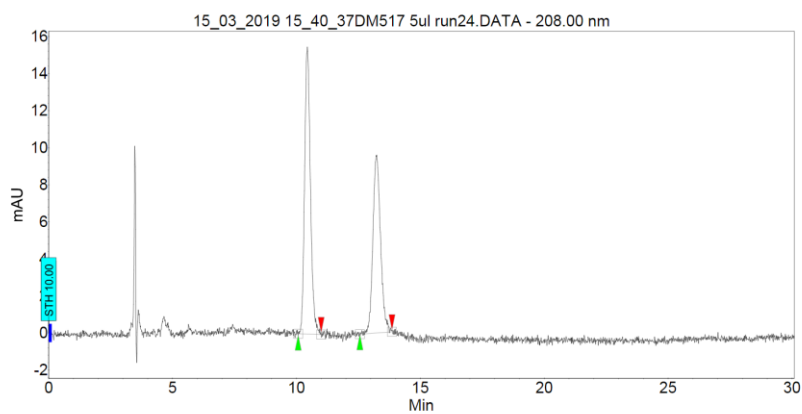
found 207.1497. IR (neat, cm^{-1}) 2942, 2979, 2885, 1657, 1452, 1443, 1413, 1393, 1369, 1360, 1027, 699.

HPLC: Chiralcel OD-H, IPA/hexane 5:95, 1 ml/min, 208 nm detection, t = 10.4 min, t = 13.2 min.



Peak results :

Index	Name	Time [Min]	Quantity [% Area]	Height [mAU]	Area [mAU.Min]	Area % [%]
1	UNKNOWN	10.279	49.33	308.8	81.0	49.328
2	UNKNOWN	12.972	50.67	244.2	83.2	50.672
Total			100.00	553.0	164.2	100.000



Peak results :

Index	Name	Time [Min]	Quantity [% Area]	Height [mAU]	Area [mAU.Min]	Area % [%]
1	UNKNOWN	10.439	55.12	15.5	4.2	55.122
2	UNKNOWN	13.226	44.88	9.5	3.4	44.878
Total			100.00	25.0	7.7	100.000

5.2 Experimental data concerning Chapter 3

5.2.1 General considerations relevant to Chapter 3

Assignment of NMR signals and coupling interactions was carried out through analogy with known compounds and by considering that ${}^3J({}^{119}\text{Sn}-{}^{13}\text{C}) > {}^2J({}^{119}\text{Sn}-{}^{13}\text{C})$.³⁰⁸

5.2.2 (–)-MenCl **170**

(–)-Menthol (50g, 320 mmol, 1 equiv.) was dissolved in 250 mL DCM. The resulting solution was cooled in an ice bath and, with stirring, SOCl_2 (35 mL, 480 mmol, 1.5 equiv.) was added. After one hour TiCl_4 (3.5 mL, 32 mmol, 0.1 equiv.) was added and the reaction stirred for a further 30 min before being quenched with water (300 mL). The aqueous phase was separated, extracted with DCM (2×200 mL) and the combined organic phases were washed with H_2O (2×300 mL) and dried on MgSO_4 for 2 days. Solvent removal yielded a black oil. The crude product was purified by distillation (58 °C at 1 mbar) to afford an almost colourless oil (46.6g, 83% yield). $[\alpha]_D^{26} = -43.4^\circ$ (neat); reported: $[\alpha]_D^{20} = -49.6^\circ$ ($c = 8.38$, EtOH).²⁷⁴ ${}^1\text{H}$ NMR (CDCl_3 , 400 MHz) 3.78 (m, 1H), 2.34 (m, 1H), 2.23 (m, 1H), 1.71 (2H, m), 1.43-1.33 (m, 3H), 1.09-0.86 (m, 3H), 0.92 (d, $J = 7.4$ Hz, 6H), 0.77 (d, $J = 7.3$ Hz, 3H). ${}^{13}\text{C}$ NMR (CDCl_3 , 125 MHz): 64, 50.6, 46.9, 34.4, 33.5, 27.3, 24.4, 22.1, 21.1, 15.3. In agreement with the literature.²⁷⁶

5.2.3 ‘MenMgCl’ **168/173** small scale preparation

Inside an inert atmosphere glovebox MenCl (29.7 mg, 0.17 mmol, 1 equiv.) and Mg powder (4.1 mg, 0.17 mmol, 1 equiv.) were mixed in a Young’s tap NMR tube using THF- d_8 (0.6 mL). The tube was sealed, removed from the glovebox, and placed in a ultrasonication bath set to 50 °C. Following sonication for 4 h the formation of a fine black suspension was observed. The tube was then moved to a heating bath set to 70 °C, where it was kept for 16 h. Mg metal was consumed and a light white precipitate was formed. The sample was taken back into the glovebox and filtered through a small anhydrous Celite® plug. ${}^1\text{H}$ NMR (400 MHz, THF- d_8): 1.91 (m, 1H), 1.83-1.49 (m, 5H), 1.27 (m, 4H), 1.09-0.66 (m, 24H), -0.14 (m, 1H).

5.2.4 'MenMgCl' **168/173** large scale preparation

Mg powder (3.28 g, 135 mmol, 8 equiv.) was weighed inside an inert atmosphere glovebox into a three-neck round bottom flask. The flask was sealed, removed from the glovebox and connected to the Schlenk line. A pressure equalising addition funnel and reflux condenser (in which the atmosphere had been replaced with nitrogen) were fitted to the flask under a stream of nitrogen. The funnel was charged with THF (~170 mL) using a double-ended needle. A large portion of the solvent was added to the flask, and to the remainder was added MenCl (23.6 g, 135 mmol, 8 equiv.) using a syringe. The reaction flask was heated to 50 °C and the MenCl solution was added with stirring over the course of an hour. During this time a black colouration developed in the reaction. The reaction was refluxed at 70 °C for 16 h. Following cooling to room temperature, the reaction mixture was transferred using a double-ended needle to an inert filtration funnel containing a bed of pre-dried Celite®. The mixture was filtered under nitrogen to give a clear brown solution. An aliquot was collected for analysis.

5.2.5 Men₃SnCl **151** small scale preparation

A MenMgCl solution was prepared from Mg powder (476 mg, 19.6 mmol, 7 equiv.) and MenCl (3.66 mL, 19.6 mmol, 1 equiv.) by heating to 70 °C with ultrasonication for 5 h in a sealed ampule. The solution was filtered through Celite® and the resulting filtrate was added with stirring to a solution of SnCl₄ (729 mg, 2.8 mmol, 1 equiv.) in benzene (2 mL). The resulting mixture was heated to 70 °C in a sealed ampule for 4 h with stirring and was then allowed to stir at room temperature for 12 h. After cooling to room temperature, a 30% HCl aqueous solution (10 mL) was added and the reaction was stirred for 1 h. Diethyl ether (250 mL) was added. The organic phase was separated, washed with a saturated sodium bicarbonate solution (100 mL), distilled water (100 mL) and dried using magnesium sulfate. The yellow oil formed after solvent removal was dissolved in absolute ethanol (11 mL) and the resulting solution placed in an ultrasonication bath, which initiates solid formation. The resulting white solid was collected by filtration, rinsed with absolute ethanol (~50 mL) and dried: Men₃SnCl (391 mg, 0.68 mmol, 24% yield). Slow evaporation of the filtrate (~1 week) yields a further crop of product (193 mg, 0.34 mmol, 12% yield). The product can be recrystallised from pentane. m.p (pentane) 128.6-

129.7 °C; $[\alpha]_D^{25} = -123.8$; ^1H NMR (400 MHz, CDCl_3): 2.16 (m, H); 1.97 (m, 1H); 1.71 (m, 2H), 1.54 (m, 1H), 1.43 (m, 1H), 1.27 (m, 2H); 1.06-0.76 (12 H); 0.97 (d, $J = 6.7$ Hz); 0.88 (d, $J = 6.5$ Hz); 0.84 (d, $J = 7.1$ Hz); ^{13}C NMR (100 MHz, CDCl_3) 46.4 ($^2J^{13}\text{C}-^{117/119}\text{Sn} = 10.4$ Hz), 43.9, 40.5 ($^2J^{13}\text{C}-^{117/119}\text{Sn} = 19.3$), 35.5, 35.5, 35.4, 27.2, 22.7, 22.3, 16.9; ^{119}Sn NMR (149 MHz, CDCl_3): 106.2; ^{119}Sn NMR (149 MHz, C_6H_6): 92.3. HRMS (ESI+) calculated for $[\text{M}(^{120}\text{Sn})\text{-Cl}+\text{CH}_3\text{CN}]^+$ 578.3748, found: 578.3768. IR (neat, cm^{-1}) 2942, 2921, 2872, 2842, 1457, 1447, 1383, 1366, 1316, 1243, 1176, 1160, 1089, 1069, 1047, 1034, 993, 933, 846, 656, 583, 503.

5.2.6 Men_3SnCl **151** large scale preparation

The MenMgCl solution (large scale preparation) was cooled using an ice bath, and with stirring was added a pre-mixed solution containing SnCl_4 (1.98 mL, 16.9 mmol, 1 equiv.) in benzene (~20 mL) using a pressure equalising addition funnel. The reaction was warmed to room temperature and then refluxed at 80 °C for 3.5 h. An aliquot was collected for analysis after 1.5 h. The reaction was cooled in an ice bath and quenched with a 30% HCl aqueous solution (100 mL). Strong gas evolution was observed. The reaction was stirred for 20 min and then diluted with diethyl ether (300 mL). The organic phase was separated, washed with distilled water (4×100 mL) and dried using sodium sulfate. Solvent removal resulted in the isolation of a clear colourless oil which was dissolved in 500 mL absolute ethanol. The resulting solution was stored at -20 °C overnight, which resulted in formation of a small amount of crystalline Men_6Sn_2 . The remaining solution was concentrated to ~200 mL and stored at -20 °C overnight, which results in the formation of a white solid. Filtration resulted in the isolation of Men_3SnCl (414 mg, 0.72 mmol, 4% yield), which was further recrystallised from pentane. The filtrate contained residual Men_3SnCl and Men_6Sn_2 however concentration and cooling did not allow further product isolation.

5.2.7 Men_6Sn_2 **148**

MenMgCl was prepared in a similar fashion to the procedure described in 'MenMgCl large scale preparation'; an additional treatment of Mg with dibromoethane (0.18 mL, 2.1 mmol, 0.07 equiv.) was

carried out at 70 °C for 30 min in THF (140 mL) before commencing addition of MenCl (29 mL, 155.4 mmol, 5.2 equiv.) in THF (30 mL). Reflux time: 3 h. Filtration was not carried out. SnCl₄ (3.5 mL, 30 mmol, 1 equiv.) was added as a solution in toluene (~30 mL) at room temperature. Reflux was carried out for 4 h, then the reaction was stirred at room temperature (12 h). Quenching was carried out at ice bath temperature using a 30% HCl aqueous solution (100 mL). Following stirring for 1.5 h, extraction was carried out with diethyl ether (300 mL). Organic phase was washed with saturated sodium bicarbonate solution (100 mL), distilled water (100 mL) and dried using magnesium sulfate. The resulting oil was crystallised from absolute ethanol (400 mL) by slow evaporation. Crystal formation starts after ~2 d and was allowed to proceed until no further progress was apparent. Crystals were collected to give Men₆Sn₂ (1g, 0.93 mmol, 6% yield) as a pale-yellow solid. $[\alpha]_D^{25} = -205.2$; m.p. decomposes at ~250 °C; ¹H NMR (400 MHz, CDCl₃) CDCl₃: 2.18 (m, 1H), 1.71 (m, 3H), 1.34 (m, 4H), 1.03-0.72 (15H): 0.91 (d, J = 6.7 Hz), 0.86 (d, J = 6.2 Hz), 0.8 (d, J = 6.7 Hz); ¹³C NMR (100 MHz, C₆H₆) 47 (³J ¹³C-^{117/119}Sn = 15.7 Hz), 46.3, 40.2 (¹J ¹³C-^{117/119}Sn = 179.8, ²J ¹³C-^{117/119}Sn = 34.8 Hz), 37.2 (³J ¹³C-^{117/119}Sn = 59.4 Hz), 36.2, 34.9, 28.2 (³J ¹³C-^{117/119}Sn = 45.7 Hz), 23, 22.6, 17.8; ¹¹⁹Sn NMR (149 MHz, C₆H₆) 19.2 (br, FWHM ~900 Hz); HRMS (ESI+) calculated for C₆₂H₁₂₀N¹¹⁶Sn¹²⁰Sn 1114.7460 ([M+CH₃CN+3H]⁺), found 1114.7490; IR (neat, cm⁻¹) 2946, 2915, 2866, 2851, 2840, 1457, 1437, 1383, 1374, 1366, 1306, 1233, 1079, 1062, 1043, 1033, 992, 962, 932, 841, 640, 628.

5.2.7.1 Crystallographic characterisation **148**

X-ray quality crystals were grown by slow cooling of a hot (100 °C) 1,4-dioxane solution (21 mg/mL).

Crystallisation occurred over 2-4 days.

Formula	C ₆₀ H ₁₁₄ Sn ₂ , C ₄ H ₈ O ₂	
Formula weight	1160.99	
Temperature	173(2) K	
Diffractometer, wavelength	Agilent Xcalibur 3 E, 0.71073 Å	
Crystal system, space group	Monoclinic, P2 ₁	
Unit cell dimensions	a = 16.9385(3) Å	α = 90°
	b = 20.9523(3) Å	β = 104.6610(16)°

	$c = 28.4464(4) \text{ \AA}$	$\gamma = 90^\circ$
Volume, Z	9766.9(3) \AA^3 , 6	
Density (calculated)	1.184 Mg/m^3	
Absorption coefficient	0.805 mm^{-1}	
F(000)	3732	
Crystal colour / morphology	Colourless blocks	
Crystal size	0.719 x 0.352 x 0.234 mm^3	
θ range for data collection	2.424 to 28.406°	
Index ranges	$-20 \leq h \leq 21$, $-28 \leq k \leq 27$, $-37 \leq l \leq 36$	
Reflections collected / unique	62854 / 38815 [R(int) = 0.0249]	
Reflections observed [$F > 4\sigma(F)$]	34105	
Absorption correction	Analytical	
Max. and min. transmission	0.873 and 0.644	
Refinement method	Full-matrix least-squares on F^2	
Data / restraints / parameters	38815 / 1 / 1675	
Goodness-of-fit on F^2	1.015	
Final R indices [$F > 4\sigma(F)$]	$R_1 = 0.0374$, $wR_2 = 0.0791$	
R indices (all data)	$R_1 = 0.0480$, $wR_2 = 0.0846$	
Absolute structure parameter	-0.024(6)	
Largest diff. peak, hole	0.655, -0.468 e\AA^{-3}	
Mean and maximum shift/error	0.000 and 0.024	

5.2.8 Men_3SnH **152**

In an inert atmosphere glovebox, Men_3SnCl (400 mg, 0.7 mmol, 1 equiv.) was suspended in diethyl ether (1 mL) in an ampule. A suspension of LiAlH_4 (26.6 mg, 0.7 mmol, 1 equiv.) in diethyl ether (~0.8 mL) was added, the flask was sealed, and the resulting reaction mixture was stirred at room temperature for 24 h. The reaction was quenched with an oxygen-free mixture of 1,4-dioxane/water (7:2, 0.8 mL) and stirred for 20 min. The workup was carried out rapidly under air. The organic phase was collected and the resulting solid residue was extracted with diethyl ether (3×2 mL). The combined organics were dried on Na_2SO_4 . Solvent removal yielded a cloudy oil, which was dissolved in pentane and filtered to give a clear colourless oil following solvent removal. The product was dried under high

vacuum and stored in an inert atmosphere glovebox. Men₃SnH (196 mg, 0.36 mmol, 52% yield). ¹H NMR (400 MHz, C₆D₆) 5.48 (1H, ¹J (¹H-^{117/119}Sn = 1374/1438 Hz), 2.19 (m, 3H), 1.97 (m, 3H), 1.76 (m, 9H); 1.55 (m, 6H), 1.28 (m, 3H), 1.15-0.81 (42H): 1.04 (d, *J* = 6.8 Hz), 0.92 (d, *J* = 6.6 Hz); ¹³C NMR (100 MHz, C₆D₆) 47.8, 43.3, 36, 35.8, 34.5, 33.9, 27.3, 23, 22.4, 16.4; ¹¹⁹Sn NMR (149 MHz, C₆D₆) -103.8; ¹¹⁹Sn NMR (149 MHz, CDCl₃) -103.5, ^{1/3/2}J (¹¹⁹Sn-¹³C) = 339.8/59/17.4 Hz.

5.2.9 Men₃SnNTf₂ 182

A solution of Men₃SnH (100mg, 0.186 mmol, 1 equiv.) in toluene (3 mL) was added to a stirred solution of HNTf₂ (52.2 mg, 0.186 mg, 1 equiv.) in toluene (3 mL). Gas evolution was observed over the course of ~10 min. Stirring was continued for 1 h at room temperature. Solvent removal under high vacuum afforded a white solid, Men₃SnNTf₂ (124 mg, 0.15 mmol, 82% yield). ¹H NMR (400 MHz, C₆D₆) 2.68-2.35 (2m, 2H), 1.47 (m, 5H), 1.14-0.58 (13 H): 0.98 (d, *J* = 6 Hz); ¹³C NMR (100 MHz, C₆D₆) 49, 46.5, 39.8 (²J ¹³C-^{117/119}Sn = 22.5 Hz), 38.9 (²J ¹³C-^{117/119}Sn = 31.8 Hz), 35.4, 35.1, 27.4, 22.5, 22.1, 17.1; ¹³C NMR (100 MHz, pentane) 118.6 (CF₃), 47.9, 45.7, 38.8 (²J ¹³C-^{117/119}Sn = 20.6 Hz), 37.3 (²J ¹³C-^{117/119}Sn = 30.8 Hz), 34.5, 34.2, 26.5 (³J ¹³C-^{117/119}Sn = 69.4 Hz), 20.9 (x2), 15.8; additional peaks: 30.8, 29, 24.9; ¹¹⁹Sn NMR (149 MHz, C₆D₆); ¹⁹F NMR (376 MHz, C₆D₆) = -77.8.

5.2.10 Gutmann-Beckett Lewis acidity measurement

Et₃PO (2.45 mg, 0.018 mmol, 1 equiv.) and Men₃SnNTf₂ (44.7 mg, 0.054 mmol, 3 equiv.) were dissolved in DCM (0.36 mL) in a Young's tap NMR tube. A capillary insert containing a solution of Et₃PO in CD₂Cl₂ was included.

$$AN = 100(76.71-41)/(86.14-41) = 79.1$$

Et₃PO · Men₃SnNTf₂

³¹P {¹H} NMR (162 MHz, CH₂Cl₂): 76.7 (²J ³¹P -^{117/119}Sn = 189/198 Hz, ¹J ³¹P -¹³C = 66 Hz); ¹¹⁹Sn 189.1 (d, ²J ¹¹⁹Sn-³¹P = 198 Hz).

5.2.11 Men₆Sn₂ cleavage using HCl

Men₆Sn₂ (25.8 mg, 0.024 mmol, 1 equiv.) was added to a Young's tap NMR tube. A commercial 4M HCl/1,4-dioxane solution (0.6 mL, 0.24 mmol, 10 equiv.) was added and the NMR tube was sealed. The reaction was heated in an oil bath to 80 °C for 49 h. NMR analysis was carried out periodically at room temperature. At the end of the reaction time the reaction mixture was homogeneous at 80 °C.

A Men₆Sn₂ (32.3 mg, 0.03 mmol, 1 equiv.) solution in benzene (0.6 mL) was prepared in a Young's tap NMR tube in the glovebox. HOTf (5.3 μL, 0.06 mmol, 2 equiv.) was added using a microsyringe and the tube sealed. Formation of a white precipitate was observed over ~45 min. The reaction was heated to 60 °C for 3 days, leading to more precipitate development. The solvent was removed under high vacuum and the resulting residue was extracted with pentane (2×~0.6 mL) under nitrogen. The extract was concentrated to give a white solid, which was analysed in benzene.

5.2.12 Men₆Sn₂ cleavage using Cp₂FeOTf

In a Young's tap NMR tube were mixed Men₆Sn₂ (25 mg, 0.024 mmol, 1 equiv.) and Cp₂FeOTf (16.1 mg, 0.048 mmol, 2 equiv.) and 1,2-difluorobenzene was added (0.6 mL) to give a deep blue solution. The tube was sealed and the reaction was analysed at the indicated time points.

5.2.13 Halide abstraction from Men₃SnCl

In a vial in the glovebox were mixed Men₃SnCl (15 mg, 0.026 mmol, 1 equiv.) and AgNTf₂ (10.2 mg, 0.026 mmol, 1 equiv.). The vial was shielded from light using Al foil and 1,2-DFB (0.6 mL) was added leading to immediate formation of a black precipitate. The reaction was allowed to stand for 24 h and was then filtered through a Celite[®] plug into a Young's tap NMR tube.

5.2.14 Hydrogen activation using Men₃SnNTf₂

In an inert atmosphere glovebox was prepared a solution containing Men₃SnNTf₂ (8.2 mg, 0.01 mmol, 1 equiv.) and DABCO (1.1 mg, 0.01 mmol, 1 equiv.) in 1,2-DFB (0.6 mL) and transferred to a Wilmad high pressure NMR tube. Analysis was carried out and then the reaction was pressurised to 10 bar with

hydrogen gas and allowed to proceed with occasional shaking. The reaction was analysed at specified time points.

5.2.15 Stoichiometric reduction of **13g**

In an inert atmosphere glovebox a solution containing **13g** (5 mg, 0.026 mmol, 1 equiv.) and HNTf₂ (7.2 mg, 0.026 mmol, 1 equiv.) in C₆D₆ (0.5 mL) was prepared in a Young's tap NMR tube. The yellow solution was analysed immediately and after 22 h. A portion (0.24 mL, 0.026 mmol, 1 equiv.) of a stock solution containing Men₃SnH (57 mg in 1 mL C₆D₆) was added. Following NMR analysis the reaction was quenched with MeOH (22 h). The resulting crude product was purified by column chromatography (pentane/EtOAc 100:1) to give the amine **36g** (1.4 mg, 0.007 mmol, 27% yield).

5.2.16 Catalytic reduction of **13g**

A solution containing **13g** (73.1 mg, 0.375 mmol, 1 equiv.), Men₃SnNTf₂ (12.3 mg, 0.015 mmol, 0.04 equiv.) and 2,4,6-collidine (2 μL, 0.015 mmol, 0.04 equiv.) was prepared in 1,2-DFB (0.6 mL) and transferred to a Wilmad high pressure NMR tube. The tube was pressurised with H₂ to a pressure of 10 bar. The temperature was increased in 20 °C increments, allowing sufficient time for reaction to occur before re-analysing. After 84 h at 60 °C the reaction was cooled, de-pressurised and quenched with methanol. The crude product was purified by column chromatography (pentane/EtOAc 100:1) to give the amine **36g** as a cloudy oil. The product was dissolved in pentane and washed with a KF solution (15% aqueous) to give a clear oil (8 mg, 0.04 mmol, 11% yield).

5.3 Experimental Section for chapter 4

5.3.1 Purification of racemic [**200**]H

Commercial racemic [**200**]H (95%, 3.25 g) was suspended in a 3.5 M aqueous HCl solution (16 mL), stirred and filtered. The recovered product was dissolved in boiling (80 °C) absolute ethanol (50 mL) and hot filtered. The solid obtained following solvent removal was suspended in boiling (80 °C) absolute ethanol (6 mL) and refluxed for 3 h. After cooling to room temperature the suspension was

filtered to give a fine beige powder and a pink filtrate. The powder was dried under high vacuum at 80 °C. Purity by ^{31}P NMR: >99%.

5.3.2 *R*-[200]Na

Prepared according to the procedure of Ishihara from commercial *R*-[200]H.³⁵⁰ Under these reaction conditions slow degradation of the product was observed to occur (degradation product ^{31}P NMR $\delta = -1.4$, DMSO- d_6).

R-[200]H (90 mg, 0.26 mmol, 1 equiv.) and NaOMe (14 mg, 0.26 mmol, 1 equiv.) were mixed and DCM and MeOH were added in approximately equal volumes (~3.5 mL). The reaction can be analysed by ^{31}P NMR, *R*-[200]H $\delta = 4.8$ (DCM:MeOH 1:1); *R*-[200]Na $\delta = 7.7$ (DCM:MeOH 1:1). The resulting solution was stirred for approximately 1 h before the solvents were removed to leave a glassy oil. DCM was added and the resulting solution was dried again under high vacuum to leave a white crystalline solid which was further dried under high vacuum (a trace of DCM remains); The solid dissolves slowly in benzene but is readily soluble in DCM or chloroform; In these solvents the ^1H NMR spectrum is not resolved; ^1H NMR (C_6D_6 , 400 MHz): 7.4 (br); ^1H NMR (DCM:MeOH 1:1, 400 MHz) 8.37 (1H), 8.3 (1H), 7.9 (1H), 7.8 (1H), 7.7 (1H), 7.6 (1H); ^{13}C NMR (DCM, 100 MHz) 148.9, 132.6, 131.4, 128.6, 127.3, 126.5, 125.2, 122.2, 121.1; ^{31}P NMR (C_6D_6 , 162 MHz): 7.7 (br).

Reaction scale-up: *R*-[200]H (300 mg), 23 h reaction time. Following solvent removal the product was re-dissolved in a small amount of DCM, filtered through Celite®, and dried to give light pink crystals (259 mg, 0.7 mmol, 81% yield, 94% purity by ^{31}P NMR). Attempted purification from DCM/pentane was unsuccessful.

^1H NMR (d_6 -DMSO, 400 MHz): 8.02 (m, 4H), 7.41 (m, 4H), 7.29 (m, 2H), 7.21 (m, 2H); ^{31}P { ^1H } NMR (162 MHz, DMSO- d_6 , externally referenced to H_3PO_4) 6.5 (s); ^{31}P { ^1H } NMR (162 MHz, THF, externally referenced to H_3PO_4) 7.5 (s).

5.3.3 Racemic [200]Li

Racemic [200]H (300 mg, 0.86 mmol, 1 equiv.) and lithium *tert*butoxide (69 mg, 0.86 mmol, 1 equiv.) were suspended in DCM (~5 mL). After stirring was started dissolution occurred immediately to give a clear solution. After 15 min at room temperature precipitation of a white solid began. After stirring for 1.5 h, the solvent was removed under high vacuum to give a fine, off white powder (contains *t*BuOH 3:2, purity by ³¹P NMR 97%). Complete removal of residual *tert*butanol was unsuccessful through azeotroping using DCM (1.5 mL) and drying under high vacuum (carried out twice). Isolated: flaky, off-white solid (283 mg, <93% yield). ¹H NMR (d6-DMSO, 400 MHz): 8.02 (m, 4H), 7.41 (m, 4H), 7.29 (m, 2H), 7.21 (m, 2H). ³¹P NMR {¹H} NMR (162 MHz, DMSO-d6, externally referenced against H₃PO₄) 6 (s).

5.3.4 *R*-[200][Bu₄N]

R-[200]Na (10.8 mg, 0.03 mmol, 1 equiv.) was dissolved in CDCl₃ (0.5 mL). [Bu₄N]Cl (8.3 mg, 0.03 mmol, 1 equiv.) was added as a solid. The solution becomes cloudy within a few minutes. Later, an extra portion of [Bu₄N]Cl (4.2 mg, 0.015 mmol, 0.5 equiv.) was added. ¹H NMR (400 MHz, CDCl₃) series of peaks in the aromatic region from which the following stand out: 7.85 (m, 3H), 7.51 (m, 1H), 7.34 (m, 3H), 7.18 (m, 1H), 2.85 (br m, 8H), 1.25 (m, 8H), 1.11 (m, 8H), 0.76 (t, *J* = 7 Hz, 12H); ¹³C NMR (125 MHz, CDCl₃) 150.8, 150.7, 132.8, 130.8, 129.7, 128.2, 127.1, 125.7, 124.3, 123.1, 122.6, 58, 23.7, 19.6, 13.7; ³¹P {¹H} NMR (162 MHz, CDCl₃, referenced externally against H₃PO₄) two clusters of peaks from which sharp singlets emerge at 8.5 and 7 ppm.

5.3.5 *R*-[201]Na

Adduct *R*-[201]Na was prepared and characterised *in situ* (0.06 mmol scale). Solids were mixed and solvent (C₆D₆ or THF) was added. In benzene, dissolution occurred after ~15 min, with vigorous shaking. The resulting solutions were transferred either to Young's tap NMR tubes or to Wilmad high pressure NMR tubes fitted with PV-ANV PTFE valves.

¹H NMR (C₆D₆, 400 MHz) 7.64 (br, m, 4H), 7.14 (br, 6H), 6.88 (br, 2H); ¹H NMR (THF, 400 MHz) 7.94 (m, 2H), 7.37 (m, 1H), 7.23 (m, 2H); ³¹P NMR (C₆D₆, 162 MHz) -2.6 (br, major), 10.9, 3.3, -10.2; ³¹P NMR

(THF, 162 MHz) -6.6; ^{19}F NMR (C_6D_6 , 378 MHz) -137 (br, 2*o*-F), -157.8 (br, 1*p*-F), -163.9 (br, 2*m*-F); ^{19}F NMR (THF, 378 MHz); -134.8 (m, 2F), -163.9 (m, 1F), -168.8 (m, 2F); ^{11}B NMR (128 MHz, THF) -4.4.

5.3.6 *R*-[202]Na

Adduct *R*-[202]Na was prepared and characterised *in situ* (0.03 mmol scale). To a solution of $\text{B}(\text{C}_6\text{F}_5)_2(\text{C}_6\text{Cl}_5)$ (17.8 mg, 0.03 mmol, 1 equiv.) in toluene-*d*₈ (0.6 mL) in a Young's tap NMR tube was added solid *R*-[200]Na (10.8 mg, 0.03 mmol, 1 equiv.). The tube was sealed and placed in a ultrasonication bath for an hour. The cloudy solution was left to stand for 15 h after which it became clear. The sample was submitted for NMR analysis.

^1H NMR (400 MHz, C_7D_8 , 300 K) series of peaks from 8.8 to 6.6 ppm; ^{31}P NMR (162 MHz, C_7D_8 , 300 K) series of peaks from 11.4 to 5 ppm from which three sharp singlets emerge: 10.2, 8.9, 6.7 and singlet at -12.6 ppm; ^{19}F NMR (378 MHz, C_7D_8 , 300 K) -127.3 (m, 2*o*-F), -141.1 (m, *p*-F), -160 (m, 2*m*-F); the ^{19}F NMR spectrum matches that of an isolated sample of $\text{B}(\text{C}_6\text{F}_5)_2(\text{C}_6\text{Cl}_5)$; ^{11}B NMR (128 MHz, C_7D_8 , 300 K) 61.1 (br s), -2.9 (s).

5.3.7 Hydrogen activation with *R*-[201]Na in benzene

The sample of *R*-[201]Na was prepared as described in section 5.3.5 and pressurised according to the general procedure. NMR analysis was carried out at room temperature after 20 h. Heating was subsequently carried out using an oil bath (120 °C).

5.3.8 Stoichiometric reductions

Chiral, enantioenriched phosphoric acids *R*-[200]H and *S*-190 (Ar = 3,5-(CF_3)₂ C_6H_3) were purchased from Sigma-Aldrich, dried under high vacuum and stored in an inert atmosphere glovebox.

($^n\text{Bu}_4\text{N}$)[$\text{HB}(\text{C}_6\text{F}_5)_3$] **204** was prepared according to the procedure by Piers on a 0.2 mmol scale.⁷⁷

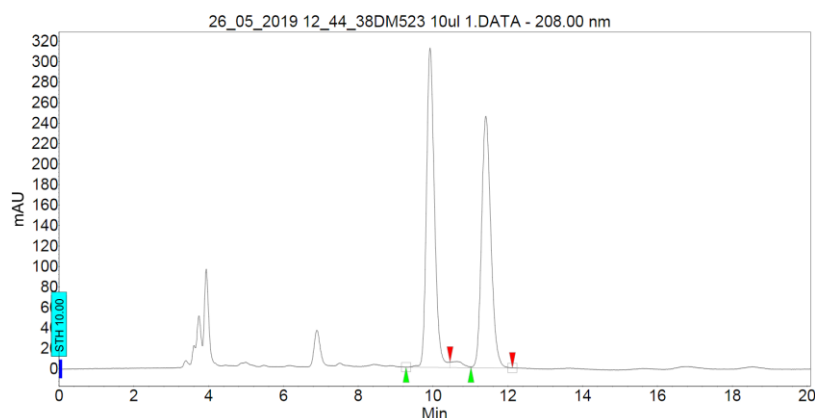
Product was obtained as a white solid (139 mg, 0.184 mmol, 92% yield). ^1H NMR (400 MHz, C_6D_6) 4.14 (br d, $J = 99$ Hz, 1H), 2.78 (br q, $J = 10.6$ Hz, 8H), 0.9 (br m, 16 H), 0.72&0.66 (2t, $J = 6.7, 6.6$ Hz, 12H); ^{19}F (376 MHz, C_6D_6) -133 (m, 2F), -163.3&-163.9 (2t, $J = 20.5, 20.3$ Hz, 1F), -166.5&-167 (2m, 2F); ^{11}B

NMR (128 MHz, C₆D₆) –24.5 (d, *J* = 77.3 Hz). Data is in agreement, the splitting observed in the ¹⁹F NMR spectrum was found to be concentration dependent.

Na[HB(C₆F₅)₃] **203** was prepared according to the procedure by Ashley and Wildgoose on a 0.6 mmol scale.³⁶⁰ Product was obtained as a white solid (218 mg, 0.41 mmol, 68% yield). ¹H NMR (400 MHz, 1,2-DFB) 3.5 (q, *J* = 80 Hz); ¹¹B NMR (128 MHz, 1,2-DFB) –26.4 (d, *J* = 84 Hz). Data is in agreement with the original reported in d₆-DMSO.

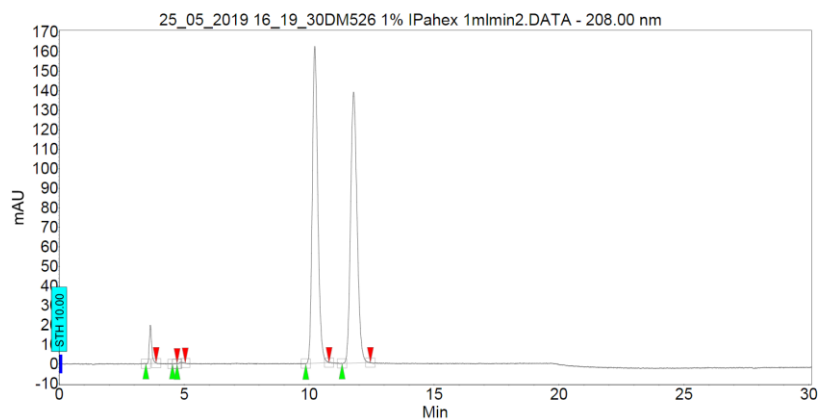
Stoichiometric reductions of imines were performed on a 0.03 mmol scale and of enamine **205** on a ~0.005 mmol scale. Solids were added sequentially (with NMR analysis of intermediate solutions), with hydride added last to the Young's tap NMR tube. Conversions were measured either by relative integration, or by integration against an external standard (capillary insert, 0.1M 1,3,5-trimethoxybenzene solution) and referenced to theoretical. Purification was carried out by flash column chromatography. e.r. values were determined by HPLC analysis on the isolated samples. Amine **206** was purified by preparative TLC (20×20 cm, 250 μm thickness). It was identified by comparison with an authentic sample by TLC, ¹H NMR and HPLC.

HPLC: Chiralcel OD-H, IPA/hexane 1:99, 1 ml/min, 208 nm detection. *t* = 9.9 min, 11.4 min.



Peak results :

Index	Name	Time [Min]	Quantity [% Area]	Height [mAU]	Area [mAU.Min]	Area % [%]
1	UNKNOWN	9.919	52.11	311.9	77.4	52.106
2	UNKNOWN	11.413	47.89	245.6	71.2	47.894
Total			100.00	557.5	148.6	100.000

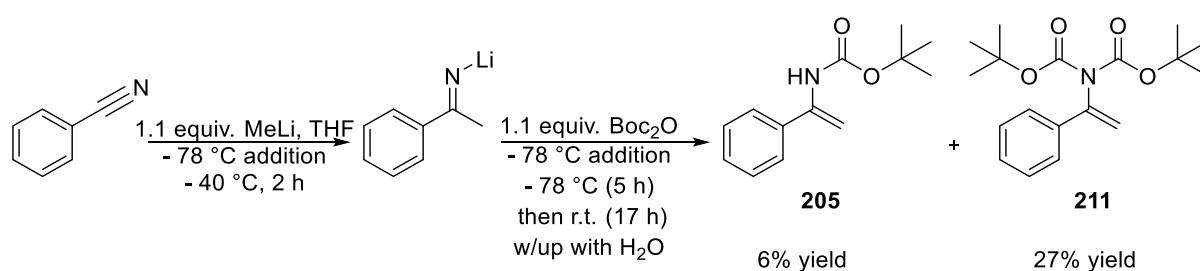


Peak results :

Index	Name	Time [Min]	Quantity [% Area]	Height [mAU]	Area [mAU.Min]	Area % [%]
1	UNKNOWN	3.653	2.50	19.5	2.1	2.504
2	UNKNOWN	4.533	0.02	0.2	0.0	0.019
3	UNKNOWN	4.853	0.10	0.5	0.1	0.096
4	UNKNOWN	10.226	48.59	162.3	41.7	48.589
5	UNKNOWN	11.772	48.79	138.8	41.8	48.793
Total			100.00	321.2	85.7	100.000

5.3.9 Preparation of enamine **205**

As described in Scheme 5.1. Intermediate iminyl lithium prepared according to the procedure of List.³⁷⁷ Direct trapping with Boc₂O was poor yielding; isolation of double *N*-Boc protected by-product **211** suggests this to be due to the intermediate iminyl lithium acting to deprotonate the mono *N*-Boc protected product **205**. This was supported by the detection of free imine and acetophenone in the crude product. Boc protecting of free imine has been reported.³⁷⁸



Scheme 5.1 Preparation of enamine **205**.

Benzonitrile (stored over activated 4 Å MS, 2.05 mL, 20 mmol, 1 equiv.) dissolved in THF (20 mL) was cooled to $-78\text{ }^\circ\text{C}$. MeLi (1.6M/Et₂O, 13.8 mL, 22 mmol, 1.1 equiv.) solution was added slowly with stirring. The reaction turns deep red. It was moved to an acetonitrile/dry ice cooling bath ($-40\text{ }^\circ\text{C}$) and stirred at this temperature for 2 h. The reaction was cooled back down to $-78\text{ }^\circ\text{C}$ and a Boc₂O (4.8 g,

22 mmol, 1.1 equiv) solution in THF (2 mL) was added slowly. The reaction was stirred at this temperature for 5 h, the colour changing from deep red to bright yellow and then to pale yellow. It was then stirred at room temperature for 17 h (large amount of precipitate formed) before being poured into water (100 mL). The aqueous phase was extracted with DCM (3×25 mL). The combined organics were washed with water (25 mL), brine (50 mL) and dried on sodium sulfate. The crude product was purified by flash column chromatography (~ 300 g silicagel) eluting with pentane/EtOAc (50:1 to 40:1, desired product elutes, then increasing polarity gradually to 15:1 to elute by-product).

205 was dried under high vacuum to remove residual acetophenone to give a very viscous pale yellow oil (250 mg, 1.14 mmol, 6% yield); ¹H NMR (400 MHz, CDCl₃) 7.44 (m, 2H), 7.36 (m, 3H), 6.12 (br s, 1H), 5.56 (br s 1H), 4.89 (d, *J* = 1 Hz, NH), 1.49 (s, 9H); ¹³C NMR (125 MHz, CDCl₃) 153.2, 141.2, 138.9, 128.7, 126.2, 98.6, 80.6, 28.4. In agreement with reported.³⁷⁸

By-product **211**, yellow oil (1.7 g, 5.32 mmol, 27% yield). ¹H NMR (400 MHz, CDCl₃) 7.42 (m, 2H), 7.32 (m, 3H), 5.6 (s, 1H), 5.17 (s, 1H), 1.35 (s, 18H); ¹³C NMR (125 MHz, CDCl₃) 151.6 (quaternary), 144.6 (quaternary), 137.8 (quaternary), 128.5 (tertiary), 128.4 (tertiary), 125.6 (tertiary), 112.6 (secondary), 82.7 (quaternary), 27.9 (primary).

5.3.10 Preparation of racemic amine **206**

Following a literature procedure.³⁷⁹ Enamine **205** (11.9 mg, 0.054 mmol, 1 equiv.) and NaBH₄ (14.4 mg, 0.38 mmol, 1 equiv.) were dissolved in absolute ethanol (0.6 mL) and the resulting solution was refluxed (80 °C) for 2 h. The reaction was cooled, the solvent was removed and the resulting residue extracted with DCM (2×5 mL). The crude product was purified by flash column chromatography (1.8 g silicagel, elution with pentane/EtOAc 20:1) to give a white solid (9.2 mg, 0.042 mmol, 77% yield). ¹H NMR (400 MHz, CDCl₃) 7.3 (m, 5H), 4.9-4.5 (br m, 1H), 1.41 (m, 12H); ¹³C NMR (125 MHz, CDCl₃) 155.2, 128.7, 127.3, 126, 79.6, 50.3, 28.5, 22.8. In agreement with the literature.³⁸⁰

5.3.11 Adduct **207**

(*R*)-[**200**]H (30.7 mg, 0.09 mmol, 1 equiv.) and B(C₆F₅)₃ (20.9 mg, 0.09 mmol, 1 equiv.) were mixed in benzene-d₆ (0.6 mL) in a Young's tap NMR tube.

¹H NMR (400 MHz, C₆D₆) 7.46 (m, 4H), 7.06 (m, 6H), 6.82 (m, 2H); ³¹P NMR (162 MHz, C₆D₆) -7.8 (br s); ¹⁹F (376 MHz, C₆D₆) -135.4 (br s), -158.3 (br s), -165.2 (br s); ¹¹B NMR (128 MHz, C₆D₆) 0.9 (br s).

5.3.12 Borane **208**

(*R*)-[**200**]H (104.5 mg, 0.3 mmol, 1 equiv.) and B(C₆F₅)₃ (153.5 mg, 0.3 mmol, 1 equiv.) were mixed in benzene (3 mL), the resulting solution was stirred at room temperature for two days. The volatiles were removed under high vacuum and the resulting solid was dissolved in a small amount of DCM and filtered through Celite®. The resulting solution was concentrated to an oil, to which was added pentane (~1 mL). After crystallisation had occurred, the brown supernatant was removed to give the product as a white crystalline solid (135 mg, 0.195 mmol, 65% yield). ¹H NMR (400 MHz, C₆D₆) 7.55 (m, 4H), 7.46 (m, 2H), 7.13 (m, 2H), 7.05 (m, 2H), 6.79 (m, 2H); ¹³C NMR (100 MHz, C₆D₆) 148.3 (dt, *J* = 245 Hz, 13 Hz), 146.1, 146, 141.2 (dt, *J* = 252 Hz, 13.8 Hz), 137.6 (dt, *J* = 249 Hz, 15.1 Hz), 132.7, 132.3, 129, 128.6, 127.1, 126.8, 121, 119.4, 114.7 (br); ³¹P NMR (162 MHz, C₆D₆) -9.4 (s); ¹⁹F (376 MHz, C₆D₆) -137.1 (dd, *J* = 23.5, 6.4 Hz, 2*o*-F), -158.1 (t, *J* = 20 Hz, 1*p*-F), -166.1 (ddd, *J* = 23.1, 20.2, 8.7 Hz, 2*m*-F); ¹¹B NMR (128 MHz, C₆D₆) 3 (br).

¹H NMR (400 MHz, *protio*-DCM, δ = 5.33) 8.12 (m, 2H), 8.03 (m, 2H), 7.57 (m, 5H), 7.34 (m, 5H); ³¹P NMR (162 MHz, *protio*-DCM) -10.7 (s); ¹⁹F (376 MHz, *protio*-DCM) -137.1 (m, 2F), -158.2 (t, *J* = 20.6 Hz, 1F), -166.2 (m, 2F); ¹¹B NMR (128 MHz, *protio*-DCM) 3 (br).

5.3.13 Hydrogen activation with **208**

Borane **208** (13.8 mg, 0.02 mmol, 1 equiv.) was dissolved in THF or 1,4-dioxane (0.6 mL) and optionally B(C₆F₅)₃ (1 mg, 0.002 mmol, 0.1 equiv.) was added. The resulting solution was transferred to a high-

pressure NMR tube. Pressurising was carried out according to the general procedure. Heating was carried out using an oil bath.

5.3.14 Attempted catalytic reduction

Imine (0.075 mmol, 10 equiv.), $B(C_6F_5)_3$ (3.8 mg, 0.0075 mmol, 1 equiv.) and chiral enantioenriched phosphoric acid (0.0075 mmol, 1 equiv.) were dissolved in solvent (toluene or benzene, 0.6 mL) and the resulting solution transferred to a Young's tap NMR tube or to a Wilmad high pressure NMR tube. The tube was pressurised with hydrogen gas to 4 bar or 10 bar, respectively. Monitoring was performed by NMR analysis at the indicated time points. Heating was carried out using oil baths at incremental temperatures, sufficient time was allowed for reaction to occur before re-analysing. Baseline and phase correction applied, however errors are expected due to the very low amounts of products formed and the use of protonated solvents.

6 References

- 1 G. C. Welch, R. R. S. Juan, J. D. Masuda and D. W. Stephan, *Science*, 2006, **314**, 1124–1126.
- 2 J. B. Van Doren, *J. Chem. Educ.*, 1967, **44**, A82.
- 3 T. M. Lowry, *J. Soc. Chem. Ind.*, 1924, **43**, 17–17.
- 4 H. C. Brown, H. I. Schlesinger and S. Z. Cardon, *J. Am. Chem. Soc.*, 1942, **64**, 325–329.
- 5 W. Tochtermann, *Angew. Chemie Int. Ed. English*, 1966, **5**, 351–371.
- 6 R. Roesler, W. E. Piers and M. Parvez, *J. Organomet. Chem.*, 2003, **680**, 218–222.
- 7 G. C. Welch and D. W. Stephan, *J. Am. Chem. Soc.*, 2007, **129**, 1880–1881.
- 8 J. S. J. McCahill, G. C. Welch and D. W. Stephan, *Angew. Chemie Int. Ed.*, 2007, **46**, 4968–4971.
- 9 F.-G. Fontaine and D. W. Stephan, *Philos. Trans. R. Soc. A Math. Phys. Eng. Sci.*, 2017, **375**, 20170004.
- 10 A. R. Jupp and D. W. Stephan, *Trends Chem.*, 2019, **1**, 35–48.
- 11 D. W. Stephan, *Org. Biomol. Chem.*, 2008, **6**, 1535.
- 12 D. W. Stephan, *Dalton Trans.*, 2009, **9226**, 3129.
- 13 D. W. Stephan and G. Erker, *Angew. Chemie Int. Ed.*, 2010, **49**, 46–76.
- 14 D. W. Stephan, *J. Am. Chem. Soc.*, 2015, **137**, 10018–10032.
- 15 D. W. Stephan, *Science*, 2016, **354**, aaf7229–aaf7229.
- 16 Z. Wang, B. J. Reinius and G. Dong, *J. Am. Chem. Soc.*, 2012, **134**, 13954–13957.
- 17 Y. Dang, S. Qu, Y. Tao, X. Deng and Z.-X. Wang, *J. Am. Chem. Soc.*, 2015, **137**, 6279–6291.
- 18 M. Liu, B. Liu, S. Zhong, L. Shi, L. Liang and J. Sun, *Ind. Eng. Chem. Res.*, 2015, **54**, 633–640.

- 19 S. D. McCann and S. S. Stahl, *J. Am. Chem. Soc.*, 2016, **138**, 199–206.
- 20 C. Zhu, Q. Xia, X. Chen, Y. Liu, X. Du and Y. Cui, *ACS Catal.*, 2016, **6**, 7590–7596.
- 21 W. Wang, C. Li, L. Yan, Y. Wang, M. Jiang and Y. Ding, *ACS Catal.*, 2016, **6**, 6091–6100.
- 22 I. E. Marko, P. R. Giles, M. Tsukazaki, S. M. Brown and C. J. Urch, *Science*, 1996, **274**, 2044–2046.
- 23 J. M. Hoover, B. L. Ryland and S. S. Stahl, *J. Am. Chem. Soc.*, 2013, **135**, 2357–2367.
- 24 H. Xu, S. J. Zuend, M. G. Woll, Y. Tao and E. N. Jacobsen, *Science*, 2010, **327**, 986–990.
- 25 J. M. Hoover and S. S. Stahl, *J. Am. Chem. Soc.*, 2011, **133**, 16901–16910.
- 26 C. Walling and L. Bollyky, *J. Am. Chem. Soc.*, 1964, **86**, 3750–3752.
- 27 A. Berkessel, T. J. S. Schubert and T. N. Müller, *J. Am. Chem. Soc.*, 2002, **124**, 8693–8698.
- 28 J. R. Khusnutdinova and D. Milstein, *Angew. Chemie Int. Ed.*, 2015, **54**, 12236–12273.
- 29 R. Noyori and S. Hashiguchi, *Acc. Chem. Res.*, 1997, **30**, 97–102.
- 30 K. Abdur-Rashid, S. E. Clapham, A. Hadzovic, J. N. Harvey, A. J. Lough and R. H. Morris, *J. Am. Chem. Soc.*, 2002, **124**, 15104–15118.
- 31 C. A. Sandoval, T. Ohkuma, K. Muñiz and R. Noyori, *J. Am. Chem. Soc.*, 2003, **125**, 13490–13503.
- 32 T. Ohkuma, H. Ooka, S. Hashiguchi, T. Ikariya and R. Noyori, *J. Am. Chem. Soc.*, 1995, **117**, 2675–2676.
- 33 R. Noyori and T. Ohkuma, *Angew. Chemie Int. Ed.*, 2001, **40**, 40–73.
- 34 S. W. Benson, *J. Chem. Educ.*, 1965, **42**, 502.
- 35 D. J. Scott, M. J. Fuchter and A. E. Ashley, *Chem. Soc. Rev.*, 2017, **46**, 5689–5700.
- 36 P. Spies, G. Erker, G. Kehr, K. Bergander, R. Fröhlich, S. Grimme and D. W. Stephan, *Chem.*

- Commun.*, 2007, **2**, 5072.
- 37 X. Wang, G. Kehr, C. G. Daniliuc and G. Erker, *J. Am. Chem. Soc.*, 2014, **136**, 3293–3303.
- 38 T. Özgün, K.-Y. Ye, C. G. Daniliuc, B. Wibbeling, L. Liu, S. Grimme, G. Kehr and G. Erker, *Chem. - A Eur. J.*, 2016, **22**, 5988–5995.
- 39 S. J. Geier, T. M. Gilbert and D. W. Stephan, *J. Am. Chem. Soc.*, 2008, **130**, 12632–12633.
- 40 H. Wang, R. Fröhlich, G. Kehr and G. Erker, *Chem. Commun.*, 2008, 5966.
- 41 A. Ramos, A. J. Lough and D. W. Stephan, *Chem. Commun.*, 2009, 1118.
- 42 P. Spies, S. Schwendemann, S. Lange, G. Kehr, R. Fröhlich and G. Erker, *Angew. Chemie Int. Ed.*, 2008, **47**, 7543–7546.
- 43 Z. Glasovac, M. Eckert-Maksić and Z. B. Maksić, *New J. Chem.*, 2009, **33**, 588–597.
- 44 V. Sumerin, F. Schulz, M. Nieger, M. Leskelä, T. Repo and B. Rieger, *Angew. Chemie Int. Ed.*, 2008, **47**, 6001–6003.
- 45 V. Sumerin, F. Schulz, M. Atsumi, C. Wang, M. Nieger, M. Leskelä, T. Repo, P. Pyykkö and B. Rieger, *J. Am. Chem. Soc.*, 2008, **130**, 14117–14119.
- 46 S. J. Geier and D. W. Stephan, *J. Am. Chem. Soc.*, 2009, **131**, 3476–3477.
- 47 M. Ullrich, A. J. Lough and D. W. Stephan, *J. Am. Chem. Soc.*, 2009, **131**, 52–53.
- 48 S. Mummadi, A. Brar, G. Wang, D. Kenefake, R. Diaz, D. K. Unruh, S. Li and C. Krempner, *Chem. - A Eur. J.*, 2018, **24**, 16526–16531.
- 49 S. Mummadi, D. K. Unruh, J. Zhao, S. Li and C. Krempner, *J. Am. Chem. Soc.*, 2016, **138**, 3286–3289.
- 50 B. Kovačević, D. Barić and Z. B. Maksić, *New J. Chem.*, 2004, **28**, 284–288.
- 51 J. W. Runyon, O. Steinhof, H. V. R. Dias, J. C. Calabrese, W. J. Marshall and A. J. Arduengo, *Aust.*

- J. Chem.*, 2011, **64**, 1165.
- 52 M. P. Boone and D. W. Stephan, *J. Am. Chem. Soc.*, 2013, **135**, 8508–8511.
- 53 E. R. Clark and M. J. Ingleson, *Angew. Chemie Int. Ed.*, 2014, **53**, 11306–11309.
- 54 A. Schäfer, M. Reißmann, A. Schäfer, W. Saak, D. Haase and T. Müller, *Angew. Chemie Int. Ed.*, 2011, **50**, 12636–12638.
- 55 T. J. Herrington, B. J. Ward, L. R. Doyle, J. McDermott, A. J. P. White, P. A. Hunt and A. E. Ashley, *Chem. Commun.*, 2014, **50**, 12753–12756.
- 56 D. J. Scott, N. A. Phillips, J. S. Sapsford, A. C. Deacy, M. J. Fuchter and A. E. Ashley, *Angew. Chemie Int. Ed.*, 2016, **55**, 14738–14742.
- 57 R. C. Turnell-Ritson, J. S. Sapsford, R. T. Cooper, S. S. Lee, T. Földes, P. A. Hunt, I. Pápai and A. E. Ashley, *Chem. Sci.*, 2018, **9**, 8716–8722.
- 58 T. vom Stein, M. Pérez, R. Dobrovetsky, D. Winkelhaus, C. B. Caputo and D. W. Stephan, *Angew. Chemie Int. Ed.*, 2015, **54**, 10178–10182.
- 59 M. Pérez, L. J. Hounjet, C. B. Caputo, R. Dobrovetsky and D. W. Stephan, *J. Am. Chem. Soc.*, 2013, **135**, 18308–18310.
- 60 C. B. Caputo, L. J. Hounjet, R. Dobrovetsky and D. W. Stephan, *Science*, 2013, **341**, 1374–1377.
- 61 J. Möbus, T. vom Stein and D. W. Stephan, *Chem. Commun.*, 2016, **52**, 6387–6390.
- 62 M. a Dureen and D. W. Stephan, *J. Am. Chem. Soc.*, 2009, **131**, 8396–8397.
- 63 C. M. Mömming, E. Otten, G. Kehr, R. Fröhlich, S. Grimme, D. W. Stephan and G. Erker, *Angew. Chemie Int. Ed.*, 2009, **48**, 6643–6646.
- 64 M. Sajid, A. Klose, B. Birkmann, L. Liang, B. Schirmer, T. Wiegand, H. Eckert, A. J. Lough, R. Fröhlich, C. G. Daniliuc, S. Grimme, D. W. Stephan, G. Kehr and G. Erker, *Chem. Sci.*, 2013, **4**,

- 213–219.
- 65 M. Sajid, G. Kehr, T. Wiegand, H. Eckert, C. Schwickert, R. Pöttgen, A. J. P. Cardenas, T. H. Warren, R. Fröhlich, C. G. Daniliuc and G. Erker, *J. Am. Chem. Soc.*, 2013, **135**, 8882–8895.
- 66 T. Wang, G. Kehr, L. Liu, S. Grimme, C. G. Daniliuc and G. Erker, *J. Am. Chem. Soc.*, 2016, **138**, 4302–4305.
- 67 M. Sajid, L.-M. Elmer, C. Rosorius, C. G. Daniliuc, S. Grimme, G. Kehr and G. Erker, *Angew. Chemie Int. Ed.*, 2013, **52**, 2243–2246.
- 68 P. A. Chase, G. C. Welch, T. Jurca and D. W. Stephan, *Angew. Chemie Int. Ed.*, 2007, **46**, 8050–8053.
- 69 P. A. Chase, T. Jurca and D. W. Stephan, *Chem. Commun.*, 2008, **2**, 1701.
- 70 D. Chen and J. Klankermayer, *Chem. Commun.*, 2008, 2130.
- 71 Z. M. Heiden and D. W. Stephan, *Chem. Commun.*, 2011, **47**, 5729.
- 72 S. J. Geier, P. A. Chase and D. W. Stephan, *Chem. Commun.*, 2010, **46**, 4884.
- 73 T. Mahdi, Z. M. Heiden, S. Grimme and D. W. Stephan, *J. Am. Chem. Soc.*, 2012, **134**, 4088–4091.
- 74 L. E. Longobardi, T. Mahdi and D. W. Stephan, *Dalton Trans.*, 2015, **44**, 7114–7117.
- 75 W. E. Piers, A. J. V. Marwitz and L. G. Mercier, *Inorg. Chem.*, 2011, **50**, 12252–12262.
- 76 J. M. Blackwell, E. R. Sonmor, T. Scoccitti and W. E. Piers, *Org. Lett.*, 2000, **2**, 3921–3923.
- 77 J. M. Blackwell, D. J. Morrison and W. E. Piers, *Tetrahedron*, 2002, **58**, 8247–8254.
- 78 J. M. Blackwell, K. L. Foster, V. H. Beck and W. E. Piers, *J. Org. Chem.*, 1999, **64**, 4887–4892.
- 79 D. Porwal and M. Oestreich, *European J. Org. Chem.*, 2016, **2016**, 3307–3309.

- 80 P.-Q. Huang, Q.-W. Lang and Y.-R. Wang, *J. Org. Chem.*, 2016, **81**, 4235–4243.
- 81 N. Gandhamsetty, J. Jeong, J. Park, S. Park and S. Chang, *J. Org. Chem.*, 2015, **80**, 7281–7287.
- 82 D. J. Parks, J. M. Blackwell and W. E. Piers, *J. Org. Chem.*, 2000, **65**, 3090–3098.
- 83 D. J. Parks, W. E. Piers, M. Parvez, R. Atencio and M. J. Zaworotko, *Organometallics*, 1998, **17**, 1369–1377.
- 84 A. Y. Houghton, J. Hurmalainen, A. Mansikkamäki, W. E. Piers and H. M. Tuononen, *Nat. Chem.*, 2014, **6**, 983–988.
- 85 T. A. Rokob, A. Hamza, A. Stirling, T. Soós and I. Pápai, *Angew. Chemie Int. Ed.*, 2008, **47**, 2435–2438.
- 86 A. Hamza, A. Stirling, T. András Rokob and I. Pápai, *Int. J. Quantum Chem.*, 2009, **109**, 2416–2425.
- 87 T. A. Rokob, I. Bakó, A. Stirling, A. Hamza and I. Pápai, *J. Am. Chem. Soc.*, 2013, **135**, 4425–4437.
- 88 N. Villegas-Escobar, A. Toro-Labbé, M. Becerra, M. Real-Enriquez, J. R. Mora and L. Rincon, *J. Mol. Model.*, 2017, **23**, 234.
- 89 M. Heshmat and T. Privalov, *Chem. - A Eur. J.*, 2017, **23**, 9098–9113.
- 90 B. Schirmer and S. Grimme, *Chem. Commun.*, 2010, **46**, 7942.
- 91 S. Grimme, H. Kruse, L. Goerigk and G. Erker, *Angew. Chemie Int. Ed.*, 2010, **49**, 1402–1405.
- 92 L. Liu, B. Lukose and B. Ensing, *J. Phys. Chem. C*, 2017, **121**, 2046–2051.
- 93 G. Skara, F. De Vleeschouwer, P. Geerlings, F. De Proft and B. Pinter, *Sci. Rep.*, 2017, **7**, 16024.
- 94 K. Sakata and H. Fujimoto, *J. Org. Chem.*, 2013, **78**, 12505–12512.
- 95 M. Heshmat and T. Privalov, *J. Phys. Chem. A*, 2018, **122**, 7202–7211.

- 96 J. Daru, I. Bakó, A. Stirling and I. Pápai, *ACS Catal.*, 2019, **9**, 6049–6057.
- 97 L. Rocchigiani, G. Ciancaleoni, C. Zuccaccia and A. Macchioni, *J. Am. Chem. Soc.*, 2014, **136**, 112–115.
- 98 A. Y. Houghton and T. Autrey, *J. Phys. Chem. A*, 2017, **121**, 8785–8790.
- 99 L. C. Brown, J. M. Hogg, M. Gilmore, L. Moura, S. Imberti, S. Gärtner, H. Q. N. Gunaratne, R. J. O'Donnell, N. Artioli, J. D. Holbrey and M. Swadźba-Kwaśny, *Chem. Commun.*, 2018, **54**, 8689–8692.
- 100 P. Spies, G. Erker, G. Kehr, K. Bergander, R. Fröhlich, S. Grimme and D. W. Stephan, *Chem. Commun.*, 2007, **51**, 5072.
- 101 M. Lindqvist, N. Sarnela, V. Sumerin, K. Chernichenko, M. Leskelä and T. Repo, *Dalton Trans.*, 2012, **41**, 4310.
- 102 L. E. Longobardi, C. Tang and D. W. Stephan, *Dalton Trans.*, 2014, **43**, 15723–15726.
- 103 P. G. Jessop, D. A. Jessop, D. Fu and L. Phan, *Green Chem.*, 2012, **14**, 1245.
- 104 T. Mahdi and D. W. Stephan, *J. Am. Chem. Soc.*, 2014, **136**, 15809–15812.
- 105 D. J. Scott, M. J. Fuchter and A. E. Ashley, *J. Am. Chem. Soc.*, 2014, **136**, 15813–15816.
- 106 T. Mahdi and D. W. Stephan, *Angew. Chemie Int. Ed.*, 2015, **54**, 8511–8514.
- 107 D. J. Scott, T. R. Simmons, E. J. Lawrence, G. G. Wildgoose, M. J. Fuchter and A. E. Ashley, *ACS Catal.*, 2015, **5**, 5540–5544.
- 108 D. J. Scott, M. J. Fuchter and A. E. Ashley, *Angew. Chemie Int. Ed.*, 2014, **53**, 10218–10222.
- 109 G. Erős, H. Mehdi, I. Pápai, T. A. Rokob, P. Király, G. Tárkányi and T. Soós, *Angew. Chemie Int. Ed.*, 2010, **49**, 6559–6563.
- 110 G. Erős, K. Nagy, H. Mehdi, I. Pápai, P. Nagy, P. Király, G. Tárkányi and T. Soós, *Chem. - A Eur. J.*,

- 2012, **18**, 574–585.
- 111 Á. Gyömöre, M. Bakos, T. Földes, I. Pápai, A. Domján and T. Soós, *ACS Catal.*, 2015, **5**, 5366–5372.
- 112 M. Bakos, Á. Gyömöre, A. Domján and T. Soós, *Angew. Chemie Int. Ed.*, 2017, **56**, 5217–5221.
- 113 É. Dorkó, M. Szabó, B. Kótai, I. Pápai, A. Domján and T. Soós, *Angew. Chemie Int. Ed.*, 2017, **56**, 9512–9516.
- 114 L. J. Hounjet, C. Bannwarth, C. N. Garon, C. B. Caputo, S. Grimme and D. W. Stephan, *Angew. Chemie Int. Ed.*, 2013, **52**, 7492–7495.
- 115 J. Paradies, *Angew. Chemie Int. Ed.*, 2014, **53**, 3552–3557.
- 116 L. Greb, P. Oña-Burgos, B. Schirmer, S. Grimme, D. W. Stephan and J. Paradies, *Angew. Chemie Int. Ed.*, 2012, **51**, 10164–10168.
- 117 Y. Segawa and D. W. Stephan, *Chem. Commun.*, 2012, **48**, 11963.
- 118 K. Chernichenko, Á. Madarász, I. Pápai, M. Nieger, M. Leskelä and T. Repo, *Nat. Chem.*, 2013, **5**, 718–723.
- 119 M.-A. Legare, M.-A. Courtemanche, E. Rochette and F.-G. Fontaine, *Science*, 2015, **349**, 513–516.
- 120 M.-A. Légaré, É. Rochette, J. Légaré Lavergne, N. Bouchard and F.-G. Fontaine, *Chem. Commun.*, 2016, **52**, 5387–5390.
- 121 J. Légaré Lavergne, A. Jayaraman, L. C. Misal Castro, É. Rochette and F.-G. Fontaine, *J. Am. Chem. Soc.*, 2017, **139**, 14714–14723.
- 122 F.-G. Fontaine, M.-A. Courtemanche, M.-A. Légaré and É. Rochette, *Coord. Chem. Rev.*, 2017, **334**, 124–135.

- 123 L. Greb, C.-G. Daniliuc, K. Bergander and J. Paradies, *Angew. Chemie Int. Ed.*, 2013, **52**, 5876–5879.
- 124 D. J. Parks and W. E. Piers, *J. Am. Chem. Soc.*, 1996, **118**, 9440–9441.
- 125 L. Süsse, J. Hermeke and M. Oestreich, *J. Am. Chem. Soc.*, 2016, **138**, 6940–6943.
- 126 S. Rendler and M. Oestreich, *Angew. Chemie Int. Ed.*, 2008, **47**, 5997–6000.
- 127 D. T. Hog and M. Oestreich, *European J. Org. Chem.*, 2009, **2009**, 5047–5056.
- 128 M. Mewald, R. Fröhlich and M. Oestreich, *Chem. - A Eur. J.*, 2011, **17**, 9406–9414.
- 129 M. Mewald and M. Oestreich, *Chem. - A Eur. J.*, 2012, **18**, 14079–14084.
- 130 J. Hermeke, M. Mewald and M. Oestreich, *J. Am. Chem. Soc.*, 2013, **135**, 17537–17546.
- 131 C. A. Willoughby and S. L. Buchwald, *J. Am. Chem. Soc.*, 1994, **116**, 11703–11714.
- 132 N. E. Lee and S. L. Buchwald, *J. Am. Chem. Soc.*, 1994, **116**, 5985–5986.
- 133 N. Arai, N. Utsumi, Y. Matsumoto, K. Murata, K. Tsutsumi and T. Ohkuma, *Adv. Synth. Catal.*, 2012, **354**, 2089–2095.
- 134 P. Schnider, G. Koch, R. Prétôt, G. Wang, F. M. Bohnen, C. Krüger and A. Pfaltz, *Chem. - A Eur. J.*, 1997, **3**, 887–892.
- 135 C. Wang, X. Wu, L. Zhou and J. Sun, *Chem. - A Eur. J.*, 2008, **14**, 8789–8792.
- 136 S. Guizzetti, M. Benaglia, F. Cozzi and R. Annunziata, *Tetrahedron*, 2009, **65**, 6354–6363.
- 137 S. Guizzetti, M. Benaglia and G. Celentano, *European J. Org. Chem.*, 2009, **2009**, 3683–3687.
- 138 V. N. Wakchaure, P. S. J. Kaib, M. Leutzsch and B. List, *Angew. Chemie Int. Ed.*, 2015, **54**, 11852–11856.
- 139 C. Wang, X. Wu, L. Zhou and J. Sun, *Org. Biomol. Chem.*, 2015, **13**, 577–582.

- 140 D. Kong, M. Li, G. Zi, G. Hou and Y. He, *J. Org. Chem.*, 2016, **81**, 6640–6648.
- 141 D. Brenna, R. Porta, E. Massolo, L. Raimondi and M. Benaglia, *ChemCatChem*, 2017, **9**, 941–945.
- 142 P. Renzi, J. Hioe and R. M. Gschwind, *J. Am. Chem. Soc.*, 2017, **139**, 6752–6760.
- 143 D. Chen, Y. Wang and J. Klankermayer, *Angew. Chemie Int. Ed.*, 2010, **49**, 9475–9478.
- 144 D. Chen, V. Leich, F. Pan and J. Klankermayer, *Chem. - A Eur. J.*, 2012, **18**, 5184–5187.
- 145 G. Ghattas, D. Chen, F. Pan and J. Klankermayer, *Dalton Trans.*, 2012, **41**, 9026.
- 146 V. Sumerin, K. Chernichenko, M. Nieger, M. Leskelä, B. Rieger and T. Repo, *Adv. Synth. Catal.*, 2011, **353**, 2093–2110.
- 147 M. Lindqvist, K. Borre, K. Axenov, B. Kótai, M. Nieger, M. Leskelä, I. Pápai and T. Repo, *J. Am. Chem. Soc.*, 2015, **137**, 4038–4041.
- 148 Y. Liu and H. Du, *J. Am. Chem. Soc.*, 2013, **135**, 6810–6813.
- 149 X. Zhu and H. Du, *Org. Biomol. Chem.*, 2015, **13**, 1013–1016.
- 150 X. Liu, T. Liu, W. Meng and H. Du, *Org. Biomol. Chem.*, 2018, **16**, 8686–8689.
- 151 S. Wei and H. Du, *J. Am. Chem. Soc.*, 2014, **136**, 12261–12264.
- 152 X. Ren, G. Li, S. Wei and H. Du, *Org. Lett.*, 2015, **17**, 990–993.
- 153 X. Ren and H. Du, *J. Am. Chem. Soc.*, 2016, **138**, 810–813.
- 154 X. Liu, Q. Wang, C. Han, X. Feng and H. Du, *Chinese J. Chem.*, 2019, **37**, 663–666.
- 155 S. Wei, X. Feng and H. Du, *Org. Biomol. Chem.*, 2016, **14**, 8026–8029.
- 156 W. Wang, X. Feng and H. Du, *Org. Biomol. Chem.*, 2016, **14**, 6683–6686.
- 157 Z. Zhang and H. Du, *Angew. Chemie Int. Ed.*, 2015, **54**, 623–626.

- 158 Z. Zhang and H. Du, *Org. Lett.*, 2015, **17**, 2816–2819.
- 159 Z. Zhang and H. Du, *Org. Lett.*, 2015, **17**, 6266–6269.
- 160 X. Tu, N. Zeng, R. Li, Y. Zhao, D. Xie, Q. Peng and X. Wang, *Angew. Chemie Int. Ed.*, 2018, **57**, 15096–15100.
- 161 X. Li, J. Tian, N. Liu, X. Tu, N. Zeng and X. Wang, *Angew. Chemie Int. Ed.*, 2019, **58**, 4664–4668.
- 162 K.-Y. Ye, X. Wang, C. G. Daniliuc, G. Kehr and G. Erker, *Eur. J. Inorg. Chem.*, 2017, **2017**, 368–371.
- 163 D. J. Parks, R. E. von H. Spence and W. E. Piers, *Angew. Chemie Int. Ed. English*, 1995, **34**, 809–811.
- 164 D. J. Parks, W. E. Piers and G. P. A. Yap, *Organometallics*, 1998, **17**, 5492–5503.
- 165 D. M. Mercea, M. G. Howlett, A. D. Piascik, D. J. Scott, A. Steven, A. E. Ashley and M. J. Fuchter, *Chem. Commun.*, 2019, **55**, 7077–7080.
- 166 P. Koelle and H. Nöth, *Chem. Rev.*, 1985, **85**, 399–418.
- 167 W. E. Piers, S. C. Bourke and K. D. Conroy, *Angew. Chemie Int. Ed.*, 2005, **44**, 5016–5036.
- 168 T. S. De Vries, A. Prokofjevs and E. Vedejs, *Chem. Rev.*, 2012, **112**, 4246–4282.
- 169 J. M. Farrell, J. A. Hatnean and D. W. Stephan, *J. Am. Chem. Soc.*, 2012, **134**, 15728–15731.
- 170 C. K. Narula and H. Nöth, *Inorg. Chem.*, 1984, **23**, 4147–4152.
- 171 C. K. Narula and H. Nöth, *J. Chem. Soc., Chem. Commun.*, 1984, 1023–1024.
- 172 E. J. Corey, T. Shibata and T. W. Lee, *J. Am. Chem. Soc.*, 2002, **124**, 3808–3809.
- 173 E. J. Corey, *Angew. Chemie Int. Ed.*, 2009, **48**, 2100–2117.
- 174 M. A. Dureen, A. Lough, T. M. Gilbert and D. W. Stephan, *Chem. Commun.*, 2008, **913**, 4303.

- 175 I. Krossing and I. Raabe, *Angew. Chemie Int. Ed.*, 2004, **43**, 2066–2090.
- 176 L. Weber, E. Dobbert, H.-G. Stammler, B. Neumann, R. Boese and D. Bläser, *Chem. Ber.*, 1997, **130**, 705–710.
- 177 T. Matsumoto and F. P. Gabbaï, *Organometallics*, 2009, **28**, 4252–4253.
- 178 D. McArthur, C. P. Butts and D. M. Lindsay, *Chem. Commun.*, 2011, **47**, 6650.
- 179 M. Valentini, H. Rügger and P. S. Pregosin, *Helv. Chim. Acta*, 2001, **84**, 2833–2853.
- 180 A. Prokofjevs and E. Vedejs, *J. Am. Chem. Soc.*, 2011, **133**, 20056–20059.
- 181 A. Del Grosso, P. J. Singleton, C. A. Muryn and M. J. Ingleson, *Angew. Chemie Int. Ed.*, 2011, **50**, 2102–2106.
- 182 A. Del Grosso, M. D. Helm, S. A. Solomon, D. Caras-Quintero and M. J. Ingleson, *Chem. Commun.*, 2011, **47**, 12459.
- 183 A. Prokofjevs, A. Boussonnière, L. Li, H. Bonin, E. Lacôte, D. P. Curran and E. Vedejs, *J. Am. Chem. Soc.*, 2012, **134**, 12281–12288.
- 184 P. Eisenberger, A. M. Bailey and C. M. Crudden, *J. Am. Chem. Soc.*, 2012, **134**, 17384–17387.
- 185 M. Horn, H. Mayr, E. Lacôte, E. Merling, J. Deaner, S. Wells, T. McFadden and D. P. Curran, *Org. Lett.*, 2012, **14**, 82–85.
- 186 D. P. Curran, A. Solovyev, M. Makhlof Brahmî, L. Fensterbank, M. Malacria and E. Lacôte, *Angew. Chemie Int. Ed.*, 2011, **50**, 10294–10317.
- 187 P. Eisenberger, B. P. Bestvater, E. C. Keske and C. M. Crudden, *Angew. Chemie Int. Ed.*, 2015, **54**, 2467–2471.
- 188 J. M. Farrell, R. T. Posaratnanathan and D. W. Stephan, *Chem. Sci.*, 2015, **6**, 2010–2015.
- 189 B. S. N. Huchenski, M. R. Adams, R. McDonald, M. J. Ferguson and A. W. H. Speed,

- Organometallics*, 2016, **35**, 3101–3104.
- 190 B. S. N. Huchenski, C. J. Christopherson, K. N. Robertson and A. W. H. Speed, *Org. Biomol. Chem.*, 2019, **17**, 6158–6164.
- 191 T. Liu, L. Chen and Z. Sun, *J. Org. Chem.*, 2015, **80**, 11441–11446.
- 192 J. E. Radcliffe, V. Fasano, R. W. Adams, P. You and M. J. Ingleson, *Chem. Sci.*, 2019, **10**, 1434–1441.
- 193 D. M. Lindsay and D. McArthur, *Chem. Commun.*, 2010, **46**, 2474.
- 194 F. Glorius, G. Altenhoff, R. Goddard and C. Lehmann, *Chem. Commun.*, 2002, 2704–2705.
- 195 G. Altenhoff, R. Goddard, C. W. Lehmann and F. Glorius, *J. Am. Chem. Soc.*, 2004, **126**, 15195–15201.
- 196 G. Altenhoff, R. Goddard, C. W. Lehmann and F. Glorius, *Angew. Chemie Int. Ed.*, 2003, **42**, 3690–3693.
- 197 C. Fliedel, A. Labande, E. Manoury and R. Poli, *Coord. Chem. Rev.*, 2019, **394**, 65–103.
- 198 M. N. Hopkinson, C. Richter, M. Schedler and F. Glorius, *Nature*, 2014, **510**, 485–496.
- 199 D. C. H. Do, S. Muthaiah, R. Ganguly and D. Vidović, *Organometallics*, 2014, **33**, 4165–4168.
- 200 H. Clavier and S. P. Nolan, *Chem. Commun.*, 2010, **46**, 841.
- 201 A. Poater, B. Cosenza, A. Correa, S. Giudice, F. Ragone, V. Scarano and L. Cavallo, *Eur. J. Inorg. Chem.*, 2009, **2009**, 1759–1766.
- 202 K. J. Iversen, D. J. D. Wilson and J. L. Dutton, *Dalton Trans.*, 2015, **44**, 3318–3325.
- 203 F. Glorius, 2004, patent *WO 2004/007465 A1*.
- 204 J.-N. Levy, C. M. Latham, L. Roisin, N. Kandziora, P. Di Fruscia, A. J. P. White, S. Woodward and M. J. Fuchter, *Org. Biomol. Chem.*, 2012, **10**, 512–515.

- 205 M. J. McKennon, A. I. Meyers, K. Drauz and M. Schwarm, *J. Org. Chem.*, 1993, **58**, 3568–3571.
- 206 S. E. Denmark, R. A. Stavenger, A.-M. Faucher and J. P. Edwards, *J. Org. Chem.*, 1997, **62**, 3375–3389.
- 207 L. Delaude, M. Szypa, A. Demonceau and A. F. Noels, *Adv. Synth. Catal.*, 2002, **344**, 749.
- 208 S. Leuthäuser, D. Schwarz and H. Plenio, *Chem. - A Eur. J.*, 2007, **13**, 7195–7203.
- 209 L. Hintermann, *Beilstein J. Org. Chem.*, 2007, **3**, 22.
- 210 S. Würtz, C. Lohre, R. Fröhlich, K. Bergander and F. Glorius, *J. Am. Chem. Soc.*, 2009, **131**, 8344–8345.
- 211 I. Krossing, *Chem - Eur. J.*, 2001, **7**, 490–502.
- 212 J. Lam, B. A. R. Günther, J. M. Farrell, P. Eisenberger, B. P. Bestvater, P. D. Newman, R. L. Melen, C. M. Crudden and D. W. Stephan, *Dalton Trans.*, 2016, **45**, 15303–15316.
- 213 J. Chen, R. A. Lalancette and F. Jäkle, *Chem. Commun.*, 2013, **49**, 4893.
- 214 U. Mayer, V. Gutmann and W. Gerger, *Monatsh. Chem.*, 1975, **106**, 1235–1257.
- 215 M. A. Beckett, G. C. Strickland, J. R. Holland and K. Sukumar Varma, *Polymer*, 1996, **37**, 4629–4631.
- 216 G. C. Welch, L. Cabrera, P. A. Chase, E. Hollink, J. D. Masuda, P. Wei and D. W. Stephan, *Dalton Trans.*, 2007, **9226**, 3407.
- 217 M. a Beckett, D. S. Brassington, S. J. Coles and M. B. Hursthouse, *Inorg. Chem. Commun.*, 2000, **3**, 530–533.
- 218 G. J. P. Britovsek, J. Ugoletti and A. J. P. White, *Organometallics*, 2005, **24**, 1685–1691.
- 219 A. E. Ashley, T. J. Herrington, G. G. Wildgoose, H. Zaher, A. L. Thompson, N. H. Rees, T. Krämer and D. O'Hare, *J. Am. Chem. Soc.*, 2011, **133**, 14727–14740.

- 220 R. J. Blagg, T. R. Simmons, G. R. Hatton, J. M. Courtney, E. L. Bennett, E. J. Lawrence and G. G. Wildgoose, *Dalton Trans.*, 2016, **45**, 6032–6043.
- 221 T. Li, A. J. Lough and R. H. Morris, *Chem. - A Eur. J.*, 2007, **13**, 3796–3803.
- 222 J. M. Blackwell, W. E. Piers, M. Parvez and R. McDonald, *Organometallics*, 2002, **21**, 1400–1407.
- 223 J. M. Farrell and D. W. Stephan, *Chem. Commun.*, 2015, **51**, 14322–14325.
- 224 R. Köster, W. Schüßler, R. Boese, M. Herberhold, S. Gerstmann and B. Wrackmeyer, *Chem. Ber.*, 1996, **129**, 503–507.
- 225 S. K. Hall and E. A. Robinson, *Can. J. Chem.*, 1964, **42**, 1113–1122.
- 226 T. R. O'Toole, J. N. Younathan, B. P. Sullivan and T. J. Meyer, *Inorg. Chem.*, 1989, **28**, 3923–3926.
- 227 A. J. Cruz-Cabeza and F. H. Allen, *Acta Crystallogr. Sect. B Struct. Sci.*, 2012, **68**, 182–188.
- 228 J. M. Kanabus-Kaminska, J. A. Hawari, D. Griller and C. Chatgililoglu, *J. Am. Chem. Soc.*, 1987, **109**, 5267–5268.
- 229 S. Keess, A. Simonneau and M. Oestreich, *Organometallics*, 2015, **34**, 790–799.
- 230 C. Wang, C. Li, X. Wu, A. Pettman and J. Xiao, *Angew. Chemie Int. Ed.*, 2009, **48**, 6524–6528.
- 231 C. D. F. Königs, H. F. T. Klare, Y. Ohki, K. Tatsumi and M. Oestreich, *Org. Lett.*, 2012, **14**, 2842–2845.
- 232 J. Mohr and M. Oestreich, *Angew. Chemie Int. Ed.*, 2014, **53**, 13278–13281.
- 233 J. Mohr, D. Porwal, I. Chatterjee and M. Oestreich, *Chem. - A Eur. J.*, 2015, **21**, 17583–17586.
- 234 M. Frutos, M. G. Avello, A. Viso, R. Fernández de la Pradilla, M. C. de la Torre, M. A. Sierra, H. Gornitzka and C. Hemmert, *Org. Lett.*, 2016, **18**, 3570–3573.
- 235 J. M. Aizpurua, M. Sagartzazu-Aizpurua, Z. Monasterio, I. Azcune, C. Mendicute, J. I. Miranda,

- E. García-Lecina, A. Altube and R. M. Fratila, *Org. Lett.*, 2012, **14**, 1866–1868.
- 236 T. Karthikeyan and S. Sankararaman, *Tetrahedron Lett.*, 2009, **50**, 5834–5837.
- 237 C. G. Arnold, S. B. Haderlein, R. P. Schwarzenbach, A. Weidenhaupt, M. M. David and S. R. Muller, *Environ. Sci. Technol.*, 1997, **31**, 2596–2602.
- 238 G. R. Whittell, E. I. Balmond, A. P. M. Robertson, S. K. Patra, M. F. Haddow and I. Manners, *Eur. J. Inorg. Chem.*, 2010, **2010**, 3967–3975.
- 239 J. S. Sapsford, D. J. Scott, N. J. Allcock, M. J. Fuchter, C. J. Tighe and A. E. Ashley, *Adv. Synth. Catal.*, 2018, **360**, 1066–1071.
- 240 R. T. Cooper, J. S. Sapsford, R. C. Turnell-Ritson, D.-H. Hyon, A. J. P. White and A. E. Ashley, *Philos. Trans. R. Soc. A Math. Phys. Eng. Sci.*, 2017, **375**, 20170008.
- 241 S. Das and S. K. Pati, *Catal. Sci. Technol.*, 2018, **8**, 5178–5189.
- 242 S. Das, S. Mondal and S. K. Pati, *Chem. - A Eur. J.*, 2018, **24**, 2575–2579.
- 243 M. Gielen, *Pure Appl. Chem.*, 1980, **52**, 657–667.
- 244 M. Gielen and Y. Tondeur, *J. Organomet. Chem.*, 1977, **127**, C75–C77.
- 245 M. Gielen and Y. Tondeur, *J. Organomet. Chem.*, 1979, **169**, 265–281.
- 246 M. Gielen and H. Mokhtar-Jamai, *J. Organomet. Chem.*, 1977, **129**, 325–330.
- 247 G. Van Koten, J. T. B. H. Jastrzebski, J. G. Noltes, W. M. G. F. Pontenagel, J. Kroon and A. L. Spek, *J. Am. Chem. Soc.*, 1978, **100**, 5021–5028.
- 248 R. S. Berry, *J. Chem. Phys.*, 1960, **32**, 933–938.
- 249 H. Schumann and B. C. Wassermann, *J. Organomet. Chem.*, 1989, **365**, C1–C5.
- 250 H. Schumann, B. C. Wassermann and J. Pickardt, *Organometallics*, 1993, **12**, 3051–3063.

- 251 J. C. Podesta and G. E. Radivoy, *Organometallics*, 1994, **13**, 3364–3365.
- 252 J. C. Podestá, A. B. Chopa, G. E. Radivoy and C. A. Vitale, *J. Organomet. Chem.*, 1995, **494**, 11–16.
- 253 C. Lucas, C. C. Santini, M. Prinz, M.-A. Cordonnier, J.-M. Basset, M.-F. Connil and B. Jousseau, *J. Organomet. Chem.*, 1996, **520**, 101–106.
- 254 D. Nanni and D. P. Curran, *Tetrahedron: Asymmetry*, 1996, **7**, 2417–2422.
- 255 K. Schwarzkopf, M. Blumenstein, A. Hayen and J. O. Metzger, *European J. Org. Chem.*, 1998, **1998**, 177–181.
- 256 V. T. Perchyonok and C. H. Schiesser, *Phosphorus. Sulfur. Silicon Relat. Elem.*, 1999, **150**, 193–199.
- 257 D. Dakternieks, K. Dunn, V. Tamara Perchyonok and C. H. Schiesser, *Chem. Commun.*, 1999, 1665–1666.
- 258 D. Dakternieks, V. T. Perchyonok and C. H. Schiesser, *Tetrahedron: Asymmetry*, 2003, **14**, 3057–3068.
- 259 D. Dakternieks, D. J. Henry and C. H. Schiesser, *J. Chem. Soc. Perkin Trans. 2*, 1998, **1**, 591–602.
- 260 M. Blumenstein, M. Lemmler, A. Hayen and J. O. Metzger, *Tetrahedron: Asymmetry*, 2003, **14**, 3069–3077.
- 261 M. B. Faraoni, A. D. Ayala, V. Vetere, M. L. Casella, O. A. Ferretti and J. C. Podestá, *Appl. Organomet. Chem.*, 2005, **19**, 465–472.
- 262 V. Vetere, M. B. Faraoni, J. C. Podestá and M. L. Casella, *Appl. Catal. A Gen.*, 2012, **445–446**, 209–214.
- 263 T. Oriyama and T. Mukaiyama, *Chem. Lett.*, 1984, **13**, 2071–2074.

- 264 N. J. Lawrence and S. M. Bushell, *Tetrahedron Lett.*, 2000, **41**, 4507–4512.
- 265 R. Krishnamurti and H. G. Kuivila, *J. Org. Chem.*, 1986, **51**, 4947–4953.
- 266 J. Otera, K. Sakamoto, T. Tsukamoto and A. Orita, *Tetrahedron Lett.*, 1998, **39**, 3201–3204.
- 267 F. Iwasaki, T. Maki, W. Nakashima, O. Onomura and Y. Matsumura, *Org. Lett.*, 1999, **1**, 969–972.
- 268 F. Iwasaki, T. Maki, O. Onomura, W. Nakashima and Y. Matsumura, *J. Org. Chem.*, 2000, **65**, 996–1002.
- 269 T. Hoshi, H. Shionoiri, M. Katano, T. Suzuki, M. Ando and H. Hagiwara, *Chem. Lett.*, 2002, **31**, 600–601.
- 270 D. Dakternieks, K. Dunn, C. H. Schiesser and E. R. T. Tiekink, *J. Chem. Soc. Dalton Trans.*, 2000, 3693–3698.
- 271 J.-D. Lee, H.-S. Kim, W.-S. Han and S. O. Kang, *J. Organomet. Chem.*, 2010, **695**, 463–468.
- 272 A. C. Tagne Kuate, R. A. Lalancette and F. Jäkle, *Dalton Trans.*, 2017, **46**, 6253–6264.
- 273 G. S. Sasin, A. L. Borrer and R. Sasin, *J. Org. Chem.*, 1958, **23**, 1366–1367.
- 274 J. G. Smith and G. F. Wright, *J. Org. Chem.*, 1952, **17**, 1116–1121.
- 275 P. Roszkowski, J. K. Maurin and Z. Czarnocki, *Tetrahedron Lett.*, 2018, **59**, 2184–2188.
- 276 D. Mondal, S. Y. Li, L. Bellucci, T. Laino, A. Tafi, S. Guccione and S. D. Lepore, *J. Org. Chem.*, 2013, **78**, 2118–2127.
- 277 M. Tanaka and I. Ogata, *Bull. Chem. Soc. Jpn.*, 1975, **48**, 1094–1094.
- 278 D. E. Pearson, D. Cowan and J. D. Beckler, *J. Org. Chem.*, 1959, **24**, 504–509.
- 279 H. M. Walborsky and A. E. Young, *J. Am. Chem. Soc.*, 1964, **86**, 3288–3296.

- 280 D. Dakternieks, K. Dunn, D. J. Henry, C. H. Schiesser and E. R. T. Tiekink, *Organometallics*, 1999, **18**, 3342–3347.
- 281 J. Klein, S. Neels and R. Borsdorf, *J. Chem. Soc. Perkin Trans. 2*, 1994, 2523.
- 282 A. C. Cope, *J. Am. Chem. Soc.*, 1935, **57**, 2238–2240.
- 283 H. W. H. J. Bodewitz, C. Blomberg and F. Bickelhaupt, *Tetrahedron*, 1973, **29**, 719–726.
- 284 H. W. H. J. Bodewitz, C. Blomberg and F. Bickelhaupt, *Tetrahedron*, 1975, **31**, 1053–1063.
- 285 H. W. H. J. Bodewitz, C. Blomberg and F. Bickelhaupt, *Tetrahedron Lett.*, 1975, 2003–2006.
- 286 H. W. J. J. Bodewitz, B. J. Schaart, J. D. Van Der Niet, C. Blomberg, F. Bickelhaupt and J. A. Den Hollander, *Tetrahedron*, 1978, **34**, 2523–2527.
- 287 H. W. H. J. Bodewitz, C. Blomberg and F. Bickelhaupt, *Tetrahedron Lett.*, 1972, 281–284.
- 288 C. Blomberg and F. A. Hartog, *Synthesis*, 1977, **1**, 18–30.
- 289 J.-C. Lahournère and J. Valade, *J. Organomet. Chem.*, 1970, **22**, C3–C4.
- 290 G. F. Smith, H. G. Kuivila, R. Simon and L. Sultan, *J. Am. Chem. Soc.*, 1981, **103**, 833–839.
- 291 D. C. McWilliam and P. R. Wells, *J. Organomet. Chem.*, 1975, **85**, 165–172.
- 292 C. Wang, C. Li, X. Wu, A. Pettman and J. Xiao, *Angew. Chemie Int. Ed.*, 2009, **48**, 6524–6528.
- 293 W. H. Glaze and C. M. Selman, *J. Org. Chem.*, 1968, **33**, 1987–1990.
- 294 D. C. McWilliam and P. R. Wells, *J. Organomet. Chem.*, 1975, **85**, 335–346.
- 295 M. J. Cuthbertson and P. R. Wells, *J. Organomet. Chem.*, 1981, **216**, 331–348.
- 296 V. Y. Lee, A. A. Basova, I. A. Matchkarovskaya, V. I. Faustov, M. P. Egorov, O. M. Nefedov, R. D. Rakhimov and K. P. Butin, *J. Organomet. Chem.*, 1995, **499**, 27–34.
- 297 D. P. Arnold and P. R. Wells, *J. Organomet. Chem.*, 1976, **108**, 345–352.

- 298 T. Birchall and J. P. Johnson, *Can. J. Chem.*, 1979, **57**, 160–166.
- 299 M. J. Cuthbertson, D. W. Hawker and P. R. Wells, *J. Organomet. Chem.*, 1985, **287**, 7–23.
- 300 I. Zharov, B. T. King, Z. Havlas, A. Pardi and J. Michl, *J. Am. Chem. Soc.*, 2000, **122**, 10253–10254.
- 301 D. Farah, K. Swami and H. G. Kuivila, *J. Organomet. Chem.*, 1992, **429**, 311–334.
- 302 N. G. Connelly and W. E. Geiger, *Chem. Rev.*, 1996, **96**, 877–910.
- 303 H. H. Anderson, *Inorg. Chem.*, 1964, **3**, 108–109.
- 304 P. A. Yeats, B. F. E. Ford, J. R. Sams and F. Aubke, *J. Chem. Soc. D*, 1969, 791–793.
- 305 P. A. Yeats, J. R. Sams and F. Aubke, *Inorg. Chem.*, 1972, **11**, 2634–2641.
- 306 J. Holeček, M. Nádvorník, K. Handlíř and A. Lyčka, *J. Organomet. Chem.*, 1986, **315**, 299–308.
- 307 J. Holeček, M. Nádvorník, K. Handlíř and A. Lyčka, *J. Organomet. Chem.*, 1983, **241**, 177–184.
- 308 M. Nádvorník, J. Holeček, K. Handlíř and A. Lyčka, *J. Organomet. Chem.*, 1984, **275**, 43–51.
- 309 J. Holeček and A. Lyčka, *Inorganica Chim. Acta*, 1986, **118**, L15–L16.
- 310 A. Lyčka, J. Jirman, A. Koloničný and J. Holeček, *J. Organomet. Chem.*, 1987, **333**, 305–315.
- 311 M. Arshadi, D. Johnels and U. Edlund, *Chem. Commun.*, 1996, 1279.
- 312 D. Parmar, E. Sugiono, S. Raja and M. Rueping, *Chem. Rev.*, 2014, **114**, 9047–9153.
- 313 D. W. Stephan, S. Greenberg, T. W. Graham, P. Chase, J. J. Hastie, S. J. Geier, J. M. Farrell, C. C. Brown, Z. M. Heiden, G. C. Welch and M. Ullrich, *Inorg. Chem.*, 2011, **50**, 12338–12348.
- 314 S. Li, G. Li, W. Meng and H. Du, *J. Am. Chem. Soc.*, 2016, **138**, 12956–12962.
- 315 S. Li, W. Meng and H. Du, *Org. Lett.*, 2017, **19**, 2604–2606.
- 316 W. Zhao, X. Feng, J. Yang and H. Du, *Tetrahedron Lett.*, 2019, **60**, 1193–1196.

- 317 Q. Zhou, W. Meng, J. Yang and H. Du, *Angew. Chemie Int. Ed.*, 2018, **57**, 12111–12115.
- 318 F. Ding, Y. Zhang, R. Zhao, Y. Jiang, R. L.-Y. Bao, K. Lin and L. Shi, *Chem. Commun.*, 2017, **53**, 9262–9264.
- 319 T. Akiyama, J. Itoh, K. Yokota and K. Fuchibe, *Angew. Chemie Int. Ed.*, 2004, **43**, 1566–1568.
- 320 T. Akiyama, Y. Saitoh, H. Morita and K. Fuchibe, *Adv. Synth. Catal.*, 2005, **347**, 1523–1526.
- 321 T. Akiyama, H. Morita, J. Itoh and K. Fuchibe, *Org. Lett.*, 2005, **7**, 2583–2585.
- 322 D. Uruguchi and M. Terada, *J. Am. Chem. Soc.*, 2004, **126**, 5356–5357.
- 323 D. Uruguchi, K. Sorimachi and M. Terada, *J. Am. Chem. Soc.*, 2004, **126**, 11804–11805.
- 324 G. B. Rowland, H. Zhang, E. B. Rowland, S. Chennamadhavuni, Y. Wang and J. C. Antilla, *J. Am. Chem. Soc.*, 2005, **127**, 15696–15697.
- 325 M. Rueping, E. Sugiono, C. Azap, T. Theissmann and M. Bolte, *Org. Lett.*, 2005, **7**, 3781–3783.
- 326 S. Hoffmann, A. M. Seayad and B. List, *Angew. Chemie Int. Ed.*, 2005, **44**, 7424–7427.
- 327 R. I. Storer, D. E. Carrera, Y. Ni and D. W. C. MacMillan, *J. Am. Chem. Soc.*, 2006, **128**, 84–86.
- 328 M. Rueping, A. P. Antonchick and T. Theissmann, *Angew. Chemie Int. Ed.*, 2006, **45**, 3683–3686.
- 329 S. Mayer and B. List, *Angew. Chemie Int. Ed.*, 2006, **45**, 4193–4195.
- 330 R. J. Phipps, G. L. Hamilton and F. D. Toste, *Nat. Chem.*, 2012, **4**, 603–614.
- 331 M. Mahlau and B. List, *Angew. Chemie Int. Ed.*, 2013, **52**, 518–533.
- 332 C. Carter, S. Fletcher and A. Nelson, *Tetrahedron: Asymmetry*, 2003, **14**, 1995–2004.
- 333 C. De, R. Mitra and B. List, *Synlett*, 2017, **28**, 2435–2438.
- 334 P. Pommerening, J. Mohr, J. Friebe and M. Oestreich, *European J. Org. Chem.*, 2017, **2017**, 2312–2316.

- 335 M. Melikian, J. Gramüller, J. Hioe, J. Greindl and R. M. Gschwind, *Chem. Sci.*, 2019, **10**, 5226–5234.
- 336 J. Greindl, J. Hioe, N. Sorgenfrei, F. Morana and R. M. Gschwind, *J. Am. Chem. Soc.*, 2016, **138**, 15965–15971.
- 337 M. Fleischmann, D. Drettwan, E. Sugiono, M. Rueping and R. M. Gschwind, *Angew. Chemie Int. Ed.*, 2011, **50**, 6364–6369.
- 338 J. P. Reid, L. Simón and J. M. Goodman, *Acc. Chem. Res.*, 2016, **49**, 1029–1041.
- 339 T. Beringhelli, D. Donghi, D. Maggioni and G. D'Alfonso, *Coord. Chem. Rev.*, 2008, **252**, 2292–2313.
- 340 A. D. Horton and J. de With, *Organometallics*, 1997, **16**, 5424–5436.
- 341 J. M. Blackwell, W. E. Piers and M. Parvez, *Org. Lett.*, 2000, **2**, 695–698.
- 342 A. D. Horton, J. de With, A. J. van der Linden and H. van de Weg, *Organometallics*, 1996, **15**, 2672–2674.
- 343 A. D. Horton and J. de With, *Chem. Commun.*, 1996, 1375.
- 344 C. Bergquist, B. M. Bridgewater, C. J. Harlan, J. R. Norton, R. A. Friesner and G. Parkin, *J. Am. Chem. Soc.*, 2000, **122**, 10581–10590.
- 345 T. Beringhelli, D. Maggioni and G. D'Alfonso, *Organometallics*, 2001, **20**, 4927–4938.
- 346 E. Martin, D. L. Hughes and S. J. Lancaster, *Inorganica Chim. Acta*, 2010, **363**, 275–278.
- 347 M. Hatano, H. Ishihara, Y. Goto and K. Ishihara, *Synlett*, 2015, **27**, 564–570.
- 348 A. Zheng, S.-B. Liu and F. Deng, *Chem. Rev.*, 2017, **117**, 12475–12531.
- 349 K. M. Diemoz and A. K. Franz, *J. Org. Chem.*, 2019, **84**, 1126–1138.
- 350 M. Hatano, K. Moriyama, T. Maki and K. Ishihara, *Angew. Chemie Int. Ed.*, 2010, **49**, 3823–3826.

- 351 P. Renzi, J. Hioe and R. M. Gschwind, *Acc. Chem. Res.*, 2017, **50**, 2936–2948.
- 352 M. Rueping, T. Theissmann, A. Kuenkel and R. M. Koenigs, *Angew. Chemie Int. Ed.*, 2008, **47**, 6798–6801.
- 353 S. Xu, Z. Wang, X. Zhang, X. Zhang and K. Ding, *Angew. Chemie Int. Ed.*, 2008, **47**, 2840–2843.
- 354 M. Klussmann, L. Ratjen, S. Hoffmann, V. Wakchaure, R. Goddard and B. List, *Synlett*, 2010, **2010**, 2189–2192.
- 355 M. Terada and K. Kanomata, *Synlett*, 2011, **2011**, 1255–1258.
- 356 S. K. Nimmagadda, Z. Zhang and J. C. Antilla, *Org. Lett.*, 2014, **16**, 4098–4101.
- 357 G. K. Ingle, Y. Liang, M. G. Mormino, G. Li, F. R. Fronczek and J. C. Antilla, *Org. Lett.*, 2011, **13**, 2054–2057.
- 358 G. K. Ingle, M. G. Mormino, L. Wojtas and J. C. Antilla, *Org. Lett.*, 2011, **13**, 4822–4825.
- 359 G. Ingle, M. G. Mormino and J. C. Antilla, *Org. Lett.*, 2014, **16**, 5548–5551.
- 360 E. J. Lawrence, V. S. Oganessian, D. L. Hughes, A. E. Ashley and G. G. Wildgoose, *J. Am. Chem. Soc.*, 2014, **136**, 6031–6036.
- 361 G. Li and J. C. Antilla, *Org. Lett.*, 2009, **11**, 1075–1078.
- 362 Z. Zhang, P. Jain and J. C. Antilla, *Angew. Chemie Int. Ed.*, 2011, **50**, 10961–10964.
- 363 R. R. Mittapalli, S. J. J. Guesné, R. J. Parker, W. T. Klooster, S. J. Coles, J. Skidmore and A. P. Dobbs, *Org. Lett.*, 2019, **21**, 350–355.
- 364 A. Turočkin, R. Honeker, W. Raven and P. Selig, *J. Org. Chem.*, 2016, **81**, 4516–4529.
- 365 J. Schneekönig, K. Junge and M. Beller, *Synlett*, 2019, **30**, 503–507.
- 366 A. G. De Crisci, K. Chung, A. G. Oliver, D. Solis-Ibarra and R. M. Waymouth, *Organometallics*, 2013, **32**, 2257–2266.

- 367 W.-S. Li, N. Zhang and L. M. Sayre, *Tetrahedron*, 2001, **57**, 4507–4522.
- 368 C.-H. Tien, M. R. Adams, M. J. Ferguson, E. R. Johnson and A. W. H. Speed, *Org. Lett.*, 2017, **19**, 5565–5568.
- 369 Y. Schramm, F. Barrios-Landeros and A. Pfaltz, *Chem. Sci.*, 2013, **4**, 2760.
- 370 P. Cazeau, F. Duboudin, F. Moulines, O. Babot and J. Dunogues, *Tetrahedron*, 1987, **43**, 2075–2088.
- 371 X. Huang, J. Huang, Y. Wen and X. Feng, *Adv. Synth. Catal.*, 2006, **348**, 2579–2584.
- 372 J. Yang, B. Chatelet, F. Ziarelli, V. Dufaud, D. Hérault and A. Martinez, *European J. Org. Chem.*, 2018, **2018**, 6328–6332.
- 373 B. Song, C.-B. Yu, W.-X. Huang, M.-W. Chen and Y.-G. Zhou, *Org. Lett.*, 2015, **17**, 190–193.
- 374 A. Chelouan, R. Recio, L. G. Borrego, E. Álvarez, N. Khiar and I. Fernández, *Org. Lett.*, 2016, **18**, 3258–3261.
- 375 A. V. Malkov, S. Stončius, K. N. MacDougall, A. Mariani, G. D. McGeoch and P. Kočovský, *Tetrahedron*, 2006, **62**, 264–284.
- 376 J. L. Peltier, R. Jazzar, M. Melaimi and G. Bertrand, *Chem. Commun.*, 2016, **52**, 2733–2735.
- 377 V. N. Wakchaure and B. List, *Angew. Chemie Int. Ed.*, 2016, **55**, 15775–15778.
- 378 J. Han, M. Jeon, H. K. Pak, Y. H. Rhee and J. Park, *Adv. Synth. Catal.*, 2014, **356**, 2769–2774.
- 379 F. Ishikawa, Y. Watanabe and J. Saegusa, *Chem. Pharm. Bull.*, 1980, **28**, 1357–1364.
- 380 J. Li, M. J. Lear, Y. Kawamoto, S. Umemiya, A. R. Wong, E. Kwon, I. Sato and Y. Hayashi, *Angew. Chemie Int. Ed.*, 2015, **54**, 12986–12990.

7 Appendix

7.1 Chapter 2

7.1.1 Catalyst synthesis

^1H NMR (CD_2Cl_2)

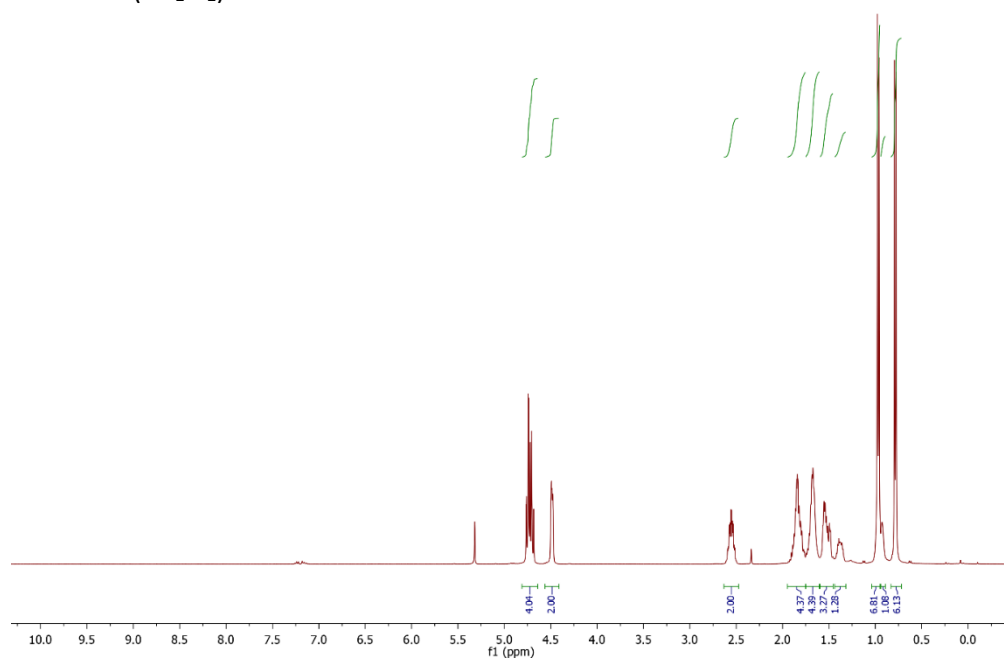


Figure 7.1 ^1H NMR for **92a**

^{13}C NMR (CD_2Cl_2)

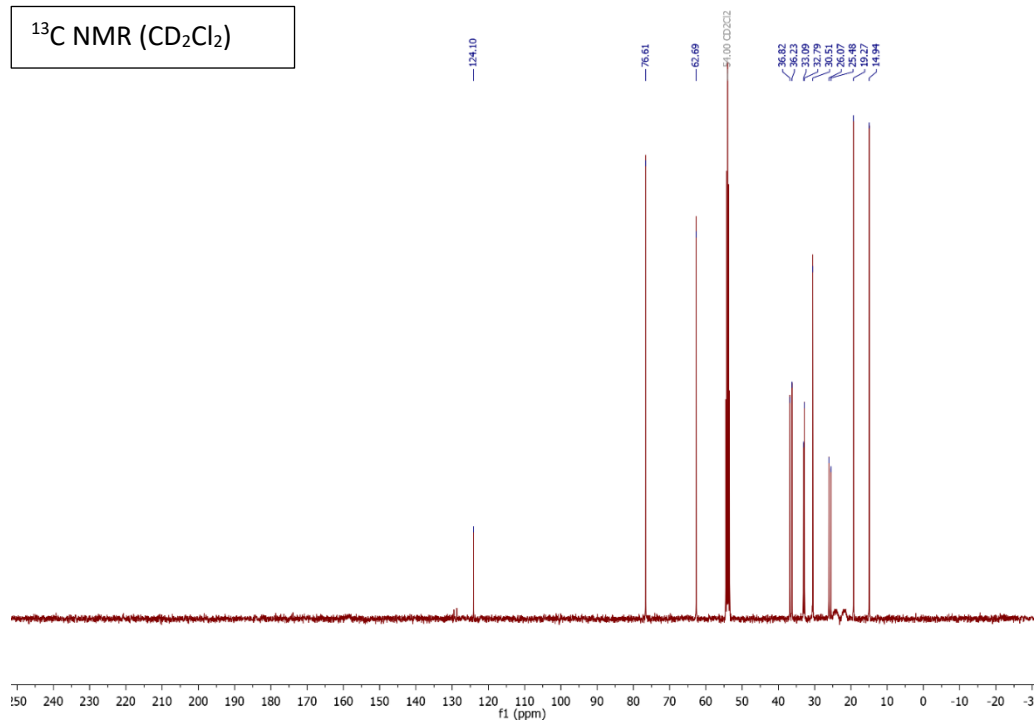


Figure 7.2 ^{13}C NMR **92a**

^{11}B NMR (CD_2Cl_2)

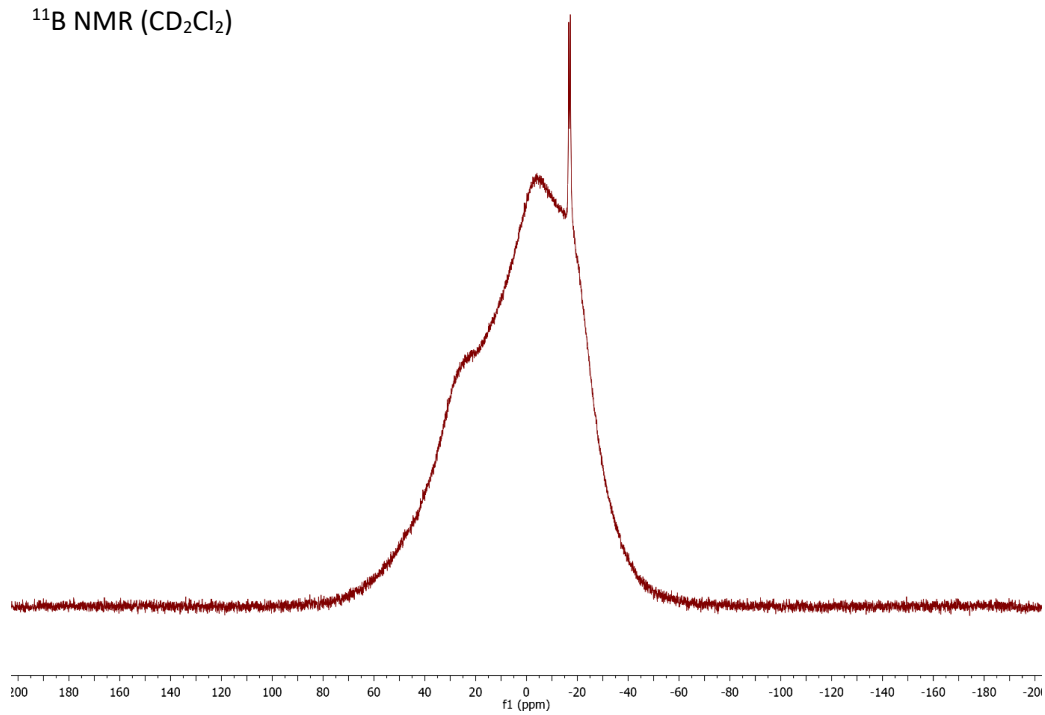


Figure 7.3 ^{11}B NMR for **92a**

^1H NMR (CD_2Cl_2)

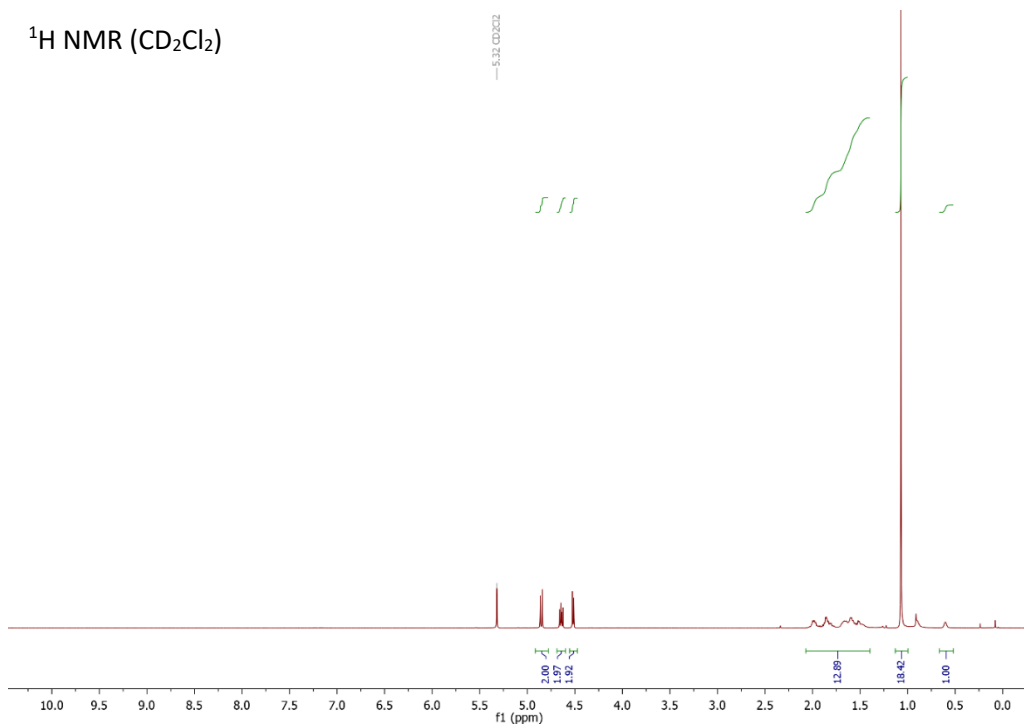


Figure 7.4 ^1H NMR for **92b**

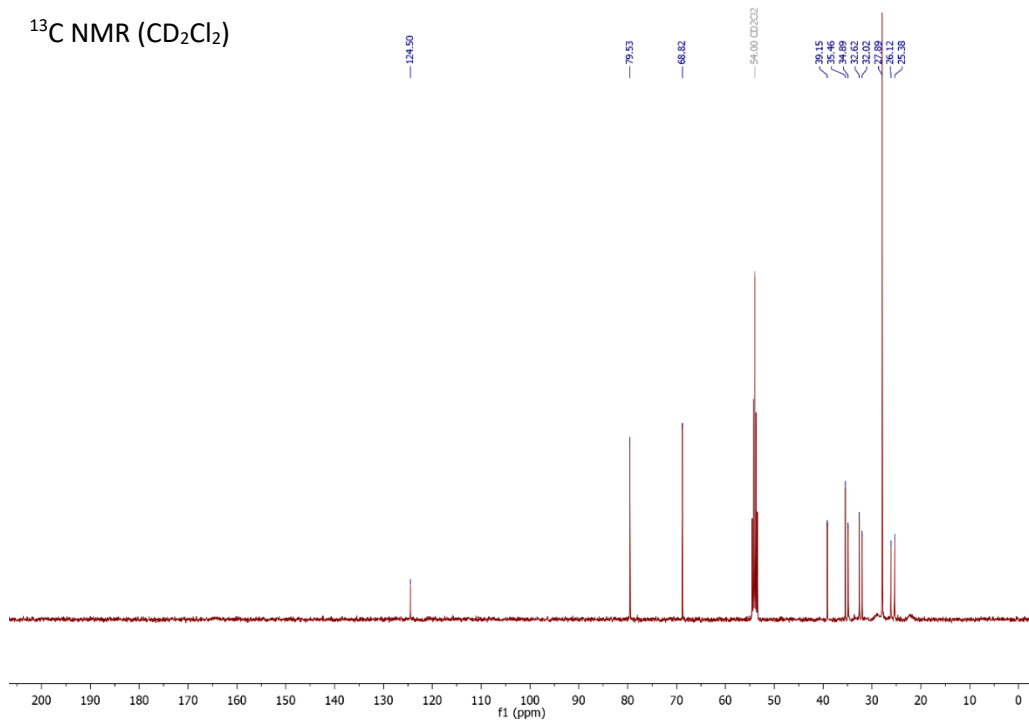


Figure 7.5 ^{13}C NMR for **92b**

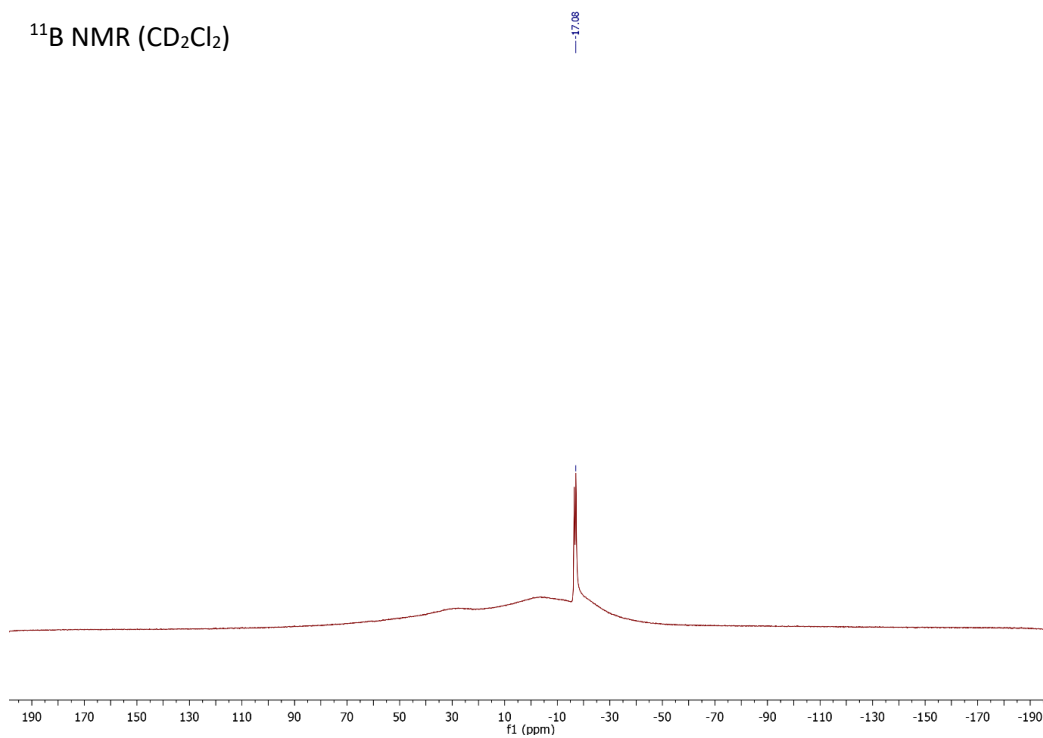


Figure 7.6 ^{11}B NMR for **92b**

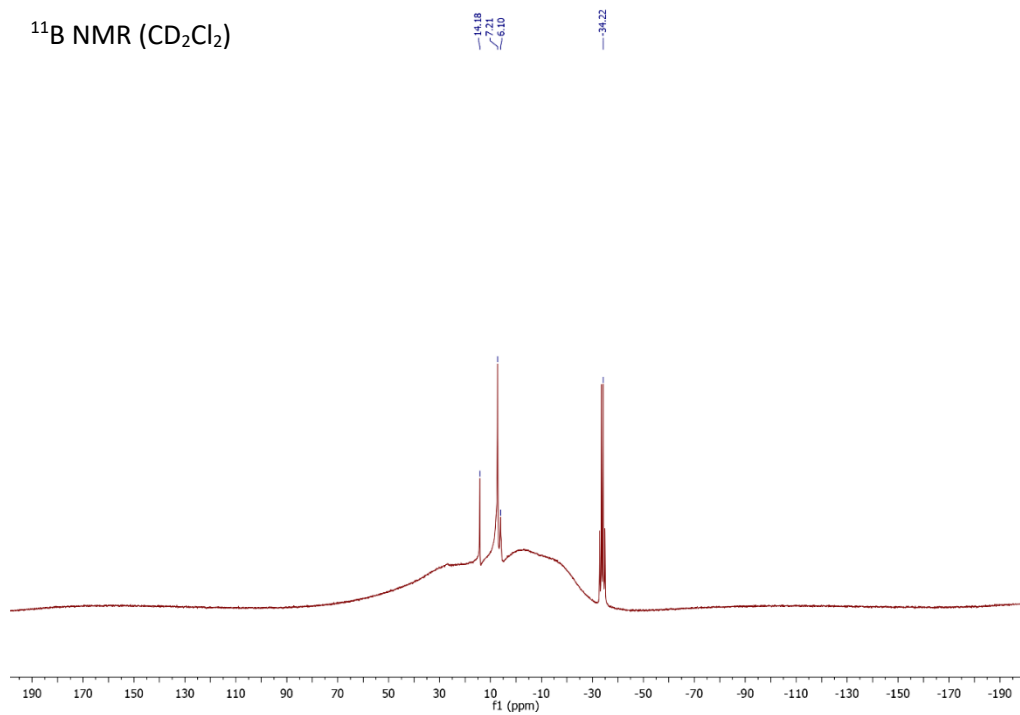


Figure 7.7 Isolated product from attempted formation of **108**

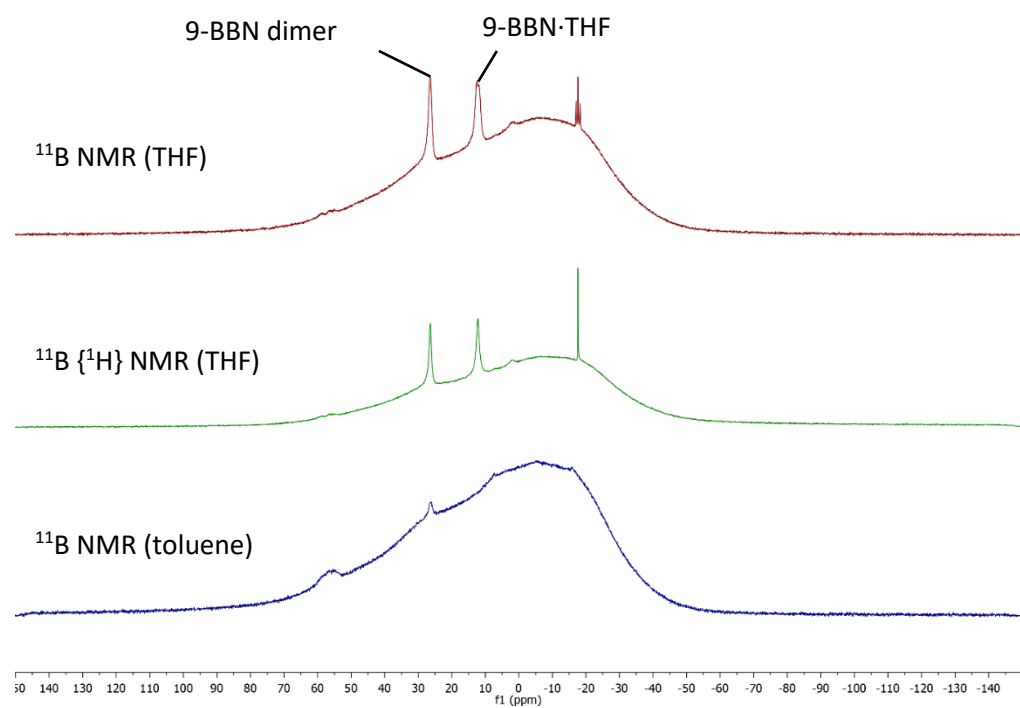


Figure 7.8 ^{11}B NMR describing attempted coupling of **110**

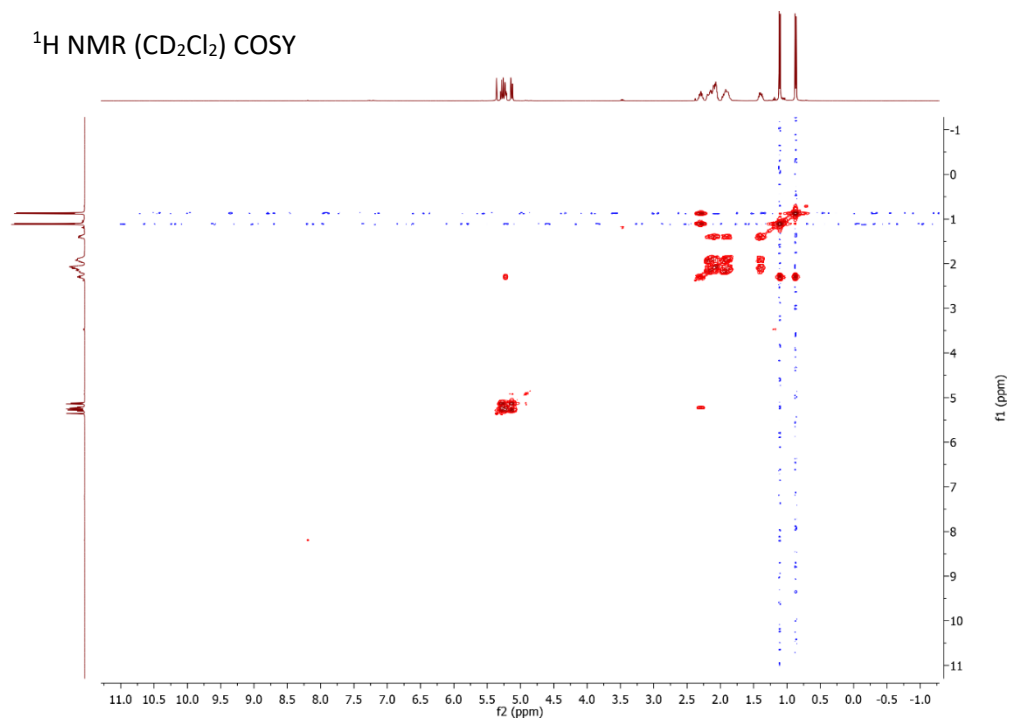


Figure 7.9 ¹H NMR COSY for **95a**

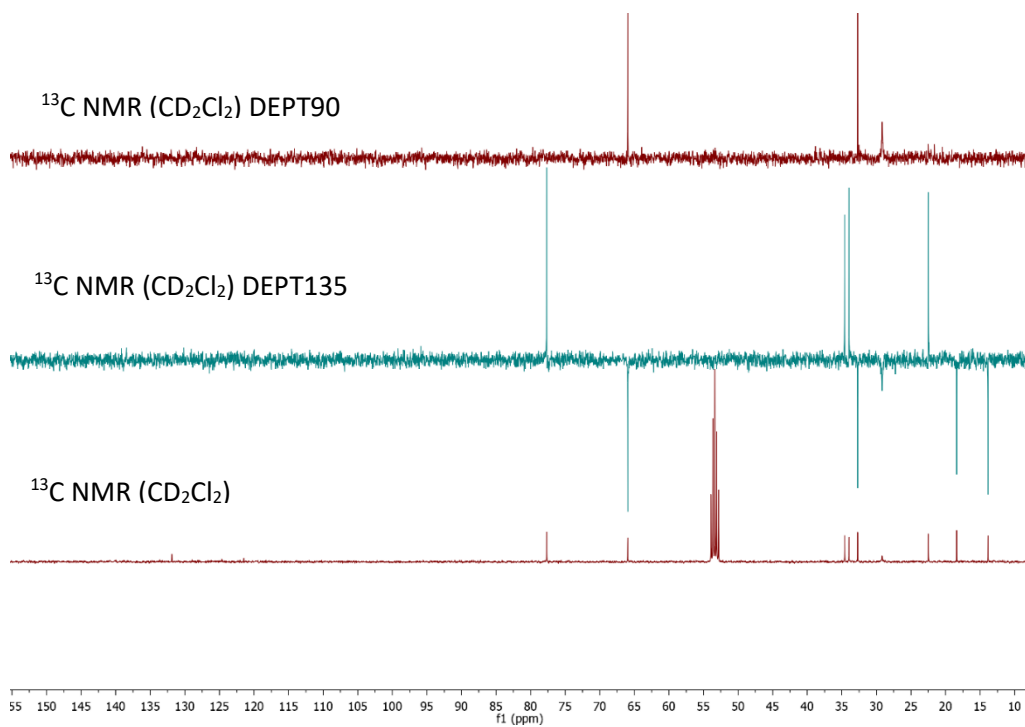


Figure 7.10 ¹³C NMR for **95a**

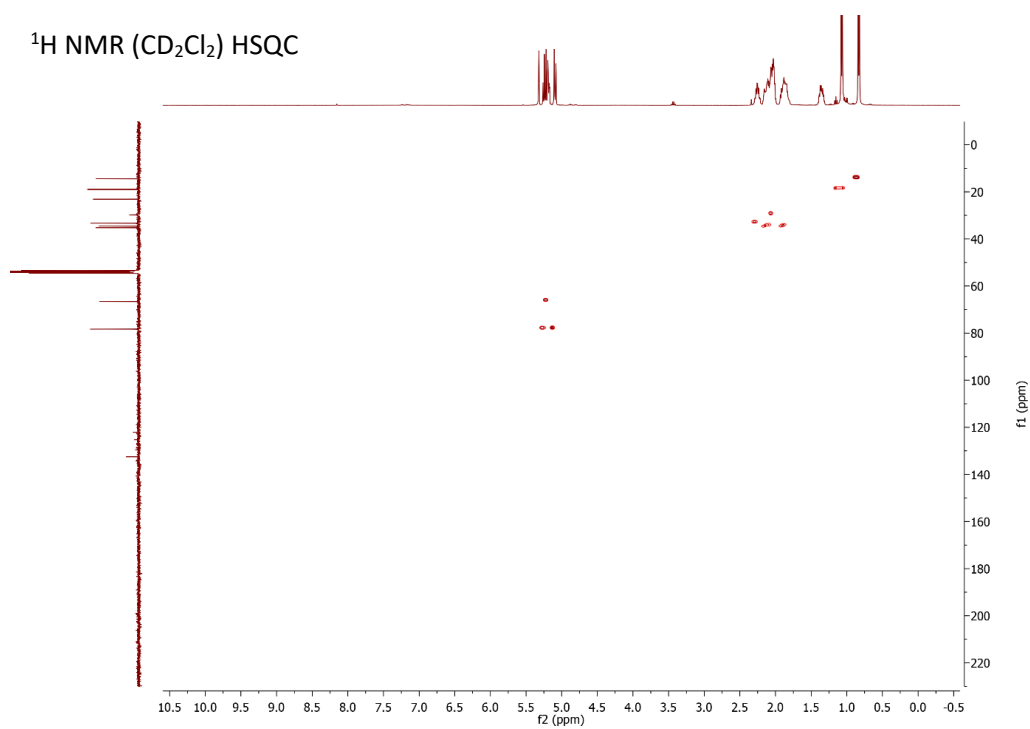


Figure 7.11 ¹H NMR HSQC for **95a**

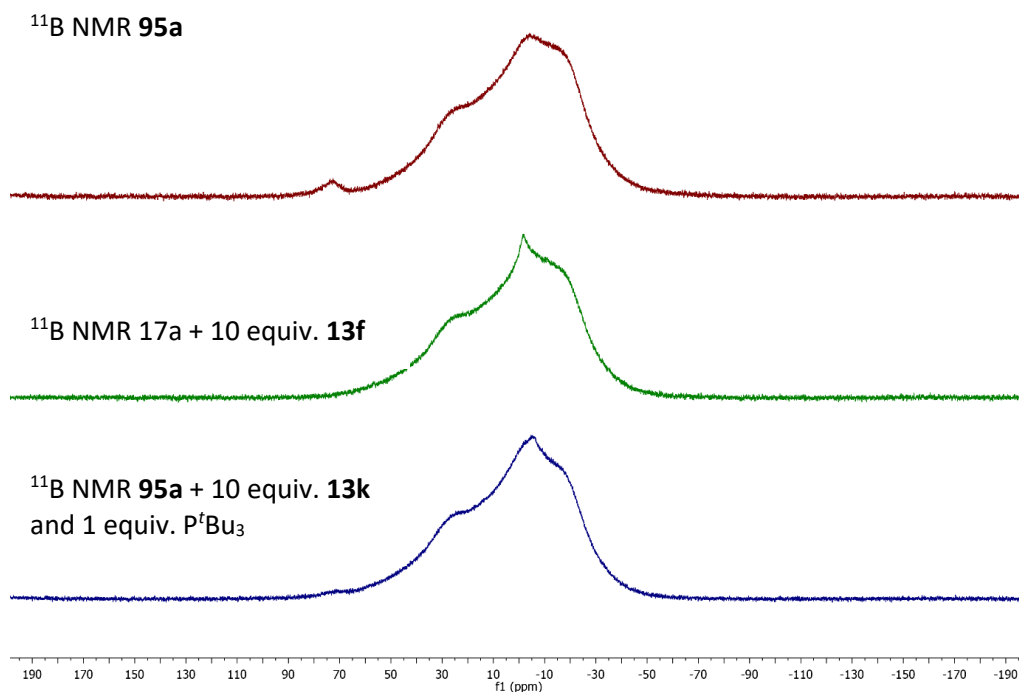


Figure 7.12 Tetrahedral adducts of **95a**

7.1.2 Proto-deborylation of **95b**

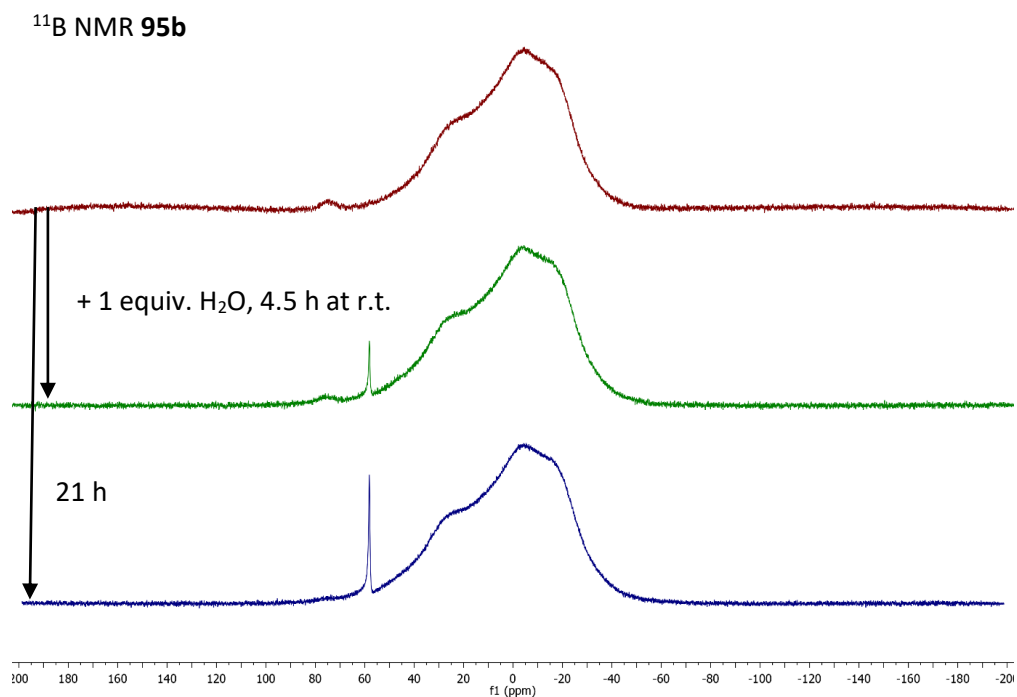


Figure 7.13 Hydrolysis of **95b**

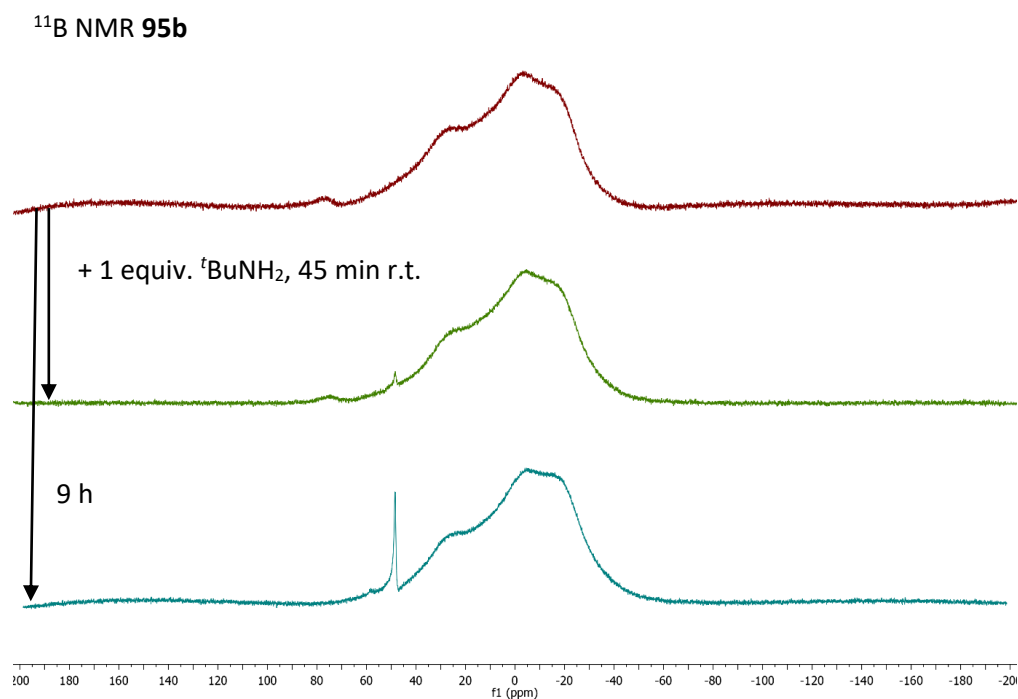


Figure 7.14 Aminolysis of **95b**

7.1.3 Stoichiometric reduction

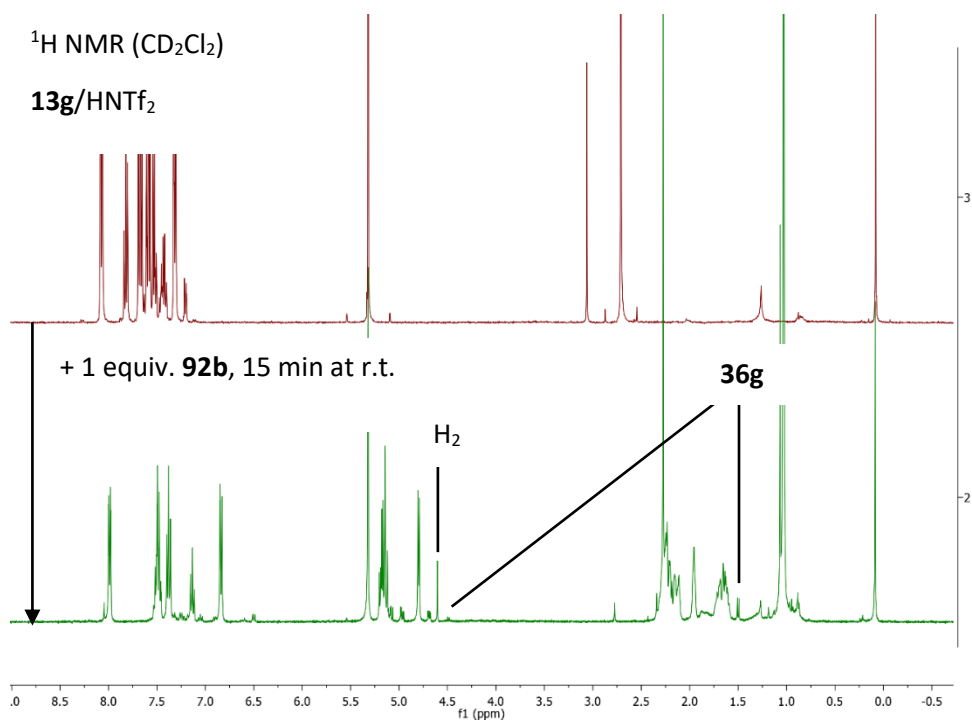


Figure 7.15 Stoichiometric reduction of **13g** with **92b**

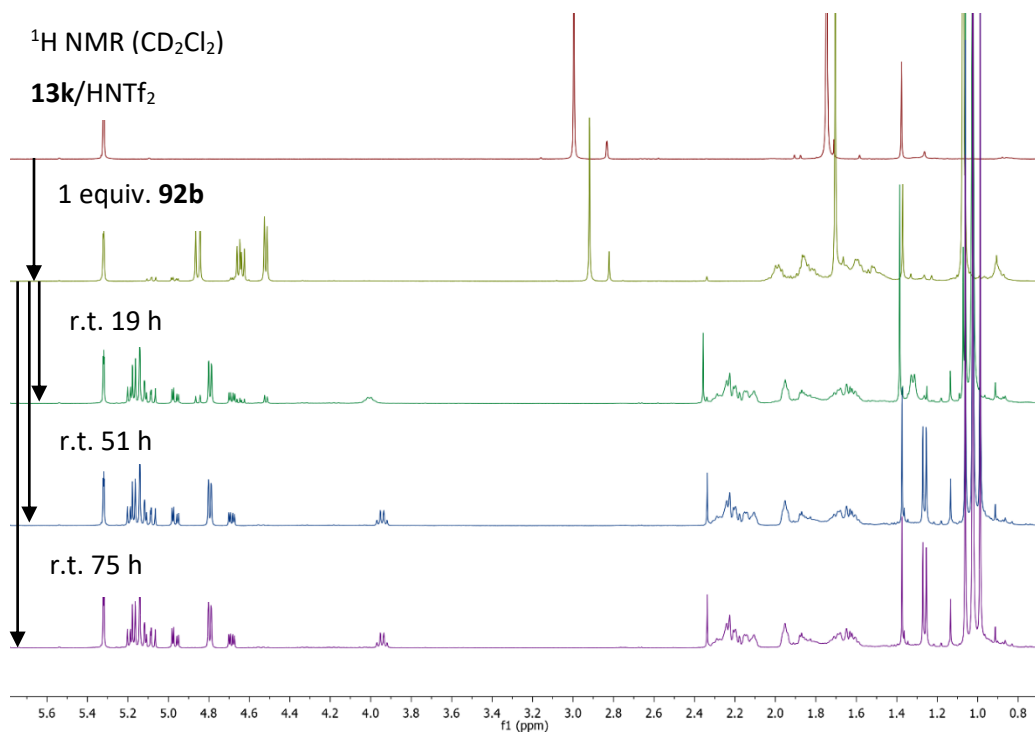


Figure 7.16 Stoichiometric reduction of **13k** with **92b**

7.2 Chapter 3

7.2.1 Catalyst synthesis and characterisation

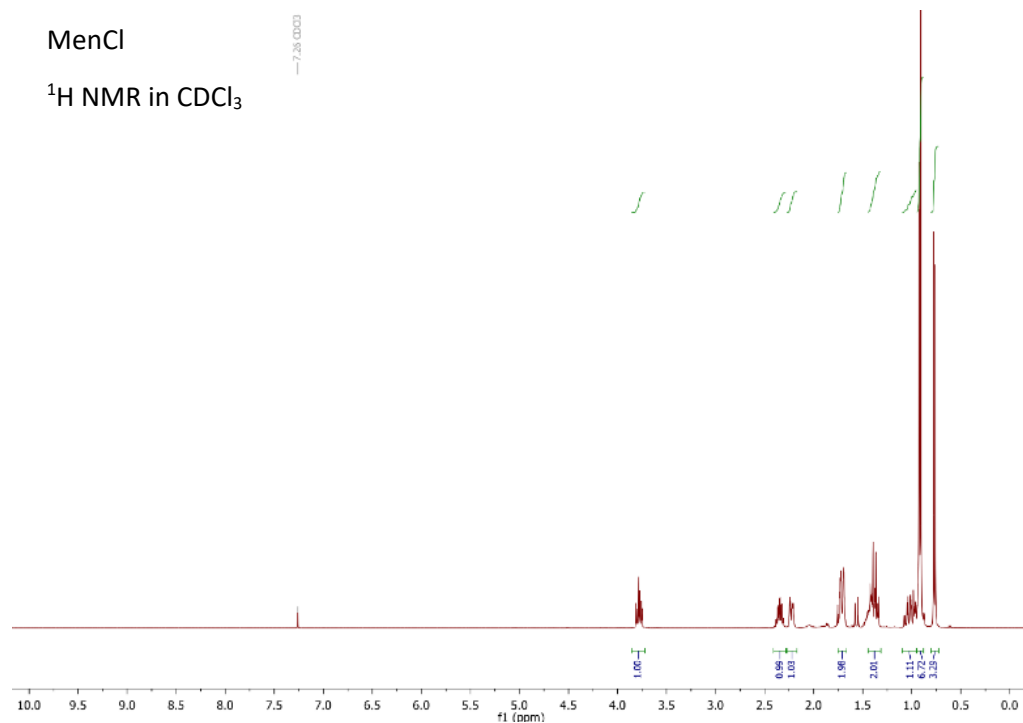


Figure 7.17 ^1H NMR for MenCl purified by column chromatography

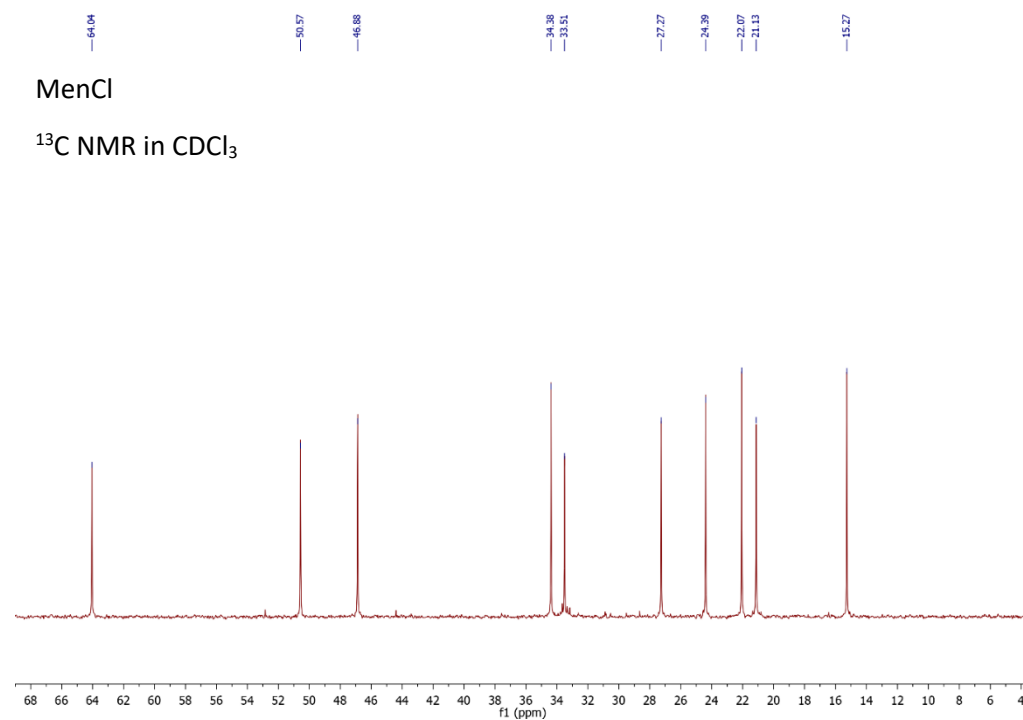


Figure 7.18 ^{13}C NMR for MenCl purified by column chromatography

MenMgCl

^1H NMR in THF-d₈

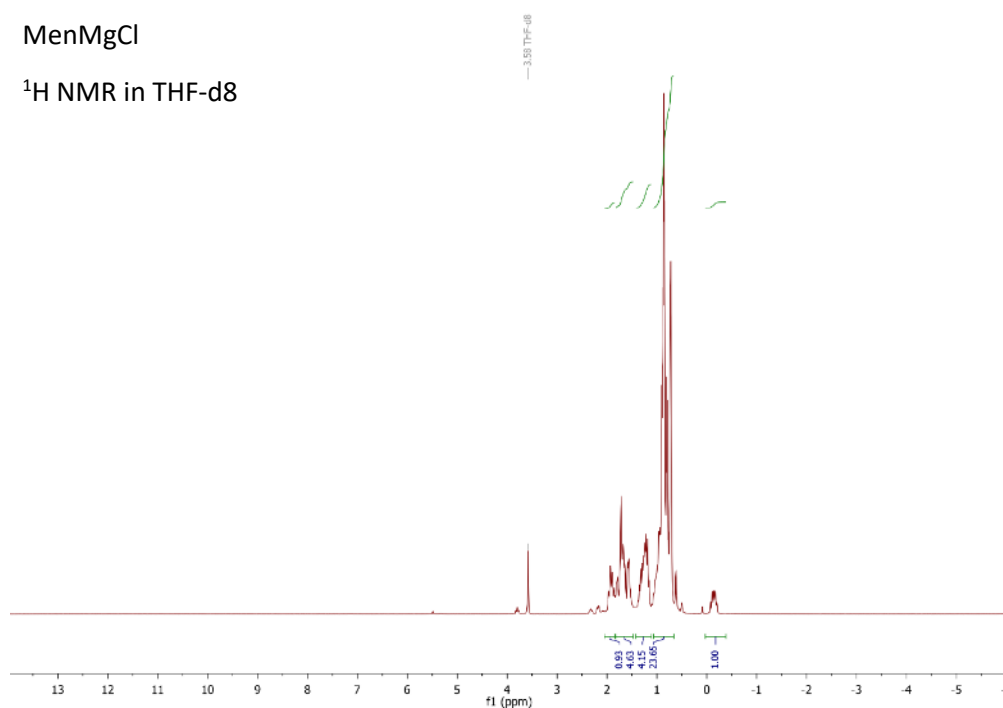


Figure 7.19 ^1H NMR for MenMgCl/Men₂Mg prepared in an NMR-scale experiment

MenMgCl formation

^1H NMR in THF-d₈

70 °C, 38 h

70 °C, 20 h

70 °C, 3 h

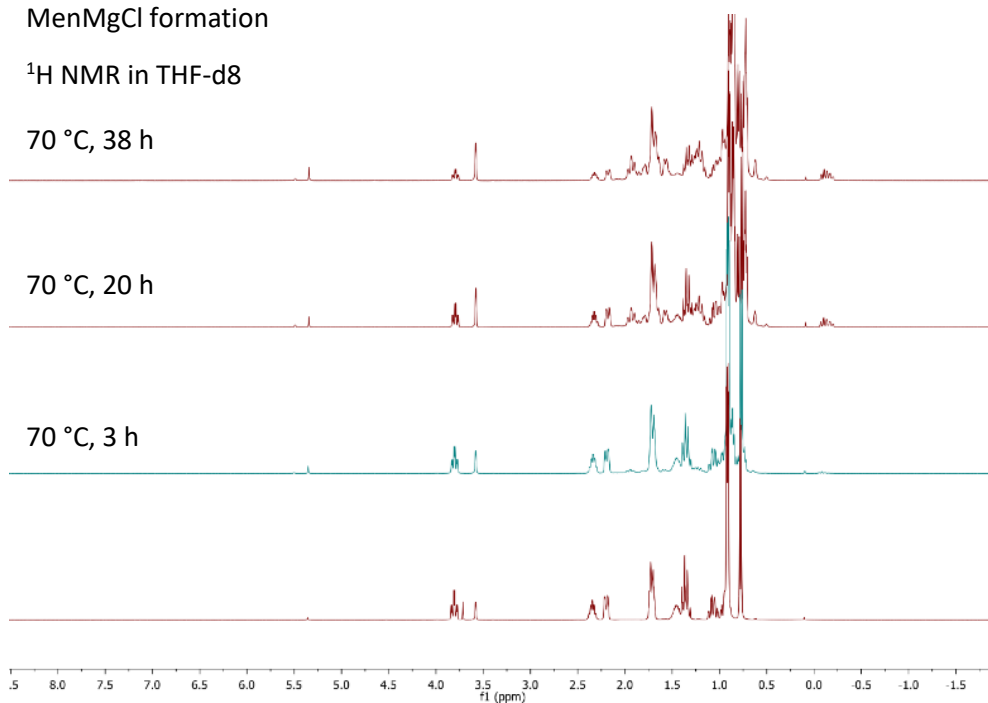


Figure 7.20 ^1H NMR spectra monitoring the conversion of MenCl to MenMgCl/Men₂Mg

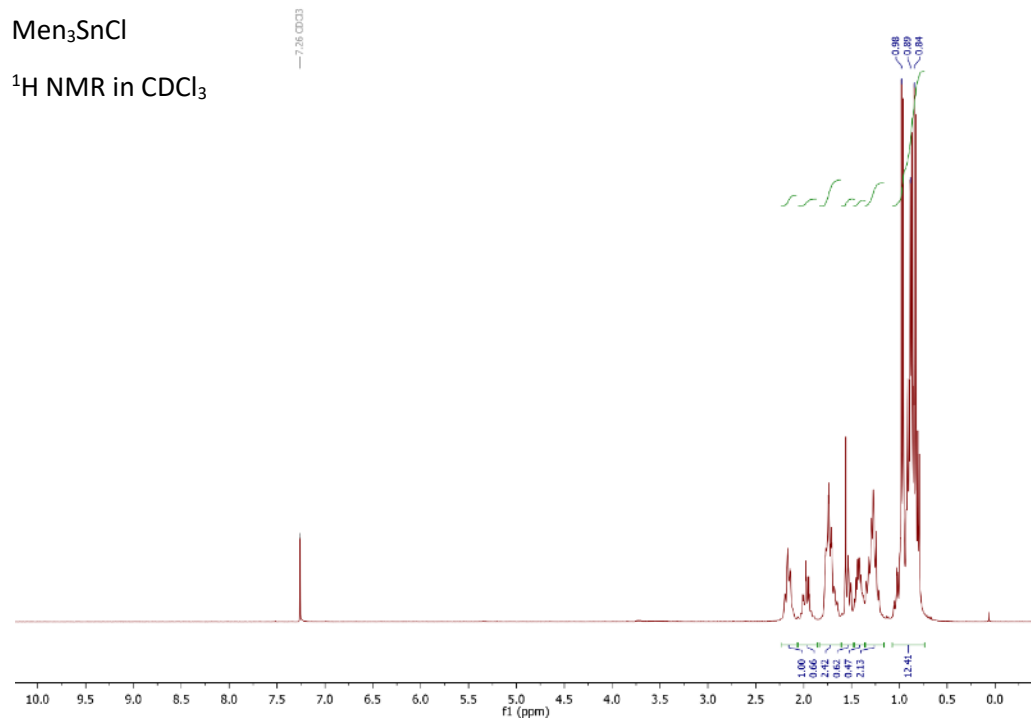


Figure 7.21 ¹H NMR spectrum for Men₃SnCl crystallised from ethanol

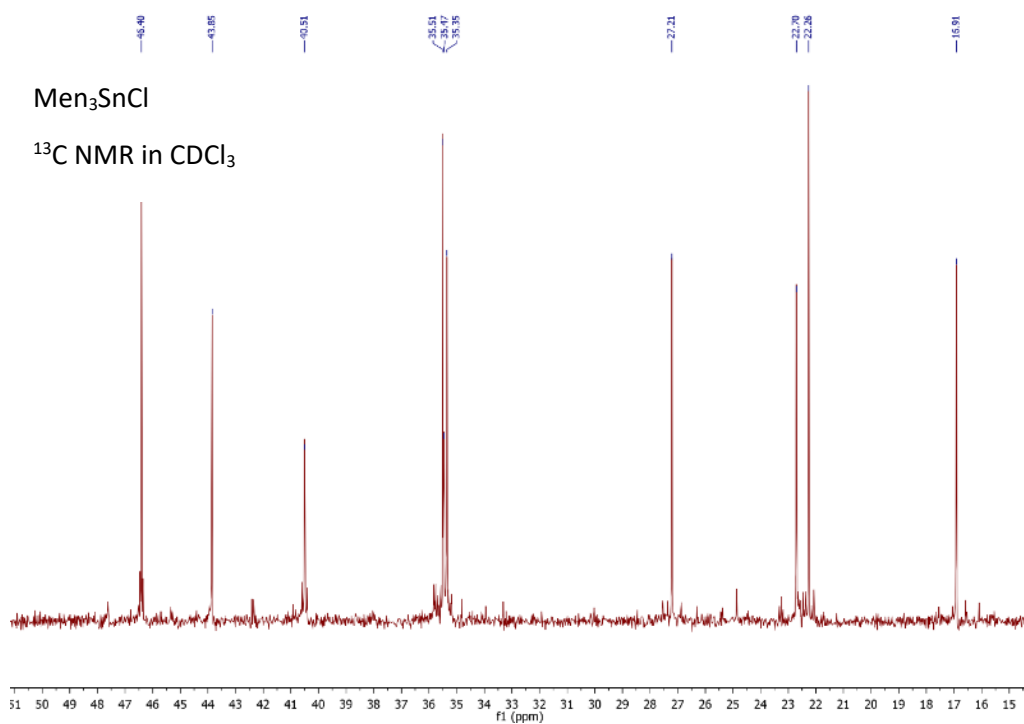


Figure 7.22 ¹³C NMR spectrum for Men₃SnCl crystallised from ethanol

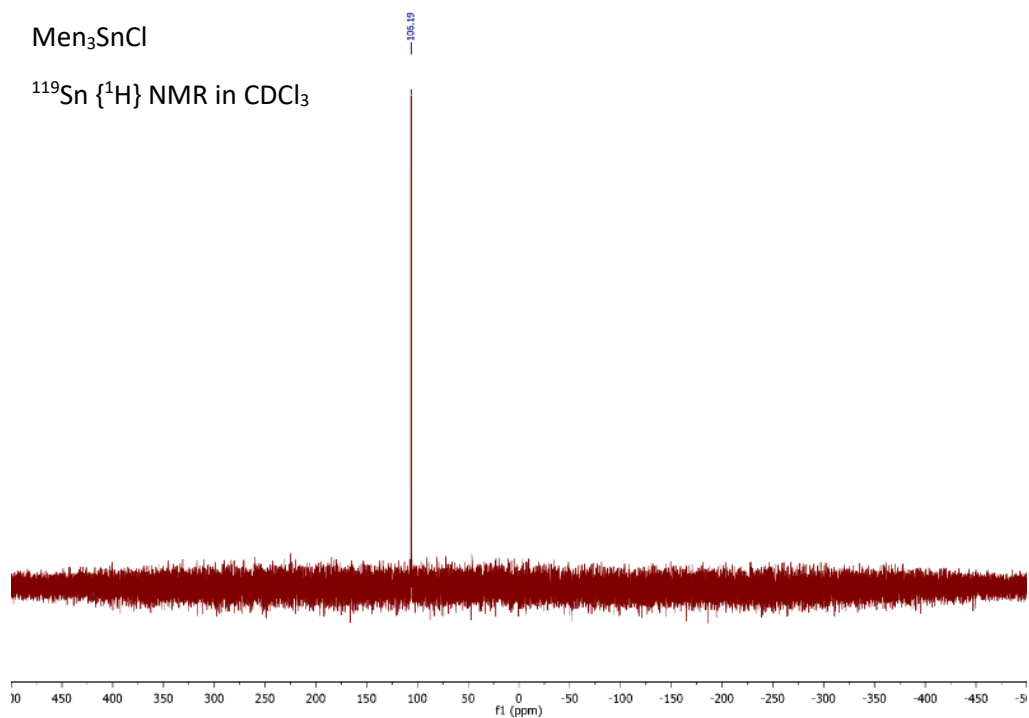


Figure 7.23 ¹¹⁹Sn NMR spectrum for Men₃SnCl crystallised from ethanol

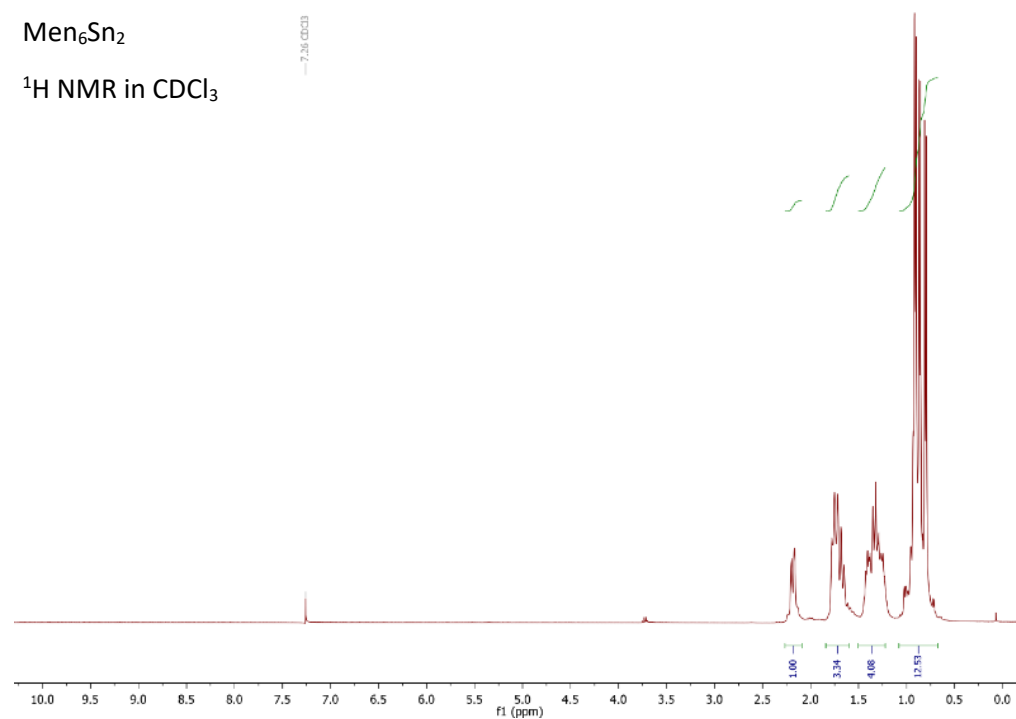


Figure 7.24 ¹H NMR for Men₆Sn₂ obtained by slow evaporation of ethanol

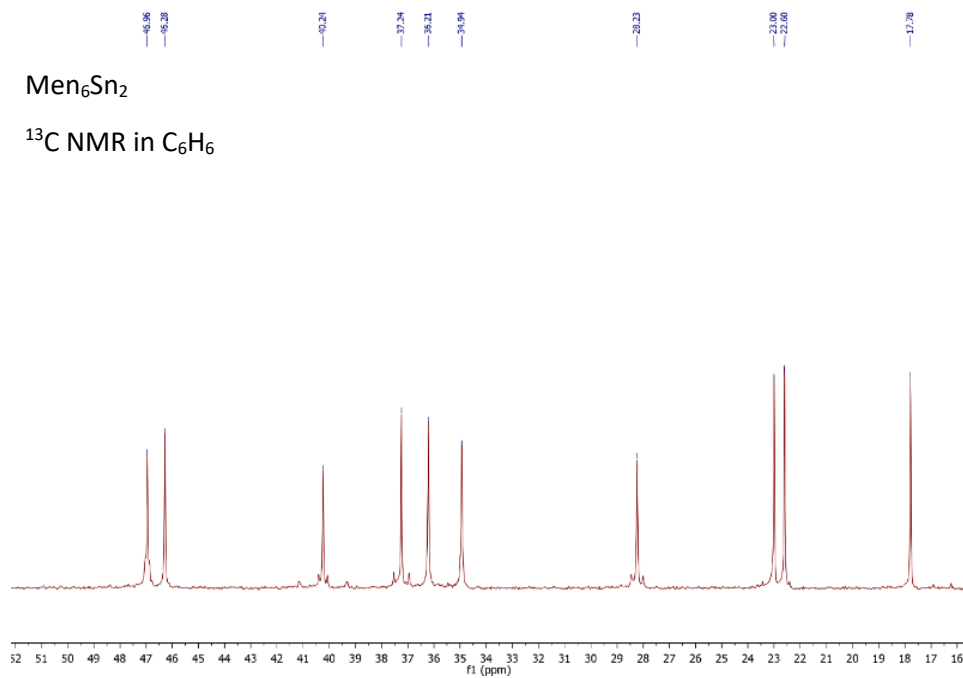


Figure 7.25 ^{13}C NMR for Men_6Sn_2 obtained by slow evaporation of ethanol

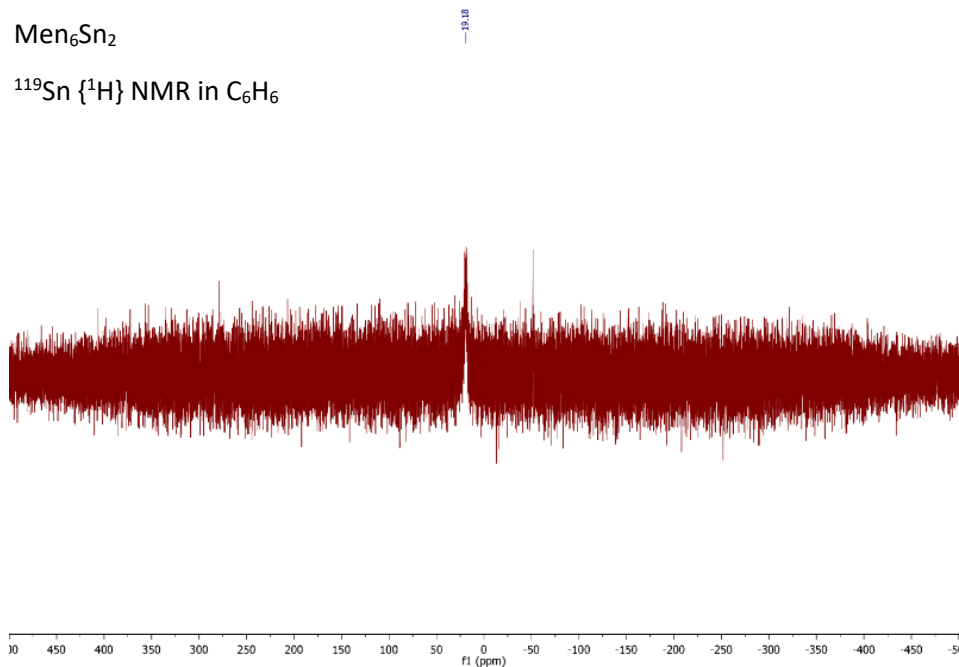


Figure 7.26 ^{119}Sn NMR for Men_6Sn_2 obtained by slow evaporation of ethanol

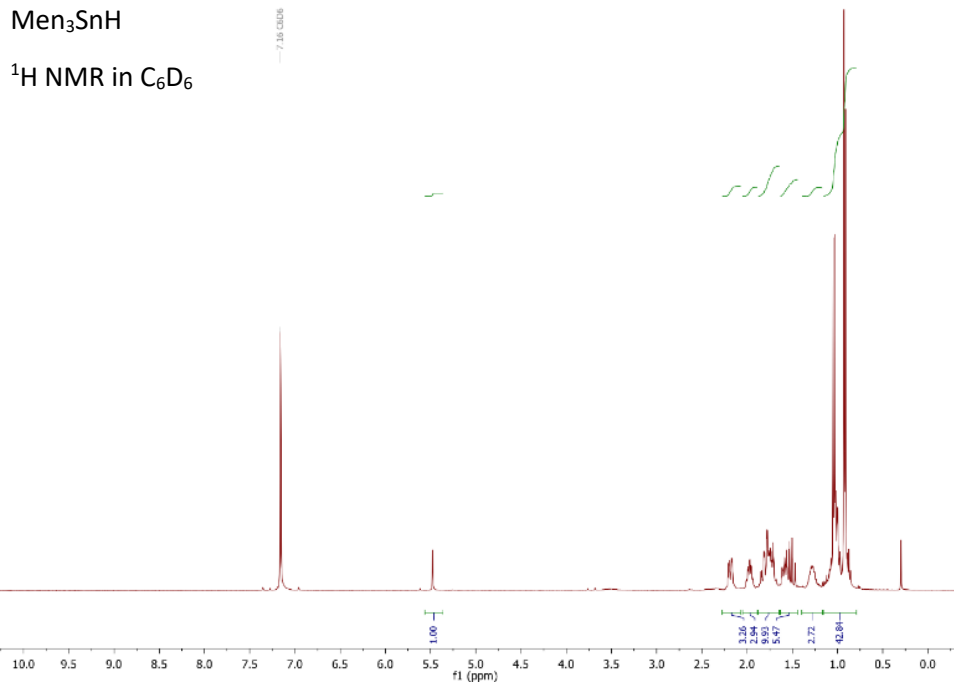


Figure 7.27 ¹H NMR for Men₃SnH

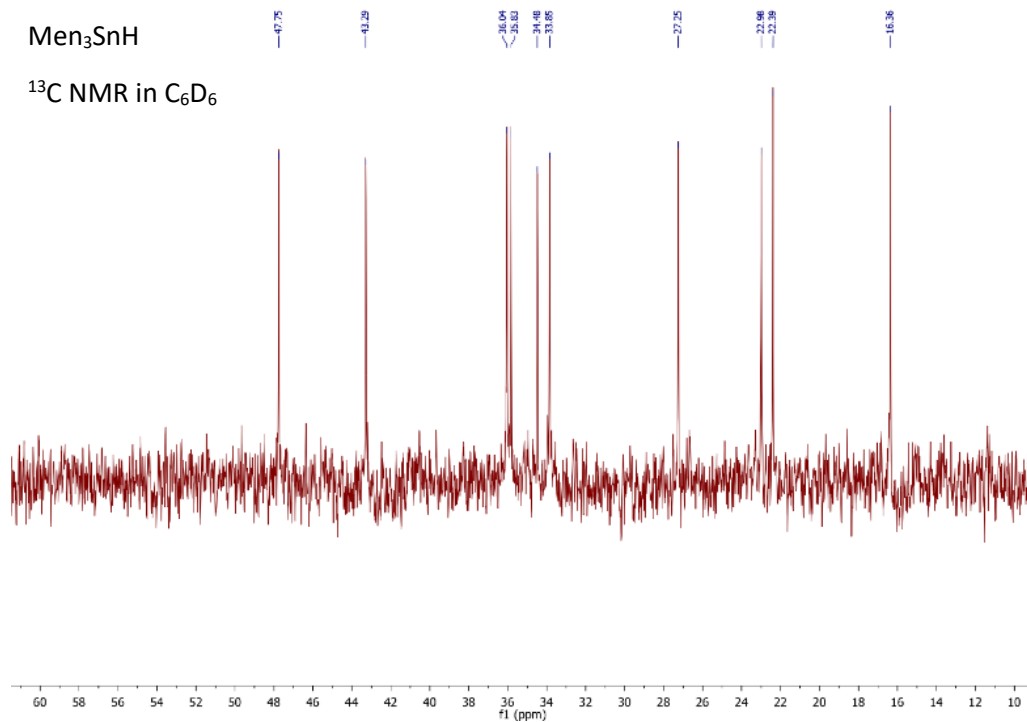


Figure 7.28 ¹³C NMR for Men₃SnH

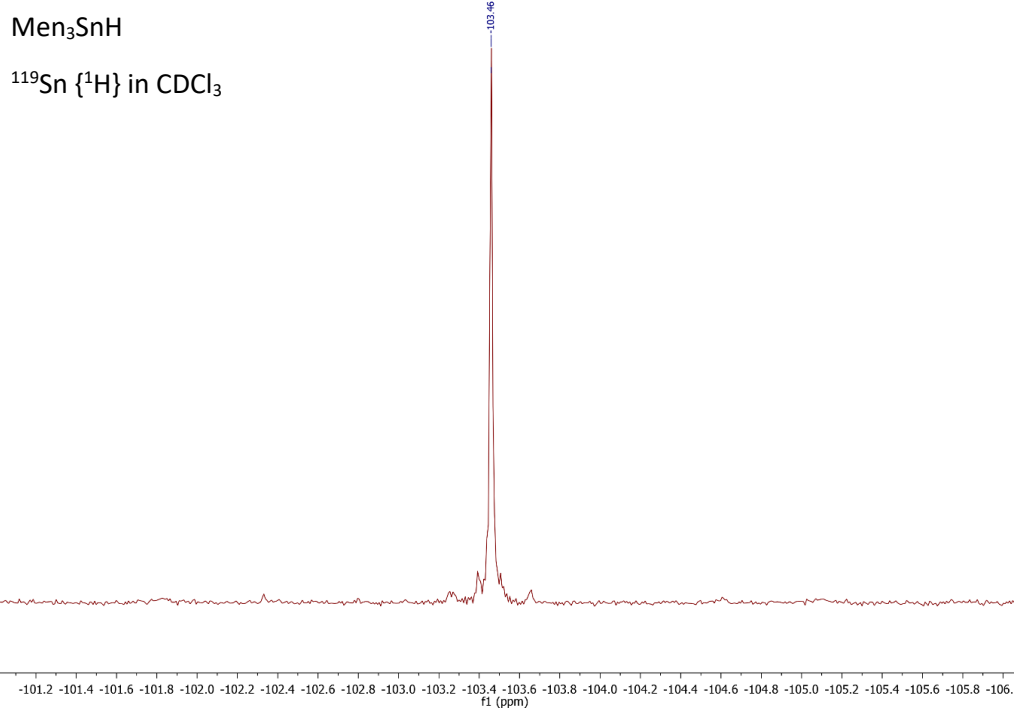


Figure 7.29 ¹¹⁹Sn {¹H} NMR for Men₃SnH in CDCl₃

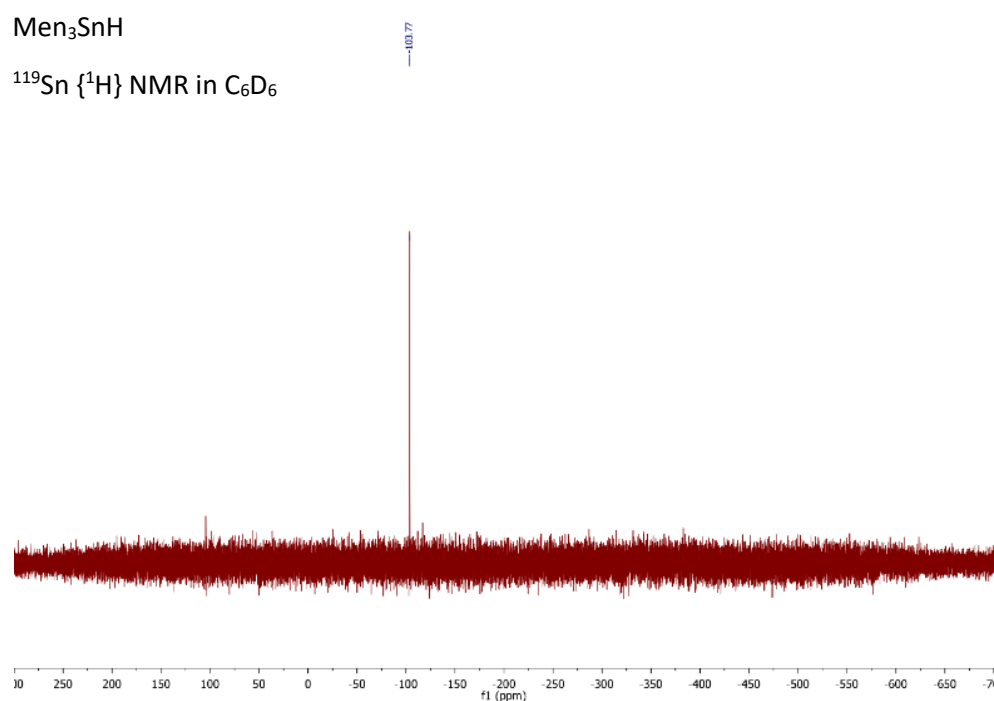


Figure 7.30 ¹¹⁹Sn {¹H} NMR for Men₃SnH in C₆D₆

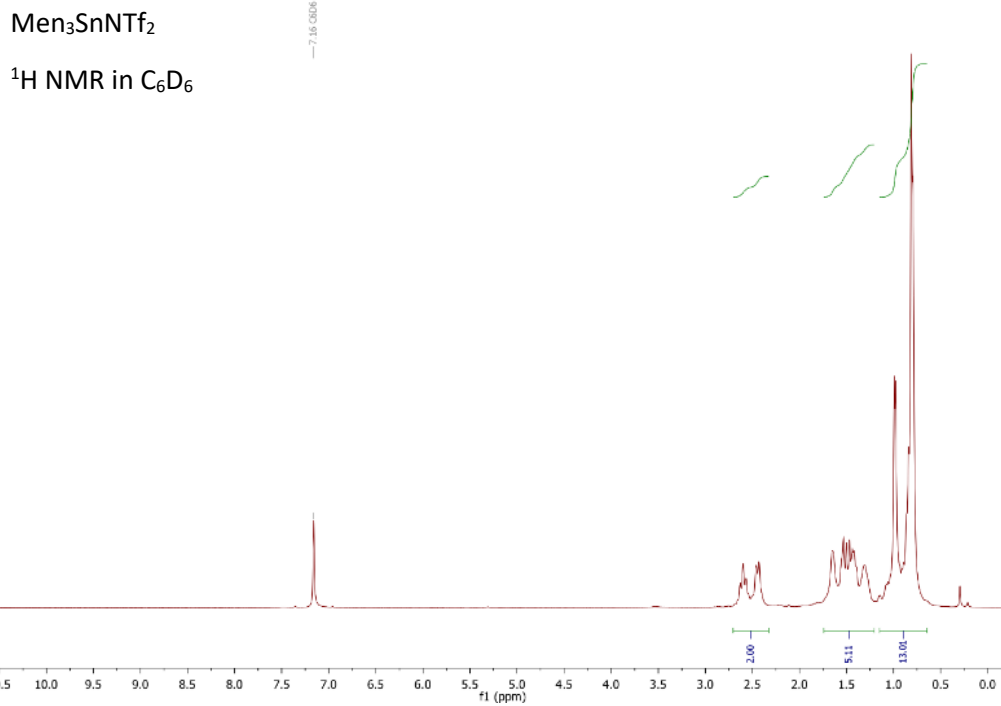


Figure 7.31 ¹H NMR for Men₃SnNTf₂

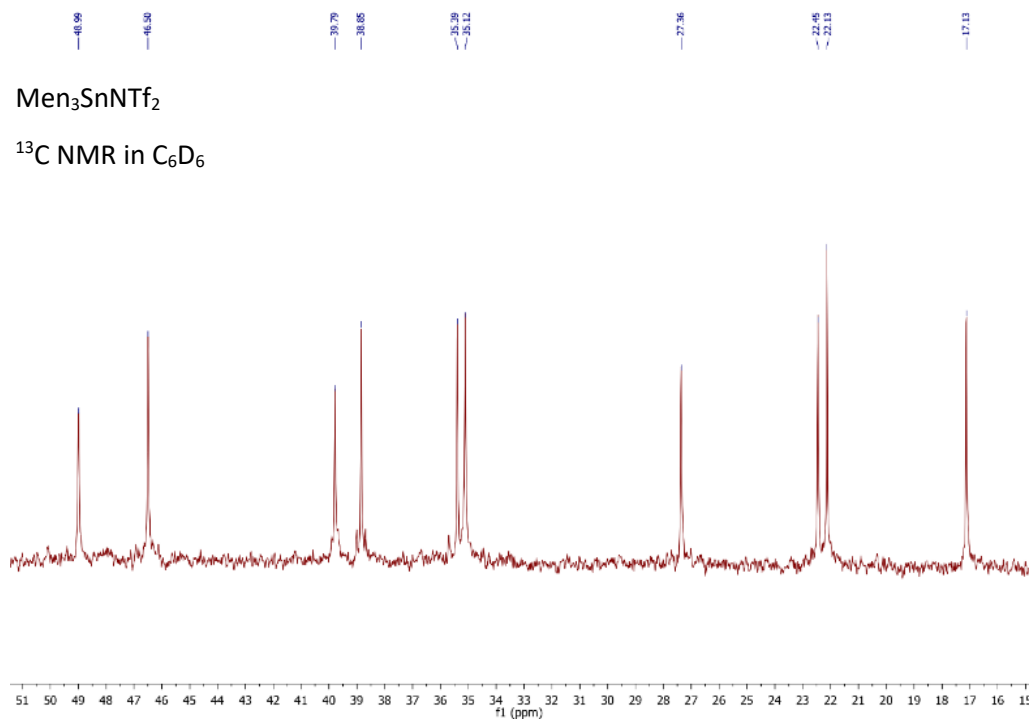


Figure 7.32 ¹³C NMR for Men₃SnNTf₂ in C₆D₆

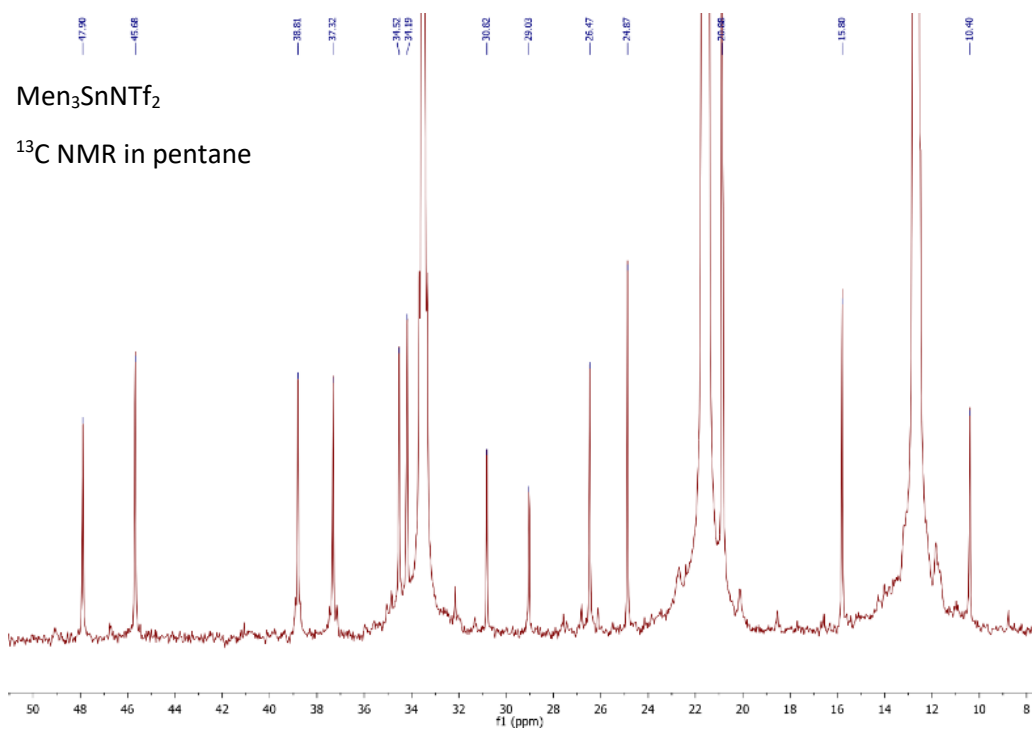


Figure 7.33 ¹³C NMR for Men₃SnNTf₂ in pentane

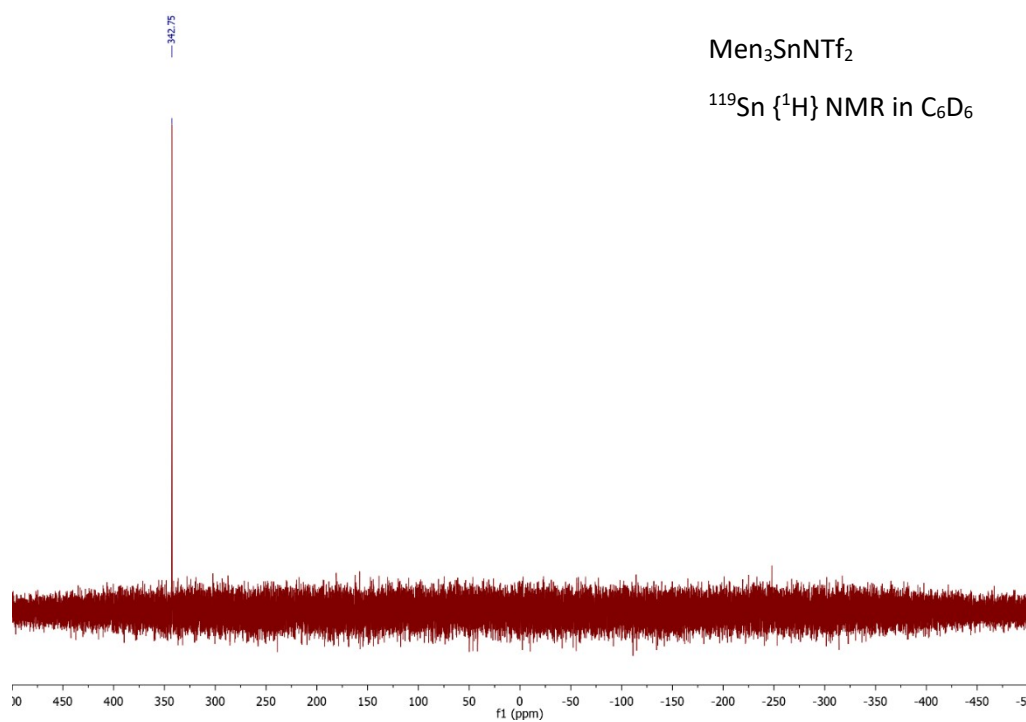


Figure 7.34 ¹¹⁹Sn {¹H} NMR for Men₃SnNTf₂ in C₆D₆

Men₃SnNTf₂

¹¹⁹Sn {¹H} NMR in pentane

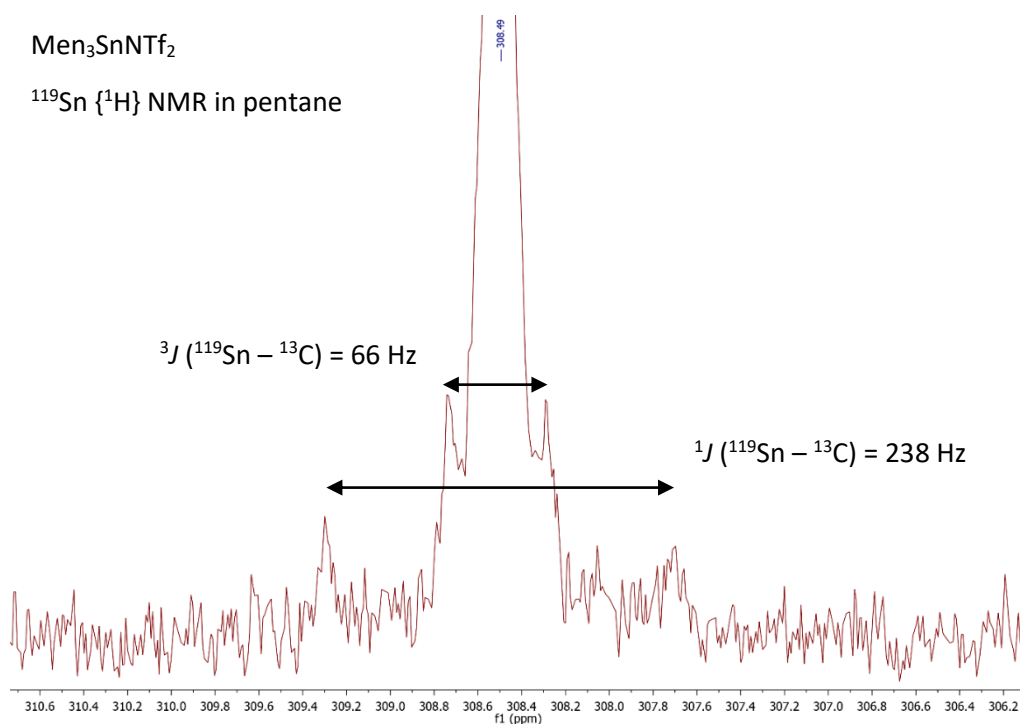


Figure 7.35 ¹¹⁹Sn {¹H} NMR for Men₃SnNTf₂ in pentane

7.2.2 Gutmann-Beckett Lewis acidity measurement

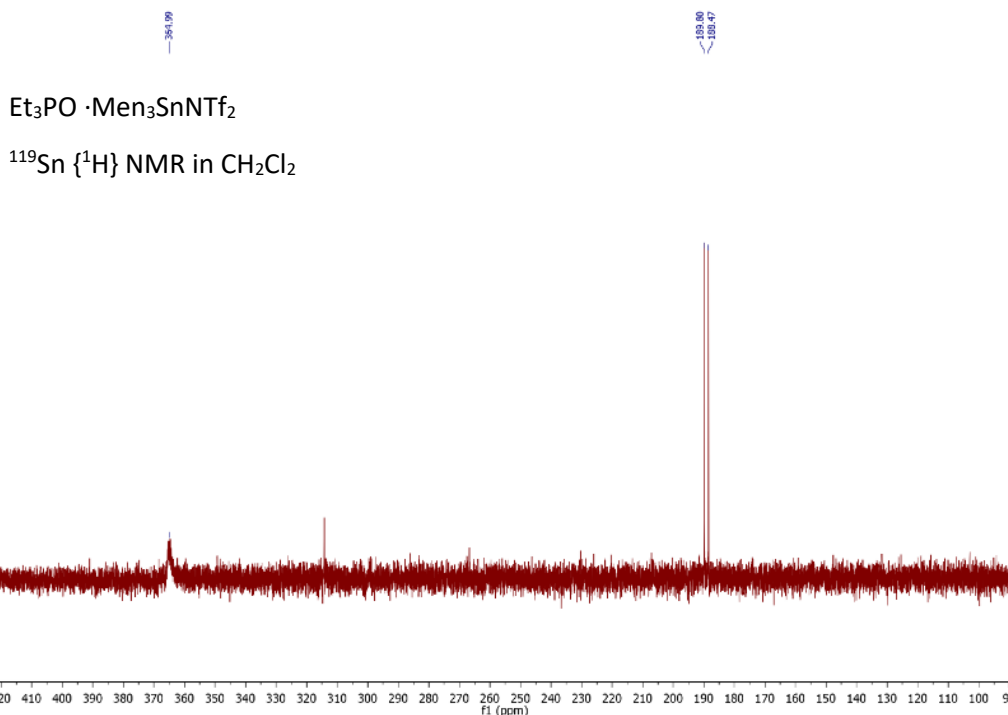


Figure 7.36 ¹¹⁹Sn {¹H} NMR recorded for Gutmann-Beckett analysis of Men₃SnNTf₂

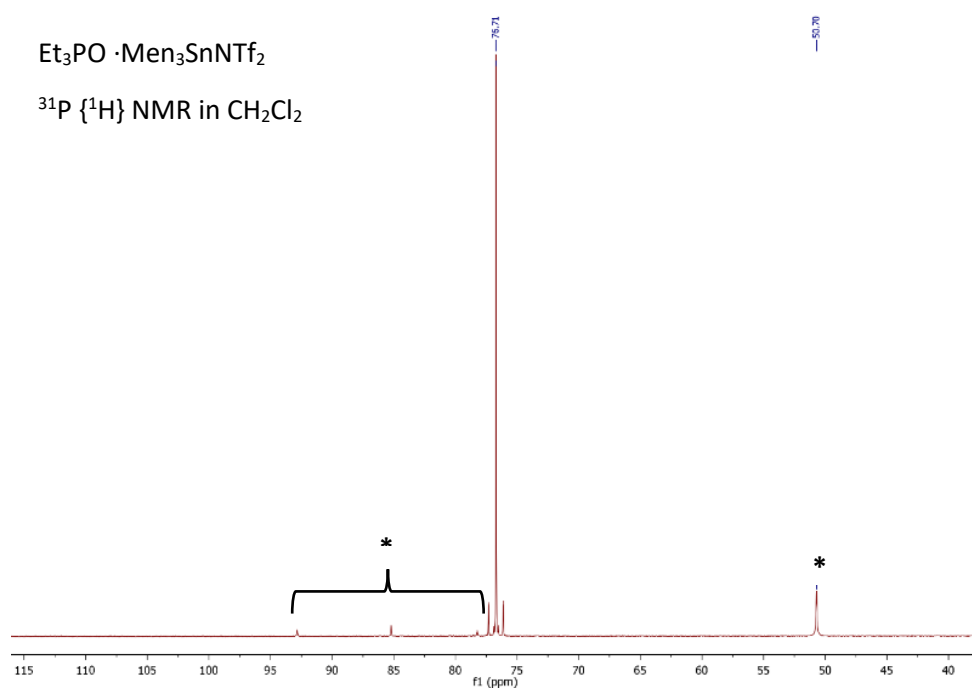


Figure 7.37 ³¹P {¹H} NMR recorded for Gutmann-Beckett analysis of Men₃SnNTf₂; * = Et₃PO external reference (capillary insert); ** = unidentified species, the peaks do not form a multiplet.

7.2.3 Men₆Sn₂ cleavage studies

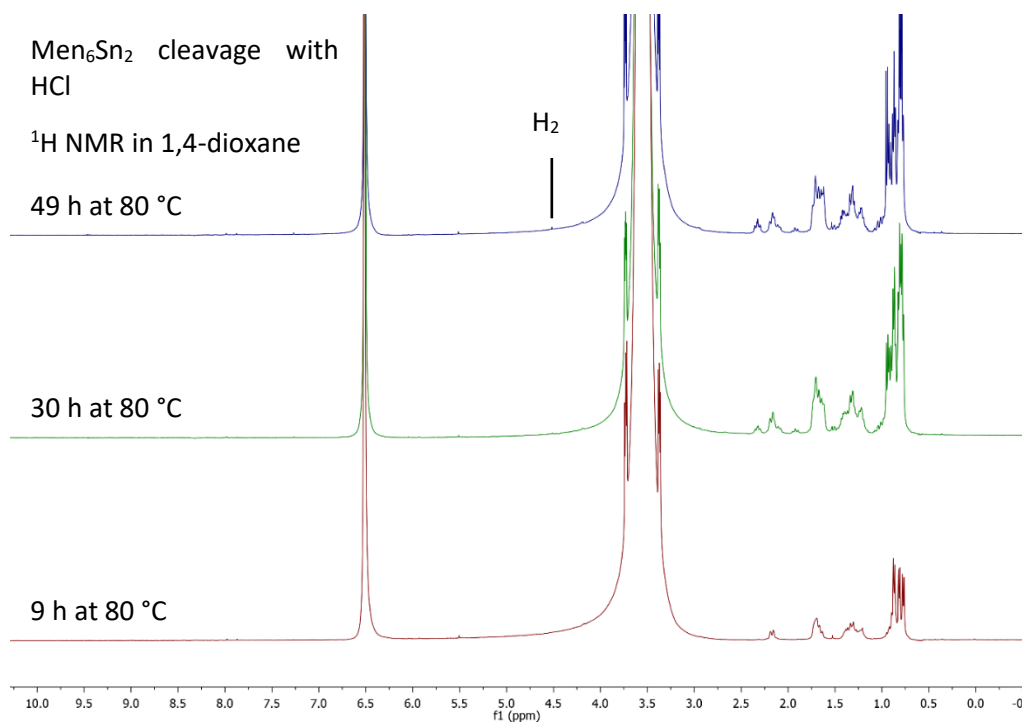


Figure 7.38 ¹H NMR showing progress of Men₆Sn₂ cleavage with HCl

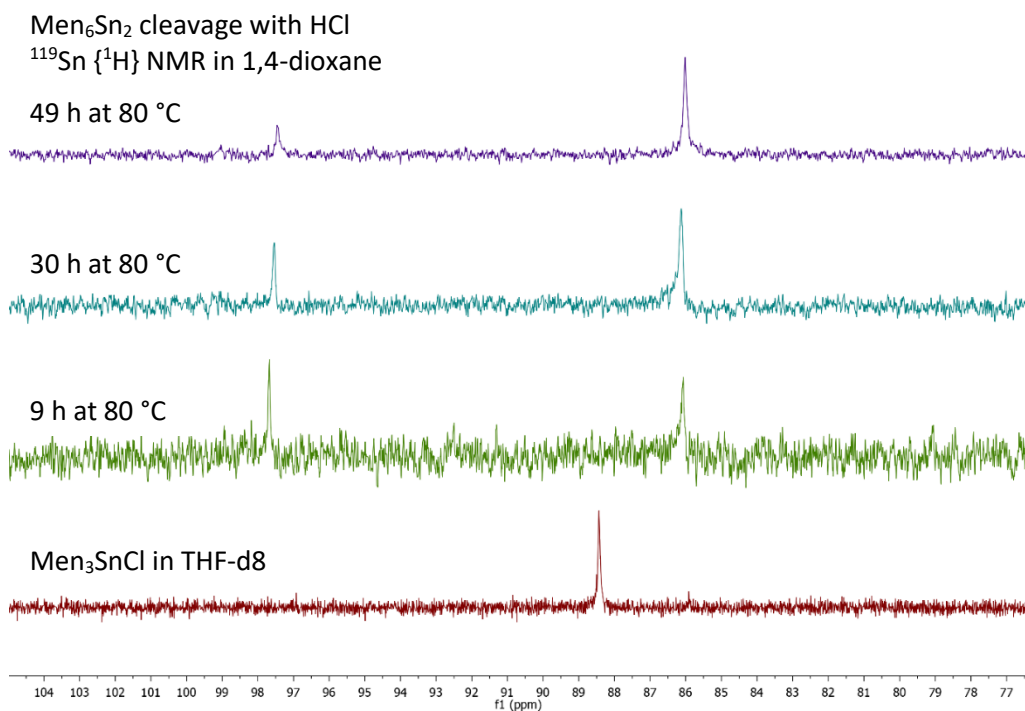


Figure 7.39 ¹¹⁹Sn {¹H} showing progress of Men₆Sn₂ cleavage with HCl

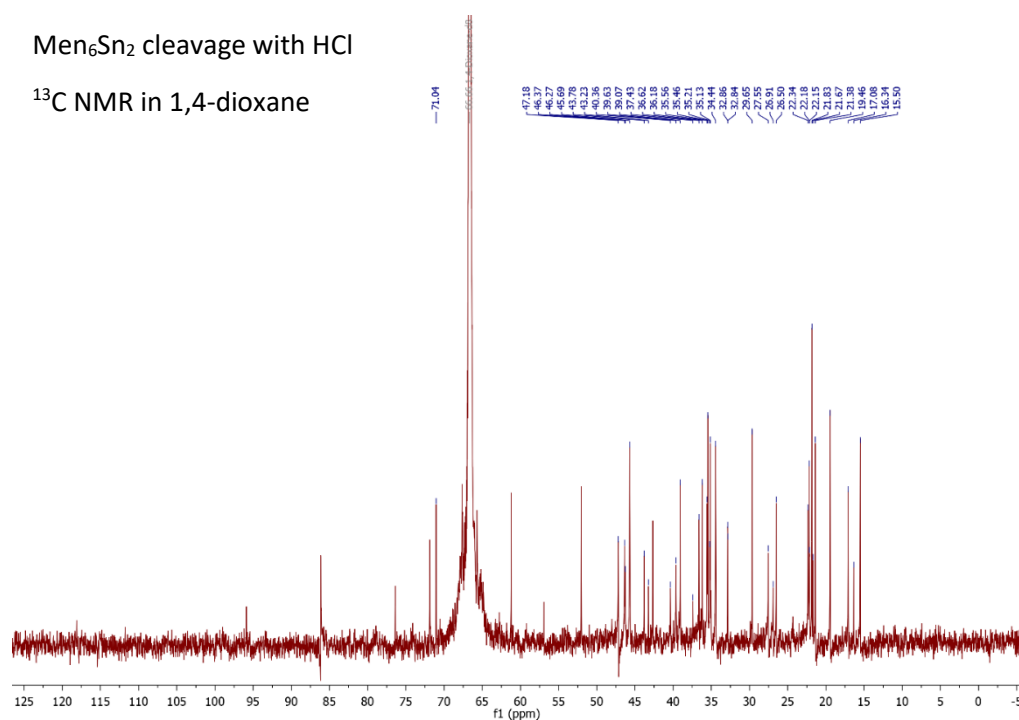


Figure 7.40 ¹³C NMR at the latest analysis time point for the Men₆Sn₂ cleavage with HCl

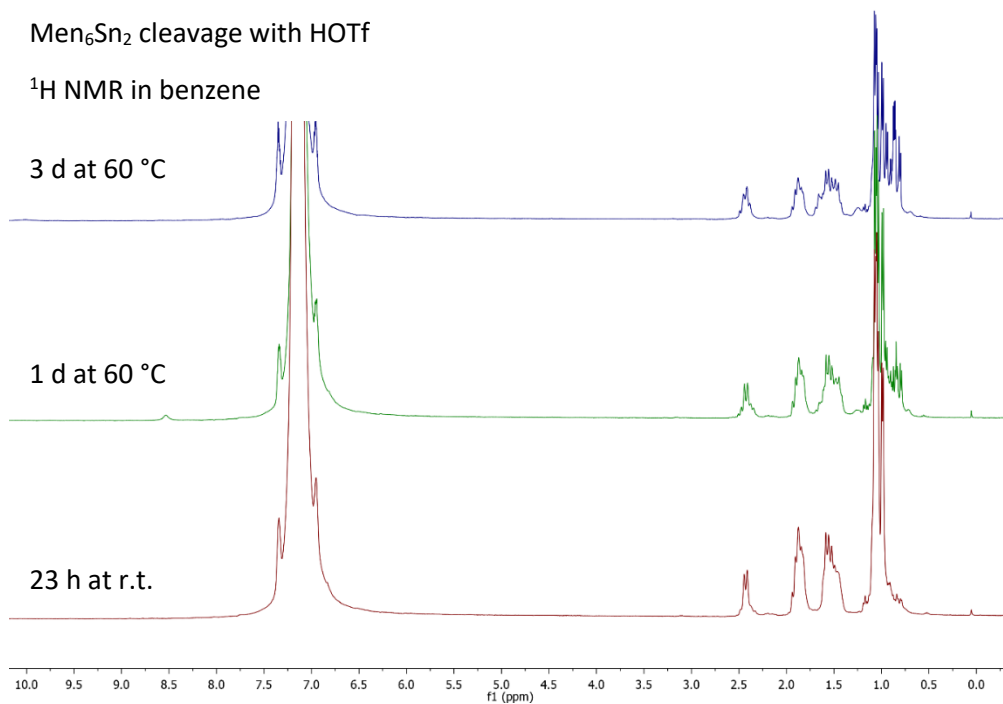


Figure 7.41 ¹H NMR showing progress of Men₆Sn₂ cleavage with HOTf

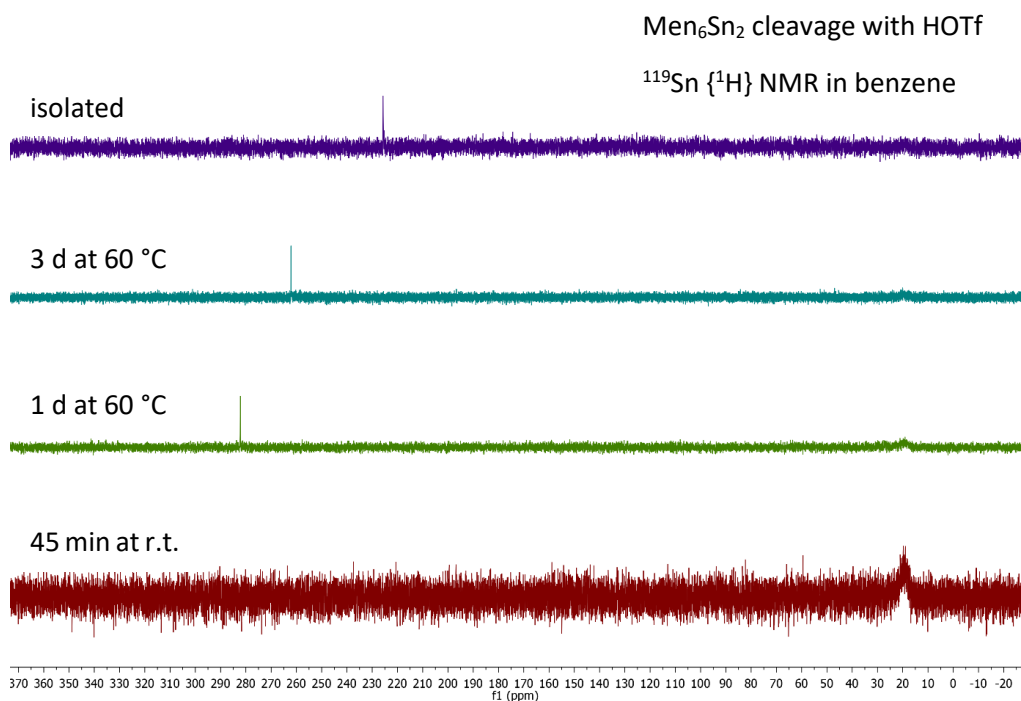


Figure 7.42 ¹¹⁹Sn {¹H} showing progress of Men₆Sn₂ cleavage with HOTf

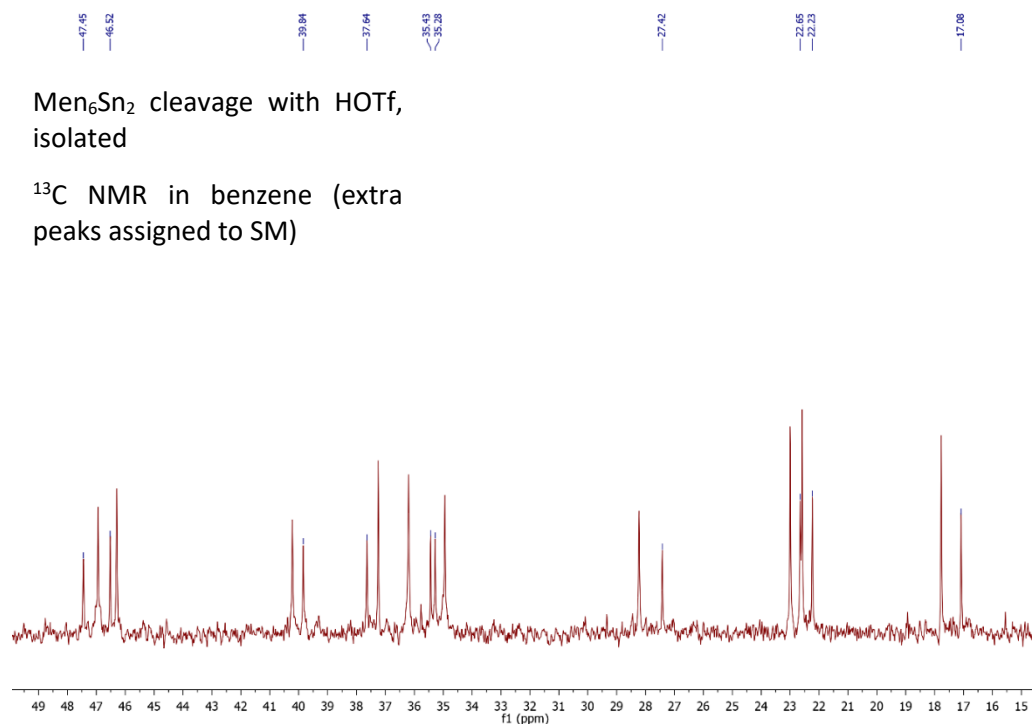


Figure 7.43 ¹³C NMR for isolated product from Men₆Sn₂ cleavage with HOTf

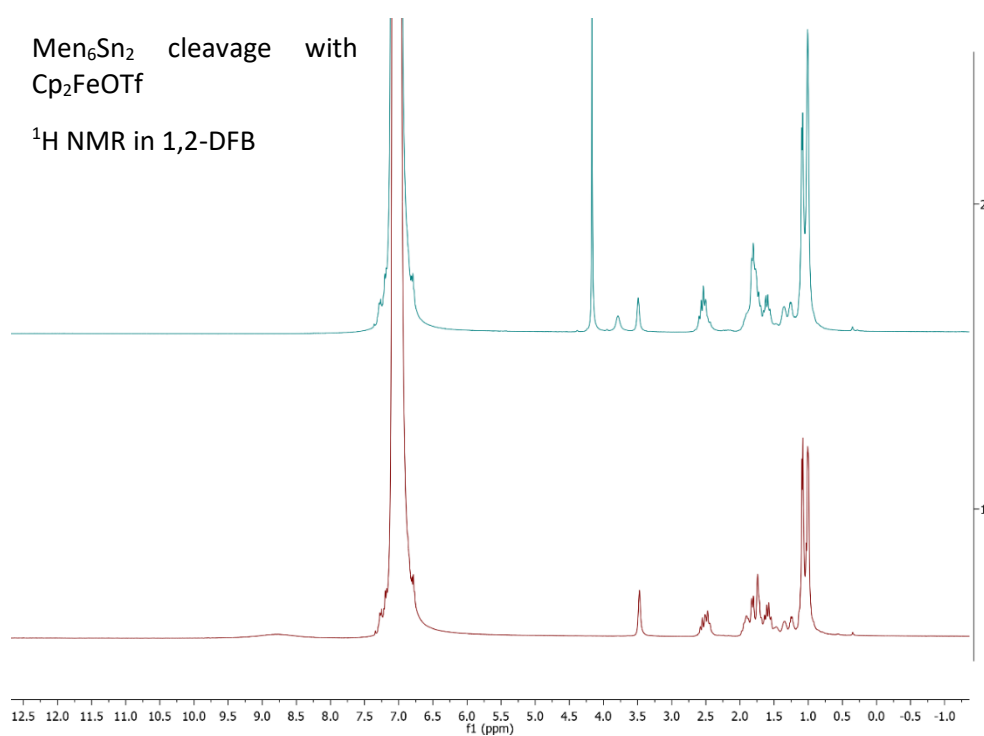


Figure 7.44 ¹H NMR monitoring Men₆Sn₂ cleavage with Cp₂FeOTf

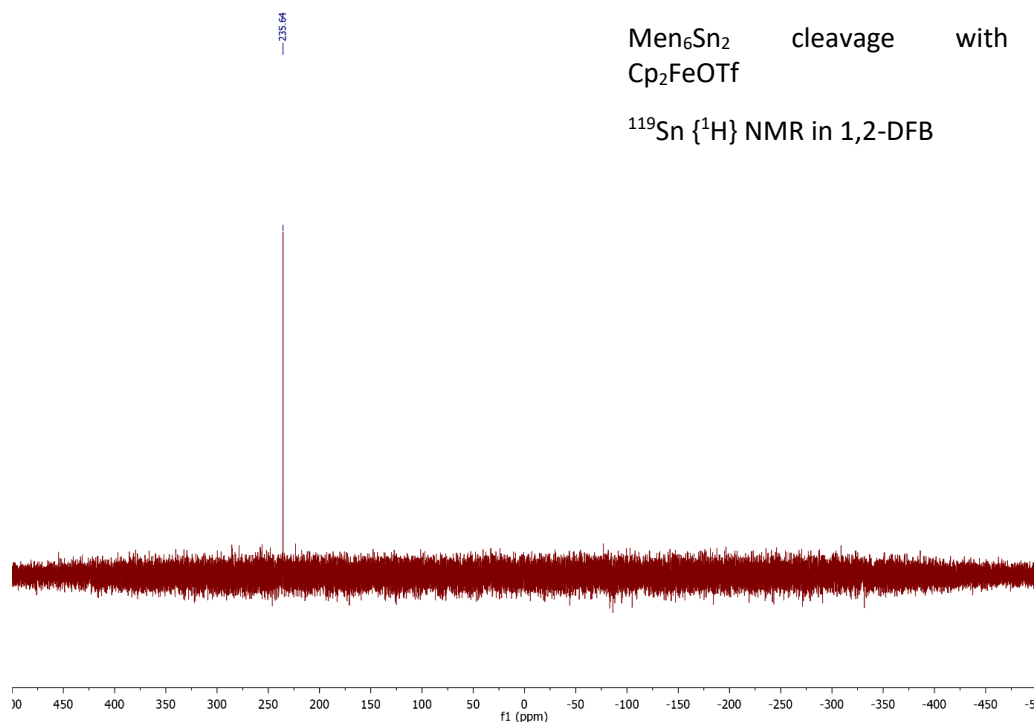


Figure 7.45 ¹¹⁹Sn {¹H} NMR for Men₆Sn₂ cleavage with Cp₂FeOTf

7.2.4 Hydrogen activation studies

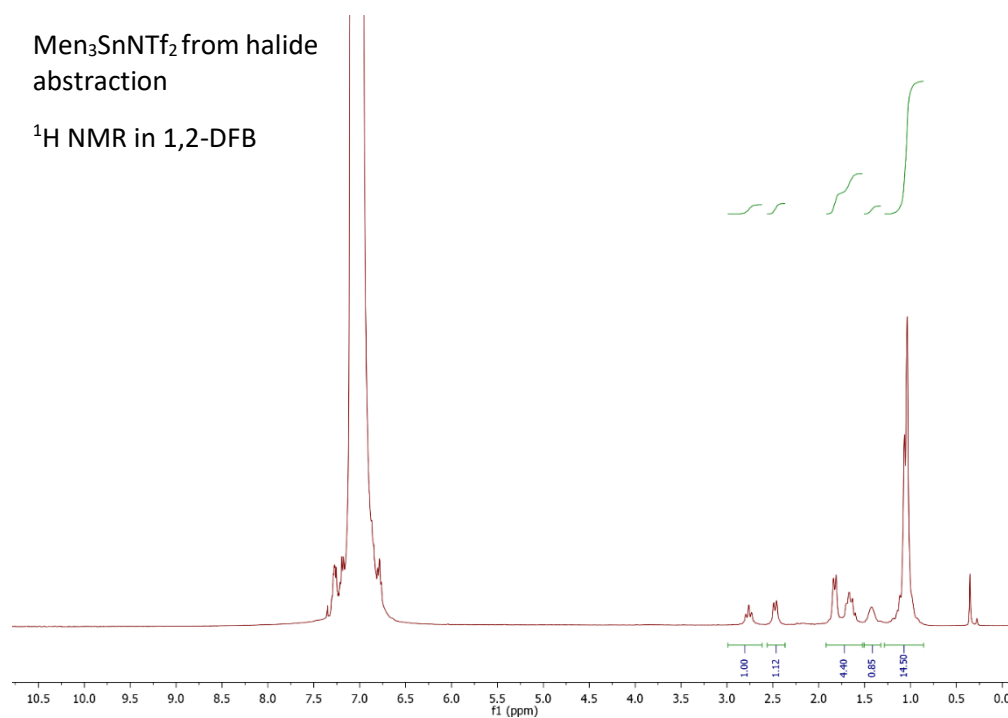


Figure 7.46 ¹H NMR for Men₃SnNTf₂ generated *via* halide abstraction from Men₃SnCl

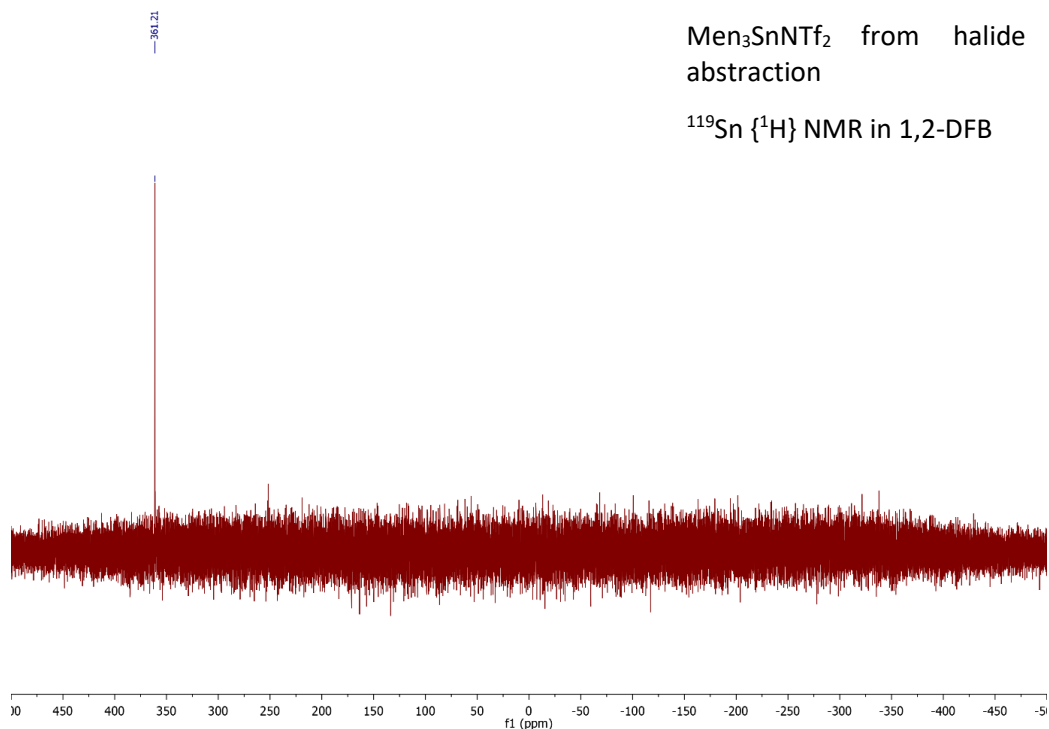


Figure 7.47 ¹¹⁹Sn {¹H} NMR for Men₃SnNTf₂ generated *via* halide abstraction from Men₃SnCl

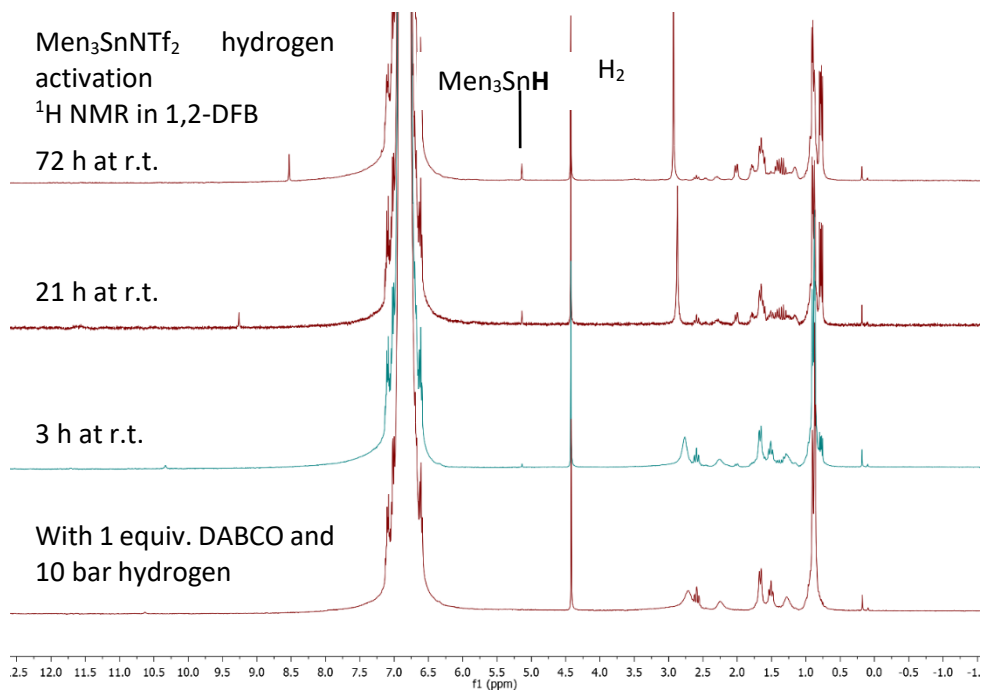
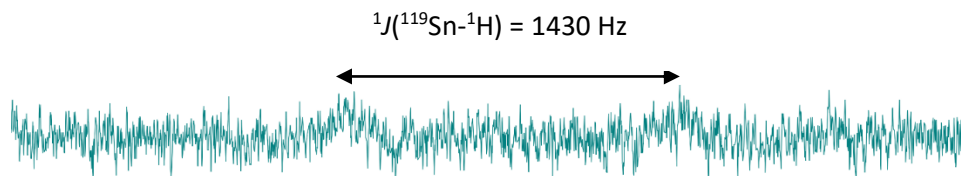


Figure 7.48 ¹H NMR monitoring hydrogen activation with Men₃SnNTf₂

Men₃SnNTf₂ hydrogen
activation
¹¹⁹Sn NMR in 1,2-DFB



Men₃SnNTf₂ hydrogen
activation
¹¹⁹Sn {¹H} NMR in 1,2-DFB

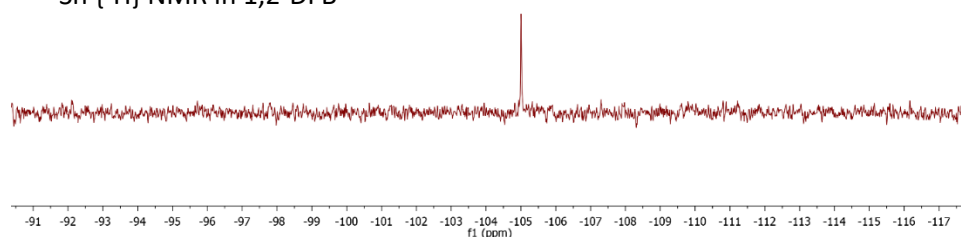


Figure 7.49 ¹¹⁹Sn NMR spectra collected after 21 h in the hydrogen activation with Men₃SnNTf₂

7.2.5 Stoichiometric and catalytic reduction of **13g**

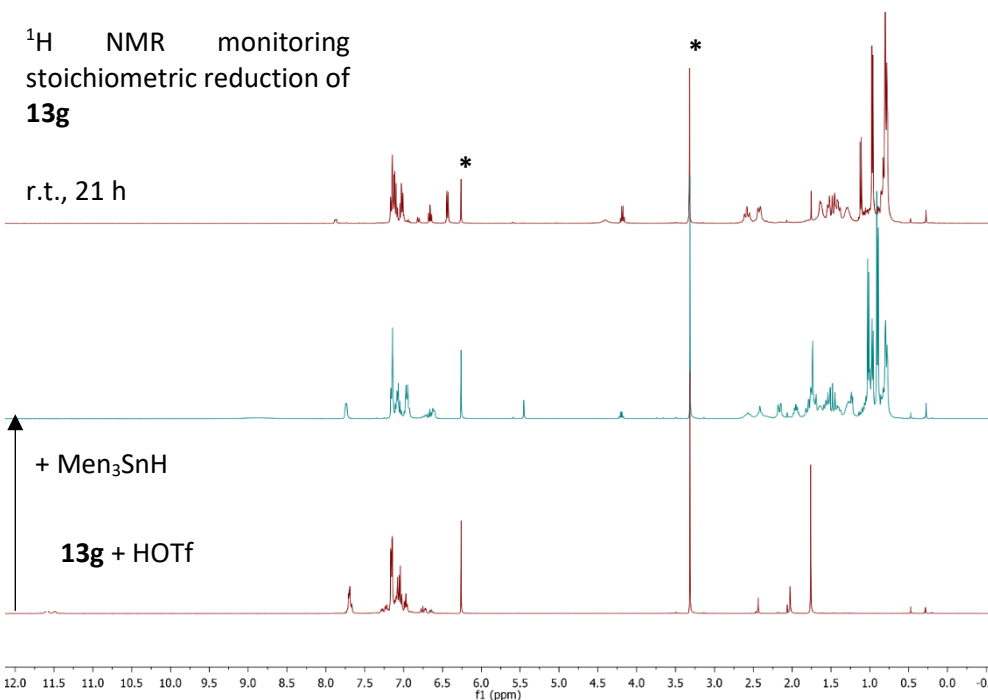


Figure 7.50 ¹H NMR monitoring stoichiometric reduction of **13g**; * = capillary insert containing 0.1 M 1,3,5-trimethoxybenzene solution in C₆D₆

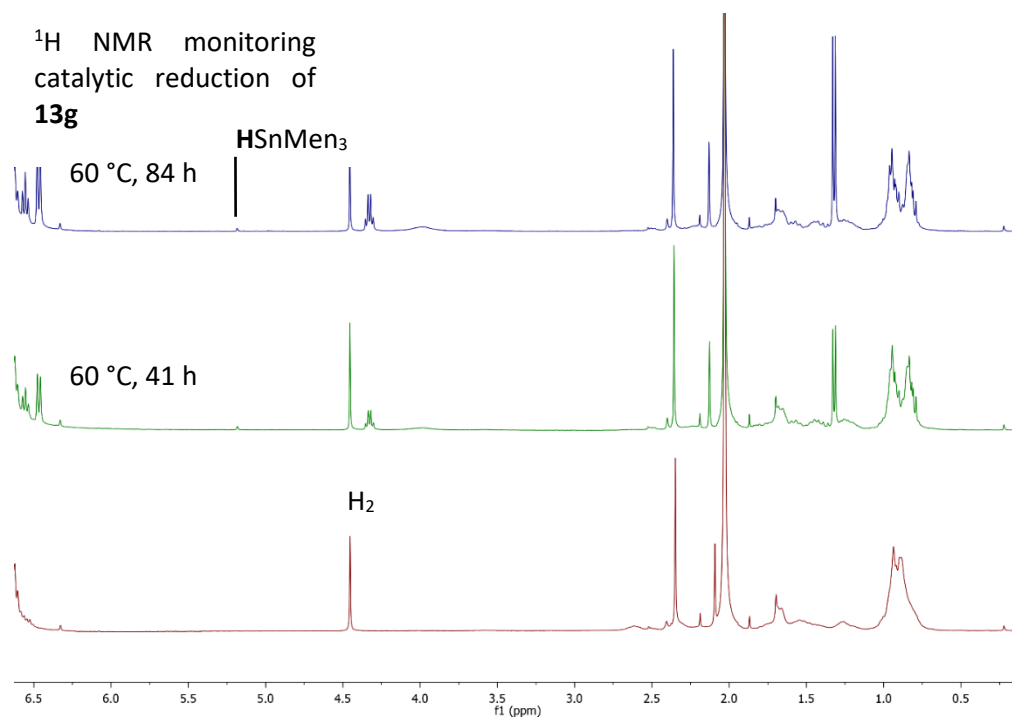


Figure 7.51 ¹H NMR monitoring catalytic reduction of **13g**

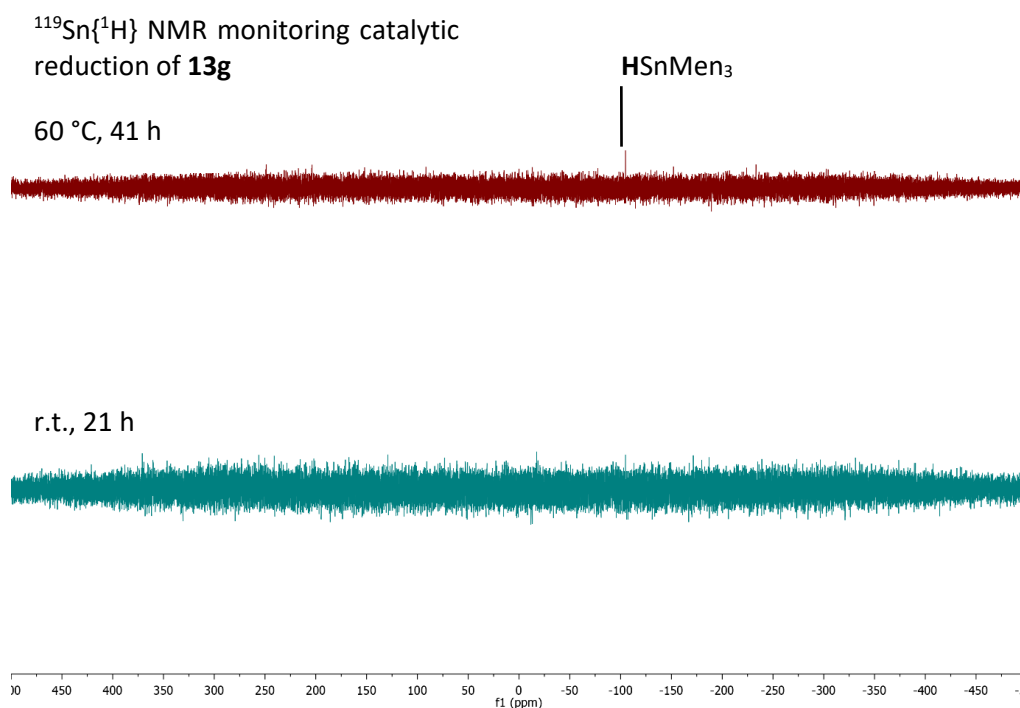
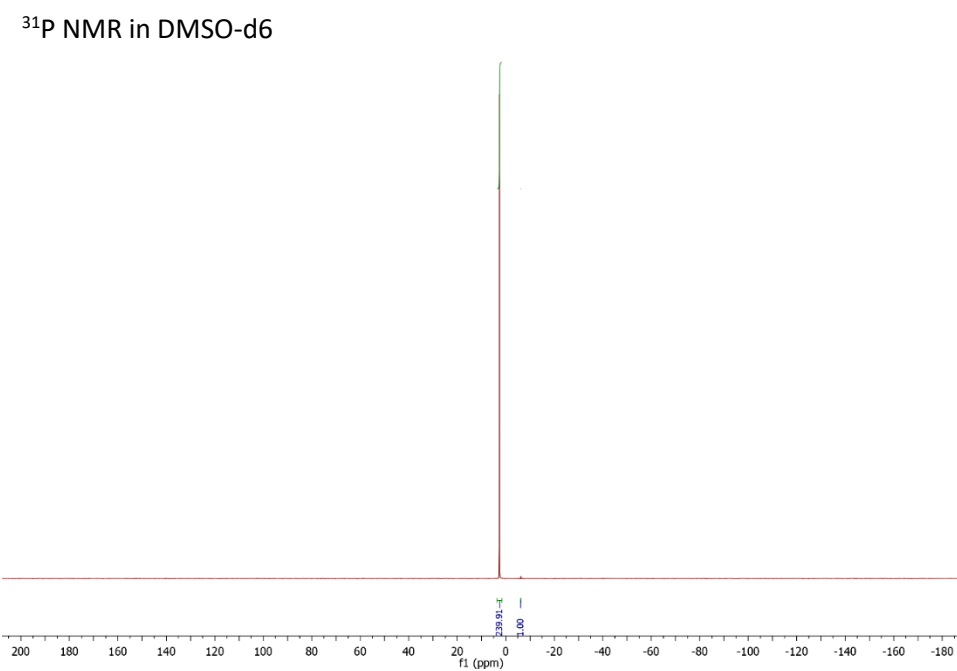
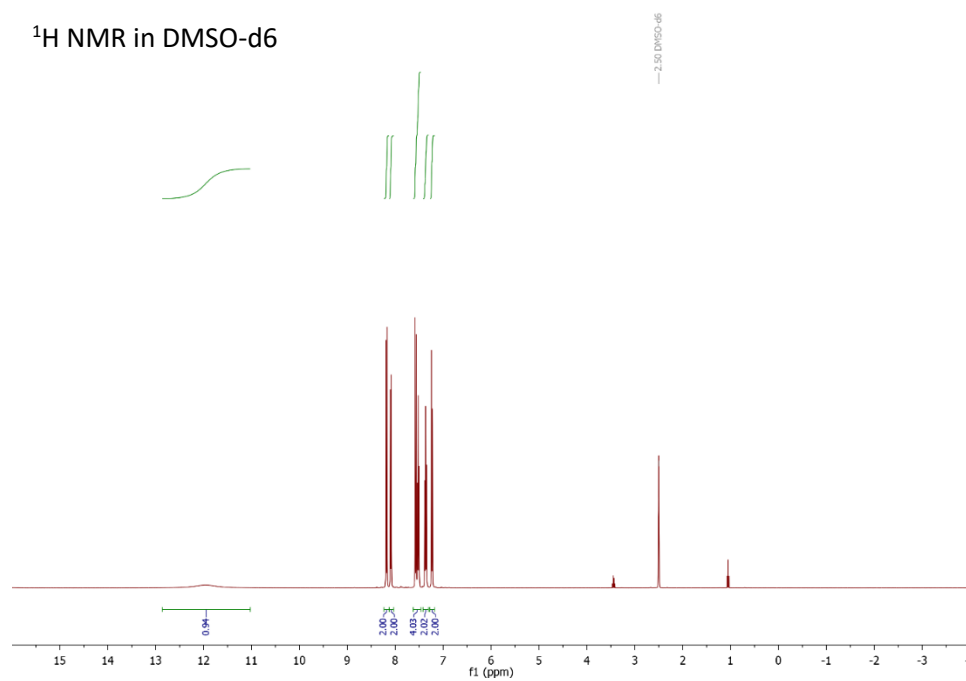


Figure 7.52 ¹¹⁹Sn{¹H} NMR monitoring catalytic reduction of **13g**

7.3 Chapter 4

7.3.1 Preparation and characterisation of phosphate salts and their adducts



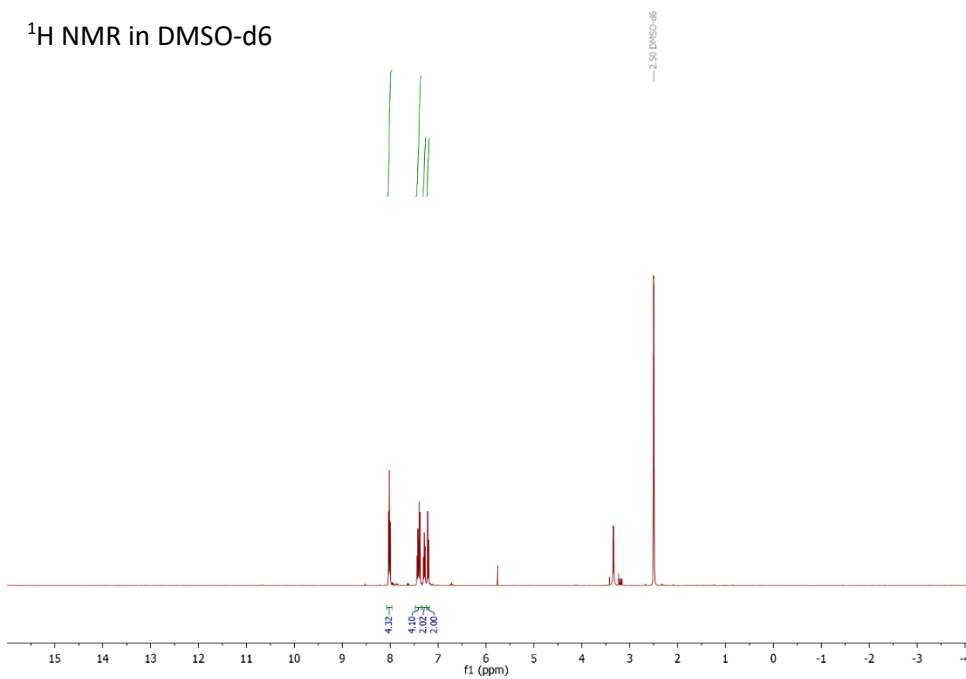


Figure 7.55 R-[200]Na

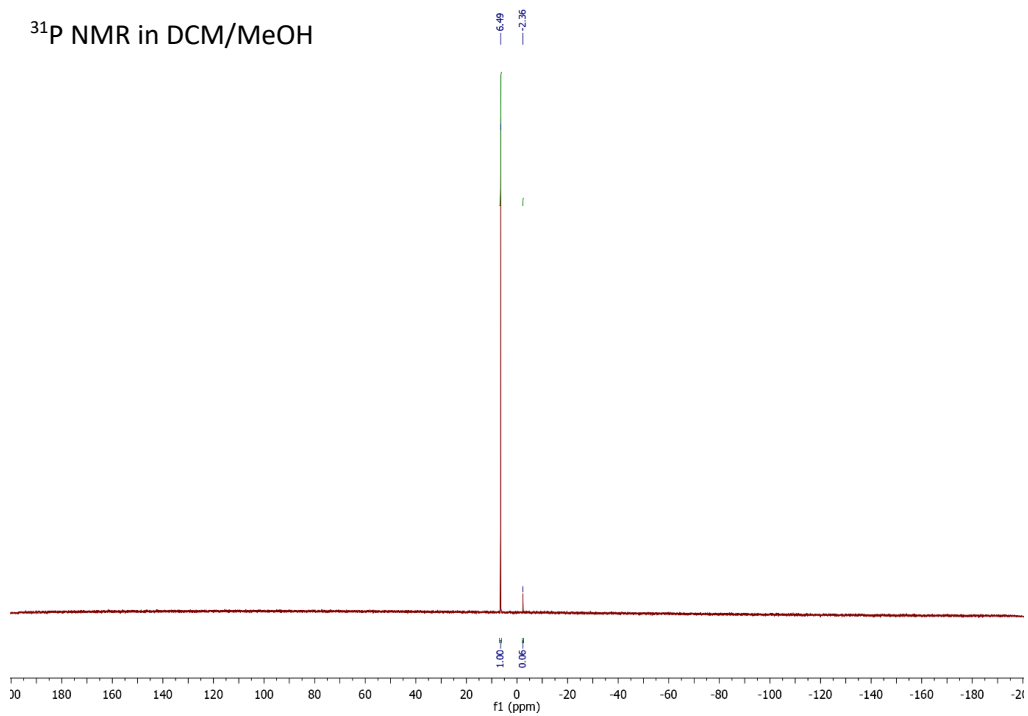


Figure 7.56 R-[200]Na

^{13}C NMR in THF

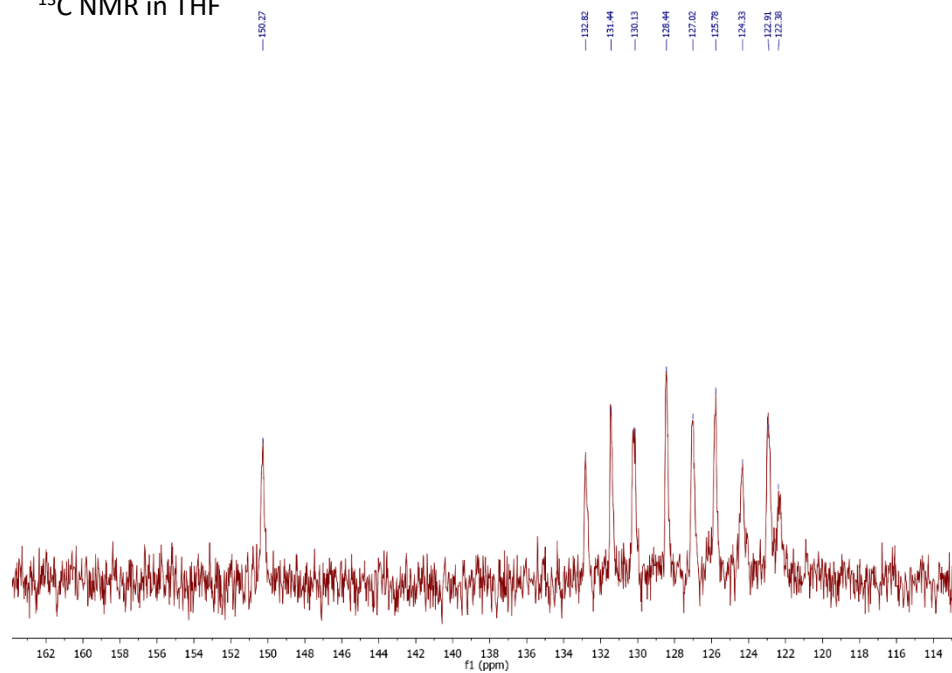


Figure 7.57 *R*-[200]Na

^1H NMR in DMSO- d_6

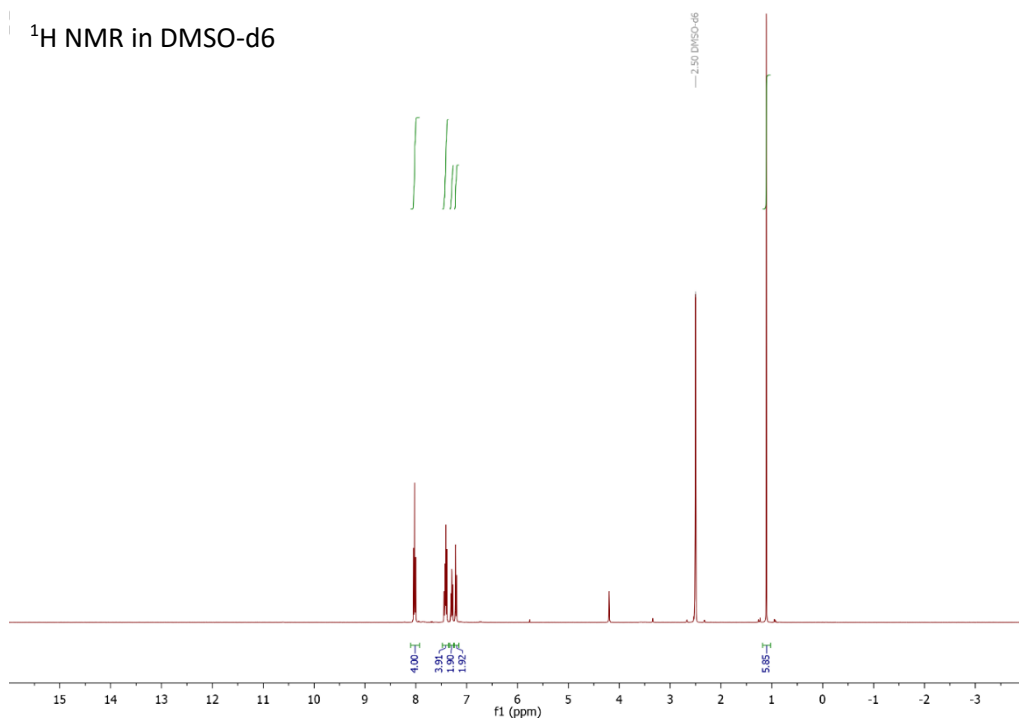


Figure 7.58 Racemic [200]Li

^{31}P NMR in DMSO-d₆

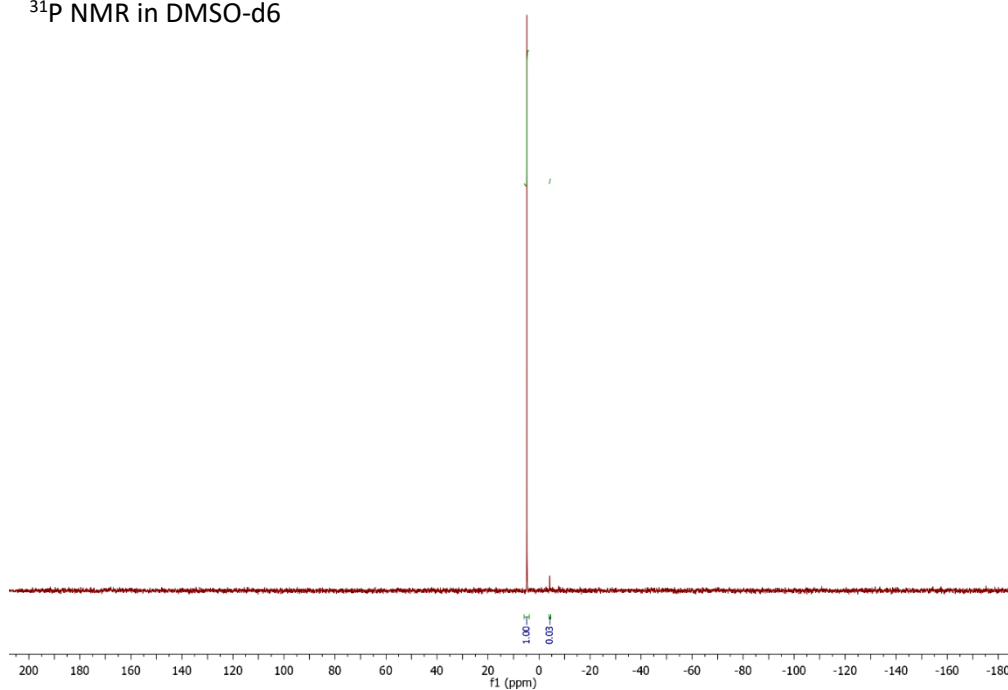


Figure 7.59 Racemic **[200]**Li

^{13}C NMR in DMSO-d₆

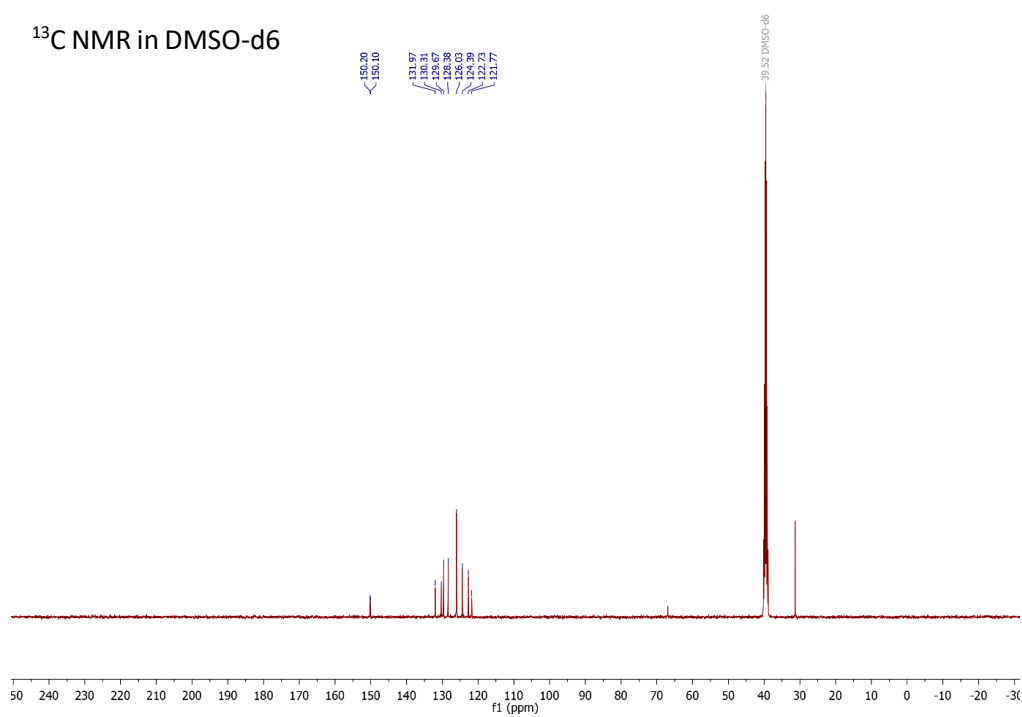
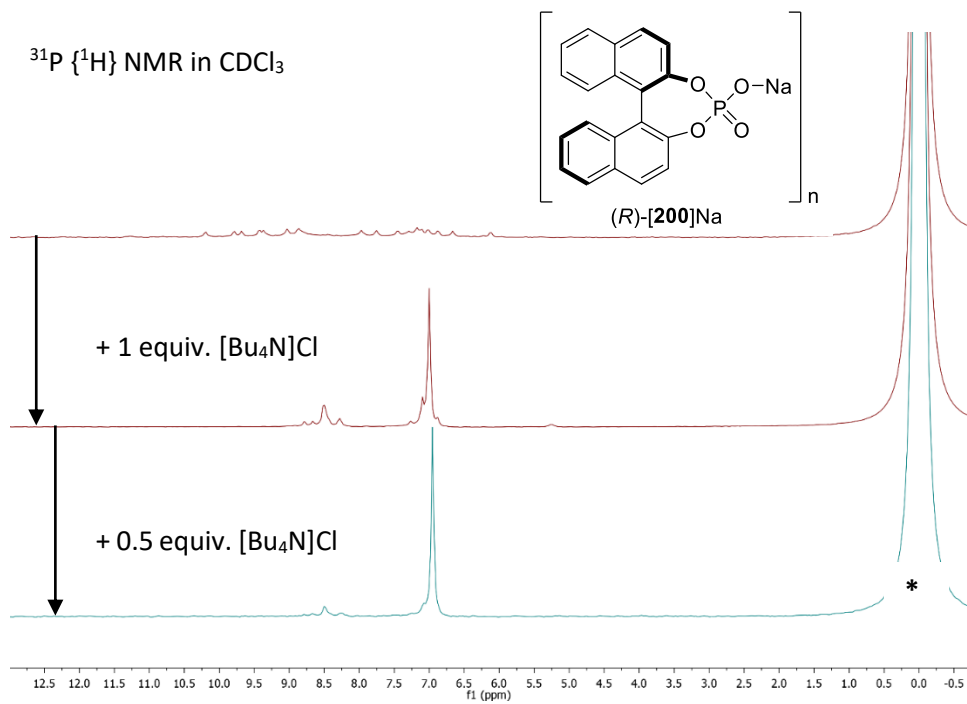
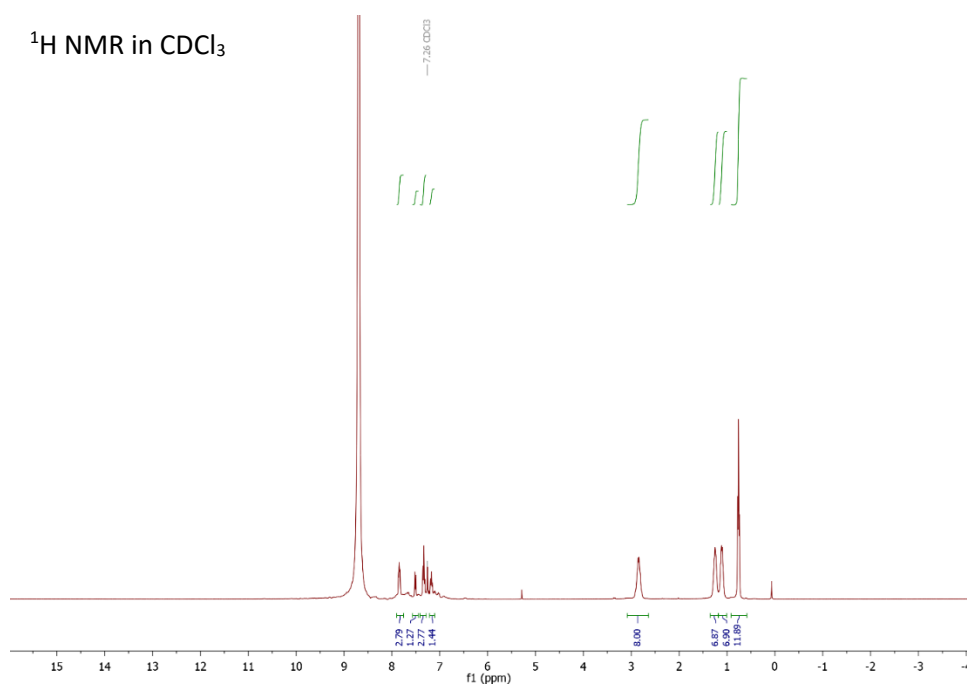


Figure 7.60 Racemic **[200]**Li



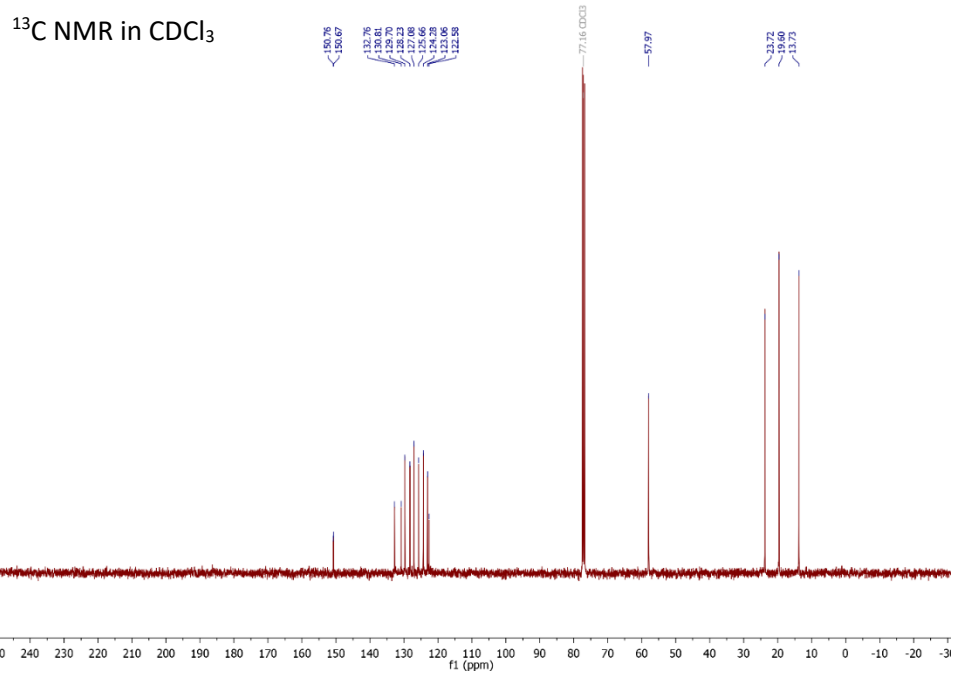


Figure 7.63 *R*-[200][Bu₄N]

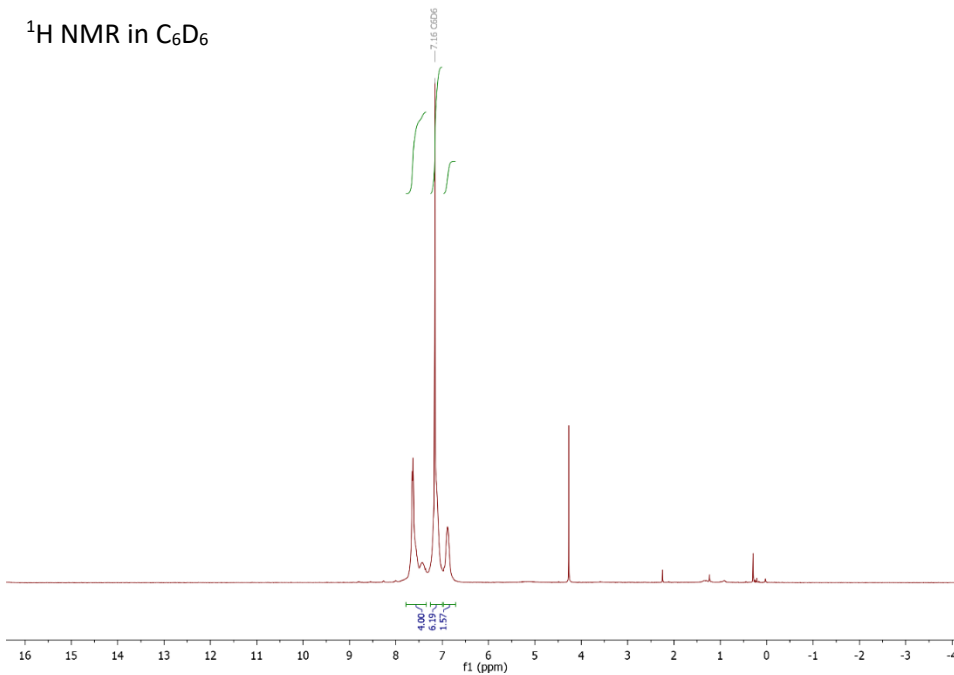


Figure 7.64 (*R*)-[201]Na

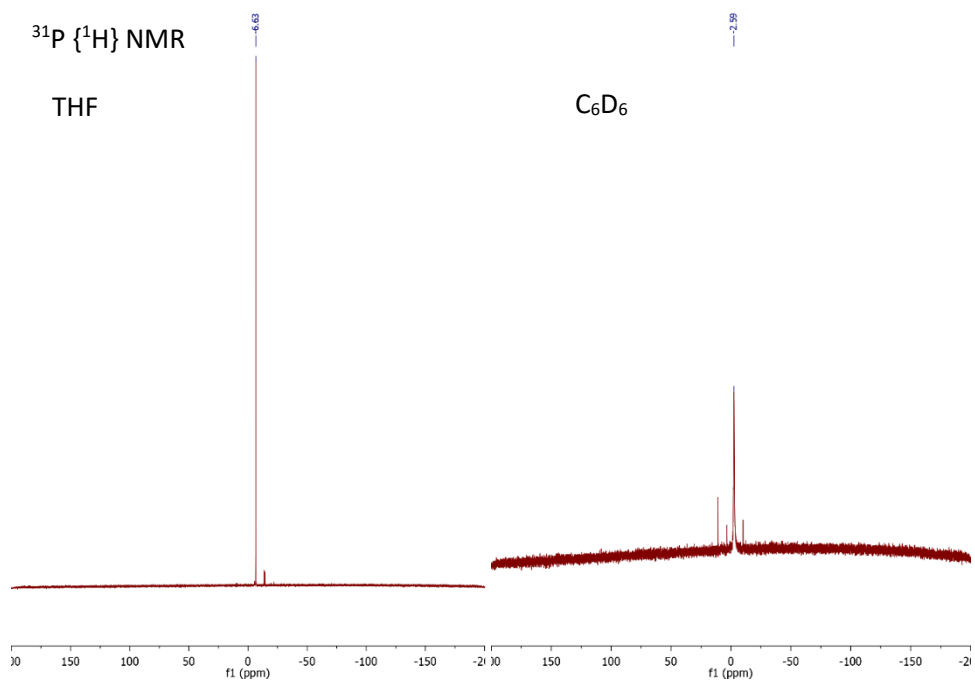


Figure 7.65 (*R*)-[201]Na

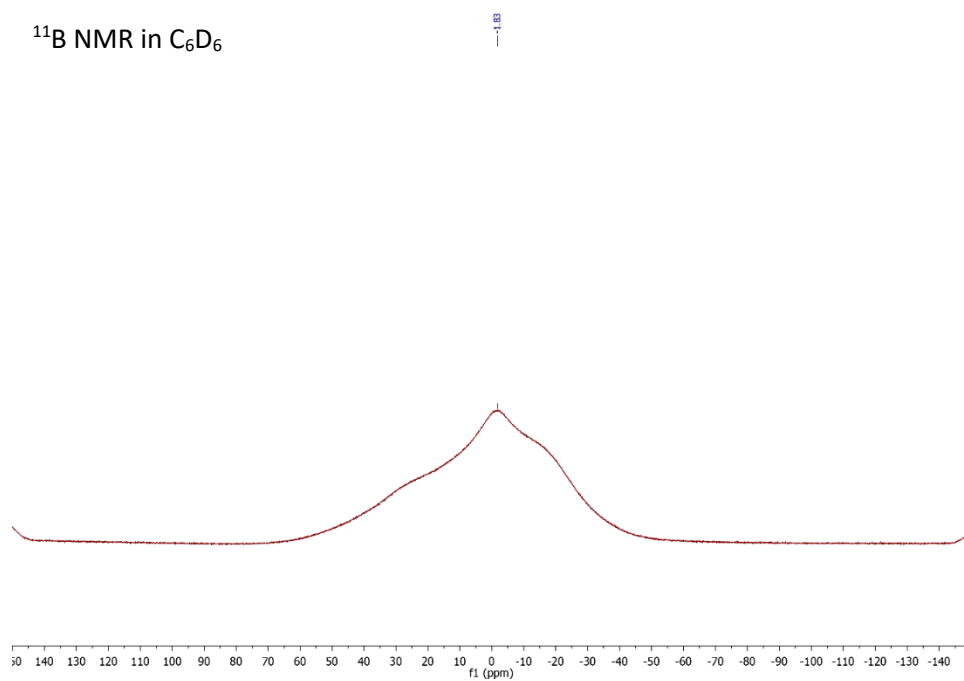


Figure 7.66 (*R*)-[201]Na

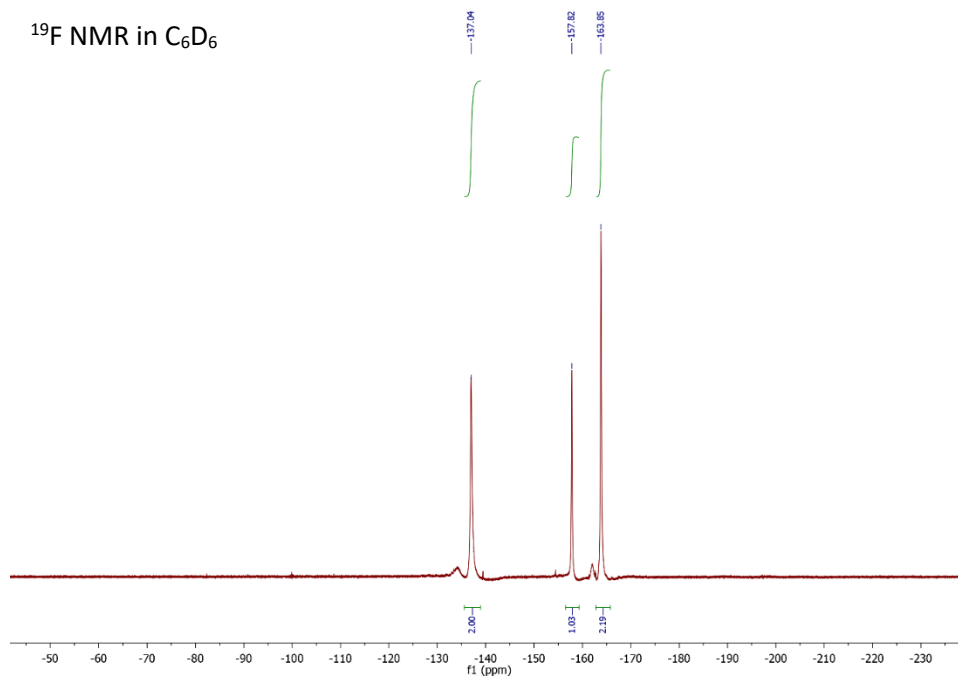


Figure 7.67 (R)-[201]Na

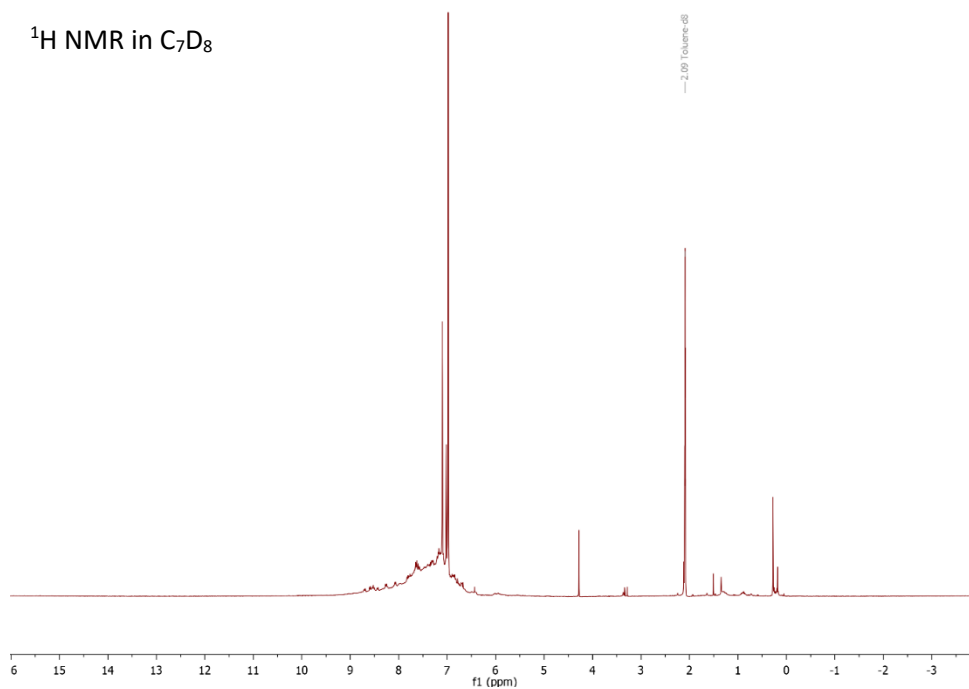


Figure 7.68 (R)-[202]Na

$^{31}\text{P} \{^1\text{H}\}$ NMR in C_7D_8

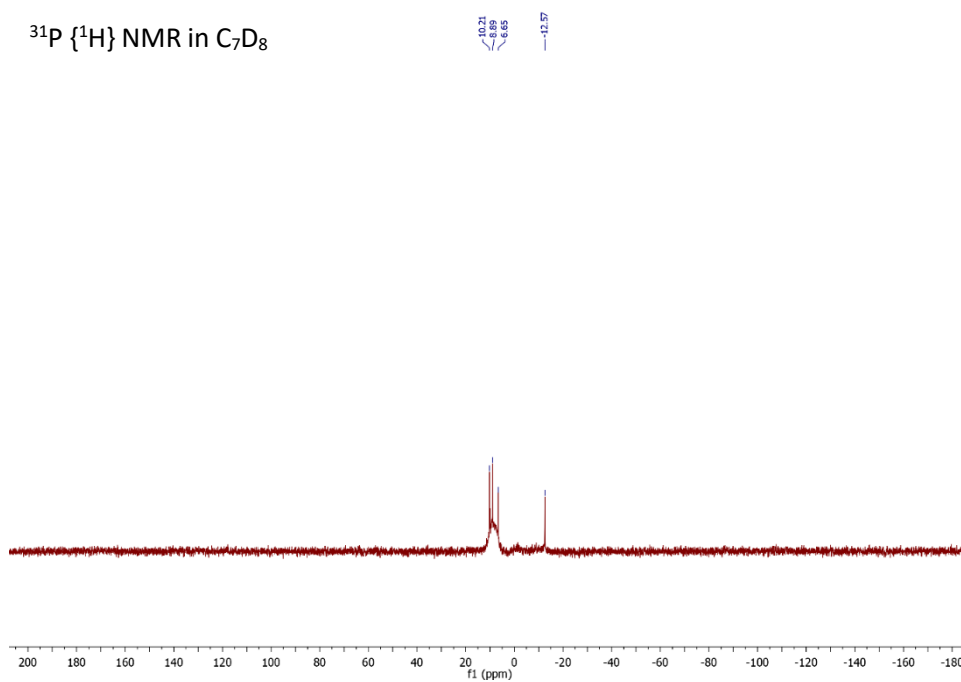


Figure 7.69 (*R*)-[**202**]Na

^{19}F NMR in C_7D_8

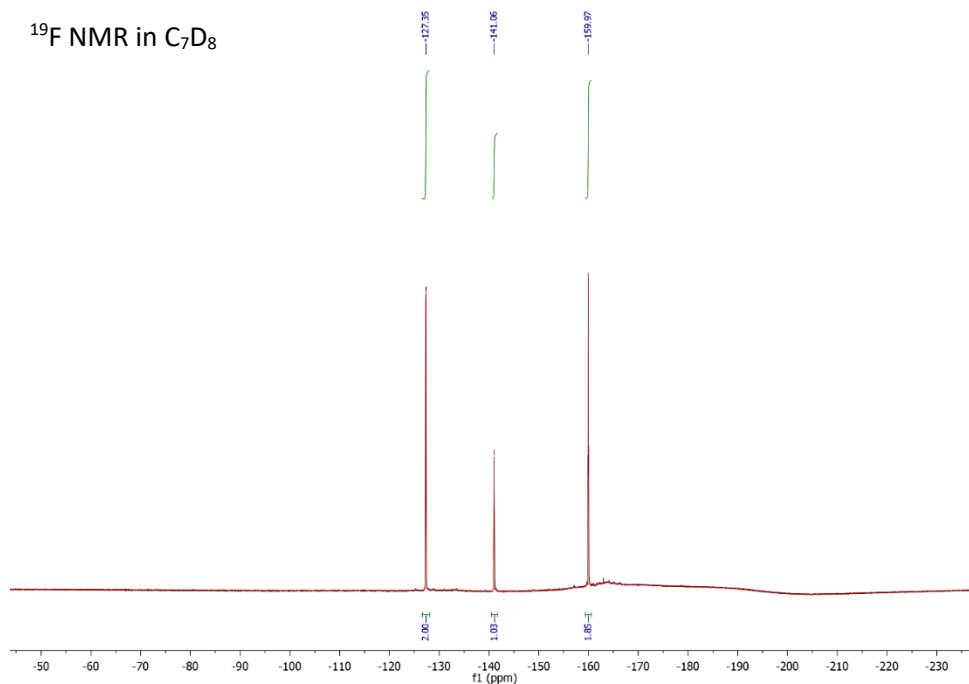
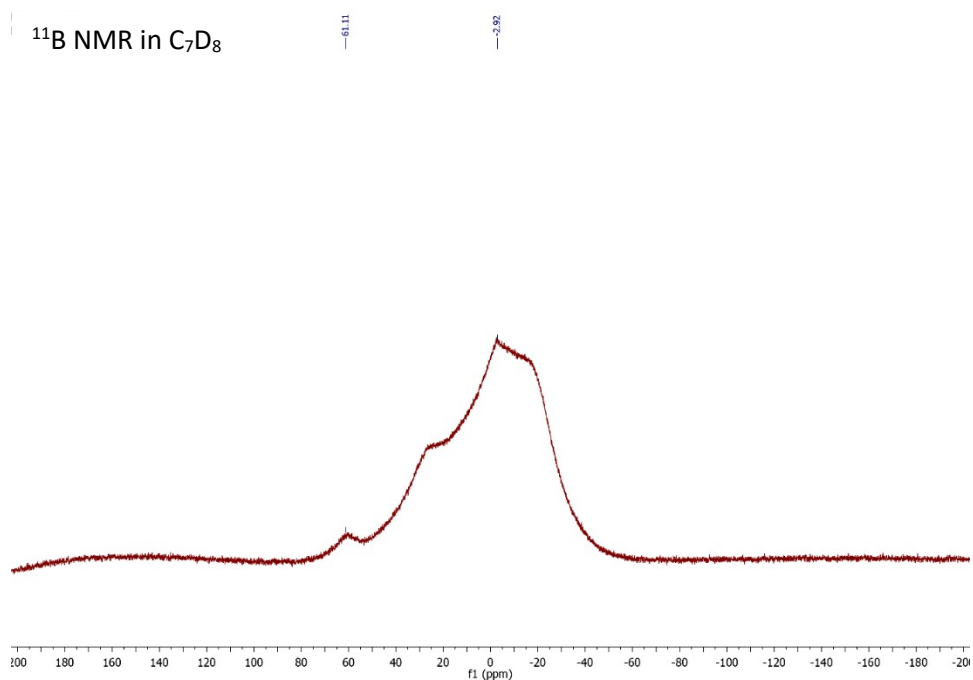
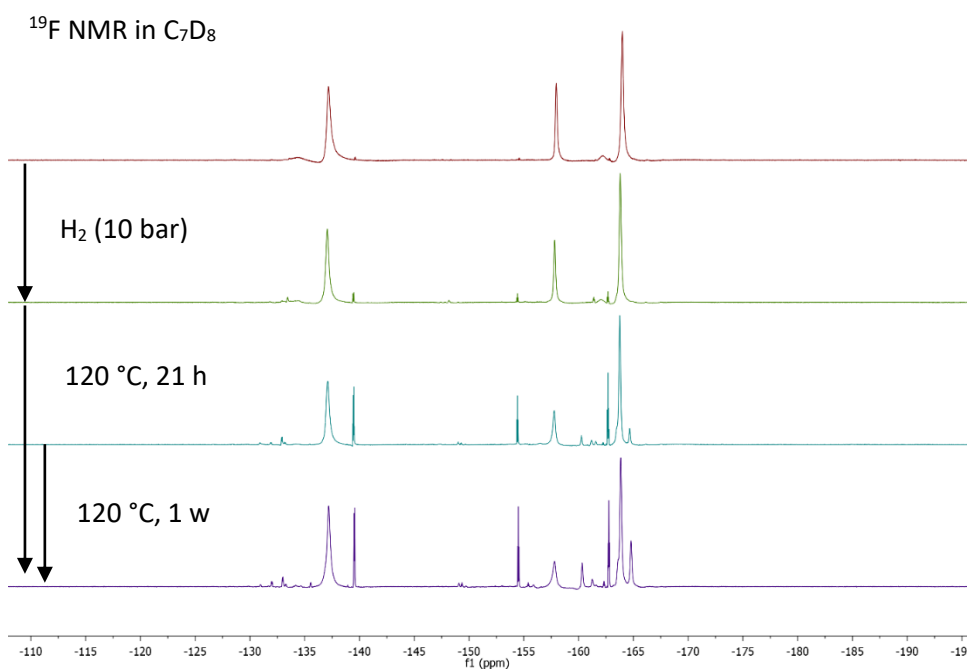


Figure 7.70 (*R*)-[**202**]Na



7.3.2 Hydrogen activation studies



^{11}B NMR in C_6D_6

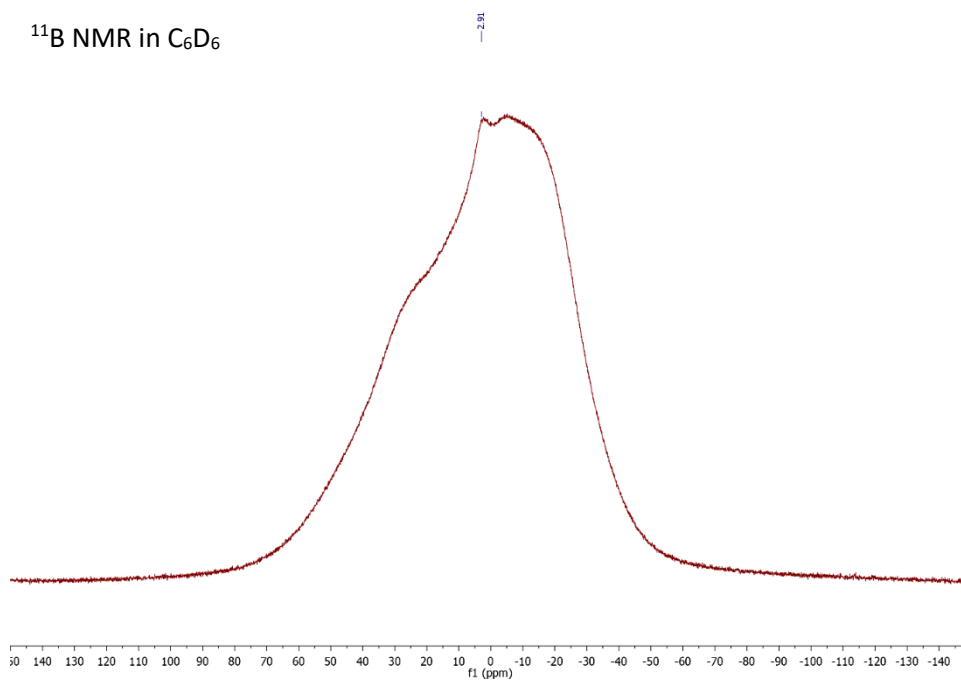


Figure 7.75 Borane **208**

^{31}P $\{^1\text{H}\}$ NMR in C_6D_6

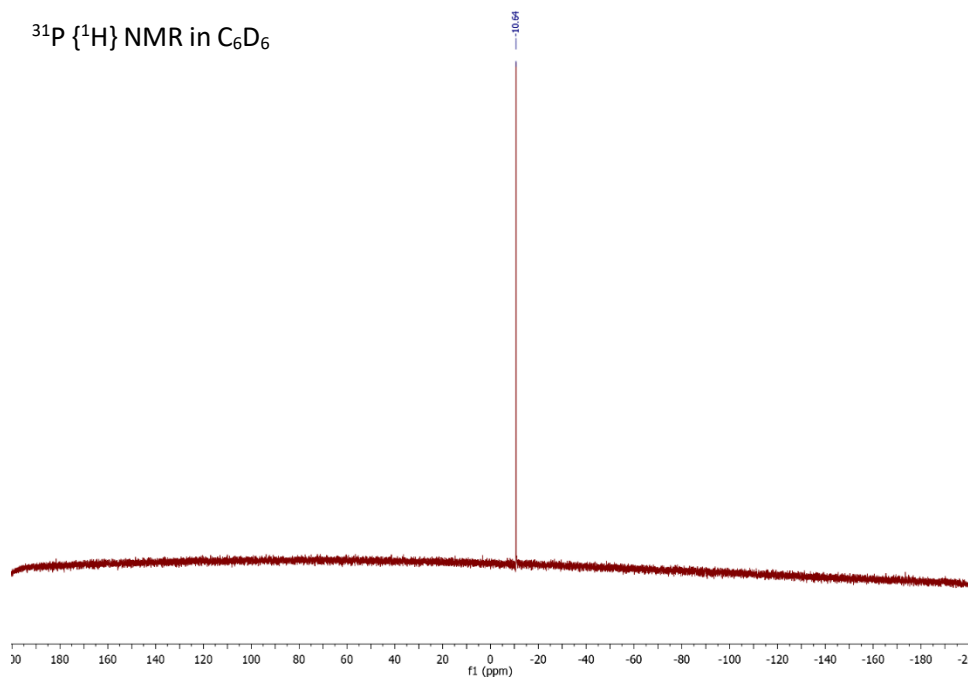


Figure 7.76 Borane **208**

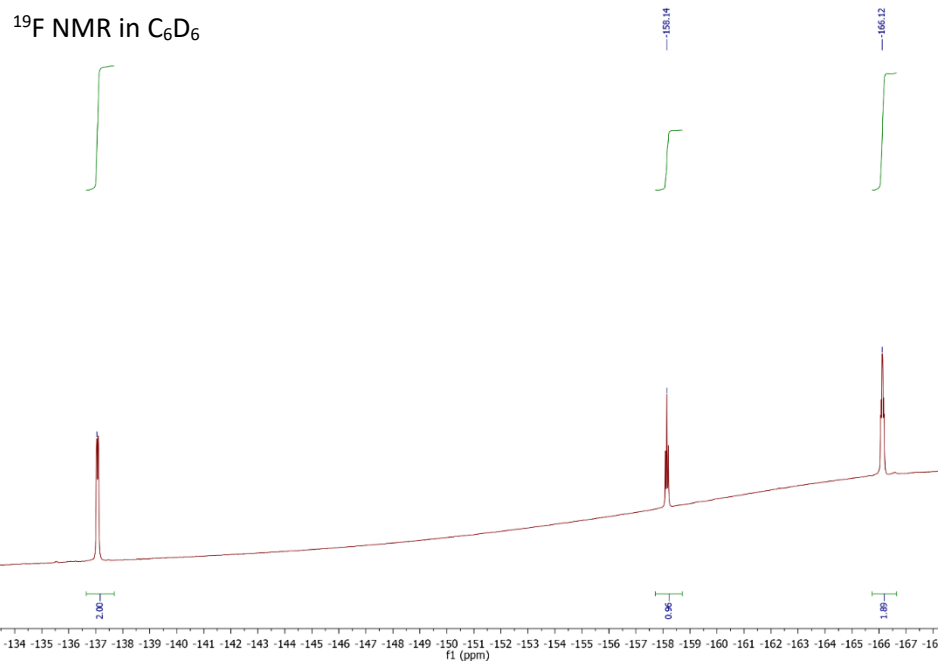


Figure 7.77 Borane **208**

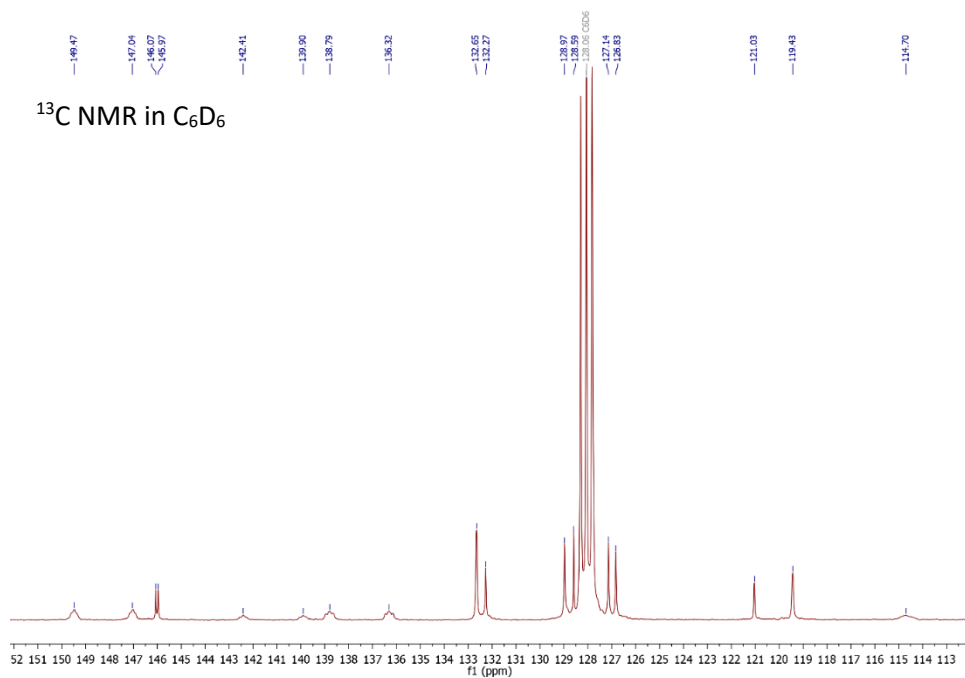


Figure 7.78 Borane **208**

7.3.4 Stoichiometric and catalytic reduction studies

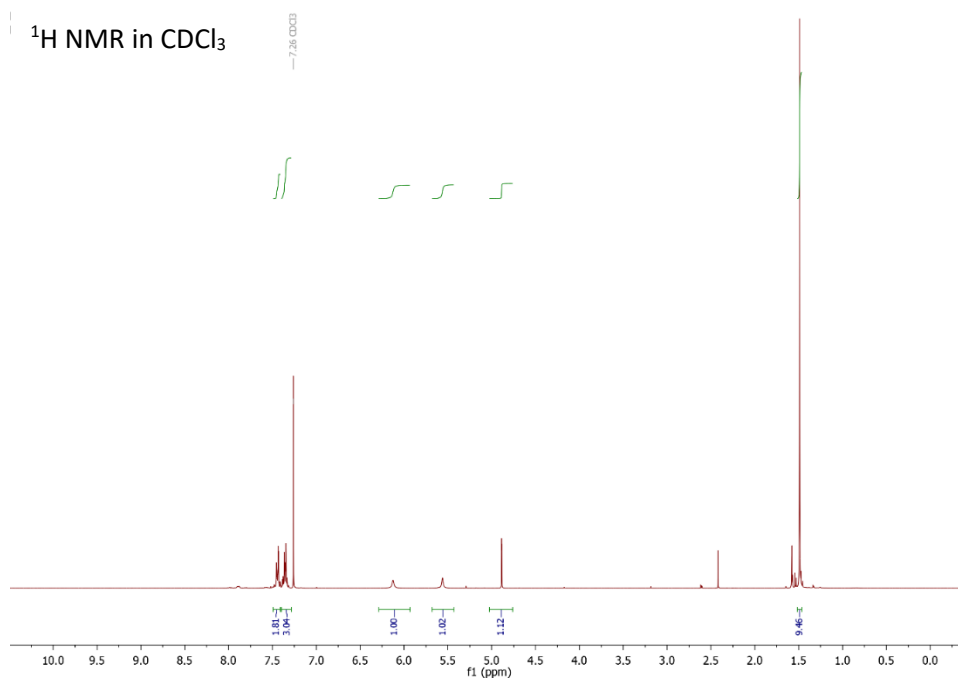


Figure 7.79 Enamine **205**

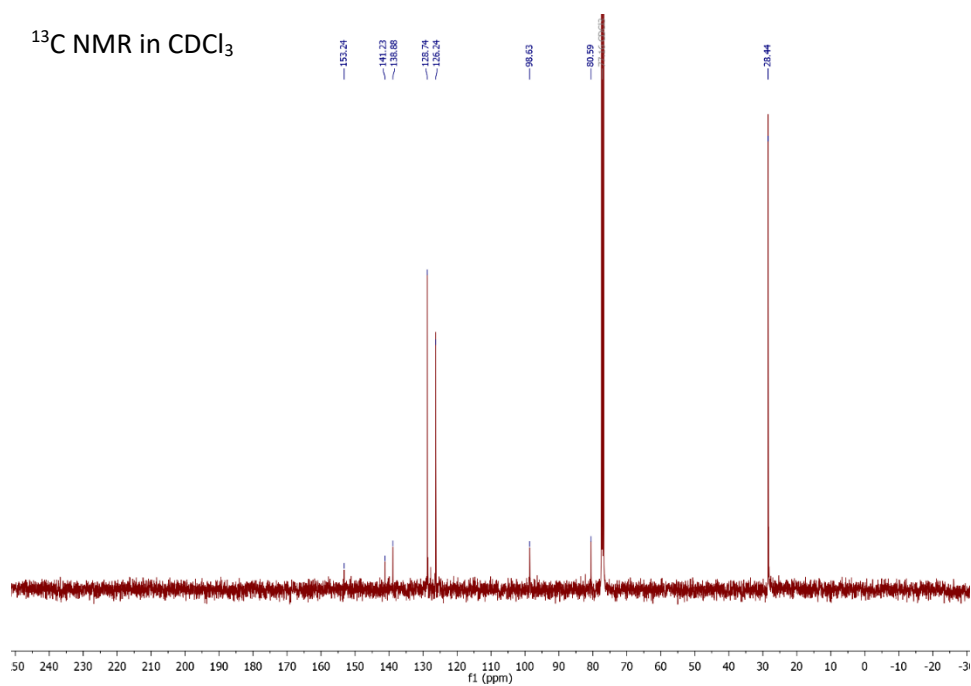


Figure 7.80 Enamine **205**

^1H NMR in CDCl_3

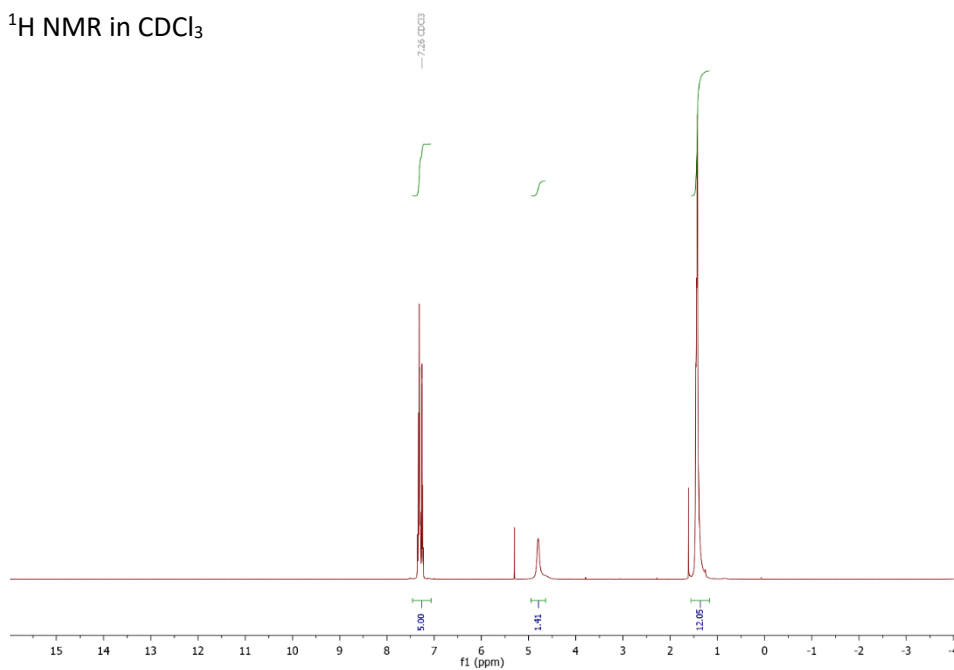


Figure 7.81 Racemic **206**

^{13}C NMR in CDCl_3

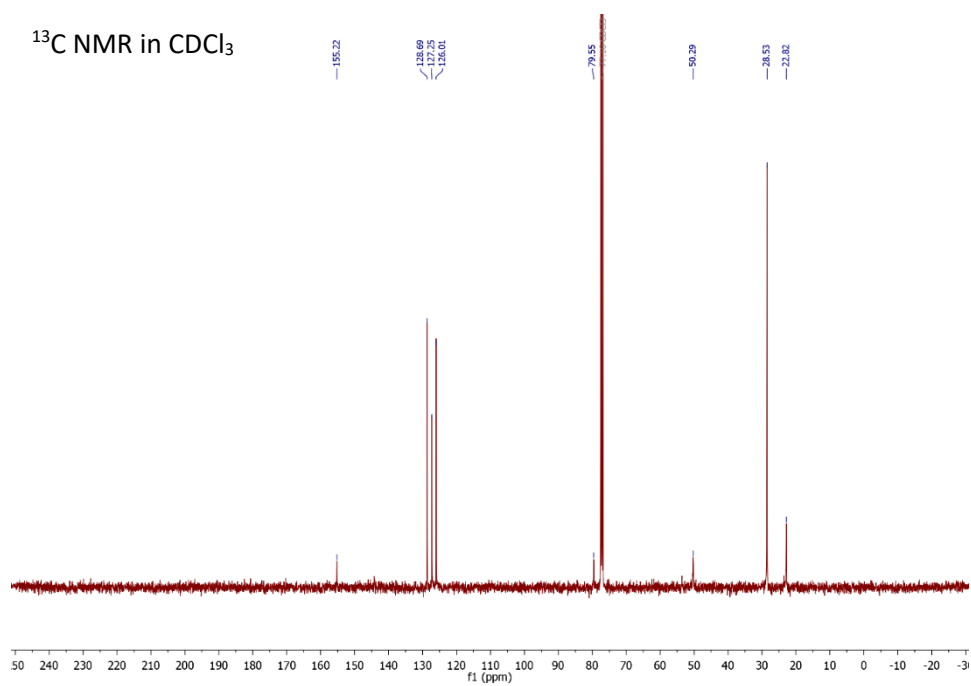


Figure 7.82 Racemic **206**

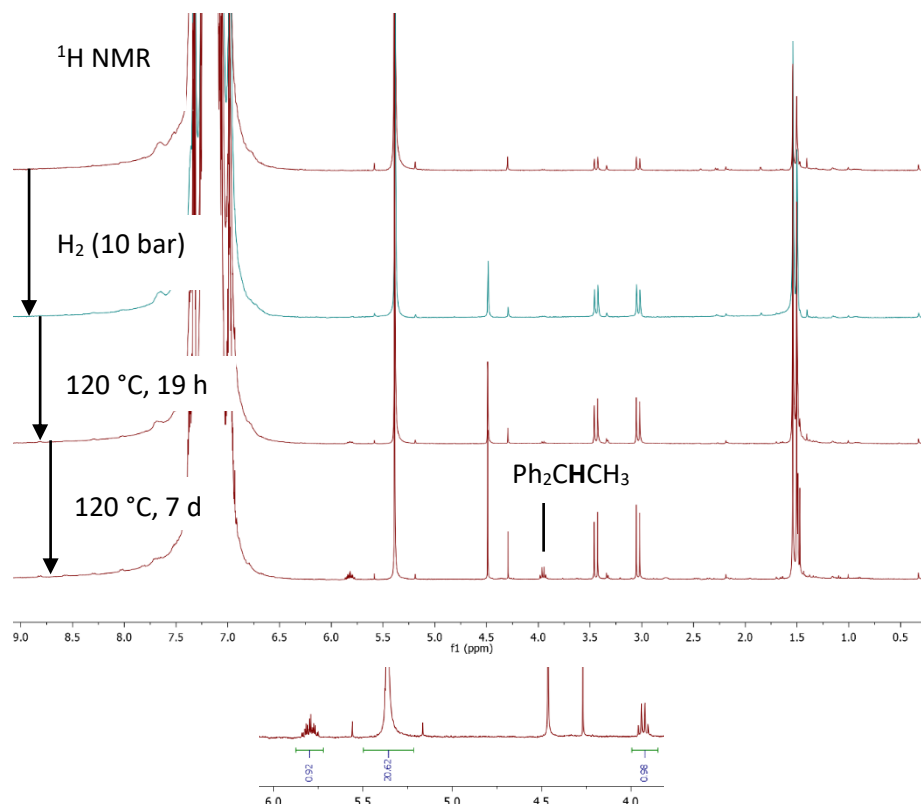


Figure 7.83 Hydrogenation of diphenylethene **210**

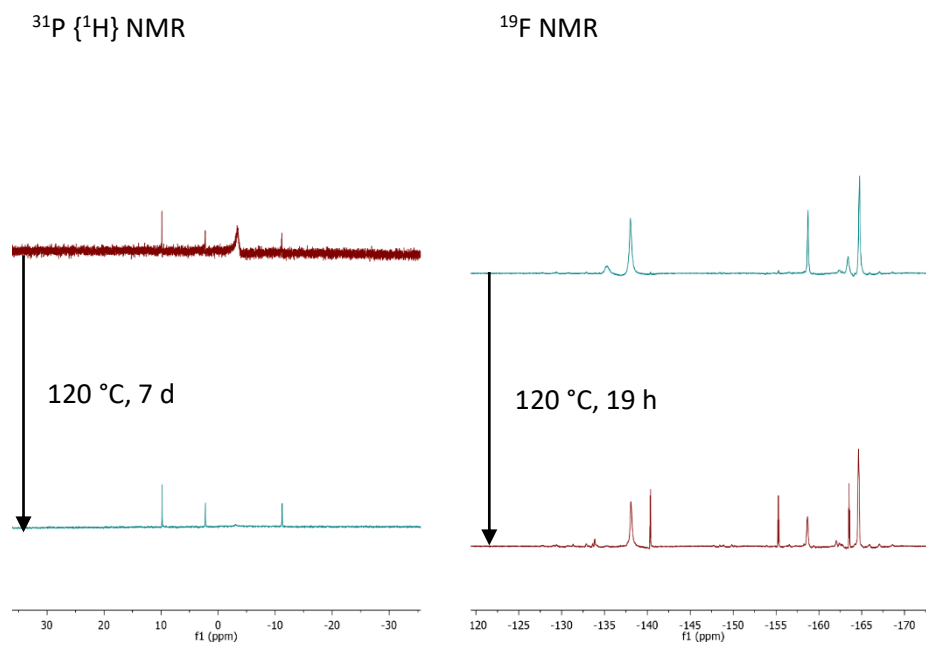


Figure 7.84 Hydrogenation of diphenylethene **210**

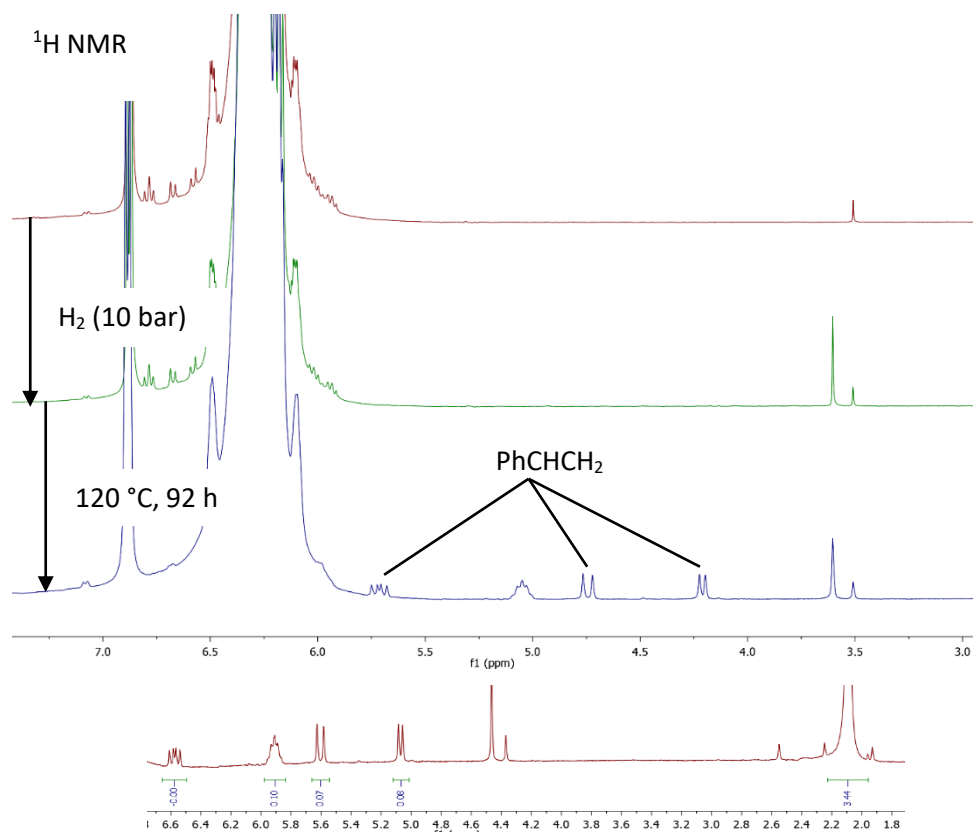


Figure 7.85 Hydrogenation of acetophenone **12c**.